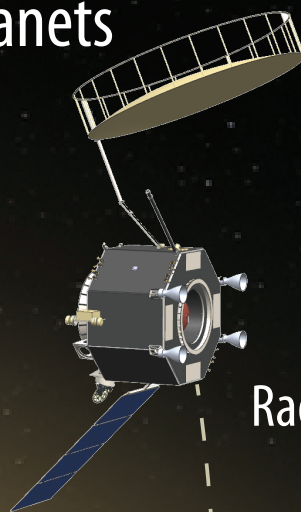




**SmallSats**  
(Loss Mechanisms,  
Particles and Fields)

# 2020 Venus Flagship Mission Study

A mission to explore the habitability of Venus  
and the origins of Earth-sized planets  
both near and far...



**Orbiter**  
(SAR, NIR, Gravity,  
Radio Science, Sub-mm)



**Aerobot**  
(Dynamics,  
Chemistry, Geophysics)



Volcano

Plains

**Lander on Descent**  
(Chemistry, Imaging)

**Lander + LLISSE**  
(Chemistry, Mineralogy,  
Weather)

Tesserae

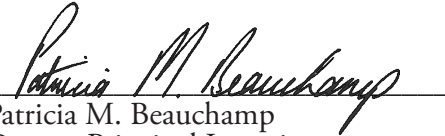
# Venus Flagship Mission Decadal Study Final Report

A Planetary Mission Concept Study Report  
Presented to the Planetary and Astrobiology Decadal Survey

08 August 2020



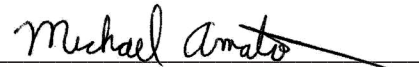
Martha S. Gilmore  
Principal Investigator  
Wesleyan University



Patricia M. Beauchamp  
Deputy Principal Investigator  
Jet Propulsion Laboratory  
California Institute of Technology




Richard Lynch  
Technical Lead  
NASA's Goddard Space Flight Center



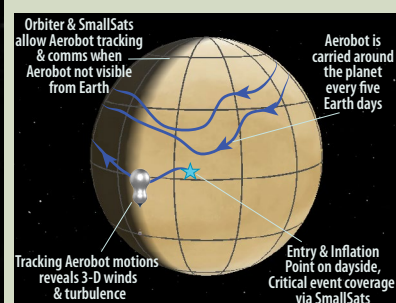
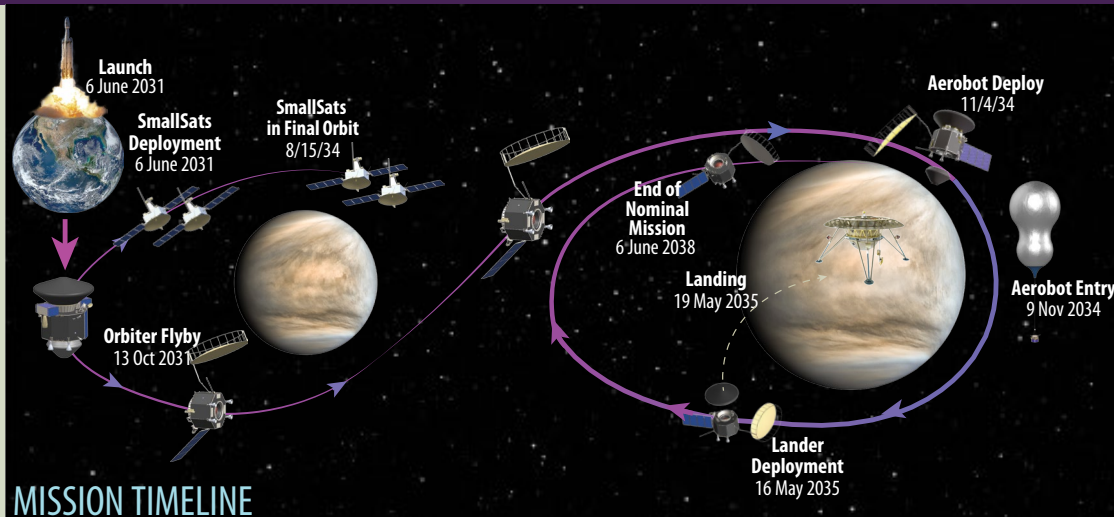
Michael J. Amato  
Planetary and Lunar Business Lead  
NASA's Goddard Space Flight Center

# Venus Flagship Mission Study

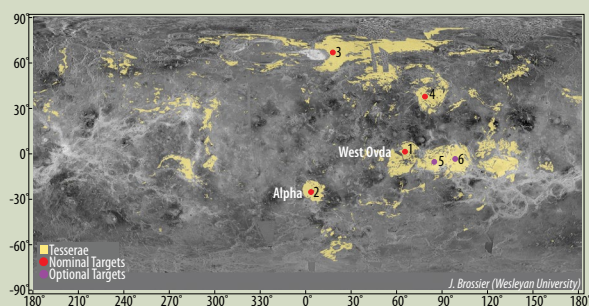
A MISSION TO EXPLORE THE HABITABILITY OF VENUS

PI: Martha Gilmore, *Wesleyan University*; D-PI: Patricia Beauchamp, *Jet Propulsion Laboratory, California Institute of Technology* 

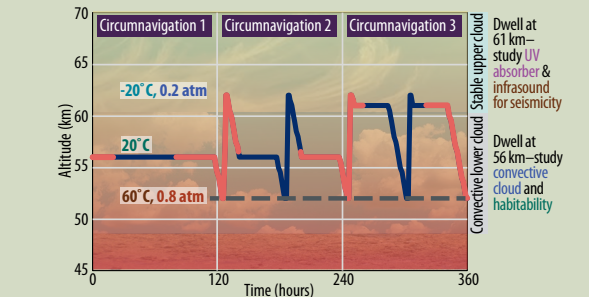
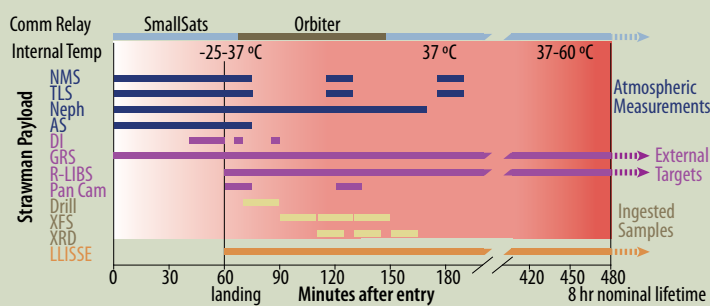
## MISSION ARCHITECTURE



The Venus Flagship mission will deliver two *in situ* assets to Venus—a Lander to newly visit the ancient tessera terrain, and a variable altitude Aerobot within the cloud layer over 60 days.



The Lander thermal design supports instrument functionality over a 1 hour descent phase and 7 hour landed phase.



The Aerobot has variable altitude capability, allowing characterization of different levels of the venusian cloud deck.

## SCIENCE GOALS & OBJECTIVES

Science Goals	Science Objectives
Understand the history of volatiles and liquid water on Venus and determine if Venus has ever been habitable.	Determine if Venus once hosted liquid water at the surface.
	Identify and characterize the origins and reservoirs of Venus's volatiles today. Place constraints on whether there are habitable environments on Venus today and search for organic materials and biosignatures.
Understand the composition and climatological history of the surface of Venus and the present-day couplings between the surface and atmosphere.	Constrain the composition of the surface and chemical markers of past and present climate.
Understand the geologic history of Venus and whether Venus is active today.	Determine if Venus shows evidence of a current or past plate tectonic regime.
	Determine whether Venus is tectonically and volcanically active today.

## SCIENCE PAYLOADS

Orbiter
Synthetic Aperture Radar (SAR)
Near-IR Imager (NIR-I)
Electron Electrostatic Analyzer (ESA-e)
Ion Electrostatic Analyzer (ESA-i)
Magnetometer (Mag)
Sub-mm Spectrometer (S-mm)
Neutral Mass Spectrometer (NMS)
EUV Sensor (EUV)

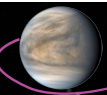
2 SmallSats
Ion Electrostatic Analyzer (ESA-i)
Electron Electrostatic Analyzer (ESA-e)
Magnetometer (Mag)
Solar Energetic Particle Detector (SEPD)
Electric Fields Detector (E-FD)
Langmuir Probe (LP)

Aerobot
Aerosol Mass Spectrometer with Nephelometer (AMS-N)
Fluorimetric Microscope (FM)
Meteorological Suite (P, T, Radiometer, 3-D Wind Sensor, Dosimeter) (MET)
Visible Imager (VI)
Magnetometer (Mag)

	Lander
Descent	Neutral Mass Spectrometer (NMS)
	Tunable Laser Spectrometer (TLS)
	Atmospheric Structure Suite (P, T, Radiometer) (AS)
	Descent NIR imager (DI)
	Nephelometer (Neph)
	Neutron Generator/Gamma Ray Spectrometer (NG/GRS)
	X-Ray Diffractometer (XRD)
	X-Ray Fluorescence Spectrometer (XFS)
	Raman-LIBS Instrument (R-LIBS)
	Panoramic Camera (PC)
	Sample Drill
	Long lived meteorologic suite (LLISSE)

## SCIENCE TEAM

Science Team Members
Sushil Atreya, <i>University of Michigan</i>
Patricia Beauchamp, <i>JPL-Caltech</i>
Penelope Boston, <i>NASA ARC</i>
Mark Bullock, <i>Science &amp; Technology Corp.</i>
Shannon Curry, <i>U.C. Berkeley</i>
Martha Gilmore, <i>Wesleyan University</i>
Robbie Herrick, <i>University of Alaska</i>
Jennifer Jackson, <i>Caltech</i>
Stephen Kane, <i>U.C. Riverside</i>
Joshua Knically, <i>University of Alaska</i>
Robert Lillis, <i>U.C. Berkeley</i>
Janet Luhmann, <i>U.C. Berkeley</i>
Alison Santos, <i>NASA GRC</i>
David Stevenson, <i>Caltech</i>
Colin Wilson, <i>Oxford University</i>



## MISSION ASSETS

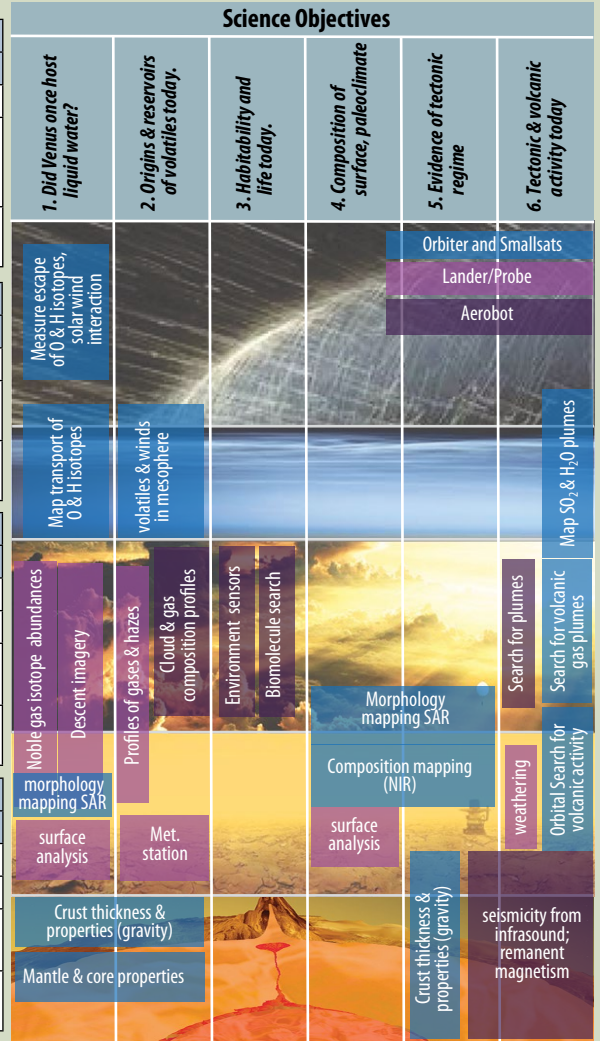


SmallSats	
Mass (MEV)	300 kg (each)
Power	Solar panels
Telecom	S-band (communication with mission assets), X-band and Ka band (Earth communication), UHF antenna (communication with long-lived station)
Functions	Science orbit (~34 months), communication relay for in situ assets

Orbiter	
Mass (MEV)	1930 kg
Power	Battery, Solar arrays
Telecom	S-band (communication with mission assets), X-band and Ka Band (Earth communication)
Functions	Science orbit (6.5 years), communication relay for in situ assets

Aerobot	
Mass (MEV)	1433 kg
Power	2 Batteries (300 Ah), Solar array
Telecom	S-band
Balloon Design	Instrument gondola, variable altitude helium balloon system
Functions	Minimum 60 day duration, variable altitude (52-62 km), global circulation

Lander	
Mass (MEV)	2002 kg
Power	9 Internal batteries (200 Ah)
Telecom	S-band to orbiter (80 mins), SmallSats (lander lifetime)
Lander Design	Ti pressure vessel, MLI insulation blankets, n-Eicosane phase change material, high vacuum environment
Functions	1 hr descent science, 7 hrs surface science, carry long lived surface meteorological package (60 days)



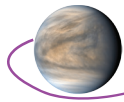
	Mass (MEV Dry, kg)	Cost (\$M, with 50% reserve)
Orbiter	1930	\$761
SmallSats (2), Wet Mass	600	\$280
Aerobot	1443	\$771
Lander	2002	\$1,238
Total Dry Mass	5965	-
Orbiter Propellant	3548	-
Launch Vehicle Adapter	71	-
Science/Management		\$662
Total	9584	\$3712

### The Venus Flagship Mission will provide major, unprecedented advancements in our understanding of the formation, evolution and habitability of terrestrial planets.

- First mission to trace volatile inventory, phase, movement, reservoirs and loss over Venus history
- First landing in tesserae thought to represent the oldest rocks on Venus
- First inventory of all major atmospheric noble gases and their isotopes
- First measurement of global surface composition from orbit
- First measurements of lower atmosphere composition with modern, high-accuracy, high-resolution instruments
- First co-located mapping of winds and composition in the mesosphere and thermosphere
- First measurement of the mineralogy and precise geochemistry of tessera terrain
- First simultaneous multipoint measurements in Venus exosphere and ionosphere
- First measurement of seismicity and remanent magnetism of Venus
- First simultaneous measurement of ion loss rates from the exosphere and thermosphere reservoirs
- First deployment of uncooled ambient temperature electronics to enable long life operation at the Venus surface

## SCHEDULE

VFM Study	Beginning	2022	2023	2024	2025	2026	2027	2028	2029	2030	2031	2032	2033	2034	2035	2042	2043
	TRL	1 2 3 4	1 2 3 4	1 2 3 4	1 2 3 4	1 2 3 4	1 2 3 4	1 2 3 4	1 2 3 4	1 2 3 4	1 2 3 4	1 2 3 4	1 2 3 4	1 2 3 4	1 2 3 4	1 2 3 4	1 2 3
		PrePhA - 12m									Launch						
ATP 1/22	ATP		PhA - 16 m														
IPDR 2/25, MPDR 6/25					PhB - 25 m												
ICDR 8/26, MCDR 12/26							PhC - 31 m				Transit to V						
IRR 12/28, LRR 5/31					IPDR	MPDR		IRR		Phase D - 42 m							
10 years						ICDR	MCDR				LRR		Phase E - 120 m				
																	Phase F
Key Mission Milestones											Small-Sats Deploy	Orbiter Venus Flyby	Small-Sats Orbit Venus	Aerobot Deploy & Entry	Lander Deploy & Entry		Orbiter Science Orbit 05/37



## **Study Team**

### **Science Team**

Sushil Atreya, University of Michigan  
Patricia Beauchamp, JPL-Caltech  
Penelope Boston, NASA ARC  
Mark Bullock, Science & Technology Corp.  
Shannon Curry, U.C. Berkeley  
Martha Gilmore, Wesleyan University  
Robbie Herrick, University of Alaska  
Jennifer Jackson, Caltech

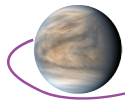
Stephen Kane, U.C. Riverside  
Alison Santos, NASA GRC  
David Stevenson, Caltech  
Colin Wilson, Oxford University  
Robert Lillis, U.C. Berkeley (Collaborator)  
Janet Luhmann, U.C. Berkeley (Collaborator)  
Joshua Knicely, University of Alaska (Student)

### **Main Technical Team at GSFC**

Naeem Ahmad	Glenn Rakow
Eric Cardiff	Rafael Rincon
Cornelis du Toit	Adan Rodriguez
Amani Ginyard	Bruno Sarli
Kyle Hughes	Marcia Segura
Art Jacques	Thomas Spitzer
Andrew Jones	David Steinfeld
Richard Lynch	Robert Thate
Paul Mason	Steve Tompkins
Ryo Nakamura	Sarah Wallerstedt
Tony Nicoletti	Miguel Benayas Penas
Eric Queen	

### **GSFC MDL Team**

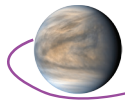
Maryam Bakhtiari-Nejad	Dick McBirney
Porfy Beltran	Frank Kirchman
Blake Lorenz	John Panek
Steve Levitski	Patrick Coronado
Kaitlyn Blair	Mark Underdown
Camille Holly	Mike Xapsos
Bob Beaman	Luis Gallo
John Young	James Sturm
Bobby Nanan	Jennifer Bracken
Sara Riall	



## **Acknowledgements**

To the many people that gave of their valuable time by participating, helping, presenting, informing and teaching us, we thank you. We could not have performed the study without you. The following are the names we captured but do not be offended if we missed citing you—at this point our memories are not quite as sharp as when we listened to you.

**Erica Aguirre, Abby Allwood, Chi Ao, Shahid Aslam, Sami Asmar, Kevin Baines, Charles Baker, Don Banfield, Bruce Bills, Dave Blake, Jeremy Brossier, Paul Byrne, Gordon Chin, Sam Clegg, Glynn Collinson, Jim Cutts, Doris Daou, Darby Dyar, Larry Esposito, Sabrina Feldman, Justin Filiberto, Stephanie Getty, Jim Greenwood, Jeff Hall, Paul Hartogh, Chris Heirwegh, Joern Helbert, Scott Hensley, Laurie Higa, Gary Hunter, Noam Izenberg, Jacob Izraelevitz, Andrew Johnson, Kandis-Lea Jessup, Attila Komjathy, Tibor Kremic, Siddharth Krishnamoorthy, Sebastian Lebonnois, Yang Liu, Earl Maize, Darby Makel, Larry Matthies, Suman Muppidi, Dragan Nikolic, Adriana Ocampo, Joe O'Rourke, Bob Pappalardo, Brian Paczkowski, Richard Quinn, Ann Parsons, Michael Pauken, Jason Rabinovitch, Bruce Milam, Miguel San Martin, Dave Senske, Raine Simons, Suzanne Smrekar, Christophe Sotin, Eric Sunada, Melissa Trainer, Allan Treiman, Ethiraj Venkatapathy, Panagiotis Vergados, Larry Wade, Michael Way, Chris Webster, Thomas Widemann.**<sub>1</sub>

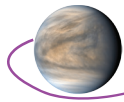


# Planetary Science Decadal Survey Venus Flagship Mission Concept Study Final Report

Fact Sheet

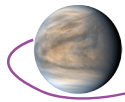
Executive Summary

1. Scientific Objectives .....	1
1.1 Science Questions and Objectives .....	1
1.2 Science Traceability Matrix.....	2
2. High-Level Mission Concept .....	3
2.1 Overview.....	3
2.2 Concept Maturity Level .....	7
2.3 Technology Maturity .....	7
2.4 Key Trades.....	7
3. Technical Overview.....	8
3.1 Instrument Payload Description.....	8
3.1.1 Lander Payload.....	8
3.1.2 Aerobot Payload.....	9
3.1.3 SmallSat Payload .....	11
3.1.4 Orbiter Payload.....	12
3.2 Flight System .....	13
3.2.1 Mission Design .....	13
3.2.2 Orbiter.....	13
3.2.3 Aerobot.....	14
3.2.4 Lander.....	16
3.2.5 SmallSats.....	18
3.3 Concept of Operations and Mission Design.....	19
3.3.1 Flight Mission Operations.....	20
3.3.2 Science Mission Operations .....	25
3.4 Risk List.....	25
4. Development Schedule and Schedule Constraints .....	26
4.1 High-Level Mission Schedule.....	26
4.2 Technology Development Plan.....	27
4.3 Development Schedule and Constraints.....	27
5. Mission Life-Cycle Cost .....	27
5.1 Costing Methodology and Basis of Estimate .....	27
5.2 Cost Estimate(s).....	28



6. Recommendations and Summary.....	28
6.1 Recommendations .....	28
6.1.1 Laboratory Measurements.....	28
6.1.2 Additional Technologies .....	28
6.2 Summary .....	29
Appendix A. Acronyms.....	A-1
Appendix B. Design Team Study Report.....	B-1
B.1 Science.....	B-1
B.1.1 The Science Rationale for Venus .....	B-1
B.1.2 Science Goals, Investigations, and Requirements of the Venus Flagship Mission.....	B-1
B.1.3 Expected Significance and Perceived Impact to State of Knowledge .....	B-24
B.1.4 Science Enhancement Options .....	B-28
B.1.5 Relationship of VFM to Other Venus Missions.....	B-28
B.2 Mission Overview.....	B-30
B.2.1 Key Architecture and Mission Trades .....	B-30
B.2.2 Mission Requirements .....	B-32
B.2.3 Planetary Protection Considerations .....	B-32
B.2.4 Mission Design Overview.....	B-34
B.2.5 Flight System.....	B-37
B.2.6 Concept of Operations .....	B-50
B.2.7 Mission Design Details.....	B-59
B.2.8 Flight System Details .....	B-73
Appendix C. Special Technical Analyses – Approaches to Safe Landing on Tessera Terrain.....	C-1
C.1 Overview .....	C-1
C.2 Approaches to Safe Landing.....	C-2
C.2.1 Regional SAR Mapping by VFM to Select Landing Site – Equatorial Mapping Orbit Study .....	C-2
C.2.2 Robust Lander Design configurations .....	C-3
C.2.3 Hazard Detection & Avoidance (HD&A) .....	C-3
C.2.4 Landing Site Analyses – Slope, Roughness, and Mantling Maps of Tessera Terrains.....	C-7
C.2.5 Recommendations for study .....	C-9
Appendix D. Additional Information on Technologies and Techniques .....	D-1
Appendix E. References .....	E-1





## Executive Summary

More than any other known planet, Venus is essential to our understanding of the evolution and habitability of Earth-size planets throughout the galaxy. **Habitability** is at the heart of our Venus Flagship Mission (VFM) study, and we approach it through tracing the history of volatile elements on Venus. We address two critical questions for planetary science: 1) How, if at all, did Venus evolve through a habitable phase? 2) What circumstances affect how volatiles shape habitable worlds? More than any other group, volatile elements have a strong influence on the evolutionary paths of rocky bodies and are critical to understanding solar system evolution. It is clear that Venus experienced a different volatile element history from the Earth thus providing the only accessible example of one end-state of habitable Earth-size planets. Venus will allow us to identify the mechanisms that operate together to produce and maintain habitable worlds like our own.

Venus is a complex planet—a highly interactive system—and, as befits a Flagship mission, the VFM concept is uniquely capable of **complementary scientific measurements to examine the synergistic behaviors of the interior, surface, atmosphere, and ionosphere**. Similar to the 2009 Venus Flagship Mission Study, but with only a **single launch on a Falcon 9 heavy expendable**, our mission architecture relies on **five collaborative platforms** to measure the factors that control the distribution of volatiles from the interior to the exosphere—volatile inventory, volcanic activity, weathering, atmosphere dynamics, cloud formation and atmospheric loss. Instruments on these platforms will assess the volatile reservoirs, inventory, and cycles over Venus history to constrain the habitability of Venus and terrestrial planets generally.

The single launch will deliver an **Orbiter, Lander, variable-altitude Aerobot, and two Small Satellites (SmallSats)** that will use multiple instruments to probe and measure the exosphere, atmosphere and surface at multiple scales with high precision. West Ovda Regio tessera will be our nominal landing site to examine rocks considered to be among the most likely to have formed in a habitable climate regime. For robustness, key measurements, such as geochemistry and mineralogy, are made with redundant instruments, with some less resource-intensive instruments duplicated on different platforms to enable risk mitigation, graceful mission degradation and low risk strategy.

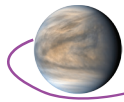
The VFM architecture is within current state-of-the-art. VFM requires minimal technology development and takes advantage of the advancements in the last 10 years, but it is also flexible to new engineering approaches as the next decade proceeds. Trade studies contributed to the architectural design. A requirement to limit the g forces on entry to < 50g enabled the use of heritage instruments. Qualification of instruments in the various Venus environments—be it the thermally isolated pressure vessel of the Lander or the relatively benign environment of the Aerobot gondola at 52–62 km altitude—is anticipated to be the major cost of most instruments.

The estimated cost (Phases A-F) of the Venus Flagship Mission is \$3.7B (2025 \$s) with the technology development costs prior to PDR totaling ~\$79M (real year \$s). The top four risks to the mission are (in order): landing on potentially steep terrain, landing hazard avoidance, Lander complexity, and overall architectural complexity. Key technologies that require development are the Terrain Relative Navigation and Landing Hazard Avoidance (TRN-LHA) system and the variable-altitude balloon. Note that what we report here is a resource-limited, 6-month study, so the depth of analysis for both the science and the engineering is commensurate with available resources. Further work that is needed is discussed in the appropriate sections. We have assumed no European or US Venus mission prior to VFM that could, if flown, reduce costs, and discuss our recommendations for potential changes in the VFM architecture should VERITAS or DAVINCI+ be selected in Discovery Step 2, or EnVision selected in the M5 competition.

The Venus Flagship Mission concept directly addresses each of the three Venus Exploration Analysis Group (VEXAG) goals as well as several objectives from the 2020 NASA Science Plan. It will inform two of the strategic objectives of the Planetary Science Division, to advance scientific knowledge of the origin and history of the solar system, and determine the potential for life elsewhere. It will also address the strategic objectives of Heliophysics to understand the Sun and its interactions with Earth, the solar system and the interstellar medium, including space weather, and it will provide data on how Venus can inform one of the Astrophysics science themes: Exoplanet Exploration.

The Planetary Decadal Survey [NRC, 2011] and Midterm report [NASEM, 2018] documented the critical importance of Venus science to understanding the origin of terrestrial planets and notes that Venus missions are necessary to address a “...lack of balance [that] undermines the compelling comparative planetology investigations recommended by the decadal survey, particularly for the terrestrial planets. The discovery of numerous Earth-size and Neptune-size exoplanets provides even greater urgency to initiate new missions to Venus and the ice giants.” The VFM is designed to fill critical gaps in our understanding of terrestrial habitable worlds.

---



# 1. Scientific Objectives

## 1.1 Science Questions and Objectives

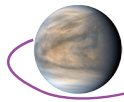
The specific goals of the Venus Flagship Mission (VFM) are: I) Understand the history of volatiles and liquid water on Venus and determine if Venus has ever been habitable, II) Understand the composition and climatological history of the surface of Venus and the present-day couplings between the surface and atmosphere and III) Understand the geologic history of Venus and whether Venus is active today. More details on these goals and the objectives can be found in **Appendix B**. To achieve these goals, **our mission architecture** relies on **five collaborative platforms**, an **Orbiter**, **Lander**, **variable-altitude Aerobot**, and **two SmallSats**, which house multiple instruments, many with heritage from prior missions, to elucidate the synergistic factors that control the distribution of volatiles from the interior to the exosphere: volatile inventory, volcanic activity, weathering, atmosphere dynamics, cloud formation and atmospheric loss. Instruments on these platforms will assess, at multiple scales with high precision, the volatile reservoirs, inventory, and cycles over Venus history, and use this to constrain the habitability of Venus. A strawman payload is shown in **Table 1**, and the Orbiter and SmallSats are also able to conduct radio science atmospheric experiments using the telecommunications system. The Long-Lived In-situ Solar System Explorer (LLISSE) will operate independently up to 60 days to demonstrate high-temperature electronics and sensor technologies. Such a flagship mission provides high-value science with minimal risk at an acceptable cost.

We have assumed no European or US Venus mission prior to VFM and discuss in more depth in **Appendix B** our recommendations for potential changes in the VFM architecture should VERITAS or DAVINCI+ be selected in Discovery Step 2 or EnVision be selected in the M5 competition. VFM complements existing proposals/concepts: if **VERITAS** is selected it would be extremely advantageous for high resolution mapping and determining the VFM Lander site; if **DAVINCI+** is selected, it would inform the descent profile at another location and characterize tessera morphology. Either mission would reduce risk and thereby cost. If **EnVision** proceeds as ESA's M5 selection in the early 2030s it could provide RADAR imagery and emissivity measurements at the same time as VFM. **Venera-D**, with a desired landing site in the plains, is synergistic and complementary to the proposed concept since it will conduct similar investigations on a vastly different terrain type.

**Table 1.** Instruments on each of the VFM Platforms with color groupings showing their scientific focus

Lander	Aerobot	Orbiter	SmallSats
Neutral Mass Spectrometer (NMS)	Aerosol Mass Spectrometer with Nephelometer (AMS-N)	Synthetic Aperture Radar (SAR)	Magnetometer (Mag)
Tunable Laser Spectrometer (TLS)	Fluorimetric Microscope (FM)	Near IR Imager (NIR-I)	Electron electrostatic analyzer (ESA-e)
Atmospheric Structure Suite [P, T, Radiometer] (AS)	Meteorological suite (P, T, Radiometer, 3-d Wind Sensor Dosimeter) (MET)	Sub-mm Spectrometer (S-mm)	Ion electrostatic analyzer (ESA-i)
Descent NIR Imager (DI)	Visible Imager (student experiment) (VI)	Magnetometer (Mag)	Langmuir Probe (LP)
Nephelometer (Neph)	Magnetometer (Mag)	Ion Electrostatic Analyzer (ESA-i)	Electric Fields Detector (E-FD)
Neutron Generator/Gamma Ray Spectrometer (GRS)	<b>Instrument Key</b> <span style="display: inline-block; width: 10px; height: 10px; background-color: #ADD8E6; border: 1px solid black; margin-right: 5px;"></span> Atmospheric <span style="display: inline-block; width: 10px; height: 10px; background-color: #FFD700; border: 1px solid black; margin-right: 5px;"></span> Mineralogy and Geology <span style="display: inline-block; width: 10px; height: 10px; background-color: #90EE90; border: 1px solid black; margin-right: 5px;"></span> Magnetic Fields <span style="display: inline-block; width: 10px; height: 10px; background-color: #DDA0DD; border: 1px solid black; margin-right: 5px;"></span> Particles <span style="display: inline-block; width: 10px; height: 10px; background-color: #FFDAB9; border: 1px solid black; margin-right: 5px;"></span> Aerosols	Electron Electrostatic Analyzer (ESA-e)	Solar Energetic Particle Detector (SEPD)
X-Ray Diffractometer (XRD)		2 each Neutral Mass Spectrometer (NMS)	EUV Sensor (EUV)
Raman-LIBS Instrument (R-LIBS)			
Panoramic Camera (PC)			
X-ray Fluorescence Spectrometer (XFS)			
Long-Lived In-Situ Solar System Explorer (LLISSE)			

VN107



Venus is a complex planet—a highly interactive system—and the Flagship mission concept is uniquely capable of **complementary scientific measurements to examine the synergistic behavior of volatiles through the multiple reservoirs on Venus**. **Figure 1** illustrates some of the processes that can be studied by the multiple VFM assets that relate to volatiles and, in various combinations, all contribute collaboratively to address the VFM’s three goals. Measuring the near-surface atmosphere and rock composition will provide clues to the weathering of surface minerals and chemical sinks, while surface samples and rocks collected at a depth of up to ~5 cm will ascertain the mineralogy and chemistry of the tessera, and look for evidence of past water. Instruments on the Lander, Aerobot and Orbiter will measure neutral and ionic volatile species, from the surface up to, and including, the haze and particles of the clouds, and directly measure their transport through the mesosphere to the thermosphere and assess the level of geological activity. To complete the picture, the SmallSat instruments will measure heavy ion escape with full spatial, energy, angular, and mass coverage during different phases of the solar activity cycle.

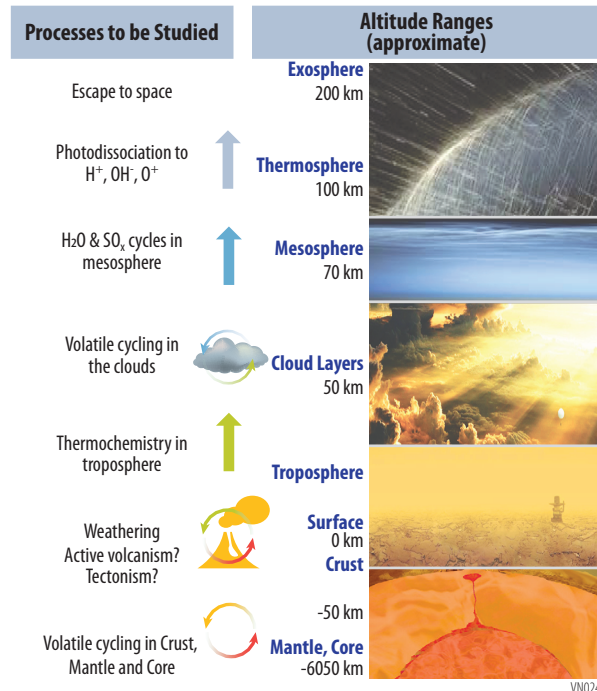


**Figure 1.** Multiple VFM assets will interrogate the interrelated processes that control the movement of volatiles through the Venus system.

## 1.2 Science Traceability Matrix

**Table 2 (STM Fold-out)** shows the full VFM Science Traceability Matrix (STM), which **describes the scientific objectives and the measurements required** to fulfill these objectives. It also presents the **performance requirements** (e.g., spatial and spectral resolution, sensitivity, timing accuracy) and their relation to the science measurements and how each instrument performs the required measurements. The STM contains the threshold performance requirements for the VFM. Of the required measurements, the most demanding will be the mineralogy and chemistry measurements made within the Lander due to the need for time-critical, autonomous, surface sample acquisition and ingestion into the instruments via the drill and sample delivery system. **Full details of the Scientific goals and objectives can be found in Appendix B.1**

Exoplanet research has progressed to the point that lessons learned from Venus are **essential for exoplanet science** in all aspects of exoplanetary data interpretation, from orbits and formation, to atmospheres and interiors. Venus is the prototype world that has transitioned from potentially habitable, with Earth-like conditions, through the inner edge of the Habitable Zone (HZ), providing a natural laboratory to study the evolution of habitability. Venus is perhaps most relevant when it comes to appreciating the diversity of terrestrial exoplanets through time and as a possible preview into Earth’s future [Kane et al. 2014]. Numerous potential Venus analogs have been discovered from Kepler [Kane et al., 2013; 2018] and Transiting Exoplanets Survey Satellite (TESS) data [Ostberg & Kane 2019], the latter of which will comprise a substantial fraction of transmission spectroscopy candidates [Kempton et al. 2018; Lustig-Yaeger et al. 2019]. All exoplanet models are currently based on the limited access to terrestrial atmospheres available within our solar system. Therefore, there is a **clear and urgent need to characterize the venusian atmosphere**, both to understand the evolution and dynamics of the Venus atmosphere [Horinouchi et al., 2020] and surface, and to provide the necessary data to correctly interpret terrestrial exoplanet atmospheric models [Kane et al. 2019]. VFM will provide comprehensive, highly targeted new measurements to fulfill this goal.

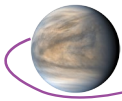


TABLE 2: SCIENCE TRACEABILITY MATRIX

Science Goals	Science Objectives	Science Investigations	Measurement Approach	Measurement Requirement	Performance Requirement	Strawman Instruments	Functional Requirements
I. Understand the history of volatiles and liquid water on Venus and determine if Venus has ever been habitable.	1. Determine if Venus once hosted liquid water at the surface	A. Determine the mineralogy and chemistry of tessera to ascertain rock type, and look for evidence of past water.	Chemical and mineralogical characterization of landing site bedrock (i.e., tessera material)	Measure elemental abundance of major, minor, and trace rock forming elements	Ingest 3 samples Element requirements: Si, Al, Ti, Mg, Fe, Ca, Mn, Cr, Na, K, P, Cl, S, F, Ni, Rb, Sr, Rare Earth Elements (REEs) Major: 0.06-0.4 wt% oxide Minor: 0.01-0.07 wt% oxide Trace: ±10%	X-ray Fluorescence (XFS)	Lander 20 mins integration time/sample
				Measure the mineralogy of surface rocks	Element requirements: Si, Al, Ti, Mg, Fe, Ca, Mn, Cr, Na, K, P, Cl, S, F, Ni, Rb, Sr, REEs, U, Th Major: 0.06-0.4 wt% oxide Minor: 0.01-0.07 wt% oxide Trace: ±10%	Gamma Ray Spectrometer (GRS)	Lander ~1.5 hr integration time. Limit interference below instrument
			Local and regional determination of landing site, drill sample site and immediate surroundings	Multispectral descent NIR imaging of lander site and drill site	Ingest 3 samples Detection limit 1%, quantify major phases within ±10%	X-ray Diffractometer (XRD)	Lander 15 mins integration time/sample
			Global and regional determination of tessera and plains composition to put landing site in context	Orbital NIR imaging	20 nested descent images from 20 km to surface at 0.9 and 1.02 microns (10 images/per band). S/N 30. FOV 90°. Resolution 100 m/pixel to 10 cm/pixel	Descent Imager (DI)	Lander Descent - dayside landing
		B. Look for evidence of surface features that might indicate a climatically different past (e.g., sedimentary structures, fluvial features)	High-resolution imaging of selected areas including tessera	RADAR imaging	S-band to match Magellan. Two modes, desired capability from near-polar orbit 1) Better than 10-m resolution with NESZ < -19dB, swath width capable of contiguous mapping, duty cycle > ~10 minutes; 2) better than 30-m resolution with NESZ < -22 dB. Surface coverage of ~5% at 30-m resolution and ~0.5% at 10-m resolution using nested imaging strategy; also high-res coverage of all previous Venera and Vega landing sites that collected surface chemistry or imaging	Synthetic Aperture RADAR (SAR) imaging	Orbiter - 300 km polar orbit. Nesting strategy for data acquisition varies depending on target and available Venus-Earth data rate.
					Local and regional imaging of landing site	Descent imaging of lander site	20 nested descent images from 20 km to surface at 0.9 and 1.02 microns (10 images/per band). S/N 30. FOV 90°. Resolution 100 m/pixel to 10 cm/pixel
			Characterize the morphology of landing site	Multispectral imaging of landing site rocks and rock formations	Panoramic images of at least 240° azimuth, 60° below nominal flat horizon, 30° above nominal flat horizon coverage in 6 filters (440, 550, 630, 780, 900 and 1020 nm). Time of Flight depth sensor for 3D information. One complete multispectral image set on landing and one set 60 mins after landing	Panoramic Camera (PC)	Lander - dayside imaging
		C. Determine isotopic ratios and abundances of hydrogen, noble gases, oxygen, nitrogen, and other elements in the atmosphere and below the cloud deck to the surface.	Characterize the atmosphere from above the clouds to the surface	Measure ≥ 5 samples at 5 different altitudes including sampling of the atmosphere at the surface	TLS: 4-channels (lasers): Channel 1: CO <sub>2</sub> and H <sub>2</sub> O for isotopic ratio of <sup>18</sup> O/ <sup>17</sup> O/ <sup>16</sup> O in CO <sub>2</sub> and H <sub>2</sub> O, D/H in H <sub>2</sub> O, and <sup>13</sup> C/ <sup>12</sup> C in CO <sub>2</sub> , all to ±1 per mil precision. Channel 2: CO and OCS for <sup>34</sup> S/ <sup>33</sup> S/ <sup>32</sup> S in OCS, <sup>13</sup> C/ <sup>12</sup> C in CO and OCS to ±5 per mil precision. Note the precision can be relaxed to ±10 or even ±20 per mil for <sup>33</sup> S. Channel 3: SO <sub>2</sub> abundance and <sup>34</sup> S/ <sup>33</sup> S/ <sup>32</sup> S isotopes to ±5 per mil. Channel 4: HCl and <sup>37</sup> Cl/ <sup>35</sup> Cl to ±10 per mil. Measure the abundances and isotopic ratios of Xe, Kr, Ar and Ne to ±5 per mil. Measure certain stable gas isotopes, in particular <sup>15</sup> N/ <sup>14</sup> N in N <sub>2</sub> to ±5 to ±10 per mil, and, for comparison with the TLS, the isotopes of S (in SO <sub>2</sub> ) C (in CO <sub>2</sub> ) and D/H (in H <sub>2</sub> O). Sampling altitudes are approximately (i) above the cloud tops (60-70 km), (ii) just below the main cloud layer (~40-50 km), (iii) lower atmosphere (~20 km), (iv) just above the surface (~5 km), and (v) from the surface. Compare with MS sampling from Aerobot and Orbiter	Tunable Laser Spectrometer (TLS)	Lander and Lander Descent
					Mass Spectrometer (NMS) and AMS-N	Lander Descent, Aerobot and Orbiter	
		D. Determine atmospheric escape rates over a full solar cycle.	Characterize ion escape	Measure the escaping ions <i>in situ</i>	Measure ions of masses 1- 60 amu (O <sup>+</sup> , O <sub>2</sub> <sup>+</sup> , CO <sub>2</sub> <sup>+</sup> ). Measure energies from 0.5 eV to 30 keV, with a delta E/E of < 15% and ~270° x 90° FOV	Electrostatic Analyzer - ions (ESA-i)	Orbiter/SmallSat constellation on a 0.5 m boom
				Measure the thermal ions and electrons	Measure thermal ions, 0.01 eV- 5 eV with 0.3 mV/m resolution Measure electron density ionosphere profiles [100-300 km]. Measure vertical & horizontal distribution and columnar density w/ accuracy <0.05 TECU every 100-500 m in altitude	Langmuir Probe (LP)	SmallSat constellation
				Measure the <i>in-situ</i> neutral constituents that are the source of escape	Measure neutral species from 2-150 amu	Neutral Mass Spectrometer (NMS)	Orbiter- RAM-pointing
				Measure the electric fields that accelerate ions to escape	Measure electric fields with resolution of 1 mV/m-50 mV/m	Electric fields (EF-D) sensor	SmallSat constellation
			Characterize solar wind conditions	Measure the solar wind protons at high energies <i>in situ</i>	Measure protons and electrons from 20 keV - 12 MeV, with a delta E/E of < 25%	Solar Energetic Particle Detector (SEPD)	SmallSat constellation
				Measure the EUV radiation	Measure Channel A: thin foil C/Al/Nb/C for 0.1-3 nm and 17-22 nm Channel B: thin foil C/Al/Ti/C for 0.1-7 nm Channel C: interference filter for 121-122 nm	Extreme Ultraviolet Monitor (EUV)	SmallSat constellation, Orbiter
				Measure the solar wind protons <i>in situ</i>	Measure solar wind ions (He <sup>+</sup> , H <sup>+</sup> , alphas). Measure energies from 0.5 eV to 30 keV, with a delta E/E of < 15% and ~270° x 90° FOV	Electrostatic Analyzer - ions (ESA-i)	Orbiter/SmallSat constellation on a 0.5 m boom
Measure the solar wind electrons <i>in situ</i>	Measure ions from 0.5 eV to 30 keV, with a delta E/E of < 15% and ~360° x 90° FOV			Electrostatic Analyzer - electrons (ESA-e)	Orbiter/SmallSat constellation on a 0.5 m boom		

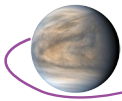


TABLE 2: SCIENCE TRACEABILITY MATRIX

Science Goals	Science Objectives	Science Investigations	Measurement Approach	Measurement Requirement	Performance Requirement	Strawman Instruments	Functional Requirements	
I. Understand the history of volatiles and liquid water on Venus and determine if Venus has ever been habitable.		E. Search for evidence of a current or past magnetic field.	Characterize the magnetic field topology and strength	Measure the magnetic fields	32 Hz sampling	Magnetometer (Mag)	Orbiter/smallsat constellation/ Aerobot on a > 1 meter boom	
				Measure the <i>in situ</i> photoelectrons (to infer magnetic topology)	Measure ions from 0.5 eV to 30 keV, ideally with a delta E/E of < 15% and ~360° x 90° FOV.	Electrostatic Analyzer - electrons (ESA-e)	SmallSat constellation on a boom	
	2. Identify and characterize the origins and reservoirs of Venus's volatiles today.	A. Determine the composition and distribution of volatiles in the atmosphere.	Characterize vertical variation of composition at 0 - 60 km altitude	Measure gaseous composition at 0 - 60 km altitude	Measure the size and amount of particulates at 0 - 48 km altitudes (below the H <sub>2</sub> SO <sub>4</sub> cloud layer) using nephelometry	Measure the abundances of SO <sub>2</sub> , SO, SO <sub>3</sub> , OCS, CO, H <sub>2</sub> O, HDO, NO, HCl, HFI and more at 0-60 km altitude during descent Measurements to be made with vertical sampling of ≤ 1 km	Mass Spectrometer and Tunable Laser Spectrometer (NMS & TLS)	Lander and Lander Descent
						Measure effective size of particles to a resolution of 0.1 μm Measure refractive index to a resolution of < 0.02 Identify non-spherical (non-liquid) particulates Measurements to be made with vertical sampling of ≤ 1 km	Nephelometer (Neph)	Lander Descent
						Mass spectrometer with dedicated aerosol sampling inlet. Measure species including SO <sub>2</sub> , SO <sub>3</sub> , HCl, CO, OCS, H <sub>2</sub> O, HDO, H <sub>2</sub> S, to a sensitivity of 1 ppm. Must be capable to measure H <sub>2</sub> SO <sub>4</sub> , H <sub>2</sub> O, FeCl <sub>3</sub> , and sulphur (S <sub>3</sub> , S <sub>4</sub> , S <sub>x</sub> ) to a sensitivity of better than 1%. Characterize diurnal variation of composition by measuring samples at all local solar times (at least 24 samples during a circumnavigation). Characterize altitude variation within the clouds by measuring samples at 1 km intervals. Require > six complete ascend/descend cycles spaced evenly around the planet	Aerosol Mass Spectrometer (AMS) Student Imager (SI)	Aerobot
			Characterize cloud-level atmospheric composition and its variability	Measure composition of cloud droplets & aerosols via repeated vertical profiles of composition in 52 - 62 km altitude range, at all local times.	Vertical absorption profiles of H <sub>2</sub> SO <sub>4</sub> (S-band) & SO <sub>2</sub> (Ka-band) with vertical resolution ~100 m	Radio Occultation (RO)	Orbiter, SmallSat constellation	
					Measure effective size of particles to a resolution of 0.1 μm Measure refractive index to a resolution of < 0.02 Identify non-spherical (non-liquid) particulates. Nephelometer must be able to measure the intensity and polarisation of scattered light at six scattering angles, to an accuracy of 1%. Measurements to be made with sampling every ≤ 1 hour interval in order to characterize spatial variability	Nephelometer (AMS-N)	Aerobot	
			Characterize mesospheric composition	Measure composition at 70 - 140 km altitude	Abundance profiles of H <sub>2</sub> O, HDO, SO <sub>x</sub> , CO, etc with sensitivities of 5 ppm. Measure pole-to-pole abundances at least twice per day during the mission	Sub-mm Spectrometer (S-mm)	Orbiter	
			B. Determine transport mechanisms from the solid surface to the upper atmosphere.	Characterize winds and determine their role in volatile transport	Measure diurnal variation of surface winds, radiance, P, T, trace gases	Measure surface winds through a solar day (118 Earth days). Measure diurnal variation of light and temperature through a solar day (118 Earth days). Measure variability of key trace gases (SO <sub>x</sub> , CO, OCS, etc) to < 1 ppm sensitivity (2 ppm for SO <sub>x</sub> ) and correlate with meteorology	Long duration Meteorology Package (LLISSE)	Lander
						Measure vertical profile (over 0 - 60 km altitude range) of horizontal winds	Track zonal (E-W) and meridional (S-N) wind velocities of descent probe to constrain tropospheric circulation patterns	Radio tracking of descent probe
					Measure vertical and horizontal wind fields at cloud level, and their correlation with composition	Determine vertical transport by correlating composition with vertical wind velocities. Characterize large-scale atmospheric circulation by measuring meridional winds as function of altitude within the cloud layer, at all local times of day. Characterize cloud-level atmospheric waves and turbulence	ASM-N, Tracking Aerobot, accelerometers, MET (anemometer)	Aerobot
					Measure winds & composition from mesosphere to lower thermosphere at 70 - 140 km	Vertical profiles in the range of 70 - 140 km with 1.5-3 km vertical resolution of wind, temperature, CO and H <sub>2</sub> O isotopologues, ClO, HCl, H <sub>2</sub> SO <sub>4</sub> , O <sub>2</sub> , O <sub>3</sub> , NO, OCS, SO and SO <sub>2</sub>	Sub-mm Spectrometer (S-mm)	Orbiter
	Vertical profiles of convective stability, and their effect on volatile transport, from surface to space	Measure P, T profiles at 0 - 60 km altitude			P, T sensors on the descent probe. Vertical resolution no worse than 100 m. Temperature absolute accuracy no worse than 0.2 K Pressure range 150 mbar - 92 bar Up- and downwelling solar and thermal fluxes, to accuracy	Atmospheric Structure Suite (AS)	Lander and Lander Descent	
					Measure P, T profiles at 40 - 90 km altitude	P, T profiles with vertical resolution in better than 100 m and < 1 K accuracy	Radio occultation	Orbiter, SmallSat constellation
					Measure P, T profiles at 60 - 140 km altitude, along with measurement of key chemical species	Vertical profiles in the range of 70 - 140 km sampled with limb viewing, 50-90 km sampled with nadir viewing, with 1.5-3 km vertical resolution of wind, temperature, CO and H <sub>2</sub> O isotopologues, ClO, HCl, H <sub>2</sub> SO <sub>4</sub> , O <sub>2</sub> , O <sub>3</sub> , NO, OCS, SO and SO <sub>2</sub>	Sub-mm Spectrometer	Orbiter
	Characterize radiative balance and its effect on circulation	Measure up-and downwelling solar and thermal fluxes as function of altitude	Up- and downwelling fluxes in broad spectral bands including UV, Vis-NIR, near-IR and thermal IR channels, over 0 - 60 km altitude range	AS Radiometer	Lander and Lander Descent			
			Up- and downwelling fluxes in broad spectral bands including UV, Vis-NIR, near-IR and thermal IR channels, over 52-62 km altitude range at all local times of day & night	MET Suite Radiometer	Aerobot			
			Measure solar and thermal fluxes reaching the surface during a full solar day (118 Earth days)	Radiance sensor	LLISSE			

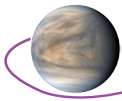


TABLE 2: SCIENCE TRACEABILITY MATRIX

Science Goals	Science Objectives	Science Investigations	Measurement Approach	Measurement Requirement	Performance Requirement	Strawman Instruments	Functional Requirements
I. Understand the history of volatiles and liquid water on Venus and determine if Venus has ever been habitable.	3. Place constraints on whether there are habitable environments on Venus today and search for organic materials and biosignatures.	A. Assess the present-day habitability of the Venus cloud environment	Measure environmental parameters which determine habitability	Environmental sensors: P, T, UV, radiation	Measure temperature, pressure, turbulence. Measure UVA, UVB, UVC up- and downwelling light. Measure ionizing radiation levels. Measure H <sub>2</sub> SO <sub>4</sub> vapor & droplet abundances	MET Suite, Radiometer, EUV Detector, Radio Occultation	Aerobot, SmallSat constellation
			Measure composition relevant to habitability	Measure composition of cloud particles; characterize availability of biologically important elements including C, H, N, O, P, S in gaseous, liquid and/or solid form	Measure effective size of particles to a resolution of 0.1 μm Measure refractive index to a resolution of < 0.02 Identify non-spherical (non-liquid) particulates Mass spectrometer with dedicated aerosol sampling inlet. Measure CHNOPS species to a sensitivity of 1 ppm, to determine chemical environment of cloud droplets	Nephelometer and Aerosol Mass Spectrometer (AMS-N)	Aerobot
		B. Determine if there are any extant or recently dead organisms or fragments present in the clouds	Collect and fluorescently characterize any biomolecules or larger fluorescing organic objects in the altitude range of 52-62 km	Identify fluorescent biomolecules, e.g. chlorophyll or other photosynthetic pigments that could allow for photosynthetic activity	Collect 7 samples over 60 days, at variable altitudes, using images (fluorescence and dark-field) of cloud droplets on 10, 1.0 and 0.2 μm pore-size filters with <0.5 μm spatial resolution at 265, 370, 470, and 530 μm to determine the difference between bio-content on day and night-sides during the course of each circumnavigation	Fluorimetric Microscope (FM)	Aerobot
II. Understand the composition and climatological history of the surface of Venus and the present-day couplings between the surface and atmosphere.	1. Constrain the composition of the surface and chemical markers of past and present climate.	A. Determine global mineralogy to distinguish major rock types and weathering regimes.	Characterize surface materials of major geomorphic units.	NIR multispectral mapper	> 6-channel (4 petrology, 2 cloud bands) between 0.8 and 1.7 microns. SNR sufficient to determine emissivity to ± 0.03 in processed data (some combination of stacking and instrument SNR). Pixel size on image < 45 km. >25% coverage to capture examples of major geomorphological terrains, 5-km elevation range, Flagship landing site and at least 1 Venera site	Near-IR Imager (NIR-I)	Orbiter
		B. Determine the oxidation state, chemistry and mineralogy of rocks in contact with the atmosphere.	Characterize surface materials in the landing site area.	Determine the oxidation state of surface materials	Ingestion of 3 samples Mineral: detection limit 1%	X-Ray Diffraction (XRD)	Lander 15 mins integration time/sample
				Measure type and variability of the mineralogy of rock surfaces	Mineralogy of a minimum of 5 samples, detection limit 1%	Raman, PC	Lander
					Mineralogy of a minimum of 5 samples, detection limit 1%	Raman, PC	Lander
				Measure type and variability of the chemistry of rock surfaces	Ingestion of 3 samples Mineralogy of a minimum of 5 samples, detection limit 1%	X-Ray Diffraction (XRD)	Lander 15 mins integration time/sample
		Element requirements: Si, Al, Ti, Mg, Fe, Ca, Mn, Cr, Na, K, P, Cl, S, F, Ni Chemistry: Major: 0.06-0.4 wt% oxide Minor: 0.01-0.07 wt% oxide Trace: ±10% Minimum of 5 samples	Laser Induced Breakdown Spectroscopy (LIBS)	Lander			
		Ingestion of 3 samples Element req'mts: Si, Al, Ti, Mg, Fe, Ca, Mn, Cr, Na, K, P, Cl, S, F, Ni Chemistry: Major: 0.06-0.4 wt% oxide Minor: 0.01-0.07 wt% oxide Trace: ±10%	X-Ray Fluorescence (XFS)	Lander 20 mins integration time/sample			
C. Determine the near surface atmospheric environment to constrain surface-atmosphere exchange and buffering.	Determine near surface atmospheric chemistry, temperature, and pressure.	Measure the chemical composition and oxidation state of the near surface atmosphere	Vertical profile of the atmosphere, down to the surface. Ingestion of at least one gas sample at surface to measure H <sub>2</sub> O, SO <sub>2</sub> , CO, HF, HCl, HCN, OCS, NO, O <sub>2</sub> , S <sub>2</sub> , H <sub>2</sub> S. Measure once per hour afterwards during landed mission Search for changes in near-surface atmospheric composition of select gas species over 60 days (H <sub>2</sub> O, SO <sub>x</sub> , CO, HF, HCl, HCN, OCS, NO, O <sub>2</sub> )	Mass Spectrometer (NMS)	Lander and Lander Descent		
Determine near surface atmospheric pressure, temperature	Measure surface pressure and temperature Measure diurnal variation of P, T over a day/night cycle	Chemical sensors	LLISSE				
Atmospheric Structure Suite (AS)	Lander + LLISSE - land during day, survive until sunset						
III. Understand the geologic history of Venus and whether Venus is active today.	1. Determine if Venus shows evidence of a current or past plate tectonic regime.	A. Constrain composition, thermal state and structure of the interior	Refine knowledge of the density structure of the lithosphere, upper mantle and core.	Improve knowledge of the gravity field	Gravity better than Magellan to uniform spherical harmonic degree 100, including love numbers. k2 requirement is +0.01 (3%)	Line of Site (LOS) tracking	Orbiter - SC <400 km altitude and in view of Earth
		B. Characterize tectonic features & establish stratigraphic relationships	Constrain the presence, spatial distribution and intensity of potential magnetic sources	Aerial magnetic field surveys over major terrains	32 Hz sampling, Magnetic field sensitivity: 0.7 nT Accuracy: 0.7 nT Precision: 0.1 nT @ ±1000 nT Range: ±1000 nT	Magnetometer (Mag)	Aerobot - altitude <62 km Magnetometer on a > 1 meter boom
			Image key surface targets in order to determine critical temporal relationships between geomorphic features	Synthetic Aperture RADAR (SAR) imaging of selected targets	S-band to match Magellan. Two modes, desired capability from near-polar orbit 1) Better than 10-m resolution with NESZ < -19dB, swath width capable of contiguous mapping, duty cycle > ~10 minutes; 2) better than 30-m resolution with NESZ < -22 dB. Surface coverage of ~5% at 30-m resolution and ~0.5% at 10-m resolution using nested imaging strategy; also high-res coverage of all previous Venera landing sites that collected surface chemistry or imaging	SAR	Orbiter

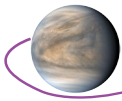
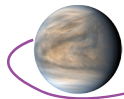


TABLE 2: SCIENCE TRACEABILITY MATRIX

Science Goals	Science Objectives	Science Investigations	Measurement Approach	Measurement Requirement	Performance Requirement	Strawman Instruments	Functional Requirements
III. Understand the geologic history of Venus and whether Venus is active today.		C. Look for evidence of crustal recycling.	Image key surface targets in order to identify landforms, stratigraphy and chemistry	SAR and NIR imaging of selected targets. Chemical and mineralogical analyses of tessera terrain	SAR requirements as above for systematic mapping of tessera, mountain belts and coronae. NIR mapping of all landforms A minimum of one chemical measurement of tessera terrain is necessary	SAR, NIR mapping (NIR-I) XFS, XRD, Raman, LIBS, GRS	Orbiter Lander
		A. Look for present day seismicity.	Search for seismic signals	Measure the pressure (P) at infrasound frequencies	Time varying measurements of pressure over freq range 0.01 - 80 Hz, Noise floor <0.001 Pa	MET (Infrasound Pressure Sensor)	Aerobot
	Search for corresponding gravity wave signals		Measure neutral T & ionospheric total electron content	T < 1 K accuracy; dual-frequency S- and Ka-band TEC w/ < 0.05 TECU accuracy every 100-500 m altitude	Radio Occultations	SmallSat Constellation	
	2. Determine whether Venus is tectonically and volcanically active today.	B. Look for present day volcanism and tectonism	Search for relatively unweathered areas on the surface.	NIR mapping, multispectral imaging	NIR surface emissivity at 0.8 - 1.7 μm. Specs are listed above for orbital NIR instrument	NIR mapping multispectral imager (NIR-I)	Orbiter
			Look for rapid changes in atmospheric chemistry or particles	Characterize cloud composition or particles (e.g., ash)	Identify any non-liquid particles in the main cloud layer, if they make up more than 1% of cloud particulates, by measuring their scattering phase function using polarimetry, to determine whether they have characteristics of volcanic ash and/or of windblown surface materials. Search for spatial and temporal variations in sulfuric acid cloud droplets indicative of volcanic plumes	Aerosol Mass Spectrometer (AMS-N)	Aerobot
				Identify and characterize any anomalous thermal anomalies, clouds and/or ash associated with volcanic plumes	Repeat-pass NIR surface emissivity at 0.8 - 1.7 μm over 2 Venus days to map thermal emission on the nightside of Venus	NIR mapping multispectral imager (NIR-I), AMS/FM	Orbiter, Aerobot
			Search for rapid changes in atmospheric composition at the surface	Measure variability over time of key trace gases (H <sub>2</sub> O, SO <sub>x</sub> , CO, OCS, HF, HCl, NO, O <sub>2</sub> , H <sub>2</sub> S, H <sub>2</sub> ) to < 1 ppm sensitivity (2 ppm for SO <sub>x</sub> ) and correlate with meteorology	Chemical Sensors	LLISSE	
			Search for new features formed during mission lifetime (and since Magellan) and observe recent surface deformation.	SAR repeat-pass imaging	Repeated imaging at 10 m resolution of volcanic targets	SAR	Orbiter



The Venus Flagship mission will provide major, unprecedented advancements in our understanding of the formation, evolution, and habitability of terrestrial planets and would be the first mission to trace volatile inventory, phase, movement, reservoirs, and loss over Venus history. It will accomplish many firsts: first landing in tesserae thought to represent the oldest rocks on Venus; first measurement of the mineralogy and precise geochemistry of tessera terrain; the first inventory of all major atmospheric noble gases and their isotopes; first measurement of global surface composition from orbit; first co-located mapping of winds and composition in the mesosphere and thermosphere; first measurements of lower atmosphere composition with modern, high-accuracy, high-resolution instruments; first simultaneous multipoint measurements in Venus exosphere and ionosphere; the first measurement of seismicity and remanent magnetism of Venus; first simultaneous measurement of ion loss rates from the exosphere and thermosphere reservoirs; and the first deployment of uncooled ambient temperature electronics to enable long-life operation at the Venus surface.

## 2. High-Level Mission Concept

### 2.1 Overview

Accomplishing the science goals presented in the STM requires interrogating Venus from the interior to the exosphere at multiple scales, which leads to performing collaborative and synergistic measurement of Venus as a system (see **Figure 2**).

From this, the architecture of the mission concept was derived: a Lander, Aerobot, Orbiter, and two SmallSats, which will launch on a Falcon 9 Heavy Expendable (Figure 3).

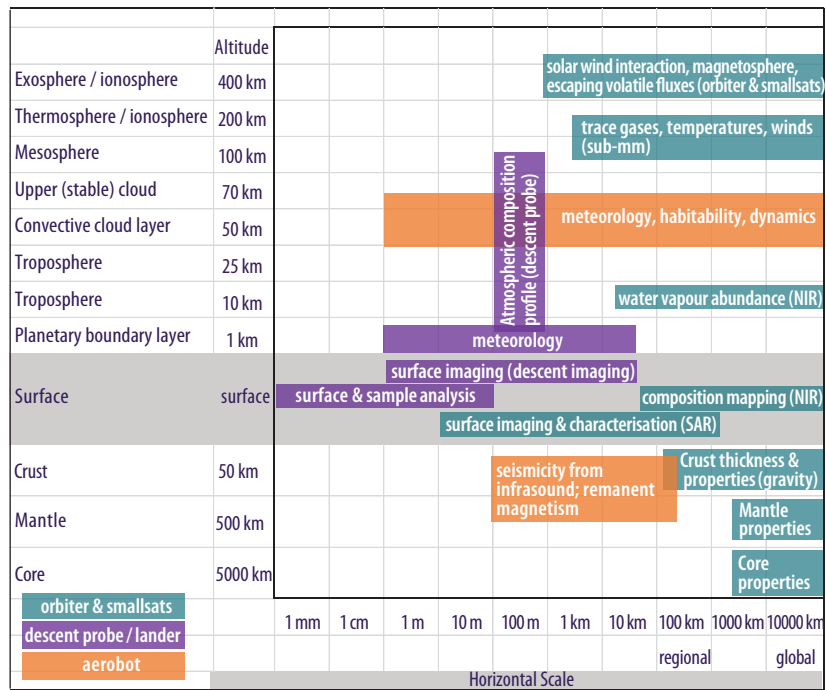


Figure 2. VFM scientific investigations on each platform illustrating scale and altitude coverage

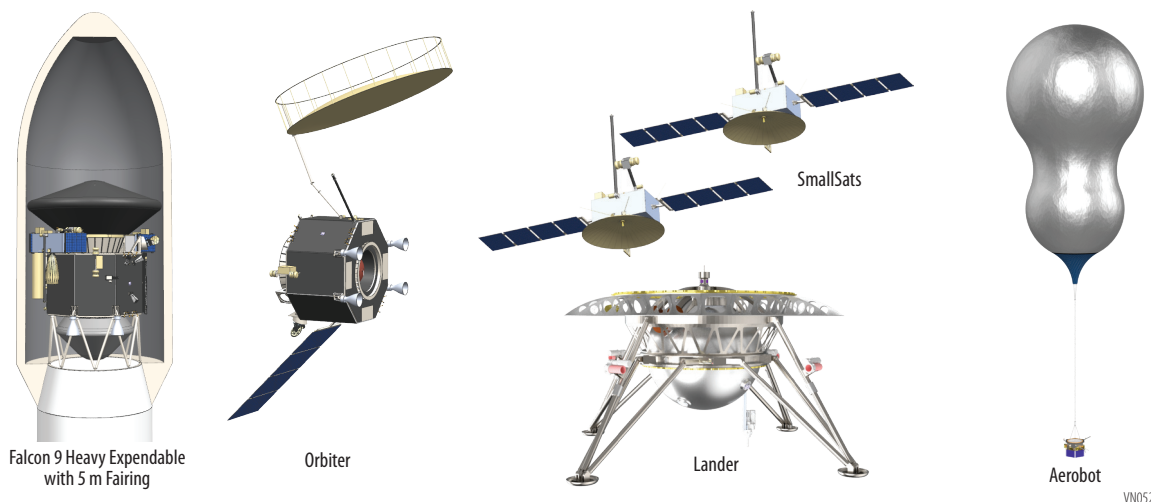
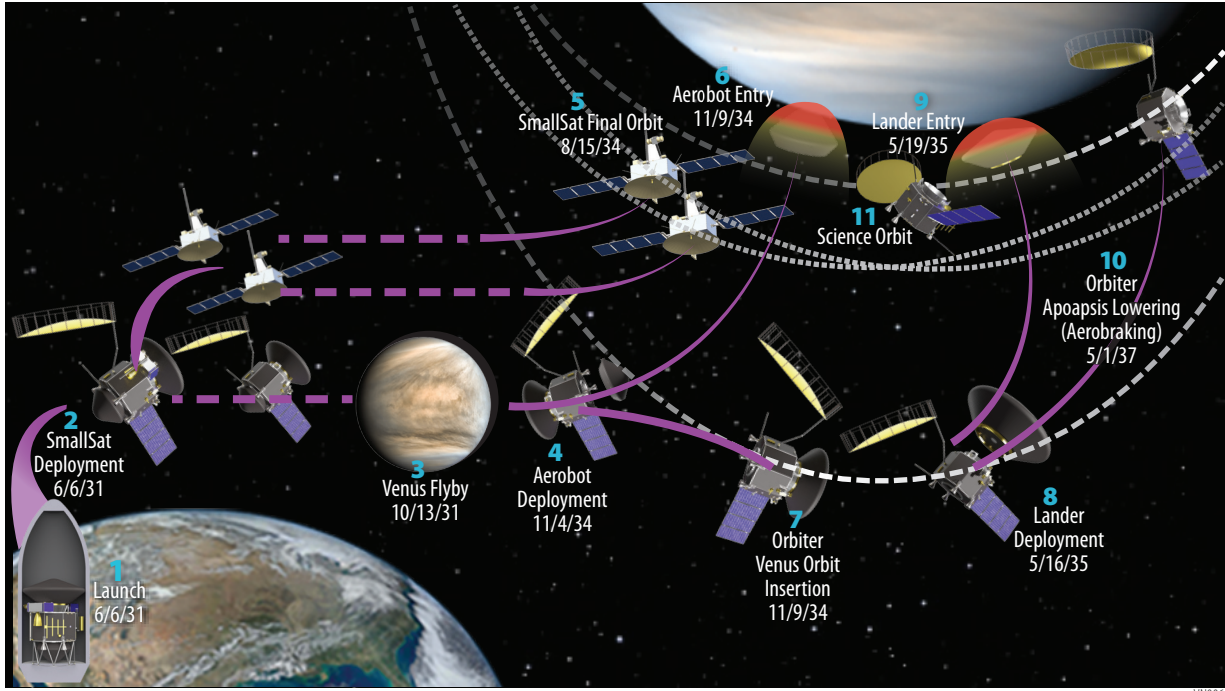


Figure 3. The VFM flight system, which addresses the VFM goals, consists of an Orbiter, Aerobot, Lander and two SmallSats (not to scale)

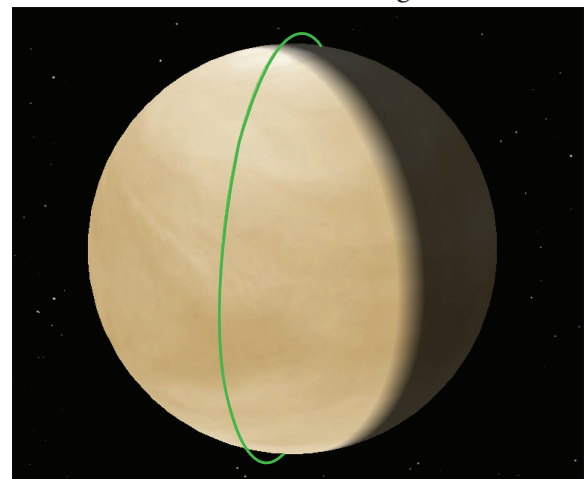




**Figure 4.** Overview of VFM mission design from launch to Lander entry and subsequent Orbiter aerobraking

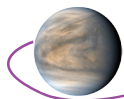
The baseline trajectory for the VFM launches in June 2031 and places the five science platforms at Venus in 2034 with the Lander released in May 2035. A backup launch opportunity in June 2032 is also identified. A similar sequence of events occurs for both trajectory options and is illustrated in **Figure 4**.

A few hours after launch (1), two SmallSats detach from the other elements (2) and follow a low-thrust transfer to Venus, each using solar electric propulsion. Once at Venus, the SmallSats spiral down to their final orbits (5). In addition to their science requirements, the SmallSats will provide essential communication with both the Aerobot and Lander. Both SmallSats will be in place, orbiting the planet, approximately 3 months prior to the arrival of the Orbiter, carrying the Aerobot and Lander, which utilizes chemical propulsion and performs a Venus flyby enroute (3). The Aerobot separates (4) from the Orbiter and Lander about 5 days prior to the Orbiter Venus Orbit Insertion (VOI) (7) maneuver directly from interplanetary space. After separation, the Aerobot enters the venusian atmosphere (6) and begins operations shortly after the balloon inflation. After VOI, the Orbiter is placed in an elliptical polar orbit for 6 months and then releases the Lander (8) after taking RADAR and emissivity measurements of tessera targets. This mission concept is flexible enough to provide the option to extend this mapping orbit to acquire additional coverage of tessera terrain as an input to landing site selection. The Lander takes approximately 3 days to reach the planet's atmosphere and 1 hour, from entry (9), to begin surface operations. The Orbiter provides communication access to the Lander for a short duration prior to handing over the relay to the SmallSats. Subsequently, the Orbiter performs a sequence of aerobraking maneuvers (10) over the course of approximately 2 years to reach its final polar science orbit (11) shown in **Figure 5**. The concept of operations is based on science, the trajectory and inter-asset communications requirements.



The overall mission concept, described briefly above and in more depth in **Section 3.2, Section 3.3,**

**Figure 5.** Final Polar Science Orbit



and **Appendix B**, was derived from the three major science goals and two cost-driven requirements that were derived early in the study: 1) Launch all elements on a single rocket and 2) limit the g-load for Venus entry to  $\leq 50g$  in order to maximize the use of state-of-the-art instruments that have high heritage or high technology levels. Both of these requirements were accomplished.

This architecture allows us to target ancient rocks, as done for Mars, to understand volatile history and whether Venus was once habitable. The Lander will nominally touchdown in tessera terrain in Western Ovda Regio, which has been covered by the highest-resolution Magellan topography and is thought to be representative of tessera terrain. The exact landing location would be selected upon examination of the **SAR** and emissivity data when the Orbiter is in its elliptical orbit phase in advance of the Lander release or, more optimally, from VERITAS, if selected. Safely landing in tessera terrain is absolutely necessary to satisfy our science objectives, so we designed a Landing Terrain Relative Navigation and Hazard Avoidance (TRN-LHA) system and self-adjusting landing struts that will help enable the Lander to touchdown at a safe velocity on a slope  $\leq 30^\circ$ , which is the maximum expected slope at 1 km spatial scales, and to control its horizontal orientation by  $\sim 10^\circ$ .

Lander instruments will determine the mineralogy and chemistry of tessera terrain to ascertain rock type, and look for evidence of past water. The depth-profiling potential of the drill system and **R-LIBS** instrument allow the lander to sample successive layers of weathering beneath the surface of the rocks to look for changes in weathering style over time, and identify any preserved record of the past climate. Such measurements also provide ground truth and calibration for orbital instruments e.g., surface composition measurements will help calibrate orbital NIR emissivity maps, and optical images from the surface will help interpret high resolution **SAR** images for tessera terrain of unknown origin. Note that VFM is *not* primarily a **SAR** mission and does not aim to return global **SAR** imagery. The **SAR** spatial resolution required to achieve the VFM science objectives includes context images at 30 m and 10 m images of critical targets (e.g., landing site), effectively Mars Orbiter Camera (MOC) at Venus.

Detailed cloud-level *in situ* investigations are required to characterize the volatile reservoir represented by the clouds, as well as astrobiological and other goals, which led to the inclusion of a cloud-level, balloon-borne Aerobot. The Aerobot has the capability to vary its altitude from 52–62 km as it circumnavigates Venus examining the aerosol and cloud composition as well as obtaining magnetic and seismicity data. It will execute multiple, controlled, vertical cycles over the altitude range to permit characterization of both the main convective cloud layer and the upper convectively stable clouds, where the UV absorber—of unknown, and possibly biological, composition—is known to be present (**Figure 6**).

Carried by Venus’s super-rotating winds, the balloon will circumnavigate the planet roughly once every five days, providing approximately 12 circumnavigations over the nominal 60-day balloon lifetime, enabling measurements of vertical and horizontal wind fields at cloud level, and their correlation with composition.

The Venus lower atmosphere is poorly known but provides critical information about the transfer of volatiles through the Venus system. The **NMS** and **TLS** on the Lander will measure chemical composition as it descends through the entire atmosphere, determining isotopic ratios and abundances of hydrogen, noble gases, oxygen, sulfur, nitrogen, and other elements in the atmosphere and from the mesosphere to the surface. Because these instruments are on the Lander, they will continue to operate on the surface during the Lander lifetime to collect samples of the atmosphere that is in direct contact with the rocks measured by the

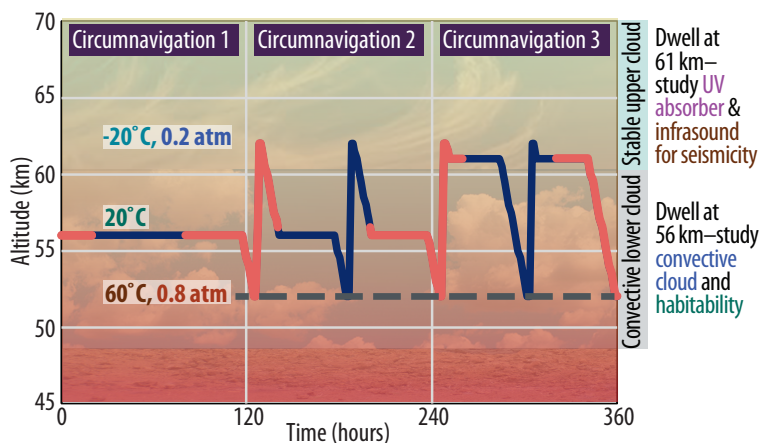
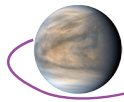


**Figure 6.** The Aerobot has variable altitude capability, allowing characterization of different levels of the venusian cloud deck



Lander instruments. Above the clouds, the **S-mm** spectrometer on the Orbiter will obtain vertical profiles in the range of 70–140 km with 1.5–3 km vertical resolution of temperature, CO and H<sub>2</sub>O isotopologues, ClO, HCl, H<sub>2</sub>SO<sub>4</sub>, O<sub>2</sub>, O<sub>3</sub>, NO, OCS, SO, and SO<sub>2</sub>—and, for the first time, co-located wind speeds measured through Doppler velocimetry, to give direct measurements of transport. These measurements will be complemented by radio science vertical absorption profiles of H<sub>2</sub>SO<sub>4</sub> (S-band) & SO<sub>2</sub> (Ka-band) with vertical resolution ~100 m on the Orbiter and SmallSats.

VFM will constrain the geophysical regime of Venus and its interior structure using a combination of gravity mapping from the Orbiter, measurement of seismicity through balloon-borne infrasound detectors, and magnetometer investigations to characterize properties of the core and search for remanent surface magnetism. These will complement the surface composition characterization from the Lander and from orbital NIR measurements, and noble gas isotope measurements of the atmosphere to form a much more comprehensive picture of Venus’s volatile inventory and distribution. Again, this illustrates the scientific complementarity of measurements from different mission elements which cannot be achieved with one platform alone.

In the exosphere of Venus, the SmallSat instruments (similar to the instruments on MAVEN) will measure heavy ion escape (e.g., atomic and molecular oxygen, carbon dioxide) with full spatial, energy, angular, and mass coverage during varying phases of the solar cycle (Figure 7). The measurements will cover the majority of solar cycle 26, including the predicted ascending and declining phases. Our approach is to deploy identical ion and magnetic field instrument suites on the **SmallSats** in two different orbits designed to obtain simultaneous information about both the *upstream solar wind conditions* in interplanetary space and escaping ion measurements in the *magnetotail*, ensuring accurate cause-and-effect interpretations of the observed escape rate variations. Based on these measurements and developing insights about the early solar wind and solar activity from observations of young Sun-like stars, VFM will provide the necessary framework for a time-integration of the oxygen escape, establishing its now uncertain role in the historical loss of water.

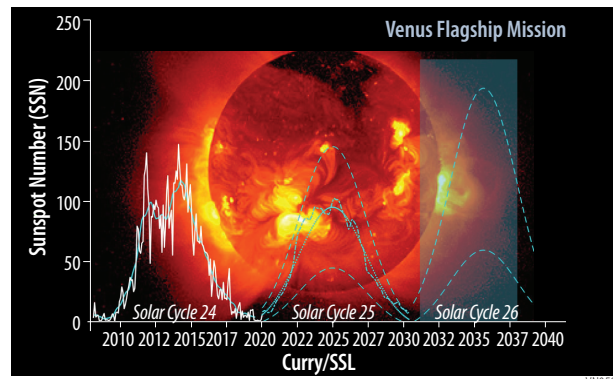


Figure 7. Illustration of the past and possible future solar cycles. The blue box is the nominal lifetime of the SmallSats.

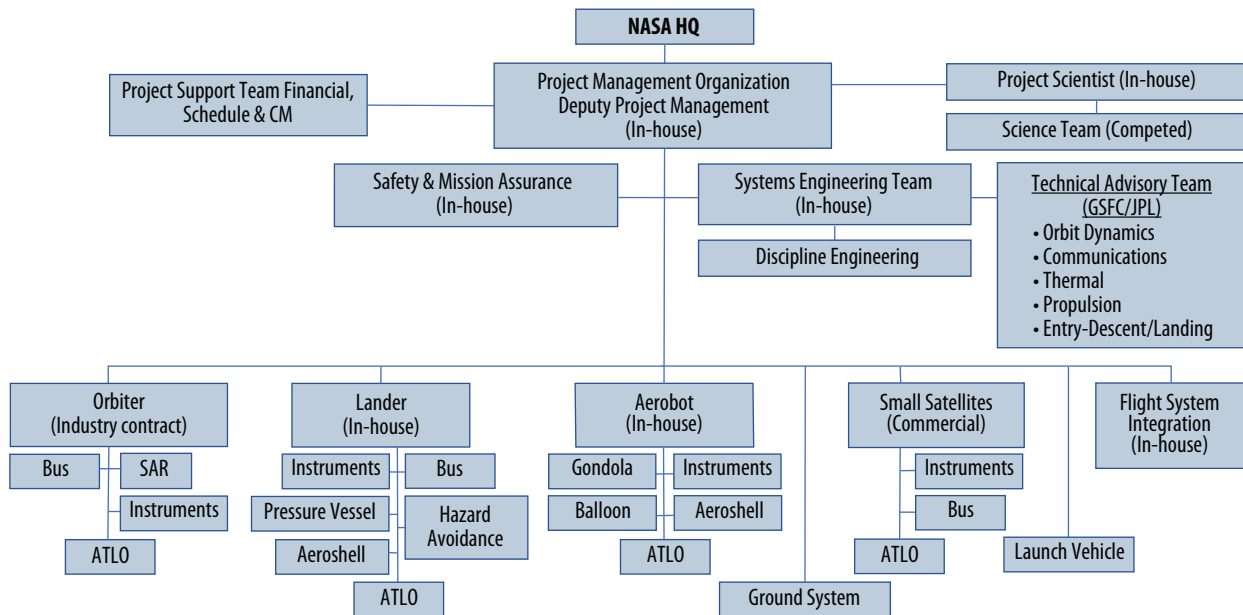
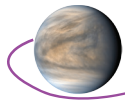


Figure 8. VFM Organization Chart. All instruments will be competed and managed within an integrated payload office.



The organization for the VFM mission is shown in **Figure 8** with overall project management done in house, commercial acquisition of the SmallSats, an industrial partner for the Orbiter, and in-house (GSFC and/or JPL) design, development and build of both the Lander and Aerobot. Assembly, Test, and Launch Operations (ATLO) will be done in-house, which entails accepting system-level deliverables, executing the integration of deliverables into the system, coordinating system-level testing, and preparing the system for launch/final testing.

## 2.2 Concept Maturity Level

Based on the Concept Maturity Level (CML) definitions in the study report template, this study achieves a **CML 5**. To support this we present an implementation concept at the subsystem level, as well as a detailed science traceability matrix, key technologies, heritage, risks and mitigations. Even though this is not a proposal, we outline management and responsibilities in implementation, provide a system make/buy option and develop detailed cost models.

## 2.3 Technology Maturity

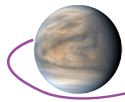
The majority of the VFM mission concept uses proven flight hardware. However, there are several areas where a technology maturity effort either enables the mission or significantly reduces mission risk. Both the Orbiter and SmallSats will be procured with little to no technology development. However, the Lander and Aerobot do require advances in specific technologies as well as some of the instruments. The main technology development is the Landing Terrain Relative Navigation and Hazard Avoidance system, which enables safe landing on the sloped tessera terrain. The three lowest TRL elements are:

1. **Lander – Integrated Terrain Relative Navigation (TRN) and Landing Hazard Detection and Avoidance (LHDA):** A high-level trade conducted as part of this study determined that the risk of landing safely could be significantly mitigated if a combination of a Terrain Relative Navigation and a Hazard Detection and Avoidance system was used with a divert system consisting of four fans. This system is estimated to be TRL 3. Development is needed for the motor and fans, terrain relative navigation and hazard avoidance algorithms. The *in situ* mineralogy instruments: **XRD**, **XFS**, **GRS** and **R-LIBS** instruments provide partial redundancy with each other, thereby providing mitigation of this risk to some degree as well.
2. **Aerobot – Balloon:** The variable-altitude Aerobot platform is currently TRL 4 but there is ongoing work at JPL to mature Venus variable-altitude balloons beyond TRL 4. Without the balloon inflating or operating as planned, the Aerobot will not float or circumnavigate Venus nor will it measure at multiple altitudes, and loss of scientific measurements will occur.
3. **Lander and Aerobot – Instruments and Sample Acquisition/Handling Systems:** Some instruments on these platforms are in need of TRL maturation for the appropriate environment they will encounter in either the constrained environment of the Lander pressure vessel or the clouds of Venus. Development is also needed for Lander and Aerobot sample ingestion systems that are at lower TRL. In some cases, field trials are needed to mature the techniques and concepts of operations. A summary of the maturation plan for the specific instruments can be found in the Technology Development Plan below in **Table 14, Section 4.2**. The effect on the mission if one of them is not developed in time varies, but much of the development is re-engineering heritage instruments rather than developing new ones. Additionally, the lowest TRL subsystems for many of those instruments are the sampling systems.

## 2.4 Key Trades

There are seven key trades that drove the VFM mission architecture and Mission Design. Key trades, additional element, and subsystem trades are discussed more fully in **Appendix B.2.1** and are summarized here. They are:

1. **Definition of the elements that are needed to fulfill the science objectives.** Numerous science trade studies contributed to the architectural design of the five platforms.
2. **Evaluation of launch architectures** to determine if current launch vehicle technology could enable a single launch. The trade settled on the use of a single Falcon 9 Heavy Expendable to reduce overall cost and complexity associated with designing, launching, tracking and operating two separate carrier platforms.



3. **Determination of how to provide communication coverage for the Aerobot and the Lander.** The third key trade was determining how to provide communication coverage for the Aerobot and the Lander. There were three options: 1) Direct to Earth, 2) Orbiter relay, and 3) SmallSat relay. Direct to Earth would require a high-power transmitter on the Lander and Aerobot. The trade determined that the optimal solution was to use both the Orbiter and SmallSats during the Lander mission to provide the coverage of the extended 8 hour lifetime. For the Aerobot, it was quickly determined that the best option would be for the SmallSats to provide daily coverage since the Aerobot would arrive at the same time as the Orbiter and Lander and the elliptical orbit of the Orbiter only provides contact with the Aerobot every 4–5 days.
4. **Selection of propulsion systems for the SmallSats and Orbiter.** This trade was driven by the results of the communication and launch trades. It was determined that the SmallSats could arrive early at Venus most efficiently using solar electric propulsion. The multiple duties for the Orbiter (lander deployment, communications, observational platform) made chemical propulsion for orbit insertion, followed by later aerobraking to a low circular orbit, the preferred solution.
5. **Evaluation of methods to reduce instrument g loads.** This trade evaluated placing a requirement that limited the g forces on the instruments to  $\leq 50g$  in order to minimize the cost of redesigning and/or requalifying heritage instruments to meet the high g loads past studies imposed on the instruments. It was determined that the Orbiter providing the  $\Delta V$  needed to place the Orbiter and Lander into an initial 5 day polar elliptical orbit prior to Lander entry would allow a low entry angle that would provide entry forces of  $\leq 50g$ . This result spawned two additional trades: Aeroshell shape and inclination of the initial orbit for the Orbiter.
6. **Determination of the aeroshell shape** to examine the benefit of a significantly lower heating rate, allowing for lighter TPS and an aeroshell shape with a  $70^\circ$  sphere-cone providing a max diameter of 4.6 m. This geometry provides significantly better packaging and drag performance than the  $45^\circ$  sphere-cone (e.g., Pioneer Venus) and has a smaller surface area for a given diameter (thereby once again reducing the mass of the thermal protection system). The diameter of 4.6m provided the added benefit of accommodating a larger distance between lander legs and thus a more stable lander.
7. **Determination of the Orbiter orbit.** We examined a) an initial elliptical orbit that was *equatorial* and b) an initial elliptical orbit that was *polar*, each followed by a polar science orbit. The initial *polar elliptical orbit* was selected to avoid the large  $\Delta V$  penalty for the inclination change to a polar orbit. The penalty for this selection was that due to the slow rotation rate of Venus, the orbit geometry no longer allows for extensive ( $\sim 70\%$ ) RADAR coverage of the primary landing site ellipse prior to Lander deployment. However, the 6 month elliptical polar orbit will allow imaging of smaller portions of tessera terrain prior to landing. This provides an opportunity to obtain a better understanding of tessera terrain which in turn improves the maps used in the feature recognition algorithms for the Terrain Relative Navigation and Hazard Avoidance systems.
8. **Determination of launch dates.** The 2031 launch date was selected to provide the needed development schedule within the decade and allows the 2032 launch date to serve as a backup.

### 3. Technical Overview

#### 3.1 Instrument Payload Description

Detailed instrument tables are provided in **Appendix B.2.8.1** for the Aerobot, **Section B.2.8.2** for the Lander, **Section B.2.8.3** for the Orbiter, and **Section B.2.8.4** for the SmallSats. Instrument operations and the level of complexity associated with analyzing the data can be found in **Appendix B.2.8**. Total Payload mass, power and data volume for each platform is provided below in **Table 3–Table 6**. All instruments have flight heritage or have been in development for some time. Concepts, feasibility, and definition studies already performed for the instruments are found in the Technology Development section below.

##### 3.1.1 Lander Payload

The Lander (**Figure 9**) was designed to conduct scientific measurements both during descent through the atmosphere and on the surface. During descent a suite of instruments will provide a profile of chemistry through measurements of gas and particles, and environmental conditions (see, for example,

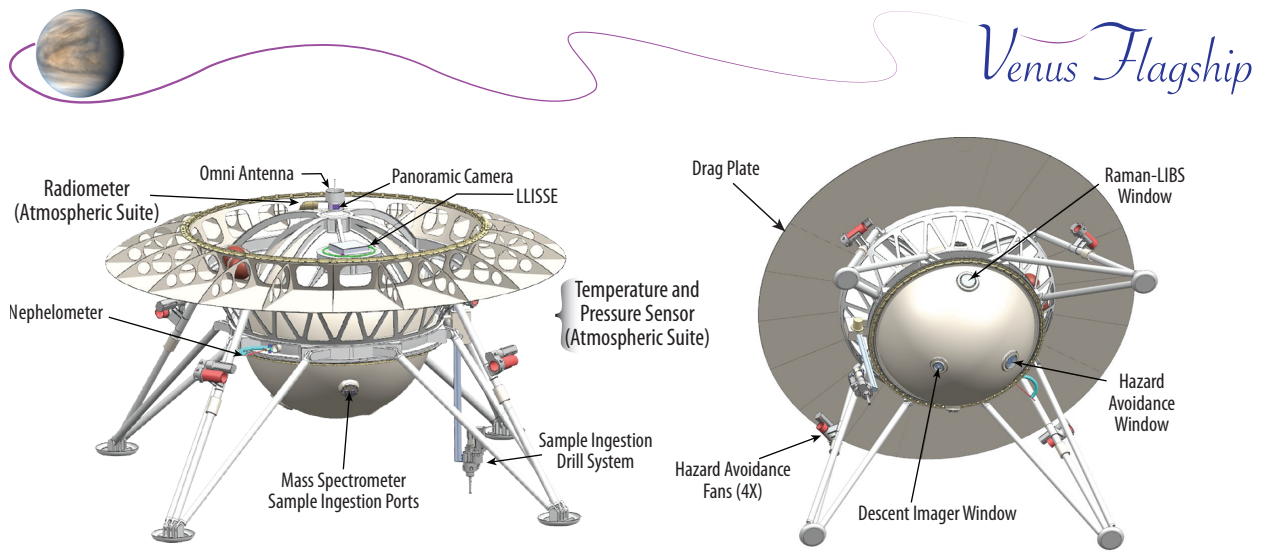


Figure 9. VFM Lander (Deployed) showing exterior features including instruments

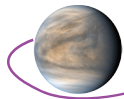
Table 3. VFM Lander Payload Mass, Power, and Mission Data Volume

Instrument	Mass			Average Power			Mission Data Volume (Mbits)
	CBE (kg)	% Cont	MEV (kg)	CBE (W)	% Cont	MEV (W)	
Neutral Mass Spectrometer (NMS)	16.5	30	21.5	60	30	78	7.3
Tunable Laser Spectrometer (TLS)	4.5	30	5.8	26.1	30	33.9	13
Atmospheric Structures Suite (AS)	4.8	30	6.2	6.9	30	8.9	2.3
Descent NIR Imager (DI)	5	30	6.5	40	30	53	463
Neutron Generator/Gamma Ray Spectrometer (GRS)	12	30	15.6	5	30	6.5	25.1
Nephelometer (Neph)	1.5	30	2.0	6.6	30	8.6	1
X-Ray Diffractometer (XRD)	5	30	6.5	29.5	30	38.3	24
X-Ray Fluorescence Spectrometer (XFS)	1	30	1.3	8	30	10.4	2.1
Panoramic Camera (PC)	3	30	3.9	12	30	15.6	2,255
Raman-LIBS (R-LIBS)	25	30	32.5	61	30	79.3	1,720
Long-Lived In Situ Solar System Explorer (LLISSE)	10	30	13	N/A	30	N/A	1,000
<b>Total Payload</b>	<b>88.3</b>	<b>30</b>	<b>114.8</b>	<b>255.1</b>	<b>30</b>	<b>332.5</b>	<b>5,513</b>

Figure 1 and Figure 2); these instruments will continue to operate on the surface providing data on the near-surface atmosphere. Additionally, the **Descent Imager (DI)** will provide images of the landing region during approach to place the landing site in context, and will continue to operate on the surface to image the drill site. The LIDAR will act as part of the Terrain Relative Navigation and Landing Hazard Avoidance (TRN-LHA) system to help the lander land safely. The instrument suite for surface operation is designed to provide quantitative chemistry (major through trace elements), mineralogy, and images of the tessera surface. Data from this suite are ideal for making geologic interpretations of the landing site (rock type, weathering style, geologic context), and when paired with the orbital dataset, can place the landing site in a broad context. The instruments chosen for these operations are capable of providing quality data over a short timescale. The drill will acquire samples to be delivered internally to the **XFS** and **XRD** instruments. The **GRS** and **R-LIBS** instruments will interrogate samples on the exterior of the Lander. The instrument suite used for measuring chemistry and mineralogy is able to provide some level of redundancy in the event of an instrument failure (e.g., multiple instruments can measure major and minor elements) but still provides unique, complementary data when all instruments perform nominally (e.g., **GRS** provides a bulk analysis, while the **LIBS** instrument is able to sample the outer surface of rocks, see Figure B-83). The stand-alone **LLISSE** payload is the only sub-system that is able to provide atmospheric data over long durations at ambient Venus surface conditions and thus supplements observations made by instruments on other mission platforms. Table 3 gives the Lander Payload Mass, Power, and Data Volume.

### 3.1.2 Aerobot Payload

The Aerobot payload (Figure 10, Table 4) is focused on three science areas: composition, meteorology, and geophysics. An **aerosol mass spectrometer (AMS)** will measure both gas composition and



aerosol/cloud composition, using dedicated inlets for each. Aerosols and cloud droplets entering the inlet pass through a **nephelometer**, a device which measures light scattered from the particles, so as to determine their shape, size, and refractive index (e.g., to distinguish sulfuric acid droplets from volcanic ash). Finally, astrobiological science is addressed by a dedicated **fluorimetric microscope (FM)**, which will examine cloud droplets for minute traces of constituents associated with past or present life.

The Aerobot also carries a suite of **meteorological sensors (MET)**. These include **barometric pressure** and **air temperature** sensors, to examine the convective stability of the atmosphere and to provide context for other measurements. A **radiometer** measuring up- and downwelling fluxes in seven channels spanning the full solar and thermal spectral ranges assesses the role of radiative balance and its relation with cloud-level dynamics. The spectral channels of the Aerobot's radiometer will overlap with those of the Lander and the LLISSE surface station's radiometer, enabling a coherent investigation of radiative processes throughout the Venus atmosphere. Vertical and horizontal **wind velocities** will be determined by tracking the trajectory of the Aerobot, utilizing the Aerobot's communication link with the Orbiter and SmallSats; tracking the Aerobot's position using ground-based telescopes (as was done for the Vega balloons) is another option to be studied. Accelerations and torques measured by an Inertial Measurement Unit (IMU) will allow trajectory reconstruction between communications passes, and facilitate the study of turbulence and waves. Like the Vega balloons, the VFM Aerobot will carry a **wind sensor** in order to distinguish vertical winds from changes in balloon buoyancy; it allows characterization of turbulence down to temporal scales which are inaccessible just by tracking the Aerobot. The **MET** also includes a **radiation dosimeter** in order to quantify the ionizing radiation levels in the cloud layer. All the meteorological sensors share a common data handling unit, which enables low-rate continuous monitoring at 0.5 Hz and occasional scheduled and event-driven acquisition of high-rate data (triggered by events such as a strong updraft or a burst of turbulence).

Finally, the Aerobot carries payloads addressing the geophysics of the solid planet below. Tectonic and volcanic activity during the mission will be monitored by the **barometric pressure (infrasound) sensor**; the high density of the atmosphere at Venus's surface ensures efficient propagation of the ground motion from seismic waves created by venusquakes or other sources into the atmosphere, making Venus well-suited for infrasound investigations of seismicity. Finally, a **3-D fluxgate magnetometer (Mag)** will carry out a number of investigations, including a search for remanent crustal magnetism; constraints on core size and properties from magnetic field draping; and a search for magnetic emissions from lightning. To involve students in this mission, the **visible imager (VI)**, which has high heritage, will take images of the balloon, gondola and atmosphere every other day.

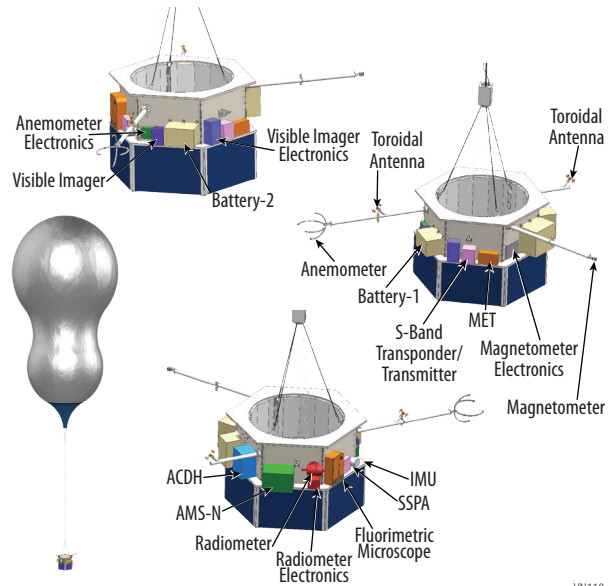
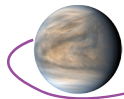


Figure 10. Aerobot with instrument complement shown

Table 4. VFM Aerobot Payload Mass, Power, and Mission Data Volume

Instrument	Mass			Average Power			Mission Data Volume (Mbits)
	CBE (kg)	% Cont	MEV (kg)	CBE (W)	% Cont	MEV (W)	
Venus Aerosol Mass Spectrometer with Nephelometer (AMS-N)	11	30	14.3	10.8	30	14.0	2,034
Fluorimetric Microscope (FM)	5	30	6.5	10	30	13	19
Magnetometer (Mag)	1	30	1.3	6.5	30	8.5	324
Meteorological Suite (MET)	3	30	3.9	5	30	6.5	2,280
Visible Imager (VI)	3	30	3.9	7	30	9.1	300
<b>Total Payload</b>	<b>23</b>	<b>30</b>	<b>29.9</b>	<b>39.3</b>	<b>30</b>	<b>51.1</b>	<b>4,957</b>



All instruments will take data throughout the 60-day nominal mission except the **FM**, which takes seven discrete samples during that time. **Table 4** shows the VFM Aerobot Payload Mass, Power, and Mission Data Volume.

### 3.1.3 SmallSat Payload

The two Venus Flagship Mission SmallSat payloads will focus on understanding atmospheric evolution and dynamics via the interaction of the venusian atmosphere and the solar wind. To accomplish this science goal, the identical payloads consist of a suite of plasma and fields instrumentation (**Figure 11**; **Table 5**), which will further our understanding of the history of volatiles and liquid water on Venus, helping to determine if Venus was habitable and if Venus once hosted liquid water on its surface. A **Langmuir Probe (LP)** will measure thermal ions and electrons, which will help characterize the spacecraft potential and wave activity. The **Ion Electrostatic Analyzer (ESA-i)** will measure *in situ* suprathermal Venus atmospheric ions and solar wind ions to study how ions are accelerated from rest. **ESA-i** will also measure minor species escape rates as well as precipitating ion flux (a proxy for sputtering). The **Electron Electrostatic Analyzer (ESA-e)** will measure *in situ* solar wind electrons and photoelectrons with the goal of characterizing the solar wind and the magnetic field topology. The electron data will aid in the search for evidence of a current or past magnetic field and assist in determining the atmospheric escape rates over a full solar cycle. The **Solar Energetic Particle Detector (SEPD)** will measure the *in situ* solar energetic particles (protons and electrons) at high energies to characterize solar activity and solar transient events in the inner heliosphere. The **fluxgate magnetometer (Mag)** data will be used to characterize the magnetic field topology and strength as well as search for evidence of a past or current magnetic field. The plasma and fields data, in concert with other comparable instruments aboard the five assets, will aid in understanding the history of the liquid water and volatiles on Venus, as well as the evolution of the solar wind interaction with Venus at 0.7 AU. The **Electric Fields Detector (E-FD)** can directly measure and map the electric fields that accelerate atmospheric plasma, contributing to wave activity, ionospheric dynamics and atmospheric escape. Finally, the **Extreme Ultraviolet (EUV)** detector will aid in characterizing the solar wind conditions and determining the solar wind radiation in the ultraviolet. The suite of instruments aboard the two SmallSats provides the means to collect data simultaneously on both the day- and night-side as well as previously unsampled low altitude, southern latitudes over the course of their expected mission. **Table 5** provides the SmallSat Payload Mass, Power, and Mission Data Volume.

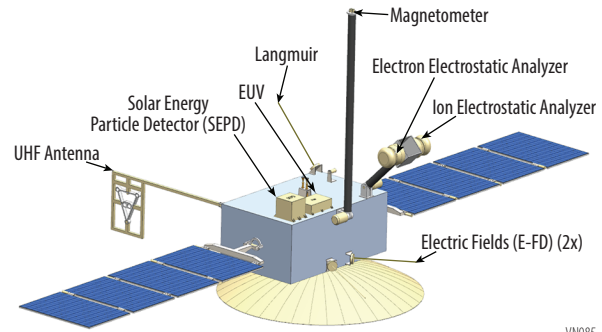


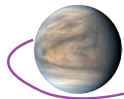
**Figure 11.** VFM SmallSat showing instrument complement

The twin satellite approach has heritage from numerous programs—MMS, THEMIS/ARTEMIS, Cluster, and Van Allen. All the instrumentation has a TRL of 6 or higher and has flight mission heritage—MAVEN, Parker Solar Probe, Juno, THEMIS, and STEREO. The SmallSats themselves are a commercial acquisition with ESCAPE heritage.

**Table 5.** A Single SmallSat Payload Mass, Power, and Mission Data Volume

Instrument	Mass			Average Power			Mission Data Volume (Mbits)
	CBE (kg)	% Cont	MEV (kg)	CBE (W)	% Cont	MEV (W)	
Langmuir Probe (LP)	2.6	30	3.4	2.7	30	3.5	18.5
Ion Electrostatic Analyzer (ESA-i)	3.2	30	4.2	3.7	30	4.8	3,067.7
Electron Electrostatic Analyzer (ESA-e)	2.2	30	2.9	2.1	30	2.7	390
Solar Energetic Particle Detector (SEPD)	2	30	2.6	2.6	30	3.4	17.7
Magnetometer (Mag)	0.5	30	0.6	1	30	1.3	176.5
Extreme Ultraviolet (EUV)	7	30	9.1	14	30	18.2	141.6
Electric Fields Detector (E-Fd)	3	30	3.9	3	30	3.9	307.8
<b>Total Payload</b>	<b>20.5</b>	<b>30</b>	<b>26.7</b>	<b>29.1</b>	<b>30</b>	<b>37.8</b>	<b>4,119.6</b>





### 3.1.4 Orbiter Payload

The Orbiter serves as a platform for a set of instruments (**Figure 12**) that achieve their science goals best by operating from a constant altitude a few hundred kilometers above the surface in a near-polar orbit. Atmospheric scattering limits the NIR resolution to  $\sim 100$  km; to meet the science requirements (high SNR,  $\sim 50$  km spatial resolution), the orbiter must integrate data taken from multiple passes of a minimum of tens of percent of the globe, including the VFM landing site. A pushbroom, **multi-band NIR camera** with a wide FOV, similar to those on the BepiColombo and proposed on VERITAS and EnVision missions [Helbert et al., 2017], can achieve the science goals with the planned orbit, and has suitable TRL, mass, and power requirements.

An **S-band SAR** was chosen to collect the nested high-resolution surface imaging needed to examine key geologic sites, including the landing site. S-band has minimal atmospheric loss, enables a **SAR** that meets TRL, mass, power, and resolution requirements and provides images that can be placed in context with and compared to those from the Magellan mission. We require only two modes of combined resolution/swath-width and a single viewing geometry (i.e., a phased array is not required), so our Soil Moisture Active Passive (SMAP) SMAP-based design [Spencer et al., 2009] provides a light-weight, high TRL solution.

Mesospheric composition of the atmosphere can be characterized in time and space using a sub-mm sounding instrument on the Orbiter operating at 1200 and 600 GHz with a narrow IFOV (1–2 arc-min) with the ability to scan over several tens of degrees while pointed in either the nadir or limb directions. The Submillimeter Wave Instrument (SWI) for ESA’s JUICE mission to the Jupiter system (scheduled launch in 2022) provides suitable scientific capability with acceptable Size, Weight, and Power (SWaP) requirements [Kotiranta et al., 2018] and is used as the basis for the sub-mm sounder for VFM. Two **neutral mass spectrometers (NMS)** (facing opposite directions to enable access to the RAM direction as we rotate the spacecraft to keep radiators away from the sun) will be able to observe *in situ* isotope and neutral constituents in the atmosphere. Finally, a fluxgate magnetometer (on a 2-m boom), two electron electrostatic analyzers (**ESA-e**) and two ion electrostatic analyzers (**ESA-i**) are on the Orbiter to provide another spatial dataset contemporaneous with the identical instruments on the SmallSat payloads discussed above (**Sec 3.1.3**) as well as additional altitude coverage. The latter two instruments will measure full 3D velocity distribution functions in both the solar wind and venusian

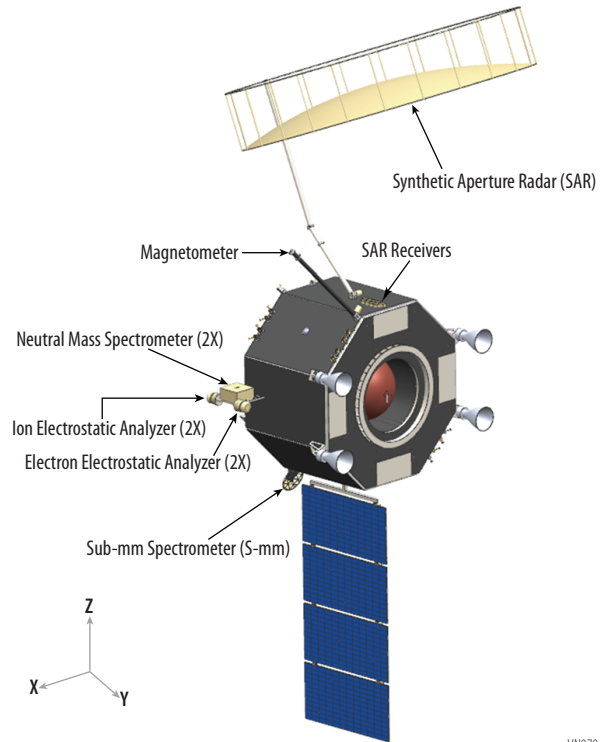
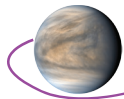


**Figure 12.** VFM Orbiter showing instrument complement

**Table 6.** VFM Orbiter Payload Mass, Power, and Mission Data Volume

Instrument	Mass			Average Power			Mission Data Volume (Mbits)
	CBE (kg)	% Cont	MEV (kg)	CBE (W)	% Cont	MEV (W)	
Synthetic Aperture RADAR (SAR)*	100.0	30	130.0	500.0	30	650.0	57,318
Near IR Imager (NIR-I)	3.4	30	4.4	13.0	30	16.9	2,707
Sub-MM Spectrometer (S-mm)	19.3	30	25.1	55.0	30	71.5	16,399
Flux Gate Magnetometer (Mag)	1.0	30	1.3	1.0	30	1.3	410
Neutral Mass Spectrometer (NMS) x2	28.0	30	36.4	2.4	30	3.1	5,931
Ion Electrostatic Analyzer (ESA-i) x2	6.4	30	4.2	3.7	30	4.8	7,094
Electron Electrostatic Analyzer (ESA-e) x2	4.4	30	2.9	2.1	30	2.7	902
<b>Total Payload</b>	<b>162.5</b>	<b>30</b>	<b>211.3</b>	<b>583.0</b>	<b>30</b>	<b>757.9</b>	<b>90,760</b>

\*SAR data in Pre-Aerobraking Orbit includes landing site mapping



plasma environment, which are especially important for better understanding the heating and acceleration of plasma throughout the induced magnetosphere and inner heliosphere. **Table 6** shows the mass, power and data volume of the Orbiter instruments, which is dominated by the SAR.

### 3.2 Flight System

The VFM flight system consists of an Orbiter, Aerobot, Lander, and two SmallSats (**Figure 3**) and fits with the 5 m diameter of the Falcon 9 Heavy Expendable fairing. The operational order (**Section 2.1** and **Figure 4**) that required the Aerobot be deployed before the Lander reduced the packaging options significantly. A custom payload attach fitting (PAF) allows the placement of the Aerobot inside its aeroshell beneath the Orbiter using commercial off-the-shelf (COTS) separation rings. The Lander inside its aeroshell is attached to the top deck of the Orbiter using COTS separation rings and the SmallSats are tucked in between the Lander and the top deck of the Orbiter. Two SmallSats are attached via separation rings to a vertical bracket, similar in concept to a Moog's Evolved Secondary Payload Adapter (ESPA).

#### 3.2.1 Mission Design

The mission requirements are derived from the Science Traceability Matrix (**Table 2**) and **Table B-5** in **Appendix B.2.2**. Key requirements that drive the mission design are limiting entry peak g loads on the Aerobot and Lander to  $\leq 50$  g, landing when the Orbiter and SmallSats can communicate with Earth, providing continuous coverage of the descent and landing of the Lander, providing communication coverage of descent, initial inflation and floating of the Aerobot, and providing daily access to the Aerobot and LLISSE. The baseline trajectory, shown in **Figure 13**, delivers the VFM elements to Venus. The mission timeline is shown in **Figure 4**. Details of the mission design are found in **Appendix B.2.7**. and the required  $\Delta V$  for the mission and orbit parameters are summarized in **Appendix B, Table B-6** and **Table B-7**.

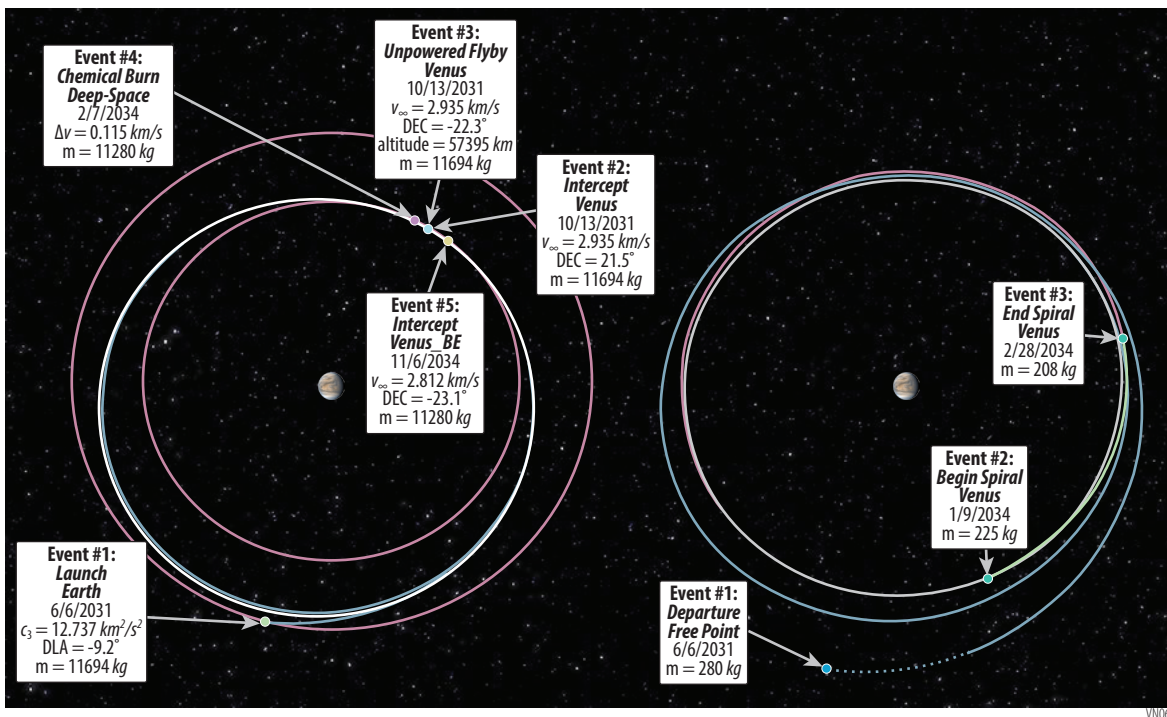
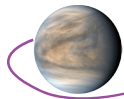


Figure 13. Orbiter (left) and SmallSats (right) Baseline Trajectories

#### 3.2.2 Orbiter

The VFM Orbiter (**Figure 12**) functions as a carrier and propulsion system for the Aerobot and Lander, as a communication relay for the Lander and Aerobot and as a science platform. It uses a 'store and forward' protocol called Delayed Tolerant Network (DTN), which has the ability to store packets from the Lander and Aerobot and forward them to Earth or receive commands from Earth and forward



**Table 7. Orbiter Mass and Power (excluding instruments)**

	Mass			Average Power		
	CBE (kg)	% Cont	MEV (kg)	CBE (W)	% Cont	MEV (W)
Structures & Mechanisms	746.6	30	970.6	N/A	N/A	N/A
Thermal Control	12.3	10	13.5	N/A	N/A	N/A
Propulsion (Dry Mass)	427.2	10	467.9	N/A	N/A	N/A
Altitude Control	85.9	10	94.5	16.3	30	21.2
Command & Data Handling	19.5	10	21.5	41.5	30	52.6
Telecommunications	12.6	16	14.7	180.0	30	234.0
Power	123.9	10	136.3	18.0	30	23.4
<b>Total Orbiter</b>	<b>1428</b>	<b>20</b>	<b>1719</b>	<b>255.8</b>	<b>30</b>	<b>331.2</b>

them to the Lander and Aerobot. Orbiter operations are discussed in **Section 3.3**. The 5 m antenna functions as both the **SAR** and the communication antenna for S-band, X-band and Ka-band systems and stows into a very compact package with enough clearance to mount on the -y panel. The antenna is a smaller version of the 6m antenna flown in 2015 on SMAP. The deployment system is the same as used on SMAP without the added turntable that SMAP required. The Orbiter also has two X-band Omni antennas and a Medium Gain X-band antenna for commanding and backup.

The Orbiter structural design was driven by carrying the launch loads of the other mission elements through to the launch vehicle. **Table 7** shows the Orbiter Mass and Power. A Master Equipment List (MEL) was developed and contingency was assigned at the component level based on TRL. Those items that have flown before and required no modification with a high TRL were assigned a contingency of 10%. Items that had to be modified were assigned 20% and new items or those that required significant modifications were assigned 30%. All structural items were assigned 30%. The total system has 23% launch mass margin on the wet mass. A conservative approach was taken with power and a 30% contingency was used on all loads. The Orbiter is three-axis stabilized with significant momentum and torque capabilities to account for the large inertia associated with the stacked configuration. All structural components are well within the state-of-the-art.

The Orbiter power system consists of solar arrays, a secondary battery, and supporting power electronics. TJGaAs solar cells with bare cell efficiency of 29.5% are used. The solar constant at Venus is 2263 W/m<sup>2</sup>, and the arrays operate at 140°C. A single two-axis tracking panel with 5.4m<sup>2</sup> active area (5.9 m<sup>2</sup> total substrate area) will provide 1,845 W of power to support loads and battery recharge. A high energy density 38AH Li Ion battery is used to support night loads. The Power System Electronics (PSE) will be a heritage 28VDC battery dominated bus included as cards in the avionics package. All Orbiter power components are greater than TRL 7. The Orbiter Attitude Control System (ACS) design is discussed in **Appendix B.2.8.3.8**. All of the ACS components are TRL 7 or greater and have significant flight heritage and can meet the mission life requirement. The avionics for the Orbiter are block redundant to meet the reliability for a Class A Flagship Mission. The avionics consists of the following functions: Command and Data Handling (C&DH), attitude control sensors and thrusters, power conditioning and distribution, mechanisms for launch locks, deployments and motors, and control of main engine propulsion.

The Orbiter thermal design has radiators on the Orbiter -z surface, bottom deck, to dissipate electronics heat while keeping the radiators out of the Sun (and out of view of the hot Venus surface). During cruise phase, the attached aeroshell will somewhat cover the radiators' view to space, but no enhancements to the thermal system are needed; the radiators can still dissipate the requisite cruise phase heat. A 'toasty' cavity approach eliminates propulsion system heaters on the tanks and lines while orbiting Venus.

### 3.2.3 Aerobot

The Aerobot is a floating platform that incorporates a helium variable-altitude balloon system that can control its altitude to a commanded profile in the venusian atmosphere. The Aerobot is based on a 15 m diameter pumped-helium balloon with a second 7.5 m diameter internal chamber (**Figure 10**). The outer chamber is at approximately equal pressure with the atmosphere (a zero-pressure balloon), while a second internal chamber is at elevated pressure with a structural, constant-volume envelope

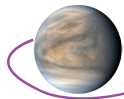


**Table 8.** Aerobot (excluding instruments) Mass and Power

	Mass			Average Power (Day)			Average Power (Night)		
	CBE (kg)	% Cont.	MEV (kg)	CBE (W)	% Cont.	MEV (W)	CBE (W)	% Cont.	MEV (W)
Aeroshell	572.8	22.3	737.6	N/A	N/A	N/A	N/A	N/A	N/A
Structures & Mechanisms	55.4	10	61.9	N/A	N/A	N/A	N/A	N/A	N/A
Balloon System	186.0	30	241.8	N/A	N/A	N/A	N/A	N/A	N/A
Inflation System	230.8	10	253.9	N/A	N/A	N/A	N/A	N/A	N/A
Thermal Control	2.6	10	2.9	3.0	30	3.9	3.0	20	3.9
Propulsion (Dry Mass)	N/A	N/A	N/A	N/A	N/A	N/A	N/A	N/A	N/A
Attitude Control (Descent & Float)	0.1	10	0.1	2.0	30	2.6	2.0	30	2.6
Command & Data Handling	10.6	10	11.7	33.0	30	42.9	8.5	30	11.1
Telecommunications	6.3	16.3	7.3	39.1	30	50.8	8.1	30	10.5
Power	78.3	10	86.2	19.0	30	24.7	6.0	30	7.8
<b>Total Aerobot Subsystems</b>	<b>1,142.9</b>	<b>23</b>	<b>1,403.5</b>	<b>96.1</b>	<b>30</b>	<b>124.9</b>	<b>27.6</b>	<b>30</b>	<b>35.9</b>

(a super-pressure balloon). Helium is pumped from the outer chamber to the inner chamber to lower the total volume and hence buoyancy and altitude, while helium is vented from the inner chamber to outer chamber to raise the altitude. The balloon system remains a sealed system for the entirety of operation; no atmosphere will be ingested. Details of the balloon design are found in **Appendix B**. Of note, lowering the altitude requires energy and is limited by the throughput of the pump, while raising the altitude can be done quickly for little energy by opening an orifice to vent the pressurized helium between the chambers. Aerobot operations are discussed in **Section 3.3**.

The Aerobot aeroshell is a 45° sphere-cone geometry with a max diameter of 2.8 m. This geometry was chosen for its good stability and packaging characteristics as well as significant flight heritage at Venus. The heat-shield TPS is a tiled single layer system of HEEET (Heat-shield for Extreme Entry Environment Technology) that is the baseline material for the Mars Sample Return Earth Entry Vehicle. PICA (Phenolic Impregnated Carbon Ablator) is the backshell TPS. The expected peak heating during the entry is 4,000 W/cm<sup>2</sup> (convective, rough wall, margined, at the shoulder) with an integrated heat load of over 53,000 J/cm<sup>2</sup>. The shoulder sees a relatively low radiative heating (peak, margined value of 11.3 W/cm<sup>2</sup> and an integrated heat load of 484 W/cm<sup>2</sup>).

The concept of operations for the Aerobot calls for two parachutes, one supersonic and the other subsonic. For the purposes of this study, the supersonic and the subsonic parachute are assumed to be identical, weighing 27.4 kg each. Details of the entry, descent, and float design are found in **Appendix B** and concept of operations are discussed in **Section 3.3**. The Aerobot provides 2 Gbits of data storage and communicates once a day for 10 minutes with the SmallSats as discussed in **Section 3.3**.

Currently, NASA classifies Venus missions under planetary protection Category II, where the surface environment of Venus presents a negligible chance of either forward or back contamination and the cloud environment presents such a slight chance of contamination that it does not require any special precautions in mission planning [PPIRB 2019]. However, given that we have a **FM** instrument to look for signs of extant life, we need to ensure that the environment of that instrument is pristine and not contaminated by terrestrial life. Consequently, measures to sterilize the instrument and possibly bag it and de-contaminate nearby gondola sub-systems have to be considered. The details of the planetary protection and contamination control plans required to remove Earth-derived live or dormant organisms and microbial debris are beyond the scope of this study and need further work.

The Aerobot uses an IMU to provide disturbance data for correlation with science measurements. It does not have an attitude control system nor a propulsion system. Ranging between the Aerobot and SmallSats provides estimates of the altitude of the Aerobot to within the required ±1 km. Avionics and electrical components all have extensive flight heritage with only minor qualification updates needed for the survivability at altitudes from 52 to 62 km. **Table 8** shows the mass, daytime average power and the night-time average power budgets for the Aerobot.

There are three deployable structures (Boom-Arms) which extend away from the Aerobot. Once deployed they provide instruments and antennas 0.5m–2.0m distance from the Aerobot structure. Boom-Arm One is for the Anemometer and Antenna One; Boom-Arm Two for Antenna Two; and the 2 m Boom-Arm Three for the Magnetometer. All of which are well within the state-of-the-art. Details on the Aerobot are in **Appendix B.2.5.1**.

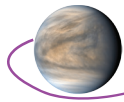


**Table 9.** Lander (excluding instruments) Mass and Power

	Mass			Average Power		
	CBE (kg)	% .	MEV (kg)	CBE (W)	% .	MEV (W)
Aeroshell	786.3	23	1,015.2	N/A	N/A	N/A
Structures & Mechanisms	448.2	30	546.2	N/A	N/A	N/A
Thermal Control	88.9	30	115.6	0	0	0
Propulsion (Dry Mass)	N/A	N/A	N/A	N/A	N/A	N/A
Attitude Control (Descent only)	72.6	10	79.9	44.0	30	57.2
Command & Data Handling	39.3	24	48.6	80.5	30	104.7
Telecommunications	5.5	11	6.1	39.0	30	50.7
Power	69.0	10	75.8	7.0	30	9.1
<b>Total Lander Subsystems</b>	<b>1,509.8</b>	<b>25</b>	<b>1,887.4</b>	<b>170.5</b>	<b>30</b>	<b>221.7</b>

### 3.2.4 Lander

The Lander is designed to operate for at least 6 hours and up to 8 hours on the surface of Venus where the temperature of the atmosphere is  $-441^{\circ}\text{C}$  and the pressure is 76 bar at West Ovda. In order to land safely, the mechanical design needs to accommodate landing terrain uncertainty, thus the Lander is designed to land on a slope up to  $30^{\circ}$  and have clearance to accommodate a 0.5 m boulder beneath the sphere. Because landing is identified as the highest risk for the mission, the Lander includes a Terrain Relative Navigation (TRN) and a Hazard Avoidance (LHA) system. The system would be used to estimate the Lander's local relative position by comparing terrain maps from the initial VFM orbit and/or other prior missions, which would be loaded into memory prior to separation, with terrain measurements from navigation sensors (LIDAR, engineering camera, laser altimeter). The TRN-LHA assesses the hazards in the projected landing site and uses fans to move the Lander laterally to avoid landing on the hazard (e.g., a steep slope or large boulder). The TRN and LHA are discussed in more detail in **Appendix B.2.8.2.5**.

The equatorial ring of the hemisphere is the primary backbone of the Lander design (**Figure 9**), providing the interface to the aeroshell, the drag plate, the legs, the **Neph**, and the instrument sphere. A bridging structure, which does not interface with the instrument sphere, is used to bridge the leg loads and isolate the sphere during landing. The bridge also provides mounting of the LLISSE instrument. The drag plate is used to control the terminal velocity during descent; the flight dynamics of the drag plate are discussed in **Section 3.3**. The **PC** uses four mirrors within the cupola to provide  $60^{\circ}$  FOV from each of the four windows (**Figure 14**). The camera views are limited by the drag plate below the windows. Additional options to increase the panoramic camera FOV, such as a drag plate that folds out of the way after landing or a deployable drag plate that sits above the lander, are left to future studies. The mass and power of the Lander are shown in **Table 9**.

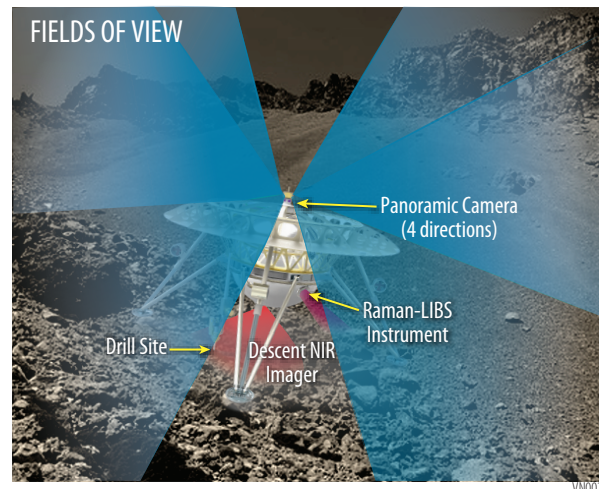


**Figure 14.** FOVs of the Lander Cameras

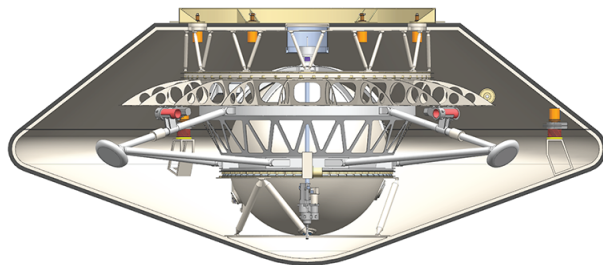
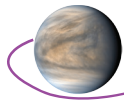


**Figure 15.** Lander Stowed in Aeroshell

The aeroshell cone angle of  $70^{\circ}$  and 4.6 m diameter provides ample volume (**Figure 15**) and enables a very simple leg design with a telescoping upper arm. This allows for both a single motion deployment and for energy absorption with the use of a crushable canister inside the leg tube. The legs provide mounting for the fan actuation system. A drive system, used to deploy the legs, can also be used to stabilize and level the landed craft after landing to within  $10^{\circ}$  of the gravity vector.



The width of the leg stance could be greatly increased, thereby increasing landing stability, by implementing a multi-fold leg design, which would also allow a smaller diameter entry system. This optimization was left for future study. At the base of the legs are landing pads. Additional studies are needed to determine the type of foot interface based upon the expected terrain; for example, spikes may be of more utility when landing on slopes to prevent sliding.

The 70° sphere-cone aeroshell geometry provides significantly better packaging and drag performance than the 45° sphere-cone (e.g., PVO) and has been successfully used at Mars (e.g., InSight). This smaller surface area for a given diameter reduces total heating, thus requiring a lighter heatshield thereby reducing the mass of the thermal protection system. The heat-shield TPS is a tiled single layer system of HEEET. PICA is used as the backshell TPS. The expected peak heating during the entry is 1734 W/cm<sup>2</sup> (convective, rough wall, with margin, at the shoulder) with an integrated heat load of 23,875 J/cm<sup>2</sup>. The shoulder also sees a peak radiative heating of 87.3 W/cm<sup>2</sup> (margin) with a corresponding heat load of 1379 J/cm<sup>2</sup>.

The aeroshell uses a supersonic parachute for deceleration prior to Lander separation and for stability near Mach 1. The parachute design is a 10.04 m diameter Disk-Gap-Band parachute deployed at Mach 1.4, and is expected to weigh 35.6 kg. This parachute design has flown many times at Earth and on every US mission to Mars since Viking [Clark and Tanner, 2017] and the loads and deployment conditions are within those recently demonstrated in the ASPIRE test program [O'Farrell et al., 2019] limits. The backshell geometry used in the current design is driven by packaging constraints: i.e. the smallest backshell that can package all the components inside the aeroshell. The backshell geometry is within the envelope of legacy backshell geometries and any of those would also meet the packaging constraints of the Lander. Details of the backshell design are in **Appendix B.2.8.2.3**.

The instrument sphere is designed in three sections (**Figure 16**). The upper hemisphere supports the sample handling tanks and the **PC** cupola and provides an access port for integration. The access port has plumbing for evacuating the sphere prior to launch. The lower hemisphere has the **TLS** and **NMS** inlet assembly and three windows. The lowest window is for the **DI** and provides a Field of View >90°. Slightly higher is the window for the hazard avoidance systems including the LIDARs, laser range finders and the supporting engineering camera. The final window is for the **R-LIBS**. The equatorial ring has the electrical connection port, and a pass-through for the **AS** mounted on the outside of the sphere. The equatorial ring supports the thermally isolating 'elephant stands', which support the upper and lower decks, and is part of the spherical geometry to maintain as consistent a spherical shape as possible, maximizing sphere strength.

The decks are thermally isolated from the sphere with a titanium flexure ring and all avionics and instruments are thermally coupled to the decks. The upper and lower decks are isogrid aluminum with pockets that are used for embedding the phase-change material, while the aluminum provides high conductivity to the boxes and instruments. Phase-change material will become liquid when it changes phase but it is contained within the decks. Structural concepts developed for this study are within the current state-of-the-art and have heritage but it is likely that high pressure sealing and ports/pass-throughs will require additional engineering development and testing.

Deck components are grouped by function whenever possible. The upper deck primarily holds the operational boxes such as communication and power boxes. Between the decks is dominated by instrument boxes with the exception of the Lander Command and Data Handling (LCDH) box. The lower volume has both instrument components and the hazard avoidance boxes. The bottom deck accommodates the sample ingestion and handling system, the **Neutron Generator/GRS**, the **XFS**, **XRD**, and **R-LIBS**.

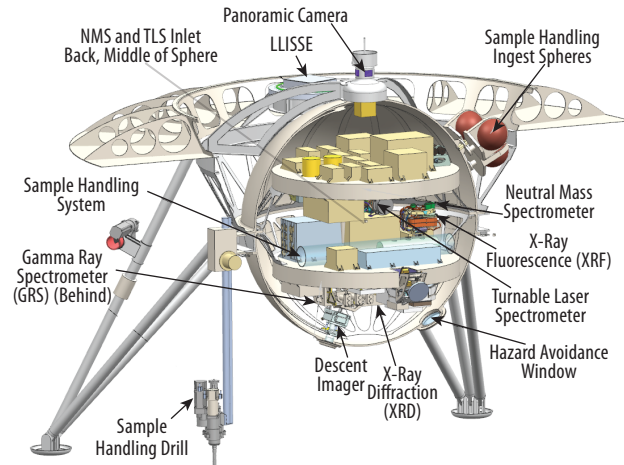
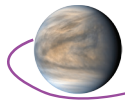


**Figure 16.** Lander Cutaway view shows packaging inside the Sphere



The outside of the Lander sphere is painted white with Z93C55 Conductive Coating. The sphere will start at  $-25^{\circ}\text{C}$  while in orbit around Venus prior to descent. During descent, temperatures will steadily increase as the Lander descends into the atmosphere, but the phase-change material (n-Eiocane ( $\text{C}_{20}\text{H}_{42}$ )  $+37^{\circ}\text{C}$ ) is used within the decks to flatten the temperature ramp.

There are 3 separate lower windows, which are triple-paned, one each for the **R-LIBS**, **HA** system, and **DI**, and the **PC** has a view through 4 small windows around the perimeter of the cupola. For the three lower windows a low emissivity coating is used to reduce heating of the instrument optics. The emissivity is 0.15 on both sides of the inner window. The sphere is evacuated to reduce convective heat transfer and allow effective MLI blanketing and will be evacuated to  $10^{-6}$  torr prior to launch, which should simplify the sealing of all ports and pass-throughs as well as the sphere segments. Zeolite is used to keep high vacuum in the sphere during transit. Both high temperature MLI blanketing and “Standard” Kapton MLI are used. A thermal model of the Lander is discussed in **Appendix B.2.8.2.8** and the model results for heating during the 1 hour of descent and 7 hours of surface operations are also discussed in **Appendix B.2.8.2.8**. All the thermal hardware has a high TRL level and has been used on many spaceflight programs.

The Lander avionics system provides Lander Command and Data Handling (LCDH) with a low power VORAGO ARM Cortex-M4 processor for commanding the instruments, sample collection and the drill. The LCDH collects, processes and stores instrument and Lander health and safety data on the 8 Gbit solid state recorder. The LCDH also includes a high performance spacecraft computing (HPSC) ARM Cortex A53 for the processing of TRN and LHA algorithms. Timing with an accuracy of  $\geq 0.1$  msec with  $10^{-6}$  stability relative to ground station is provided by an ultrastable oscillator. A Mechanism and Propulsion Unit (MPU) provides cards that interface with the aeroshell separation hardware and control deployments including: parachute, heat shield, backshell, leg deployments, and fans. Communication links are shown in **Table B-17** in **Appendix B.2.6.1**.

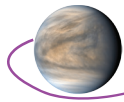
The Lander power system consists of a primary non-rechargeable battery and supporting power electronics. The power system configuration is driven by lack of any usable solar flux at the Venus surface prohibiting power generation to support loads or recharge a secondary battery. Saft LSH20 D 13000mAh 3.6V Lithium-Thionyl Chloride cells are used in a 9 series 9 parallel (9s9p) configuration to provide 117AH of energy at 32V. Due to the nature of the primary battery, all Lander subsystems remain off until just prior to separation from the Orbiter. The Power System Electronics (PSE) will be a heritage 28VDC battery-dominated bus included as cards in the avionics package. The PSE will control switching and power distribution.

### 3.2.5 SmallSats

The Venus Flagship Mission includes two SmallSats (**Figure 11**) that house the science instruments listed in **Table 5** and communications coverage for the Aerobot and Lander. A majority of the SmallSat spacecraft and subsystems are expected to be procured commercially. The study focused on developing a concept that meets the data storage and communication requirements, including defining a feasible propulsion subsystem. As a result, the SmallSat concept is at CML 2 but has leveraged the ESCAPEDE architecture and mission design with similar instruments that are on a SIMPLEX-II twinsat plasma mission to Mars.

The SmallSats are expected to be physically identical, but they will be deployed in different orbits as described in **Section 3.2.1**. The requirement to act as data relays for the Aerobot and Lander drives the need for the SmallSats to be orbiting Venus prior to the arrival of the other elements. SmallSats separate from the Orbiter a few hours after launch and guide themselves to Venus, each using solar electric propulsion. After arrival at Venus they follow a low-thrust spiral down to their final Venus orbits. Details of the trajectory design for the SmallSats is shown in **Appendix B.2.7**. The Communication subsystem was sized to provide the capabilities listed in **Table B-17** in **Appendix B** and the data storage needed was derived from the concept of operations. A preliminary mass estimate is shown in **Table 10** and the SmallSat power will be determined by the commercial provider. Due to the nature and focus of the current study only the propulsion, communication and data storage needed were explored. Details of the other SmallSat subsystems are left to future studies, as the technological innovations are moving quickly and should be revisited closer to flight.

The VFM flight platform characteristics are shown in **Table 11** with more details in **Appendix B**.



### 3.3 Concept of Operations and Mission Design

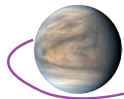
**Table 10.** A Single SmallSat (excluding Instruments) Mass and Power

	Mass			Average Power		
	CBE (kg)	% .	MEV (kg)	CBE (W)	% .	MEV (W)
Structures & Mechanisms	33.0	30	49.4	–	–	–
Thermal Control	6.9	30	9.0	–	–	–
Propulsion (Dry Mass)	27.0	30	35.1	–	–	–
Attitude Control (Descent only)	12.0	30	15.6	–	–	–
Command & Data Handling	11.2	30	9.3	–	–	–
Telecommunications	10.0	30	14.6	–	–	–
Power	14.0	30	18.2	–	–	–
<b>Total SmallSat Subsystems</b>	<b>114.1</b>	<b>30</b>	<b>148.3</b>	–	–	–

**Table 11.** VFM System and Sub-system Characteristics

Flight System Element Parameters (as appropriate)	Aerobot	Lander	Orbiter	SmallSats
<b>General</b>				
Design Life	60 Days	6 Hours	10 years	6 years
<b>Structure</b>				
Structures material (aluminum, exotic, composite, etc.)	Composite, AL, Honeycomb, Ti	Composite, AL, Honeycomb, Ti	Composite, AL, Honeycomb, Ti	–
Number of articulated structures	0	4 Sample Handling system, Drill, Raman/LIBS minor, Leg Leveler	2 (Solar Arrays, Rotation Platform)	–
Number of deployed structures	3 (Anemometer and Antenna, Antenna and Mag booms)	5 (4 Legs, Mass Spec Inlet Caps)	7 (Aerobot, Lander, 2 SmallSats, Antenna, Mag & S/A)	–
Aeroshell diameter, m	2.8	4.6	N/A	N/A
<b>Thermal Control</b>				
Type of thermal control used	Convection and radiation white painted radiator	Ti flexures and Phase Change Material	Passive thermal radiator	–
<b>Propulsion</b>				
Estimated $\Delta V$ budget, m/s	N/A	N/A	1642.8	
Propulsion type(s) and associated propellant(s)/oxidizer(s)	N/A	N/A	Regulated Bipropellant, MMH, NTO	SEP
Number of thrusters and tanks	N/A	N/A	4 Main Engines 16 ACS Engines 1 MMH Tank 4 NTO Tanks 2 Press. Tanks	2 BHT600
Specific impulse of each propulsion mode, seconds	N/A	N/A	293	1750
<b>Attitude Control</b>				
Control method (3-axis, spinner, grav-gradient, etc.)	None	Roll Axis with 2-Axis Translational Control	3-Axis	3-Axis
Control reference (solar, inertial, Earth-nadir, Earth-limb, etc.)	None	Local Vertical	Inertial	LVLH, Inertial
Attitude control capability, degrees	None	15	3 arcmin 3-axis 3-sigma	2 deg 3-axis 3-sigma
Attitude knowledge limit, degrees	None	10	0.5 arcmin 3-axis 3-sigma	-0.5 deg 3-axis 3-sigma
Agility requirements (maneuvers, scanning, etc.)	None	3-DOF maneuver	Antenna Pointing	3-DOF maneuver
Articulation/#-axes (solar arrays, antennas, gimbals, etc.)	0	0	2	2
Sensor and actuator information (precision/errors, torque, momentum storage capabilities, etc.)	IMU	IMU, Fans	IMU, ST, RCS, RWA, CSS	RWA, ST, IMU CSS





Flight System Element Parameters (as appropriate)	Aerobot	Lander	Orbiter	SmallSats
<b>Command &amp; Data Handling</b>				
Housekeeping data rate, kbps	2	2	2	–
Data storage capacity, Mbits	2,000	8,000	4,000,000	100,000
Maximum storage record rate, kbps	30,000	30,000	500,000	–
Maximum storage playback rate, kbps	30,000	30,000	30,000	–
<b>Power</b>				
Type of array structure (rigid, flexible, body mounted, deployed, articulated)	Fixed	N/A	Two-Axis	–
Array size, meters x meters	1.9 m <sup>2</sup> Active	N/A	5.4 m <sup>2</sup> Active	–
Solar cell type (Si, GaAs, Multi-junction GaAs, concentrators)	TJGaAs	N/A	TJGaAs	–
Expected power generation at Beginning of Life (BOL) and End of Life (EOL), watts	448 (BOL) 380 (EOL)	N/A	2,181 (BOL) 1,845 (EOL)	–
On-orbit average power consumption, W	0	0	902	–
Day Power Consumption, watts	360	400	902	–
Night Power Consumption, watts	120	N/A	902	–
Battery type (NiCd, NiH, Li-ion)	Li Ion	Primary Lithium-Thionyl Chloride	Li Ion	–
Battery storage capacity, aH	300	200	38	–

The mission design was previously discussed in **Section 3.2.1**. A summary of the VFM mission design is shown in **Table 12** and more fully in **Appendix B.2.6.3**.

**Figure 17** shows the VFM ground architecture. The Orbiter and SmallSats both command and receive science data, health and safety data from the Lander and Aerobot using S-band. The SmallSats also receive science, health and safety data from **LLISSE** using UHF. The Orbiter and SmallSats store the data they receive from the Aerobot, Lander, and LLISSE and then add their own science, health, and safety data and transmit to DSN via X-Band for the SmallSats and via Ka-Band for the Orbiter. The Orbiter has a high gain antenna (HGA), medium gain antenna (MGA) and a low gain antenna (LGA) X-Band link with DSN in addition to the Ka-Band link. During critical events, such as launch, Deep Space Maneuvers (DSMs), Venus Orbital Insertion (VOI), Entry, Descent, and Landing of the Aerobot and Lander, DSN coverage is expected 24 hours a day for the duration of each critical event. Delta Differential One-way Ranging (DDOR) will be required on the X-Band links with the SmallSats and Orbiter. During the mission phases routine daily contacts are required between DSN and the Orbiter and SmallSat as shown in **Table B-17** in **Appendix B**.

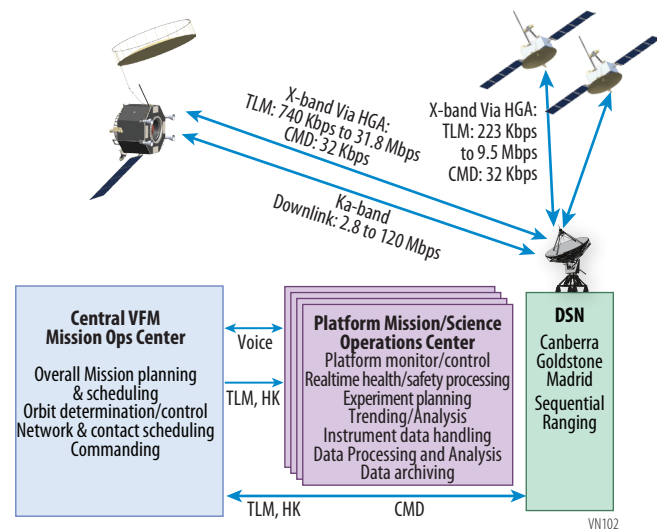


**Figure 17. Ground Systems Architecture**

### 3.3.1 Flight Mission Operations

Mission operations has three phases: 1) Launch and Cruise to Venus operations, 2) Venus Orbit, Atmosphere and Surface operations, 3) Aerobraking and Science Orbit operations. Venus Orbit, Atmosphere and Surface operations are divided into the operations performed by each element.

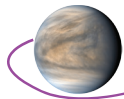


Table 12. Mission Design

Parameter	Orbiter Elliptical	Orbiter Circular	SmallSat 1	SmallSat 2
Orbit Parameters (apogee, perigee, inclination, etc.)				
Apoapsis (km)	116,108.4	300	18,661	18,661
Periapsis (km)	300	300	500	500
Eccentricity	0.95	0	0.578	0.578
Inclination (deg)	90	90	22.5	65
Orbital Period	5 days	1.6 hours	6 hours	6 hours
RAAN (deg)	334.4	334.4	251.0	339.9
Argument of Periapsis (deg)	188.6	188.6	86.7	359.5
Mission Lifetime	10 years		6 years	
Maximum Eclipse Period (minutes)	22.2	22.3	87.7	90.0
Launch Site	Cape Canaveral, FL			
Total Mass <b>with</b> contingency (includes instruments)	1,930.2		300.0	300.0
Propellant Mass <b>without</b> contingency	3,193.2		112.5	112.5
Propellant contingency	354.8		12.5	12.5
Propellant Mass <b>with</b> contingency	3,548.0		125	125
Launch Adapter Mass <b>with</b> contingency	71			
Total Launch Mass	9,584.6			
Launch Vehicle	Falcon 9 Heavy Expendable 5 m fairing			
Launch Vehicle Lift Capability	11,694.0			
Launch Vehicle Mass Margin	2,109.4			
Launch Vehicle Mass Margin (%)	22.0			

### 3.3.1.1 Launch and Cruise to Venus Operations

The VFM launches from Cape Canaveral, Florida, on a single Falcon 9 Heavy Expendable vehicle with 5m fairing on June 6, 2031. The launch window is 14 days long. There is a backup launch opportunity in June of 2032. The mission timeline is shown in **Figure 4**, with details in **Appendix B.2.7**.

### 3.3.1.2 Venus Orbit, Atmosphere, and Surface Operations

#### 3.3.1.2.1 Aerobot Operations

Five days after release by the Orbiter the Aerobot enters the venusian atmosphere on November 9, 2034, and begins the Entry, Descent, and Float (EDF) sequence shown in **Figure 18**. The SmallSats

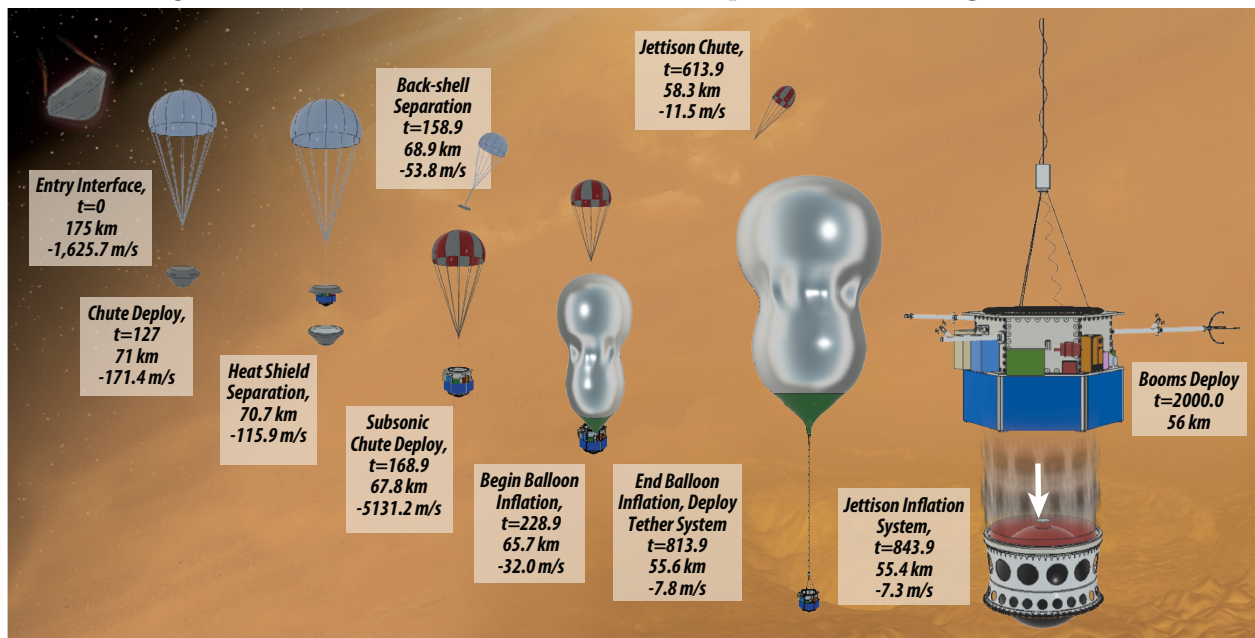
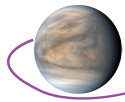


Figure 18. Aerobot Entry, Descent, and Float Operational sequence



will have arrived 3 months earlier and will provide communication for the EDF sequence and the 60 days of float operations.

Once the Aerobot is fully deployed after atmospheric entry and descent, the Aerobot altitude will be set to a nominal 56 km, where the temperature is  $\sim 20^{\circ}\text{C}$ . Carried by ambient winds, the Aerobot will circumnavigate Venus every 5 days on average. During the first circumnavigation, the altitude control system will be used to maintain a near-constant altitude, and thus a near-constant temperature, for sensitive characterizations of atmospheric composition including the isotopic ratio of noble gases. In later circumnavigations, the Aerobot's altitude control will be used to descend to 52 km, rise over 2 hours to 62 km altitude, and then descend again to the chosen float altitude, allowing quasi-vertical profiles of atmospheric parameters to be measured (**Figure 6**). One ascent is planned during each dayside pass and during nightside pass, for a total of 24 vertical profiles, distributed over all times of day and night, over the 60 day nominal mission duration. Altitude cycling can be stopped or reduced at night if desired to conserve power. The nominal mission lifetime for the Aerobot is 60 days, but if it lasts longer communication to the SmallSats is available. The Aerobot will communicate with the SmallSats at least once a day to receive a new 4–5 day observation plan from the ground and to downlink science and health and safety data.

The balloon's meteorological instrumentation (**MET**) will be powered on at all times, measuring continuously at sampling rates varying from 0.02 Hz (radiometer) to 60 Hz (infrasound sensor). A low rate meteorological data set recorded at 0.2 Hz will be returned for the whole mission duration. To characterize turbulence, power spectra of meteorological parameters will be calculated onboard for each half hour interval. Onboard autonomous event detection will be performed to identify possible seismic, volcanic, lightning or other transient events; high-rate data from these candidate events will be downlinked to Earth. The **AMS-N** is powered on for seven minutes, once per hour on average (with a higher measurement cadence during vertical ascents). During each operational period after a 2-minute warm up period, the mass spectrometer will measure composition of the atmosphere for five minutes, and then measure the composition of cloud/aerosol particles which are separated from atmospheric gas using an aerodynamic aerosol separator. The incoming atmosphere passes through a nephelometer that optically interrogates cloud and aerosol particles entering the mass spectrometer to constrain their size, shape, and composition. The mass spectrometer data are integrated over 10 second periods in order to reduce data rate. After each operational period, the instrument will remain in standby power until it is ready to ingest the next sample.

The **FM** will characterize 7 samples during the 60-day mission. Each time it is switched on, a pump draws atmosphere in and the sample is then pumped via a bypass line in the fluidic manifold to 1-of-7 particle-capture filter sets located on a rotatable sample-stage. A stepper-motor positions the stage and directs the sample to a set of particle-capture filters as it aligns each filter set beneath the microscope objective. The **MET** and **Mag** operate continuously during the day and night side of Venus. The meteorological suite is sampled at 0.2 Hz background, the radiometer at 0.02 Hz, including additional 20 high-rate events per day of 3 minutes each. Magnetometer data are downsampled to 0.5 Hz, which is sufficient for measurement of remanent magnetism and occasional high-rate data for investigations such as Schumann resonances characterization and the search for lightning. The **VI** will take 1 image every other day on the day side to show the balloon and cloudscapes, for student and public outreach purposes. The collection time is 1 minute for each image. The mission data volume generated by the Aerobot instruments is shown above in **Table 4**.

### 3.3.1.2.2 Lander Operations

On May 16, 2035, the Orbiter performs a Lander entry targeting maneuver, spins up to 3 rpm and deploys the lander with a separation velocity of  $\geq 1$  m/s. The Lander has two operational sub-phases: 1) Lander Entry, Descent, and Landing Operations and 2) Surface Operations.

#### 3.3.1.2.2.1 Lander Entry, Descent, and Landing Operations

The Entry, Descent, and Landing sequence is shown in **Figure 19**. The Lander transmits data from entry through landing as shown in **Figure 20**. The parachute deploys 125.3 seconds after entry and slows the Lander in its aeroshell down from Mach 1.4 to Mach 0.7 at 358.6 seconds. At that time, the heat shield is jettisoned and the Lander and backshell remain attached until 388.6 seconds when the Lander jettisons the parachute and backshell. The parachute and backshell are blown westerly by the

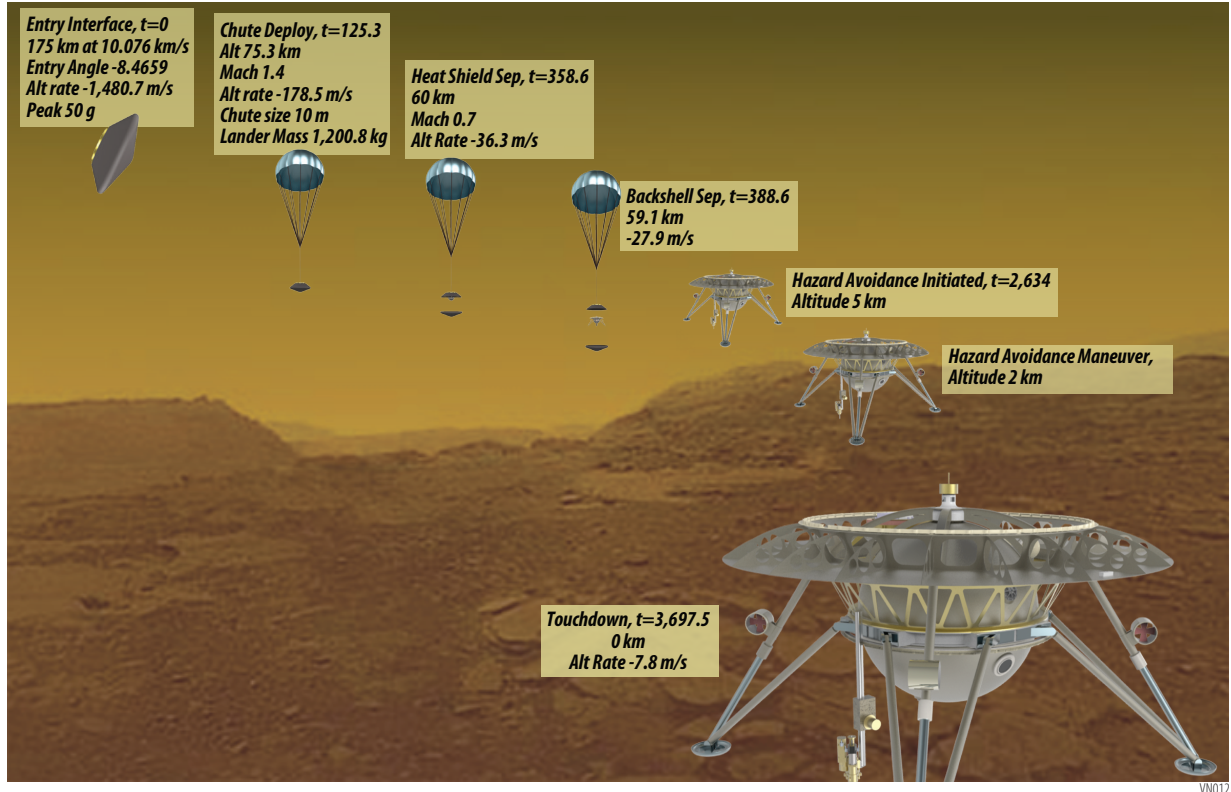
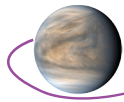


Figure 19. Lander Entry, Descent and Landing Operations

Venus winds while the Lander begins free fall with its drag plate used to slow it down for landing with a velocity of less than 8 m/s. Lander science operations commence upon entry into the Venus atmosphere and continue throughout descent to obtain a full meteorological and spectroscopic atmospheric profile. The **NMS** and **TLS** sample above the cloud tops, below the main cloud layers, in the lower atmosphere and just above the surface. The **Neph** and **AS** obtain samples at 100 m increments. The **GRS** records data continuously in passive mode throughout descent. Below 9 km the **DI** captures the landing area by virtue of the slow rotation (2–3 RPM) of the lander as it touches down. Safe landing is achieved through the use of TRN-LHA as described in **Appendix B.2.6.3** and **Appendix B.2.8.2**.

### 3.3.1.2.2 Lander Surface Operations

The **TLS** and **NMS** sample the atmosphere upon touchdown, at landing+1 hour and landing+2 hours. Passive **GRS** science continues on the surface for 30 minutes after landing, then the **Neutron Generator** turns on to begin active **GRS** measurements, which continue until the end of surface operations. The **AS** continues to take data after landing (see **Figure 20**). A full set of panoramic images is taken upon landing and at landing+60 minutes. Imaging is completed, and images uploaded, while the lander is in communication range of the Orbiter. The **R-LIBS** Instrument begins surface interrogation upon landing and continues until the end of surface science operations at landing+7 hours, although the sampling rate is reduced after landing+2 hours in order for the full lander data to be uploaded to a SmallSat.

Once on the surface and with the lander leveled, sample science can begin. The **DI** images the drill area prior to and post drilling. Drill deployment and sample acquisition to 5 cm depth commences

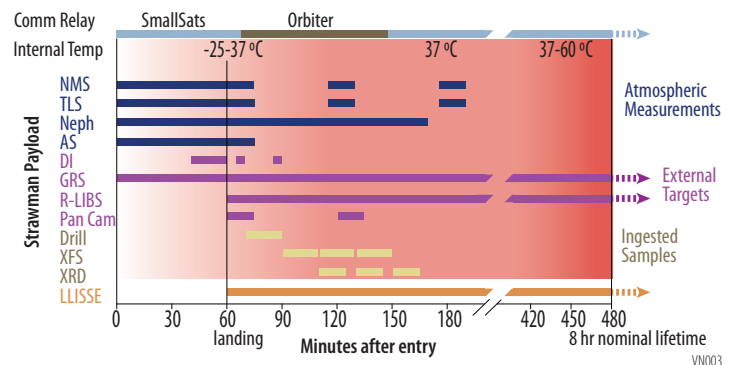
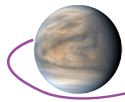


Figure 20. Lander Surface Operations of the Strawman Payload



after landing and takes approximately 15–20 minutes to acquire the 3 samples from three different depths. Each sample will be ingested into the Lander interior and placed in an individual cup for analyses by the **XFS** and **XRD**, which will take 20 and 15 minutes to do their respective analyses. The sample ingestion system facilitates direct interrogation by the **XFS** while in the sample ingestion cup. Once this analysis is complete, the sample drops into a hopper that feeds the **XRD**. While the diffractometer analyzes the first sample, the **XFS** analyzes the second. This parallel sample analysis continues until all 3 samples are analyzed by both X-Ray instruments. Full sample science operations are complete at landing+105 minutes.

LLISSE operates continuously on the surface for 60 days from landing, sending data at regular 6 hour intervals to the SmallSats to be received whenever they are overhead. **Figure 20** illustrates the timeline established by using a set of specific instruments to represent the strawman payload. The mission data volume generated by the Lander instruments is shown in **Table 3**.

### 3.3.1.2.3 Orbiter Operations

#### 3.3.1.2.3.1 Transitional Aerobraking Orbit

The Orbiter goes through a series of maneuvers to circularize the initial eccentric polar orbit that results from VOI into a circular polar orbit of 300 km altitude above the venusian surface (the science orbit). Circularization is achieved via aerobraking, which is performed using a sequence of steps. First, periapsis is lowered to ~130 km altitude. At this altitude, the Venus atmosphere can dissipate orbital energy to facilitate lowering the apoapsis to an altitude of 300 km. During the actual mission, orbit determination is performed by the MOC as frequently as possible and the maneuver cadence is decided based on contact schedule and limitations on the allowable density corridor and maneuver plans are uploaded to the Orbiter. The aerobraking phase is expected to last ~2 years. Details on aerobraking are discussed in **Appendix B.2.6.3.3.2**.

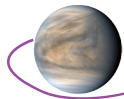
Most of the Orbiter instruments take advantage of the time spent in the aerobraking orbit to conduct valuable science operations and are continuously operating during the aerobraking process. However, in order to maintain the aerobraking drag profile, the **SAR** does not conduct science operations during aerobraking. The data generated by the payload in a typical aerobraking orbit, assuming 95% operational efficiency, is approximately 38 Gb, allowing for ample margin on data downlink capacity.

#### 3.3.1.2.3.2 Circular Science Orbit

Once in the circular science orbit, the full Orbiter suite, excluding the **SAR**, continues to operate at 100% duty cycle (**NIR camera** only images the night side). The **S-mm** spectrometer is mounted on a rotation platform allowing for alternate views of the limb of the planet on successive orbits. The **SAR** surface coverage requirement of 5% at 30-m resolution and 0.5% at 10-m resolution results in a very low duty cycle (See **Figure B-41** in **Appendix B**), assuming wide-swath mode, yielding flexibility in the timing of the RADAR operations. At close Earth-Venus range, full data downlink can occur over several DSN passes; more data buffering is required if RADAR operations occur at longer ranges. The mission data volume generated by the Orbiter instruments is shown in **Table 6**.

#### 3.3.1.2.4 SmallSat Operations

The two SmallSats play various roles in the Venus Flagship Mission; not only does the payload provide crucial science data about the venusian magnetosphere and solar wind, the satellites themselves play a critical part in communications with the Aerobot and the Lander and are used as relays for both uplink and downlink to both assets. The first key role that the SmallSats play is providing 8 hours of coverage for the Lander mission in combination with the Orbiter. The second role that they play is in providing at least one contact daily to downlink LLISSE data during its 60 day mission. They also play a role in the Aerobot's 60-day nominal mission by providing at least 1 contact per day and total contact duration of at least 100 minutes to downlink the nearly 5,000 Mbits of data produced by the Aerobot. In addition, the SmallSats' contacts with the Aerobot provide positioning information for the Aerobot science and operations staff. Finally, the SmallSats themselves have a payload consisting of seven instruments—**Langmuir Probe (LP)**, **Ion Electrostatic Analyzer (ESA-i)**, **Electron Electrostatic Analyzer (ESA-e)**, **Solar Energetic Particle Detector (SEPD)**, **Magnetometer (Mag)**, **Extreme Ultraviolet (EUV)**, and **Electric Fields Detector (E-FD)**—that are powered on and collecting data continuously as downlink and support for the other VFM assets allow for their entire mission.



It is anticipated that each SmallSat will have a 2-hour downlink with a DSN 34 meter station each day during normal operations (supporting the Lander and Aerobot may require additional time). When commanding from the ground is required, the duration of the viewing period would be adjusted to accommodate round-trip light time. One of the challenges faced by the SmallSats is the amount of data that can be collected versus what can be returned given the downlink allocation and onboard data storage. See **Table 5** for the total 34-month mission data volume per SmallSat payload.

### 3.3.2 Science Mission Operations

Due to the variety of platforms and multiple suites of instruments, we believe that a distributed operations approach with one institution managing the effort will provide the best scientific outcome and reduce risk. There will be one central VFM mission operations center (at managing institution) with a maximum of four element mission/science operations centers housed at the institution/facility that provided the element. Each element mission/science operations center is responsible for interaction with each instrument on their payload which has the potential to add one more layer of distributed operations. The benefit of using this model for operations is that the science teams, who have a vested interest in the data return and intimately understand the instrument, will be actively engaged in developing the observing plans and designing the observations. Students can also become engaged on the project. To ensure that the science teams are mindful of the big science picture and the synergistic science goals, working groups of project/programs scientists should be established to oversee those efforts. This approach has been successfully used on previous flagship missions such as Cassini.

### 3.4 Risk List

Risks identified during the VFM study are listed below. Proposed mitigation of these risks is also presented. **Figure 21** summarizes the risks.

1. **Landing:** The landing on tessera terrain, which may have local slopes >30 degrees. Landing on a large boulder and/or steep slope is possible, causing damage and/or tip-over. If tip-over is severe, communication may be impaired or lost.

**Mitigation** (also see extended discussion in Appendix C)

- 1.1. Study of imagery of landing sites to select the most favorable.
- 1.2. Design of lander provides for clearance of 0.5m boulders.
- 1.3. Leg design includes crushable material and the location of center of gravity of lander provides stable configuration for slopes of up to 30°.
- 1.4. Use of LHA subsystem to avoid hazards within 50 m of projected landing site.
- 1.5. Model and test of leg and fan system designs.
- 1.6. The trajectory design has a margin for completing the Aerobot mission and then conducting the orbital mapping campaign before releasing the Lander (1 year delay to landing).

2. **Landing Terrain Relative Navigation and Hazard Avoidance Subsystem:** The hazard avoidance subsystem consists of a LIDAR sensor, engineering camera, control electronics and processor, and a divert subsystem composed of four fans for direction control as well as algorithms for terrain relative navigation. The hazard avoidance algorithms and sensors must be able to determine the Lander's relative position, detect a hazard and determine the appropriate action to perform a divert maneuver. The divert subsystem is a TRL 2 technology for the Venus lander that requires development of the design and qualification of the motor and fan assemblies to operate in Venus atmosphere. Further, the Venus atmosphere, entry loads and environment could potentially compromise the LIDAR, resulting in an undesired orientation of the Lander for sample ingestion.

**Mitigations:**

- 2.1. Develop and demonstrate necessary performance during Phase A for the algorithms, LIDAR and fan/directional control subsystem in concert with the Venus Terrain Relative Navigation

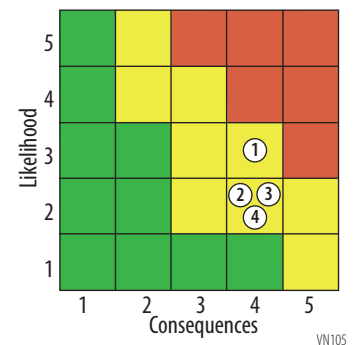
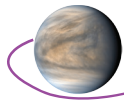


**Figure 21.** Risk Summary showing the four top Risks



algorithms (informed by M2020 TRN) and divert maneuver strategies, see **Appendix B.2.6** and **B.2.8**.

- 2.2. Put in place a technology development plan that achieves TRL-6 demonstration by PDR.
- 2.3. Implement a rigorous testing program to verify landing dynamics.

3. **Lander Pressure Vessel complexity:** The pressure vessel hardware integration and test is a complex blend of stepwise I&T and modeling of the densely packed avionics, batteries, instruments and phase change material that cannot be exposed to thermal vacuum. There is a risk that the integration and test program may take longer than planned.

**Mitigations:**

- 3.1. This risk is mitigated by implementing a technology development program to design and demonstrate a robust surface Lander payload that achieves TRL-6 BY PDR.
- 3.2. Additionally, there are embedded cost reserves (>30%) and funded schedule reserves for each instrument (4 months) and the Lander (4 months).

4. **Mission Complexity:** VFM contains five distinct flight elements (Lander, Aerobot, SmallSats (2), and the Carrier/Orbiter Spacecraft). Integrating five elements together may be challenging. There is a risk that integration problems will occur that affect the launch schedule and the cost of the mission.

**Mitigations:**

- 4.1. There are embedded cost reserves (>30%) and funded schedule reserves for each instrument (4 months) and the Lander (4 months).
- 4.2. Implement a technology development plan for low TRL items.

**4. Development Schedule and Schedule Constraints**

**4.1 High-Level Mission Schedule**

An overall (Phase A through Phase F) high-level schedule highlighting the key design reviews is shown in **Table 13**, with the length of time for each phase shown in **Figure 22**.

The more detailed schedule including the critical path and the development time for delivery required for each instrument, the spacecraft, development of ground and mission/science operations is shown in the **Fold-out Figure 23**.

**Table 13. High Level Schedule with key design reviews**

Project Phase	Duration (Months)
Phase A – Conceptual Design	16
Phase B – Preliminary Design	25
Phase C – Detailed Design	31
Phase D – Integration, Test, & 12m Commissioning	42
Phase E – Primary Mission Operations	120
Phase F – Decommissioning and Final Reporting	16
Start of Phase B to PDR	15
Start of Phase B to MPDR	19
Start of Phase B to CDR	27
Start of Phase B to MCDR	31
Start of Phase B to Delivery of Instruments (all instruments delivered by 10/2028)	54
Start of Phase B to Delivery of Flight Elements	82
System Level & Platforms Integration & Test	28
Project Total Funded Schedule Reserve	12
Total Development Time Phase B - D	98

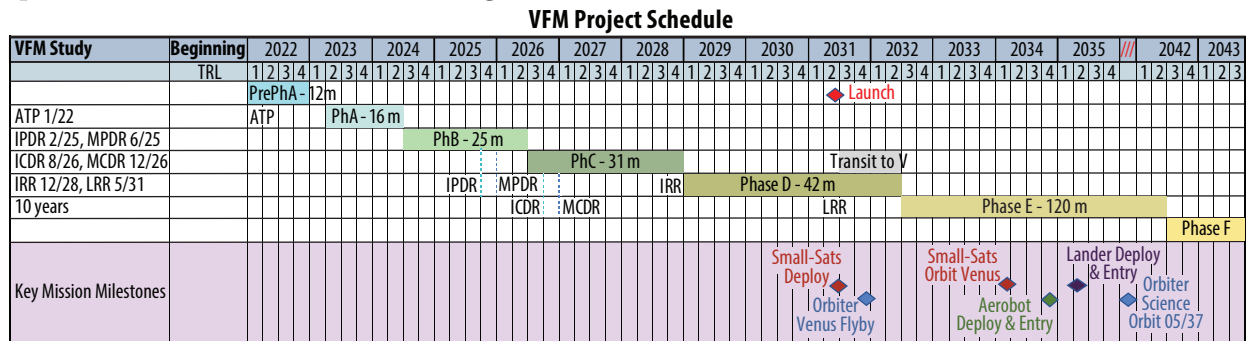
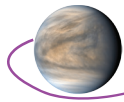


**Figure 22. Key project phases detailing specific mission durations.** The mission, as outlined in this concept, does not represent a high development risk mission.



## 4.2 Technology Development Plan

Table 14 shows the development plan for the technologies required for VFM.

**Table 14.** Technology Development schedules and cost estimates for VFM Instrument and Subsystems below TRL 6 for completion prior to PDR

	Instrument/Subsystem	Current TRL	Funding Source	Duration and Time Frame to TRL 6	Est. Cost (\$M)
<b>Lander</b>	Terrain Relative Navigation	5	VFM Mission	1 year	3
	Landing Hazard Avoidance and Divert System (Fans and Motors)	2	VFM Mission	3 years	5
	Radiometer in AS and Met suites	5	VFM Mission, MatISSE submission anticipated	2 years Beginning VFM Mission Phase A	3
	Nephelometer	4	VFM Mission, MatISSE submission anticipated	32 Months beginning VFM Mission Phase A	3
	CheMin-V (X-ray Diffractometer)	5	VFM Mission, MatISSE submission	2 years	3.5
	VEMCam (R-LIBS)	5	VICI and MatISSE proposal submitted	2 years	5
	Rotary Percussion Drill	5	VFM Mission	24 month year beginning VFM Mission Phase A	5
	Sample Handling System	5	VFM Mission		
	Long-Lived Surface Lander	3	NASA PSD Direct Funding	In Progress – Completion Mid 2024	18
<b>Aerobot</b>	Fluorimetric Microscope	4	MatISSE submission anticipated	4 years	4
	Meteorological Suite	5/4 (P sensor – Infrasond)	PSTAR awarded and MatISSE submitted	3.5 years	3
	Aerosol Mass Spectrometer with Nephelometer	2	DALI19	End before 2024	6.5
	Balloon	4	JPL internal and VFM	3 years	8
	Inflation/System	4	VFM	1 year	12
				<b>Total</b>	<b>79</b>

## 4.3 Development Schedule and Constraints

The schedule is shown in **Fold-out Figure 23**. Phase A includes development effort for the Lander pressure vessel and is 18 months in duration. Other mission systems are mature enough to not need additional development prior to Phase B. The Phase B duration is approximately 25 months and includes the Preliminary Design Review, by which time all technologies are planned to be at TRL 6. Phase C runs for 31 months and concludes with all the mission system elements fabricated, tested, and ready for mission integration. Phase D lasts approximately 42 months and includes mission integration, test, and launch site activities as well as commissioning of the instruments and platforms for one full year. Phase E begins 12 months after the June 2031 launch with mission operations at Venus beginning in July 2032 and lasting 120 months, followed by a Phase F of 16 months.

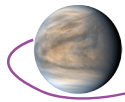
## 5. Mission Life-Cycle Cost

### 5.1 Costing Methodology and Basis of Estimate

Costing methodology for the VFM study is based on a combination of cost modeling and historic cost wrap factors (to account for program support, mission operations, ground systems, etc.). The cost models used are Price H and NASA Instrument Cost Model (NICM). Price H parametric model cost use Master Equipment Lists (MELs) and known pass-through costs. MEL item masses, type of materials, TRLs, and complexity are inputs to this model. NICM estimates instrument costs using various instrument parameters. Science costs were developed after discussion with planetary flagship mission science offices and reflect FTE required for the mission phases.

These estimates are combined with mission-level cost-wrap factors to derive an initial estimated mission cost. A reserve of 50% on Phases A-D and 25% on Phase E and Phase F is added to the total estimated mission cost. The 50% reserve equates to an approximate 70% confidence level in the cost





certainty in conventional cost risk analysis. All costs are in Fiscal Year (FY) 2025 dollars. No grassroots costs were developed for the study.

## 5.2 Cost Estimate(s)

Based on the Price H and NICM results, the team estimated a VFM mission concept Phase A to Phase F total cost of \$3.7B in 2025 dollars (including 50% margin) at 70% confidence level, (**Foldout Table 15**). The Orbiter, Aerobot, and Lander costs were derived from the CEMA Mission Development Lab (MDL) models, with aeroshell cost inputs from ARC, but with a 50% A-D reserve versus 30%; the SmallSat costs are for a commercial bus with 50% A-D reserves. Science costs (with reserves) from pre-Phase A–Phase F are \$185M in 2025 dollars. The VFM mission costs are within the range of a flagship mission. A major engineering development cost for this mission is the packaging and design for the Lander/Payload. In addition, there are technologies that require development, which are described in **Table 14**. To advance these technologies, the mission cost estimate includes \$79M including instrument development prior to pre-Phase A through PDR, which is estimated at \$56M in Real Year dollars. We assumed that the mission is totally funded by NASA and all significant work is performed in the US. Please note that the costs presented in this report are preliminary, limited by the nature of the study.

## 6. Recommendations and Summary

### 6.1 Recommendations

The VFM study successfully matured a concept to deliver high-value science data that uses technology achievable in the next decade for input to the Decadal Survey. Along with the technology developments that are cited above (**Table 14**) that require funding, the study identified several investments beyond the direct scope of the study that NASA could make ahead of such a mission to reduce the cost of the mission and/or increase the science return.

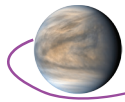
#### 6.1.1 Laboratory Measurements

Resources need to be available for scientists and instrument developers to carry out laboratory experiments (e.g., facilities, *in situ* metrology sensors, and supplies), which should start prior to pre-Phase A. Ideally, NASA would institute a funded, coherent Venus Program that would enable coordinated scientific research and technology developments. This Program would include resources for scientists and instrument suppliers to carry out laboratory experiments, which should start prior to pre-Phase A. The Program should also include resources for improving models (e.g., wind models that would allow better prediction of aerobot trajectories). Such resources would allow the community to prepare for the scientific results and ensure instruments and technologies are developed that can achieve the VFM goals and objectives and reduce the cost of *in situ* Venus missions.

*In situ* Venus missions require additional investment, beyond those that Mars or lunar missions require, because there are no field sites on Earth that mimic the specific challenges of the venusian surface environment. In order to do the work to prepare for, and in support of, anticipated VFM Lander results, we must replicate the conditions of the Venus environment to be encountered in the laboratory using experimental chambers. Experimental work in such chambers will help understand mission data on weathering of surface rocks and minerals, the chemical and physical properties of Venus's deep atmosphere, and environmental conditions required to support candidate UV absorbing species, including biogenic sources [Treiman et al., 2020]. Multiple Venus chambers are necessary because of the long time scales required for some of these experiments and the varying required capabilities to execute them [Santos et al., 2020]. These can provide the “field tests” necessary to learn how to operate on Venus and interpret the data from *in situ* instruments. Additionally, chambers are required to qualify flight hardware. All of these experimental and test chambers require excellent metrology to interpret results correctly, so a Venus program should also support sensor development and calibrations to make the most of these efforts. Field tests *are* possible for Venus Aerobots and resources should be made available to conduct precursor instrument experiments and technology flight tests.

#### 6.1.2 Additional Technologies

Although the VFM can be accomplished with limited technology developments that are identified in the Technology Development Plan (**Table 14**) in **Section 4.2**, the mission could benefit substantially



from sustained investment in ancillary technologies that could reduce the cost and complexity of the mission. Some of them are described in detail in the 2009 Flagship Mission Study and **Appendix D** updates the community on the advancements of those technologies since that time. For example, in the last decade, development in high-temperature electronics, sensors and batteries have proceeded under the HOTTech program, although further work is needed before a scientifically viable, stand-alone Venus surface mission can be accomplished, particularly in the area of computing, memory and communications. The VEXAG Technology Plan [Hunter et al., 2019] also details technologies needed for future Venus exploration. Additional specific technologies that would reduce cost and/or improve science data return for this specific VFM are:

## Lander

1. Investments in Autonomy; both system (including goal-based sequencing and fault protection) and functional level to operate on the surface for eight hours without substantial communication with Earth [VDRT, 2018].
2. Passive thermal management techniques to enable longer-lived surface vehicles.
3. Higher density batteries – higher W-hr/kg performance, higher operating temperature.
4. High Performance Computing.

## Orbiter

1. Next generation reprogrammable RF transponders with reduced SWaP dual-band architecture, supporting UHF, S, X, and Ka-band options, a multitude of modulation types, turbo and LDPC coding, regenerative ranging, and open-loop recording.
2. Optical Communications and ground-based assets needed to support it.
3. Spaceborne atomic clocks to revolutionize spacecraft tracking methods.
4. Compression for **SAR** and other targeted data types.

## SmallSats

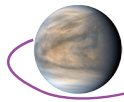
1. Next generation reprogrammable RF transponders with reduced SWaP.

## 6.2 Summary

The importance of Venus to the understanding of habitable terrestrial planets and the evolution of our solar system cannot be overstated. Due to its size and proximity, more than any other known planet, Venus is essential to our understanding of the evolution and habitability of Earth-size planets throughout the galaxy. Over the past 60 years, more than 40 spacecraft have been launched to explore Venus with flybys, orbiters and *in situ* probes, balloons and landers, but none by the US since Magellan in 1989. Analysis of our current data underscore the critical role of Venus in planetary evolution. Our knowledge of planetary processes predicts that Venus, like Earth is now, was and may still be a habitable planet. Our limited knowledge of the inventory and history of volatiles recorded in the Venus atmosphere and surface represents a significant gap in our understanding of the acquisition of volatiles in the inner solar system. Studying Venus will allow us to identify the mechanisms that operate together to produce and maintain habitable worlds like our own. As on Earth, the processes on Venus are dynamic and interrelated and their understanding requires multiple investigations throughout the Venus system. It is clearly time for Venus.

**Habitability** is at the heart of our Venus Flagship Mission (VFM) study, and we approach it through tracing the history of volatile elements on Venus. We address two critical questions for planetary science: 1) How, if at all, did Venus evolve through a habitable phase? 2) What circumstances affect how volatiles shape habitable worlds? More than any other group, volatile elements have a strong influence on the evolutionary paths of rocky bodies and are critical to understanding solar system evolution. It is clear that Venus experienced a different volatile element history from the Earth, thus providing the only accessible example of one end-state of habitable Earth-size planets. Venus will allow us to identify the mechanisms that operate together to produce and maintain habitable worlds like our own.

The VFM has a multi-platform architecture, with an Orbiter to deliver an Aerobot and Lander to Venus as well as two SmallSats, which guide themselves to Venus. Instruments for the various mission platforms were selected to address the science goals and objectives of the VFM. This mission concept study successfully demonstrates the feasibility of a scientifically viable mission to explore the habitability of Venus using existing technologies and flight heritage from previous missions for the science



payload and for the various mission elements. It should be noted, however, that many elements of this mission concept study have not been optimized, which likely results in an oversizing of various instruments and mission elements. Future studies and mission proposals could benefit from continuing development of instruments and Venus related technologies. Such development could increase the overall science return and improve confidence in the cost estimates.

For the current VFM concept, the estimated cost for Phases A-F is in the range of a flagship mission (\$3.7B, 2025 dollars). While technology maturation and engineering development of some sub-systems is needed, no high-risk elements have been identified, given the 50% margin provides a ~70% confidence level.

**Venus is the closest planet to Earth in size and heliocentric distance. Yet it stands in striking contrast to our home planet in terms of its habitability. Still largely untapped for its scientific value, Venus is the key to understanding what leads to conditions hospitable to life on terrestrial planets. We therefore recommend that NASA institute a funded, coherent Venus Program of missions, scientific research and technology developments, culminating in a Venus Flagship mission.**

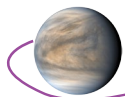


FIGURE 23: SCHEDULE



Critical Path  
 - - - Primary  
 - - - Secondary

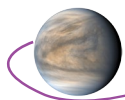
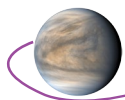
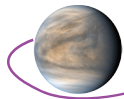


TABLE 15: COST BY FISCAL YEAR

	Item	Pre-Phase-A FY22	FY23	FY24	FY25	FY26	FY27	FY28	FY29	FY30	FY31	F32	E/F	Total A-D FY20 (\$M)	Total FY25 (\$M) A-D	Total (\$M) plus 50% Reserve
Phase A Concept Study																
Technology Development																
WBS 1, 2 & 3: Mission PM/SE/MA			2.37	8.41	26.95	29.65	40.43	36.87	18.87	18.87	18.87	14.34		\$125.0	\$143.8	\$215.6
WBS 4: Science		0.78	3.96	2.27	6.34	8.37	10.04	14.70	10.77	10.77	10.77	4.83			\$55.2	\$83.6
WBS 5 - Instruments																
Lander Descent Operations																
5.1.1	Neutral Mass Spectrometer		0.41	2.76	9.32	17.66	24.50	6.35	3.45	3.45	1.10			\$40.0	\$46.0	\$69.0
5.1.2	Tunable Laser Spectrometer		0.25	1.69	5.71	10.82	15.00	3.89	2.11	2.11	0.68			\$24.5	\$28.2	\$42.3
5.1.3	Atmosphere Structures	3.00	0.04	0.28	0.93	1.77	2.45	0.63	0.35	0.35	0.11			\$4.0	\$4.6	\$9.9
5.1.4	Descent NIR Imager		0.04	0.28	0.93	1.77	2.45	0.63	0.35	0.35	0.11			\$4.0	\$4.6	\$6.9
5.1.5	Neutron Generator/Gamma Ray Spectrometer		0.26	1.73	5.82	11.04	15.31	3.97	2.16	2.16	0.69			\$25.0	\$28.8	\$43.1
5.1.6	Nephelometer	3.00	0.06	0.41	1.40	2.65	3.67	0.95	0.52	0.52	0.17			\$6.0	\$6.9	\$13.4
Surface Operations																
5.1.7	X-ray Diffractometer	3.50	0.41	2.76	9.32	17.66	24.50	6.35	3.45	3.45	1.10			\$40.0	\$46.0	\$72.5
5.1.8	X-Ray Fluorescence Spectrometer		0.36	2.42	8.15	15.46	21.43	5.55	3.02	3.02	0.97			\$35.0	\$40.3	\$60.4
5.1.9	Raman-LIBS Instrument	5.00	0.47	3.11	10.48	19.87	27.56	7.14	3.88	3.88	1.24			\$45.0	\$51.8	\$82.6
5.1.10	Panoramic Camera		0.16	1.04	3.49	6.62	9.19	2.38	1.29	1.29	0.41			\$15.0	\$17.3	\$25.9
5.1.11	Rotary Percussion Drill	2.50	0.16	1.04	3.49	6.62	9.19	2.38	1.29	1.29	0.41			\$15.0	\$17.3	\$28.4
5.1.12	Sample Handling System	2.50	0.16	1.04	3.49	6.62	9.19	2.38	1.29	1.29	0.41			\$15.0	\$17.3	\$28.4
5.1.13	Descent Sphere		0.97	6.49	21.89	41.51	57.56	14.92	8.11	8.11	2.59			\$94.0	\$108.1	\$162.2
5.1.14	Long Lived Surface Lander	18.00	0.43	2.90	9.78	18.55	25.72	6.67	3.62	3.62	1.16			\$42.0	\$48.3	\$90.5
5.1.15	Hazard Avoidance Subsystem	8.00	0.04	0.24	0.82	1.55	2.14	0.56	0.30	0.30	0.10			\$3.5	\$4.0	\$14.0
Balloon/Aerobot																
5.2.1	Venus Aerosol Mass Spectrometer															
5.2.1.1	Spectrometer Optics & Amplifier Board		0.44	2.92	9.85	18.68	25.90	6.71	3.65	3.65	1.17			\$42.3	\$48.6	\$73.0
5.2.1.2	Nephelometer	6.50	0.07	0.50	1.68	3.18	4.41	1.14	0.62	0.62	0.20			\$7.2	\$8.3	\$18.9
5.2.2	Fluorimetric Microscope	4.00	0.41	2.76	9.32	17.66	24.50	6.35	3.45	3.45	1.10			\$40.0	\$46.0	\$73.0
5.2.3	Magnetometer		0.04	0.28	0.93	1.77	2.45	0.63	0.35	0.35	0.11			\$4.0	\$4.6	\$6.9
5.2.4	Anemometer - Wind Sensor		0.04	0.28	0.93	1.77	2.45	0.63	0.35	0.35	0.11			\$4.0	\$4.6	\$6.9
5.2.5	Meteorology Suite (MET)	3.00	0.11	0.76	2.56	4.86	6.74	1.75	0.95	0.95	0.30			\$11.0	\$12.7	\$22.0
5.2.6	Visible Imager (Student Exp)		0.02	0.14	0.47	0.88	1.22	0.32	0.17	0.17	0.06			\$2.0	\$2.3	\$3.5
Small Satellites (2)																
5.3.1	Langmuir Probe x 2		0.02	0.14	0.47	0.88	1.22	0.32	0.17	0.17	0.06			\$2.0	\$2.3	\$3.5
5.3.2	Magnetometer x 2		0.03	0.21	0.70	1.32	1.84	0.48	0.26	0.26	0.08			\$3.0	\$3.5	\$5.2
5.3.3	Electron Electrostatic Analyzer x 2		0.10	0.69	2.33	4.42	6.12	1.59	0.86	0.86	0.28			\$10.0	\$11.5	\$17.3
5.3.4	Ion Electrostatic Analyzer x 2		0.13	0.90	3.03	5.74	7.96	2.06	1.12	1.12	0.36			\$13.0	\$15.0	\$22.4
5.3.5	Solar Energetic Particle Detector x 2		0.10	0.69	2.33	4.42	6.12	1.59	0.86	0.86	0.28			\$10.0	\$11.5	\$17.3
5.3.7	Electric Fields Detector x 2		0.08	0.55	1.86	3.53	4.90	1.27	0.69	0.69	0.22			\$8.0	\$9.2	\$13.8
5.3.8	Solar Extreme Ultraviolet		0.17	1.10	3.73	7.07	9.80	2.54	1.38	1.38	0.44			\$16.0	\$18.4	\$27.6
Orbiter																
5.4.1	Synthetic Aperture RADAR (SAR)															
5.4.1.1	RADAR Electronics		0.72	4.83	16.30	30.91	42.87	11.11	6.04	6.04	1.93			\$70.0	\$80.5	\$120.8
5.4.1.2	RADAR Aperture		0.36	2.42	8.15	15.46	21.43	5.55	3.02	3.02	0.97			\$35.0	\$40.3	\$60.4
5.4.2	Magnetometer		0.05	0.35	1.16	2.21	3.06	0.79	0.43	0.43	0.14			\$5.0	\$5.8	\$8.6
5.4.3	Electron Electrostatic Analyzer		0.05	0.35	1.16	2.21	3.06	0.79	0.43	0.43	0.14			\$5.0	\$5.8	\$8.6
5.4.4	Ion Electrostatic Analyzer		0.07	0.45	1.51	2.87	3.98	1.03	0.56	0.56	0.18			\$6.5	\$7.5	\$11.2
5.4.5	NIR Imager		0.06	0.41	1.40	2.65	3.67	0.95	0.52	0.52	0.17			\$6.0	\$6.9	\$10.4
5.3.6	Neutral Mass Spectrometer		0.09	0.62	2.10	3.97	5.51	1.43	0.78	0.78	0.25			\$9.0	\$10.4	\$15.5
5.4.7	Sub-mm Spectrometer		0.31	2.04	6.87	13.03	18.07	4.68	2.54	2.54	0.81			\$29.5	\$33.9	\$50.9
WBS 6																
6.1	Orbiter		2.09	11.67	45.07	57.40	106.73	101.99	59.77	59.77	29.89			\$275.0	\$316.3	\$474.4
6.2	SmallSat#1/#2		0.76	4.24	16.39	20.87	38.81	37.09	21.74	21.74	10.87			\$100.0	\$115.0	\$172.5
6.3	Aerobot	Balloon \$25M, Inflation ss \$12M	1.12	6.28	24.25	30.89	57.44	54.89	32.17	32.17	16.08			\$148.0	\$170.2	\$255.3

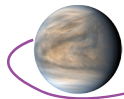


		Item	Pre-Phase-A FY22	FY23	FY24	FY25	FY26	FY27	FY28	FY29	FY30	FY31	F32	E/F	Total A-D FY20 (\$M)	Total FY25 (\$M) A-D	Total (\$M) plus 50% Reserve
6.3.1	Balloon & Inflation subsystem		20.00	0.28	1.57	6.06	7.72	14.36	13.72	8.04	8.04	4.02			\$37.0	\$42.6	\$83.8
6.3.2	Entry Aeroshell & Paerachute			1.00	5.60	21.63	27.55	51.23	48.96	28.69	28.69	14.35			\$132.0	\$151.8	\$227.7
6.4	Lander			1.14	6.37	24.58	31.31	58.22	55.63	32.60	32.60	16.30			\$150.0	\$172.5	\$258.8
6.4.1	Entry & Descent Aerooshell & Parachute			1.01	5.64	21.80	27.76	51.62	49.33	28.91	28.91	14.45			\$133.0	\$153.0	\$229.4
<b>WBS 7 Mission Operations</b>				0.00	0.22	1.08	2.37	7.55	8.62	9.31	9.31	4.66			\$25.0	\$28.8	\$43.1
<b>WBS 8 LV/Services (5m High Performance)</b>				0.00	0.00	0.00	0.00	0.00	0.00	0.00	0.00	0.00			\$0.0	\$0.0	\$0.0
<b>WBS 9 Ground Data System</b>				0.00	0.13	0.65	1.42	4.53	5.17	5.59	5.59	2.79			\$15.0	\$17.3	\$25.9
<b>WBS 10 System I&amp;T</b>				0.00	0.52	2.59	5.69	18.11	20.70	22.36	22.36	11.18			\$60.0	\$69.0	\$103.5
																\$2,293.7	\$3,520.3
<b>Total Development w/o Reserves</b>			79.78	14.31	69.61	247.48	387.11	610.81	377.43	228.80	228.80	116.55	12.78			\$2,373.5	
<b>Development Reserves (50%)</b>			0.00	7.15	34.81	123.74	193.56	305.40	188.71	114.40	114.40	58.28	6.39			\$1,146.8	
<b>Total A-D Cost</b>			79.78	21.46	104.42	371.22	580.67	916.21	566.14	343.20	343.20	174.83	19.17				\$3,520.3
<b>Phase-E/F Science</b>																\$80.2	\$100.2
<b>Phase E Cost - Mission Operations</b>																\$72.0	\$90.0
<b>Total Costs Phases A-F:</b>																\$2,525.6	\$3,710.5
<b>Science FTE/Yr</b>			2.25	8.52	8.31	8.82	10.82	11.26	15.95	8.92	8.92	8.92	4.00	14/yr			



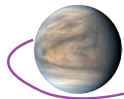
## Appendix A. Acronyms

9s9p	9 series 9 parallel
ACDH	Aerobot Command and Data Handling
ACS	Attitude Control System
ADC	Analog Digital Converter
AH	Amp Hour
ALHAT	Autonomous Landing Hazard Avoidance Technology
AMS	Aerosol mass spectrometer
AMS-N	Aerosol Mass Spectrometer with Nephelometer
AO	Announcement of Opportunity
AOS	Acquisition of Signal
APE	Attitude and Position Estimate
ARC	Ames Research Center
ARM	Advanced RISC (reduced instruction set computer)
ARTEMIS	Acceleration, Reconnection, Turbulence and Electrodynamic of the Moon's Interaction with the Sun
AS	Atmospheric Structure Suite
ASPIRE	Advanced Supersonic Parachute Inflation Research Experiment
ASRG	Advanced Stirling Radioisotope Generator
ATC	Analog Telemetry Card
ATLO	Assembly, Test, and Launch Operations
ATP	Authority To Proceed
B	Billion
BCM	Battery Charge Module
BECA	Bulk Elemental Composition Analyzer
BLDT	Balloon Launched Decelerator Test
BM	Breaking Manuever
BOL	Beginning of Life
BPSK	Binary Phase Shift Keying
C	Celsius
C3	launch energy
CBE	Current Best Estimate
CAD	Computer Aided Design
CADRe	Cost Analysis Data Requirement
CBE	Current Best Estimate
CCD	Charge Coupled Device
CCSDS	Consultative Committee for Space Data Systems
Cd	Coefficient of Drag
CDF	Cumulative Distribution Function
C&DH	Command and Data Handling
CDR	Critical Design Review
CEMA	Cost Estimating, Modeling & Analysis
CFD	Computational Fluid Dynamics
cg	center-of-gravity
CheMin-V	Chemistry and Mineralogy - Venus
CLPS	Commercial Lunar Payload Services
cm	centimeter
CM	Configuration Management
CMCP	Chopped Molded Carbon Phenolic
CMD	Command
CML	Concept Maturity Level
CMOS	Complementary metal-oxide-semiconductor
COEL	Committee on Origin and Evolution of Life
CoM	Center of Mass

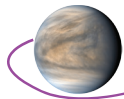


ConOPS	Concept of Operations
COSPAR	Committee on Space Research
COTS	Commercial off the Shelf
CP	Carbon Phenolic
cPCI	Compact Peripheral Component Interface
CSR	Concept Study Report
CSS	Coarse Sun Sensors
CTE	Controlled Thermal Expansion, Coefficient of Thermal Expansion
DAVINCI+	Deep Atmosphere of Venus Investigation of Noble gases, Chemistry, & Imaging, Plus
dB	Decibel
DDOR	Delta Differential One-way Ranging
DEA	Digital Electronics Assembly
Dec	Declination
$\Delta V$	Delta Velocity
DEM	Digital Elevation Model
DGB	Disk-Gap-Band
D/H	Deuterium/Hydrogen
DI	Descent NIR Imager
DIMES	Descent Image Motion Estimation System
DInSAR	Differential Interferometric SAR
DLA	Declination of Launch Asymptote
DOD	Depth Of Discharge
DOF	Degrees of Freedom
DPDT	Double Pull Double Throw
DPU	Data Processing Unit
DSM	Deep Space Manuever
DSN	Deep Space Network
DTE	Direct to Earth
DTN	Delayed Tolerant Network
EDE	Entry and Descent Element
EDF	Entry, Descent and Float
EDL	Entry, Descent and Landing
EEV	Earth Entry Vehicle
E-FCM	Evolutionary Fuzzy Cognitive Map
E-FD	Electric Fields Detector
EFPA	Entry Flight Path Angle
EM	Engineering Model
EMTG	Evolutionary Mission Trajectory Generator
EOL	End of Life
ESA	European Space Agency
ESA	Electrostatic Analyzer
ESA-e	Electrostatic Analyzer - electrons
ESA-i	Electrostatic Analyzer - ions
ESCAPEDE	Escape and Plasma Acceleration and Dynamics Explorers
ESPA	Evolved Secondary Payload Adapter
EUV	Extreme Ultraviolet
EUV-D	Extreme Ultraviolet detector
FDIR	Fault detection, isolation, and recovery
FEC	Forward Error Correction
FEP	Fluorinated Ethylene Propylene
FETS	Field Effect Transistors
FM	Fluorimetric Microscope
FOV	Field of View
FPA	Flight Path Angle

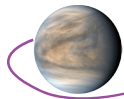




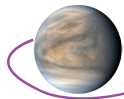
FSW.....	Flight Software
FTE .....	Full Time Equivalent
FWHM.....	Full Width at Half Maximum
FY .....	Fiscal Year
g.....	Earth gravitational acceleration (9.81 m/s <sup>2</sup> )
Ga.....	Giga annum (billion years)
GaAs .....	Gallium Arsenide
Gbits .....	Gigabits
Gbps .....	Gigabits per second
GFIC .....	Goddard Fellow Innovation Challenge
GMSL.....	Gaussian Minimum Shift Keying
GN&C .....	Guidance Navigation and Control
GOI.....	Goals, Objectives, and Investigations
GPR.....	Goddard Procedural Requirements
GRS.....	Gamma Ray Spectroscopy/Spectrometer
GSDR.....	Global Slope Data Record
GSFC.....	Goddard Space Flight Center
GSM.....	Generic Switch Module
GTDR.....	Global Topographic Data Record
HA.....	Hazard Avoidance
HD&A .....	Hazard Detection and Avoidance
HEEET.....	Heat-shield for Extreme Entry Environment Technology
HiPAT .....	High Performance Apogee Thruster
HGA.....	High Gain Antenna
HK.....	Housekeeping
HOTLINE.....	Hot Operating Temperature Lithium combustion IN situ Energy
HOTTech .....	High Operating Temperature Technology
HPSC .....	High Performance Spacecraft Computing
HZ.....	Habitable Zone
Hz.....	Hertz
I2C .....	Inter-Integrated Circuit
I&T .....	Integration and Test
IAU.....	International Astronomical Union
ICDR.....	Instrument Critical Design Review
ICRF.....	Inertial Centered Reference Frame
IFOV .....	Instantaneous Field of View
IMU.....	Inertial Measurement Unit
InSAR .....	Interferometric SAR
InSight.....	Interior Exploration using Seismic Investigations, Geodesy and Heat Transport
IPDR .....	Instrument Preliminary Design Review
IR.....	Infrared
JPL.....	Jet Propulsion Laboratory
JUICE.....	Jupiter Icy Moons Explorer
K.....	Kelvin
Ka-band .....	Ka-band Communication frequencies of 26.5-40GHz
KE .....	Kinetic Energy
kg.....	kilogram
KISS.....	Keck Institute for Space Studies
km/s.....	kilometers per second
kN .....	KiloNewtons
kPa.....	KiloPascals
kpbs .....	kilobits per second
KSC.....	Kennedy Space Center
kW.....	kilowatt



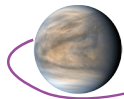
LaRC .....	Langley Research Center
LCDH .....	Lander Command and Data Handling
LDPC .....	Low Density Parity Check
LGN .....	Low Gain Antenna
LHA.....	Landing Hazard Avoidance
LHD&A .....	Landing Hazard Detection and Avoidance
LIBS.....	Laser Induced Breakdown Spectroscopy
LiDAR.....	Light Detection And Ranging
LLISSE.....	Long-Lived In Situ Solar System Explorer
LOS .....	Line Of Sight
LNT.....	lithium nitrate trihydrate
LP .....	Langmuir Probe
LRD.....	Launch Readiness Date
LRO.....	Lunar Reconnaissance Orbiter
LTRNHA.....	Landing Terrain Relative Navigation and Hazard Avoidance
LV .....	Launch Vehicle
LVDS.....	Low Voltage Differential Signaling
LVLH.....	Local Vertical, Local Horizontal
LVPS.....	Low Voltage Power Supply
LVS .....	Lander Vision System
m .....	meter
M.....	million
Ma .....	Mega annum (millions of years)
Mag.....	Magnetometer
MatISSE .....	Maturation of Instruments for Solar System Exploration
MAVEN.....	Mars Atmosphere and Volatile Evolution
m/s.....	meters per second
Mbits .....	Megabits
Mbps.....	Megabits per second
MCC .....	Motor Controller Card
MCDR .....	Mission Critical Design Review
MCU .....	Mechanism Control Unit
MDL.....	Goddard Space Flight Center's Mission Design Lab
MEL .....	Master Equipment List
MER.....	Mars Exploration Rover Mission
MET .....	Meteorological Suite/Mission Elapsed Timer
MEV .....	Maximum Expected Value
MGA .....	Medium Gain Antenna
MGS .....	Mars Global Surveyor
MIC.....	Multi-Interface Cards
mJ .....	millijoules
MLI .....	Multi-Layer Insulation
mm .....	millimeter
MMH .....	Monomethylhydrazine
MMS .....	Magnetospheric Multiscale Mission
MOC.....	Mission Operations Center
MOCET.....	Mission Operations Cost Estimating Tool
MOSFETS.....	Metal–Oxide–Semiconductor Field-Effect Transistor
MPDR.....	Mission Preliminary Design Review
MPU.....	Mechanism and Propulsion Unit
MPR .....	Mean Planetary Radius; 6051.84 km for Venus
MRC.....	Mechanism Release Card
MSC/NASTRAN .....	MacNeal-Schwendler Corp (mechanical analysis software)
MSL.....	Mars Science Laboratory
MSPS.....	Million Symbols Per Second



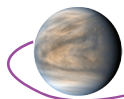
MSR .....	Mars Sample Return
Mw .....	Moment Magnitude Scale
NASA .....	National Aeronautics and Space Administration
NASEM.....	National Academies of Sciences and Engineering
NEA.....	Non-Explosive Actuator
Neph.....	Nephelometer
NESZ.....	noise-equivalent-sigma-nought
NFR.....	Net Flux Radiometer
NFT.....	Natural Feature Tracker
NiCd.....	Nickel Cadmium
NICER .....	Neutron star Interior Composition Explorer
NICM.....	NASA Instrument Cost Model
NIMS .....	Near Infrared Mapping Spectrometer aboard Galileo
NIR .....	Near Infrared
NIR-I.....	Near Infrared Imager/Imaging
nm .....	nanometer
NMS.....	Neutral Mass Spectrometer
NRC .....	National Research Council
ns .....	nanosecond
NTO.....	Dinitrogen tetroxide
OD .....	Orbit Determination
OSIRIS-Rex .....	Origins, Spectral Interpretation, Resource Identification, Security, Regolith Explorer
OSAM-1 .....	On-orbit Servicing, Assembly, and Manufacturing Mission 1
OSR.....	Optical Solar Reflectors
Pa.....	Pascals
PAF.....	Payload Attach Fitting
PC.....	Panoramic Camera
PCM.....	Phase Change Material
PDC .....	Propulsion Drive Card
PDR.....	Preliminary Design Review
PEPP.....	Entry Parachute Program
PI .....	Principal Investigator
PICA.....	Phenolic Impregnated Carbon Ablator
PIPS.....	Pulsed Injection Position Sensor
PM.....	Project Management
PMCS .....	Planetary Mission Concept Studies
PPS .....	Pulse Per Second
PSE .....	Power System Electronics
PV.....	Pioneer Venus
PVLP .....	Pioneer Venus Large Probe
PVO.....	Pioneer Venus Orbiter
RAAN.....	Right Ascension of the Ascending Node
RADAR .....	Radio Azimuth Direction and Ranging
RADARSAT .....	Radar Satellite; Canadian Space Agency
RAM.....	Random Access Memory
RAO .....	Resource Analysis Office
REE .....	Rare Earth Elements
RF.....	Radio Frequency
R-LIBS.....	Raman-Laser Induced Breakdown Spectroscopy
RMS .....	Root Mean Square
RO.....	Radio Occultation
ROM .....	Rough Order of Magnitude
rpm .....	rotations per minute
RWA .....	Reaction Wheel Assembly



SA, S/A .....	Solar Array
SARM.....	Solar Array Regulation Module
S-band.....	2 to 4 GHz (15 to 7.5 cm wavelength) Communications Band
SBC .....	Single Board Computer
S/C .....	spacecraft
S/W .....	Software
S:N .....	Signal-to-Noise
SAR.....	Synthetic Aperture Radar
SBC .....	Single Board Computer
SEP .....	Solar Electric Propulsion
SEPD .....	Solar Energetic Particle Detector
SEU .....	Single Event Upset
SiAPD.....	Silicon avalanche photodiodes
SiC.....	Silicon Carbide
SIFT .....	Scale Invariant Feature Transform
SIMPLEx .....	Small Innovative Missions for Planetary Exploration
SINDA .....	Systems Improved Numerical Differencing Analyzer
SLS .....	Space Launch System
SmallSat .....	Small Satellite
SMAP .....	Soil Moisture Active Passive
S-mm .....	Sub-mm Spectrometer
SNR.....	Signal to Noise Ratio
SOC.....	Science Operations Center
SOI.....	Silicon on Insulator
SPED.....	Supersonic Planetary Entry Decelerator
SPENVIS.....	Space Environmental Effects and Education System
SPICAV .....	Spectroscopy for Investigation of Characteristics of the Atmosphere of Venus
SPENVIS.....	Space Environmental Effects and Education System
SPLICE.....	Safe and Precise Landing-Integrated Capabilities Evolution project
SQPSK.....	Staggered Quadrature Phase-Shift Keying
SRR .....	System Requirements Review
SSN .....	Sunspot Number
SSPA.....	Solid State Power Amplifier
SSR.....	Solid-State Recorder
STEREO.....	Solar Terrestrial Relations Observatory
STM .....	Science Traceability Matrix
SWaP .....	Size, Weight and Power
SWI .....	Submillimeter Wave Instrument
T.....	Tesla; e.g. mT - microTesla, nT - nanoTesla.
TCM.....	Trajectory Correction Maneuver
TESS.....	Transiting Exoplanets Survey Satellite
THEMIS .....	Thermal Emission Imaging System
TJGaAs .....	Triple Junction Gallium Arsenide
TLM .....	Telemetry
TLS.....	Tunable Laser Spectrometer
TMR.....	Triple Modular Redundant
TOF.....	Time of Flight
TPS.....	Thermal Protection System
TRL.....	Technology Readiness Level
TRN .....	Terrain Relative Navigation
TRN-LHA.....	Terrain Relative Navigation and Landing Hazard Avoidance
TWCP .....	Tape Wrapped Carbon Phenolic
TWTA.....	Traveling Wave Tube Amplifier
UART .....	Universal Asynchronous Receiver/Transmitter



UHF .....	Ultra High Frequency
ULA.....	United Launch Alliance
ULDB.....	Ultra Long Duration Balloon
USN .....	Universal Space Network
UTC .....	Coordinated Universal Time
UTCG .....	Coordinated Universal Time Grennwich
UV .....	ultraviolet
V.....	Volt
VEM.....	Venus Emissivity Mapper
VEMCam .....	Venus Elemental and Mineralogical Camera
VERITAS.....	Venus Emissivity, Radio Science, InSAR, Topography, And Spectroscopy
VEx.....	Venus Express
VEXAG .....	Venus Exploration Analysis Group
VFM .....	Venus Flagship Mission
VGA .....	Venus Gravity Assist
VI .....	Visible Imager
VICI .....	Venus In Situ Composition Investigations
VIRA .....	Venus International Reference Atmosphere
VIRTIS .....	Visible and Infrared Thermal Imaging Spectrometer on VEx
VISAGE.....	Venus In Situ Atmospheric and Geochemical Explorer
VITaL .....	Venus Intrepid Tessera Lander
VIXL.....	Venus Instrument for X-ray Lithochemistry
VME.....	Venus Mobile Explorer
VMTF .....	Venus Materials Test Facility (JPL)
VOI .....	Venus Orbit Insertion
VS.....	Vision System
VTF .....	Venus Thrust Fan
W.....	Watt
WBS .....	Work Breakdown Structure
X-band.....	2.5–3.5 cm; 7.0 to 11.2 GHz communications band
XFS.....	X-Ray Fluorescence Spectrometer
XRD .....	X-Ray Diffractometer
XFS.....	X-Ray Fluorescence
µm .....	micrometer



## Appendix B. Design Team Study Report

### B.1 Science

#### B.1.1 The Science Rationale for Venus

The importance of Venus to the understanding of habitable terrestrial planets cannot be overstated. It is well known that the size and orbit of Venus makes it a critical comparison to the evolution of the Earth and to Earth-size exoplanets. Modeling shows that Venus should have accreted from similar materials as the Earth [e.g., Morbidelli et al., 2012], including refractory and volatile elements. Venus should have a similar amount of heat as the Earth, a planet with rigorous volcanic activity and plate recycling, and indeed the evidence for active volcanism on Venus is mounting [Smrekar et al., 2010; Shalyglin et al., 2015; Gülcher et al., 2020]. The atmospheric D/H ratio of Venus demonstrates the loss of significant amounts of water at some point in its history [e.g., de Bergh et al., 1991; Donahue et al., 1997; Taylor et al., 2018], and recent calculations show that oceans may have persisted on Venus for several billion years [Way et al., 2016; Way and Del Genio, 2020]. Our knowledge of planetary processes, then, predicts that Venus was once a habitable planet as Earth is now. The presence of microbes in the clouds of Earth [e.g., Delort and Amato, 2017] forces us to reconsider the possibility that the Venus clouds may be inhabited today [Morowitz and Sagan, 1967; Limaye et al., 2018; Seager et al., 2020]. **Venus provides the single most accessible example of an end-state of habitable Earth-size planets and it will allow us to identify the mechanisms that operate together to produce and maintain habitable worlds like our own.**

**Venus data are essential to advance our fundamental understanding of solar system evolution.** For example, one of the major outstanding questions in solar system research is from where and how did the Earth acquire its volatiles? Is the Earth's water a product of nebular processes, the accretion of water-rich planetesimals, or does it depend on delivery from the outer solar system? How do magma oceans, oxidation state, plate recycling and loss mechanisms determine the water inventory of terrestrial planets over time? Each terrestrial planet provides additional insight into these questions, but because of its size and proximity, Venus, *more than any other world in our solar system*, allows us to control for some of the factors that contribute to the geologic evolution of the Earth, e.g., the role of surface gravity, heat budget, plate tectonics and potentially long-lived oceans. **It is imperative to study Venus to understand the delivery of water to the inner solar system.**

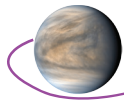
The key scientific importance of Venus is clearly stated across the scientific community and the Agency. The VFM will address parts of each of the three Venus Exploration Analysis Group (VEXAG) science goals [VEXAG, 2020] as well as several objectives from the 2020 NASA Science Plan across all three divisions. It will inform two of the strategic objectives of the Planetary Science Division, to advance scientific knowledge of the origin and history of the solar system, and to determine the potential for life elsewhere. It will also address the strategic objectives of the Heliophysics Science Division to understand the Sun and its interactions with Earth, the solar system and the interstellar medium, including space weather, and will provide data on how Venus can inform one of the Astrophysics Division's science themes: Exoplanet Exploration. The Planetary Decadal Survey [NRC, 2011] and Midterm report [NASEM, 2018] documented the critical importance of Venus science to understanding the origin of terrestrial planets and notes that Venus missions are necessary to address a "...lack of balance [that] undermines the compelling comparative planetology investigations recommended by the decadal survey, particularly for the terrestrial planets. The discovery of numerous Earth-size and Neptune-size exoplanets provides even greater urgency to initiate new missions to Venus and the ice giants."

#### B.1.2 Science Goals, Investigations, and Requirements of the Venus Flagship Mission

The Venus Flagship Mission Science Traceability Matrix is found in **Foldout Table 2.**

**Goal I. Understand the history of volatiles and liquid water on Venus and determine if Venus has ever been habitable.**

**Objective I.1: Determine if Venus once hosted liquid water at the surface**



**Investigation I.1.A – Determine the mineralogy and chemistry of tessera to ascertain rock type, and look for evidence of past water.**

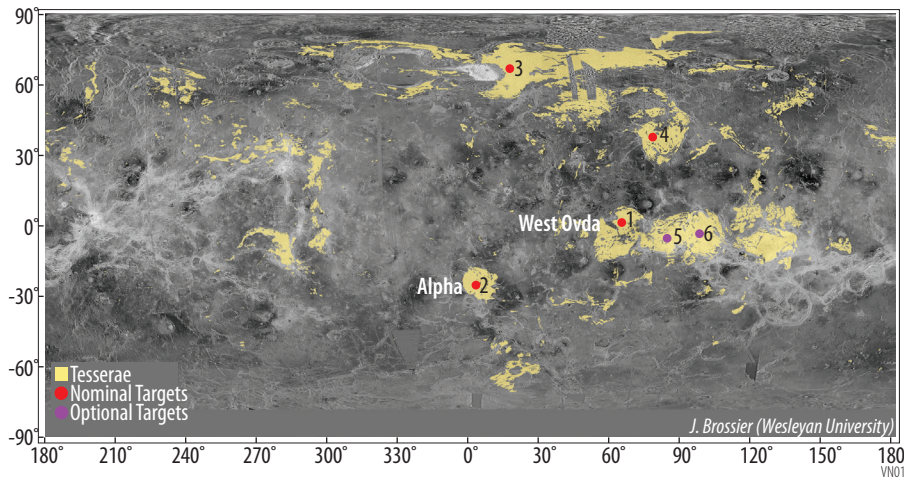


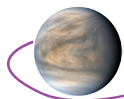
**Figure B-1.** Distribution of tessera terrain on Venus and potential VFM landing sites. Landing sites include tessera occurrences that are morphologically representative of tessera terrain generally and are near equatorial to ensure a high sun angle during Lander operations.

In the last decade, we have made major advances regarding our understanding of the habitability of Venus. For the first time, we have evidence that rocks in tessera terrain (identified in yellow in **Figure B-1**) on Venus may have formed in the presence of significant amounts of water (summarized in Gilmore et al. [2017]). Independently, climate modeling has shown that oceans may have persisted on Venus for

2–3 Ga [Grinspoon and Bullock, 2003; Way et al., 2016; Way and Del Genio, 2020]. Combined, this information is the strongest suggestion yet that the tesserae may have existed during a time when Venus had liquid water. We can now target these ancient rocks, as we do for Mars, to understand volatile history and whether Venus was once habitable.

The suite of instruments enabled by a Flagship mission allows a sweeping investigation into these hypotheses. A lander reaching the tessera terrain must carry instruments to make geochemical and mineralogical measurements of rocks at a range of depths and scales. Because the detailed geochemistry of the surface of Venus, in particular the yet unvisited tesserae, is largely unknown to us, this suite of measurements will help ensure the desired data are collected by this single lander opportunity. These measurements of chemistry and mineralogy are essential for determining rock type, and will settle the question of tessera composition. Heterogeneous reactions with atmospheric gases also produce secondary mineral assemblages which may have occurred under older and more water-rich atmospheric conditions.

Both sub-surface and surface mineralogy and chemistry will be determined with Lander instruments. A bulk geochemical measurement of the ground beneath the lander (~20–30 cm depth over a ~75 cm radius area (see **Section 2.8.2.1**)) will be conducted using a **Pulsed Neutron Generator** and **Gamma Ray Spectrometer (GRS)** to determine major, minor, and trace element chemistry (including the key elements U, K, and Th). This bulk measurement eliminates any potential issues caused by sampling bias that can arise in techniques using smaller samples (i.e., grain size and weathering rind thickness of tessera rocks are unknown). In addition, paired geochemistry and mineralogy measurements will be performed on powdered samples brought inside the lander vessel by drilling into the surface using the drill and sample ingestion system. The drill and sampling system is capable of delivering three aliquots of sample from different depths along a single drill hole, targeted to be ~5 cm depth in total. This depth should provide a sample of pristine rock material, and allow assessment of weathering profiles depending on thickness of the weathering rind (see **Investigation II.1.B**). The powdered drill samples will be analyzed successively by an **X-ray Fluorescence Spectrometer (XFS)** and an **X-ray Diffractometer (XRD)** to determine major, minor, and trace element chemistry, along with quantitative mineralogy. Pairing the chemistry and mineralogy for the same samples allows for better assessment of mineral compositions, and also aids in the identification of any X-ray amorphous materials, should they be present (as seen in data from the Curiosity rover, [Morrison et al. 2018]). The **XRD** will provide, for the first time, the detection of crystalline mineral phases on Venus, as well as quantification of their proportions in the sample, and mineral formulae for phases present at high enough abundance using lattice parameter refinement. The analysis of powdered samples by **XFS**, **XRD**, and interrogation of



### Box 1. The Importance of Tessera Terrain in the History of Venus

Venus tessera terrain is defined as having two or more sets of intersecting ridges and/or grooves that contribute to high RADAR backscatter [Sukhanov, 1992]. Tessera terrain covers about ~8% of the surface of Venus (**Figure B-1**) and is the stratigraphically oldest material on the planet [Ivanov and Head, 1996]. This stratigraphic position is crucial for the understanding of Venus as these are the oldest accessible rocks on Venus and the best, and perhaps only, chance to access rocks that are derived from the first ~80% of the history of the planet [see also Whitten et al., 2020]. The tessera crater age of 1.4x the average surface crater retention age of ~1 Ga [Ivanov and Basilevsky, 1993; McKinnon et al. 1997] overlaps in time with recent estimates of the lifetime of an ocean on Venus [Way et al., 2016; Way and Del Genio 2020, **Figure B-2**]. The tesserae were present during the eruption of global volcanic plains which are expected to have changed the volatile inventory and temperature of the atmosphere [Bullock and Grinspoon, 2001]. Additionally, the structural geology of the tessera records an extinct tectonic regime perhaps related to ancient crustal movement and recycling processes on Venus [e.g., Smrekar et al. 2007]. Analysis of the NIR radiance of Alpha Regio tessera using VEx VIRTIS data show that the tessera differs from the plains materials in a manner that is consistent with a lower FeO (more felsic) content [Gilmore et al., 2015], corroborating earlier measurements by Galileo NIMS during its Venus flyby [Hashimoto et al., 2008]. The formation of felsic continental crust on Earth is facilitated by the introduction of water-rich sediments into the mantle via subduction [e.g., Campbell and Taylor, 1983]. Felsic tessera would, therefore, record an extinct plate tectonic regime on a water-rich planet. **The direct, high-precision measurements of the mineralogy and chemistry of tessera terrain taken by the VFM Lander, coupled with morphologic information from the Lander and Orbiter, are essential to assess the thermal and volatile history and budget of the planet and to help determine whether Venus was once a habitable world.**

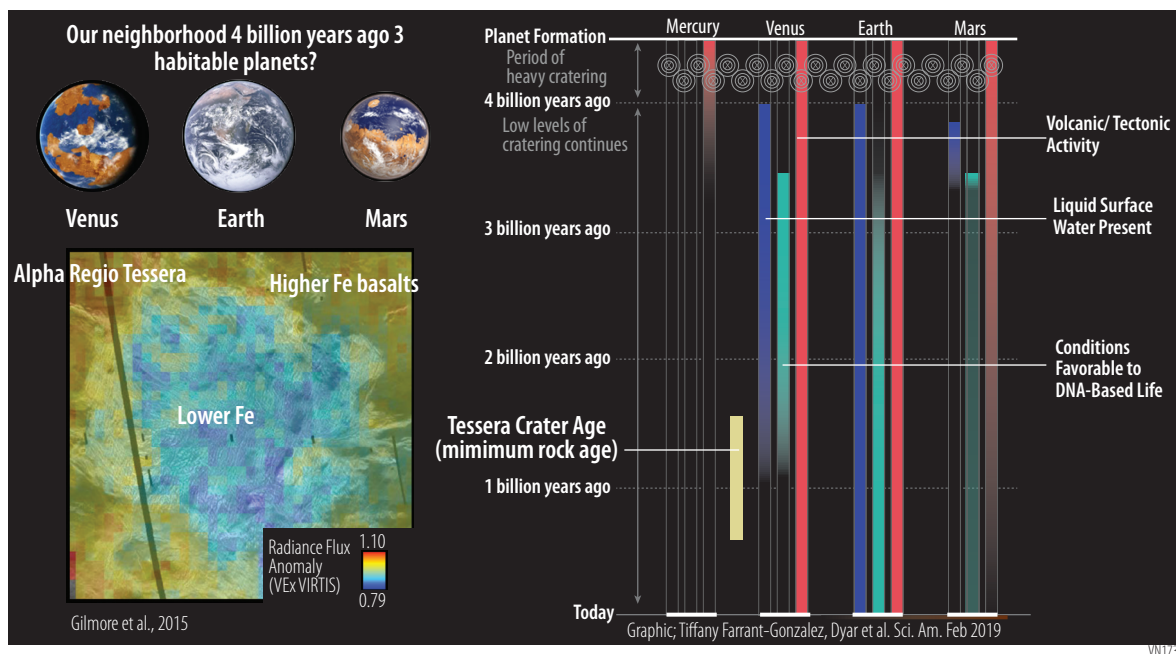
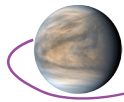


**Figure B-2.** Tessera terrain is the oldest accessible material on Venus and may overlap with a time when Venus had liquid water.

the subsurface by the **GRS** instrument best ensures the high precision measurement of unaltered rock, the standard for the analysis of rock composition on Earth. If weathering rinds in the landing site are thin enough, chemical and mineralogical information on unaltered rocks can be collected remotely for numerous additional samples outside of the Lander vessel by the **Raman-Laser Induced Breakdown Spectroscopy (R-LIBS)** Instrument (see *Investigation II.1.B* for more discussion).

The required precisions for chemical measurements by these instruments are given in the **STM (Foldout Table 2)**. The VFM requirements will provide data to allow sophisticated petrologic analyses





to constrain rock origin and are based on suggestions by Treiman and Filiberto [2016]. The large uncertainties in the Venera and Vega chemical measurements (**Table B-1** and **Table B-2**) limit their ability to constrain igneous provenance, thus this critical area of Venus science is largely unexplored. If the science goals of the mission were simply to distinguish if the tessera were mafic or felsic in composition, the precision requirements given in the **STM** could be less stringent, however. **Table B-1** and **Table B-2** show the chemical detection limits and relative precision of potential heritage **XFS**, **LIBS**, and the compositional uncertainty for the **GRS** instrument we identified in the strawman payload, while **Table B-3** illustrates the capability of the mineralogy instruments.

To provide local geologic context for the chemical and mineralogical measurements, the Lander will obtain 240° multi-color, stereo panoramic imagery of the landing site from a **Panoramic Camera (PC)** with four view directions. Additionally, the **Descent NIR Imager (DI)** on the bottom hemisphere of the vessel is set at an angle to include the drill site in its field of view after landing, to acquire images of the drill sampling location before and after sample acquisition (at ~200 microns/pixel resolution). The **R-LIBS** is equipped with a context imager to provide images of its sampling locations at <80 μrad spatial resolution, and thus is capable of providing images of rock texture and grain or clast morphology. This imaging suite provides a range of views to place the geochemical and mineralogical data in the appropriate geologic and stratigraphic context. The combination of chemical and mineralogical data paired with images capturing rock textures and the surrounding landscape can help distinguish rock type (e.g., igneous vs. sedimentary) at the landing site because different geologic environments concentrate elements and minerals in different ways, and different types of rocks have characteristic textures and grain morphologies.

The orbital assets of this mission will allow the local and regional data gathered by the Lander to be placed in a global context. A **Near-Infrared Imager (NIR-I)** on the Orbiter will produce a global map of the NIR emissivity at several wavelengths and in an orbit optimized for surface study. It will provide global mineralogical information for Venus, and provide the opportunity to extrapolate the detailed

**Table B-1.** GRS Instrument Performance. The instrument used as part of a strawman payload in this study is the Bulk Elemental Composition Analyzer (BECA) [Schweitzer et al., 2017]. Performance data provided by A. Parsons, pers. comm. Elements in italics are required by the VFM to address the Science Traceability Matrix. BECA can measure a range of elements including: Al, S, C, O, Si, Ca, Fe, Mg, H, B, Cl, Ti, Mg, K, Na, Gd, Ni, V, U, Th, REEs, if present at high enough concentrations. Measurement uncertainty decreases with longer integration times for the detector.

Elements	Venera/Vega <sup>1</sup> Uncertainty (wt%)	BECA Composition Uncertainty (wt%) For Integration Times		
		30 Min	60 Min	90 Min
		<i>Si</i>	~3	0.33
<i>Ti</i>	0.1–0.5	0.02	0.01	0.01
<i>Al</i>	2–3	0.63	0.44	0.36
<i>Fe</i>	2–3	0.19	0.13	0.11
<i>Cr</i>	–	0.06	0.04	0.03
<i>Mn</i>	0.1–0.2	0.02	0.01	0.01
<i>Mg</i>	4–7	0.31	0.22	0.18
<i>Ca</i>	1–2	1.17	0.83	0.67
<i>K</i>	0.1–1	0.05	0.04	0.03
<i>Na</i>	–	0.33	0.24	0.19
<i>P</i>	–	0.07	0.05	0.04
<i>S</i>	0.2–0.8	0.10	0.07	0.06
<i>Cl</i>	–	0.04	0.03	0.02
<i>F</i>	–			
<i>O</i>	–	0.75	0.53	0.43
<i>REEs</i>	–	*	*	*
<i>U, Th</i>	0.3–2.4 ppm 0.4–2.4 ppm	*, 0.80	*, 0.57	*, 0.46

<sup>1</sup>range from data from all Venera and Vega missions given in Treiman, 2007, \*elements able to be measured with this technique, but uncertainty data not available at this time.

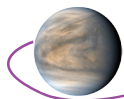


**Table B-2. XFS and LIBS Instrument Performance.** The instruments used to bound this VFM study are the Venus Instrument for X-ray Lithochemistry (VIXL) [after Allwood et al., 2015] and Venus Elemental and Mineralogical Camera (LIBS) [Clegg et al., 2019]. Performance data provided by L. Wade (VIXL) and S. Clegg (LIBS), pers. comm. Elements in italics are required by VFM to address the Science Traceability Matrix. The LIBS technique is capable of measuring a wide range of elements, including light elements like H and heavy elements such as actinides, if present at high enough concentrations. VIXL can detect elements from Na through U, with the addition of lighter elements if using a polymer window.

Elements	Venera/Vega <sup>1</sup>	VIXL		LIBS	
	Relative Precision	Detection Limits	Relative Accuracy and Precision	Detection Limits (2 m)	Relative Accuracy and Precision
<i>Si</i>	13–15%	0.5 wt%	±10%*	<1000 ppm	±10%*
<i>Ti</i>	56–100%	100 ppm	±10%*	<1000 ppm	±10%*
<i>Al</i>	23–38%	0.2 wt%	±10%*	<1000 ppm	±10%*
<i>Fe</i>	29–47%	0.1 wt%	±10%*	<1000 ppm	±10%*
<i>Cr</i>	–	100 ppm	±10%*	<1000 ppm	±20%*
<i>Mn</i>	100–171%	100 ppm	±10%*	<1000 ppm	±20%*
<i>Mg</i>	64–109%	0.2 wt%	±10%*	<1000 ppm	±10%*
<i>Ca</i>	19–28%	0.1 wt%	±10%*	<1000 ppm	±10%*
<i>K</i>	30–160%	100 ppm	±10%*	<1000 ppm	±10%*
<i>Na</i>	–			<1000 ppm	±10%*
<i>P</i>	–	100 ppm		<5%	±20%*
<i>S</i>	63–171%	100 ppm	±10%*	<5%	±20%*
<i>Cl</i>	–	0.2 wt%		<5%	±20%*
<i>F</i>	–			<5%	±20%*
<i>O</i>	–			<1000 ppm	±10%*
<i>U, Th</i>	6–160%			<5%	±20%*
<i>C</i>				<5%	±20%*
<i>Ni, Cu, Zn, Rb, As, Cd, Pb</i>				<1000 ppm	±20%*
<i>Li, Sr, Ba, H</i>				<100 ppm	±20%*

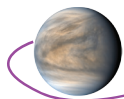
<sup>1</sup>calculated based on data from all Venera and Vega missions given in Treiman, 2007, \*VIXL accuracy at 10 wt% oxide concentration in a vacuum environment, +VIXL accuracy at 1 wt% oxide concentration in a vacuum environment

**Table B-3. Detection and quantification limits for instruments measuring mineralogy.** XRD instrument performance used in this study as part of the strawman payload is from CheMin-V [Blake et al., 2019]. Performance data provided by D. Blake, pers. comm. Similarly, Raman specifications used in this study are from the Venus Elemental and Mineralogical Camera (VEMCam; Clegg et al., 2019). Performance data provided by S. Clegg, pers. comm.

CheMin-V	
Detection of xtalline phases	All minerals present at ≥ 1 wt%
Quantification of proportions of xtalline phases	All minerals present at ≥ 3 wt%
Lattice parameter refinement of xtalline phases	All minerals present at ≥ 5 wt%
Detection/quantification of clay minerals	Detection if ≥ 5 wt%, quantification if ≥ 10 wt%
Quantification of proportions of amorphous component	If present at ≥ 10 wt%, ± 30% of amount present
Raman	
Mineral Group	Detection Limit at 2 m (vol %)
Oxides	< 10
Chain silicates	5
Sheet silicates, framework silicates	< 5
Olivine, Aragonite, magnesite, talc, quartz, sulfates, phosphates	1
Calcite, pyrite	< 1

landing site data to the global scale to assess variability among the tesserae. Having both the lander and orbital mapping allows unprecedented ground truthing of orbital data from Venus by comparing *in situ* mineralogy and chemistry data with orbital measurements, an opportunity with extra significance for a planet from which we have no samples in hand for analysis on Earth.

Determining the composition of the tesserae themselves using measurements of pristine rock chemistry and mineralogy provides insight into ancient crust-building processes on Venus, processes



that are significantly influenced by the presence of water (see **Box 1**). Certain igneous rock compositions require water to form; large scale occurrences of granitoid rocks being one of them [Campbell and Taylor, 1983]. Orbital spectroscopic data suggest that the tesserae are more felsic in composition than the surrounding plains [e.g., Hashimoto et al., 2008; Gilmore et al., 2015], and the chemical and mineralogical data from the Lander would speak directly to this hypothesis, with granitic tesserae indicating both a past crustal recycling mechanism and widespread liquid water [e.g., discussion in Gilmore et al., 2017]. It is also possible that the tesserae hold other types of rock that are formed with the aid of volatiles and tectonism (e.g., sedimentary, metamorphic), and the mineralogy and detailed imagery of the landing site will help in identification of these types of rocks, if present.

The rocks of a planet also record processes, like weathering, that have acted upon them since their formation. Weathering of rocks is a function of the climate, and thus secondary minerals are important tracers of the current and past climate on Venus. If an ancient climate regime with stable liquid surface water did occur, water-related weathering may be recorded in the tesserae. The depth-profiling potential of the drill system and LIBS instrument allow the Lander to sample successive layers of weathering beneath the surface of the rocks to look for changes in weathering style over time, and identify any preserved record of the past climate. Together, the composition of the tessera and presence of any ancient secondary mineral phases help establish the conditions on the venusian surface billions of years ago when water, and a habitable environment, are most likely to have been present.

### ***Investigation I.1.B*** – Look for evidence of surface features that might indicate a climatically different past (e.g., sedimentary structures, fluvial features)

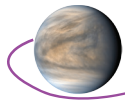
Results from the Magellan mission demonstrate that erosional processes are minimal under the current climatic regime because the high surface temperatures prohibit fluvial processes. Magellan images show some wind streaks and a few dune fields, whose spatial association with impact craters support crater ejecta as the likely sediment source [Greeley et al., 1992]. Venera lander images and modeling suggest that surface winds on Venus are below a few m/s, in part due to the planet's slow rotation and massive atmosphere [Schubert et al., 1980]. Large portions of the planet are clearly volcanic terrains that have not eroded significantly since emplacement.

Tessera terrain, however, are stratigraphically older than the plains and display a distinct deformation pattern as indicated by folds, faults, and lineaments, indicating an extinct tectonic regime. The RADAR brightness of the tessera surfaces also indicates roughness elements at the cm-scale. In several tesserae, RADAR data reveal patterns that could be interpreted as horizontal layering that would require both deposition and erosional processes to expose the layers [Senske and Plaut, 2000; Byrne et al., 2020]. The 100 m resolution Magellan data do not allow us to discern the origin of these lineaments and roughness elements.

Experience from the Earth and Mars suggests that image resolutions of around 10 m or better are capable of revealing layered sedimentary sequences, drainages, small alluvial fans, and other erosional and depositional features that might be indicative of different past climatic regimes. If we were to find evidence of erosional products in older terrains, this would certainly be indicative of dramatically different surface and atmospheric conditions, and evidence of past fluvial activity would be a strong indicator of past habitability. The VFM Orbiter **Synthetic Aperture Radar (SAR)** will enable imaging of selected targets around the globe at better than 10 m resolution. The tessera landing site and immediate surroundings will further be imaged by the **DI** during descent from the km to the cm scale at 0.9 and 1.02  $\mu\text{m}$ . Finally, the lander will collect images down to the sub-cm scale from three cameras: the **PC**, the **DI** images of the drill site and the context imager associated with the **R-LIBS** instrument. The result will be a set of image data for the tessera that spans cm–km scale and can be compared to Magellan or other RADAR sets to better interpret the RADAR signatures of major terrain types. These VFM imaging systems are well understood, high-TRL technology and can be immediately incorporated into a mission.

### ***Investigation I.1.C*** – Determine isotopic ratios and abundances of hydrogen, noble gases, oxygen, nitrogen, and other elements in the atmosphere and below the cloud deck to the surface.

The **D/H** ratio in atmospheric  $\text{H}_2\text{O}$  provides an essential constraint on the original water abundance. Donahue et al. [1982] derived a value of D/H that was 100 times greater than the terrestrial D/H



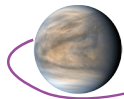
ratio, and suggested that this result implied that Venus had lost the equivalent of a terrestrial ocean of water. However, this measurement was likely compromised by sulfuric acid droplets clogging the instruments. Telescopic observations done from the ground [Bezard et al., 1990; Bjoraker et al., 1992] find D/H ratios that differ from the Pioneer Venus (PV) result. The recent measurements made with the SPICAV instrument on VEx also find a different result where the D/H varies from 3–4 times the PV value and changes with altitude [Bertaux et al., 2007]. As the atmosphere is well-mixed up to the homopause at ~120 km, the above variation in D/H was not expected, since any fractionation due to preferential condensation of HDO over H<sub>2</sub>O would mean a decrease, not increase, in D/H with height. The VEx results and ground-based data also have a relatively large uncertainty.

The VFM will therefore measure the D/H ratio, in water and other species, at all altitudes from the surface to the thermosphere. The VFM will use a **Neutral Mass Spectrometer (NMS)** and **Tunable Laser Spectrometer (TLS)** on the Lander to measure D/H profile from 63 km down to the surface; it will employ an **Aerosol Mass Spectrometer (AMS-N)** on the Aerobot to measure multiple vertical profiles of D/H in both liquid and gaseous phases in the cloud layer, to characterize fractionation processes in the clouds. A heterodyne **Sub-mm Spectrometer (S-mm)** on the VFM Orbiter will map the D/H ratio from the cloud layer (70 km) up to the turbopause (140 km), in order to determine transport through the mesosphere and mesosphere-thermosphere turbulent transition region. Finally, instrumentation on the SmallSats will measure the escape fluxes of D and H to space and characterize how this is mediated by solar wind interaction. Together, these investigations enable a complete characterization of the D/H from surface to space, to enable a reconstruction of its implications for the history of water on Venus. Similar studies will also be possible by measuring isotopic abundances of oxygen, carbon, sulfur isotopes, again from a Lander, Orbiter, and Aerobot. Comparisons of the variability of the different isotopic ratios will help to determine fraction mechanisms (such as those associated with condensation/evaporation or photochemistry) dominating at different altitudes.

**Noble gas isotopes** provide strong constraints on models of the origin and evolution of the atmospheres of terrestrial planets, providing clues to the history of the planet in epochs older than those preserved in the geological record. Does that imply a far greater loss of neon and argon from Earth and Mars or that Venus was endowed with a greater inventory of volatiles? In the absence of measurements of the heavy noble gases, Kr and Xe, this mystery remains unresolved to this day. Though Kr was measured on PV, its uncertainty is so large (by a factor of 15 [von Zahn et al., 1983]) that it spans the whole range of values from the Earth to CI chondrites. Xe has not even been measured at Venus except for possible upper limits. It is essential to carry out the measurements of the heavy noble gases to altitudes *well below* the average homopause altitude of ~110–125 km on Venus, to accommodate their much heavier mass relative to the CO<sub>2</sub> atmosphere. A comparison between the isotopic ratios of Ne, Ar, Kr, and Xe in the atmosphere of Venus with their values in the atmospheres of Earth and Mars is crucial for distinguishing between formation scenarios of the terrestrial planets as well as understanding the loss of atmosphere over time. If the atmosphere of Venus suffered a giant impact as Earth did, its Xe isotopic ratios would be similar to Earth's. If the noble gas isotopic ratios are similar to the solar/Jovian values, this would indicate a dramatically different processing and evolution of the atmosphere of Venus compared to Earth.

Venus is a critical data point to understand the chemistry of the solar system generally and the history of accretion and origin of planetary water, both important aspects of the Earth/Venus dichotomy. For instance, Greenwood and Anand [2020] note that Venus makes up 41% of the inner planets by mass, making Earth and Venus likely the most representative bodies for the composition of the inner solar system (for reference Mars is 5%). Therefore, a better understanding of Venus can shed significant insight into such questions as the degree of compositional homogeneity in the inner solar system (e.g., is Mars anomalously different from the rest of the inner solar system, or is each planet unique?; discussion in Greenwood and Anand [2020]). If the inner solar system planets formed from a heterogeneous reservoir, then perhaps Venus and Earth diverged at their beginning.

However, we know processes occurring after initial accretion can affect the composition of planetary bodies, such as the Moon-forming giant impact on Earth. Venus can therefore also provide insight into how such processes influence planetary evolution, and conditions of habitability. Noble gas isotopes record volatile acquisition and loss. For example, the Earth's mantle has a <sup>20</sup>Ne/<sup>22</sup>Ne close to the solar value, but its atmospheric ratio is lower, indicating atmospheric loss of Ne since Earth's formation. If Venus experienced an episode of vigorous atmospheric loss, this should be reflected in



its atmospheric  $^{20}\text{Ne}/^{22}\text{Ne}$ . Similarly, hydrodynamic loss of an atmosphere should strongly fractionate Kr, so  $^{82}\text{Kr}/^{86}\text{Kr}$  measurements will shed light on whether Venus lost an ocean's worth of water in the past [Zahnle 1993]. Further constraints on the original inventory of volatile elements on Venus are provided by the non-radiogenic Ar isotopes. Atmospheric loss of Ar from Earth has resulted in a lower  $^{36}\text{Ar}/^{38}\text{Ar}$  than the Sun, for example. The escape of Ar from Venus's atmosphere over time is therefore recorded in the ratio  $^{36}\text{Ar}/^{38}\text{Ar}$ . Atmospheric radiogenic  $^{40}\text{Ar}$ , produced from the radioactive decay of  $^{40}\text{I}$  in the crust and mantle, is often interpreted as an indicator of the degree to which the mantle has degassed over geologic time [O'Rourke and Korenaga, 2015]. However, an alternative explanation is that  $^{40}\text{Ar}$  is derived from the hydrologic weathering of planetary crust [Watson et al., 2007].  $^{40}\text{Ar}$  is about  $\frac{1}{4}$  as abundant in Venus's atmosphere as in the Earth's. Therefore, measurements of  $^{40}\text{Ar}$  in Venus's atmosphere constrain sources and sinks such as the efficiency of mantle degassing and crustal weathering and recycling, integrated over time.

Accurate determination of the noble gas isotopes and **light element isotopes** in  $\text{N}_2$ , C in  $\text{CO}_2$ , and O in  $\text{CO}_2$  and  $\text{H}_2\text{O}$ , in particular, would provide the robust constraints required for distinguishing between models of formation of Venus, atmospheric evolution, past habitability and the timing of the loss of water [Baines et al., 2013].

Atmospheric **oxygen isotopes** record the history of fractionating loss and atmospheric interactions with the surface. Both of these processes are poorly understood for Venus, but crucial for understanding how Venus evolved after it lost Earth-oceans worth of hydrogen. Recent ground-based spectroscopy shows that at the level of Venus cloud tops,  $^{17}\text{O}$  is enriched and  $^{18}\text{O}$  is depleted compared with terrestrial ocean water oxygen isotopes [Iwagami et al., 2015]. However, the error bars of these measurements overlap the Earth-Moon fractionation line, so the authors concluded that the Earth, Moon, and Venus were formed from a well-mixed solar nebula.  $^{16}\text{O}/^{17}\text{O}/^{18}\text{O}$  measurements are crucial for understanding the history of this important volatile.

The fractionation of atmospheric **sulfur isotopes** by photolysis of sulfur-bearing gases is mass independent, with distributions highly sensitive to atmospheric concentrations of  $\text{O}_2$ ,  $\text{O}_3$ ,  $\text{H}_2\text{O}$ ,  $\text{CS}_2$ ,  $\text{N}_2\text{O}$ ,  $\text{H}_2\text{S}$ , and  $\text{OCS}$ . *In situ* measurements of atmospheric  $^{32}\text{S}/^{33}\text{S}/^{34}\text{S}$  therefore provide constraints on recent atmospheric composition and processes. Fractionation of atmospheric sulfur is driven by photolysis, condensation, and reactions with surface minerals. For example, negative  $\Delta^{33}\text{S}$  in Archean sulfate deposits is most likely due to the UV shielding provided by increased levels of atmospheric  $\text{OCS}$  during the Archean [Ueno et al., 2009].

Because of the importance of these critical measurements, the VFM will make these measurements using **mass spectrometers** on the Lander (NMS), Aerobot (AMS-N) and the Orbiter (NMS). This will allow us to put the data from a single entry location, the lander, into context with the Aerobot and Orbiter data collected over multiple locations and at different times of day to confirm any variation (or expected invariance) in the distribution of noble gases and isotopic species.

**Investigation I.1.D – Determine atmospheric escape rates over a full solar cycle.**

VFM will measure heavy ion escape (atomic and molecular oxygen, and carbon dioxide) with full spatial, energy, angular, and mass coverage during different phases of the solar activity cycle (Figure B-3).

Our approach is to deploy identical payloads on the **SmallSats** in orbits designed to obtain simultaneous information about both the *upstream* solar wind conditions in interplanetary space and escaping ion measurements in the solar wind *magnetotail*, ensuring accurate cause-and-effect interpretations of the observed escape rate variations. The highly elliptical orbit for the SmallSats was chosen in order to sample the venusian atmosphere simultaneously with the solar wind to better understand the response of the atmosphere to solar wind drivers. The orbit also was designed to provide dual sampling of specific regions behind the venusian bow shock

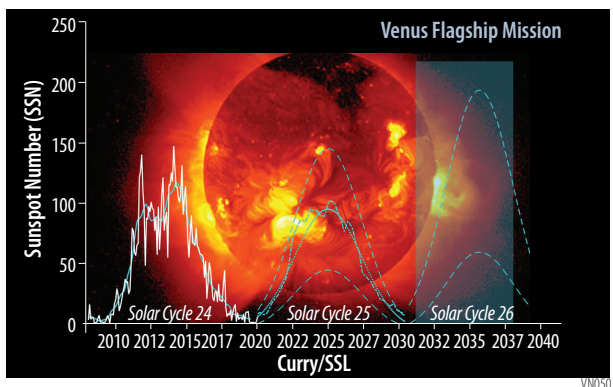
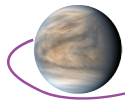


Figure B-3. Illustration of the past and predicted future solar cycles. The blue box is the nominal lifetime of the SmallSats.



in order to characterize the temporal changes and fine-scale structures in the atmosphere (akin to a ‘string or pearls’ configuration as the Mars Thermal Emission Imaging System (THEMIS), Cluster and other multi-platform plasma missions have historically used). Additionally, the orbits will be able to observe the southern hemisphere at low latitudes in order to examine the potential for remanent crustal magnetism or weak dipole magnetic field signatures in concert with magnetometer measurements at lower altitudes collected by the Aerobot. To complement the SmallSat measurements, the Orbiter carries a **NMS** that will measure the *in situ* neutral constituents from 2–150 Dalton that are the source of escaping ions.

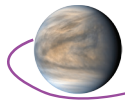
Each payload consists of ion and electron **Electrostatic Analyzers (ESA-i, ESA-e, respectively)** that will observe solar wind ions and electrons as well as planetary ions and electrons in the suprathermal energy range (i.e., 1 eV–25 keV). Ion and electron observations are critical for science investigations into atmospheric escape (bulk ion escape), magnetic topology and reconnection (plasmoid escape), and the response of the atmosphere to changes in the solar wind and solar transient events. The payload will also have a **Langmuir Probe (LP)** to characterize the thermal population (< 5 eV) and better estimate the spacecraft potential. A **Solar Energetic Particle Detector (SEPD)**, a solid state detector, will also be aboard both SmallSats that will observe high energy charged particles (>25 keV), which will characterize the space weather effects and high energy input into the venusian atmosphere. In order to understand how the charged particles are accelerated, the SmallSat payloads will also have an **Electric Fields detector (E-FD)** to directly measure the electric fields potentials. The other fields instrument on the payload will be a fluxgate **Magnetometer (Mag)** to measure the vector components of the magnetic field, which will characterize the interplanetary magnetic field, potential remanent crustal magnetic fields, and the induced magnetic field at Venus. Finally, an **EUV (Extreme Ultraviolet) detector (EUV-D)** will be aboard both spacecraft to measure the EUV changes from the sun over the course of the solar cycle.

The measurements will cover the majority of solar cycle 26, including the predicted ascending and declining phases. Based on these measurements and the development of insights about the early solar wind and solar activity from observations of young Sun-like stars, **the VFM will provide the necessary framework for a time-integration of the oxygen escape, establishing its role in the historical loss of water.**

D/H measurements from PVO indicate that Venus once had a substantial inventory of water that has either been lost to space or been taken up by subsurface processes [e.g., Futaana et al., 2017 and references therein]. That neutral H is removed from the atmosphere by the thermal process of Jeans escape is well-established, and the growing body of knowledge regarding the EUV history of Sun-like stars can be used to estimate the total loss of H over time. A problem remains in understanding the mechanism or mechanisms that remove the oxygen left behind from the loss of potentially an Earth ocean’s worth of water. The ionization of oxygen atoms and molecules accelerates them to velocities exceeding the ~10 km/s escape speed for Venus at altitudes where conditions are effectively collisionless, allowing solar wind interaction-related erosion processes. What is *not established* is their ability to remove a sufficient amount of oxygen over time.

Previous measurements of escaping oxygen ions have been obtained on Venera, PVO, and VEx missions [e.g., Brace et al., 1987; Barabash et al., 2007]. The instruments used to make and interpret these measurements are a combination of ESAs and magnetometers. The PVO mission’s instrument had several serious shortcomings in that the composition of the ions had to be inferred from their energy/charge and the measurements missed both the low and high-energy populations of the escaping oxygen, which VEx determined were important, if not dominant, contributors to atmospheric escape. Also, the VEx measurements were made during a relatively low activity solar cycle [Luhmann et al., 2008] and in an orbit that was not ideally suited for ion escape measurements. On each VFM SmallSat an **ESA-i** and **ESA-e** provide the solar wind velocity and dynamic pressure that have been demonstrated to be key factors in controlling observed escape rates in available measurements. A **Mag** provides information both about the solar wind and solar activity conditions as well as an understanding of the principal mechanisms for accelerating oxygen away into space.

Opportunistic **Radio Occultation (RO)** soundings can also constrain the structure of the Venus ionosphere. Differential Doppler shift measurements of X- and S-band signals, between Mariner 10 and Earth stations captured the vertical structure of Venus’s ionosphere identifying two distinct electron density peaks around 120 km ( $7 \times 10^3$  electron/cm<sup>3</sup>) and 140 km ( $9 \times 10^3$  electrons/cm<sup>3</sup>) during



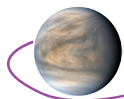
night-time close to the equator; these electron density peaks increase by two-orders of magnitude to a peak density ( $2.9 \times 10^5$  electrons/cm<sup>3</sup>) at 142 km on the day side [Fjeldbo et al., 1975]. The Akatsuki RO observations also captured a peak electron density around 140 km ( $3 \times 10^5$  electrons/cm<sup>3</sup>) on 6 May 2016 showing a gradual decrease to  $10^4$  electrons/cm<sup>3</sup> from 200 km up to 1,000 km [Imamura et al., 2017]. There is clear evidence of a variable degree of ionization with altitude that is also subject to solar input. Crosslink RO soundings between the two SmallSats at two frequency bands (options include X-, S-, or ultra high frequency (UHF)) will allow retrievals of the vertical structure of the venusian ionosphere every 100–500 m with better than 10% accuracy. The increased number of such ionospheric RO observations, in combination with the unique RO geometry, will enable increased spatial coverage that will allow understanding the Sun-Venus ionospheric coupling, its 3D spatial variability, and the underlying physical processes that modulate Venus's ionization over time. An increased number of opportunistic RO soundings can also be obtained between the Orbiter and the SmallSats, as well as between each of the three orbiting spacecraft and Earth stations.

### ***Investigation I.1.E* – Search for evidence of a current or past magnetic field.**

Measurements by multiple missions [e.g., Russell et al., 1979] have demonstrated that Venus does not currently have an intrinsic magnetic field. Despite the high surface temperatures, remanent magnetism may exist in the uppermost crust of Venus [O'Rourke et al., 2019], likely confined to a thinner layer than that detected on Mars because of the high temperatures. Previous spacecraft have lacked magnetometers with an adequate combination of sensitivity and proximity to the surface to adequately evaluate the presence of a remanent magnetic field. Permanent magnetism might be observed from low orbit or from a balloon if it is sufficiently strong. The VFM will measure the magnetic field from several vantage points. **Mags on the SmallSats and Orbiter** will measure the strength of the field with unprecedented precision from multiple altitudes in three different orbits, thereby constraining the strength and shape of the magnetic field. Additionally, a **Mag on the Aerobot** will perform a magnetic survey from ~55 km. These data can be compared to the orbital data to further specify the contributions to the magnetic field. The 60 day lifetime of the Aerobot will enable **mapping of the field strength from equator to the pole** of one of the hemispheres of Venus. This will allow mapping the distribution, field strength and direction of crustal magnetic sources if present. Similar mapping for Mars from Mars Global Surveyor (MGS) in low orbit showed strong magnetic fields of varying polarity in the ancient crust, allowing calculation of the thickness and possible mineralogy of the magnetic layer, indicating the presence of a core dynamo in the early history of Mars, and suggesting crustal spreading [e.g., Connerney et al., 1999]. The detection of remanent magnetism on Venus would constitute a major scientific discovery as it would indicate the presence of a dynamo in a past epoch.

On Earth, a dynamo field has existed for at least 3.5 Ga based on the rock record. Earth's dynamo has been important in shielding organisms from some of the most harmful effects of solar radiation [e.g., Dogliani et al., 2016]. It may also have a role, though not well understood, in the evolution of the atmosphere since the magnetic field affects the interactions of incident solar and cosmic particles with the atmosphere. For these reasons, as well as for a fundamental understanding of the whole planet, it is of great interest to know whether Venus exhibits any remanent magnetism.

There are three possible explanations for why Venus currently lacks a global field: (1) absence of an inner core [Stevenson et al, 1983], possibly because Venus is smaller and possibly hotter. Compositional convection arising from inner core growth is believed by many to be responsible for sustaining Earth's dynamo [e.g., Loper and Roberts, 1983]; (2) a transition in mantle convection within Venus because of the hypothesized resurfacing event about 700 Ma ago [e.g., Nimmo and McKenzie, 1998]. In this picture, Venus's mantle is not currently cooling sufficiently fast to allow for core convection; (3) lack of a late giant impact during formation. This kind of impact may have favored homogenization of Earth's core and thus allowed for the terrestrial dynamo. It may also affect the likelihood of core-mantle interactions such as the magnesium precipitation prosed for Earth [O'Rourke and Stevenson, 2016]. In this third case, unlike the other two, it is possible that Venus never had a global field. Contrary to what is sometimes said, the slow rotation is, in fact, not relevant. Venus rotates fast enough for core convection (i.e., the Coriolis force dominates the inertial terms in the equation of motion despite the 243 day current spin period).



Dynamo models predict that surface fields on Mars, Earth, and Venus would be similar (~30–50 mT), so crustal rocks with similar mineralogy would have similar magnetization intensities on all three planets [O’Rourke et al., 2019]. Thus the requirements for the sensitivity of the magnetometer on the Aerobot are designed to detect anomalies of this strength from lava flows that are at least 200 m thick (based on dark floor crater data) over a spatial resolution of 150 km [O’Rourke et al., 2014; O’Rourke et al., 2020].

**Objective I.2: Identify and characterize the origins and reservoirs of Venus’s volatiles today.**

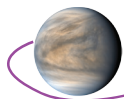
***Investigation I.2.A* – Determine the composition and distribution of volatiles in the atmosphere.**

The composition of the atmosphere below the clouds, at 0–50 km altitude, is poorly known. This is where the bulk of the chemistry of the sulfur cycle takes place, and where a large number of as yet undetected trace constituents are predicted to form [Yung and Demore, 1982]. The sulfur cycle and the distribution of trace constituents are crucial for understanding the energetics, mixing and dynamics of the Venus atmosphere. They also likely hold the secret of the stability of the atmosphere of Venus [Yung and Demore, 1982], considering that, unlike Mars, the catalytic role of hydroxyl to recycle CO<sub>2</sub> is absent on Venus due to its low water vapor abundance. Measurements in the lowest few kilometers of the atmosphere are particularly needed in order to understand surface-atmosphere chemical interactions. During descent, the VFM’s Lander will use a **NMS** and **TLS to measure atmospheric composition** with unprecedented sensitivity and vertical resolution **over the full 0–60 km altitude range**. The **Long-Lived In situ Solar System Explorer (LLISSE)** [Kremic et al., 2020] will characterize the **variability of key trace gases at the surface over its 60 day** lifetime. These data will be correlated with measurements by the **AMS-N on the Aerobot** and the **NMS on the Orbiter**.

Chemical cycles occurring in the cloud layers, both in the main layer at ~50–60 km and in the convectively stable layer lying above at 60–70+ km, are very poorly understood, largely because the clouds themselves block efforts to observe composition from orbit. The primary constituent of the clouds is likely to be sulfuric acid, mixed with 5%–25% water, but there are several pieces of evidence hinting at more complex constituents, from the blue/UV absorption at cloud-tops by an as-yet-unidentified substance, to unexplained X-ray fluorescence results from Soviet probes finding large abundances of P, Cl, and Fe in lower and middle clouds, to the presence of particulates at altitudes too hot for sulfuric acid. The **VFM will obtain repeated multiple profiles of cloud and gas composition using the AMS-N on a balloon-borne Aerobot**, which will execute multiple controlled vertical cycles over a 52–62 km altitude range, to permit characterization of both the main convective cloud layer and the upper convectively stable cloud, where the UV absorber is known to be present. To support the characterization of cloud particles, a **nephelometer within the AMS-N** will be used to characterise the refractive index and size distribution of aerosol particles, and a net flux radiometer in the **MET** will allow correlation of composition measurements with measurements of UV flux absorption. By measuring the composition of cloud particles during its 60 day lifetime in the clouds of Venus, and executing multiple vertical excursions through the clouds, the VFM aerobot’s payload is likely to be able to solve the long-standing mystery of the nature of the Venus UV absorber. Carried by Venus’s super-rotating winds, the Aerobot will circumnavigate the planet roughly once every five days; its dataset will, therefore, span all times of day and night and cover a range of latitudes, ideal for characterization of cloud-level chemical processes. Further information will be gained by using the student **Imager (VI)** to monitor the effect of cloud and gas composition on the balloon as it circumnavigates Venus. This imager will look at both the clouds and monitor targets composed of chemically reactive materials on balloon and gondola as a function of time to look for possible oxidation/sulfurization reactions that might occur.

Additional insights into the process of cloud convection will be obtained using **RO** of X- and Ka-band signals from the VFM orbiters to Earth. Over the lifetime of the mission, these measurements will return vertical profiles of both liquid and vapor of sulfuric acid at altitudes of 35–90 km, in hundreds of vertical profiles distributed around the planet. Recent RO observations from VEx identified latitudinal and time-dependent distributions of the H<sub>2</sub>SO<sub>4</sub> mixing ratio, which are not reproduced in numerical models [Oschlisniok et al., 2012]. By exploiting not only Orbiter to Earth occultations, but also occultations using the SmallSats, the number of occultations is increased by over an order of magnitude, and will be more evenly distributed over the planet.





Compared to the atmosphere below the clouds, the mesosphere of Venus (at 60–100 km altitude) is relatively well studied by Venus Express. The mid-IR solar occultations, and UV stellar occultations, executed by Venus Express measured the vertical profiles of species including SO<sub>2</sub> and H<sub>2</sub>O, but only in a few hundred profiles in total, and only for a relatively small number of species. The VFM will

**Box 2. VFM Unravels Venus Volatile History**

The volatile inventory of the solar system remains vexing (e.g., Greenwood et al., [2018], and references therein): where did the Moon’s water come from? Why is Mercury rich in volatile elements, like Cl, S and C? The evolving story of Mars tells us several ways its evolution congenitally differs from that of the Earth. Its water inventory is affected by closer proximity to the water-rich outer asteroid belt [e.g., O’Brien et al., 2018]. As a smaller planet, its crust solidified earlier than that of the Earth, such that its mantle was isolated from accretion processes such as the late veneer [Bouvier et al., 2018]. Both Mars and Venus have high D/H values indicating loss of water, but Mars lost a substantial atmosphere and Venus did not. To understand these elements that are so critical in determining the climate and habitability of any planet, the VFM will examine the sources and sinks of different volatile species and study the processes by which they are exchanged between different parts of the Venus system. Water is the key volatile species for habitability, but sulfur species (SO<sub>x</sub>), carbon dioxide and monoxide (CO<sub>x</sub>), nitrogen and halogen species all play important roles. To understand how Venus diverged from Earth, VFM will characterize **volatiles today** using complementary measurements covering altitudes from the surface to space; and it will constrain **past volatiles** by examining the geochemistry and morphology on ancient tessera terrain (See Box 1), noble gas and light element isotopic abundances, and searching for evidence of a past magnetic field (**Figure B-4**).

The 5 platforms of VFM allow measurement of volatiles throughout the Venus system over space and time. The origin of Venus’s water will be addressed by measuring noble and trace gases and their isotopes, which must be measured by *in situ* measurements directly in the atmosphere. The rate of volcanism will be assessed via SAR and NIR imaging from the Orbiter, which will be aided by monitoring of the atmospheric variability over 60 days by the Aerobot and the Lander. Surface-atmosphere interactions will be constrained

by direct and simultaneous measurements of surface rocks and the atmosphere with which they are in contact. Volatile circulation will be constrained by measurement of the dynamics of the atmosphere within the clouds by the Aerobot and throughout the atmosphere by the Lander on descent. The two SmallSats carry instruments and are in orbits to best understand the complex loss mechanisms of volatile species at Venus, and can be put in context of magnetic field measurements by the Aerobot and three orbiting platforms.

VFM objectives explore the abundance, type, and movement of volatiles, the chemical sources and sinks between the surface and atmospheric reservoirs and constrain the loss at the top of the atmosphere. Such data are the basis for a new understanding of the present day Venus carbon, sulfur and water cycles. Noble gases, tessera geochemistry and geophysics measurements will constrain original and ancient volatile abundances. VFM data will add the essential story of Venus to bear on the major question of how terrestrial planets acquire and maintain their volatiles and thus their habitability.

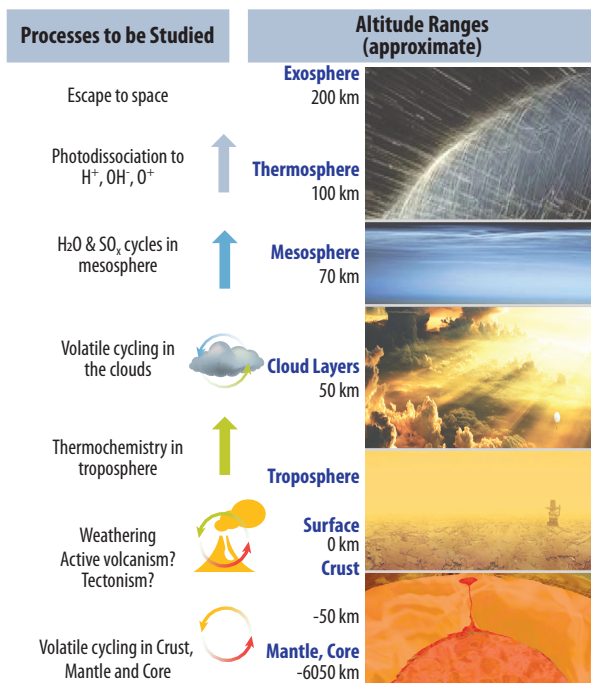
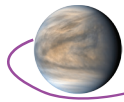


**Figure B-4.** Multiple VFM assets will interrogate the interrelated processes that control the movement of volatiles through the Venus system.



extend the mesospheric characterization started by Venus Express by using a limb-viewing **S-mm** to measure species including SO<sub>2</sub>, SO, SO<sub>3</sub>, OCS, CO, H<sub>2</sub>O, HDO, NO, HCl, HF. While the occultation techniques used by Venus Express could obtain typically one or two profiles per Earth day, the sub-mm limb sounding technique used by the VFM will return several profiles every minute; it will obtain complete pole-to-pole coverage in its comprehensive mapping. Combined with this instrument’s measurements of atmospheric temperature structure and wind fields, as will be described in the next section, these measurements will dramatically improve our understanding of the variability of trace species in the mesosphere and its causes.

**Investigation I.2.B – Determine transport mechanisms from the solid surface to the upper atmosphere.**

Following the measurement of composition—as discussed above in *Investigation I.2.A – Investigation I.2.B* focuses on measurements of atmospheric temperature structure, radiant fluxes and winds.

The atmospheric temperature profile determines how volatiles are transported through the atmosphere; it determines where convection can occur or where it is inhibited; it is inextricably linked with the atmospheric circulation. The temperature structure in the lower atmosphere is poorly known; temperature profiles from most Venera probes have large uncertainties, and those from the PV probes all stopped working at around 12 km altitude [Seiff et al., 1987]. Only one reliable temperature profile all the way to the surface is available, from the Vega 2 probe, and even that appears to show an unpredicted steep temperature gradient near the surface, which may indicate exotic fluid dynamical processes related to carbon dioxide’s supercritical nature at these high pressures [Lebonnois and Schubert, 2017]. Recent mesoscale atmospheric modelling has shown a surprisingly dynamic lower atmosphere, with upslope/downslope wind circulation patterns and convective updrafts reaching several kilometers high in some locations [Lebonnois et al., 2018]. These near-surface circulations will govern surface-atmosphere exchange and transport of volatile or aeolian materials into the atmosphere. The multiple assets of the VFM offers the ability to measure these interrelated processes over space and time (**Figure B-5**).

Instruments on the Lander will measure Venus’s atmospheric temperature profile from the cloud layer down to the surface using a range of complementary techniques in the **AS**, which consists of **temperature and pressure sensors and a radiometer**. The Aerobot **Meteorological suite (MET)** will obtain repeated temperature profiles during its vertical cycling between 52–62 km altitudes at all times of day and night and at a range of latitudes, and will study their relation to vertical winds, turbulence, radiative balance and composition. Additional vertical profiles covering the altitude range of 40–90 km will be obtained by **RO**; this vertical range includes the cloud layers and the tropopause. ROs between the Orbiter and SmallSats would allow vastly more occultations (and thus better coverage) to be obtained than relying solely on Orbiter-to-Earth communications; this is an option which should be investigated in greater detail in Phase A. Temperature profiles at 70–140 km will be measured from orbit using a **S-mm**; this range covers the turbulent and difficult to observe transition between retrograde zonal super-rotation in the mesosphere to subsolar-to-antisolar flow in the thermosphere.

The VFM will also measure up- and downwelling **solar and thermal radiant fluxes** in the atmosphere, as it is the balance of radiant fluxes in the atmosphere which drives atmospheric circulation. Multichannel **radiometers**, covering broad spectral bands from UV through to thermal infrared, are included in the **AS** on the Lander and the **MET** on the Aerobot, and on the long-life surface package, **LLISSE**. Convection in the lower- and middle-cloud layer is driven by radiant heating of the cloudbase from below, and radiative cooling of the cloud tops to space [e.g., Imamura et al.,

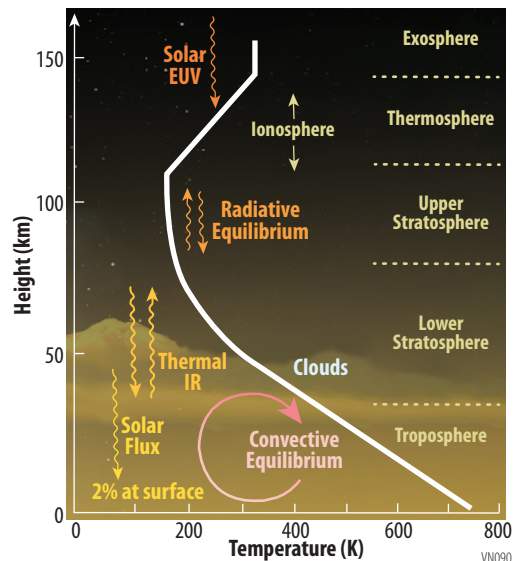
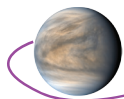


**Figure B-5.** VFM will measure the temperature structure and dynamics of the Venus atmosphere from the surface to the exosphere. After Taylor [2014].



2014]; there will be complex feedback between radiative fluxes, vertical winds and microphysics (cloud droplet growth and development) and chemistry. The Aerobot's radiance measurements will explore the radiative-convective-microphysical feedback associated with convective processes in the clouds. Radiance measurements throughout the Lander descent, using the same spectral bands, will enable the identification of particulate layers below the clouds and their effect on circulation. These will be complemented by solar and thermal flux measurements from LLISSE over 60 days to identify the radiative forcing of deep atmosphere circulation.

Instruments will also directly measure **wind velocities (MET)**. A vertical profile of horizontal winds in the lower atmosphere will be obtained by tracking the Lander during its descent; this will then be followed by a full diurnal cycle (60 days) of wind measurements at the surface by **LLISSE**. Winds in the cloud layer will be measured by tracking the Aerobot during its circumnavigations of the planet. This can be done both from Earth (as was done previously for the Vega balloons in 1985, but also from our own Orbiter and SmallSats, which provide the capability of position determination even when the Aerobot is on the side of Venus not visible from Earth. The Aerobot will carry a **3-D anemometer (MET)** to provide improved capability to disambiguate vertical motions due to buoyancy changes from those due to vertical winds, and to provide improved sensitivity to turbulence and atmospheric waves. Winds in the upper atmosphere have been previously determined indirectly from temperature structure using the thermal wind equation [e.g., Mendonca et al., 2012]; we will directly measure line-of-sight winds in the upper atmosphere using the **S-mm**. From its polar orbit, the **S-mm** sounder will alternate between an orbit of along-track limb viewing, to enable it to map meridional (north-south) wind velocities, and across-track limb viewing, which enables zonal (east-west) velocity mapping. The velocity measurements will cover an altitude range of 70–140 km, allowing measurement of transport of volatile materials from the cloud tops up through the mesosphere-thermosphere boundary at 100 km altitude as discussed above.

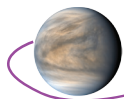
Taken together, this suite of measurements of temperature structure, radiative fluxes and wind velocities, collocated with composition measurements, will provide a detailed set of measurements constraining the transport of volatile materials from surface to space.

### **Objective I.3: Place constraints on whether there are habitable environments on Venus today and search for organic materials and biosignatures.**

#### ***Investigation I.3.A – Assess the present-day habitability of the Venus cloud environment***

With its Earth-like temperatures, abundant sunlight, and water-containing cloud droplets, Venus's cloud-level environment is one of the most benign environments for life to be found in the solar system. Water makes up only 5%–25% of the cloud droplet composition, with much of the rest composed of sulfuric acid. However, there is also ample evidence for further cloud constituents: an as-yet-unidentified substance absorbs UV-blue light in the upper clouds; Soviet XFS results from four different entry probes showing iron, chlorine and phosphorus in the lower clouds; particulates have been detected below the cloudbase at temperatures above the boiling temperature of sulfuric acid [see review in Titov et al., 2018].

The Aerobot instruments will characterize the habitability of this environment in four ways. Firstly, they will undertake a detailed compositional analysis, using an **AMS-N**, equipped with an aerodynamic lens allowing cloud/particulate composition and gas composition to be measured independently. This will identify the abundances and molecular forms of the key astrobiological elements C, H, N, O, P, and S, as well as further elements, such as metals and halogens, which may have been brought to the cloud layer by processes such as volcanism, aeolian processes, or meteoritic infall. Secondly, the physical environment of cloud droplets will be characterized using **nephelometry**; the optical interrogation of cloud and aerosol particles to measure their size distribution and their shape (spherical for liquid droplets or jagged for crystalline or fractal solid particulates). This will allow the longevity of individual droplets—potentially individual habitable sites—to be assessed. Thirdly, availability and variability of UV and visible radiation—potential sources of energy—will be characterized by the radiometers in the MET. Finally, the **MET** will include a dosimeter to verify model predictions of ionizing radiation fluxes in the cloud layer. The 52–62 km altitude range to be explored by the VFM Aerobot corresponds to atmospheric temperatures of  $-20^{\circ}$  to  $+60^{\circ}\text{C}$  and so includes all biologically relevant temperatures



### Box 3. The Search for Life on Venus

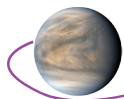
Morowitz and Sagan [1967] were the first to recognize that the characteristics of the Venus clouds:  $-20^{\circ}$  to  $+60^{\circ}\text{C}$ ,  $\sim 1$  atm pressure, and the presence of  $\text{CO}_2$ ,  $\text{N}_2$ , and  $\text{H}_2\text{O}$  are compatible with photosynthetic organisms and hypothesized that such organisms may have evolved on the surface of Venus during a more clement epoch. They then could have been lofted upwards by winds and might persist still in the refugium of the cloud deck given its density and inferred vigorous dynamical properties. Furthermore, they speculated that such life could be the cause of the UV absorption in clouds. Versions of this set of interrelated ideas has been explored many times over the intervening decades [e.g., Dartnell et al 2015, Grinspoon 1997], and most recently by Limaye et al. [2018] who pointed out that the spectral signature of some common bacteria are consistent with Venus UV spectra and presented three lines of support for the Venus cloud deck hypothesis. First, terrestrial bacteria have been widely recognized for more than 100 years that exist in S-rich, low pH, and high-radiation environments (e.g., Waksman and Joffe [1922], Anderson et al. [1956], Wasmund et al. [2017]); secondly, lofted microbes are observed to survive in the clouds of Earth for extended periods of time (e.g., Smith [2013], Pepper and Dowd, [2009]; Delort and Amato, [2017]), and thirdly, atmospheric gravity waves, discovered by Akatsuki [Fukuhara et al. 2017], may be one of several large scale vertical transport mechanisms available to effectively send surface particles aloft including trace metals and minerals useful to life biochemistry as we understand it. On Earth, sulfur is one of the biogeochemical cycles to be vitally dependent upon microorganism activities [Klotz et al 2011] and has been suggested as part of the earliest metabolisms at the dawn of life (cf. Wächtershäuser [1988, 2007]; Canfield and Raiswell, [1999]; Canfield et al. [2006]) and for which there are ancient indicators in the rock record [Wacey et al 2011].

**The hypothesis that Venus may host extant life can be tested only by extended observations within the Venus clouds.** Adequate time to detect potentially very low concentrations of organisms or fragments in a gas “ocean” is paramount to optimizing the life detection effort. The VFM Aerobot is designed to make a suite of environmental measurements that bear directly on the life hypothesis including the chemistry of the atmosphere (nutrient availability or potential toxicity), the nature and shape of cloud particles (droplets as host for liquids and/life [Seager et al., 2020], temperature, pressure, radiance and radiation environment, and wind movement, strength and variability (residence times of particles). A Fluorimetric microscope, also in consideration for life detection on icy moons, will recognize live or dead cells, the presence of fluorescent photosynthetic pigments (the most likely mode of nutrition of a hypothetical Venus cloud biosphere), and other fluorescent particles of interest like certain minerals. The VFM aerobot will collect these data over the course of 60 days over half of the globe at variable altitudes and times of day. This platform uniquely addresses one of the major strategic objectives of the Planetary Science Division and NASA, to determine the potential for life elsewhere. We must add Venus to the membership of solar system worlds that may yet host extant life, and we are compelled to investigate.

while the Aerobot’s planet-encircling trajectory enables characterization of habitability at all times of day and at a range of latitudes.

#### ***Investigation I.3.B* – Detect any extant or recently dead organisms or fragments present in the clouds**

It has long been known that the Venus clouds exhibit absorption in the blue-UV spectral range, at 320–400 nm wavelength [e.g., Pollack et al., 1980; Krasnopolsky, 2006; Perez-Hoyos et al., 2018], but the chemical identity of this “**unknown UV absorber**” still eludes us, with possible candidate materials including  $\text{FeCl}_3$ ,  $\text{S}_x$ , or many other possible materials. As was discussed above in **Section I.2.A**, the instruments aboard the Aerobot will measure cloud particle composition and measure size (**AMS-N**), shape and refractive index of cloud particles (**Neph**), and a net flux radiometer in the **MET** will measure local UV absorption. These simultaneous measurements, carried out during a 60-day lifetime at a range of altitudes and latitudes over all times of day, are likely to be able to identify the chemical composition of the UV absorber. The **Fluorimetric Microscope (FM)** carried by the Aerobot complements this investigation by specifically examining the possibility that the UV absorption is due to a biological source [Limaye et al., 2018] or fluorescence from disulfur dioxide [OSSO; Wu et al., 2018].



Using the **FM** capability will elucidate whether there is any merit to some type of biological interpretation or whether we must focus on unusual or unique chemistry to explain the presence of the UV-absorber. Lofted fluorescent mineral micro-grains deriving from the Venus surface could conceivably be a source of the UV absorbance and would be a valuable non-biological indicator of surface-atmosphere interactions that may be occurring, or a signal of meteoritic infall with some residence time in the cloud decks. Both mineral, fluid aerosol, and biological sources of this UV absorbance phenomenon are amenable to analysis with the **FM** and the **AMS-N** instruments.

The use of the **FM** builds on the idea that photosynthesis is the most likely energy-providing mechanism for a venusian cloud biosphere [Morowitz and Sagan, 1967] and that on Earth photosynthetic light-trapping pigments are commonly inherently fluorescent. Intrinsic fluorescence is widespread in biological materials, critically including pigments mentioned, and can be measured in the atmosphere and clouds on Earth [Rost et al., 1992, Hill et al., 1999, Delort et al., 2010]. In the venusian clouds, the potential for detection of extant organisms, or fragments of such organisms, depends upon direct measurement of fluorescence of aerosol particles in the range of naturally fluorescing biomolecules. Biological materials should display excitation wavelengths ranging from blue to deep UV (< 250nm), and an emissions peak between 270–400nm [Bhartia et al., 2008, 2010; Mazel & Fuchs, 2003]. Such fluorescence must be distinguished from any naturally fluorescent mineral particles that might be aloft in the cloud decks using a combination of the fluorescence measurements with an analysis of particle size and shape provided by the **FM**, which will image cloud particles collected by drawing ambient air through a series of size-sorting, collecting filters. The in-line filter-set captures successively smaller particle sizes on 10, 1.0, and 0.2  $\mu\text{m}$  pore-size filters for sample imaging by the microscope. In Earth's clouds, organisms can be found in small clusters adhered to dust grains and in aerosol droplets [Failor et al., 2017; Pereira et al., 2017]. This is a more likely presentation than unattached individual organisms; thus the size of object being interrogated will be closer to the tens of micrometer range than typical sizes of individual Earth microorganisms ( $\sim 0.5\text{--}20 \mu\text{m}$ ).

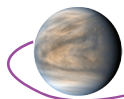
## **Goal II. Understand the composition and climatological history of the surface of Venus and the present-day couplings between the surface and atmosphere.**

### **Objective II.1: Constrain the composition of the surface and chemical markers of past and present climate.**

#### ***Investigation II.1.A* – Determine global mineralogy to distinguish major rock types and weathering regimes.**

Orbital measurements of NIR radiance (and derived emissivity) from the venusian surface show distinct spectral signatures that correlate with specific terrains and landforms. The tesserae were observed by Galileo NIMS and VEx VIRTIS to have a lower emissivity than the plains, which has been interpreted to indicate rocks in the region have a lower ferrous iron content [Hashimoto et al., 2008; Mueller et al., 2008; Gilmore et al., 2015]. Several volcanoes have been observed to have higher emissivity than surrounding plains suggesting they have greater ferrous iron (in silicates) and are thus less weathered than the surrounding plains where  $\text{Fe}^{2+}$  is predicted to convert to  $\text{Fe}^{3+}$  in oxides [Smrekar et al., 2010]. With the help of high-temperature emissivity spectral libraries in development [Helbert et al., 2017], these variations in radiance can be tied to specific mineralogy of surface rocks on Venus. These differences imply either different modes of magmatism and volcanism over time, different climate regimes and/or differences in surface age. Improved spatial resolution (10–30 m) targeted **SAR** imagery, global multispectral measurement of NIR radiance (**NIR-I**) (limited by atmospheric scattering to  $\sim 50$  km resolution), both on the Orbiter, and pairing of orbital observations with chemical measurements at the surface will allow better definition of volcanic units, possibly identification of sedimentary rock types, and classification and distribution of weathering products. By correlating compositional data with geographic location and indicators of relative age, we can understand how these rocks and minerals are distributed over time. These data will give insight into the flux history of volcanic volatiles to the atmosphere, cycling of volatiles between the interior, crust, and atmosphere, and changes in global weathering, all of which influence global climate.

This mission offers the unique capability of using data from the Lander to better interpret and provide simultaneous ground truth measurements for surface emissivity observations from orbit. The **DI**



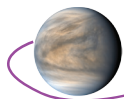
will observe the landing site below the bulk of the atmosphere at  $\sim 1 \mu\text{m}$  to assist in atmospheric correction and calibration of the data collected from orbit. The Lander will also collect surface mineralogy data using **XRD** of ingested samples and **Raman** interrogation of multiple, weathered surfaces. The **PC** will observe surface emissivity at 5 wavelengths to allow direct comparison between spectral radiance and mineralogy. For example, the kinetics of weathering of venusian basalts is poorly constrained and leaves us to guess at what the weathering products are and the thickness of these products with time. This question can be addressed directly by comparison of the **R-LIBS** data to the mineralogy of ingested, fresher, samples. The 7 hour lifetime on the surface will provide an opportunity to “drill” surfaces with the **LIBS** instrument, where repeated interrogation of a single target with the **LIBS** laser will probe deeper layers of the surface with each laser pulse, a technique that has been used on Mars [e.g., Wiens et al., 2013]. These Lander data will allow critical tests of our interpretation of the global NIR datasets which can be extrapolated across the planet. The measurement of global mineralogy has revolutionized our understanding of the other solar system bodies and will be a fundamental and unprecedented measurement for Venus.

### ***Investigation II.1.B*** – Determine the oxidation state, chemistry and mineralogy of rocks in contact with the atmosphere.

A planet’s surface and atmosphere influence each other through the chemical reactions that take place at their interface. The conditions of climate determine what minerals are stable on the planet’s surface, and through global weathering reactions that cause changes in atmospheric chemistry, minerals can change the climate. For this reason, weathering reaction products can be used as indicators of past climate conditions, as has been done on Earth and Mars. Modern weathering reactions are critical to understand in order to assess current volatile cycling and reservoirs, as well as to interpret modifications to the ancient rock record by the modern climate, for example, potential overprinting of a new weathering signature on top of one from a past climate regime.

Weathering of the surface on modern Venus takes place in the presence of a hot, almost waterless, supercritical fluid, which is one of the most unique weathering regimes in our solar system. Numerous reactions between minerals and venusian atmospheric gases have been proposed based on thermodynamic modeling and experimental studies, such as carbonation, oxidation, and sulfurization (summarized in Zolotov [2018]), but a major barrier to our understanding of these reactions as possible climate feedbacks on Venus is our lack of data from the surface and near-surface environment. Almost all parameters required to accurately model weathering are poorly constrained for the venusian surface: near-surface atmospheric chemistry, detailed composition of common rock types, and composition of weathering products (e.g., discussions in Zolotov, [2018]; Treiman, [2007]). By measuring the mineralogy and composition of the surface, we will be able to infer the mineral-atmosphere reactions currently active on Venus. This will also allow recognition of weathering caused by past climate conditions, as these products will differ from the secondary minerals currently forming on the surface.

The Lander will conduct measurements of secondary minerals using the mineralogy and chemistry instruments **R-LIBS**, **XRD**, and **XFS**. These data will reveal which of the several proposed surface-atmosphere reactions are currently occurring on Venus, and which ones dominate the weathering cycle. Descent and surface imaging from the **DI** and **R-LIBS context imager** will also help constrain the extent of weathering in the crust by examining thickness and porosity of weathering rinds. Measurements of secondary minerals produced by weathering will be conducted primarily using a **R-LIBS** housed inside the Lander vessel looking out of a window in the lower side of the vessel. This instrument will autonomously scan its view area to measure materials outside the Lander. The **R-LIBS** is uniquely suited to probe surface chemistry and mineralogy as both techniques have shallow interaction depths. The remote nature of this method also means the **R-LIBS** is only restricted by time in the number of materials it can analyze (as compared to methods reliant on sample delivery through a finite number of sampling cups), so it has the ability to probe 10s and perhaps 100s of targets within view outside the Lander (e.g., soils, dust, rock surfaces) although not at a great depth. The drill system, however, is designed to bring powdered samples from three depth ranges up to  $\sim 5$  cm into the Lander for analysis by the **XFS** and **XRD**. Depending on the thickness of weathering rinds present on the surface, these instruments may also be able to provide information on the weathered surface layers. All of these techniques will provide data on the chemistry (**XFS**, **LIBS**) and mineralogy (**XRD**, **Raman**)



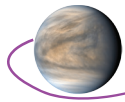
of the rocks and subsurface materials. This combination of approaches is able to address either a thin or thick weathering rind because of their different ranges of depth profiling. It is not known how thick weathering rinds are on tessera rocks, and the small analytical point of the **LIBS** will allow for detection of very thin rinds that the other methods may miss due to their coarser sampling. Rapid succession of **LIBS** points also allow for finer scale depth profiling than the drill system to look at chemical gradients in the outer rock layers caused by weathering but may not get through the weathering rind..

These chemical and mineralogical measurements, combined with simultaneous measurements of the near surface atmosphere, pressure, and temperature, will constrain the weathering regime currently operating in the tessera, revealing insights about chemical exchanges between the surface and atmosphere. The oxidation state of the near surface environment can also be determined by these measurements based on which secondary minerals are present (e.g., hematite vs magnetite). Additional detail on oxidation state may potentially be gleaned from lattice parameter refinement using the **XRD** should the current weathering layer be thick enough to be able to be sampled by this technique. **The oxidation state of surface materials is also relevant to interpreting the orbital NIR data** (discussed in previous section) and identifying the possible magnetic phases present in the crust (*Investigation I.I.E*). The sampling drill and **LIBS** will also be able to constrain weathering extent and depth through profiling into the rock surfaces. This will be aided by surface imaging from the **R-LIBS context images**, **PC** images, and **DI** images of the ground around the lander, which can examine porosity and lateral extent of weathering. The measurement requirements for these instruments are given in the **STM**, while instrument performance for our strawman payload is given in **Table B-1** and **Table B-2**. The VFM chose mineral detection limits that are needed to measure small quantities of minerals on the surface in anticipation of thin weathering rinds, however these detection limits could be modified if results from experimental studies on venusian weathering products and processes determined the need for different limits.

### ***Investigation II.1.C* – Determine the near surface atmospheric environment to constrain surface-atmosphere exchange and buffering.**

Venus atmospheric chemistry is maintained in part through surface-atmosphere chemical buffering reactions which are as yet unidentified. Buffer systems have been proposed (e.g., calcite-anhydrite and pyrite-magnetite) but there is little observational constraint on the solid-surface or near-surface atmospheric composition to separate these claims (discussion in Zolotov 2018). To constrain the reactions and exchanges between the solid-surface and the atmosphere, measurements of both solids and gases must be undertaken. The previous two investigations under this objective serve to constrain both the local solid-surface near the Lander, as well as constrain the mineralogy of the global surface. The global data will show if the surface-atmosphere reactions seen at the landing site are representative of conditions across the planet, or if other lithologies or secondary minerals are present elsewhere, leading to alternate weathering reactions. These surface solids analyses serve to identify possible minerals available to buffer atmospheric gases, and to identify the signature of the current Venus climate in the geologic record. However, it is important to also understand what aspects of the current climate are responsible for these reactions, and for that the near surface atmosphere composition, pressure, and temperature must also be measured.

Meteorological conditions at the Venus surface, which mediate any atmospheric weathering interactions, are very poorly understood. The only prior measurements of the near surface atmosphere were provided by the Venera landers for periods of up to two hours, and these measurements did not have sufficient resolution in their chemical measurements to elucidate important parameters such as the oxygen fugacity of the atmosphere. Thus current calculations of the atmospheric oxygen fugacity fall within the error of the magnetite-hematite stability boundary, and it is not clear which minerals are stable at the surface of Venus [Zolotov 2018]. Many other potential mineral buffer reactions depend on the fugacity of minor gas species to determine which way the reaction progresses. VFM will determine these atmospheric parameters using the Lander **NMS** during descent **and on the surface**, the **AS**, and **LLISSE**. During Lander descent, the **NMS** and **AS** will provide a profile through the atmosphere of the chemical species present as well as the pressure and temperature. These data relate to the transport and cycling of gas to the near surface environment, and how the gas products of reactions may affect the atmosphere as a whole. Once landed, the **NMS** will sample the near surface atmosphere to monitor



chemical species present during the Lander lifetime. Such data will provide needed constraints on gas abundances and speciation of the atmospheric layer in contact with the surface. Starting at the time of landing, **LLISSE** will provide data for 60 days on the concentration of a selection of important gas species (e.g., SO<sub>2</sub>, CO, O<sub>2</sub>) using chemical sensors [Hunter et al., 2006], as well as atmospheric pressure and temperature. This will be the longest duration measurement of the near-surface atmosphere of Venus, and will capture a day/night cycle on Venus, providing information on any changes during that transition. The long lifetime of **LLISSE** will provide insight into how stable the near surface atmosphere layer is over time, since variation in this layer can influence which surface-atmosphere reactions are taking place.

### **Goal III. Understand the geologic history of Venus and whether Venus is active today.**

#### **Objective III.1: Determine if Venus shows evidence of a current or past plate tectonic regime.**

##### **Investigation III.1.A – Constrain composition, thermal state and structure of the interior.**

Our knowledge of the formation, evolution and structure of the terrestrial planets (including Earth) and exoplanets is currently impeded by our very limited understanding of Venus. Currently the size and state of the core are unknown. **Geodetic measurements by the Orbiter using LOS tracking** will provide constraints on crust, mantle and core structure. Measurement of the spin and librations of Venus will constrain the first-order structural units of Venus as has been done recently at Mercury [Genova et al., 2019]. Improved **gravity mapping** is essential to identify anomalies related to changes in density that are a product of the composition, thermal state and structure of the lithosphere. These data are fundamental to our understanding of whether Venus and Earth have similar compositions, the origin and maintenance of magnetic fields, the rheology of the mantle, core and crust, heat flow and the state of the lithosphere.

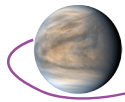
A critical element of distinguishing between various hypotheses for Venus's geodynamic history, which are in turn tied to habitability scenarios, is understanding how surface topography relates to conditions in the crust and upper mantle. For example, if areas of widespread felsic crust are identified, are they all isostatically supported, and did they form on a thick or thin elastic lithosphere? A particularly important component of evaluating surface-subsurface relationships on Venus is studying the wavelength-dependent relationship between gravity and topography for features on spatial scales of a few hundred kilometers, as this enables assessing elastic lithospheric thicknesses of several km to tens of kilometers, which in turn provide critical constraints on crust and upper mantle thermal structure. In the absence of improved global topography as proposed by the VERITAS mission, VFM gravity measurements can be combined with Magellan topography to investigate these questions.

While the long-wavelength topography from Magellan is mostly adequate for these assessments [Rappaport et al., 1999], the mostly Magellan-derived gravity field varies from a few hundred to several hundred kilometers in spatial resolution, with poorest resolution in the southern hemisphere over longitudes corresponding to many of the important chasmata regions [Konopoliv and Sjogren, 1996]. To first order, for line-of-sight gravity data (collected during data transmission to Earth) the spatial resolution is determined by the altitude of the spacecraft. One example gravity field, derived from the combination of gravity data from numerous Venus missions, is considered accurate up to degree and order 70, which corresponds to a spatial resolution of ~270 km [James et al., 2013]. From a long-duration circular orbit of 300 km, the VFM mission will be able to improve the global gravity field globally to approximately degree and order 100, which will correspond to a spatial resolution of ~200 km and an error of a few mGal. To complement the gravity data the **Mag** aboard the Aerobot will acquire aerial magnetic field surveys over major terrains from equator to pole to constrain the presence, spatial distribution and intensity of potential magnetic sources.

##### **Investigation III.1.B - Characterize tectonic features & establish stratigraphic relationships**

Magellan imaging and topography was sufficient to show that Venus does not currently have an organized system of plate tectonics [Solomon et al., 1992]. However, unlike the moon, Mars, and Mercury, there is clear evidence of horizontal movement of crustal material [Solomon et al., 1992] and perhaps subduction [Davaille et al, 2017]. Venus has linear mountain ranges, transform faults, and other de-





formational features that require up to tens of kilometers of relative displacement. There is a diversity of geomorphic terrains on Venus, and it is unclear whether or not some of these terrains, especially tessera, are formed by geologic processes today or whether they are from a bygone era of a different geodynamic regime [e.g., Basilevsky and Head, 1998; Hansen and Young, 2007]. While the organization of geologic features on the surface is distinctly nonrandom, the overall spatial distribution of impact craters, which are used to date surfaces and time stratigraphic markers, by itself is nearly indistinguishable from random [Phillips et al., 1992]. Almost all of the craters that have been identified are nearly circular, indicating minimal deformation, but there is clear evidence that the vast majority have experienced at least partial filling by later volcanism [Herrick and Rumpf, 2011]. A variety of big-picture explanations have been developed to explain the crater distribution observations [e.g., Turcotte, 1993; Solomatov and Moresi, 1996; Basilevsky and Head 1998; Phillips and Hansen 1998; Guest and Stofan 1999; Turcotte et al., 1999; Hansen and Young, 2007; Romeo and Turcotte, 2008]. Some explanations require significant changes with time in the geodynamic regime controlling mantle and lithospheric behavior (e.g., plate tectonics to stagnant lid convection), but other, more steady-state, explanations can also be made congruent with the current state of knowledge. Of the explanations that involve a major change in the planet's surface-interior interaction, some also cause a dramatic change in the atmosphere and surface habitability [e.g., Bullock and Grinspoon, 2001; Way and Del Genio, 2020].

Distinguishing between these big-picture ideas requires **nested SAR imaging** (a small area at 10 m resolution surrounded by a much larger area at 30 m resolution) of a few percent of the planet that contains critical terrains and geologic contacts. Such data will allow the **detection, classification and stratigraphic position of tectonic and volcanic structures** that are not interpretable in the Magellan data (Figure B-6), and are critical to understanding the evolution of tesserae, for which we have no

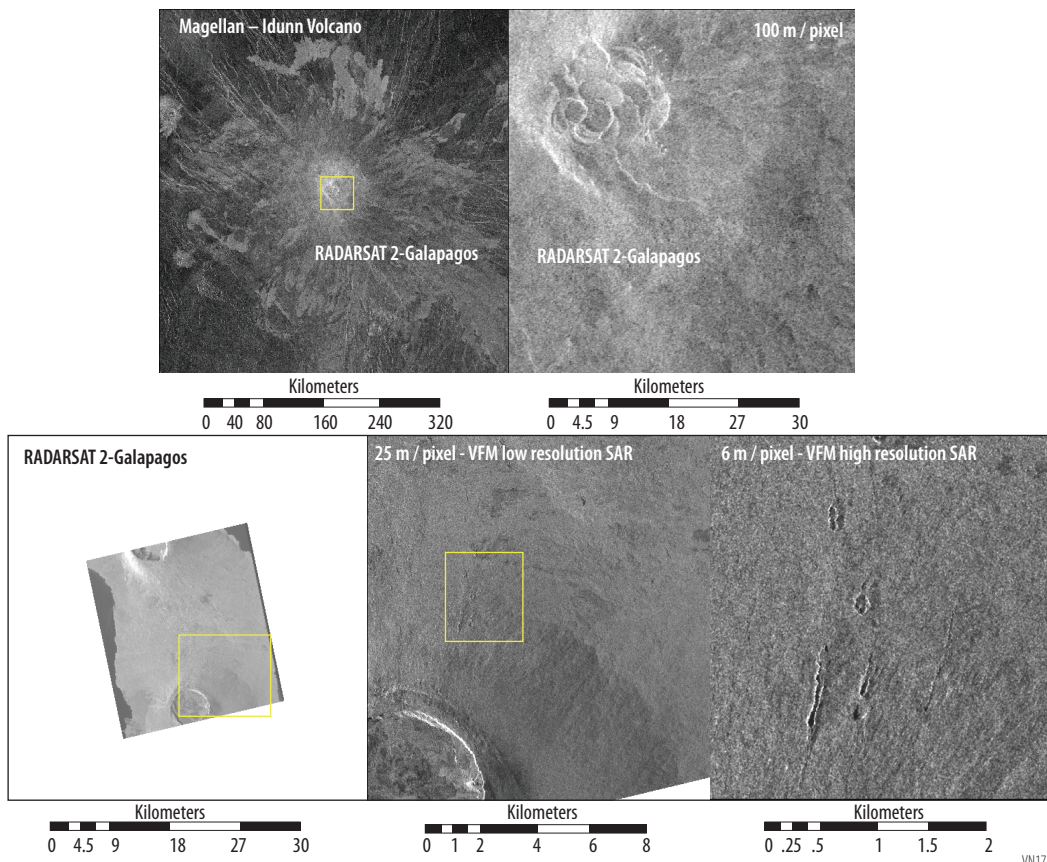
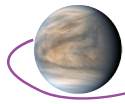


**Figure B-6.** The top panel shows the venusian volcano Idunn, and to the right, the next image shows the caldera region at full Magellan resolution. The bottom row of images are RADARSAT SAR data terrestrial analog from the Galapagos at Magellan resolution, and illustrates the critical details that can be observed with higher resolution imagery. At 25 m resolution (bottom center image), radial vents indicative of the local stress regime of the volcano are evident. At 6 m resolution (bottom right image), spatter cones indicative of pyroclastic activity are visible. Modified from Herrick et al. [2009].



clear analogue on Earth. Establishing the relative timing of tectonic deformation and deposition of different geomorphological units at these key locations will constrain formation mechanisms for the tesserae (i.e., uplift via primarily volcanic vs tectonic processes) and whether or not the style of deformation or volcanism has changed with time.

### ***Investigation III.1.C. – Look for evidence of crustal recycling***

The topography of Venus as revealed by Magellan shows no obvious global system of plate boundaries (spreading centers, subduction zones) that are the hallmark of plate tectonics on Earth. The current perceived lack of plate tectonics on Venus is generally ascribed to two related causes [e.g., Phillips et al., 1991]. First, the higher surface temperature on Venus compared to Earth makes it less likely that the lithosphere will become denser than the underlying convecting mantle, and thus subduction would be inhibited. Second, if the crust and upper mantle are also dry, a relatively inviscid layer, called the asthenosphere on Earth, does not exist to serve as a bottom lubricant to enable rigid surface plates to move semi-independently of underlying mantle convection. The lack of asthenosphere is suggested by the geoid to topography ratio at hotspots on Venus [Smrekar and Phillips, 1991], although it is unclear if this can be extrapolated to the rest of the lithosphere and does not consider the effect of large errors associated with current crustal thickness estimates [Smrekar et al., 2018]. Elkins-Tanton et al. [2007] argue that a fertile mantle may retain its water over geologic time and participate in some manner of crustal recycling via delamination events. The annuli of some large coronae have trenches similar to terrestrial subduction zones and have been modeled to form via plume-initiated subduction [Davaille et al., 2017]. Observing either structural or chemical indicators of plate tectonics would thus suggest a past with a lower surface temperature and a recycling mechanism to reintroduce water in the lithosphere and uppermost mantle. Structurally, such evidence comes from geologic processes that can only be associated with plate-tectonics, or at least a highly mobile crust. This would include formerly connected terrains now separated by hundreds of kilometers, and/or a lack of continuity of terrains across the venusian features identified in Magellan as resembling Earth's subduction trenches. Large expanses of felsic rock in the continents of Earth are formed in association with subduction that introduces excess water into the Earth's interior to lower mantle melting temperatures.

Thus, identifying evidence of crust recycling includes chemical (**XFS**, **LIBS**, **GRS**) and mineralogical data (**XRD**, **Raman**) obtained by the Lander on tessera terrain that will identify rock type at the landing site. These data and the **DI** frames serve as ground truth for global NIR radiance (**NIR-I**) with enough fidelity to distinguish between felsic and mafic rocks across the planet. If large regions of felsic rock exist, this would provide compelling evidence of past crustal recycling in the presence of water. Additionally, **nested SAR imaging** (30 and 10 m) of selected locales on Venus can assess structural movements and offsets on opposite sides of possible spreading ridges, transform faults, and subduction zones. This can constrain the style and state of and lithospheric motions today.

### ***Objective III.2 – Determine whether Venus is tectonically and volcanically active today.***

#### ***Investigation III.2.A – Look for present day seismicity.***

Venus quakes will produce strong infrasonic signals that can be detected as pressure waves at altitudes in the Venus atmosphere where long duration observations are possible with existing technology [KISS, 2015]. Infrasonic pressure signals emanate either directly above the epicenter of a seismic event or from surface motions excited by the Rayleigh wave that radiates from the epicenter. A barometer (**MET**) deployed on the Aerobot gondola can identify pressure variations resulting from an upwardly propagating Rayleigh wave from the surface as demonstrated on Earth [Krishnamoorthy et al., 2018b; Martire et al., 2018]. The platform would circumnavigate Venus every few days, potentially enabling detection of Venus quakes of magnitude  $\geq 3$ .

Measuring the seismic properties would provide crucial information to constraining Venus's interior dynamics and past evolution. However, the extremely harsh surface temperature and pressure conditions pose serious technical challenges by preventing the use of traditional long-duration seismic techniques to examine the planet's interior from the surface [e.g., Cutts et al., 2015]. Analogous to Earth, venusian seismic events are expected to generate infrasound waves (pressure waves with frequency  $< 20$  Hz) that couple with the planet's atmosphere via wave dynamics, thus providing a remote-sensing approach to understand the planet's interior processes. However, on Venus, the dense

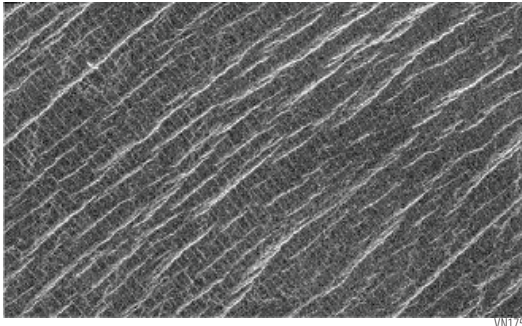
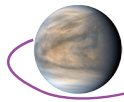


**Figure B-7.** Ridges and cracks of the Lakshmi plains. Radar image of a region within the Lakshmi Plains on Venus. This region has been fractured by tectonic activity to produce a cross-hatched grid of cracks and ridges (brightness of the ridges indicates their relative height). This image shows a region about 80 kilometers wide and 37 kilometers high. (credit: modification of work by Magellan Team, JPL, NASA).

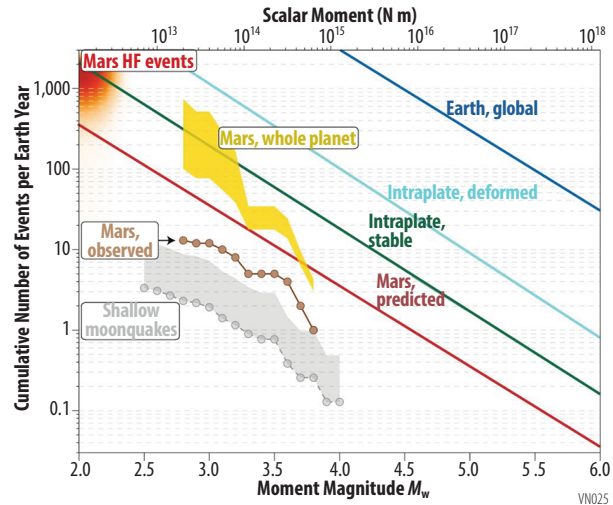


**Figure B-8.** Predicted vs. measured Marsquakes vs. seismicity on the Moon and Earth (from Banerdt et al. [2020]). The range of Venus seismicity is predicted to be similar to intraplate deformation on Earth [Krishnamoorthy et al., 2020].

atmosphere means that the coupling of seismic waves into the atmosphere is approximately 60x more efficient than Earth. The morphology of the structural features as well as the youthfulness of the planet's surface testify to the potential for seismic activity. Evidence of recent volcanism [Smrekar et al., 2010] and that the crust of Venus has experienced stress, causing stress release expressed in a wide range of structural features (**Figure B-7**), point to specific targets of present day seismicity on Venus. Estimated levels of seismicity on Venus suggest that they fall between that of Mars and Earth [e.g., Lognonné and Johnson, 2007; Lorenz and Panning, 2018; Giardini et al., 2020] (**Figure B-8**). Stress relief in the form of volcanic sources contribute to detectable surface deformation and explosive eruptions [e.g., Fee et al., 2013; Johnson et al., 2004]. Using multiple approaches (e.g., seismic waveform analysis, moment tensor inversion, and infrasound simulation) the 2018 Kilauea summit/Lower East Rift Zone eruption/deformation activity was analyzed. Interpretations point to a connected magmatic plumbing system from the summit caldera to the lower rift zone [Lai et al., 2019]. Venus has 100s of Kilauea analogs [McGovern et al., 2013] that could potentially be active.

There are competing conditions on Venus that will influence the likelihood of stress release in the deeper parts of the planet. On one hand, if Venus's interior is dry, a larger fraction of seismic energy release could be expected; on the other hand, higher temperatures could limit the magnitude of stress release events, rendering them aseismic. Potential sources of deep seismicity are regions of crustal thickening [e.g., Li et al., 2018; Zhan and Kanamori, 2016], subduction, and lithospheric dripping. Hydrated minerals could be retained in Venus's interior during subduction or lithospheric delamination/dripping events, thus, influencing processes related to plate dynamics on planetary bodies [e.g., Elkins-Tanton et al., 2007; Perez et al., 2020]. Transformational faulting, in which a metastable nominally anhydrous mineral, such as olivine, transforms into a denser phase could trigger instability by strain localization and stress concentration in the upper mantle [e.g., Shen and Zhan, 2020], and cause deep-focus earthquakes.

*Seismic wave propagation into Venus's atmosphere.* For many decades it has been recognized that Earth's atmosphere dynamics are affected by interactions with solid Earth [e.g., Wolcott et al., 1984]. Volcanic eruptions inject clouds of ash into the stratosphere with climate-modifying effects. Earthquakes also produce atmospheric disturbances. Ground motion near the epicenter of an earthquake produces a broad spectral range of infrasonic waves propagating upward. Far from the epicenter, long-period Rayleigh surface waves couple at the surface to create atmospheric gravito-acoustic waves propagating upward in the atmosphere [e.g., Lognonné et al., 2006; Occhipinti et al., 2011; Hickey et al., 2009].

Modeling surface-atmosphere coupling during seismic events and propagation of infrasound waves incorporates state-of-the-art Global Circulation Model outputs for Venus's atmospheric conditions

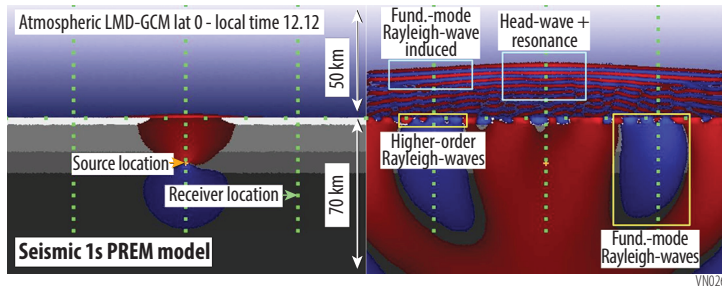
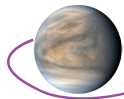


**Figure B-9.** Simulated seismically-induced acoustic waves in Venus's atmosphere. Normalized vertical velocity perturbations for a Gaussian isotropic source (depth 20 km - period 0.1 s) after 12.5 s (left) and 62.5 s (right); Left: Variations in P-wave velocity (blue shades), S-wave velocity (gray shades); Right: positive (red) and negative (blue) amplitudes. Above the epicenter, one observes a head wave followed by reflected seismic waves. On both sides of the epicenter, the higher-order Rayleigh-wave modes generate quasi-plane acoustic waves. (credits: Q. Brissaud and J.M. Jackson, Caltech).

and Earth-based estimates on seismic sources [e.g., Brissaud et al., 2017]. The modeling includes attenuation processes and has the potential to resolve the propagation of seismically-induced acoustic and gravity waves in a visco-elastic medium coupled to a compressible fluid (**Figure B-9**), although uncertainties remain. Analogue experiments on Earth point toward the feasibility of such measurements on a balloon-based platform floating in Venus's atmosphere [e.g., Krishnamoorthy et al., 2018a, 2018b, 2019; Martire et al., 2018]. The suite of instruments and measurements on the Aerobot to identify quakes are the atmospheric temperature sensor, a barometer to measure absolute atmospheric pressure, a differential pressure

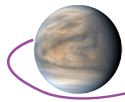
sensor for detecting infrasound, a 3-D sonic anemometer to measure wind velocity and turbulence relative to the balloon, and an inertial measurement unit to filter motion-induced noise.

*Synergy of seismicity detection with surface mineralogy, near-surface atmosphere composition, gravity, and topography.* Assessing the mineralogy/petrology and gas composition data acquired by the Lander instruments provides a way to identify (and potentially provide an age estimate for) recent seismicity from volcanism. Limited data on surface composition, lower atmospheric chemistry, and weathering on Venus, combined with the challenges of conducting experiments under Venus conditions, have resulted in a dearth of much needed experimental constraints on surface-atmosphere chemical interactions [e.g., Filiberto et al., 2020; Gillman et al., 2020; Semprich et al., 2020]. For example, experimental studies of the mixing of CO<sub>2</sub> and N<sub>2</sub> under conditions found at the surface of Venus suggest that extrinsic processes (e.g., volcanism) are likely required to explain the compositional vertical gradient deduced from the Vega-2 temperature profiles [Lebonnois et al., 2020]. Thus, seismically-detected signals on the balloon could be corroborated by compositional measurements of gas and particle variability in the clouds (**AMS-N, FM**) and/or near-surface atmosphere gas concentrations (**LLISSE**). Constraints on the thickness of the seismogenic layer can come from the gravity data from the orbiter combined with other topographic data [e.g., James et al., 2013].

Observations from a spacecraft in orbit around Venus enable a broad range of techniques for investigating the perturbations of the neutral atmosphere and ionosphere by seismic waves. The acoustic waves generated during an earthquake vertically propagate through the Earth's neutral atmosphere (causing air pressure and, in turn, temperature variations) into the Earth's ionosphere, disturbing the local electron density [Vergados et al., 2019; Meng et al., 2019, Meng et al., 2018]. High sampling rate (20 Hz) ionospheric electron density observations were used to detect Moment Magnitude Scale (Mw) 3.2 Earthquakes (most recent event in May 2020). In an analogous fashion for Venus, where the atmospheric coupling is 60 times stronger than that on Earth, quake-generated acoustic waves from Mw > 3.0 quakes will cause ionospheric electron density variations that can be detected from dual frequency (X- and S-band and preferably UHF) crosslink **ROs**. Due to Venus's small rotational period, the Orbiter and SmallSat crosslink **ROs** will allow monitoring of specific regions over prolonged periods of time to catch a Venusquake, providing long-term variability observations. Opportunistic **ROs** between the Orbiter and the SmallSats, as well as between each SmallSat and the Earth stations and between the Orbiter and the stations, will allow planet-wide scanning for Venusquakes.

***Investigation III.2.B. – Look for present day volcanism and tectonism***

Many global geodynamic scenarios for the history of Venus, including those that invoke a late “catastrophe” to end a multi-billion year period of habitability, predict a current low level of volcanic activity compared to present day Earth, even in comparison to intraplate volcanism levels [e.g., Solomatov and



Moresi, 1996; Basilevsky and Head, 1998; Ivanov and Head, 2011]. It is important to constrain both the level and locations of current volcanism and tectonics. Through **repeat-pass imaging** of areas of likely volcanism or tectonic deformation, the **SAR** can be used to identify new volcanism or tectonic activity. At the simplest level, images collected with similar viewing geometries can be used to identify new flows, faults, and other features. Through **SAR** interferometry (a possible science enhancement option, see **Section 1.4.1**), images taken with near-identical viewing geometries within a critical baseline can be used to measure cm-scale deformation associated with volcanic and tectonic activity. **NIR imaging** by the Orbiter will be able to identify large areas (at least several thousand square kilometers) of relatively unweathered, and thus recently formed, volcanic terrains [Smrekar et al., 2010; Shalygin et al., 2015]. It is also possible that large regions of active volcanism will produce thermal anomalies identifiable with repeat imaging by the NIR camera on the Orbiter.

Mesospheric  $\text{SO}_2$  abundances have been observed to exhibit sharp increases, followed by gradual decreases [Marcq et al., 2013], a pattern which could arise from episodic volcanic activity. Furthermore, some modelling suggests that maintenance of the sulfuric acid clouds requires sources of out-gassed sulfur within the last 20–50 My [Bullock and Grinspoon, 2001]. The Orbiter's **S-mm** will not only map mesospheric  $\text{SO}_2$ , but also  $\text{SO}$ ,  $\text{H}_2\text{O}$ , and further related species, to allow the mechanisms governing the  $\text{SO}_2$  variations to be studied. Nightside spectroscopy in the near infrared from orbit will allow the mapping of water vapor in the lower atmosphere, and cloud thickness variations, which could reveal volcanic plumes. The Aerobot **AMS-N** will measure the composition and shape of cloud particles in the cloud layers, looking for evidence of volcanic ash or sulfate aerosols associated with volcanic activity. The Lander will measure atmospheric composition from the clouds down to the surface; it will carry a **Neph** to identify whether particulate matter below the cloud layers exhibits properties consistent with volcanic ash or condensed volatiles. The descent probe's **NMS** and **TLS** will measure vertical profiles of atmospheric composition, seeking evidence of near-surface gradients consistent with volcanic emission. Finally, the **LLISSE** platform will monitor the presence and variation of potentially volcanogenic trace gases at the surface over its 60 day lifetime.

## B.1.3 Expected Significance and Perceived Impact to State of Knowledge

### B.1.3.1 Critical Need for a Flagship Class Mission to Venus

The exploration of Venus is long overdue. It has been over 40 years since the last US mission, Magellan. A reticence to study Venus comes from the perception that because of the high surface temperature it is uninhabitable, inactive and too difficult to explore. Yet Venus is the key for understanding terrestrial planets. It is the only Earth-size planet in our solar system and the only accessible example of an Earth-size exoplanet. Careful study since Magellan has also shown that it is likely that Venus possessed an ocean for a long part of its history. We have the information to target the oldest rocks on Venus that are most likely to record that extinct regime, an exploration tactic we have successfully used for Mars.

Also like Mars, the exploration of Venus will require the deployment of multiple spacecraft in all mission classes. Even a Flagship mission, like VFM, cannot address all of the open issues about Venus. An improved global map of the Venus surface, topography and gravity, as could be provided by VERITAS, is absolutely essential for Venus as higher resolution data have shown for Mars. NIR imaging as baselined for VERITAS, DAVINCI+, and EnVision will yield a first look at global surface composition, a measurement shown to be so essential to understanding other worlds that it has become common practice. A probe mission like DAVINCI+ is the *only* way to collect information about the lower atmosphere—the critical interface between the surface and the clouds that we can see from orbit. What the Flagship budget allows is **multiple, powerful long-lived *in situ* assets** and **the ability to make measurements through the interconnected Venus system, from the sub-surface to the exosphere, at the same time**. As one example, while the Aerobot and Lander instruments directly measure composition of and magnetic field strength within the atmosphere, the three VFM orbiters will make measurements of the loss of volatiles, magnetic field shape and strength and solar particles. The response of the Venus system to any variation in solar activity will be measured simultaneously and in real time by these platforms.

The mission components and architecture of the VFM are designed to address the central question of habitability, which requires multiple measurements throughout the Venus system. The ad-

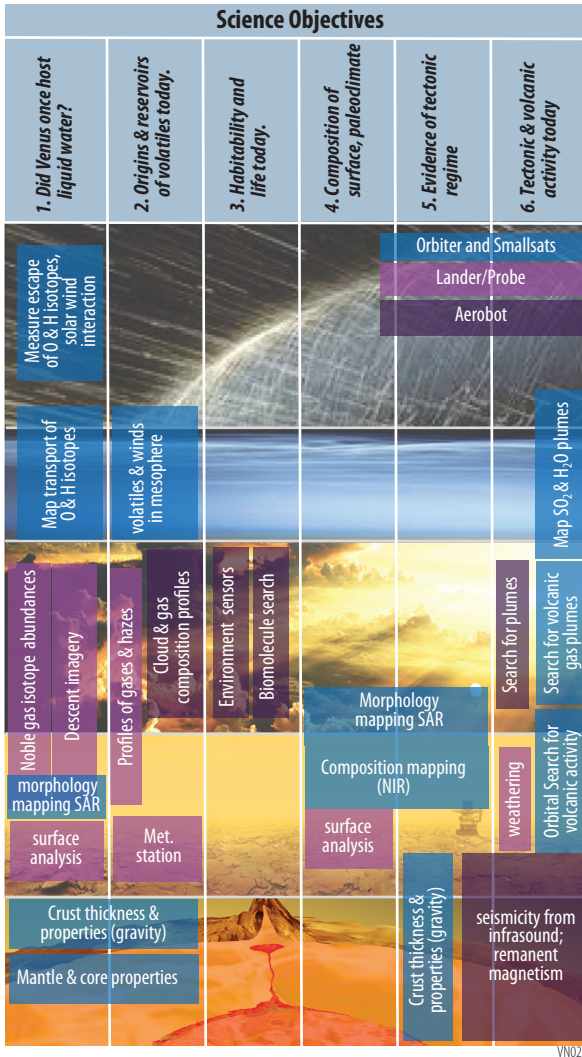
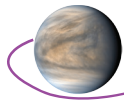


**Figure B-10.** The six VFM science objectives can only be addressed by measurements by five platforms that interrogate the multiple reservoirs of the complex Venus system allowing comparative and collaborative measurements of Venus phenomena.

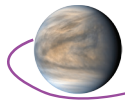
vantage of sending multiple assets in one mission to address our six Objectives is shown in **Figure B-10. Objective 1, Did Venus once host liquid water?**, is interrogated by all assets at all levels of the planetary system. This allows measurements both of the state and distribution of water in rock, air and space, but, importantly its sources (volcanism), fluxes (variability through the system), and loss from the Venus system. **Alone, each of these measurements is significant, but the measurements must be integrated to most fully address the objective. This can be accomplished with a single Flagship-class mission.**

Objectives 2, 5, and 6 also utilize measurements from all platforms. These objectives explore the type of chemical sources and sinks and movement of volatiles between the surface and atmospheric reservoirs. These data are the basis for an understanding of the present day Venus carbon, sulfur and water cycles. The chemical composition of the rocks and their weathering processes, on the tessera specifically, will for the first time, allow us access to Venus's ancient history. **SAR, NIR, and Lander** imaging will place these measurements in context and can be extrapolated to reinterpret Magellan data and augment data from missions to come. Multiple assets allow measurement of volcanic and tectonic activity via seismicity, atmospheric chemistry and imaging.

The central question of the habitability of Venus today (Objective 3) can only be addressed with a long-lived aerial platform as is proposed here. As was done by the Viking Landers, **we propose what would be the first life detection instrument at Venus to interrogate what could be an inhabited world.**

The larger budget of a Flagship class is what makes it possible to execute this systems approach. It not only allows more assets to be sent to the

planet, but also allows higher cost mission assets to be employed in our investigation of Venus. For example, a key element of this mission is the Lander, costed at ~\$1.2 billion with 50% reserves, which alone is just over the budget cap of a New Frontiers mission. This Lander carries an ambitious payload in order to serve dual purpose as a descent probe and surface analyzer, and this mass and volume requirement contributes to the cost. This payload, however, is capable of performing the most thorough, accurate, and precise characterization of the Venus surface to date, and thus can significantly advance our understanding of Venus. The ability to define the composition of rock, solid weathering products, and atmosphere from measurements in a single location is powerful; this provides all the data needed to look at surface-atmosphere interactions at that location without needing to rely on assumptions or calculations for part of the weathering equation. The ability to measure all parts of this phenomenon comes from the multitude of instruments carried by the lander. This large suite of instruments is also a risk-reduction tactic, as key measurements needed to address the questions in the **STM** are acquired by multiple instruments, so these data may be obtained despite single instrument failure, but the dataset is enhanced if all instruments function properly, since each instrument provides either additional elements or access to different layers of the surface (see **Section B.2.8.2.1**).



Autonomous hazard avoidance and navigation is an essential component of and cost to the Lander because we may not know the detailed terrain properties of the tessera until the mission arrives at Venus. **The global, high-resolution RADAR, imaging spectroscopy and topography that could be provided by VERITAS and meter-scale imaging and spectroscopy of tessera terrain that could be provided by DAVINCI+ prior to VFM would critically enable site selection both scientifically and by reducing hazard risk.**

This mission offers an unprecedented length of time for *in situ* exploration of Venus. The VFM study team has successfully designed a mission with several long-lived *in situ* assets. The Lander lifetime of 7 hours at the surface is a factor of 3 improvement over previous landers and we have devised a communication relay that accommodates that lifetime and more. This extended lifetime allows for instruments to make repeated observations to look for short timescale changes in conditions (e.g., mass spectrometer) or to improve data quality. Instruments can also integrate over longer durations, also allowing improved data quality as shown for the GRS. The R-LIBS instrument, if verified, also makes use of this time, as it is the only instrument sent to measure rocks that is capable of measuring multiple discrete samples on the surface, and each individual measurement is very rapid, **allowing 100s of targets to be measured**, providing a benefit of “mobility” at the Venus surface.

The unprecedented 60-day lifetime of the variable-altitude Aerobot allows time to measure the dynamics and composition of the clouds over several Venus days from equator to pole. A station in the cloud deck will allow the detection of geophysical phenomena, such as seismicity, and a survey over one Venus hemisphere for remanent magnetism which can be compared to magnetic measurements collected simultaneously in orbit.

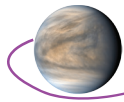
Finally, the Lander will carry LLISSE, the first station to use NASA’s investments in high-temperature electronics to survive for 60 days at the Venus surface. This will provide meteorology and atmospheric composition data across a period of time orders of magnitude greater than any previous surface sensor sent to Venus. LLISSE could be the pathfinder for a new era of Venus surface exploration.

The VFM study has shown that **multiple communications satellites are required to maintain contact with *in situ* elements over months**. The Flagship cost envelope provides the ability to insert three orbiters at Venus to provide telecommunications infrastructure and redundancy at Venus in a single launch. The VFM would provide orbital assets at Venus for 7 years from 2034–2041, which could be leveraged by other missions at Venus, as has been done so successfully at Mars.

A Flagship class mission can address many, but not all, of the critical questions we have about Venus that still remain after the last US mission over 40 years ago. The Venus Flagship Mission addresses several of the criteria for large strategic missions outlined in NASEM [2017], including 1) “Focus on reconnaissance and on conducting a broad suite of objectives”, 2) “Travel to hard-to-reach destinations or challenging environments”, 3) “Operate with an evolving science program that responds to what has been learned as the mission proceeds” and 4) “Answer many of the most compelling scientific questions facing the scientific fields supported by NASA’s Science Mission Directorate, and most importantly develop and deepen humanity’s understanding of Earth, our solar system, and the universe.” **The simultaneous, synergistic measurements of the solid body, surface, atmosphere and space environment provided by the VFM will allow us to target Venus, the most accessible Earth-size planet in our galaxy, and gain a profound new understanding of the evolution of our solar system and habitable worlds.**

### B.1.3.2 Relevance to Exoplanet Research

Exoplanet research has also progressed to the point that lessons learned from Venus are *essential* for **exoplanet science** to utilize in all aspects of exoplanetary data interpretation, from orbits and formation, to atmospheres and interiors. Venus is the prototype for a world that has transitioned from habitable and Earth-like conditions through the inner edge of the Habitable Zone (HZ), providing a natural laboratory to study the evolution of habitability. Venus is perhaps the most relevant when it comes to appreciating the variety of terrestrial exoplanets in habitable zones and how Earth could have ended up—or may become [Kane et al., 2014]. This includes studying the complex interaction between the Venus surface and the atmospheric dynamics [Horinouchi et al., 2020], a topic which is highly relevant to correct assessment of climate studies for tidally-locked exoplanets [Sergeev et al., 2020]. Numerous potential Venus analogs have been discovered from Kepler [Kane et al., 2013; 2018] and Transiting Exoplanets Survey Satellite (TESS) data [Ostberg and Kane, 2019], the latter of which



will comprise a substantial fraction of transmission spectroscopy candidates [Kempton et al., 2018; Lustig-Yaeger et al., 2019]. Therefore, there is a clear and urgent need to characterize the venusian atmosphere, both to understand the evolution and dynamics of the Venus atmosphere [Horinouchi et al., 2020] and surface, to understand the evolution of secondary atmospheres generally and in relation to exoplanets [Kite and Barnett, 2020] and to provide the necessary data to correctly interpret terrestrial exoplanet atmospheric models [Kane et al. 2019]. VFM will provide comprehensive, highly targeted new measurements to fulfill this goal.

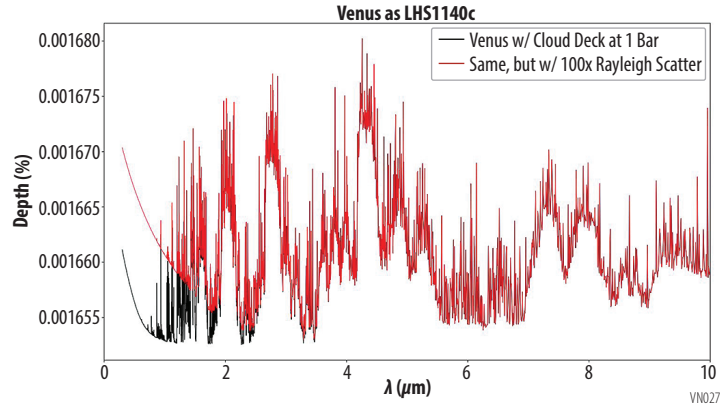


Figure B-11. Derived spectrum of a Venus analog orbiting the known exoplanet host LHS1140. The red spectrum includes enhanced Rayleigh scatter.

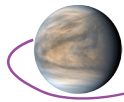
A critical feature of exoplanet atmosphere models is their dependence on the uncertainties in the currently available Venus data that informs the transmission spectra generation. Shown in **Figure B-11** is a simulated transmission spectrum for a Venus analog orbiting the nearby star LHS1140. The clouds used in the model are fully grey, or opaque, and raising the cloud deck will raise the level of the continuum of the spectrum and decrease the depth of spectral features. Our models utilize T-P and mixing ratio data from the Venus International Reference Atmosphere (VIRA), which has a broad range of values depending on the data source and latitude of the probe deployment in the atmosphere. The models are highly dependent on these data and generally require better than 5% precision on the T-P values to avoid degeneracy below the cloud deck that leads to incorrect predictions of surface conditions. Given the trajectory of exoplanetary science towards exoplanet atmospheric characterization and the expected prevalence of Venus analog environments, the study of Venus represents the highest priority synergistic target shared by the planetary science and exoplanet communities. **Therefore it is a matter of high priority that crucial pressure, temperature, and compositional atmospheric measurements of the nearest Earth-size planet are obtained.**

An important aspect of **Figure B-11** is the effect of uncertainties in the currently available data that informs the models of exoplanet transmission spectra. A critical component of atmospheric measurements are thus composition and pressure-temperature profiles as a function of altitude, particularly in the deep atmosphere where such measurements are relatively uncertain. This will be accomplished by the **NMS, TLS, MET suite and AS investigation** on the VFM Lander. These measurements can be obtained over a range of latitudes and longitudes, with the **MET suite on the Aerobot**, to allow an approximate integrated compositional model of the Venus atmosphere to best represent exoplanet-related spectra. Measurements of species lost from the Venus exosphere collected by the **NMS on the Orbiter** will help interpret transmission spectra of exoplanets as well as atmospheric loss models. The acquired data will result in revised atmospheric models that will aid considerably in the removal of degeneracy in the interpretation of exoplanet spectra.

### B.1.3.3 Constraints for Meteorites

VFM data are also critical because they are necessary to help identify potential venusian meteorites discovered on Earth. Venusian rocks can be transported to Earth, although their volumes are estimated to be low due to the difficulty of ejecting rocks from a large body towards Earth and through the Venus atmosphere [Melosh and Tonks, 1993; Gladman et al., 1996]. If found, a Venus meteorite would be invaluable, as many critical techniques such as age-dating using radiogenic isotopes can only be performed in Earth-based labs, and sample return missions from Venus are far off into the future. Data to be collected by the VFM that would aid in identifying a venusian meteorite would include atmospheric chemical and isotopic composition [e.g., Bogard and Johnson, 1983], which can be compared to gases trapped in glass within a meteorite sample, and determination of typical venusian weathering products, as parent-body weathering has been preserved in many meteorites, including those from Mars [e.g., Borg et al. 1999]. Venus is likely to have a unique weathering style compared to that seen





on other terrestrial planets, moons, or asteroids due to its hot, sulfur- and CO<sub>2</sub>-bearing atmosphere, and as a result weathering products may be more useful in linking meteorites to Venus. Chemical and mineralogical measurements of venusian rocks, specifically basalts, would also be helpful as they can define element ratios (e.g., FeO/MnO) or mineral compositions (e.g., percent anorthite in feldspar) that are characteristic of Venus [Papike et al., 2003; Treiman et al., 2000]. It is not certain what rock type will be encountered in the tessera landing site, but such chemical and mineralogical signatures of parent bodies are best defined as trends derived from several data points, so the measurements from this mission will only serve as a beginning of the definition of Venus's traits.

### B.1.4 Science Enhancement Options

#### B.1.4.1 InSAR Campaign

As discussed briefly for *Investigation III.2.b*, images taken with near-identical viewing geometries within a critical baseline, and with compatible pulse timing and bandwidth, can be used to conduct SAR interferometry (InSAR). In terms of increasing complexity in the data gathering, some potential uses of InSAR are as follows:

- New volcanic flows can be identified in a semi-automated method from phase decorrelation in an InSAR pair. This can be done with essentially any InSAR pair.
- With S-band baselines of a few hundred meters, or longer with offset of the center frequency, InSAR pairs can be used to obtain topography with spatial resolutions a few times the image resolution and vertical precision of a few meters.
- If sufficient-quality topography exists (e.g., from a previous InSAR pair), then a relatively short-baseline pair can be used to measure cm-scale deformation of the surface over the time interval between images (commonly referred to as Differential InSAR (DInSAR)). Likely places with active deformation are Venus's volcano-rift-coronae zones.

These techniques can provide critical information about the surface geology and the nature and amount of current volcanic and tectonic activity. However, InSAR requires considerable advance planning, particularly with respect to navigation, and fuel resources are expended in order to maintain cycle-cycle orbits within acceptable baselines. In some cases near the poles, InSAR can also be conducted using adjacent orbits of imaging [Meyer and Sandwell, 2012]. At least one of the images in an InSAR pair must also be collected using continuous pulsing, and for both images the full single-look-complex image must be returned. Thus, an InSAR campaign generates large data volumes.

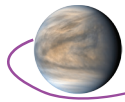
#### B.1.5 Relationship of VFM to Other Venus Missions

Venus Flagship does not obviate the need for other classes of missions to Venus. The focus of the Flagship proposed here, habitability, prescribes a particular implementation that will not deliver other critical data sets, for example high resolution global SAR and topography, orbital multispectral remote sensing of the clouds (particularly the UV), or chemical measurements of plains materials, each of which is absolutely critical to our understanding of the planet as outlined in the VEXAG Goals, Objectives, and Investigations (GOI). Like Mars, the study of Venus requires multiple, complementary missions that can build on discoveries and provide key infrastructure about Venus—a Venus Program.

Any of the proposed missions would serve as pathfinders for a Flagship class mission, by collecting critical datasets that are not collected by VFM as studied, reduce risk for all future missions, particularly *in situ* assets, and enhance and focus science objectives based on new discoveries. Below we describe the relationship between VFM and proposed missions, and make recommendations for possible descopes for VFM if these missions are selected (Table B-4).

Table B-4. Synergistic relationships between VFM and proposed Venus Missions

Mission	2020 Status	Nominal Launch	VFM Synergies	Possible VFM Descope if Flown
VERITAS	Discovery Phase A	2026	Pathfinder for VFM lander	NIR emissivity, gravity
DAVINCI+	Discovery Phase A	2026	Pathfinder for VFM lander	None
EnVision	ESA M5 Candidate	2032	Would observe simultaneously	NIR emissivity/SAR
Venera-D	JSDT Report	Post 2026	Plains landing	None

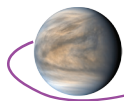


**DAVINCI+, Discovery Phase A, Launch 2026.** The DAVINCI+ mission seeks to send an instrumented probe through the Venus atmosphere to the surface and is accompanied by an orbiter that will collect NIR data of the planet's surface [Garvin et al., 2020]. The probe instruments and science goals are similar to those on the VFM Lander and include detection of noble and trace gases and their isotopes as well as descent imaging. The VFM descent profile would collect similar critical data at another location and potentially time of day on Venus, which would bolster our understanding of the variability of the type and volume of these gas species at different locations on the planet. Differences in the temperature and pressure profiles of the Venera and Vega landers and the PVO probes show that there is substantial variability in these values at different locations and times of day [e.g., Seiff et al., 1987] which may affect the stability of chemical species. Especially because so little is known about the lowest scale height of the atmosphere, each probe provides important constraints on atmospheric dynamics and variability. The VFM Lander instruments will operate throughout descent but also collect data on the surface to gather critical information that, when paired with the surface chemistry, can constrain local surface-atmosphere interactions. Orbital NIR images collected by both missions at 1  $\mu\text{m}$  increase the chances of detecting transient phenomena, as well as provide more opportunity to secure global NIR coverage at a potentially greater number of wavelengths. Both missions would provide important ground truth data to calibrate existing and planned orbital NIR images. If DAVINCI+ is selected, a possible VFM descope would be to remove the mass spectrometer on the lander to eliminate the noble gas measurement, based on the assumption that noble gases do not vary throughout the atmosphere. However, recent measurements of  $\text{N}_2$  abundance during the MESSENGER flyby of Venus show unexpected differences between the upper and lower atmosphere [Peplowski et al., 2020]. Our stance is that every (relatively costly) descent into the Venus lower atmosphere should carry a full complement of instruments to better understand the lowest scale height and its spatial variability at as many locations and times as possible.

**VERITAS, Discovery Phase A, Launch 2026.** The VERITAS mission [Smrekar et al., 2020] is an orbiter carrying an X-band Interferometric SAR and the VEM instrument [Helbert et al., 2016] to perform global SAR mapping at 30 m resolution; acquire topography, gravity, InSAR, and NIR emissivity data; and characterize the atmosphere. These global datasets would significantly advance our ability to test several major hypotheses, derived from the Magellan data, about the geology, stratigraphy, and geophysics of Venus. The global NIR radiance map calibrated with improved topography would provide, for the first time, a compositional map of the Venus surface. VERITAS would be a critical and enabling pathfinder for VFM, particularly for the selection of the VFM landing site and high resolution (10 m) **SAR** targets. If VERITAS flies, a possible VFM descope would be to eliminate the orbital NIR emissivity, although VFM emissivity would offer additional opportunity to detect transient thermal anomalies. The VFM high resolution **SAR** would provide additional imaging to the VERITAS high resolution data set. The VERITAS gravity mapping would release VFM from the need to collect those data.

**EnVision, ESA M5 candidate, Launch 2032.** EnVision [Ghail et al., 2019] is an orbiter mission being studied in collaboration with NASA. Its current design has an S-band SAR, a subsurface RADAR sounder, and a spectrometer suite [Helbert et al., 2019]. It will produce targeted RADAR imagery, topography, spectral radiance, thermal emissivity, sub-surface and gravity field mapping and atmosphere characterization. Because EnVision would nominally be at Venus concurrently with VFM, it is possible that EnVision could provide the SAR and NIR observations to support some VFM objectives, including landing site selection and characterization, allowing the VFM **SAR** and **NIR** emissivity mapper to be descope.

**Venera-D**, has been studied by a joint NASA, IKI STDT [Venera-D JSDT, 2019]. It consists of a Vega-like lander that would target the plains, and an orbiter that observes the atmosphere at several wavelengths, including NIR. The lander is synergistic and complimentary to VFM because it will be conducting similar investigations on a different terrain type—the Venus plains. The combination of chemical and mineralogical data from both the plains and tesserae would significantly advance our understanding of the venusian crust, mantle and igneous processes, the evolution of volcanism with time and the range of surface-atmosphere interactions on modern Venus.



## B.2 Mission Overview

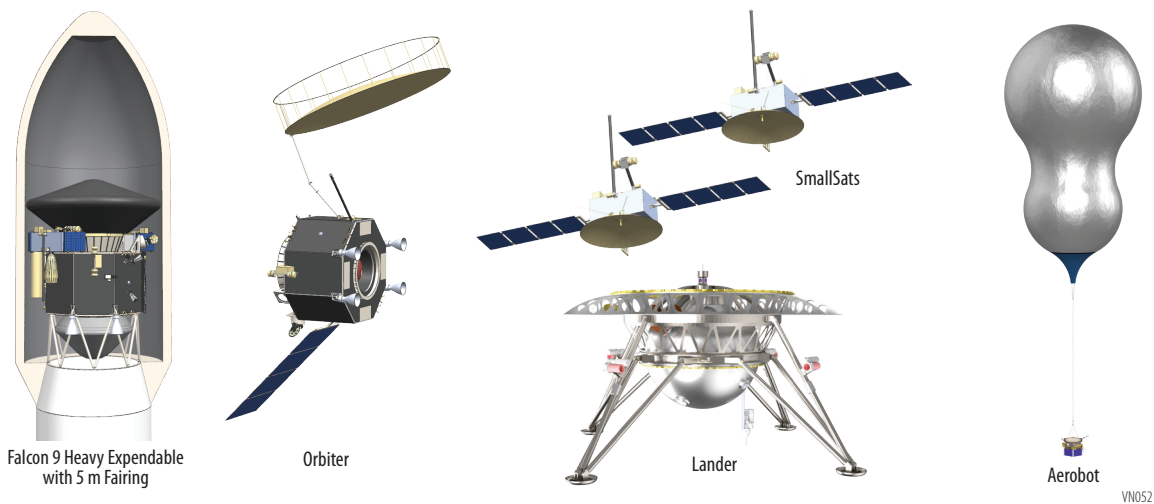


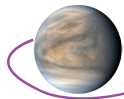
Figure B-12. Venus Flagship Mission Flight System

The VFM flight system consists of an Orbiter, Aerobot, Lander, and two SmallSats as shown in **Figure B-12**. VFM fits within the 5 m diameter of the Falcon 9 heavy fairing. While not a specific design driver, the consideration of the center-of-mass height limit of the Falcon 9 nudged the design to be as squat in height as possible. The operational order requirement that the Aerobot be deployed before the Lander, reduced the packaging options significantly. A custom payload attach fitting (PAF) allows the placement of the Aerobot inside its aeroshell beneath the Orbiter using commercial off-the-shelf (COTS) separation rings. The Lander inside its aeroshell is attached to the top deck of the Orbiter using COTS separation rings. The SmallSats are tucked in between the Lander and the top deck of the Orbiter and are attached via separation rings to a vertical bracket, similar in concept to a Moog's Evolved Secondary Payload Adapter (ESPA).

### B.2.1 Key Architecture and Mission Trades

Seven key trades drove the VFM mission architecture and Mission Design (**Figure B-13**). They are:

1. **Defining the platforms required to fulfill the science objectives in the Science Traceability Matrix (STM) (Foldout Table 2).** Using the 2009 Flagship Mission Study as a starting point it quickly became clear that an architecture composed of an Aerobot, Lander, Orbiter, and two SmallSats would achieve all of the science objectives. This architecture is within the current state-of-the-art with modest technology development needs and takes advantage of advancements in the last 10 years, but also has the flexibility to adapt to new engineering approaches as the next decade proceeds.
2. **Evaluating the launch architecture**—should the two-launch architecture in the 2009 Venus Flagship Mission Study be used or could current launch vehicle technology enable a single launch. The trade settled on the use of a single Falcon 9 Heavy Expendable. Using a single launch vehicle reduces overall cost and complexity associated with designing, launching, tracking and operating two separate payloads.
3. **Determining how to provide communication coverage for the Aerobot and the Lander.** There were three options available: (1) Direct to Earth, (2) Orbiter relay and (3) SmallSat relay. Direct to Earth would require a high-power transmitter on the Lander and Aerobot. To minimize power dissipation on the Lander as well as minimize battery size on the Lander and Aerobot, the decision was made to use option (2) and option (3)—the Orbiter and SmallSats—as communication relays. The trade determined that the optimal solution was to use communication with the Orbiter during a portion of the Lander mission to take advantage of its larger bandwidth to return the imagery data and use the SmallSats to provide the coverage for the extended 8-hour life-



time. For the Aerobot, it was quickly determined that the best option would be for the SmallSats to provide daily coverage since the Orbiter's elliptical orbit only enables contact with the Aerobot once every 4–5 days.

4. **Deciding which propulsion systems to use for the Small-Sats and Orbiter.**

This trade was driven by the results of the communication and launch trades. It was determined that the SmallSats could arrive early at Venus most efficiently using solar electric propulsion. Due to the large delta Velocities (delta V or  $\Delta V$ ) and the mass of the Aerobot, Lander, Orbiter and SmallSat stack a bi-prop pressurized system would be needed on the Orbiter.

5. **Evaluation of methods to reduce instrument loads.**

In past studies and proposals, including the 2009 Venus Flagship Mission Study, direct entry from the interplanetary trajectory was selected to avoid the mass of propellant required to get into orbit with the consequence of higher g loads during entry. This impacted the development cost due to the need to qualify instruments, electronics and the pressure vessel for the peak g-load of 99g. For the current effort, we established a requirement to

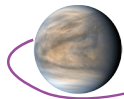
limit the g forces to < 50g to reduce the cost of completely redesigning heritage instruments. In addition, the need to have the landing occur with sunlight for the **DI**, Terrain Relative Navigation (TRN) and Landing Hazard Avoidance (LHA) sensors during landing resulted in selection of an architecture that uses an initial elliptical orbit before releasing the Lander. This decision spawned two additional key trades: Entry angle and inclination for the initial orbit of the Orbiter.

6. **Determination of the Aerobot shape and entry-angle trade** to evaluate if low entry angles could meet the <50g requirement with the benefit of a significantly lower heating rate, allowing for a lighter thermal protection system (TPS) and an aeroshell shape with a 70° sphere-cone providing a max diameter of 4.6 m. This geometry provides significantly better packaging and drag performance than the 45° sphere-cone (e.g., Pioneer Venus) and has a smaller surface area for a given diameter (thereby once again reducing the mass of the TPS). The maximum diameter of 4.6 m provided the added benefit of a larger distance between Lander legs and thus a more stable Lander.

Architecture			
Single Launch		< Lower Complexity and cost	
Multiple Launch		<b>X</b> Higher Complexity and cost	
Elements	Aerobot	< Meets Science Objectives	
	Lander	< Meets Science Objectives	
	Orbiter	< Meets Science Objectives	
	Rover	<b>X</b> Not Required by Science Objectives	
	SmallSat	< Meets Science Objectives	
Aerobot and Lander Communication	Direct to Earth	<b>X</b> Requires higher power transmitters	
	Orbiter	< Minimizes transmitter power	
	SmallSat	< Minimizes transmitter power	
Propulsion	Orbiter	Solar Electric	<b>X</b> Capability insufficient for required $\Delta V$
		Bi-Prop	< Provides all $\Delta V$ for Aerobot, Lander and Orbiter
	SmallSats	Solar Electric	< Enables arrival at Venus before Aerobot
		Bi-Prop	<b>X</b> Does not arrive at Venus in time
Mission Design			
Launch Date	2031	< Minimum $\Delta V$	
	2032	<b>X</b> Requires higher $\Delta V$	
Initial Elliptical Orbit	Equatorial	<b>X</b> Requires higher $\Delta V$ to achieve science polar orbit	
	Polar	< Minimum $\Delta V$	
Aerobot and Lander Entry Angle	Heritage of -19°	<b>X</b> g loads exceed requirement	
	Shallow	< Provides required 50g load	
<b>LEGEND</b> <span style="background-color: #d9e1f2; padding: 2px;">Traded Item</span> <span style="background-color: #d9ead3; padding: 2px; margin-left: 10px;">Option Baselined</span> <span style="background-color: #f2dede; padding: 2px; margin-left: 10px;">Option Rejected</span> <span style="background-color: #fff2cc; padding: 2px; margin-left: 10px;">Option Not Selected, but worthy of further study</span>			

Figure B-13. Architecture and Mission Design Trade Tree

VN020



7. **Examining the type and order of the orbits to achieve a polar science orbit;** an *initial* equatorial elliptical orbit that was followed by a polar science orbit vs an *initial* polar elliptical orbit so that the transition to the polar science orbit would minimize the required  $\Delta V$ . The initial polar elliptical orbit option was selected as it avoided the large  $\Delta V$  penalty for the inclination change to a polar orbit. The penalty for this selection was that the orbit geometry no longer allows for SAR mapping of the primary landing site prior to landing due to the slow rotation rate of Venus. However, we are able to map the remaining potential landing sites prior to landing at the primary site and this provides an opportunity to obtain a better understanding of the tessera which in turn improves the maps used in the feature recognition algorithms for the Terrain Relative Navigation and Hazard Avoidance systems. This mission concept is flexible enough to provide the option to extend this mapping orbit to acquire additional coverage of tessera terrain as an input to landing site selection if necessary.
8. **Determining the launch date.** This trade was driven by the programmatic need to have a realistic development schedule and the need to minimize the  $\Delta V$  that the Orbiter had to provide. The 2031 launch date was selected since it provides the needed development schedule and allows the 2032 launch date to serve as a backup.

## B.2.2 Mission Requirements

The mission requirements are derived from the STM (Fold-out Table 2) and the architecture and mission trades. The mission requirements are shown in Table B-5. Key requirements that drive the mission design are the limiting entry peak g loads on the Aerobot and Lander to less than 50 g, providing communication coverage of critical events, such as when the Orbiter performs Venus Orbit Insertion (VOI), entry, descent, and landing of the Lander, entry, descent and initial float of the Aerobot, as well as providing daily access to the Aerobot and the LLISSE.

## B.2.3 Planetary Protection Considerations

As was discussed in the 2009 Venus Flagship Mission Study, studies of planetary protection issues have concluded that the surface environment of Venus presents a negligible chance of either forward or back contamination and that the cloud environment presents such a slight chance of contamination that it does not require any special precautions in mission planning [NASEM, 2006; PPIRB, 2019].

In 2005, in light of advances in astrobiology, including expanding discovery of extremophile organisms in ever more diverse niches on Earth, new ideas about the possible viability of cloud-based life on Venus (e.g., Schulze-Makuch et al., [2004]), and the prospect of a new generation of Venus spacecraft, NASA's Office of Planetary Protection asked the Space Studies Board's Committee on Origin and Evolution of Life (COEL) to provide advice on planetary protection concerns related to missions to and from Venus. A Task Group on Planetary Protection Requirements for Venus Missions was formed and heard expert testimony at several meetings. The Task Group concluded that no significant risk of forward contamination exists in either landing on the surface of Venus or exposing spacecraft to the venusian clouds, and recommended that the previous COSPAR Category II planetary protection classification of Venus be retained [NASEM, 2006]. Category II includes missions to those bodies where there is "significant interest relative to the process of chemical evolution and the origin of life, but where there is only a remote chance that contamination carried by a spacecraft could jeopardize future exploration." For category II bodies, the legal requirements are only for simple documentation. This required documentation includes a short planetary protection plan, primarily to outline intended or potential impact targets; brief pre-launch and post-launch analyses detailing impact strategies; and a post-encounter and end-of-mission report providing the location of inadvertent impact, if such an event occurs.

For planetary protection concerns, the relevant question is ultimately not the probability of any habitable niche existing on present day Venus, but the likelihood of such a niche, if it does exist, possessing physical conditions which overlap the conditions under which terrestrial organisms can survive, grow and reproduce [Cockell, 1999; Limaye et al., 2018]. The judgment of the ad hoc Task Group was that the chance of such overlap is too slight to significantly impact planning for future Venus missions. This history is reviewed, and the rationale behind these studies discussed in more detail by Grinspoon and Bullock [2007].

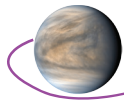
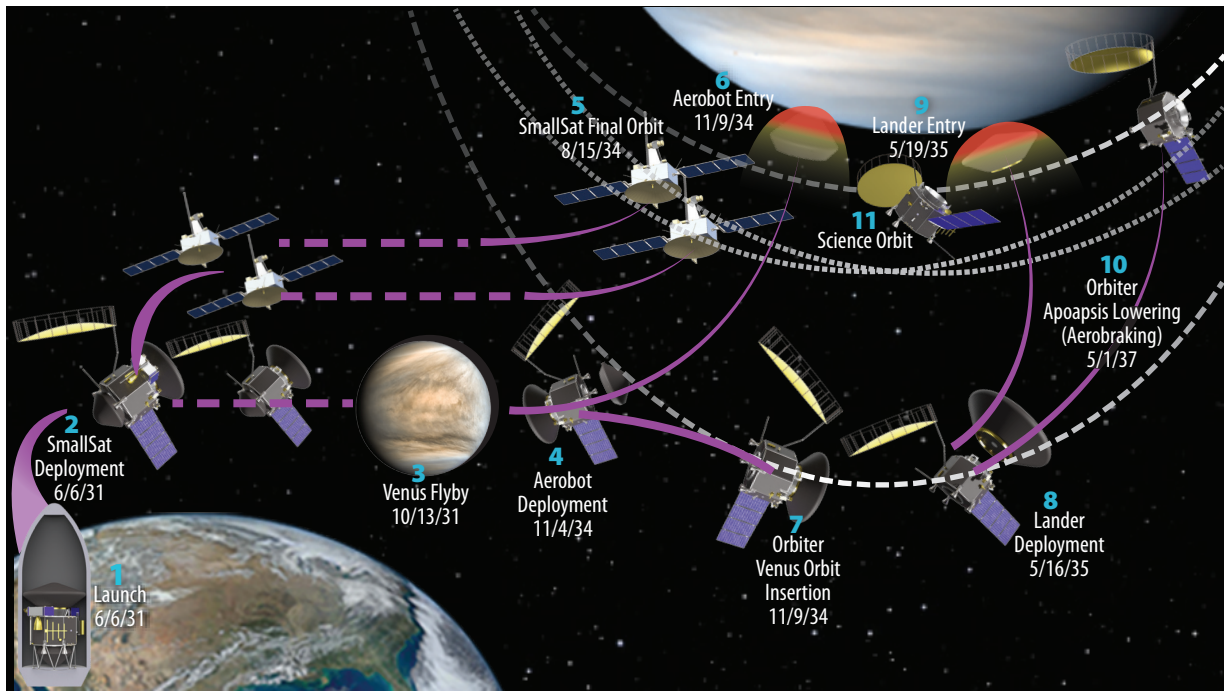
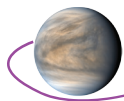


Table B-5. Mission Requirements

Mission Requirement (Top Level)	Mission Design	Aerobot	Lander	Orbiter	SmallSat	Ground System Requirements	Operations Requirements
<ul style="list-style-type: none"> <li>• Mission Reliability Category 1, Class A</li> <li>• Mission Lifetime 10 years</li> <li>• Aerobot 60 days</li> <li>• Orbiter 10 years</li> <li>• Lander 6 hours, 8 hour goal</li> <li>• SmallSats 6 years</li> <li>• Provide communication with Earth via Orbiter and SmallSat during all critical events</li> </ul>	<ul style="list-style-type: none"> <li>• Falcon Heavy Expendable with 5m fairing</li> <li>• Launch mass (kg): 11,694</li> <li>• Launch date: 6/6/2031</li> <li>• Launch C3: 12.737 km<sup>2</sup>/s<sup>2</sup></li> <li>• Launch Window of at least 14 consecutive days</li> <li>• Landing done in sunlight</li> <li>• Landing done when Orbiter and SmallSats can communicate with Lander and Earth</li> <li>• Provide continuous communication of the descent and landing of the Lander</li> <li>• Provide communication coverage of descent and initial float of Aerobot.</li> <li>• Provide daily communication for at least 10 minutes with the Aerobot and LLISSSE</li> <li>• Final Orbiter science orbit of 300 km circular polar</li> <li>• Provide Access with a 300 (N-S) × 150 km (E-W) landing ellipse to Landing Sites: <ul style="list-style-type: none"> <li>• West Ovda 0.3412, 62.5327</li> <li>• Alpha -26.3206, 0.7381</li> <li>• Fortuna 66.0976, 15.1338</li> <li>• Tellus 36.8398, 75.6959</li> <li>• Mid Ovda -6.3498, 81.8099</li> <li>• East Ovda -4.4522, 95.5453</li> </ul> </li> <li>• Place Aerobot into a float altitude of 52–62 km at a low latitude</li> <li>• Max Entry G-Load of ≤50 g for Aerobot and Lander</li> </ul>	<ul style="list-style-type: none"> <li>• Reliability Category 2, Class B</li> <li>• Data Storage of 2 Gbits</li> <li>• S-band to SmallSats and Orbiter</li> <li>• 28 V power System</li> <li>• Accommodate Instruments</li> <li>• Control operational altitude between 52 km and 62 km</li> <li>• Maintain commanded altitude within 1 km</li> <li>• Survive altitudes down to 50 km and as high as 64 km</li> </ul>	<ul style="list-style-type: none"> <li>• Reliability Category 2, Class B</li> <li>• ≥ 1 m/s separation velocity from Orbiter</li> <li>• Landing Velocity of ≤ 8 m/s vertical and ≤ 2 m/s horizontal.</li> <li>• Land Safely with clearance for 0.5 m boulder.</li> <li>• Land and operate on a ≤30° slope.</li> <li>• Post-landing adjustability to orient the instrument deck within 10° of the gravity vector</li> <li>• Operate in Venus atmosphere for at least 6 hours (8 hour goal)</li> <li>• &lt;1 bar to 92 bar pressure range</li> <li>• 30 °C to 452 °C temperature range</li> <li>• Accommodate instruments</li> <li>• Cameras Images</li> <li>• Descent</li> <li>• Panoramic of site</li> <li>• Deployments and drilling</li> <li>• Descent Camera Field of View &gt; 90°</li> <li>• Data Storage 8 Gbits</li> <li>• Panoramic Camera Field of View ≥60° per mirror (4) with 240° azimuth coverage and 30° above horizon and 60° below</li> <li>• 28 V power System</li> <li>• 0.1 ms timing accuracy with 10<sup>-6</sup> stability relative to ground station</li> </ul>	<ul style="list-style-type: none"> <li>• Reliability Category 1, Class A</li> <li>• Perform Venus Orbit Insertion</li> <li>• Provide orbit maneuvers for station keeping and release of the Lander</li> <li>• Land Lander with a solar angle of ≥15°</li> <li>• Land Lander with elevation of the Earth greater than 10°</li> <li>• Provide ≥1 m/s separation velocity for Aerobot and Lander separations</li> <li>• Provide spin rate to Aerobot and Lander at separation of 5 rpm</li> <li>• Accommodate Instruments</li> <li>• Data Storage 4 Tbits</li> <li>• Ka-Band ≥ 2.8 Mbps to Earth</li> <li>• X-Band ≥ 740 kbps to Earth with two way tracking</li> <li>• S-Band ≥ 31 kbps from Lander</li> <li>• S-Band ≥ 740 bps from Aerobot</li> <li>• UHF ≥ 700 bps from LLISSSE</li> <li>• 1 ms timing accuracy with 1e<sup>-15</sup> stability relative to ground station</li> </ul>	<ul style="list-style-type: none"> <li>• Reliability Category 1, Class B</li> <li>• Two SmallSats with Wet Mass ≤300 kg each</li> <li>• Arrive at Venus at least 2 months prior to Aerobot</li> <li>• Science orbit: <ul style="list-style-type: none"> <li>• Apoapsis altitude &gt;5000 km</li> <li>• Periapsis altitude &lt;500 km</li> </ul> </li> <li>• At least one SmallSat with Inclination ≥65°</li> <li>• Provide 8 hours of continuous access starting at the Lander entry interface (altitude of 175 km)</li> <li>• Provide daily access for a minimum of 10 minutes to Aerobot</li> <li>• 3-Axis Stabilized</li> <li>• Receive from Aerobot and Return to Earth 200 Mb/s/Earth Day of data</li> <li>• X-Band ≥200 kbps to Earth</li> <li>• S-Band ≥14 kbps from Lander</li> <li>• S-Band ≥18 kbps and Aerobot</li> <li>• Accommodate Instruments</li> <li>• Data Storage 50 Gbit</li> <li>• 28 V power System</li> </ul>	<ul style="list-style-type: none"> <li>• 34m DSN Antenna, Ka-Band at maximum of 100 Mbps</li> <li>• Receive housekeeping &amp; science data telemetry</li> <li>• Provide commanding</li> <li>• Record/Store science data</li> <li>• DDOR Tracking of Orbiter and SmallSats, Tracking of Aerobot from release through end of mission, Tracking of Lander from release through landing</li> <li>• Provide critical event telecom coverage: Launch, Separation from Launch Vehicle, SmallSat separation, Flyby targeting, DSM, Balloon entry Targeting, Balloon separation, Orbit insertion targeting, Instrument Deployments, Descent of Balloon, Descent and Landing of Lander</li> </ul>	<ul style="list-style-type: none"> <li>• Implement required DDO</li> <li>• Manage time correlations</li> <li>• Maneuvers</li> <li>• Support DSN passes</li> <li>• Monitor Lander state of health</li> <li>• Implement contingency procedures</li> <li>• Implement science sequences</li> <li>• Manage Lander operations</li> <li>• Perform ops sim testing</li> </ul>



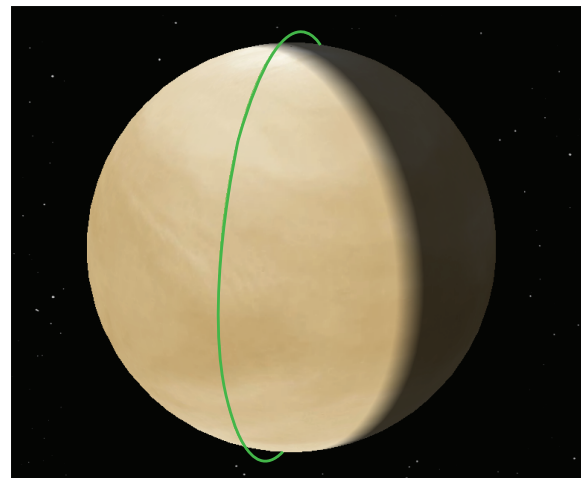
VN006

Figure B-14. Mission Timeline

Although NASA classifies Venus missions under planetary protection Category II, given that we have a **FM** to specifically look for signs of extant life, we need to ensure that the environment of that instrument is pristine and not contaminated by terrestrial life. Consequently, measures to sterilize the instrument and possibly bag or shroud it and decontaminate nearby gondola sub-systems must be considered. The details of the planetary protection and contamination control plans required to remove Earth-derived live or dormant organisms and microbial debris are beyond the scope of this study and need further work.

### B.2.4 Mission Design Overview

The mission timeline is shown in **Figure B-14**. A few hours after launch (1), two SmallSats detach from the other platforms (2) and follow a low-thrust transfer to Venus, each using solar electric propulsion. Once at Venus, the SmallSats spiral down to their final orbits (5). In addition to their science requirements, the SmallSats provide essential communication with both the Aerobot and Lander. Both SmallSats will be in place, orbiting the planet, approximately 3 months prior to the arrival of the Orbiter, carrying the Aerobot and Lander, which utilizes chemical propulsion and performs a Venus flyby enroute (3). The Aerobot separates (4) from the Orbiter and Lander about 5 days prior to the Orbiter VOI (7) maneuver directly from interplanetary space. After separation, the Aerobot enters the venusian atmosphere (6) and begins operations shortly after the balloon inflation. After VOI, the Orbiter is placed in an elliptical polar orbit for 6 months and then releases the Lander (8) after taking RADAR and emissivity measurements of tessera targets. This mission concept is flexible enough to provide the option to extend this mapping orbit to acquire additional coverage of tessera terrain as an input to landing site selection. The Lander takes approximately 3 days to reach the planet’s atmosphere and 1 hour, from entry (9), to begin operations. The Orbiter provides communication access to the Lander for a short duration prior to handing over the relay to the SmallSats. Subsequently, the Orbiter performs a sequence of aerobraking maneuvers (10) over the course



VN116

Figure B-15. Final Polar Science Orbit

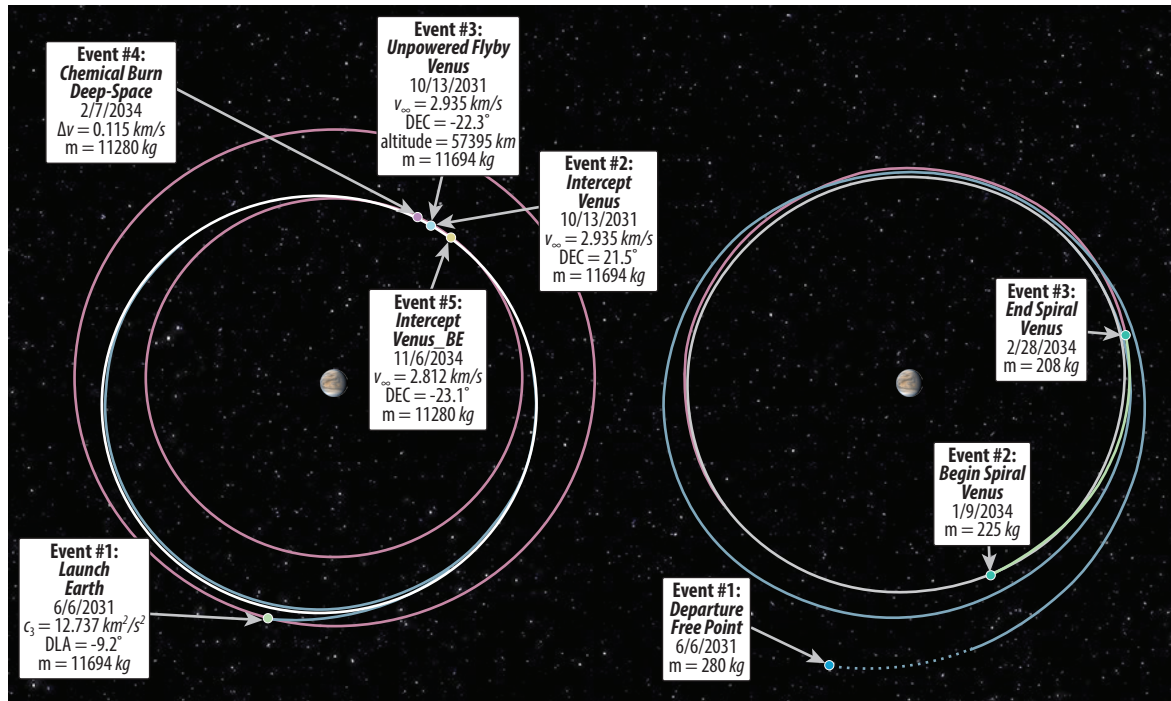
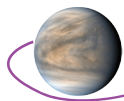


Figure B-16. Orbiter and SmallSats Baseline Trajectory.

Table B-6. Mission Design Table

Parameter	Orbiter Elliptical	Orbiter Circular	SmallSat 1	SmallSat 2
Orbit Parameters (Venus-centered Inertial Centered Reference Frame (ICRF))				
Apoapsis (km)	116,108.4	300	18,661	18,661
Periapsis (km)	300	300	500	500
Eccentricity	0.95	0	0.578	0.578
Inclination (°)	90	90	22.5	65
Orbital Period	5 days	1.6 hours	6 hours	6 hours
RAAN (°)	334.4	334.4	251.0	339.9
Argument of Periapsis (°)	188.6	188.6	86.7	359.5
Mission Lifetime	10 years		6 years	
Maximum Eclipse Period (minutes)	22.2	22.3	87.7	90.0
Launch Site	Cape Canaveral, FL			
Total Mass <b>with</b> contingency (includes instruments)	1,930.2		300.0	300.0
Propellant Mass <b>without</b> contingency	3,193.2		112.5	112.5
Propellant contingency	354.8		12.5	12.5
Propellant Mass <b>with</b> contingency	3,548.0		125	125
Launch Adapter Mass <b>with</b> contingency	71			
Total Launch Mass	9,584.6			
Launch Vehicle	Falcon 9 Heavy Expendable 5 m fairing			
Launch Vehicle Lift Capability	11,694.0			
Launch Vehicle Mass Margin	2,109.4			
Launch Vehicle Mass Margin (%)	22.0			

of approximately 2 years to reach its final 300 km polar science orbit (11) shown in **Figure B-15**. The concept of operations is based on science, trajectory and inter-asset communications requirements. Details of the mission design are found below in **Table B-6** and **Section B.2.7**. Required  $\Delta V$  for the mission and orbit parameters are summarized in **Table B-6** and **Table B-7**. The baseline trajectory shown in **Figure B-16** delivers the VFM platforms to Venus .



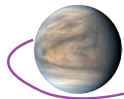
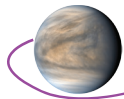


Table B-7. VFM Characteristics Table

Flight System Element Parameters (as appropriate)	Aerobot	Lander	Orbiter	SmallSats
<b>General</b>				
Design Life	60 Days	6 Hours	10 years	6 years
<b>Structure</b>				
Structures material (aluminum, exotic, composite, etc.)	Composite, AL, Honeycomb, Ti	Composite, AL, Honeycomb, Ti	Composite, AL, Honeycomb, Ti	–
Number of articulated structures	0	4 Sample Handling system, Drill, Raman/LIBS mirror, Leg Leveler	2 (Solar Arrays, Rotation Platform)	–
Number of deployed structures	3 (Anemometer, and Antenna, Antenna and Mag booms)	5 (4 Legs, Mass Spec Inlet Caps)	7 (Aerobot, Lander, 2 SmallSats, Antenna, Mag Boom and S/A)	–
Aeroshell diameter, m	2.8	4.6	N/A	N/A
<b>Thermal Control</b>				
Type of thermal control used	Convection and radiation white painted radiator	Ti flexures and Phase Change Material	Passive thermal radiator	–
<b>Propulsion</b>				
Estimated $\Delta V$ budget, m/s	N/A	N/A	1,642.8	
Propulsion type(s) and associated propellant(s)/ oxidizer(s)	N/A	N/A	Regulated Bipropellant, MMH, NTO	SEP
Number of thrusters and tanks	N/A	N/A	4 Main Engines 16 ACS Engines 1 MMH Tank 4 NTO Tanks 2 Press. Tanks	2 BHT600
Specific impulse of each propulsion mode, seconds	N/A	N/A	293	1750
<b>Attitude Control</b>				
Control method (3-axis, spinner, gravity-gradient, etc.)	None	Roll Axis with 2-Axis Translational Control	3-Axis	3-Axis
Control reference (solar, inertial, Earth-nadir, Earth-limb, etc.)	None	Local Vertical	Inertial	LVLH, Inertial
Attitude control capability, °	None	15	3 arcmin 3-axis 3-sigma	2 ° 3-axis 3-sigma
Attitude knowledge limit, °	None	10	0.5 arcmin 3-axis 3-sigma	-0.5 ° 3-axis 3-sigma
Agility requirements (maneuvers, scanning, etc.)	None	3-DOF maneuver agility	Antenna Pointing	3-DOF maneuver agility
Articulation/# –axes (solar arrays, antennas, gimbals, etc.)	0	0	2	2
Sensor and actuator information (precision/errors, torque, momentum storage capabilities, etc.)	IMU	IMU, Fans	IMU, ST, RCS, RWA, CSS	RWA, ST, IMU CSS
<b>Command &amp; Data Handling</b>				
Flight platform housekeeping data rate, kbps	2	2	2	–
Data storage capacity, Mbits	2,000	8,000	4,000,000	100,000
Maximum storage record rate, kbps	30,000	30,000	500,000	–
Maximum storage playback rate, kbps	30,000	30,000	30,000	–
<b>Power</b>				
Type of array structure (rigid, flexible, body mounted, deployed, articulated)	Fixed	N/A	Two-Axis	–
Array size, meters x meters	1.9 m2 active	N/A	5.4 m2 Active	–
Solar cell type (Si, GaAs, Multi-junction GaAs, concentrators)	TJGaAs	N/A	TJGaAs	–
Expected power generation at Beginning of Life (BOL) and End of Life (EOL), watts	448 (BOL) 380 (EOL)	N/A	2,181 (BOL) 1,845 (EOL)	– –



Flight System Element Parameters (as appropriate)	Aerobot	Lander	Orbiter	SmallSats
On-orbit average power consumption, watts	0	0	902	–
Day Power Consumption, watts	360	400	902	–
Night Power Consumption, watts	120	N/A	902	–
Battery type (NiCd, NiH, Li-ion)	Li Ion	Primary Lithium-Thionyl Chloride	Li Ion	–
Battery storage capacity, amp-hours	300	200	38	–

### B.2.5 Flight System

The VFM flight system consists of an Orbiter, Aerobot, Lander and two SmallSats as shown in **Figure B-12** and fits within the 5 m diameter of the Falcon 9 Heavy Expendable fairing. **Table B-7** shows the VFM characteristics. **Table B-8** below shows the total mass of the VFM flight system, the launch vehicle performance and the launch vehicle margin. The following sections provide an overview of each of the platforms. Further details on each platform can be found in **Section B.2.8**. The mission design (**Section B.2.7**) provides the  $\Delta V$  estimates for the mission. The propulsion (**Section B.2.8.4.**) uses the  $\Delta V$  from the mission design section and a conservative knock down on the engine Isp to determine the Orbiter propellant and size the tanks to cover both the 2031 and 2032 launch opportunities.

**Table B-8. VFM Mass and Launch Margin**

Platform/Item	MEV (kg)
Aerobot	1,433.2
Orbiter (dry)	1,930.2
Lander	2,002.2
SmallSats (wet)	600
Total Mass (pseudo dry)	5,965.6
Orbiter Propellant	3,548.0
Launch Vehicle Adapter	71
Total Launch Mass	9,584.6
Launch Capability	11,694.0
Margin	22%

#### B.2.5.1 Aerobot

The Aerobot is a floating platform that incorporates a helium variable-altitude balloon system which has the capability to control its altitude to a commanded profile in the venusian atmosphere. Important design characteristics of the Aerobot are shown in **Table B-7**. The instruments on the Aerobot are shown in **Table B-9** and the total mass and power of the Aerobot is given in **Table B-10**.

The VFM Aerobot uses a 15 meter diameter pumped-helium balloon with a second 7.5 m internal chamber (**Figure B-17**). The outer chamber is at approximately equal pressure with the atmosphere

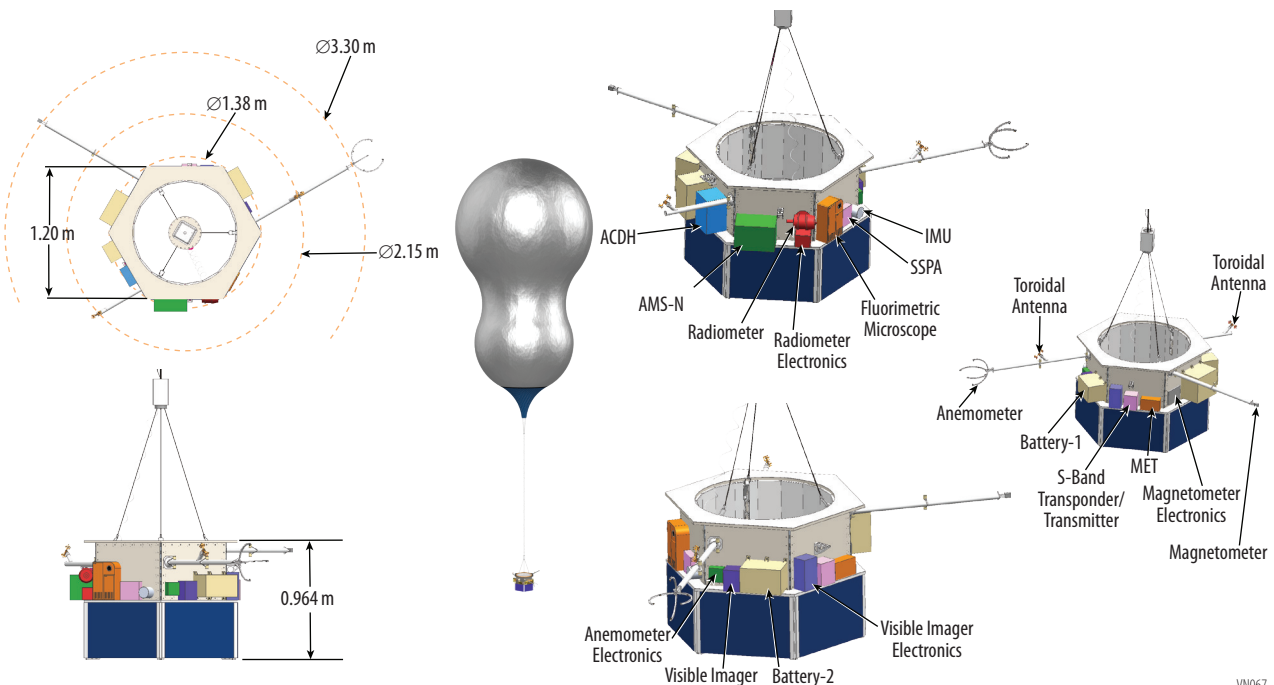


**Figure B-17. Aerobot showing subsystems and instruments**

VN067

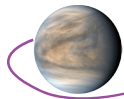


**Table B-9.** VFM Aerobot Payload Mass, Power, and Mission Data Volume

Instrument	Mass			Average Power			Mission Data Volume (Mbits)
	CBE (kg)	% Cont.	MEV (kg)	CBE (W)	% Cont.	MEV (W)	
Aerosol Mass Spectrometer with Nephelometer (AMS-N)	11	30	14.3	10.8	30	14.04	2,034
Fluorimetric Microscope (FM)	5	30	6.5	10	30	13	19
Magnetometer (Mag)	1	30	1.3	0.5	30	0.65	324
Meteorological Suite (MET)	3	30	3.9	5	30	6.5	2,280
Visible Imager (VI)	3	30	3.9	7	30	9.1	300
<b>Totals</b>	<b>23</b>	<b>30</b>	<b>29.9</b>	<b>39.3</b>	<b>30</b>	<b>51.1</b>	<b>4,957</b>

**Table B-10.** Aerobot Mass and Power Table

	Mass			Average Power (Day)			Average Power (Night)		
	CBE (kg)	% Cont.	MEV (kg)	CBE (W)	% Cont.	MEV (W)	CBE (W)	% Cont.	MEV (W)
Aeroshell	572.8	22.3	737.6	N/A	N/A	N/A	N/A	N/A	N/A
Structures & Mechanisms	55.4	10	61.9	N/A	N/A	N/A	N/A	N/A	N/A
Balloon System	186.0	30	241.8	N/A	N/A	N/A	N/A	N/A	N/A
Inflation System	230.8	10	253.9	N/A	N/A	N/A	N/A	N/A	N/A
Thermal Control	2.6	10	2.9	3.0	30	3.9	3.0	30	3.9
Propulsion (Dry Mass)	N/A	N/A	N/A	N/A	N/A	N/A	N/A	N/A	N/A
Attitude Control (Descent & Float)	0.1	10	0.1	2.0	30	2.6	2.0	30	2.6
Command & Data Handling	10.6	10	11.7	33.0	30	42.9	8.5	30	11.1
Telecommunications	6.3	16.3	7.3	39.1	30	50.8	8.1	30	10.5
Power	78.3	10	86.2	19.0	30	24.7	6.0	30	7.8
<b>Total Aerobot Subsystems</b>	<b>1,142.9</b>	<b>23</b>	<b>1,403.5</b>	<b>96.1</b>	<b>30</b>	<b>124.9</b>	<b>27.6</b>	<b>30</b>	<b>35.9</b>
Aerobot Payload	23	30	29.9	39.9	30	43.3	16.4	30	21.4
<b>Total Aerobot</b>	<b>1,165.8</b>	<b>23</b>	<b>1,433.2</b>	<b>206.4</b>	<b>30</b>	<b>268.3</b>	<b>71.0</b>	<b>30</b>	<b>91.7</b>

(a zero-pressure balloon), while a second internal chamber is at elevated pressure with a structural, constant-volume envelope (a super-pressure balloon). Helium is pumped from the outer chamber to the inner chamber to lower the total volume and hence buoyancy and altitude, while helium is vented from the inner to outer chamber to raise the altitude. The balloon system remains a sealed system for the entirety of operation; no atmosphere need be ingested. Details of the balloon design are found in **Section B.2.8.1**. Of note, lowering the altitude requires energy and is limited by the throughput of the pump, while raising the altitude can be done quickly for little energy by opening an orifice to vent the pressurized helium between the chambers. Operation of the Aerobot is discussed in **Section B.2.6.3.1**.

The variable-altitude balloon is currently TRL 4, and there is ongoing work at JPL to mature it further. Venus-relevant early prototype testing is scheduled for the summer of 2020. Helium tank plumbing release mechanisms and the helium pumps will require some development for the unique venusian atmosphere as well. **Figure B-17** shows the overall dimension as well as the placement of science instruments and electronics on the Aerobot's gondola.

Throughout the nominal 60-day mission, the balloon system will allow changes in the flight altitude of the Aerobot by transferring helium between a large, low pressure chamber and a small, high pressure chamber. The operational range of the Aerobot is 52–62 km above the surface of Venus and can survive brief excursions as low as 50 km and as high as 64 km and the Aerobot is expected to completely circle Venus once every 4–5 days. The structure is made of Aluminum with all environmentally exposed materials using common coatings to mitigate atmospheric corrosion.

The Aerobot's stowed configuration, **Figure B-18**, packages the main parachute, balloon system and single helium storage tank inside and

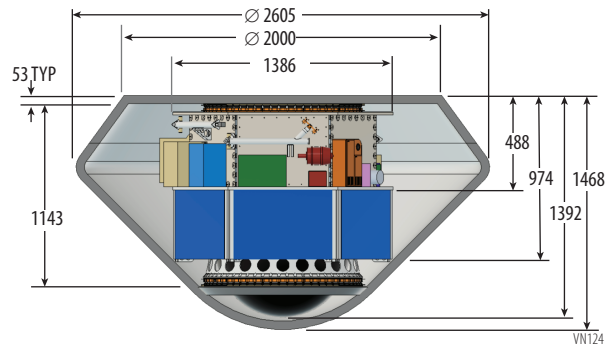
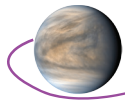


**Figure B-18.** Aerobot Stowed in aeroshell



along the centerline of the Aerobot's interior structure. The tank assembly is attached via a COTS separation system. All Aerobot instruments and systems are mounted around the external faces of the main structure's honeycomb panels. Signal and power harnesses will be mounted and routed on both external and internal panel surfaces. The aeroshell is a 45° sphere-cone geometry with a maximum diameter of 2.8 m. This geometry was chosen for its good stability and packaging characteristics as well as significant flight heritage at Venus. The heat shield TPS is a tiled, single-layer system of HEEET (Heat Shield for Extreme Entry Environment Technology) that is the baseline material for the Mars Sample Return Earth entry vehicle. PICA (Phenolic Impregnated Carbon Ablator) is the backshell TPS. The tiles are expected to be bonded to the structure using HT-424, while RTV-560 fills the gaps, using the same techniques as Mars Science Lab and Mars 2020. The Thermal Protection System (TPS) is designed not to let the temperature at the bondline between it and the structure exceed 260°C during the entry pulse. The expected peak-heating during the entry is 4,000 W/cm<sup>2</sup> (convective, rough wall, margined, at the shoulder) with an integrated heat load of over 53,000 J/cm<sup>2</sup>. The shoulder sees a relatively low radiative heating peak, margined value of 11.3 W/cm<sup>2</sup>, and an integrated heat load of 484 W/cm<sup>2</sup>.

The Entry, Descent, and Float concept for the Aerobot calls for two parachutes, one supersonic and the other subsonic. For the purposes of this study, the supersonic and the subsonic parachute are assumed to be identical, weighing 27.4 kg each. Details of the Entry, Descent, and Float design are found in **Section B.2.8.1.3.2** and concept of operations are discussed in **Section B.2.6.3.1**.

The Aerobot uses a power subsystem that includes a battery and solar arrays with characteristics shown in **Table B-7**. The Aerobot provides 2 Gbits of data storage and communicates at least once a day with a total contact time of at least 100 minutes with the SmallSat, as discussed in **Section B.2.6.3**.

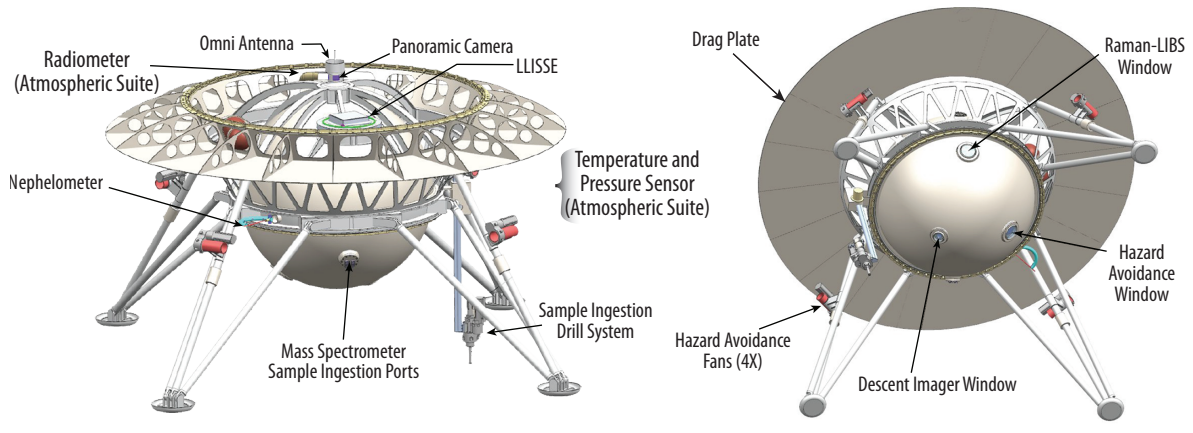
The Aerobot uses an IMU to provide disturbance data for correlation with science measurements. The Aerobot does not have an attitude control system or propulsion system and uses pressure measurements from the science instruments to determine its altitude and to inform altitude changes. Avionics and electrical components all have extensive flight heritage with only minor qualification updates needed for the survivability at altitudes of 50 and 64 km. **Table B-9** shows the Aerobot payload mass, average power and mission data volume while **Table B-10** shows the mass, daytime average power, and the night time average power budgets for the Aerobot. A Master Equipment List (MEL) was developed and contingency was assigned at the component level based on TRL. Those items that have flown before and required no modification, with a high TRL, were assigned a contingency of 10%. Items that had to be modified were assigned 20% and new items or those that required significant modifications were assigned 30%. All structural items were assigned 30%. The total system has 23% Launch mass margin on the wet mass. A conservative approach was taken with power and 30% contingency was used on all loads.

There are three deployable structures (Boom-Arms) which extend away from Aerobot. Once deployed they provide instruments and antennas 0.5 m–2.0 m distance from the Aerobot structure; Boom-Arm One is for the Anemometer and Antenna One, Boom-Arm Two is for Antenna Two, Boom-Arm Three (2 m) is for the **Mag**. All of these components are well within the state-of-the-art. Details on the Aerobot are in **Section B.2.8**.

## B.2.5.2 Lander

The VFM Lander is shown in **Figure B-19**. Important characteristics are shown in **Table B-7** and **Table B-11** shows the Lander payload mass, power and data volume. **Table B-12** shows the Lander subsystem masses and the total Lander mass and power.

The VFM Lander is designed to safely land the instrument payload in a tessera region of Venus and survive for at least 6 hours, with a goal of 8 hours. In order to land safely, the mechanical design needs to accommodate landing terrain uncertainty. To account for the uncertainty, the Lander is designed to land on a slope of up to 30° and accommodate a 0.5 m boulder beneath the sphere. With landing as the highest risk for the mission, the Lander includes both a Terrain Relative Navigation (TRN) and a Landing Hazard Avoidance (LHA) system. The TRN would be used to estimate the Lander's local relative position by comparing terrain maps, which would be loaded into memory prior to separation, with terrain measurements from navigation sensors (LIDAR, optical engineering camera, laser altimeter). The LHA assesses the hazards in the projected landing site and uses fans to move the Lander laterally to avoid landing on a hazard. The TRN and LHA are discussed in more detail in **Section B.2.8.2.5**.



VN101

**Figure B-19. VFM Deployed Lander Exterior Features**

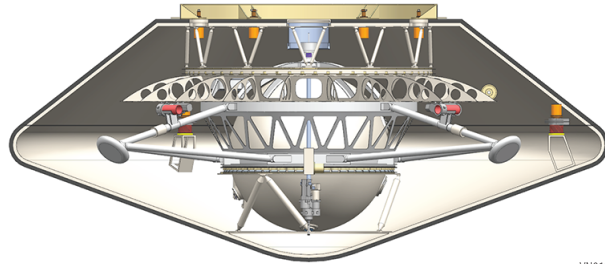
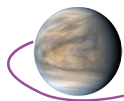
The equatorial ring of the hemisphere is the primary backbone of the Lander design (**Figure B-19**). On the exterior, it provides the interface to the aeroshell, drag plate, legs, Nephelometer, and the instrument sphere. A bridging structure, which does not interface with the instrument sphere, is used to bridge the leg loads and isolate the sphere during landing. The bridge also provides mounting of the **LLISSSE** payload. The drag plate is used to control the terminal velocity during descent. Detailed flight dynamics of the drag plate have not been performed, but some approximate calculations were done and used in the entry descent and landing design that is discussed in **Section B.2.8.2.3**. The **PC** uses four mirrors within the cupola to provide 60° FOV from each of the four windows. The camera views

**Table B-11. VFM Lander Payload Mass, Power, and Mission Data Volume**

Instrument	Mass			Average Power			Mission Data Volume (Mbits)
	CBE (kg)	% Cont	MEV (kg)	CBE (W)	% Cont	MEV (W)	
Neutral Mass Spectrometer (NMS)	16.5	30	25	60	30	78	7.3
Tunable Laser Spectrometer (TLS)	4.5	30	5.9	26.1	30	33.9	13
Atmospheric Structures Suite (AS)	4.8	30	6.2	697	30	8.1	2.3
Descent NIR Imager (DI)	5	30	6.5	40	30	53	463
Neutron Generator/Gamma Ray Spectrometer (GRS)	12	30	15.6	5	30	6.5	25.1
Nephelometer (Neph)	1.5	30	2.0	6.6	30	8.6	1
X-Ray Diffractometer (XRD)	5	30	6.5	29.5	30	38.4	24
X-Ray Fluorescence Spectrometer (XFS)	1.0	30	1.3	8	30	10.4	2.1
Panoramic Camera (PC)	3	30	3.9	12	30	15.6	2,255
Raman-LIBS (R-LIBS)	25	30	32.5	61	30	79.3	1,720
LLISSSE	10	30	13	N/A	30	N/A	1,000
<b>Total Payload</b>	<b>88.3</b>	<b>30</b>	<b>114.8</b>	<b>316.8</b>	<b>30</b>	<b>411.8</b>	<b>5,513</b>

**Table B-12. Lander Mass and Power Table including Payload**

	Mass			Average Power		
	CBE (kg)	% .	MEV (kg)	CBE (W)	% .	MEV (W)
Aeroshell	786.3	23	1,015.2	N/A	N/A	N/A
Structures & Mechanisms	448.2	30	546.2	N/A	N/A	N/A
Thermal Control	88.9	30	115.6	0	0	0
Propulsion (Dry Mass)	N/A	N/A	N/A	N/A	N/A	N/A
Attitude Control (Descent only)	72.6	10	79.9	44.0	30	57.2
Command & Data Handling	39.3	24	48.6	80.5	30	104.7
Telecommunications	5.5	11	6.1	39.0	30	50.7
Power	69.0	10	75.8	7.0	30	9.1
Total Lander Subsystems	1,509.8	25	1,887.4	170.5	30	221.7
Lander Payload totals	88.3	30	114.8	316.8	30	411.8
<b>Total Lander</b>	<b>1,598.1</b>	<b>25.3</b>	<b>2,002.2</b>	<b>1,193.3</b>	<b>30</b>	<b>1,551.3</b>



VN013

Figure B-20. Lander Stowed in Aeroshell

are limited by the drag plate below the windows. Additional options to increase the PC FOV, such as a drag plate that folds out of the way after landing or a deployable drag plate that sits above the Lander, are left to future studies.

The aeroshell cone angle of 70° and 4.6 m diameter provides ample volume (Figure B-20) and allows a very simple leg design with a telescoping upper arm. This allows for both a single motion deployment and for energy absorption with the use of a crushable canister inside the leg tube. The

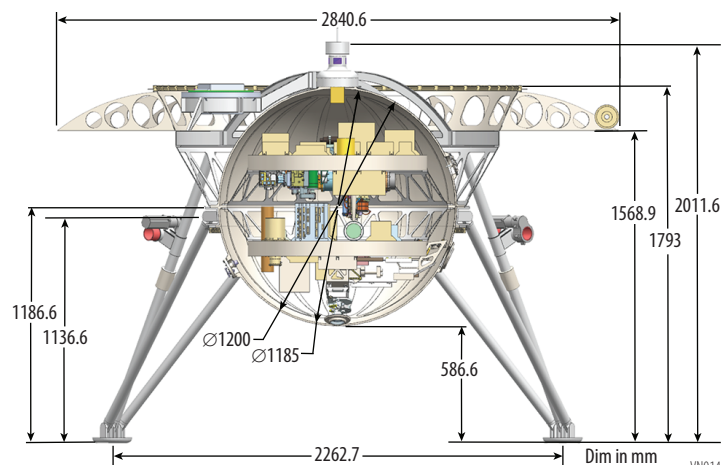
legs provide mounting for the fan actuation system. The addition of hazard avoidance capability for the Lander opened up the possibility for a smaller, simpler leg design. A drive system, used to deploy the legs, can also be used to stabilize the landed craft after landing to within 10° of the gravity vector. This leveling ensures the omni antenna on top of the Lander has the maximum field of view and thus maximum data transfer. It should be noted that the width of the leg stance could be greatly increased, thereby increasing landing stability, by implementing a multi-fold leg design. This would also allow a smaller diameter entry system. This optimization was left for future study. At the base of the legs are landing pads. Additional studies are needed to determine the type of foot interface based upon the expected terrain; for example, spikes may be of more utility when landing on slopes to prevent sliding.

The 70° sphere-cone aeroshell geometry provides significantly better packaging and drag performance than the 45° sphere-cone (e.g., Pioneer Venus) and has a smaller surface area for a given diameter (thereby reducing the mass of the thermal protection system). The 70° sphere-cone geometry has been successfully used at Mars (with similar upper atmospheric composition as Venus). Aerothermal analysis shows that while there is higher radiative heating near the shoulder compared to the 45° geometry, the total heating is still within the capability of the thermal protection system. A benefit of the 70° sphere-cone, by virtue of smaller surface area, results in a lighter heatshield than for a 45° sphere-cone. The heatshield TPS is a tiled, single-layer system of HEEET. PICA is used as the backshell TPS. The tiles are expected to be bonded to the structure using HT-424, with RTV-560 filling the gaps, using the same techniques as Mars Science Lab and Mars 2020. The Thermal Protection system is designed to not let the internal/bondline temperature exceed 260°C during the entry pulse. The expected peak heating during the entry is 1734 W/cm<sup>2</sup> (convective, rough wall, margined, at the shoulder) with an integrated heat load of 23,875 J/cm<sup>2</sup>. The shoulder also sees a peak radiative heating of 87.3 W/cm<sup>2</sup> (margined) with a corresponding heat load of 1379 J/cm<sup>2</sup>.

The aeroshell utilizes a supersonic parachute for deceleration prior to Lander separation and for stability near Mach 1. The parachute design is a 10.04 m diameter Disk-Gap-Band parachute deployed at Mach 1.4, and is expected to weigh 35.6 kg. This parachute design has flown many times at Earth and Mars and the loads and deployment conditions are within recently demonstrated limits.

The backshell geometry used in the current design is driven by packaging constraints: i.e., the smallest backshell that can package all the components inside the aeroshell. The backshell geometry is within the envelope of legacy backshell geometries and any of those would also meet the packaging constraints of the Lander. Details of the backshell design are in Section B.2.8.1.2.8.

The instrument sphere is built in three sections as shown in Figure B-21. The upper hemisphere supports the sample handling evacuation spheres and the PC cupola and provides an access port for integration. The PC cupola



VN014

Figure B-21. VFM Cutaway view shows packaging inside the Sphere

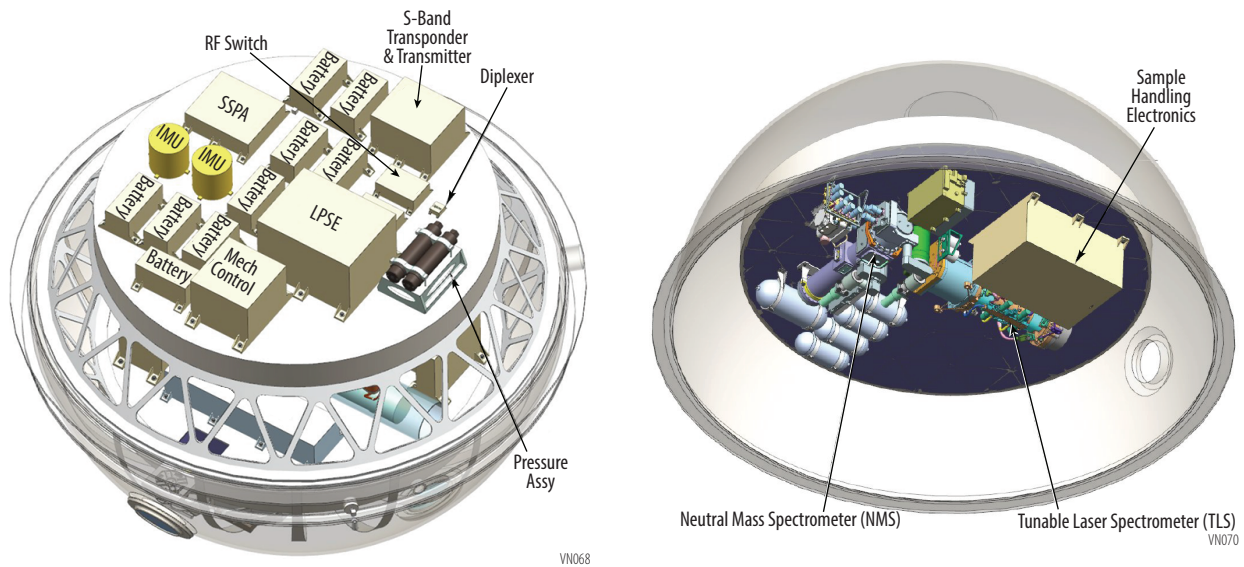
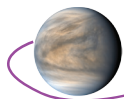


Figure B-22. VFM Sphere Top Deck Details

provides a FOV  $\geq 60^\circ$  per mirror (4) with  $240^\circ$  azimuth coverage and  $60^\circ$  below the nominal flat horizon and  $30^\circ$  above. An access port has plumbing for evacuating the sphere prior to launch. The lower hemisphere has the TLS and NMS inlet assembly and three windows. The lowest window is for the DI and provides a Field of View  $> 90^\circ$ . Slightly higher is the window for the hazard avoidance sensors including the LIDARs, laser range finders and the engineering camera. A final window is for the R-LIBS. The equatorial ring has the electrical connection port, and a pass-through for the AS mounted on the outside of the sphere, and is the structural interface to the drag plate and legs. On the inside, it supports the thermally isolating ‘elephant stands’ which support the upper and lower decks. The equatorial ring is part of the spherical geometry to maintain as consistent a spherical shape as possible, maximizing sphere strength.

The upper and lower decks are isogrid aluminum. The isogrid pockets are used for embedding the phase-change material; and the aluminum provides high conductivity to the boxes and instruments. The phase-change material will become liquid when it changes phase and is contained within the decks. As required for thermal isolation of the decks, the ‘elephant stands’ are titanium, which will require a flexure interface with the decks to mitigate CTE mismatch issues. Each deck has mounting interfaces on both top and bottom sides. A sheet metal aluminum retainer supports the sphere insulation. Metal C-seals will be required at all sphere ports and separation planes. The sphere will be launched evacuated which should simplify the sealing of all ports and pass-throughs as well as the sphere segments. Structural concepts developed for this study are within the current state-of-the-art and have heritage. It is likely that high pressure sealing and ports/pass-throughs will require additional development and testing.

Deck components are grouped by function whenever possible (Figure B-22 and Figure B-23). An upper deck primarily holds the Lander operational boxes such as communication and power boxes. Between decks is dominated by instrument boxes with the exception of the Lander Command and Data Handling (LCDH) box. The lower volume has both instrument components and the landing hazard avoidance boxes. Characteristics of the Lander subsystems are discussed briefly below, in detail in Section B.2.8.2 and an overview is provided in Table B-7.

The bottom deck (Figure B-23) accommodates the sample ingestion and handling system, the GRS, XFS, XRD, and R-LIBS.

The Lander is designed to operate for at least 6 hours and up to 8 hours on the surface of Venus where the temperature of the atmosphere is  $\sim 440^\circ\text{C}$  and the pressure is 76 bar at West Ovda. The sphere is painted white with Z93C55 conductive coating. The sphere will start at  $-25^\circ\text{C}$  in orbit around Venus before descent. During descent temperatures will steadily increase as the Lander descends into the atmosphere. As mentioned above, phase-change material (n-Eiocane ( $\text{C}_{20}\text{H}_{42}$ )  $+37^\circ\text{C}$ ) is used within the decks to flatten the temperature ramp.

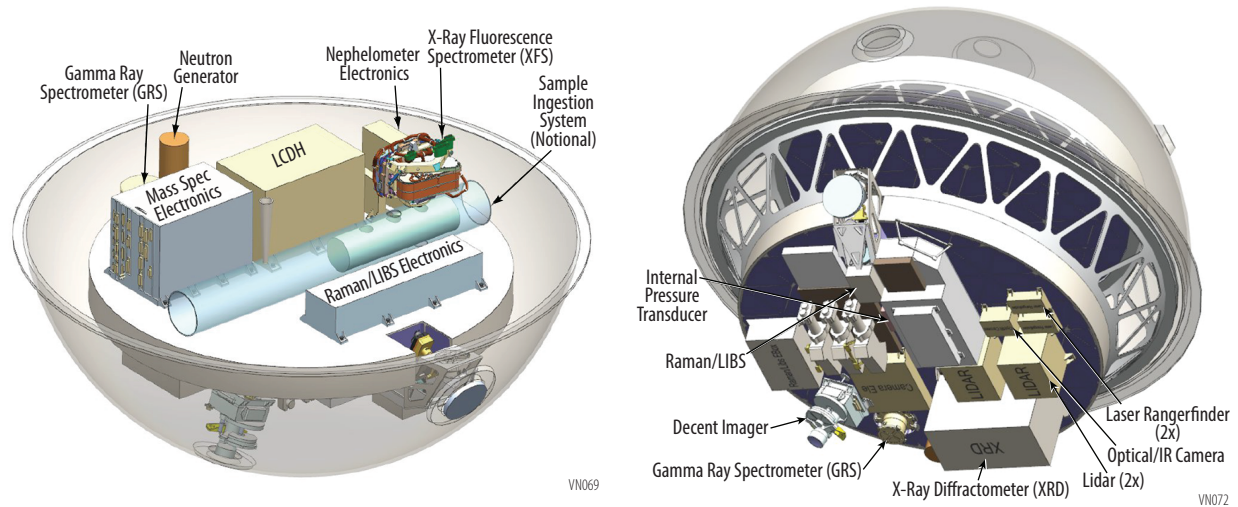
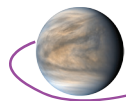


Figure B-23. VFM Bottom Deck Details

The decks are thermally isolated from the sphere with a titanium flexure ring and all avionics and instruments are thermally coupled to the decks. For the three windows, each of which is triple-paned, a low emissivity coating is used to reduce heating of the instrument optics. The emissivity is 0.15 on both sides of the inner window. The sphere is evacuated to high-vacuum conditions ( $10^{-6}$  torr) to reduce convective heat transfer and allow effective MLI blanketing. Zeolite is used to keep high vacuum in the sphere during outgassing. Both high temperature MLI blanketing and “Standard” Kapton MLI are used. High temperature MLI blanketing is used on the inner walls of the sphere with MLI used on the decks.

A thermal model of the Lander is discussed in **Section B.2.8.2.8** and the model results for heating during the 1 hour of descent and 7 hours of surface operations are discussed in **Section B.2.8.2.8.2**. All the thermal hardware has a high TRL level and has been used on many spaceflight programs.

The Lander avionics system provides a Lander Command and Data Handling (LCDH) with a low power VORAGO ARM Cortex-M4 processor for the commanding instruments, sample collection and the drill. The LCDH collects, processes and stores science data as well as health and safety data on the 8 Gbit solid state recorder. The LCDH also includes a High Performance Spacecraft Computing (HPSC) ARM Cortex A53 for the processing of TRN and LHA algorithms. Timing with an accuracy of  $\geq 0.1$  msec with  $10^{-6}$  stability relative to a ground station is provided by an ultrastable oscillator. A Mechanism and Propulsion Unit (MPU) provides cards that interface with the aeroshell separation hardware and control deployments including: parachute, heat shield, backshell, leg deployments and fans. Communication links are discussed in **Section B.2.1**.

The Lander power system consists of a primary (non-rechargeable) battery and supporting power electronics. The power system configuration is driven by lack of any usable solar flux at the Venus surface yielding no way to generate power to support loads or recharge a secondary battery. Saft LSH20 D 13000mAh 3.6V Lithium-Thionyl Chloride cells are used in a 9 series 9 parallel (9s9p) configuration to provide 200 AH of energy at 32V. Due to the nature of the battery (it cannot be recharged), all Lander subsystems remain off until just prior to separation from the Orbiter. The Power System Electronics (PSE) will be a battery-dominated bus included as cards in the avionics package. The PSE will control switching and power distribution.

### B.2.5.3 Orbiter

The VFM Orbiter (**Figure B-24**) functions as a carrier and propulsion system for the other mission platforms, communication relay for the Lander and Aerobot as well as an important science platform. The instruments on the Orbiter are listed in **Table B-13** along with their mass, power, and mission data volume and include a SAR, NIR-I, S-mm, Mag, 2 ESA-i and 2 ESA-e, with 2

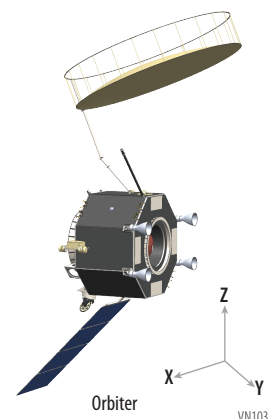
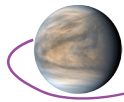


Figure B-24. VFM Orbiter





**Table B-13.** VFM Orbiter Payload Mass, Power, and Mission Data Volume

Instrument	Mass			Average Power			Mission Data Volume (Gbits)
	CBE (kg)	% Cont	MEV (kg)	CBE (W)	% Cont.	MEV (W)	
Synthetic Aperture Radar (SAR)	100	30	130	500	30	650	57,318
Near IR Imager (NIR-I)	3.4	30	4.42	13	30	16.9	2,707
Sub-MM Spectrometer (S-mm)	19.3	30	25.1	55	30	71.5	16,399
Flux Gate Magnetometer (Mag)	1	30	1.3	1	30	1.3	410
Neutral Mass Spectrometer (NMS) x2	28	30	36.4	2.4	30	3.1	5,931
Ion Electrostatic Analyzer (ESA-i) x2	6.4	30	4.16	3.7	30	4.81	7,094
Electron Electrostatic Analyzer (ESA-e) x2	4.4	30	2.86	2.1	30	2.73	902
<b>Total Payload</b>	<b>162.5</b>	<b>30</b>	<b>211.3</b>	<b>583.0</b>	<b>30</b>	<b>757.9</b>	<b>90,760</b>

**Table B-14.** Orbiter Mass and Power Table

	Mass			Average Power		
	CBE (kg)	% .	MEV (kg)	CBE (W)	%.	MEV (W)
Structures & Mechanisms	746.6	30	970.6	N/A	N/A	N/A
Thermal Control	12.3	10	13.5	N/A	N/A	N/A
Propulsion (Dry Mass)	427.2	10	467.9	N/A	N/A	N/A
Attitude Control (Descent only)	85.9	10	94.5	16.3	30	21.2
Command & Data Handling	19.5	10	21.5	41.5	30	52.6
Telecommunications	12.6	16	14.7	180.0	30	234.0
Power	123.9	10	136.3	18.0	30	23.4
<b>Total Orbiter Subsystems</b>	<b>1,428.0</b>	<b>20</b>	<b>1,719.0</b>	<b>255.8</b>	<b>30</b>	<b>331.2</b>
<b>Total Payload</b>	<b>162.5</b>	<b>30</b>	<b>211.3</b>	<b>580.6</b>	<b>30</b>	<b>754.8</b>
<b>Total Orbiter</b>	<b>1,590.5</b>	<b>21</b>	<b>1,930.2</b>	<b>836.4</b>	<b>30</b>	<b>1,085.9</b>

NMS facing opposite directions (to enable sampling in the RAM direction as we rotate the spacecraft to keep the radiators from seeing the sun). **Table B-14** shows the Orbiter subsystems masses and power as well as the total Orbiter mass.

The **S-mm** instrument has a wide field of view (45°) perpendicular to the spacecraft velocity vector and its boresight is pointed at nadir. The **S-mm** is mounted on a table to provide the ability to look at the limb in the + and - z direction. The **Mag** is deployed on a 2 m boom. Two sets of the **ESA-i** and **ESA-e** are mounted on the + and -x panels in order to measure full 3D velocity distribution functions in both the solar wind and venusian plasma environment. These distributions are especially important to better understand heating and acceleration of plasma throughout the induced magnetosphere and inner heliosphere.

The 5 m antenna functions as both the **SAR** and the communication antenna for S-band, X-band and Ka-band systems. The Orbiter also has two X-band omni antennas and a medium gain X-band antenna for commanding and backup. The 5 m antenna stows into a very compact package with enough clearance to mount it on the -y panel. The antenna is a smaller version of the 6 m antenna flown in 2015 on Soil Moisture Active Passive (SMAP). The deployment system is the same as used on SMAP without the added turntable that SMAP required.

The Orbiter structural design was driven by carrying the launch loads of the other mission platforms through to the launch vehicle. The Aerobot is mounted beneath the Orbiter and inside the 3.1m PAF used to attach to the upper stage of the Falcon 9 Heavy Expendable. The Orbiter structural radials are the transition load path from the 3.1 m interface to the launch vehicle and the central cylinder, which carries the launch loads for both the Lander and the Aerobot. The Orbiter structure was designed with composite face sheet/aluminum honeycomb core panels using the clip and post method employed on other composite structures such as Lunar Reconnaissance Orbiter (LRO). The basic structure of a central cylinder, upper and lower deck, radials and equipment panels is very common and well understood. The dry mass efficiency of the structure is approximately 12%.

To accommodate the placement of the Aerobot under the Orbiter the main engines were moved outboard (**Figure B-25**). This had the added benefit of providing significant ACS capability. The octagon design provided an efficient mount for the large oxidizer tank and the central cylinder and

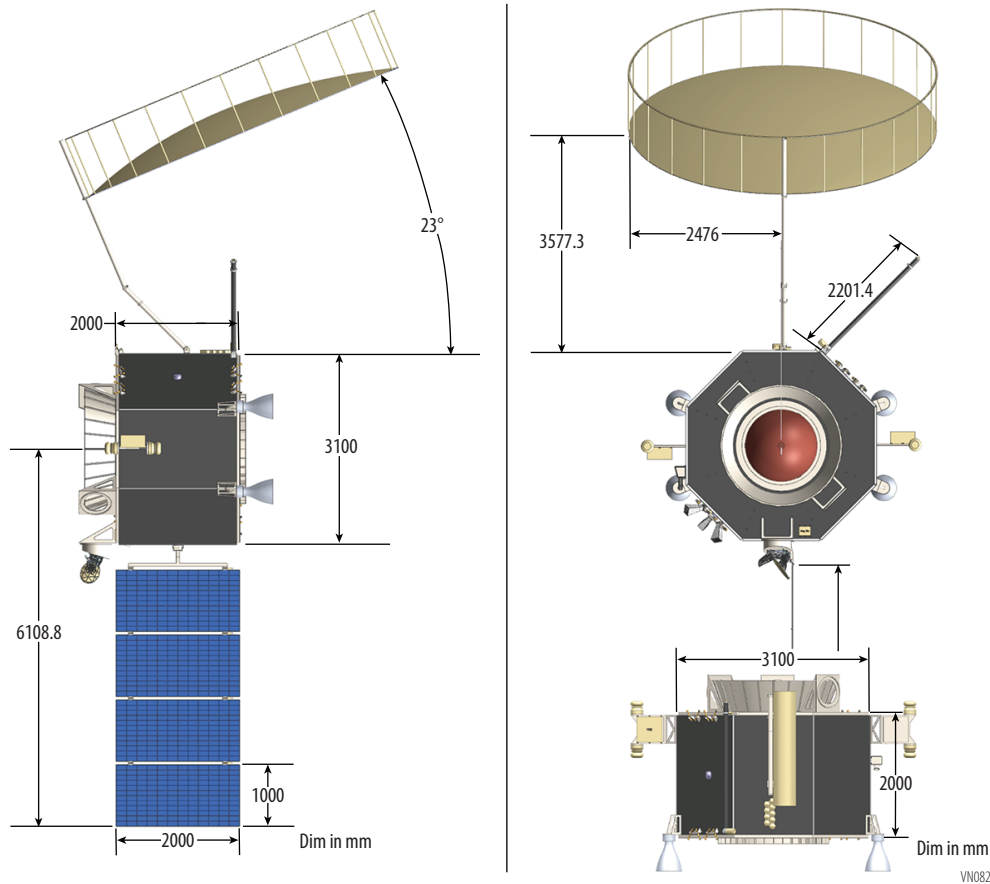
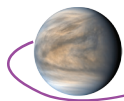


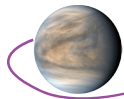
Figure B-25. Orbiter Dimensions

bays for mounting the four fuel tanks. The central cylinder is the primary support for the Lander. The Lander inside its aeroshell is attached to the top deck of the Orbiter using COTS separation rings and the SmallSats are tucked in between the Lander and the top deck of the Orbiter. The SmallSats are attached via separation rings to a vertical bracket, similar in concept to a Moog's Evolved Secondary Payload Adapter (ESPA). All structural components are well within the state-of-the-art.

The Orbiter power system consists of solar arrays, a secondary battery, and supporting power electronics. TJGaAs solar cells with bare-cell efficiency of 29.5% are used. The solar constant at Venus is 2263 W/m<sup>2</sup>, and the arrays operate at 140°C. Space Environmental Effects and Education System (SPENVIS) solar array degradation factors were used to derive the array area. A single two axis tracking panel with 5.4m<sup>2</sup> active area (5.9 m<sup>2</sup> total substrate area) will provide 1,845 W End-of-Life (EOL) and 2181W Beginning-of-Life (BOL) power to support loads and battery recharge. A high energy density 38AH Li Ion battery is used to support night loads. The Power System Electronics (PSE) will be a battery-dominated bus included as cards in the avionics package. All Orbiter power components are greater than TRL 7.

The avionics for the Orbiter are a block redundant system to meet the reliability for a Class A Flagship Mission. The avionics consists of the following functions: Command and Data Handling (C&DH), attitude control sensors and thrusters, power conditioning and distribution, mechanisms for launch locks, deployments and motors, and control of main engine propulsion. The avionics implementation consists of three enclosures, C&DH Unit, the Power System Electronics (PSE) and the Mechanism, and Propulsion Unit (MPU) and is detailed in **Section B.2.8.3.6**. All avionics components are TRL 7 or greater with significant heritage.

The Orbiter, for most of the mission, functions as a communication relay between Earth and the Lander, and the Aerobot. The Orbiter utilizes a store and forward protocol called Delayed Tolerant Network (DTN), which has the ability to store packets from the Lander, and Aerobot and forward



them to Earth or receive commands from Earth and forward them to the Lander and Aerobot. Orbiter operations are discussed in **Section B.2.6.3.3**.

The Orbiter is three-axis stabilized with significant momentum and torque capabilities to account for the large inertia associated with the stacked configuration. The Orbiter ACS design is discussed in **Section B.2.8.3.8**. All of the ACS components have significant flight heritage and can meet the life mission requirement.

The VFM Orbiter thermal design has radiators on the  $-z$  surface, bottom deck, to dissipate electronics heat while keeping the radiators out of the Sun (and view of the hot Venus surface). During cruise phase, the attached aeroshell will somewhat cover the radiators' view to space, but no enhancements to the thermal system are needed; the radiators can still dissipate the requisite heat during the cruise phase. A 'toasty' cavity approach eliminates propulsion system heaters on the fuel tanks and lines while orbiting Venus.

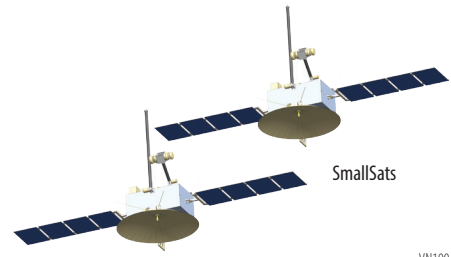


**Figure B-26.** Two SmallSat in operational configuration showing deployed solar arrays and antennae

### B.2.5.4 SmallSats

The Venus Flagship Mission uses two SmallSats (**Figure B-26**) that provide science data from the instruments listed in **Table B-15** and communications coverage for the Aerobot and Lander. The SmallSat payload mass, power, and mission data volume are shown in **Table B-16**. SmallSats are expected to be identical and procured commercially. The study focused on developing a concept that meets the data storage and communication requirements including defining a feasible propulsion subsystem since the SmallSat subsystems are rapidly evolving and a decade from now commercial availability will drastically change. As a result, the SmallSat concept is at CML 2 although a preliminary mass estimate was made and is shown in **Table B-16**. Due to the nature and focus of the current study, only the propulsion, communication and data storage needs were explored. Since the component heritage is unknown, all mass estimates were assigned a 30% contingency. Details of the other SmallSat subsystems are left to future studies.

The SmallSats (**Figure B-27**) are expected to be physically identical, but will be deployed in different venusian orbits as described in **Section B.2.7.4**. The requirement to provide access to the Aerobot and Lander drives the need for the SmallSats to be orbiting Venus prior to the arrival of the other platforms. SmallSats separate from the Orbiter a few hours after launch and guide themselves to Venus, each using solar electric propulsion. After arrival at Venus they follow a low-thrust spiral down to their final Venus orbits.

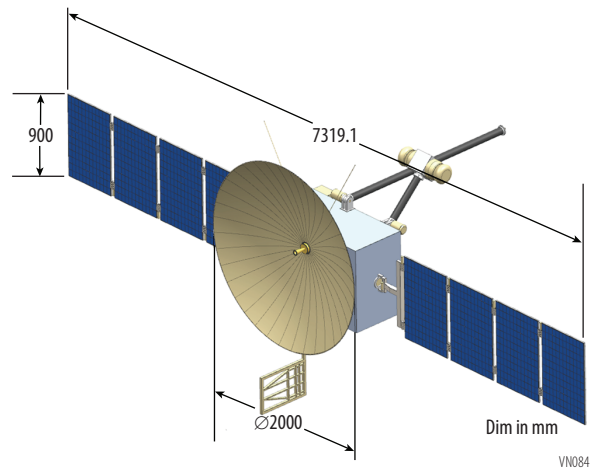


**Figure B-27.** SmallSat Dimensions

**Table B-15.** Single SmallSat Payload Mass, Power, and Mission Data Volume

Instrument	Mass			Average Power			Mission Data Volume (Mbits)
Langmuir Probe (LP)	2.6	30	3.4	2.7	30	3.5	18.5
Ion Electrostatic Analyzer (ESA-i)	3.2	30	4.2	3.7	30	4.8	3,067.7
Electron Electrostatic Analyzer (ESA-e)	2.2	30	2.9	2.1	30	2.7	390
Solar Energetic Particle Detector (SEPD)	2	30	2.6	2.6	30	3.4	17.7
Magnetometer (Mag)	0.5	30	0.7	1	30	1.3	176.5
Extreme Ultraviolet (EUV)	7	30	9.1	14	30	18.2	141.6
Electric Fields Detector (E-Fd)	3	30	3.9	3	30	3.9	307.8
<b>Total Payload</b>	<b>20.5</b>	<b>30</b>	<b>26.7</b>	<b>29.1</b>	<b>30</b>	<b>37.8</b>	<b>4,119.6</b>

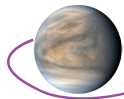


**Table B-16.** Single SmallSat Mass and Power

	Mass			Average Power		
	CBE (kg)	%	MEV (kg)	CBE (W)	%	MEV (kg)
Structures & Mechanisms	33.0	30	49.4	-	-	-
Thermal Control	6.9	30	9.0	-	-	-
Propulsion (Dry Mass)	27.0	30	35.1	-	-	-
Attitude Control (Descent only)	12.0	30	15.6	-	-	-
Command & Data Handling	11.2	30	9.3	-	-	-
Telecommunications	10.0	30	14.6	-	-	-
Power	14.0	30	18.2	-	-	-
<b>Total SmallSat Subsystems</b>	<b>114.1</b>	<b>30</b>	<b>148.3</b>	-	-	-
<b>Total Payload</b>	<b>20.5</b>	<b>30</b>	<b>26.7</b>	<b>29.1</b>	<b>30</b>	<b>37.8</b>
<b>Total SmallSat</b>	<b>134.6</b>	<b>30</b>	<b>175.0</b>	-	-	-

The communication subsystem was sized to provide the capabilities listed in **Table B-16** and the data storage needed was derived from the concept of operation with ample margin applied.

### B.2.5.5 Platform and Subsystem Trades

The subsystem trade studies are illustrated in **Figure B-28** for the Lander and **Figure B-29** for the Aerobot, Orbiter, and SmallSats. The trades are discussed later with additional lower level trades in each of the flight platform sections.

### B.2.5.6 Technology Maturity

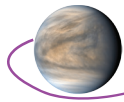
The majority of the VFM mission concept uses proven flight hardware. However, there are several areas where a technology maturity effort either enables the mission or significantly reduces mission risk. Both the Orbiter and SmallSats will be procured commercially with little to no technology development. However, the Lander and Aerobot do require advances in specific technologies as well as some of the instruments. The main technology development is for the Landing Terrain Relative Navigation and Hazard Avoidance system, which enables safe landing on the sloped tessera terrain. The three lowest TRL platforms are described here.

#### B.2.5.6.1 Lander Technology Maturity

**Integrated Terrain Relative Navigation and Landing Hazard Detection and Avoidance:** Extreme environmental conditions make safe landing on the Venus tessera terrain challenging because the tesserae present an irregular, hazardous topography and VFM sample ingestion and surface interrogation instrumentation rely on appropriate Lander orientation. A high-level trade study conducted as part of this concept development resulted in the combination of a TRL 2 Terrain Relative Navigation and Landing Hazard Avoidance system and a divert system composed of four fans. However, further study and technology maturity is needed for an integrated system that avoids hazards, controls Lander orientation and minimizes overall risk to landing on the Venus surface. Terrain Relative Navigation (TRN) on Mars has been developed for Perseverance with the Europa Lander pre-project extending that technology to Landing Hazard Avoidance (LHA) on an airless body, but to date neither TRN nor LHA have been attempted at Venus. Some of the technology *may* be developed for Dragonfly, which will land on Titan, but Venus has a thicker, denser atmosphere, so the technology would have to be adapted to Venus conditions. In addition, the fan hardware, needed to perform the divert maneuvers for the LHA, needs further development to bring it to TRL 6. Without LHA the risk to landing safely increases, which could result in loss of scientific measurements, although the instruments with the greatest dependence on Lander orientation, e.g., the **XRD** and the **XFS**, which require ingested samples, are partially redundant with the **Raman** and **LIBS/GRS**, respectively, thereby mitigating this risk somewhat.

#### B.2.5.6.2 Aerobot Technology Maturity

**Balloon:** The variable-altitude Aerobot platform is currently TRL 4. Constant-altitude platforms have been flown on Venus before (i.e., Vega Missions) and naturally have a higher TRL, but VFM has selected variable-altitude in keeping with recommendations of enhanced science return benefits de-



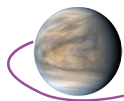
Lander			
Spin up for entry	Orbiter roll		< Simple, minimal
	Turntable		X Added mechanism, mass
	Self Spin		X No RCS system on lander
Thermal Control	Hi Temp Electronics		X Very low TRL, possible for future missions
	Phase Change Material	n-Eiocene (C <sub>20</sub> H <sub>42</sub> )	< Simple, low cost
		ISRU Dry Ice (CO <sub>2</sub> )	X Very low TRL
		Li Nitrate Trihydrate	X Not needed to meet requirements, viable if needed
Autonomy	Limited Commands		< Enables variable transmission rates and prioritized data
	Sequencer		X Resources available for limited commanding
	Full Autonomy		X low TRL
Sample Method	Ingest	Drill and Pneumatic	< Simple, minimal impact on pressure vessel
		Drill and Scoop	X Complex sample handling
	Remote Measure	Autofocus	< Provides needed sensitivity
		No focus	X LIBS would be less sensitive
Panoramic Camera FOV	Unblocked 360		X Need drag plate for landing
	Internal rotation with Cupola		< Provides required 360, some blockage due to drag plate
	Fixed < 360		X Does not meet science objectives
Support Structure	Legs		< Best stability on required 30° slope
	Ring		X Needs outriggers, self righting system
Safe Landing	Hazard Avoidance	Thrusters	X Exceeds state of the art
		Flaps	X Winds make this not practical
		Fans	< Provide needed force
	Landing Site Selection		X Not sufficient for Tessera landing
Power	ASRG		X Sink Temperature makes them poor design for Venus
	Secondary Batteries		X Lower energy/mas density ratio
	Lithium-Thionyl Chloride Primary		< Provide needed power with lowest mass
Communication	Omni		< Lowest cost, works with uncertainty in position
	Actuated HGA		X Requires hi-temp mechanisms, very low TRL
	Shaped Antenna		X Uncertainty in landing position

LEGEND			
Traded Item	Option Baselined	Option Rejected	Option Not Selected, but worthy of further study

VW021

Figure B-28. Lander Subsystem Trades

scribed in the NASA Aerial Vehicles Study [Cutts et al., 2018]. Variable-altitude balloons are already highly developed in terrestrial applications, Google Loon being the most well-known, so this TRL gap largely represents a need to adapt to the Venus environment. There is ongoing work at JPL to mature Venus variable-altitude balloons beyond TRL 4. Venus-relevant early prototype testing is scheduled for the summer of 2020. Past JPL efforts also provide a baseline of material testing [Hall et al., 2008] that have been leveraged into the VFM design. Metalized Fluorinated Ethylene Propylene (FEP) has been validated against concentrated sulfuric acid and resistance to pinhole growth. Vectran fabric, used for the MER airbags, has similarly been tested for acid resistance and integrated into several Venus balloon



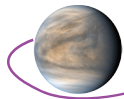
Aerobot			
Spin up for entry	Orbiter roll	< Simple, minimal	
	Turntable	X Added mechanism, mass	
	Self Spin	X No RCS system on lander	
Autonomy	Commands	< Enables variable transmission rates and prioritized data	
	Sequencer	X Resources available for commanding	
	Full Autonomy	X low TRL	
Power	ASRG	X Sink Temperature issues, not needed	
	Solar Array and Battery	< Provide needed power	
Communication	Omni	X Significant blockage by Balloon	
	Actuated HGA	X Requires hi-temp mechanisms, very low TRL	
	Shaped Antenna	< Two provide needed FOV with max gain	
Orbiter			
Communication	Separate X and Ka Band Antennas	X Mass inefficient	
	X, Ka and RADAR share Antenna	< Mass efficient, provides large X-band and minimizes Aerobot and lander communication systems	
SmallSat			
Orbits	Optimized for SmallSat Science	X After communication role will adjust orbit for science	
	Optimized for Communications	< Optimized to initially provide data return from Aerobot and Lander	
Communication	DTE X-Band	< Provides tracking and supports gravity science	
	DTE Ka-Band	X Does not support gravity science	
LEGEND			
Traded Item	Option Baselined	Option Rejected	Option Not Selected, but worthy of further study

Figure B-29. Aerobot, Orbiter, and SmallSat Subsystem Trades

prototypes. Without the balloon operating as planned, the Aerobot will not circumnavigate Venus nor measure at multiple altitudes, and loss of scientific measurements will occur.

### B.2.5.6.3 Instruments and Sample Acquisition/Handling Systems

The instruments that require technology development were selected for their innovation and ability to achieve the required groundbreaking measurements. Many are heritage instruments from Mars missions, however, some instruments are in need of TRL maturation for the appropriate environment they will encounter in either the constrained environment of the Lander pressure vessel or the clouds of Venus. Others are in need of developing specific sample ingestion systems that are at lower TRL. The strawman instrument teams have provided technology maturation plans to ensure their development and, if required, that of their aerosol or particulate sample acquisition/ingestion system, to reach TRL 6 before PDR. In many cases, applications are in process for independent technology development funding mechanisms, such as MatISSE. Where there is no approved external funding mechanism in place it is assumed the TRL development costs fall on the VFM mission and technology maturity efforts begin in Pre-Phase A. The main purpose of the Pre-Phase A development effort



will be to design efficient packaging methods to minimize volume, power and mass for emerging low TRL ( $\leq$  TRL-5) technologies. The design requirements will be driven by the thermal and structural loads acting on these systems during Venus atmospheric entry and descent through the atmosphere. A rigorous test program will be instituted to verify the packaging designs are capable of performing successfully at Venus. The effect on the mission if one of them is not developed in time varies but much of the development is re-engineering heritage instruments rather than developing new ones. The lowest TRL sub-systems for many of those instruments are the sampling systems.

### B.2.6 Concept of Operations

The Venus Flagship Mission would be managed in-house, and the platforms would be built in house (Lander and Aerobot)—either at JPL and/or GSFC, provided by industry contract (Orbiter), or purchased commercially (2 SmallSats). Due to the variety of sources and the large suite of instruments, we believe that a distributed science mission operations approach with one institution managing the effort will provide the best scientific outcome and reduce risk. There will be one central VFM science mission operations center (at managing institution) with a maximum of four platform mission/science operations centers housed at the institution/facility that provided the platform. Each platform mission/science operations center is responsible for interaction with each instrument on their payload which has the potential to add one more layer of distributed operations. The benefit of using this model for operations is that the science teams, who have a vested interest in the data return and intimately understand the instrument, will be actively engaged in developing the observing plans and designing the observations. To ensure that the science teams are mindful of the big science picture and the synergistic science goals, working groups of project/programs scientists will be established to oversee those efforts. This approach has been successfully used on previous flagship missions such as Cassini.

Flight mission operations are composed of three phases: 1) Launch and Cruise to Venus operations, 2) Venus Orbit, Atmosphere and Surface operations, 3) Aerobraking and Science Orbit operations. Venus Orbit, Atmosphere and Surface operations are divided into the operations performed by each platform.

#### B.2.6.1 Mission Operations

Figure B-30 shows the VFM Communication architecture and Figure B-31 shows the VFM ground architecture. The Orbiter and SmallSats both command and receive science data and health and safe-

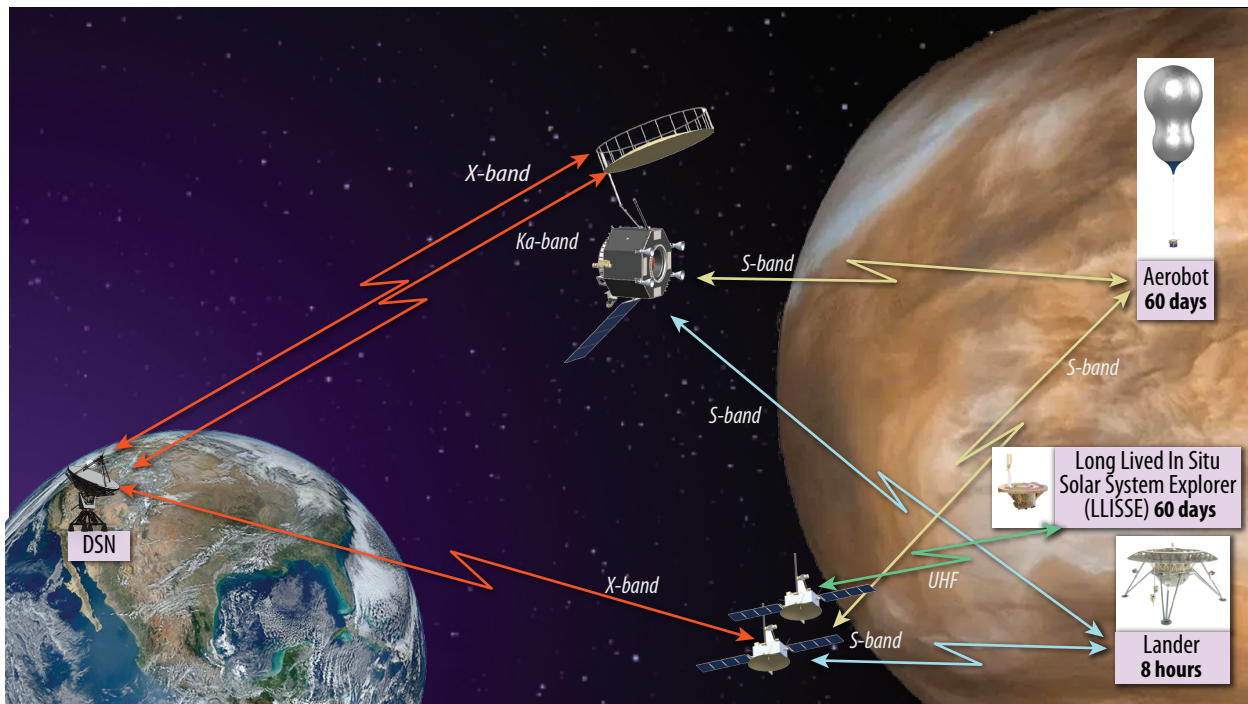
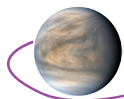


Figure B-30. VFM Communication architecture



# Venus Flagship

ty data from the Lander and Aerobot using S-Band. The SmallSats receive science and health and safety data from the **LLISSE** using UHF. The Orbiter and SmallSats store the data they receive from the Aerobot, Lander, and **LLISSE** and then add their own science, health, and safety data and transmit to DSN via X-Band for the SmallSats and via Ka-Band for the Orbiter. The Orbiter has a HGA, MGA and LGA X-Band link with DSN in addition to the Ka-Band link. Critical events such as launch, Deep Space Maneuvers (DSMs), VOI, Entry, and Descent and Float/Landing of the Aerobot/Lander are expected to be covered 24 hours a day for the duration of the critical event. Delta Differential One-way Ranging (DDOR) will be required on the X-Band links with the SmallSats and

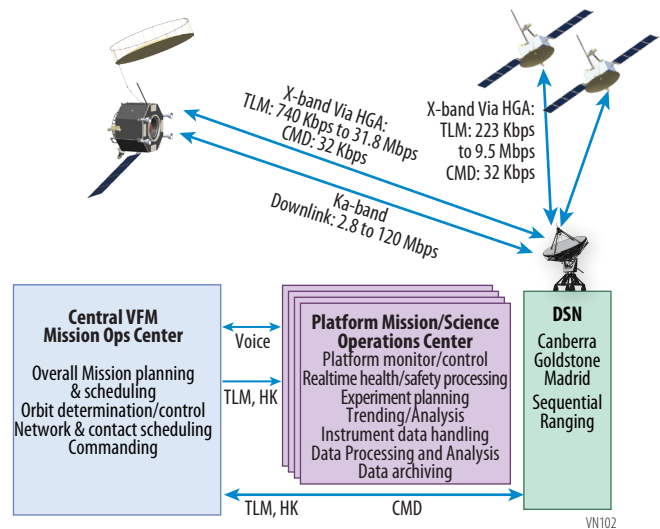
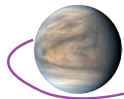


Figure B-31. Ground Systems Architecture

Table B-17. Mission Operations and Ground Data Systems Table

Down link Information	Mission Phase 1 Launch and Cruise to Venus	Mission Phase 2 Venus Orbit, Atmosphere, and Surface	Mission Phase 3 Aerobraking and Science Orbit
Number of Contacts per Day			
Orbiter	1	1	1
SmallSat 1 and 2	1	1	1
Number of Weeks for Mission Phase, weeks			
Orbiter	179	27	209
SmallSat 1 and 2	167	39	209
Downlink Frequency Band, GHz			
Orbiter	8.4, 32.0	8.4	8.4
SmallSat 1 and 2	8.4	8.4	8.4
Telemetry Data Rate(s)			
Orbiter Ka-Band Minimum	> 2,800 Kbps	2,800 Kbps	2,800 Kbps
Orbiter Ka -Band Mean	> 2,900 Kbps	2,900 Kbps	2,900 Kbps
Orbiter Ka -Band Maximum	> 120 Mbps	120 Mbps	120 Mbps
Orbiter X-Band HGA Minimum	> 740 Kbps	740 Kbps	740 Kbps
Orbiter X-Band HGA Mean	> 760 Kbps	760 Kbps	760 Kbps
Orbiter X-Band HGA Maximum	> 31.8 Mbps	31.8 Mbps	31.8 Mbps
Orbiter X-Band MGA Minimum	> 1,175 bps	1.1 Kbps	1.1 Kbps
Orbiter X-Band MGA Mean	> 1,210 bps	1.2 Kbps	1.2 Kbps
Orbiter X-Band MGA Maximum	> 50 Kbps	50 Kbps	50 Kbps
Orbiter X-Band LGA Minimum	> 41 bps	41 bps	41 bps
Orbiter X-Band LGA Mean	> 42 bps	42 bps	42 bps
Orbiter X-Band LGA Maximum	> 1,740 bps	1,740 bps	1,740 bps
SmallSat 1 and 2 HGA X-Band Minimum	> 223 Kbps	223 Kbps	223 Kbps
SmallSat 1 and 2 HGA X-Band Mean	> 226 Kbps	226 Kbps	226 Kbps
SmallSat 1 and 2 HGA X-Band Maximum	> 9,500 Kbps	9,500 Kbps	9,500 Kbps
SmallSat 1 and 2 MGA X-Band Minimum	> 1,325 bps	1,325 bps	1,325 bps
SmallSat 1 and 2 MGA X-Band Mean	> 1,350 bps	1,350 bps	1,350 bps
SmallSat 1 and 2 MGA X-Band Maximum	> 56 Kbps	56 Kbps	56 Kbps





Down link Information	Mission Phase 1 Launch and Cruise to Venus	Mission Phase 2 Venus Orbit, Atmosphere, and Surface	Mission Phase 3 Aerobraking and Science Orbit
Transmitting Antenna Type(s) and Gain(s), DBi			
Orbiter Ka-Band HGA		63.1	
Orbiter X-Band HGA		51.5	
Orbiter X-Band MGA		22.0	
Orbiter X-Band LGA		7.4	
SmallSat 1 and 2 HGA X-Band		44.3	
SmallSat 1 and 2 MGA X-Band		22.0	
Transmitter peak power, Watts			
Orbiter Ka-Band HGA		100.0	
Orbiter X-Band HGA		100.0	
Orbiter X-Band MGA		100.0	
Orbiter X-Band LGA		100.0	
SmallSat 1 and 2 HGA X-Band		100.0	
SmallSat 1 and 2 MGA X-Band		100.0	
Downlink Receiving Antenna G/T, dB/K		51.9	
Nominal Total Daily Data Volume, (MB/day)			
Orbiter Ka-Band	32	80,702	80,702
SmallSat 1 and 2 HGA X-Band	32	5,846 each	5,846 each
<b>Uplink Information</b>			
Number of Uplinks per Day	1	1	1
Uplink Frequency Band, GHz	7.2	7.2	7.2
Telecommand Data Rate, kbps			
Orbiter X-Band HGA, gain 51.5	8	8	8
Orbiter X-Band MGA, gain 22.0	8	8	8
Orbiter X-Band LGA, gain 7.4	0.5	0.5	0.5
SmallSat X-Band HGA, gain 44.26	8	8	8
SmallSat X-Band MGA, gain 22.0	8	8	8

Orbiter. During the mission phases routine daily contacts are required between DSN and the Orbiter and SmallSat as shown in **Table B-17**

### B.2.6.2 Launch and Cruise to Venus Operations.

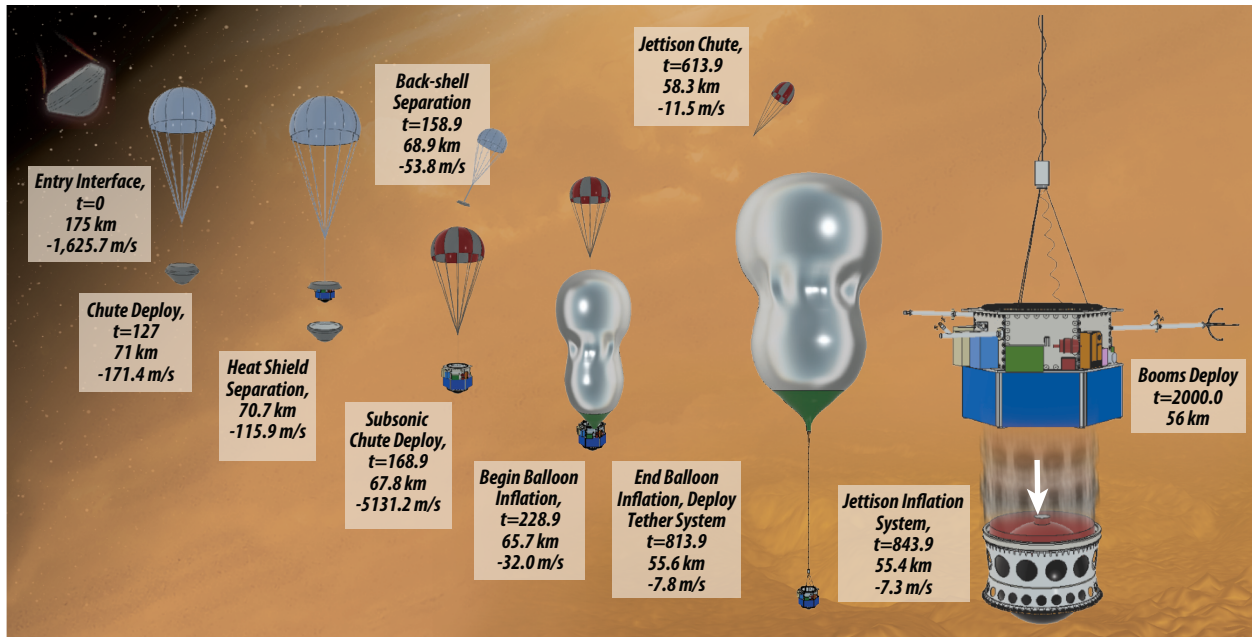
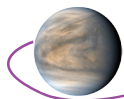
The VFM launches from Cape Canaveral, Florida on a single Falcon 9 Heavy vehicle with 5m fairing on June 6, 2031. The launch window is 14 days long. There is a backup launch opportunity in June of 2032. The mission timeline is shown in **Figure B-14**. As previously discussed in **Section B.2.4** and shown in **Figure B-14**, the SmallSats use their electric propulsion to arrive at Venus ahead of the Orbiter that has the Aerobot and Lander attached. The SmallSats arrive on August 15, 2034. Meanwhile, the Orbiter does a flyby of Venus on October 12, 2031. The Orbiter continues on to Venus and on November 4, 2034 the Orbiter spins up to 5 rpm and releases the Aerobot with a  $\Delta V$  of  $\geq 1$  m/s. One day later the Orbiter performs a Venus Orbit Insertion (VOI) targeting maneuver in preparation for VOI. On November 9, 2034 the Orbiter performs the VOI and begins science operations in the initial elliptical polar orbit.

### B.2.6.3 Venus Orbit, Atmosphere, and Surface Operations

#### B.2.6.3.1 Aerobot Operations

Five days after release by the Orbiter, the Aerobot enters the venusian atmosphere on November 9, 2034 and begins the Entry, Descent and Float (EDF) sequence shown in **Figure B-32**. The SmallSats, having arrived 3 months earlier, will provide communication for the EDF sequence and the 60 days of float operations.

Once the Aerobot is fully deployed after atmospheric descent, during the first circumnavigation the altitude control system will be used to maintain a near-constant altitude of 56 km, and thus a near-constant temperature of 20°C, for sensitive characterizations of atmospheric composition including isotopic ratio of noble gases.

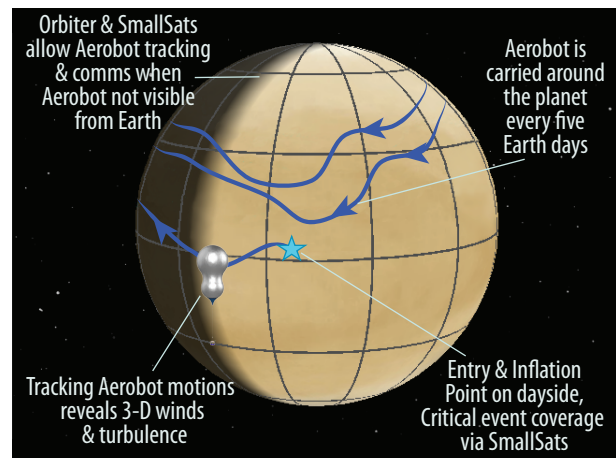


VN083

Figure B-32. Aerobot Entry, Descent, and Float Operations

In later circumnavigations, the Aerobot's altitude control will be used to descend to 52 km, rise rapidly (over 2 hours) to 62 km altitude, and then descend again to the chosen float altitude, allowing quasi-vertical profiles of atmospheric parameters to be measured. One rapid ascent is planned during each dayside and nightside pass, for a total of 24 vertical profiles, distributed over all times of day and night, over the 60 day nominal mission duration. Altitude cycling can be stopped or reduced at night. The nominal mission lifetime for the Aerobot is 60 days, although communication relays will be available for longer.

Carried by ambient winds, the Aerobot will circumnavigate Venus every 5 days, on average. **Figure B-33** shows an example of what the trajectory would look like. The entry time and location was chosen to allow sufficient time for the Aerobot batteries to be charged to full capacity prior to entering the venusian night.



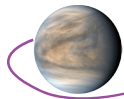
VN083

Figure B-33. Example Aerobot Trajectory around Venus

The balloon's meteorological instrumentation will be powered on at all times, measuring continuously at sampling rates varying from 0.02 Hz (radiometer) to 60 Hz (infrasound sensor). A low rate meteorological data record at 0.2 Hz will be returned for the whole mission duration (0.02 Hz for the radiometer). For characterization of turbulence, power spectra of meteorological parameters will be calculated onboard for each half hour interval, and scheduled periods of high rate data at 1 Hz will be scheduled. Onboard event detection will be performed, to identify possible seismic, volcanic, lightning or other events; high-rate data from these candidate events will be downlinked to Earth.

**Figure B-34** shows the Aerobot power profile from entry through the first circumnavigation of Venus and completion of the first day of the repeating five day cycle of circumnavigation. The maximum depth of discharge is 33% during the night.

The AMS-N is powered on for seven minutes, once per hour on average (with a higher measurement cadence applying during vertical ascents). At each time, after a 2-minute warm up period, the mass spectrometer will measure composition of the atmosphere for five minutes, and then of cloud/



aerosol particles which are separated from atmospheric gas using an aerodynamic aerosol separator. The incoming atmosphere passes through a nephelometer that optically interrogates cloud and aerosol particles that will enter the mass spectrometer to constrain their size, shape, composition. The mass spectrometer data are integrated over 10 second periods in order to reduce data rate. After each operational period, the instrument will remain in standby power until it is ready to ingest the next sample.

The **FM** will characterize 7 samples during the 60-day mission. Each time it is switched on, a pump draws atmosphere through filters to collect cloud/aerosol for analysis. The 1-of-7 particle-capture filter sets are located on a rotatable sample-stage. A stepper-motor positions the stage and directs the sample to a set of particle-capture filters as it aligns each filter set beneath the microscope objective. The in-line filter-set captures successively smaller particle sizes on 10, 1.0, and 0.2  $\mu\text{m}$  pore-size filters for sample imaging.

The **MET** and **Mag** operate continuously during the day and night side of Venus. The **MET** is sampled at 0.2 Hz background, **radiometer** at 0.02 Hz, including additional 20 high-rate events per day of 3 minutes each. Magnetometer data is down sampled to 0.5 Hz, which is sufficient for measurement of remnant magnetism and occasional high-rate data for investigations such as Schumann resonances characterization and search for lightning.

The **VI**, located on the side of Aerobot as shown in **Figure B-17**, will take 5 images every other day to show the balloon and cloudscape, as well as examine the Aerobot for signs of oxidation or sulfurization and is for student and public outreach purposes. The collection time is 1 minute for each image.

The mission data volume generated by the Lander instruments is shown above in **Table B-11**. **Table B-17** and **Figure B-30** shows the communication links between the Aerobot and the SmallSats and the Aerobot and the Lander. The Aerobot has at least one contact per day for 10 minutes. Contacts are limited to 1 during the night to conserve battery charge. The daily average data volume is ~83 Mbits, which takes a minimum of 73 minutes to downlink per day. **Section B.2.6.3.2** shows that there are multiple daytime contacts between the Aerobot and the SmallSats as well as a contact with the Orbiter every 5 days, all of which provide significant contact time to download the daily data volume with significant margin. The Aerobot data storage of 2 Gbits provides ample storage of data collected at night to be sent during the day.

### B.2.6.3.2 Lander Operations

On May 16 2035, the Orbiter performs a Lander entry targeting maneuver, spins up to 3 rpm and deploys the Lander with a separation velocity of  $\geq 1$  m/s. The Lander has two operational subphases: 1) Lander Entry, Descent, and Landing Operations and 2) Surface Operations.

#### B.2.6.3.2.1 Lander Entry, Descent, and Landing Operations

The Entry, Descent, and Landing sequence is shown in **Figure B-35**. The Lander transmits data from entry through landing as shown in **Figure B-36**. The parachute deploys 125.3 seconds after entry and slows the Lander in its aeroshell down from Mach 1.4 to Mach 0.7 at 358.6 seconds. At that time the heat shield is jettisoned and the Lander and backshell remain attached until 388.6 seconds when the Lander jettisons the parachute and backshell. The parachute and backshell are blown westerly by the Venus winds while the Lander begins free fall with its drag plate, which is used to slow it down for landing with a velocity of less than 8 m/s. Lander science operations commence upon entry into the Venus atmosphere and continue throughout descent to obtain a full meteorological and spectroscopic atmospheric profile. The **NMS** and **TLS** sample above the cloud tops, below the main cloud layers, in the lower atmosphere and just above the surface. The **Neph** and **AS** obtain samples at better than a 100 m increment. The **GRS** records data continuously in passive mode throughout descent. Below 9 km

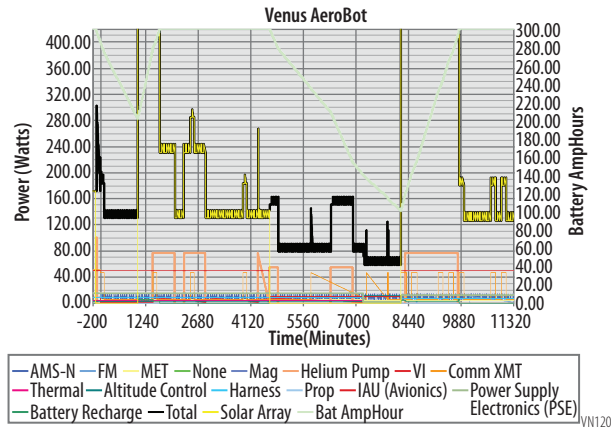


**Figure B-34.** Aerobot Power profile showing ample power for the mission

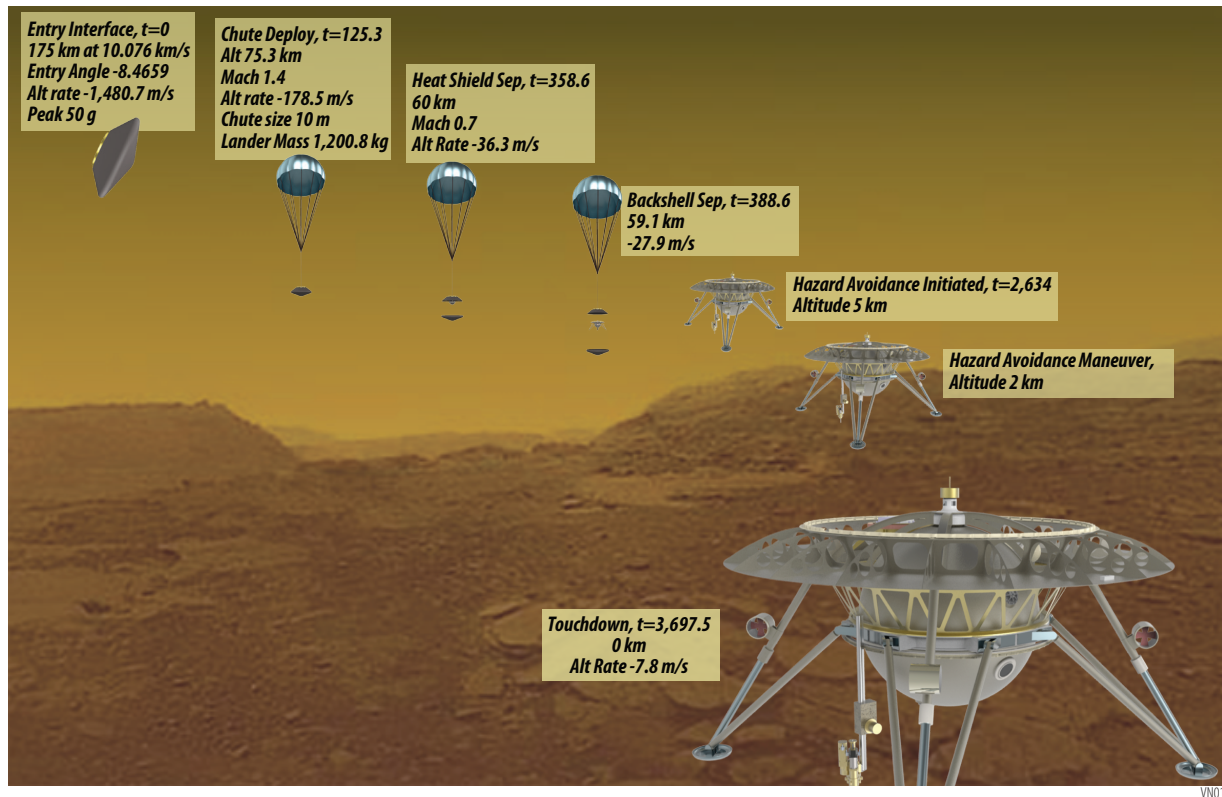
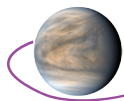


Figure B-35. Lander Entry, Descent, and Landing Operations

the DI captures the landing area by virtue of the slow rotation (2–3 RPM) of the Lander as it touches down. Figure B-36 shows the instrument operations timeline during descent and once landed.

### B.2.6.3.2.2 Lander Surface Operations

Figure B-37 shows the power usage from Lander entry until end of mission plus 60 minutes for the surface operations sequence shown in Figure B-36. The spike from 70–90 minutes is due to the use of the drill.

Figure B-38 shows the temperature response of the Lander decks, from descent and into Lander operations. Phase-change material embedded in the decks slows down the temperature rate of change (due to instrument/avionics heating and parasitic heating from the Venus atmosphere). Enough phase-change material is embedded into the two decks to ensure electronics stay under their maximum operating temperature limit for approximately 6.5 hours after landing.

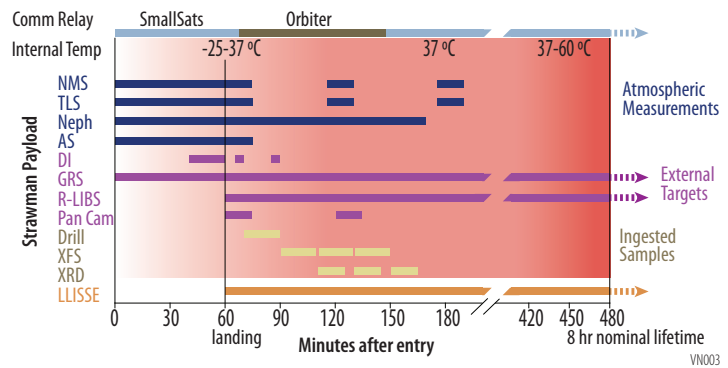


Figure B-36. Lander Surface Operations of the Strawman Payload

The TLS and NMS sample the atmosphere upon touchdown, at landing +1 hour and landing +2 hours. Passive GRS science continues on the surface for 30 minutes after landing, then the Neutron Generator turns on to begin active GRS measurements, which continue until the end of surface operations. The AS continues to take data after landing. A full set of panoramic images is taken upon landing and at landing plus 60 minutes. Imaging is completed while the Lander is in communication range of the Orbiter. The R-LIBS begins surface interrogation upon landing and continues until the end of surface science operations, nominally at landing +7 hours.

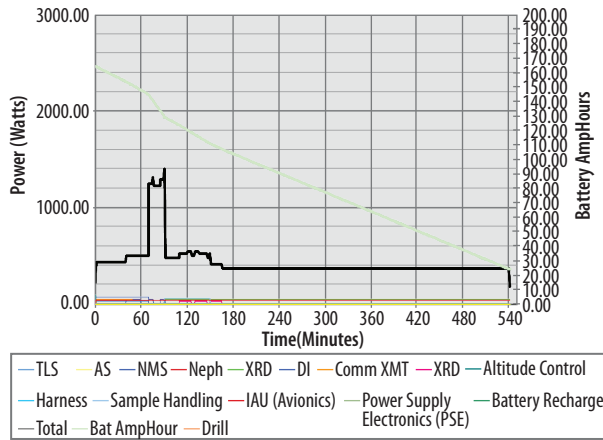
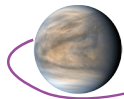


Figure B-37. Lander Power, starting on descent. Landing Time= 60 minutes

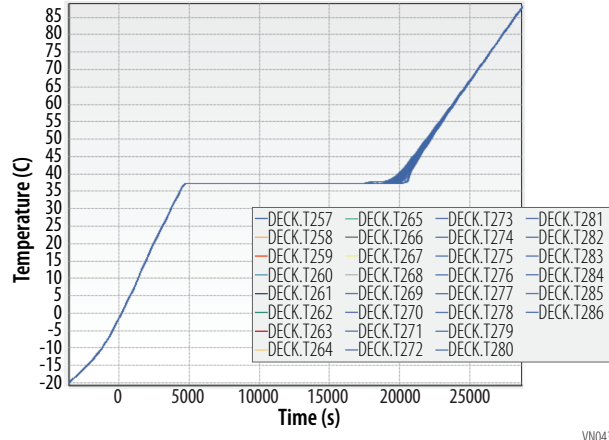


Figure B-38. Deck Temperature during Descent and Surface Operations

### B.2.6.3.2.3 Surface Sample Science

Once on the surface, and with the Lander leveled, sample science can begin. The **DI** images the drill area prior to and post drilling. Drill deployment and sample acquisition to 5 cm depth takes approximately 15–20 minutes, so 30 minutes after landing 3 samples from three different depths are available for analysis by the **XFS** and **XRD** with the instruments taking 20 and 15 minutes to do their respective analysis. The sample ingestion system facilitates direct interrogation by the **XFS** while in the sample ingestion cup. Once this analysis is complete, the sample drops into a hopper that feeds the **XRD**. While the **XRD** analyzes the first sample, the **XFS** analyzes the second. This parallel sample analysis continues until all 3 samples are analyzed by both X-Ray instruments. Full sample science operations are complete at landing plus 105 minutes.

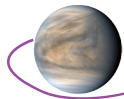
**LLISSE** nominally operates continuously on the surface for 60 days from landing, transmitting data every 6 hours for 6 minutes to the SmallSats. The SmallSats are not always available for transmissions from **LLISSE** over the 60 days but this best effort approach is deemed acceptable due to the nature of **LLISSE** communication protocol and the lack of memory on-board.

The mission data volume generated by the Lander instruments is shown in **Table B-11**. The SmallSats have a total of 8 hours of contact time with the Lander and the Orbiter has 80 minutes of contact time. All image data is sent to the Orbiter since it has the highest data rate. **Table B-17** shows the data rates, contact times and data transmission capabilities of the SmallSats and Orbiter. All the data collected during the 8 hour life of the lander is collected with ample margin.

### B.2.6.3.3 Orbiter Operations

#### B.2.6.3.3.1 Elliptical Polar Orbit

Upon arrival at Venus the Orbiter performs VOI and enters an elliptical polar orbit for 6 months prior to releasing the Lander. The VFM mission takes advantage of the time spent in the elliptical polar orbit to conduct valuable science operations. The **NIR-I** is assumed here to be a pushbroom with a field of view optimized for orbital operations and only images when the entire field of view is in darkness. The **DI**, **Mag**, **S-mm**, and **NMS** are on at essentially 100% duty cycle while **ESA-i** and **ESA-e** are on at ~50% duty cycle and the **SAR** is utilized when below 1,000 km (13 minutes out of 5 days). **Figure B-39** shows the ground track of the **SAR** during this time. The option exists to delay the release of the Lander an additional 234 days to acquire additional coverage of tessera terrain as an input to landing site selection. **Table B-18** shows a breakdown of the data generated by the Orbiter in the different orbits. The **SAR** generates data during the months prior to lander separation, but does not generate any data during aerobraking. The majority of **SAR** data is generated during the circular orbit. During the elliptical orbit and during the circular orbit a daily total contact time of 5 hours is needed with DSN.



The Orbiter, as shown in **Figure B-40**, is oriented in its orbit such that the NMS are in the velocity direction (+x) and the SAR antenna is pointed at a look angle of 45° from the +z axis. The radiators are kept pointed away from the sun in the -y axis. As Venus orbits the sun the VFM orbit remains inertially fixed and thus the Orbiter must rotate about the +z axis twice per Venus year to maintain the radiators pointing away from the sun. This is also true for the aerobraking and circular orbits. The Orbiter uses a two-axis, gimballed solar array to track the sun. The array moves forward and backward about the x-axis every orbit on the sun-side and rotates about the z-axis over the course of the year. The SAR is placed such that it has a viewing cross-track of 45° off-nadir. The SAR antenna is also used to communicate with the Aerobot, Lander, and Earth as shown in **Table B-17**. The NIR-I is pointed nadir with a 45° FOV, pushbroom. The S-mm views the limb and uses a turntable to allow both along-track scanning and across-track scanning.

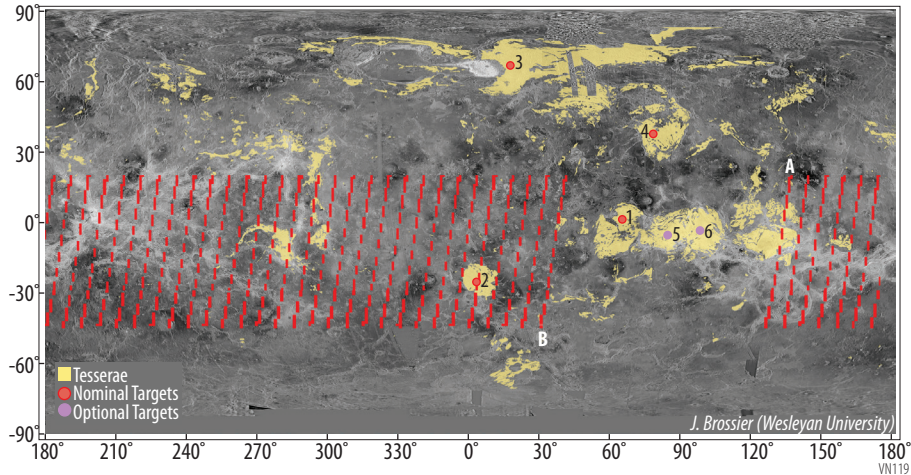


**Figure B-39.** SAR Ground Coverage during the Elliptical Polar Orbit. For the baseline missions, coverage starts at 120° longitude (point A) and moves eastward to point B. Coverage can be increased by extending the length time the Orbiter is in the initial elliptical orbit.

### B.2.6.3.3.2 Aerobraking and Science Orbit Operations

The Orbiter goes through a series of maneuvers to circularize the initial elliptical polar orbit into a circular polar orbit of 300 km altitude above the venusian surface (the science orbit, see **Figure B-15**). Circularization is achieved via aerobraking, which is performed using a sequence of steps. First, periapsis is lowered to 130 km altitude, where the Venus atmosphere can dissipate orbital energy to facilitate lowering the apoapsis to an altitude of 300 km. The required  $\Delta V$  to lower the periapsis is 116 m/s. With this periapsis altitude, the apoapsis decreases to the required altitude of 300 km over the course of 2–4 years. During aerobraking, the Orbiter uses 215 m/s of  $\Delta V$  to maintain its periapsis altitude. Maneuvers for periapsis-keeping are performed at the apoapsis. During the actual mission, orbit determination is performed by the Mission Operations Center (MOC) as frequently as possible and the maneuver cadence is decided based on contact sched-

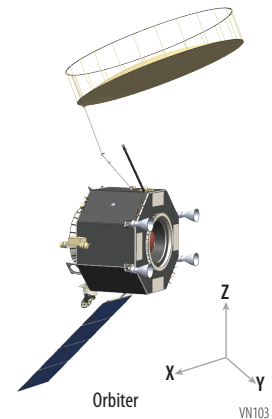
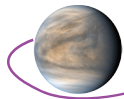


**Figure B-40.** VFM Orbiter with Two axis gimballed Solar Array

**Table B-18.** Orbiter Data Generation by Orbit

Instrument	Circular Orbit		Elliptical Orbit				Mission Total
	Gbit/Orbit	Total	Pre-Aerobraking Orbit		Aerobraking Orbit		
			Gbit/Orbit	Total	Gbit/Orbit*	Total	
NIR Imager (NIR-I)	0.1	2658	0.1	4.2	0.1	44	2707
Flux Gate Magnetometer (Mag)	0.01	252	0.9	31.5	0.3	126	410
SAR	2.4	53611	103	3707	0.0	0	57318
Sub MM	0.4	10092	35	1261.4	13.4	5046	16399
Mass Spectrometer	0.161	3650.0	12.7	456.3	4.8	1825	5931
Ion Electrostatic Analyzer (ESA-i)	0.19	4365	15.2	545.7	5.8	2183	7094
Electron Electrostatic Analyzer (ESA-e)	0.02	555	2	69.4	0.7	277	902
	<b>3.3</b>	<b>75183</b>	<b>169</b>	<b>6075</b>	<b>25.2</b>	<b>9501</b>	<b>90760</b>



ule and limitations on the allowable density corridor and maneuver plans are uploaded to the Orbiter. Details on aerobraking are discussed in **Section B.2.6.4.3.2**.

The **NIR-I**, **Mag**, **NMS**, **S-mm**, **ESA-i**, and **ESA-e** collect data during the entire aerobraking process. In order to maintain the required aerobraking drag profile the **SAR** does not conduct science operations during that time. As Venus orbits the sun the VFM orbit remains inertially fixed and thus the Orbiter must rotate about the +z axis twice per Venus year to maintain the radiators pointed away from the sun. This means that the **NMS** is used 50% of the time.

### B.2.6.3.3 Circular Science Orbit

Once in the circular science orbit, the full Orbiter suite, excluding the **SAR**, continues to operate at 100% duty cycle, with the same thermal rotational maneuvers causing the **NMS** to be used 50% of the time. The **S-mm** spectrometer is mounted on a rotation platform allowing for alternate views to the different limbs on successive orbits. During the entire first orbit, **S-mm** would be looking at the cross-track limbs (eastward or westward) so that it is sensitive to East-West wind velocity and during the entire second orbit, it would be looking along track (northwards or southwards), so that it is sensitive to North-South wind velocity.

The **STM SAR** surface coverage requirement of 5% at 30m resolution and 0.5% at 10m resolution results in a very low duty cycle (**Figure B-41**), assuming wide swath mode. Thus, there is a lot of flexibility in timing the **RADAR** operations. At close Earth-Venus ranges, full data downlink can occur over several DSN passes and more data buffering is required if **RADAR** operations occur at larger ranges. The mission data volume generated by the Orbiter instruments is shown above in **Table B-13**. Data collected during the circular orbit and requiring DSN contact time are given in **Table B-17**.

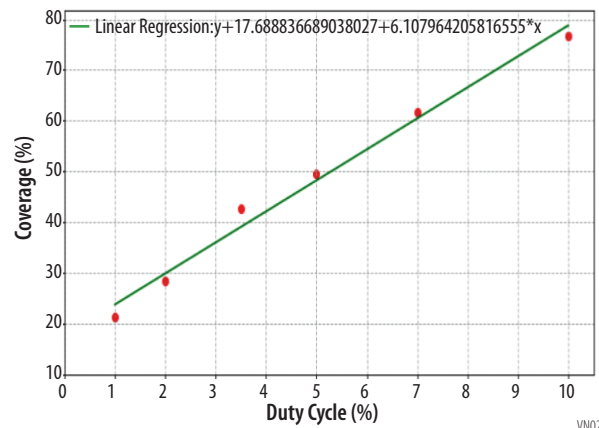


**Figure B-41.** Low SAR Duty Cycle Required to achieve STM coverage requirements

### B.2.6.3.4 SmallSat Operations

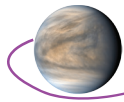
The two SmallSats play several roles in the Venus Flagship Mission; not only does the payload provide crucial science data about magnetosphere and solar wind, the satellites themselves play a critical part in communications with the Aerobot and the Lander. The satellites are used as relays for both uplink and downlink to both assets.

The first key role the SmallSats play is providing 8 hours of coverage for the Lander mission in combination with the Orbiter. They also play a role in the Aerobot’s 60 day nominal mission by providing at least 1 contact per day and total contact duration of at least 100 minutes to downlink the nearly 5,000 Mbits of data produced by the Aerobot. In addition, the SmallSats contacts with the Aerobot provide positioning information for the Aerobot science and operations staff. The final role they play is in providing at least one contact daily to downlink **LLISSE** data during its 60 day nominal mission.

Importantly, the SmallSats themselves have 7 science instruments—**LP**, **ESA-i**, **ESA-e**, **SEPD**, **Mag**, **EUV**, and **E-FD**—that are powered on and collecting data near to continuously as downlink and support for the other VFM assets allow for the entire mission.

It is anticipated that each SmallSat will have a 2 hour downlink with a DSN 34 meter station each day during normal operations (supporting the Lander and Aerobot may require additional time). When commanding from the ground is required, the duration of the viewing period would be adjusted to accommodate round-trip light time.

One of the challenges faced by the SmallSats is the amount of data that can be collected versus what can realistically be returned given the downlink allocation and onboard data storage. See **Table B-15** for the SmallSat total mission data volume.



## B.2.7 Mission Design Details

### B.2.7.1 Mission Design Requirements

The Mission Timeline was discussed in **Section B.2.4** and shown in **Table B-7**. The Mission Design Requirements are taken from and derived from the Mission Requirements in **Table B-5** and are shown in **Table B-19**.

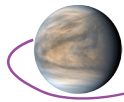
**Table B-19.** VFM Mission Design Requirements

Platform	Higher-level requirement	Lower-level requirements
Aerobot	Be safely placed on Venus's atmosphere	Assuming 45° cone-angle capsule, maximum g-load during entry must be less than 50-g Deployment latitude: low latitude
SmallSats	Be safely placed in orbit around Venus	Science orbit requirement : Apoapsis altitude > 5000 km Periapsis altitude < 500 km Inclination > 65° Communication requirement with the Lander: 8 hours of continuous access starting at the Lander entry interface (altitude of 175 km) Communication requirement with the Aerobot: daily access for a minimum of 10 minutes
Orbiter	Be safely placed in orbit around Venus	Need elliptical orbit Science orbit requirement: 300 km x 300 km polar orbit Communication requirement with the Lander: 80 minutes of continuous access starting at the Lander entry interface (altitude of 175 km)
Lander	Be safely placed on the surface of Venus	Assuming 70° cone-angle capsule, maximum g-load during entry Orbiter must be less than 50-g Landing site: West Ovda Landing Ellipse: 300 km (East - West) x 150 km (North - South)

**Table B-20.** VFM Baseline Trajectory Timeline

Mission Event	Time [UTC]	Navigation constraints	Maneuver	Platforms
Launch	06 Jun 2031 10:46:29			SmallSat1, SmallSat 2, Orbiter, Lander, Aerobot
SmallSat deployment and separation		Hours after the upper stage clears the spacecraft	1 m/s (separation mechanism)	SmallSat1, SmallSat 2
Orbiter Venus flyby targeting	28 Sep 2031 18:44:06	15 days prior to Orbiter flyby	not evaluated	Orbiter, Lander, Aerobot
Orbiter Venus flyby	13 Oct 2031 18:44:06			SmallSat1, SmallSat 2
DSM	07 Apr 2032 14:00:21	Targeting Aerobot entry	114.54 m/sec	Orbiter, Lander, Aerobot
Orbiter post-DSM OD end	27 Apr 2032 14:00:21	for at least 20 days after DSM		
SmallSat Venus arrival and begin of spiral down	28 Feb 2034 20:51:47.97		SEP system	SmallSat1, SmallSat 2
SmallSats end of spiral down	02 Apr 2034 12:26:47.16		SEP system	SmallSat1, SmallSat 2
SmallSats orbit arrival	15 Aug 2034 12:30:40.44	Arrive before the Aerobot entry	SEP system	SmallSat1, SmallSat 2
Aerobot targeting TCM for entry	03 Nov 2034 12:42:36	6 days prior to Aerobot entry	2 m/sec	
Aerobot deployment and separation	04 Nov 2034 12:42:36	5 days prior to Aerobot entry	5 m/s (separation mechanism)	Aerobot
Orbiter VOI targeting	05 Nov 2034 00:00:00	4.5 days prior to Aerobot entry	2.02 m/sec	Orbiter, Lander
Orbiter VOI targeting TCM	06 Nov 2034 12:47:21	3 days to update OD, plan, command TCM	not evaluated	
Aerobot entry	09 Nov 2034 12:42:36			Orbiter, Lander





Mission Event	Time [UTC]	Navigation constraints	Maneuver	Platforms
Orbiter VOI	09 Nov 2034 12:47:21		529.648 m/sec	Aerobot
Orbiter post-VOI OD end	04 Dec 2034 12:47:21	5 orbits (~25 days) after Orbiter VOI		Orbiter, Lander
Last periapsis keeping maneuver	06 May 2035 21:35:03		6.905039 m/sec	Orbiter, Lander
Orbiter post-maneuver OD end	11 May 2035 21:35:03	for at least 5 days after periapsis adjustment		Orbiter, Lander
Lander entry targeting	16 May 2035 02:49:04		0.694762 m/sec	Orbiter, Lander
Lander deployment	16 May 2035 14:49:04	12 hours after entry targeting	1 m/s (separation mechanism)	Lander
Orbiter divert	17 May 2035 02:49:10		126.01 m/sec	Orbiter
Lander entry interface	19 May 2035 14:14:11			Lander
Orbiter science orbit	(estimated) May 2037			Orbiter

### B.2.7.2 Mission Design Summary

Venus Flagship Mission (VFM) aims to deploy an Aerobot, an Orbiter, two SmallSats, and a Lander on Venus. The target landsite is West Ovda, whose coordinates are 0.3412° latitude and 62.5327° longitude. The baseline trajectory for VFM is summarized in **Table B-20** and illustrated in **Figure B-15**.

The two SmallSats detach from the other platforms a few hours after launch to follow a solar-electric propulsion (SEP)-powered trajectory to Venus. The SmallSats arrive in Venus orbit approximately 8 months before the Aerobot entry date. The trajectories of the SmallSats are detailed in **Section B.2.7.4**.

The Orbiter, with the Aerobot and Lander follow the heliocentric trajectory summarized in **Table B-21** and illustrated in **Figure B-42**. The

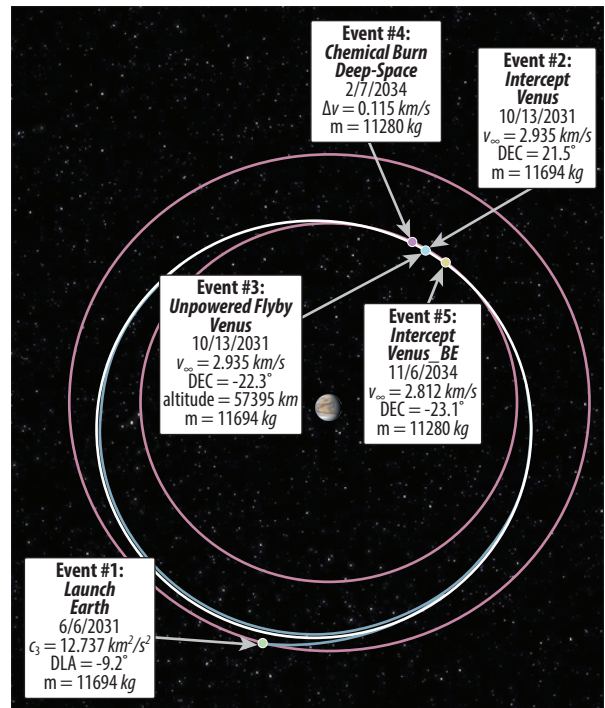


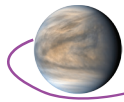
Figure B-42. Illustration of the baseline heliocentric phase for the Orbiter.

Table B-21. Main events of the baseline heliocentric phase for the Orbiter.

Event	Date	Mass (kg)	$\Delta V$ (m/s)
Launch	6/6/2031	11694	$C3 = 12.737 \text{ km}^2/\text{s}^2$
Venus Flyby	10/13/2031	11694	–
DSM	2/7/2034	11280	115
Venus Arrival	11/6/2034	11280	–

Table B-22.  $\Delta V$  budget (in m/s) for the baseline (2031 launch) and backup (2032 launch) trajectories

Propellant Sizing	Platforms in Mass	Launch date	
		Jun. 2031	Jun. 2032
Science Orbit Maintenance	Orbiter	0 m/s	0 m/s
Aerobraking Operations	Orbiter	331 m/s	331 m/s
Divert Maneuver after releasing Lander	Orbiter	130 m/s	130 m/s
Lander Deployment	Orbiter	-	-
Lander Entry Targeting	Orbiter plus Lander	1.7 m/s	9.8 m/s
Orbiter Periapsis Adjustment	Orbiter plus Lander	45 m/s	20 m/s
VOI Insertion	Orbiter plus Lander	530 m/s	158 m/s
Orbiter VOI Targeting	Orbiter plus Lander	10 m/s	17 m/s



Propellant Sizing	Platforms in Mass	Launch date	
		Jun. 2031	Jun. 2032
Aerobot Deployment	Orbiter plus Lander	-	-
Aerobot TCM for Entry	Orbiter, Lander and Aerobot	2 m/s	2 m/s
Aerobot Targeting	Orbiter, Lander and Aerobot	10 m/s	10 m/s
DSM	Orbiter, Lander and Aerobot	115 m/s	966 m/s
<b>Total ΔV</b>		<b>1,174.7 m/s</b>	<b>1642.8 m/s</b>
<b>Total propellant*1</b>		<b>1,671.2kg</b>	<b>3287.5kg</b>

\*1) propellant is estimated based on dry mass of each asset and Isp of 300s with 10% margin

**Table B-23.** Mass budget of the platforms for the baseline trajectory

Asset	CBE Mass (kg)	MEV Mass (kg)
Launch	4,799.7 (Dry)	5,924.1 (Dry) 9,510.1 (Wet) – assumes SmallSat Wet is 300kg each
Orbiter	1,580.0 (Dry) 5,095.0 (Wet)	1,916.6 (Dry) 5,431.6 (Wet)
Lander	1,576.7 (Dry)	1974.4 (Dry)
Aerobot	1,665.8 (Total Entry Mass) 176.2.2 (Total Float Mass)	1,433.2 (Total Entry Mass) 199.9 (Total Float Mass)
SmallSats	175.1 (Dry) 279.9 (Wet)	175.1 (Dry) 300.0 (Wet)

**Table B-24.** Main events of the heliocentric phase for the Orbiter (backup launch opportunity).

Event	Date	Mass (kg)	ΔV (m/s)
Launch	6/6/2032	13,020	$C_3=7.287 \text{ km}^2/\text{s}^2$
Venus Flyby	8/29/2033	13,020	-
DSM	5/28/2034	9,608	966
Venus Arrival	9/12/2034	9,608	-

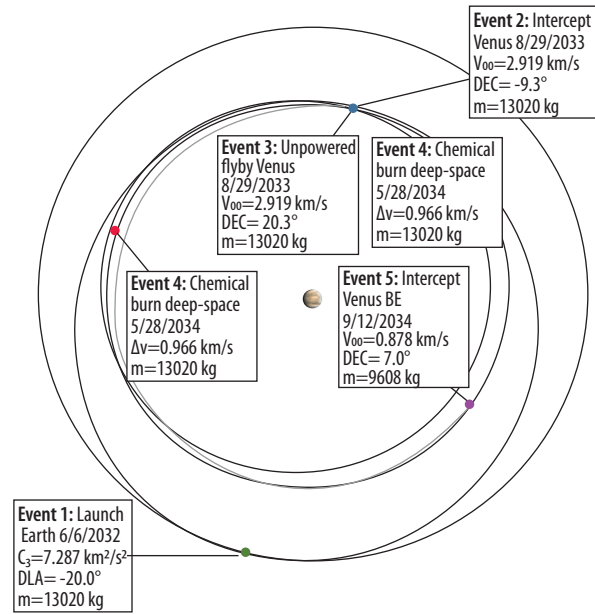


**Figure B-43.** Illustration of the heliocentric phase for the Orbiter (backup launch opportunity).

Aerobot separates from the Orbiter and Lander about 5 days prior to the Orbiter Venus orbit insertion (VOI) maneuver. After VOI, the Orbiter releases the Lander 6 months later, although as described earlier this can be postponed for a year for site imaging, and then begins an aerobraking maneuver that lasts approximately 2 years to reach its science orbit. The Orbiter’s trajectory is more fully described in **Section B.2.7.3**. This concept of operations is based on trajectory requirements.

The ΔV budget for the mission with the primary and backup trajectory are provided in **Table B-22**, where the events are ordered backward in time. The VFM mass budgets for the platforms of the baseline trajectory are given in **Table B-23**. The details of the orbit science design are covered in **Section B.2.7.7**.

As described in **Table B-22**, there is a backup launch opportunity in 2032. Despite providing an extra year of schedule margin compared to the baseline, this opportunity is kept as a backup rather than baseline due to its higher total ΔV. The event timeline for the backup trajectory mimics that of the baseline, though dates and ΔV requirements are different. The details of the heliocentric phase for the Orbiter are given in **Table B-24** and **Figure B-43**.

The compliance against other requirements are also shown in **Table B-25**.

### B.2.7.3 Orbiter Mission Design

The Orbiter is inserted into a 5-day period elliptic polar orbit. This particular orbit is a mission enabler for it allows Venus insertion with smaller ΔV. The elliptical orbit is also important for the Lander deployment sequence, providing 2-day orbit determination for the entry targeting and release of the Lander. Later, an 80-minute communication access with the Lander can be achieved by a reasonably small divert maneuver (130 m/s, see **Table B-22**), performed at the orbit’s apoapsis after the Lander

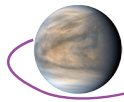


Table B-25. Mission design compliance matrix

Platform	Requirements	Design / Compliance
Aerobot	Aerobot deployment latitude: low latitude	<ul style="list-style-type: none"> <li>• Direct entry from interplanetary orbit</li> <li>• Targeting with VGA, DSM, and TCM by Orbiter propulsion system.</li> </ul> Baseline result : 8.8°
	Assuming 45° cone capsule entry, maximum g-load during entry must be less than 50-g	<ul style="list-style-type: none"> <li>• Direct entry from interplanetary orbit</li> <li>• Targeting with VGA, DSM, and TCM by Orbiter propulsion system. TCM must be 6 days before the entry and the magnitude must be less than 2m/s (assuming the magnitude error of 1%, 3-sigma), and the direction error must be less than 1° (3-sigma).</li> <li>• Aerobot separation must be done 5 days before the entry with a separation Δv, whose error is less than 0.1m/s (3-sigma) and direction error is less than 1° (3-sigma).</li> <li>• Aerobot capsule performs a small TCM for final targeting.</li> </ul> Baseline result: FPA range is -8°±0.9°(3-sigma). The resulting g-load must be analyzed by EDL simulation
Lander	Landing site: West Ovda	<ul style="list-style-type: none"> <li>• Entry from polar orbit (the periapsis direction should align with the landing site direction)</li> <li>• Targeting with a maneuver by Orbiter propulsion system</li> </ul>
	Assuming 70 ° cone capsule entry, maximum g-load during entry must be less than 50-g	<ul style="list-style-type: none"> <li>• The error of the targeting maneuver must be less than 0.2m/s (3-sigma), and the error of the maneuver direction must be less than 1° (3-sigma).</li> <li>• Lander separation must be done with a separation Δv, whose error is less than 0.1m/s (3-sigma) and direction error is less than 1° (3-sigma)</li> </ul>
	Landing Ellipse : 300 km (east-west) x 150 km (north - south)	Baseline result: FPA range is -8.34°+/-0.24° (3-sigma). The resulting g-load and landing ellipse must be analyzed by EDL simulation
Orbiter	Science orbit requirement : 300 km x 300 km polar orbit	Requirement baselined.
	Communication requirement with Lander: 80 minutes continuous access from Lander entry at altitude of 175 km	<ul style="list-style-type: none"> <li>• Lander deployment from polar eccentric orbit (at least 24 hours before the Lander entry) and periapsis raise (at least 12 hours before the Lander entry) after Lander deployment.</li> <li>• The polar orbit before Lander deployment must be 3 to 5 days orbit</li> </ul>
	Communication requirement with Aerobot: daily access for a minimum of 10 minutes	Baseline result : 80 minutes access to Lander, with a divert maneuver of 126 m/s.
SmallSats	Science orbit requirement : - Apoapsis altitude > 5000 km - Periapsis altitude <= 500 km - Inclination > 65°	<ul style="list-style-type: none"> <li>• Each SmallSat reaches its orbit utilizing electric propulsion before other platforms arrive at Venus.</li> </ul> Baseline result :
	Communication requirement with Lander: total 8 hours (4 hours each) continuous access from Lander entry at altitude of 175 km	<ul style="list-style-type: none"> <li>• 8 hours (2 x 4 hours) continuous access to Lander</li> </ul>
	Communication requirement with Aerobot: daily access for a minimum of 10 minutes	

separation. A depiction of the aforementioned sequence is shown in **Figure B-44**, and it is a well-known fact in orbital dynamics that an apoapsis maneuver in the direction of the velocity vector is the most fuel-efficient method to change the height of an orbit's periapsis. The Orbiter goes through a series of maneuvers to circularize the initial eccentric polar orbit into a polar orbit of 300 km altitude above the venusian surface (the science orbit). Circularization is achieved via a sequence of aerobraking maneuvers combined with chemical maneuvers to keep the spacecraft within the designed density corridor.

This study's first proposed mission design explored a Venus insertion that resulted in an elliptical orbit, similar to the current baseline, but *equatorial* instead of *polar*. That design required the initial orbit to be later rotated into a polar orbit by means of a maneuver. The equatorial elliptical orbit allows better access to the landing sites near the equator and maximizes the number of observations of these sites. However, as a drawback, this strategy requires roughly 500 m/s of ΔV to perform an inclination

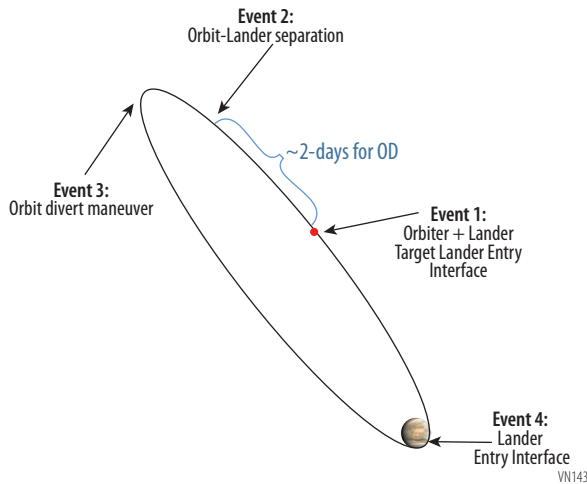
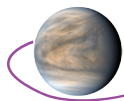


Figure B-44. Lander deployment sequence

change of nearly 90°. This extra propellant mass required for the inclination change drove the design, ultimately resulting in a very poor mass margin to the Orbiter. As a result, the current baseline, which consists of an initial *elliptical polar orbit* with direct polar insertion, was selected to avoid the inclination change maneuver. Another important component of the orbit is the ground analysis. Although this analysis is the focus of the science orbit, it is also performed during the elliptical orbit. A detailed description of the ground analysis for the polar elliptical orbit is provided later in this section. The amount of surface measurements that would be obtained in the elliptical equatorial orbit are fundamentally the same as the ones obtained by the elliptical polar orbit, but essentially flipped 90° (longitude to latitude and latitude to longitude). This happens because both orbits are the same with the only difference being a 90° offset in inclination; therefore, the swaths over the planet have the same width and frequency. **Table B-26** shows the Orbiter venusian orbital parameters.

After the Lander deployment and in order to achieve the desired science orbit (circular and polar), the Orbiter goes through a series of maneuvers to circularize the initial eccentric polar orbit that results from the VOI maneuver (**Figure B-45**) into a polar orbit of 300 km altitude above the venusian surface (the science orbit). Circularization is achieved via aerobraking.

The key advantage of aerobraking is that energy dissipation does not exclusively rely on propellant expenditure but also on aerodynamic drag. However, there are technical challenges associated with aerobraking, such as setting the density corridor (i.e., the periapsis altitude) accurately. If the periapsis altitude is too high, orbital energy dissipates too slowly. On the other hand, if periapsis altitude is too low, the spacecraft could experience unacceptably high dynamic pressure and heat flux. It is thus necessary to have reliable models of the Venus gravity field and atmosphere and of associated dynamical processes, such as atmospheric winds.

As discussed earlier, after the Lander is released the Orbiter performs a divert maneuver that raises its periapsis so as not to plummet into Venus (as the Lander does) and to reach a sufficient altitude that provides 80 minutes of communication access to the Lander. This resulting periapsis altitude is 7,000 km altitude from Venus surface. Having completed communications with the Lander, the Orbiter is ready to move to the aerobrake sequence. The aerobraking is performed using a sequence of steps: first, the periapsis is lowered to an appropriate level such that the venusian atmosphere is dense enough to generate a sizable drag force. This altitude is set to 130 km<sup>[1]</sup>. At this altitude, the Venus atmosphere is enough to dissipate the vehicle's energy (drag force) at the periapsis, which over time lowers the

Table B-26. Orbiter venusian orbital parameters

Orbit Parameters (Venus Inertial Frame)	Orbiter Elliptical	Orbiter Circular
Apoapsis (km)	116,108.4	300
Periapsis (km)	300	300
Eccentricity	0.945	0
Inclination (°)	90	90
Orbital Period	5 days	1.55 hours
RAAN (°)	334.4	334.4
Argument of Periapsis (°)	188.6	188.6

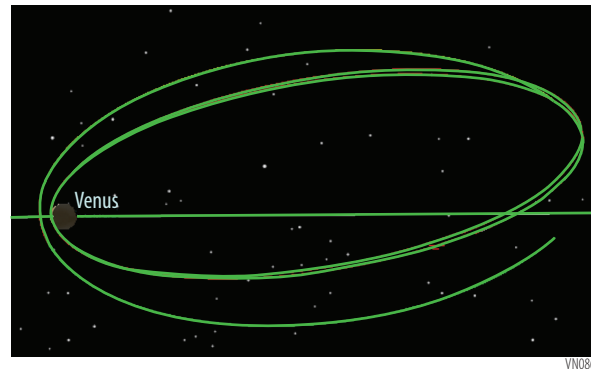


Figure B-45. Orbiter arrival at Venus and beginning of the circularization phase.

[1] The MAVEN mission was used as a benchmark for selecting appropriate aerobraking conditions. As a flight mission with published data, MAVEN is used as a base to loosely drive the aerobrake conditions. venusian atmospheric density at 130 km is 6.85 kg/km<sup>3</sup> on the dayside and 49.7 kg/km<sup>3</sup> on the night side. (The maximum atmospheric density MAVEN encountered was about 5 kg/km<sup>3</sup>). Maximum velocity at periapsis for VFM is 10.1 km/s. (MAVEN's maximum velocity was about 4.2 km/s).

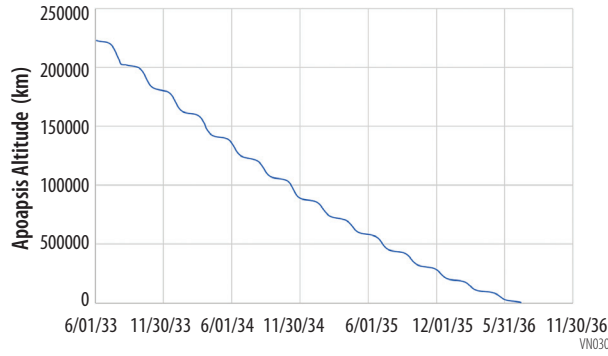
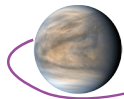


Figure B-46. Apoapsis decay as a function of time for the Orbiter baseline trajectory, from Venus arrival to achievement of the science orbit.

apoapsis. The required  $\Delta V$  to lower the periapsis from 7000 km to 130 km is 116 m/s. Chemical maneuvers are inserted along the way to account for atmospheric changes and keep the Orbiter within the designed density corridor. This process continues until the spacecraft's apoapsis reaches an altitude of 300 km. With this periapsis altitude, it takes ~2 years for the apoapsis to lower to the desired altitude. To conclude the sequence, a final maneuver is performed at the apoapsis to raise the periapsis to 300 km altitude, thus circularizing it.

The evolution of the apoapsis altitude over time is shown in **Figure B-46**. During aerobraking, the Orbiter uses 215 m/s of  $\Delta V$  to maintain its periapsis altitude and a maneuver for periapsis-keeping is performed at the apoapsis. During the actual mission, orbit determination is performed as frequently as possible and the maneuver cadency is decided upon based on contact schedule and violation of the pre-defined density corridor. The analysis performed here, assumed that a maneuver is placed at the apoapsis every time the periapsis violates an altitude equal or lower than 130 km. The apoapsis maneuver is performed in such a way to raise the periapsis back to 132 km altitude.

Prior to the aerobraking phase, between VOI and Lander release (roughly 6 months), the Orbiter performs two tasks. Firstly, it approximately covers 4.47% of the surface of Venus (**Figure B-47**), collecting scientific measurements before reaching its science orbit. The criteria for the ground coverage is a minimum ground-elevation of 15° in the daylight side of Venus with a maximum altitude of 1000 km to ensure that the RADAR can obtain and process images. Secondly, it provides 80 minutes of communications with the Lander.

Station-keeping maneuvers are required between VOI and Lander release to maintain the periapsis altitude value of 300 km. This periapsis altitude decay is due to solar gravity, which pushes the periapsis down toward the venusian surface. Nevertheless, the total  $\Delta V$  used by these station-keeping maneuvers is small for both the baseline (**Table B-27**) and backup (**Table B-28**) launch opportunities.

### B.2.7.4 SmallSats Mission Design

The trajectories of the two SmallSats were designed to strike a balance between (1) communications with the Lander and the Aerobot and (2) orbits that are relevant to the science experiments to be conducted by the onboard instruments. The SmallSats are physically identical, but will be deployed in different

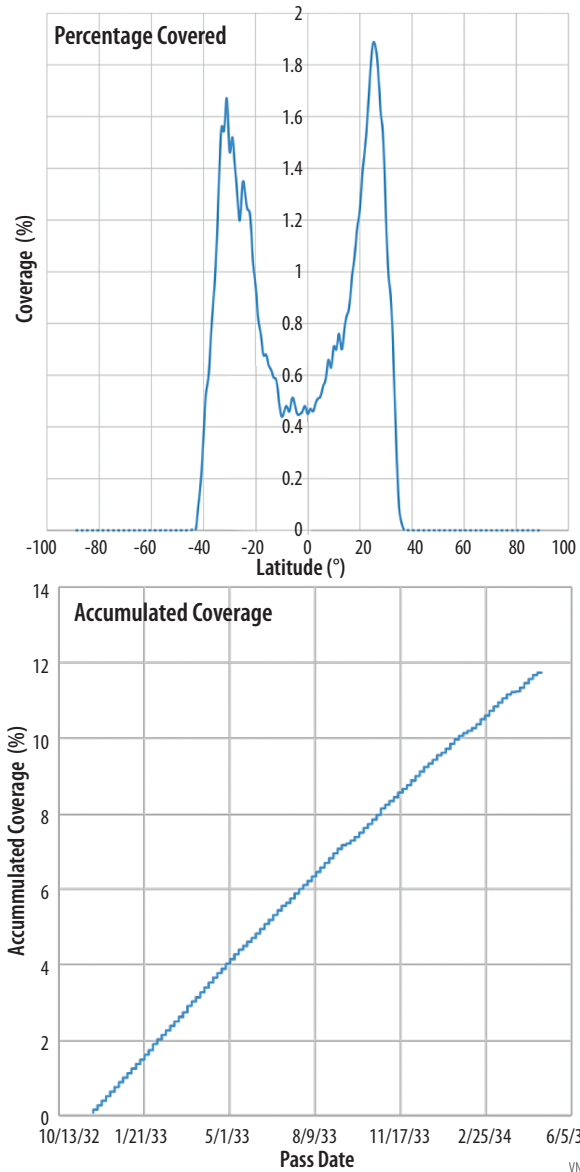
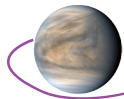


Figure B-47. Venus coverage prior to achievement of science orbit.



**Table B-27.** Periapsis station keeping maneuvers: pre-science phase of the baseline trajectory. Total value does not include VOI.

Date [UTC]	$\Delta V$ [m/s]	
9 Nov 2034 12:47:08.745	529.8	Orbiter VOI
31 Dec 2034 23:04:45.432	5.1	
11 Jan 2035 00:09:28.996	5.2	
21 Jan 2035 01:33:08.849	7.1	
31 Jan 2035 03:08:57.403	6.8	
10 Feb 2035 04:47:11.189	4.5	
11 Apr 2035 13:44:51.732	4.3	
26 Apr 2035 18:06:29.645	5.4	
6 May 2035 21:36:14.781	6.9	
Total	45.3	

**Table B-28.** Periapsis station keeping maneuvers: pre-science phase of the backup trajectory. Total value does not include VOI.

Date [UTC]	$\Delta V$ [m/s]	
20 Sep 2034 17:36:44.053	157.6	Orbiter VOI
13 Oct 2034 08:06:19.636	5.8	
23 Oct 2034 09:54:21.387	4.7	
2 Nov 2034 11:52:05.301	5.0	
17 Nov 2034 14:36:02.725	4.4	
11 Jan 2035 22:39:47.718	4.86	
27 Jan 2035 02:59:18.864	4.5	
Total	29.2	

venusian orbits: SmallSat 1’s orbit inclination is  $0.0^\circ$  (Venus Inertial Frame), and SmallSat 2’s orbit inclination is  $65^\circ$ . The  $65^\circ$  inclination of SmallSat 2 is the minimum inclination requirement for science operations. The orbital parameters of the venusian orbits of both SmallSats are provided in **Table B-29**.

**Table B-29.** SmallSat venusian orbital parameters.

	SmallSat 1	SmallSat 2
Apoapsis altitude (km)	18,661	18,661
Periapsis altitude (km)	500	500
Orbit Period (hr)	5.985	5.985
Inclination ( $^\circ$ )	0.0	65.0
RAAN ( $^\circ$ )	251.0	339.9
Argument of Periapsis ( $^\circ$ )	86.6	359.5

The two SmallSats detach from the rest of the platforms a few hours after launch to follow their own interplanetary trajectory toward Venus. Separate trajectories are used for the SmallSats and the rest of the platforms because each of the two SmallSats needs to be in place before the Aerobot arrival (11/9/2034), and the SmallSats must provide 4 hours of communication to the Lander for entry, descent, and landing (EDL) (5/19/2035). In addition, SmallSat 1 is required to provide communication access to the Aerobot during the its 60-day mission.

The interplanetary portions of the SmallSats’ trajectories for the baseline and backup launch opportunities are shown in **Figure B-48** and **Figure B-49**, respectively. The SmallSat physical characteristics and the main events of their interplanetary trajectories are given in **Table B-30**.

Upon arrival in the Venus system, the SmallSats use their SEP systems to spiral down to their target Venus orbits. (It is worth noting that the SmallSats’ low-thrust interplanetary trajectories allow the

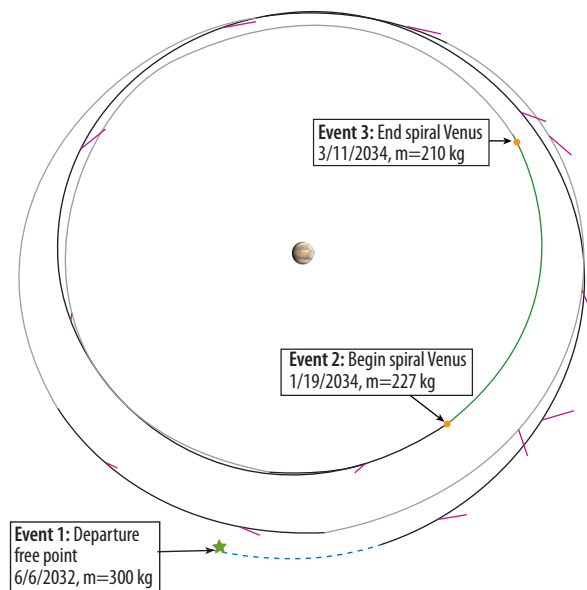


**Figure B-48.** SmallSats baseline trajectory.

VN140

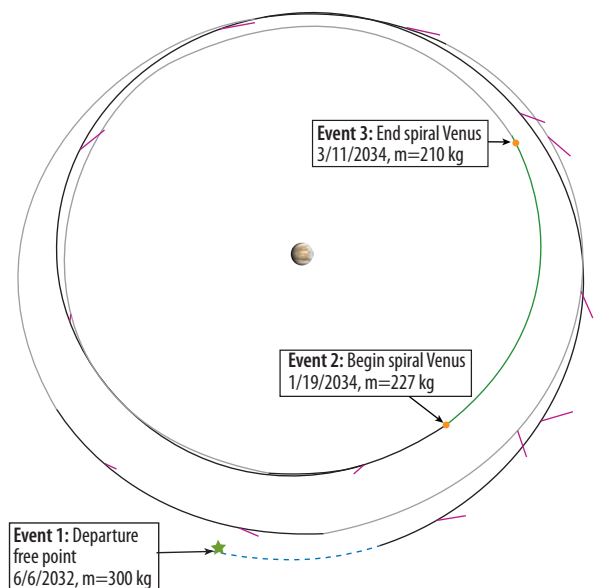
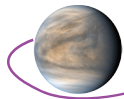


**Figure B-49.** SmallSats backup trajectory.

111111



SmallSats to reach practically any venusian orbit inclination because the SmallSats' arrival C3 with respect to Venus is zero.)

### B.2.7.5 Communication Access

The computed accesses for communication between couples of platforms are provided in **Table B-31** assuming a minimum ground elevation of 15° for the SmallSats and the Orbiter. Due to atmospheric effects, S-Band communication below a ground elevation of 15° suffers from a large absorption as shown in the Orbiter communication **Section B.2.8.3.7**.

**Table B-30.** Main events and spacecraft parameters for the two SmallSats.

	Baseline	Backup
Earth Departure	6/6/2031	6/6/2032
Wet mass (kg)	238.6	300
Dry mass (kg)	134	175
Venus Spiral Beginning Date	1/9/2034	1/19/2034
Wet Mass (kg)	102	101
Venus Spiral End (Venus Arrival)	8/15/2034	8/24/2034
Wet Mass (kg)	93	92
Engine thrust (N)	0.0337 each	0.0337 each
Propellant Isp (s)	1500	1500

**Table B-31.** Access between platforms of VFM (baseline launch opportunity).

Access	Start Time (UTC) Range (km)	End Time (UTC) Range (km)	Duration
Lander to SmallSat 1	05/19/2035 14:16:52.538 13576.46	05/19/2035 18:16:52.538 12726.65	4 hour
Lander to SmallSat 2	05/19/2035 18:16:52.538 13215.77	05/19/2035 22:16:52.538 13053.76	4 hour
Lander to Orbiter	05/19/2035 15:16:53.539 16842.76	05/19/2035 16:36:53.539 13138.77	80 min
Aerobot to SmallSat 1 <sup>1</sup>	11/09/2034 12:42:36.196 20933.27	05/19/2035 14:43:42.374 15512.00	60 days
Aerobot to SmallSat 2 <sup>1,2</sup>	11/09/2034 12:42:36.196 21123.78	05/19/2035 13:58:48.975 20235.32	60 days
Aerobot to Orbiter <sup>8</sup>	11/09/2034 19:09:22.056 76087.25	01/08/2035 11:17:38.858 11363.05	60 days

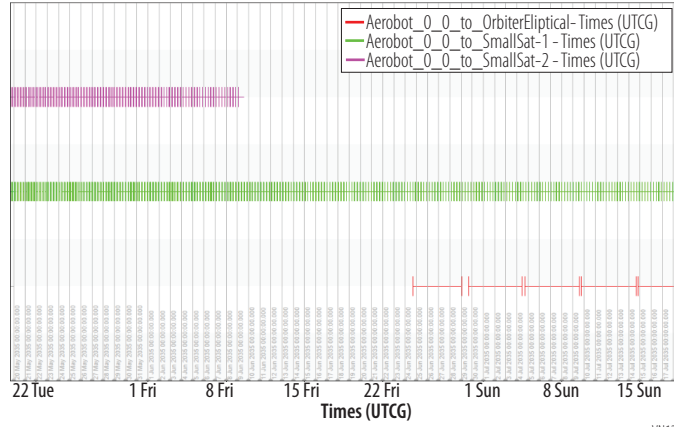
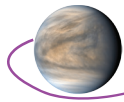
<sup>1</sup> Access computed for four different positions (latitude, longitude) of the Aerobot (angles in °): (0, 0), (0, 90), (0, 180) and (0, 270). The Aerobot trajectory has not yet been modeled.

<sup>2</sup> The contact times are intermittent.

#### B.2.7.5.1 Contact Times Evaluation from SmallSats and Orbiter to Aerobot

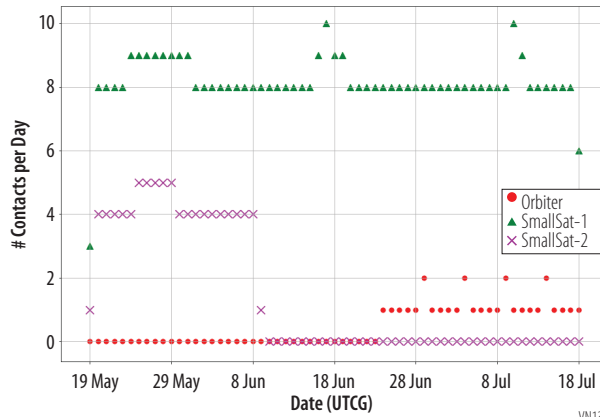
The number of contacts per day along with the total contact time per day was assessed for SmallSats and Orbiter with respect to Aerobot. It consisted of a 60-day evaluation, i.e., the Aerobot's nominal lifetime, having May 19, 2035, 16:56:53.539 UTCG as the start of the epoch. The Aerobot has an elevation mask of 15° that only allows contacts from 15° to 75°, and 105° to 165° due to the S-band absorption of the atmosphere from 0° to 15° and 165° to 180° as well as the balloon blocking signal from 75° to 105°.

As the Aerobot's trajectory over the surface of Venus is not defined, the communication link evaluation was performed using four different Aerobot latitude/longitude configurations: (0°,0°), (0°,90°), (0°,180°), and (0°,270°) with the Aerobot's altitude fixed at 62 km. The Aerobot's operational altitude interval is set to 52 to 62 km, as required by the science payload; this small difference in altitude does not play a significant role in defining the communication link—the range difference to the platforms varies little with the Aerobot's altitude. The communications link evaluation is presented in the next figures; in them the Orbiter results are depicted in red, SmallSat-1 in green, and SmallSat-2 in purple. **Figure B-50**, **Figure B-53**, **Figure B-56**, and **Figure B-59** depict the full timeline of access during the Aerobot's 60-day lifetime. **Figure B-51**, **Figure B-54**, **Figure B-57**, and **Figure B-60** show the number of contacts per day per platform. **Figure B-52**, **Figure B-55**, **Figure B-58**, and **Figure B-61** show the total contact time for each platform per day.



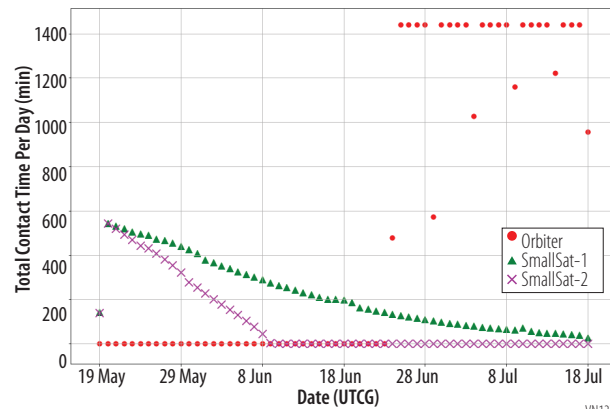
VN139

Figure B-50. Contact times for Aerobot at position (0°, 0°)



VN138

Figure B-51. Number of contacts per day to Aerobot (0°, 0°) during the 60-day period



VN137

Figure B-52. Total contact time per day to Aerobot (0°, 0°) during the 60-day period.



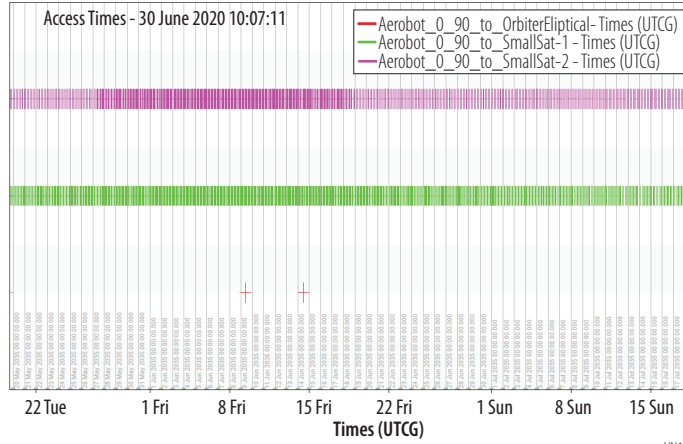
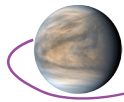


Figure B-53. Contact times for Aerobot at position (0°, 90°)

VN136

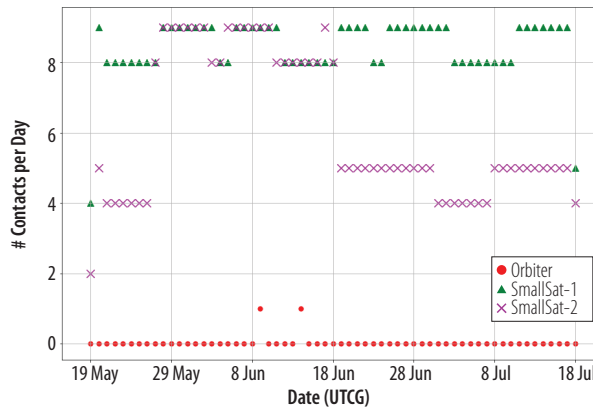


Figure B-54. Number of contacts per day to Aerobot (0°, 90°) during the 60-day period.

VN135

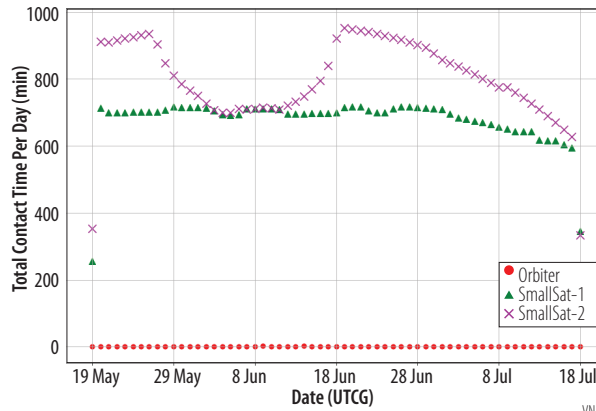


Figure B-55. Total contact time per day to Aerobot (0°, 90°) during the 60-day period.

VN134

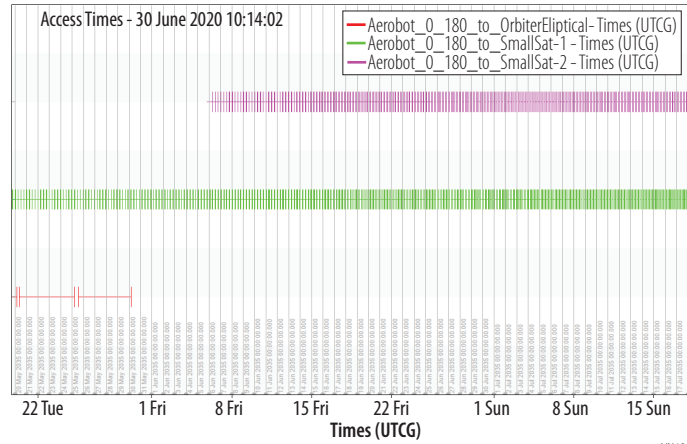
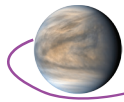


Figure B-56. Contacts times for Aerobot (0°, 180°) during the 60-day period

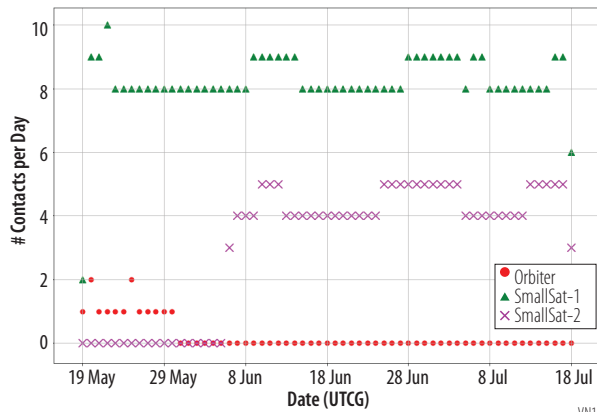


Figure B-57. Number of contacts per day to Aerobot (0°, 180°) during the 60-day period

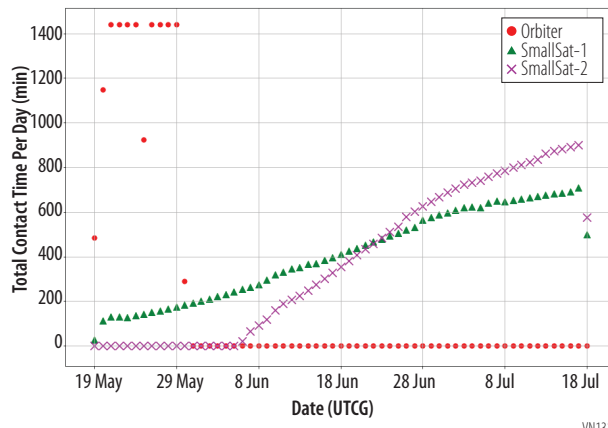


Figure B-58. Total contact time per day to Aerobot (0°, 180°) during the 60-day period

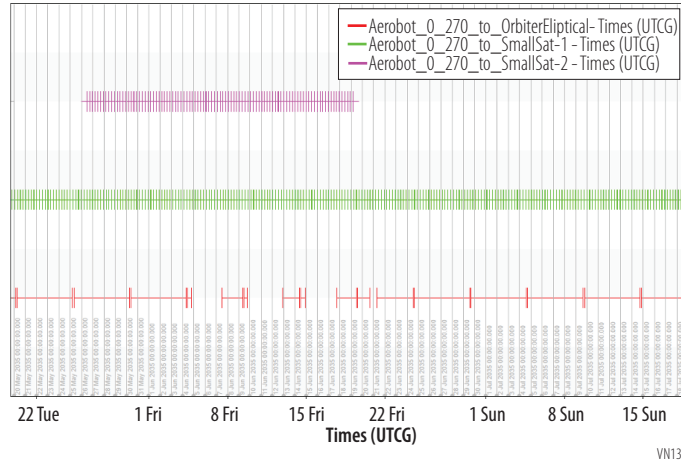
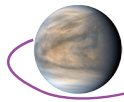


Figure B-59. Contacts times for Aerobot (0°, 270°) during the 60-day period

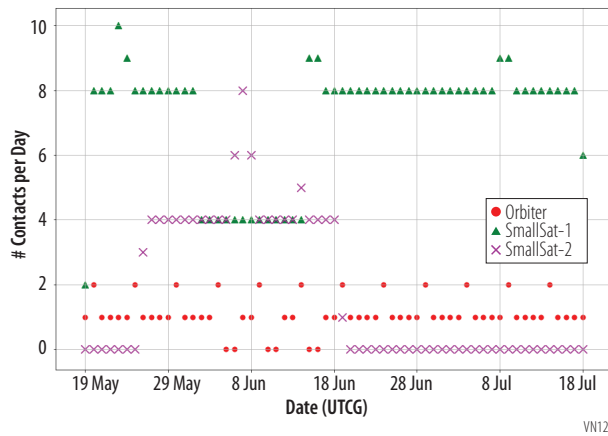


Figure B-60. Number of contacts per day to Aerobot (0°, 270°) during the 60-day period

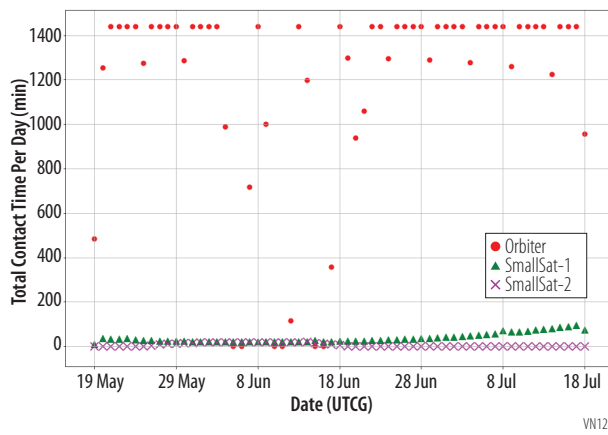


Figure B-61. Total contact time per day to Aerobot (0°, 270°) during the 60-day period

### B.2.7.6 Landing Conditions Analysis

VFM requires venusian daytime access between Earth and the target site, West Ovda, at the landing epoch. To do that, accesses were computed for possible landing epochs from 01/01/2033 to 01/01/2036. The analysis had a solar exclusion angle of 5° as a constraint. The results are shown in **Figure B-62**. In it, the orange lines outline landing opportunities where the site is visible from Earth, on the daylight side of Venus, and no Sun conjunction is present. The x-axis presents the dates in UTC format and

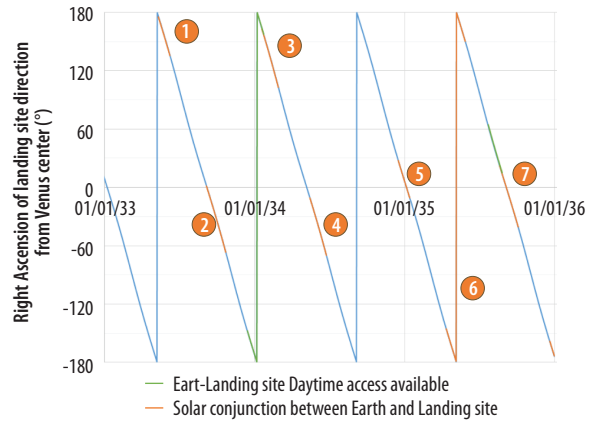
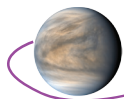


Figure B-62. Right ascension of landing site as function of daytime access available between Earth and West Ovda.

Table B-32. Landing opportunities.

Opportunity	Start Time (UTC)	Stop Time (UTC)
1	05/12/2033 17:01	06/09/2033 14:44
2	09/06/2033 19:30	10/23/2033 09:15
3	01/18/2034 19:32	02/28/2034 17:40
4	05/16/2034 21:39	06/25/2034 00:38
5	12/17/2034 16:56	01/14/2035 20:29
6	04/13/2035 08:54	05/29/2035 14:21
7	08/21/2035 14:13	10/05/2035 00:32

Table B-33. Launch opportunities

Opportunity	Launch Date	Max. Delivered Mass to Venus (kg)	Landing Opportunity
1	Jun. 2030	9403	2
2	Dec. 2030	9128	1
		9646	2
		9084	3
		9654	4
		9342	5
3	Jun. 2031	9637	6
		9427	7
4	Jun. 2032	9174	5
		9331	7
5	Dec. 2032	9356	4

the y-axis gives the right ascension of the landing site with respect to the venusian Inertial Centered Reference Frame (ICRF) frame.

At the time of landing, the landing site must be in the venusian daytime and have a direct communication link with Earth (ground station not specified). As a result, the landing windows are limited to several periods (Figure B-63). Since the periapsis direction of the orbit before Lander separation needs to be aligned in the direction of the landing point, the periapsis direction of the Venus insertion orbit must be changed for each landing window. Therefore, a launch window analysis was necessary for each landing period because the optimum launch and orbit insertion timing are different depending on the periapsis direction (dominated by right ascension) of the insertion orbit. The resulting acceptable landing opportunities are shown in Table B-32. Trajectory solutions were generated to find feasible<sup>[2]</sup> heliocentric trajectories that arrive at Venus during these opportunities, leading to the launch

[2] Trajectories able to deliver the required mass for the computed landing opportunities, with TOF less than 4 years. The objective function of the Evolutionary Mission Trajectory Generator (EMTG) analysis was to maximize the final mass delivered to Venus.

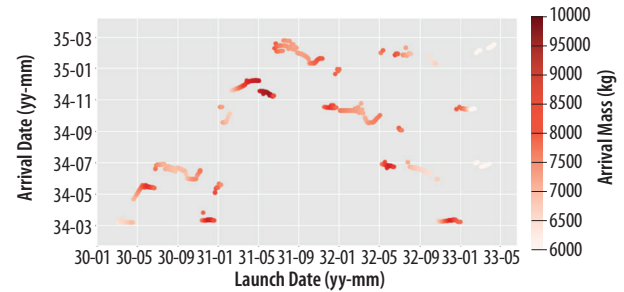


Figure B-63. Baseline launch opportunity, landing opportunity 6. RA of periapsis = 155°–205°; latitude of periapsis = -9°; TOF < 4 years.

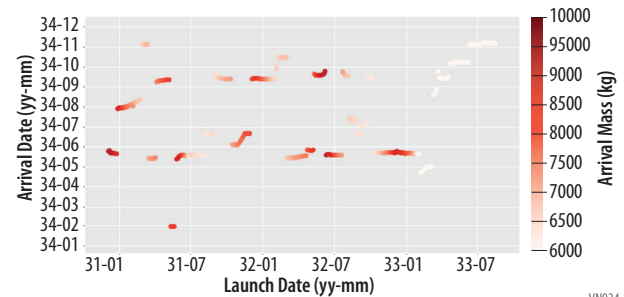


Figure B-64. Backup launch opportunity, landing opportunity 5. RA of periapsis = -5°–20°; latitude of periapsis = -9°; TOF < 4 years.

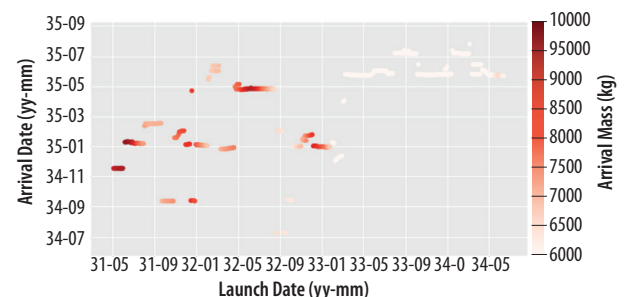
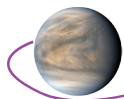


Figure B-65. Backup launch opportunity, landing opportunity 7. RA of periapsis = -5°–20°; latitude of periapsis = -9°; TOF < 4 years.



opportunities given in **Table B-33**. Note that **Table B-33** shows only those launch opportunities with an arrival mass of more than 9,000 kg (Aerobot, Orbiter, and Lander), assuming launch on a Falcon Heavy Expendable. Similar launch and landing opportunities exist in every subsequent synodic period (Earth-Venus synodic period 583.92 days).

This result is a combination of the trajectory flight time and arrival dates, which were defined by the feasible landing opportunities. The launch period solutions are presented with respect to launch and arrival date. These trajectories insert at Venus already with the periapsis direction determined by the right ascension of the land site, shown in **Figure B-63**, **Figure B-64**, and **Figure B-65**. The launch date of 2031 was selected as the earliest feasible launch date with an adequate mission development schedule.

### B.2.7.7 Orbiter Coverage Analysis

**Table B-34.** Orbital parameters for the two orbits assessed. Coordinate system for Circular Orbit: Venus Inertial, coordinate system for Elliptical Orbit: Venus-centered ICRF.

Orbital Parameter (Venus Inertial Frame)	Circular Orbit	Elliptical Orbit
Semi Major Axis (km)	6351.8	116108.38
Eccentricity	0	0.945
Inclination (°)	90.0	90.0
Argument of Periapsis (°)	188.6	188.6
RAAN (°)	334.42	334.42
True anomaly at Initial Epoch (°)	0	0
Initial Epoch (UTCG)	May 1 2037 00:00:00.000	May 1 2037 00:00:00.000
Orbit Propagation Time Step (sec)	60	60

**Table B-35.** Results of the simulations conducted for Science Orbit, assuming a 100% duty cycle. Daylight constraint.

Venus Days	Lat/Long Discretization (deg)	Sensor Vertical Half Angle (Deg)	Sensor Horizontal Half Angle (deg)	Coverage (%)
2	2	3.65	1.6	78.36
2	6	3.65	1.6	78.73
4	6	3.65	1.6	91.85
6	6	3.65	1.6	100.00
2	6	4.65	2.6	78.73
4	6	4.65	2.6	91.85

Two orbits were assessed for RADAR coverage analysis during the Orbiter science phase. The analysis evaluated duty cycles lower than a hundred percent in terms of Field of View (FOV). The orbital parameters of the two orbits used throughout the trade are provided in **Table B-34**.

Several analyses were conducted assuming a 100% duty cycle for circular orbit, in order to set a latitude/longitude (lat/lon) discretization value for the Venus surface and to explore the effect of slightly increasing the beam width of the RADAR, with respect to the nominal values. The results are presented in **Table B-35**.

Three preliminary conclusions were extracted for the aforementioned analysis:

- The 6° discretization provides similar results than the 2° discretization. Therefore, a 6° discretization was used in the rest of the simulations to avoid high computational times.<sup>[3]</sup>
- The 1° increase of the sensor FOV with respect to the nominal configuration does not affect coverage results.
- A 100% coverage can be obtained in the 4 Earth-year (6-venusian day) interval. Lower intervals lead to lower total accumulated-coverage values.

As a final remark, the ground track is repeated every two venusian days. Nonetheless, more venusian days have to pass before getting 100% coverage due to the imposed daylight constraint.

[3] This is a coarse discretization. Higher coverage may be expected with finer lat/lon discretization, so results using a 6° discretization are conservative.

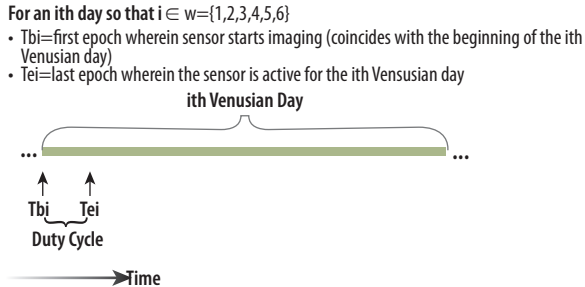
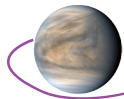


Figure B-66. First RADAR duty cycle policy concept

The next step was to come up with a duty cycle policy to get the approximate coverage stipulated in the requirements: 3.5% for wide beam and 2% for the narrow beam. Three different policies were studied:

- P1. The RADAR is on at the beginning of each venusian day.
- P2. The RADAR is on at different epochs in each venusian day.
- P3. The RADAR is on at the beginning of each Orbiter revolution.

The three policies are depicted in **Figure B-66**, **Figure B-67**, and **Figure B-68**, respectively. The input values assumed for the coverage comparison among the three duty cycle policies are given in **Table B-36**.

The results of the duty cycle comparison are given in **Table B-37**. Policy 3 leads to the highest coverage and, therefore, it is the chosen policy for the coverage analysis. It is important to note that the results obtained are conservative, as better policies could be found on top of implementing a finer latitude/longitude discretization for the Venus surface.

The final step is to perform the actual coverage analysis, after having performed a non-exhaustive parameter tuning in terms of latitude/longitude discretization and duty cycle policy. The coverage analysis inputs are provided in **Table B-38**.

The elliptical orbit was first evaluated yielding a coverage of 34.13%, significantly outperforming the wide/narrow beam requirements of 3.5 and 2% respectively. Based on this promising result, a more thorough coverage analysis was performed for the circular orbit as a project decision leading to the results illustrated in **Figure B-69**.

### B.2.8 Flight System Details

The packaging of all the platforms of the VFM launch stack was driven by the Falcon 9 heavy fairing size. The diameter of the fairing is within scope of standard 5m fairings used on the Delta IV, Atlas

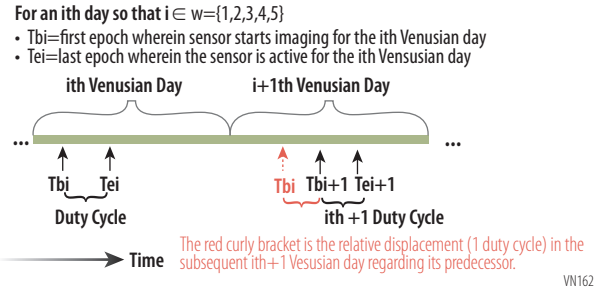


Figure B-67. Second RADAR duty cycle policy concept

For every orbital period in Science Orbit:

- $T/2$  = half orbital period
- $T_{bi}$  = first epoch sensor starts imaging (coincides with the beginning of every orbital period)
- $T_{ei}$  = last epoch the sensor is active

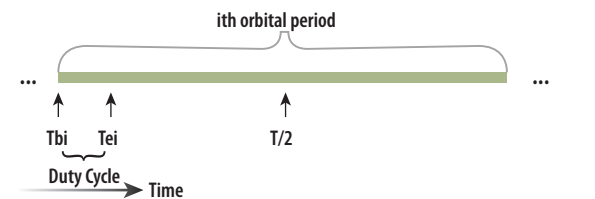


Figure B-68. Third RADAR duty cycle policy concept.

Table B-36. Values used for the duty cycle comparison regarding coverage. Circular Orbit.

Input	Value
Duty Cycle (%)	5
Daylight Constraint	Yes
Lat/Lon Discretization (°)	6
Interval (Earth Years)	4
RADAR V/H Half Angles (°)	3.65/1.6

Table B-37. Results of the duty cycle comparison.

# Duty Cycle Policy	Coverage (%)
1	9.8
2	41.1
3	49.48

Table B-38. Coverage analysis inputs.

	Circular Orbit	Elliptical Orbit
Duty Cycles Evaluated (%)	1, 2, 3.5, 5, 7, 10	5
Daylight Constraint	Yes	No
Lat/Lon Discretization (°)	6	6
Start Epoch (UTC)	May 1, 2037	May 1, 2037
Analysis Duration (Earth years)	4	4
Sensor Vertical/Horizontal Half Angles (°)	3.65/1.6	3.65/1.6
Altitude Constraint for Measurements	No	Yes (1000 km)

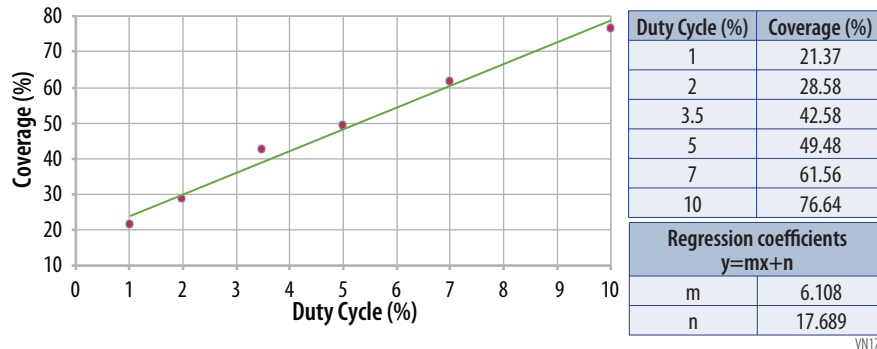
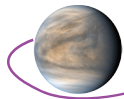


Figure B-69. Coverage analysis results for Circular orbit.

and baselined for the Block 1 SLS but the height is significantly smaller. Baselining the smaller fairing ensures that, from a packaging standpoint, a broad spectrum of fairings are viable. All current launch vehicles have a limited center-of-mass offset. Although this was not a specific design driver, it was a consideration that nudged the design to as squat a height as possible. This had the additional advantage of a more efficient mass design.

Various concepts were studied for accommodating the Aerobot. The operational order required that the Aerobot be deployed before the Lander which reduced the packaging options significantly. The discovery during the MDL study that a 3.1m diameter PAF was being developed by SpaceX for upcoming flight missions allowed the placement of the Aerobot beneath the Orbiter within the PAF/ Orbiter interface thrust cone. This required the outboard placement of the main engines which had the added benefit of providing significant ACS capability. This interface concept also suggested that the Orbiter be an octagon with an upper and lower deck, equipment panels, a large central cylinder and radials to better provide a robust load path to the Lander and SmallSats. The layout provided an efficient mount for the large oxidizer tank to the central cylinder and bays for mounting the four fuel tanks.

The central cylinder became the primary support for the Lander/Entry System. The decks provided mounting for the SmallSats and the **S-mm** instrument. The compact octagonal shape also allowed clearance for the 5m antenna and deployment system and other instruments and hardware. Both the Aerobot and Lander are depicted being mounted with notional separation rings such as Marmon clamp-bands or Lightbands. These are considered notional since no attempt was made to look at other mount/release systems. They were merely used to provide a mass within the range of viable options with the expectation that detailed design of these would be future work all well within the state-of-the-art.

### B.2.8.1 Aerobot

The VFM Aerobot is a variable-altitude balloon-based platform, and can control this altitude to a commanded profile. In contrast, passive constant-altitude balloons that have been flown on Venus before (i.e., Vega Missions), are naturally higher TRL, and have been a more popular platform in prior NASA mission proposals and Decadal Studies [Klaasen, 2003; Balint, 2008; Grinspoon et al., 2010], but VFM has selected variable-altitude in keeping with the recent recommendations of NASA 2018 Venus Aerial Platforms Study [Cutts et al., 2018] and the need to fulfill the requirements in the **STM**. Variable-altitude Aerobots can carry instrument payloads at multiple altitudes and multiple times of day independently, allowing targeted science investigations not possible with a passive system. Additionally, variable altitude balloons are already highly developed in terrestrial applications—the Google Loon project [<https://loon.com/>] is most well-known, among others [World View, 2019; De Jong, 2017], so the TRL gap largely represents a need to adapt this technology to the Venus environment rather than a unknown control method. Past JPL efforts, though concentrating on constant-altitude balloons and passive cycling balloons, also provide a baseline of material testing [Hall et al., 2008] that have been leveraged into the VFM design. Metalized fluorinated ethylene propylene (FEP) has been validated against concentrated sulfuric acid and resistance to pinhole growth. Vectran fabric, used for the MER airbags, has similarly been tested for acid resistance and integrated into several Venus balloon prototypes.

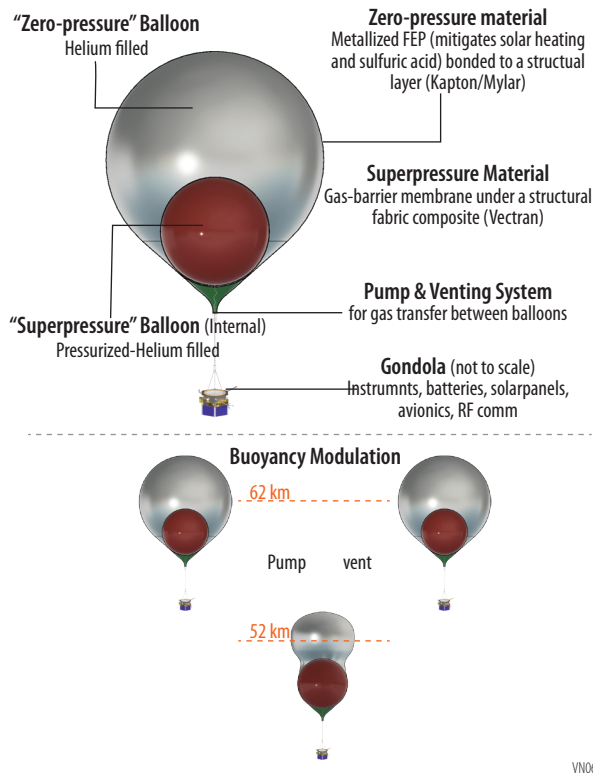
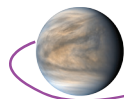


Figure B-70. Balloon-in-a-balloon Pumped Helium Venus Aerobot Concept

Many forms of altitude control exist, but not all are suitable for a long-duration mission on Venus. The long-duration Venus case is unique in that expendables (ballast drops and venting) must be avoided and pumping the outside atmosphere into the Aerobot as ballast (the technique used by Google Loon) is undesirable due to the sulfuric acid aerosol content of Venus atmosphere. A comparison of options for Venus can be found in Hall et al. [2019], with the pumped-helium method [e.g., Voss, 2009] shown to be least mass and power of the options considered for active altitude-control on Venus.

The Aerobot uses a 15-m diameter pumped-helium balloon with a second 7.5-m internal chamber (**Figure B-70**). The outer chamber is at approximately equal pressure with the atmosphere (a zero-pressure balloon), while the internal chamber is at elevated pressure with a structural, constant-volume envelope (a super-pressure balloon). Helium is pumped from the outer chamber to the inner chamber to lower the total volume and hence buoyancy and altitude, while helium is vented from the inner to outer to raise the altitude. The Aerobot therefore remains a sealed system for the entirety of operation; no sulfuric acid aerosols need be ingested. Of note, lowering the altitude requires energy and is limited by the

throughput of the pump, while raising the altitude can be done quickly for little energy by opening an orifice to vent the pressurized helium between the chambers.

The Aerobot pump and vent systems share the solar power provided by the gondola (payload module), and are controlled by the central avionics. The pump, as a mobility system, is a significant power driver that affects the mission design and concept-of-operations. At night, all descents must be performed on battery power only, while ample sunlight during the day supports wider operation.

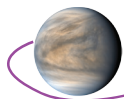
In summary, the requirements of this balloon are to:

- Deploy and inflate aerielly while suspended from the main parachute after atmospheric entry.
- Carry a 200 kg gondola (MEV).
- Control the flight altitude to a commanded profile cycling between 52 and 62 km in both day and night.
- Resist sustained vertical wind perturbations and solar heating that would push the balloon outside its designed altitude range.
- Support long duration flights by both minimizing helium loss to the atmosphere, and resisting sulfuric acid aerosols that would degrade the envelope over time.

Hall et al. [2019] describe the design method for such Aerobots in detail, which can be easily scaled up or down for various payloads, structural margins, or predicted environmental conditions. Large payloads require larger Aerobots and more pumping energy to vary the altitude.

The two envelopes of the Aerobot, one for each balloon, are important subsystems with distinct functions. The zero-pressure envelope acts as a helium gas barrier, sulfuric acid barrier, and solar heating barrier. Accordingly, it is made from a metallized (vapor deposited) FEP layer bonded to a structural plastic of Kapton or Mylar. The metallized FEP provides sulfuric-acid resistance and is a second-surface mirror of low solar absorptivity and high IR emissivity. The structural plastic below it provides strength for handling and deployment, and the bi-laminate construction lowers the probability of aligned material defects between layers that could leak gas.





The internal superpressure envelope acts as a pressure vessel (operating in the tens of kPa range), but need not be acid-resistant as it is protected by the outer balloon. This envelope is accordingly made from a gas barrier membrane beneath an inflatable structure—Vectran composite fabric as currently designed but an array of tendons (pumpkin balloon construction) has also shown success in the NASA ULDB program [Cathey, 2007].

The Aerobot has the following performance metrics:

- Maximum descent rate of 0.5 km/hr at 26W (night) and 77W (day) assuming a 70% efficient flight pump. This slow descent rate is designed to minimize the pump power and mass, while still allowing multiple descents as desired by mission operations.
- A 110kg zero pressure balloon envelope, 62kg superpressure balloon envelope, and 39kg of helium (CBE). The larger zero pressure balloon is a lower areal density (100g/m<sup>2</sup>) than the superpressure material (225g/m<sup>2</sup>), consistent with its lighter loading.
- Maximum expected pressurization of 30kPa in full equatorial solar heating, with balloon designed to a structural safety margin of 2.

The variable-altitude Aerobot platform is currently TRL 4, and there is ongoing work at JPL to mature it further. Venus-relevant early prototype testing is scheduled for the summer of 2020. Past JPL efforts, though concentrating on constant-altitude balloons and passive cycling balloons, also provide a baseline of material testing [Hall et al., 2008] that have been leveraged into the VFM design. Metalized FEP has been validated against concentrated sulfuric acid and resistance to pinhole growth. Vectran fabric, used for the MER airbags, has similarly been tested for acid resistance and integrated into several Venus balloon prototypes.

### B.2.8.1.1 Instrument Accommodations

The Aerobot payload is focused in three science areas: composition, meteorology, and geophysics. For composition, the key instrument is an **aerosol mass spectrometer** with a **nephelometer (AMS-N)**. It will measure both gas composition and aerosol/cloud composition, using dedicated inlets for each. Astrobiological science is addressed by a dedicated **FM**, which will examine cloud droplets for minute traces of constituents associated with past or present life. The Aerobot also carries a suite of **meteorological sensors-barometric pressure and air temperature sensors, radiometer, wind sensor, and a radiation dosimeter** to address the meteorology questions. Finally, the Aerobot carries payloads addressing the geophysics of the solid planet below. Tectonic and volcanic activity during the mission will be searched for by an infrasound pressure sensor. A **3-D fluxgate magnetometer** will carry out a number of investigations, including a search for remnant crustal magnetism; constraints on core size and properties from magnetic field draping; and a search for magnetic emissions from lightning. A **visible imager** is the final instrument on the payload—its purpose is to take images of the balloon and Venus clouds as well as support public outreach activities.

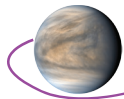
### B.2.8.1.2 Aerobot Instruments

#### B.2.8.1.2.1 Aerosol Mass Spectrometer with Nephelometer (AMS-N)

The **AMS-N** is a mass spectrometer with a dedicated aerosol sampling inlet. **AMS-N** measures species including SO<sub>2</sub>, SO<sub>3</sub>, HCl, CO, OCS, H<sub>2</sub>O, HDO, H<sub>2</sub>S, to a sensitivity of 1 ppm. The instrument must be capable to measure H<sub>2</sub>SO<sub>4</sub>, H<sub>2</sub>O, FeCl<sub>3</sub>, and sulfur (S<sub>3</sub>, S<sub>4</sub>, S<sub>X</sub>) to a sensitivity of better than 1%. The goal is to characterize diurnal variation of composition and altitude variation within the clouds. **AMS-N** will characterize cloud-level atmospheric composition and its variability. The instrument will measure particle size and identify non-liquid particulates. The objective is to determine the chemical environment and composition of the cloud particles searching for evidence of previous habitability and current surface volcanic activity.

Table B-39. Aerosol Mass Spectrometer with Nephelometer Characteristics

Item	Value	Units
Type of instrument	Mass Spectrometer	
Number of channels	1–150	Daltons
Size/dimensions (for each instrument)	30 x 20 x 20	cm x cm x cm



Item	Value	Units
Instrument mass <b>without</b> contingency (CBE)	11	kg
Instrument mass contingency	30	%
Instrument mass <b>with</b> contingency (CBE+Reserve)	14.3	kg
Instrument average payload power <b>without</b> contingency	10.8	W
Instrument average payload power contingency	30	%
Instrument average payload power <b>with</b> contingency	14.04	W
Instrument average science data rate <sup>^</sup> <b>without</b> contingency	0.392	kbps
Instrument average science data <sup>^</sup> rate contingency	30	%
Instrument average science data <sup>^</sup> rate <b>with</b> contingency	0.51	kbps
Instrument Fields of View (if appropriate)	RAM direction	
Pointing requirements (knowledge)	N/A	
Pointing requirements (control)	N/A	
Pointing requirements (stability)	N/A	

<sup>^</sup>Instrument data rate defined as science data rate prior to on-board processing

### B.2.8.1.2.2 Fluorimetric Microscope (FM)

The **FM** is an instrument on board the Aerobot designed to search for bio-content in Venus's clouds and will collect 7 samples over 60 days, at variable altitudes, using images (fluorescence and dark-field) of cloud droplets on 10, 1.0, and 0.2  $\mu\text{m}$  pore-size filters with  $<0.5 \mu\text{m}$  spatial resolution at 265, 370, 470, and 530 nm to determine the difference between bio-content on day and night-sides during the course of circumnavigation (1 circumnavigation takes about 5 days). These data will identify fluorescent biomolecules, e.g., chlorophyll or other photosynthetic pigments that could allow for photosynthetic activity. The **FM** will collect and fluorescently characterize any biomolecules or larger fluorescing organic objects in the altitude range of 52–62 km to determine if there are any extant or recently dead organisms or fragments present in the clouds.

**Table B-40.** Fluorimetric Microscope Characteristics

Item	Value	Units
Type of instrument	Fluorescence and Dark-field Microscope	
Number of channels (filters)	7 x 3 pore sizes (10, 1, 0.2)	micrometers
Size/dimensions (for each instrument)	10 x 10 x 33	cm x cm x cm
Instrument mass <b>without</b> contingency (CBE)	5	kg
Instrument mass contingency	30	%
Instrument mass <b>with</b> contingency (CBE+Reserve)	6.5	kg
Instrument average payload power <b>without</b> contingency	10	W
Instrument average payload power contingency	30	%
Instrument average payload power <b>with</b> contingency	13	W
Instrument average science data rate <sup>^</sup> <b>without</b> contingency	0.03125	kbps
Instrument average science data <sup>^</sup> rate contingency	30	%
Instrument average science data <sup>^</sup> rate <b>with</b> contingency	0.0406	kbps
Instrument Fields of View (if appropriate)	RAM direction	
Pointing requirements (knowledge)	N/A	
Pointing requirements (control)	N/A	
Pointing requirements (stability)	N/A	

<sup>^</sup>Instrument data rate defined as science data rate prior to on-board processing

### B.2.8.1.2.3 Magnetometer (Mag)

The **Mag** is an instrument capable of measuring the magnetic field of Venus. The instrument is part of the payload for 4 of the 5 Venus Flagship Mission assets—the Aerobot, Orbiter, and the two Small-Sats. The magnetometer instrument will perform aerial magnetic field surveys over major terrains to constrain the presence, spatial distribution and intensity of potential magnetic sources. These data will determine if Venus shows evidence of a current or past plate tectonic regime. The instrument must be magnetically clean and requires a  $> 1$  meter boom with 32 Hz sampling and a resolution of  $\pm 5$  nT. The **flux-gate magnetometer** data will be used to characterize the magnetic field topology and strength as

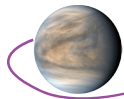


**Table B-41. Magnetometer Characteristics**

Item	Value	Units
Type of instrument	Fluxgate Magnetometer	
Number of channels (filters)	N/A	
Size/dimensions (for each instrument)	4 x 3 x 3	cm x cm x cm
Instrument mass <b>without</b> contingency (CBE)	1	kg
Instrument mass contingency	30	%
Instrument mass <b>with</b> contingency (CBE+Reserve)	1.3	kg
Instrument average payload power <b>without</b> contingency	0.5	W
Instrument average payload power contingency	30	%
Instrument average payload power <b>with</b> contingency	0.65	W
Instrument average science data rate <sup>^</sup> <b>without</b> contingency	0.0625	kbps
Instrument average science data <sup>^</sup> rate contingency	30	%
Instrument average science data <sup>^</sup> rate <b>with</b> contingency	0.8125	kbps
Instrument Fields of View (if appropriate)	N/A	
Pointing requirements (knowledge)	N/A	
Pointing requirements (control)	N/A	
Pointing requirements (stability)	N/A	

<sup>^</sup>Instrument data rate defined as science data rate prior to on-board processing

well as search for evidence of a past or current magnetic field. These data, in concert with other instruments aboard the five assets will aid in the understanding the history of the liquid water and volatiles on Venus. The instrumentation used as a baseline for this mission study is currently at TRL 9 and has heritage on three flight missions—MAVEN, Parker Solar Probe, and Juno.

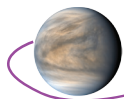
#### **B.2.8.1.2.4 Visible Imager (VI)**

The **VI** is an instrument on the aerobot payload which has multiple purposes. The imager will be able to provide context for data from other instruments as well as collect visible data of the cloudscapes. The data collection plan will enable the ability to see the impacts of the Venus atmosphere on the balloon over the course of its 60 day mission. The imager also will be utilized for students and public outreach purposes.

**Table B-42. Visible Imager Characteristics**

Item	Value	Units
Type of instrument	Imager	
Number of channels (filters)	3	
Size/dimensions (for each instrument)	15 x 11 x 11	cm x cm x cm
Instrument mass <b>without</b> contingency (CBE)	3	kg
Instrument mass contingency	30	%
Instrument mass <b>with</b> contingency (CBE+Reserve)	3.9	kg
Instrument average payload power <b>without</b> contingency	7	W
Instrument average payload power contingency	30	%
Instrument average payload power <b>with</b> contingency	9.1	W
Instrument average science data rate <sup>^</sup> <b>without</b> contingency	0.05787	kbps
Instrument average science data <sup>^</sup> rate contingency	30	%
Instrument average science data <sup>^</sup> rate <b>with</b> contingency	0.07523	kbps
Instrument Fields of View (if appropriate)	120	
Pointing requirements (knowledge)	n/a	
Pointing requirements (control)	n/a	
Pointing requirements (stability)	n/a	

<sup>^</sup>Instrument data rate defined as science data rate prior to on-board processing



### B.2.8.1.2.5 Meteorological Suite (MET)

The Aerobot carries a suite of **meteorological sensors**, including **barometric pressure** and **air temperature** sensors, to examine the convective stability of the atmosphere and to provide context for other measurements. A **radiometer** measuring up- and downwelling fluxes in seven channels spanning the full solar and thermal spectral ranges enables the role of radiative balance and its relation with cloud-level dynamics. The spectral channels of the Aerobot’s radiometer will overlap with those of the descent probe and the **LLISSE** surface station’s radiometer, enabling a coherent investigation of radiance balance throughout the Venus atmosphere. Vertical and horizontal **wind velocities** will be determined by tracking the trajectory of the Aerobot, utilizing the Aerobot’s communication link with the orbiters and SmallSats; tracking the balloon’s position using ground-based telescopes (as was done for Vega balloons) is another option to be studied. Accelerations and torques measured by an Inertial Measurement Unit (IMU) will allow trajectory reconstruction between communications passes, and facilitate the study of turbulence and waves. Like the Vega balloons, the VFM Aerobot will carry a **wind sensor** in order to distinguish vertical winds from changes in balloon buoyancy; it allows characterization of turbulence down to temporal scales which are inaccessible just by tracking the balloon. The **MET** also includes a **radiation dosimeter** in order to quantify the ionizing radiation levels in the cloud layer. All the meteorological sensors share a common data handling unit, which enables low-rate continuous monitoring at 0.5 Hz and occasional scheduled and event-driven acquisition of high-rate data (triggered by events such as a strong updraft or a burst of turbulence).

**Table B-43.** Meteorological Suite Characteristics

Item	Value	Units
Type of instrument	Pressure Temperature, Wind, Radiometer, Dosimeter	
Number of channels (filters)	24	
Size/dimensions (for each instrument)	20x12x8	cm x cm x cm
Instrument mass <b>without</b> contingency (CBE)	3	kg
Instrument mass contingency	30	%
Instrument mass <b>with</b> contingency (CBE+Reserve)	3.9	kg
Instrument average payload power <b>without</b> contingency	5	W
Instrument average payload power contingency	30	%
Instrument average payload power <b>with</b> contingency	6.5	W
Instrument average science data rate <sup>^</sup> <b>without</b> contingency	0.4398	kbps
Instrument average science data <sup>^</sup> rate contingency	30	%
Instrument average science data <sup>^</sup> rate <b>with</b> contingency	0.5717	kbps
Instrument Fields of View (if appropriate)	clear of gondola	
Pointing requirements (knowledge)	N/A	
Pointing requirements (control)	N/A	
Pointing requirements (stability)	N/A	

<sup>^</sup>Instrument data rate defined as science data rate prior to on-board processing

### B.2.8.1.3 Entry, Descent, and Float

#### B.2.8.1.3.1 Overview and Requirements

The entry sequence is shown in **Figure B-32** and was driven by: (1) the final altitude/destination of the aerobot, (2) the assumed balloon inflation timeline, (3) dynamic pressure through balloon inflation, (4) and need to have the heat shield separation occur prior to balloon inflation/deployment.

To keep the design simple, the baseline deployment sequence has the 1st parachute inflated/deployed at Mach 1.4 to avoid transonic deployment conditions in the range of Mach 0.75 and Mach 1.25. A second option is to wait a few more seconds (+27) and deploy the (first/drogue) parachute at subsonic speeds. Almost immediately the heatshield separates (here, the parachute is used to ensure a positive separation during heat shield jettison). Roughly 30 s later, the backshell and the parachute separate from the aerobot/gondola. The rest of the events are very similar, if later in time. The dynamic

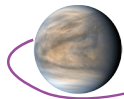


**Table B-44. Aerobot Entry Table**

	Item	Values	Units
Aeroshell	Aeroshell Geometry	45	° (sphere cone)
	Aeroshell max diameter	2.8	m
	Entry Mass	1450	kg
Entry Vector	Entry Interface	175	km
	Entry Velocity	10.56	km/s
	Peak Deceleration		
	Requirement. Less than	50	Earth-g
	Entry Flight Path Angle	-8.86	°
	Heading	270	° (relative to North)
	Entry Latitude	0	° (relative to equator)
	Entry Longitude	70	°
	Entry time(s)	2463414.155	JED

\* The entry design assumes an entry flight path angle of  $-8.86^\circ$  (which results in a peak deceleration of 50-earth g) with the assumption that the nominal EFPA is  $-7.86^\circ$ , and the uncertainty is  $\pm 1^\circ$ .

pressure through the balloon inflation is still under 100 Pa. The final altitude is slightly lower at 54.36 km. Future studies should consider this second option as it may allow slower landing velocities.

The EDF subsystem includes the forebody and afterbody aeroshells with Thermal Protection System (TPS) and the parachute(s), and within the mission's concept of operations its primary performance is from entry interface to initial float altitude. This EDF subsystem protects the payload/probe/instruments from entry heating and deceleration forces during the entry into the Venus atmosphere and was designed to meet the following requirements:

1. Temperatures at the bondline not to exceed  $260^\circ\text{C}$ . This is driven by the temperature limits on the adhesive that bonds the TPS to the aeroshell structure.
2. Peak deceleration not to exceed 50 g. This requirement stems from the science instruments. This lower value (compared to prior missions) enables a wider array of science instrumentation to be used as part of this mission.
3. Achieve flight conditions acceptable for balloon extraction and inflation at an altitude of 52 to 62 km.

The EDF subsystem must meet these requirements subject to entry conditions consistent with the interplanetary approach trajectory. The requirement on peak deceleration (for the nominal entry velocity of 10.56 km/s) yields an Entry Flight Path Angle of  $-8.5^\circ$ , significantly shallower than prior missions (such as Pioneer Venus Large Probe,  $-32.4^\circ$ ) and mission concepts (such as VITaL,  $-23.5^\circ$ ). The entry mass of 1450 kg used for the analysis and design results in a ballistic coefficient of  $224.3 \text{ kg/m}^2$  (compared to the value of  $188 \text{ kg/m}^2$  for Pioneer Venus Large Probe).

The baseline concept of operations for the Aerobot calls for two parachutes, one supersonic and the other subsonic. For the purposes of this early design, the supersonic and the subsonic parachute are assumed to be identical, weighing 27.4 kg each.

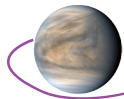
The aeroshell is a  $45^\circ$  sphere-cone geometry with a max diameter of 2.8 m. This geometry was chosen for its good stability and packaging characteristics as well as significant flight heritage at Venus. The aeroshell structure is composite with a mass of 226 kg (not including the TPS), based on preliminary

**Table B-45. Heat Shield Thermal Protection System characteristics**

TPS Material	TPS Thickness	Recession Layer Thickness	Insulative Layer Thickness	Aerial Density	Area	Mass
	(inch)	(inch)	(inch)	( $\text{kg/m}^2$ )	( $\text{m}^2$ )	(kg)
T/SL HEEET	1.33	-	1.33	27.7	8.52	235.8

**Table B-46. Backshell Thermal Protection System characteristics**

TPS Material	TPS Thickness	Aerial Density	Area	Mass
	(inch)	( $\text{kg/m}^2$ )	( $\text{m}^2$ )	(kg)
PICA	0.40	2.74	7.66	21.0



analysis. This estimate is conservative and a detailed design could provide avenues for optimization and a reduction in mass.

The heat shield TPS is a tiled single layer system of HEEET (Heat shield for Extreme Entry Environment Technology) with a mass of 236 kg and a uniform thickness of 1.33 inches. HEEET is a 3-dimensional woven TPS system developed for extreme entry environments, and the single-layer HEEET (as proposed here) only utilizes the insulation layer (versus the standard dual layer HEEET). This single layer (insulation layer only) HEEET is the baseline material for the Mars Sample Return Earth Entry Vehicle, that will bring the samples back from Mars and land them safely on Earth.

PICA (Phenolic Impregnated Carbon Ablator) is used as the backshell TPS. The tiles are expected to be bonded to the structure using HT-424 while RTV-560 fills gaps using the same techniques as Curiosity and Perseverance. The backshell TPS mass is estimated to be 20 kg.

### B.2.8.1.3.2 Aerobot Aeroshell Structure

The Aeroshell structure is designed to withstand the deceleration loads of 50 g during entry. The Thermal Protection system is designed not to let the temperature at the bondline between the TPS and the structure exceed 260° C during the entry pulse. Expected peak heating during the entry is 4,000 W/cm<sup>2</sup> (convective, rough wall, margined, at the shoulder) with an integrated heat load of over 53,000 J/cm<sup>2</sup>. The shoulder sees a relatively low radiative heating (peak, margined value of 11.3 W/cm<sup>2</sup> and an integrated heat load of 484 W/cm<sup>2</sup>).

### B.2.8.1.3.3 Concept of Operations

Table B-47 provides a summary of main events and concept of operations from entry interface to the descent of the Aerobot to the desired altitude.

Table B-47. Aerobot Entry, Descent, and Float Timeline

Event	Time from Entry sec	Altitude km	Sink Rate m/s	Mass kg
Entry Interface	0	174.837482	-1625.728676	1450
Supersonic Chute Deploy	127	70.9936445	-171.4217487	1450
Supersonic Chute Full	127.33	70.9376271	-164.8801176	1450
Heatshield Sep	128.9	70.7233224	-115.8840058	953.8
Backshell Sep	158.9	68.9014938	-53.7712862	570.3
Subsonic chute Deploy	168.9	67.9636378	-131.2215976	570.3
Begin Balloon Inf	228.9	65.7184215	-32.0285	570.3
Jettison Subsonic Chute	613.9	58.267672	-11.4840038	562.5
End Balloon Inf	813.9	55.6338495	-7.8383447	562.5
Jettison Inf Sys	843.9	55.4082738	-7.2597464	270.1

The entry vehicle enters the atmosphere, at a relative velocity of 10.5 km/s five days after release. The steepest, dispersed entry flight path angle cannot be steeper than -8.5° to limit the peak deceleration to 50g. The entry heat pulse lasts for about 2 min, slowing down the capsule (Figure B-71 and Figure B-72).

The supersonic parachute deploys at Mach 1.4 and an altitude of about 71 km. This is followed by separation of the heatshield triggered by Mach number, and separation of the backshell half a minute later, at just under 69 km altitude.

The subsonic parachute is deployed 10 seconds later (to minimize chances of recontact), followed by the beginning of the balloon inflation—at ~65 km of altitude. Four hundred seconds later, while the balloon is partly inflated, the main chute is jettisoned. The balloon is assumed to be fully inflated in 10 min and the inflation system is jettisoned half a minute later, leaving the Aerobot at an altitude of 54 km.

This sequence is designed to deliver the Aerobot to the altitude of interest, and to keep the dynamic pressure low during balloon inflation (currently peaking at 108 Pa).

Previous missions (and studies) to Venus were designed with a requirement on peak deceleration much higher than the current value of 50 g. This requirement imposes a significantly different entry flight path angle; -8.9°, as opposed to Pioneer Venus's value of -32.4°. Lofting (the vehicle flying “up”

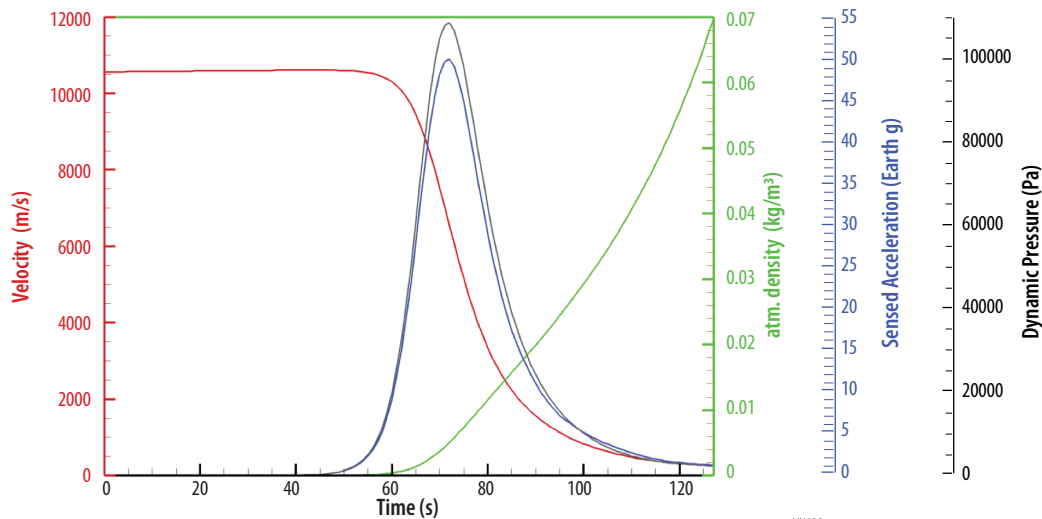
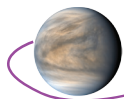


**Figure B-71.** Trajectory of the capsule from entry interface through the end of the heat pulse. Curves show temporal variation of velocity, atmospheric density and the resulting freestream dynamic pressure and the deceleration on the capsule. The EDL design is driven by the requirement on peak deceleration.

relative to Venus's surface) was used as a conservative upper limit on the Entry Flight Path Angle (EFPA). This upper limit precludes skip-out and limits the size of the “footprint” when the balloon is released. The lofting limit angle for the nominal entry velocity at entry interface is about  $-6.4^\circ$ . This implies a flyable corridor of just over  $2^\circ$  in EFPA. This  $\pm 1^\circ$  in flight path must be met at the end of a long, uncontrolled flight phase after the Aerobot separates from the launch vehicle/Orbiter. It is recommended that the addition of a cold gas ACS system should be evaluated.

### B.2.8.1.3.4 Aeroshell Technology Maturity

#### B.2.8.1.3.4.1 Thermal Protection System

Entry into the Venus atmosphere is challenging due to the high atmospheric density and resulting heating. Typical entry trajectories result in heat fluxes in excess of  $2000 \text{ W/cm}^2$  and pressures in excess of  $100 \text{ kPa}$ . To withstand these challenging entry environments, previous missions/studies to Venus have used Carbon Phenolic (tape-wrapped, or chop-molded) as the heatshield material (e.g., Pioneer Venus, ViTAL). However, heritage Carbon-Phenolic is no longer available due to unavailability of raw material and atrophy of manufacturing capabilities.

The Heat shield for Extreme Entry Environment Technology (HEEET) system was developed as an alternative to Heritage Carbon Phenolic for missions with extreme entry environments (e.g., to Venus, Saturn, Ice Giants, high speed Earth re-entry). It is a novel, three-dimensional, woven TPS technology consisting of layers of carbon (and/or phenolic) mechanically woven together. HEEET TPS can be either single-piece or tiled, and either dual-layer or single-layer. A dual-layer TPS has a high-density all-carbon weave (recession layer) on the outside and a low-density (blended carbon and phenolic) weave (insulation layer) underneath. The single-layer HEEET TPS, featured in the Aerobot design, is composed of the insulation layer only. HEEET TPS technology has demonstrated exemplary performance when subject to arc jet conditions of  $\sim 3,600 \text{ W/cm}^2$  and 5 atmospheres of pressure in both the single- and dual-layer configurations.

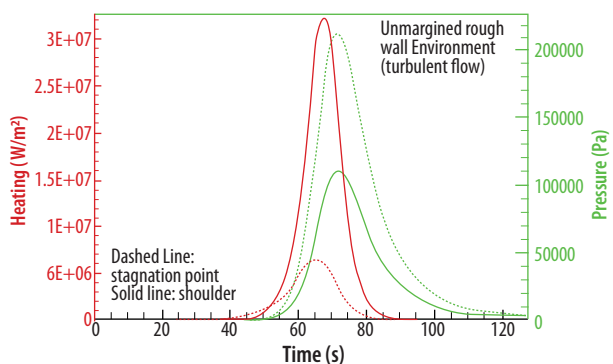
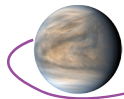


**Figure B-72.** Aerothermal environment (convective heating and pressure) on the capsule-stagnation point and the shoulder. While the stagnation pressure is higher, the shoulder heating drives the TPS design.



The tiled dual-layer TPS has been matured to TRL 6 and is ready for flight infusion. Single-layer HEEET is currently the baseline TPS for the Mars Sample Return (MSR) Earth Entry Vehicle (EEV), resulting in ongoing improvements in loom and weaving capabilities. The geometries proposed here for the Aerobot and Lander are likely beyond the capability of existing looms to weave a single-piece heat shield. Therefore the baseline design assumes a tiled insulation layer configuration. As a result, the TPS design requires some early engineering work in terms of demonstration, build and testing of seams with gap-fillers for single-layer HEEET tiled design. It is expected that this activity will be less challenging and complex than the gap/seam design that has already been demonstrated for the dual-layer HEEET TPS. Finally, the TPS thickness for the current design is 1.33 inches, well within the demonstrated capability of current weaving vendors.

**B.2.8.1.3.4.2 Parachute**

The supersonic parachute is a standard Disk-Gap-Band (DGB) design used in many previous planetary missions. Material selection will take into consideration the caustic nature of the Venus atmosphere. Since the subsonic parachute is deployed by the supersonic parachute separating the backshell, opening loads should not be excessive and several options exist for the subsonic parachute design.

**B.2.8.1.3.5 EDL ConOps Trigger(s)**

The parachute deployment, and possibly heatshield separation, events are triggered on navigated velocity. All other events are triggered on 'time' from those events. The EDF sequence is not expected to be sensitive to reasonable errors in the navigated state.

**B.2.8.1.3.6 Key Trades**

Early in the design process, trades examined entry flight path angle and the resulting heating and the peak deceleration. Steeper entries resulted in higher peak deceleration and higher heating while reducing the entry pulse width. At an entry velocity of 10.5 km/s, an EFPA of -8.5 provided 50 g of peak deceleration, with a narrow entry corridor (between the designed EFPA and lofting, at -6.4°). Particularly since the Aerobot is released so long before entry, the narrow entry corridor is a concern (i.e., EFPA accuracy needs to be within ± 1°).

**B.2.8.1.3.7 Suggested Later Trade: Drogue Parachute, or Mortar Deployment**

We suggest an early analysis and design trade of the parachute deployment system: whether the main supersonic parachute is extracted through a drogue parachute (supersonic, above Mach 1.4) or is deployed by a mortar. Both are viable and have been shown to be successful at Mars, at Venus, and at Earth.

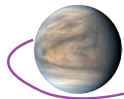
**B.2.8.1.3.8 Backshell Geometry**

The backshell geometry used in the current design, shown in **Figure B-73** is driven by packaging constraints: i.e., the smallest backshell that can package all the components inside the aeroshell. The TPS mass estimates (**Table B-48**) are consistent with this geometry. This being a novel geometry, an aerodynamic database has to be generated early in the project (likely including CFD, wind tunnel testing and ballistic range testing) both to establish the aerodynamic characteristics as well as to ensure desired static and dynamic stability features. Use of a legacy backshell geometry permits taking advan-

**Table B-48.** Areas and Backshell TPS masses corresponding to various backshell geometries.

Backshell Geometry	Area [m <sup>2</sup> ]	Backshell TPS mass [kg]
VFM Aerobot	7.66	21.0
M2020	8.68	23.8
Mars Insight	8.53	23.4
Mars Phoenix	8.53	23.4
Stardust	10.21	28.0
Dragonfly	9.40	25.7
Pathfinder	7.99	21.9





tage of existing knowledge and aerodynamic databases. **Figure B-73** also shows radial distance as a function of axial distance for a few legacy geometries, scaled appropriately. These geometries provide larger packing volume and exhibit a larger surface area (increasing the backshell TPS mass). For the same backshell TPS thickness, the TPS masses for these other geometries range from 21.9 kg to 28.0 kg.

### B.2.8.1.4 Aerobot Structure

The Aerobot is a variable-altitude, floating platform housing a broad range of scientific instruments and the structural design for it provides for various configurations needed for launch, flight, entry, deployment, and mission operations. Aluminum is the baseline material used for Aerobot's primary and secondary structures. All environmentally exposed materials used in the Aerobot and its subsystems will require optimized coatings to mitigate corrosive, atmospheric conditions which may be encountered during the mission. The Aerobot's stowed configuration packages the main parachute, balloon system and single helium storage tank inside and along the centerline of its interior structure. Aerobot's hexagonal framework and tank support structure provide for the primary load path for both launch and entry. The interface between Aerobot and the aeroshell are 38 inch diameter, commercial-off-the-shelf (COTS) Lightband separation rings. These separation rings are the current baseline for this design. Additional work is required to keep both the Aerobot and aeroshell's flight and deployment configurations from being over-constrained. All instruments and systems are mounted around the external faces of the main structure's honeycomb panels. Signal and power harnesses will be mounted and routed on both external and internal panel surfaces. A third Lightband is used to connect the tank structure assembly to Aerobot.

the Aerobot and its subsystems will require optimized coatings to mitigate corrosive, atmospheric conditions which may be encountered during the mission. The Aerobot's stowed configuration packages the main parachute, balloon system and single helium storage tank inside and along the centerline of its interior structure. Aerobot's hexagonal framework and tank support structure provide for the primary load path for both launch and entry. The interface between Aerobot and the aeroshell are 38 inch diameter, commercial-off-the-shelf (COTS) Lightband separation rings. These separation rings are the current baseline for this design. Additional work is required to keep both the Aerobot and aeroshell's flight and deployment configurations from being over-constrained. All instruments and systems are mounted around the external faces of the main structure's honeycomb panels. Signal and power harnesses will be mounted and routed on both external and internal panel surfaces. A third Lightband is used to connect the tank structure assembly to Aerobot.

#### B.2.8.1.4.1 Parachute, Balloon, Tether System Canister

During flight and entry, the Aerobot's parachute, balloon, and tether system is stored inside the Aerobot's structure. The area for this storage consists of an upper and lower canister. The upper canister platform is integral to the Aerobot structure, while the lower canister is connected to the tank support structure. The canister volume is sufficient to provide room for these platforms, including volume margin for any helium residue trapped inside the balloon after testing, which can cause small pockets of the balloon to expand during flight. The current design meets volume requirements for all platforms described in this section. The tether system will be stowed beneath the balloon in the canister, using layered blankets and hook and loop fastener strips. These blankets and fasteners are designed to organize and manage the tether system during flight; and provide an orderly, tangle-proof, release during the balloon and tether deployment sequence.

#### B.2.8.1.4.2 Tether System

The tether system comprises three mechanical sections; section one is a three-point mount from the balloon to a union buckle; section two is a single main cable [8 m long] which spans between section 1 and section 3; and section 3 of the tether system incorporates an inertial braking system for the deployment of the main cable in section 2. This includes a three-point mount tether configuration between the gondola and the union buckle that is integral with the inertial braking assembly.

The entire tether system is stowed inside the balloon canister, beneath the balloon, during flight. There are three swivel mounts connecting the termination of the tether system to the gondola. Additional work is needed to mitigate sudden deceleration events of individual components and/or backlash activity during tether system deployment.

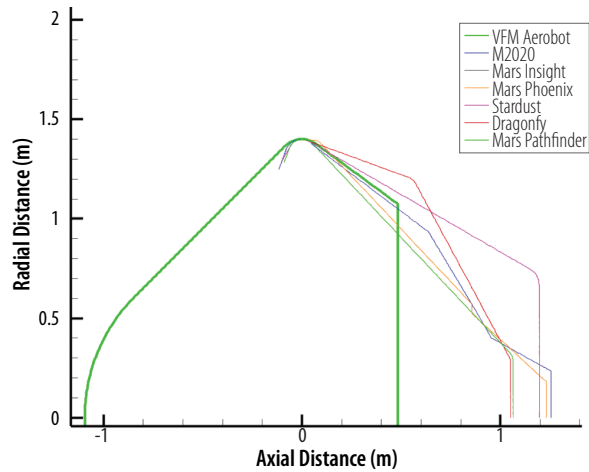
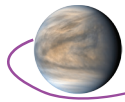


**Figure B-73.** Geometry of the current design of the backshell along with a few legacy backshells scaled up to match the aerobot's diameter

VN049



#### **B.2.8.1.4.3 Tank and Balloon Separation**

After the balloon-fill is complete, a non-explosive actuator (NEA) will separate the balloon assembly from the helium storage tank. As the balloon lifts upward and away from Aerobot's gondola, the tether system is deployed. Following the complete deployment of the tether system, the separation ring between the tank support structure and Aerobot is ready for activation. Following separation ring activation, the tank and support structure will jettison underneath the Aerobot and fall away. The bracket design used in the solar array assembly serves as a passive guide and barrier to prevent a collision with the solar panels during tank/structure jettison activity.

#### **B.2.8.1.4.4 Solar Panel Array**

The solar array is a 6 panel section, dual-sided solar panel array, which provides a physical solar collection surface area of 3.18 m<sup>2</sup>. The requirement is 1.6 m<sup>2</sup> (with margin, 1.9 m<sup>2</sup>). The outward facing surface of the array assembly provides a physical area of 1.614 m<sup>2</sup>. The obverse side provides an additional surface area of 1.566 m<sup>2</sup>. Assigning a conservative efficiency of just 20% for the inside surface area, the combined surface area is 1.927 m<sup>2</sup>. The solar array is static mounted and does not require deployment. This structure is also isolated from flight and entry load paths. The solar array assembly brackets are designed to protect the arrays and serve as passive guide rails for the helium tank and structure assembly during jettison.

#### **B.2.8.1.4.5 Deployable Structures**

There are three deployable structures (Boom-Arms) which extend away from Aerobot. Once deployed they provide instruments and antennas 0.5 m–2.0 m distance from the Aerobot structure; Boom-Arm One is for the **Anemometer** and Antenna One; Boom-Arm Two is for Antenna two; Boom-Arm Three for the **Mag**. The current design for the three deployable structures and their respective release mechanisms are considered notional. They were merely used to provide a mass within range of viable options, with the expectation that detailed design of these would be future work, all of which are well within the state-of-the-art.

#### **B.2.8.1.4.6 Key Trades**

##### Helium tank

A multiple spherical tank design and a single toroidal tank design were studied. However, the use of one large, individual helium storage tank was deemed optimal for the overall Aerobot design. Utilizing a single-tank design provided flight heritage, and eliminated the need for a more complicated helium transfer plumbing, separation and structure jettison systems. Options studied included:

- Toroidal tank design (no flight heritage, TRL development).
- Multi-tank design (gas transfer plumbing, structure and separation complexities).
- Singular tank design (flight heritage, simple gas transfer plumbing, structure and separation).

##### Gondola

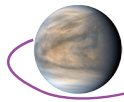
Instrument support concepts for mounting on a horizontal tray and mounting on the panel faces were studied. Mounting the instruments on the hexagonal panel faces was chosen as it provided better packaging and thermal control.

For packaging the parachute and balloon we looked at both an exterior and an interior canister design. The interior design was selected because it uses the existing structure and simplifies the load path.

For the tether system we assessed the use of existing space flight deployment systems used on Mars and evaluated a single-tether concept and a three-tether concept with electronic controls as well as a three-point mount on the balloon and gondola with a single main tether in between with a mechanical inertia break. This last option was selected because it greatly simplified deployment, reduced system mass and because it has heritage to deployment for the Perseverance rover.

##### Aeroshell shape

The selection of the aeroshell shape was motivated to minimize development cost by selecting a shape that was within past experience. There are two heritage options 45° and 70°. The size of the Aerobot and the available volume for packaging the Aerobot on the Orbiter led to selection of the 45° heritage.



This allowed placement of the Aerobot beneath the Orbiter for launch while maintaining a design with flight heritage.

#### Deployable Structures

Deployment of the booms and the jettison of the helium tank: we evaluated multiple concepts during the iterative design study and selected simple deployment hinges for the booms and a lightband system for the helium tank.

#### Solar Array Assembly

We conducted an iterative design study for packaging, solar collection area, packaging inside the aeroshell and compatibility with launch & entry loads, which resulted in a fixed solar array mounted to the gondola that required no mechanisms for deployment.

#### Antenna

An iterative design study was conducted to determine antenna type and placement. The ideal design would be an omni-antenna placed on top of the balloon. However, concerns with cable loss and issues with structural support on top of a balloon that is not fully inflated made this an unattractive option. Placement of two omnis on panels 180° apart were evaluated but due to the absorption characteristics of the atmosphere and the size of the balloon much of the omni coverage is unusable. It was determined that two high gain toroidal antennas placed 180° apart would provide the maximum gain in the allowable field of view.

### **B.2.8.1.5 Aerobot Attitude Control and Avionics Subsystems**

The Aerobot does not have an Attitude Control Subsystem. It does have an IMU that is used to measure disturbance for correlation with science observations, but there are no control actuators.

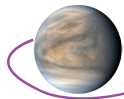
The avionics for the Aerobot portion of the mission is a single string system because of the short mission duration of 60 days and because of the power restrictions of the Aerobot. The avionics consists of the following functions: Command and Data Handling (C&DH), attitude control sensors, power conditioning and distribution, mechanisms for launch locks, deployments and motors. The avionics implementation consists of two enclosures, C&DH Unit and the Mechanism Control Unit (MCU). All units are single string.

The C&DH portion of the avionics performs basic command and control functions for the Aerobot. C&DH is comprised of a low-power processor based upon the VORAGO ARM Cortex-M4, the processor chip has a power of less than 1W (the board peripherals are about 3W additional), which is necessary to meet the power requirements of the mission. During this phase of the mission, the processor gathers science data and stores it for transmission to the Orbiter. The processor executes stored commands and gathers telemetry during the science phase of the mission. The processor performs CCSDS AOS transfer frame generation of telemetry data and passes it to the Multi Interface Card (MIC), which has the communication interface function and performs Forward Error Correction (FEC) encoding (Reed Solomon or Turbo) and has the interface to the S-band transponder.

The MIC has the interface to the instruments, many of which are low data-rate (10s of kilobits per second average) while some are high data-rate (several Mbps). The C&DH has the ability to handle the typical spacecraft interfaces such as RS-422 UART interface, I2C, LVDS interfaces, SpaceWire and Mil-Std 1553B. The lowest power option is RS-422 UART option so this will probably be the solution unless there is a heritage subsystem or instrument that dictates a different one. The instrument interfaces reside on the MIC along with the communication interface. The MIC board also has the GN&C sensor interfaces such as sun sensors, IMU, accelerometers, star tracker, etc., as well as Mil-Std 1553B, I2C, RS-422, or SpaceWire data interfaces for other avionic units.

#### **B.2.8.1.5.1 C&DH Unit**

The C&DH uses the VORAGO ARM Cortex-M4 processor, which runs the flight software to command GN&C effectors based upon the GN&C sensors and algorithms, the power conditioning of solar array and battery, and distribution switches to various spacecraft loads. The Aerobot runs on a scheduled timeline uploaded in advance to perform autonomous operations. The processor works as the file manager for the memory on the MIC that stores the packets from the Aerobot for reliable



forwarding to the Orbiter, i.e., DTN bundle protocol operations for reliable communication. The functions of the various cards in the C&DH system are internally redundant.

The MIC is a multi-function card. It has the high-speed Mil-Std 1553B and RS-422 interfaces to support the nominal interfaces found on a spacecraft. It also has the communication functions (transfer frame FEC encoding, hardware command decoding and execution as well transponder interface and transmitter interface for the different RF bands). It has GN&C interfaces for sun sensors and IMU. It has non-volatile memory of 8 Gbits to serve as the SSR. The MIC also has the Mission Elapsed Timer (MET) and provides the One Pulse Per Second interface (1 PPS) to spacecraft subsystems as well. The Analog Telemetry Card (ATC) has the analog digital converter (ADC) and analog multiplexers to gather temperature and other analog telemetry for the spacecraft. The Analog Telemetry Card (ATC) has the analog digital converter (ADC) and analog multiplexers to gather temperature and other analog telemetry for the spacecraft.

The Solar Array Regulation Module (SARM) has the Field Effect Transistors (FETS) to switch the solar array strings for current regulation. There is one SARM card in the PSE. The Battery Charge Module (BCM) card performs battery charge control. There is one BCM for a single battery. The power switch function uses three Generic Switch Module (GSM) cards. Lastly, the C&DH enclosure has the Low Voltage Power Supply (LVPS) to power the cards in the C&DH.

#### **B.2.8.1.5.2 Mechanism Control Unit (MCU)**

The MCU has the functions for mechanisms, which include the launch locks, deployment actuators and motors. Note that the pressure sensor telemetry goes to the C&DH unit. All cards have Inter-Integrated Circuit (I2C) interfaces. The Motor Controller Card (MCC) has the H-bridge circuits and the relays to control 3 phase stepper motors. Each MCC has the ability to drive four motors. Currently one MCC is baselined for the antenna and solar array gimbals. Two MCC are baselined. The Mechanism Release Card (MRC) has the ability to control eight mechanisms switching both high and low sides with an arm switch. Two MRC are currently baselined. Lastly, the MCU has a LVPS card to provide secondary voltages to the MCU cards.

#### **B.2.8.1.5.3 Technology Maturity**

The board designs are based upon the Eurocard form factor 3U and 6U. For the C&DH Unit, the backplane is Compact Peripheral Component Interface (cPCI). For the MCU the backplane is based upon an I2C interface. Board level products exist and have heritage from the Lucy mission.

#### **B.2.8.1.6 Aerobot Power**

The Aerobot power system consists of solar arrays, a secondary battery, and supporting power electronics. The Aerobot mission requirement is 60 days in the venusian atmosphere at various altitudes and positions around the planet. TJGaAs solar cells with a bare-cell efficiency of 29.5%, a solar constant of 200 W/m<sup>2</sup>, array operating temp at 120°C were modelled. A fixed panel with 1.9 m<sup>2</sup> active area will provide 380 W EOL and 448 W BOL of power to support loads and battery recharge. A high energy density 300 AH Li Ion battery is used to support night loads. The Power System Electronics (PSE) will be a heritage 28VDC battery-dominated bus included as cards in the avionics package and will control battery charging and power distribution. The Aerobot solar array is TRL 6. The Aerobot battery, PSE 28 VDC battery dominated bus and harness are all TRL 7.

#### **B.2.8.1.7 Aerobot Thermal**

##### **B.2.8.1.7.1 Thermal Requirements**

The Venus Flagship Mission (VFM) Balloon descends through a progressively warmer, high pressure atmosphere, as it floats between 52 km and 62 km altitudes. For added thermal margin, the thermal design was modified to include a range of 50 km and 64 km altitudes.

**Figure B-74** shows a plot of altitude vs. temperature for the altitude range of interest. **Figure B-75** shows the solar flux at the same altitude range. Both the air temperature and solar flux are needed to determine Aerobot temperatures.

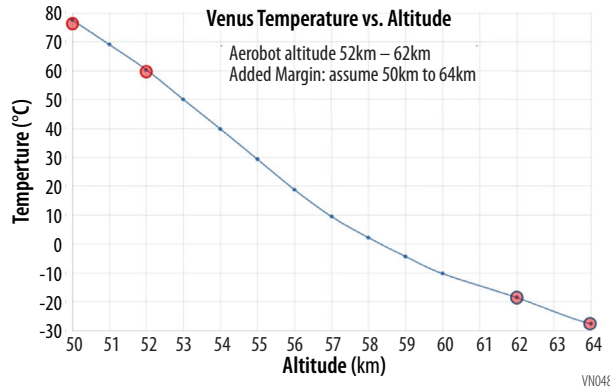
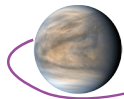


Figure B-74. Venus Temperature vs. Altitude

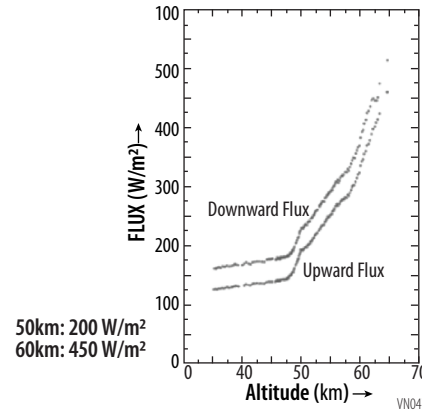


Figure B-75. Venus Solar Flux from the Pioneer Venus Probe. After Tomasko et al. [1980].

### B.2.8.1.7.2 Thermal Model and Design

A summary of the Aerobot's thermal design is shown below:

- **Balloon cycles between 52 km and 62 km altitude**
  - Thermal model assumes 50 km to 64 km for added margin.
- **Pressure is 0.12 bar to 1.07 bar (88 torr to 810 torr)**
  - High enough where the MLI blanketing will not work. Needs rigid insulation.
- **Forced Convection overcomes radiation heat transfer.**
  - Relative wind velocity is assumed to be around 1.5 m/s.
- **Balloon painted white to reduce solar loading (esp. at low altitudes)**

A thermal model of the Aerobot is shown in **Figure B-76**. It consists of a 6-sided gondola with electronics/instruments mounted on each of the 6 outer surfaces. The outer face of each electronics box has a radiator to convect/radiate the heat away. Two of the boxes, the C&DH box, and the SSPA need extra finned surfaces in order to get enough surface area for adequate heat removal. The solar panels are included in the model. A single solar array panel is shown as a blue rectangle in **Figure B-76** through **Figure B-79** with the others removed for clarity.

**Table B-49** shows the electronics power assumed for all instruments and avionics for the thermal model.

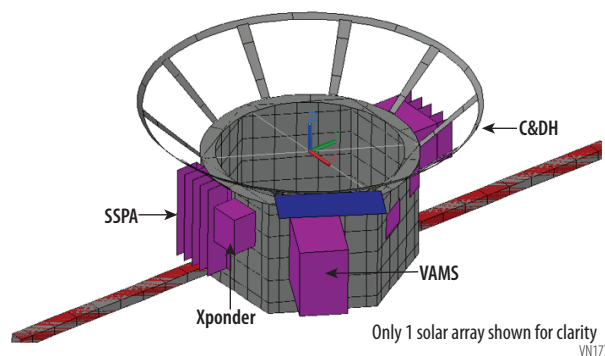
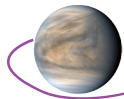


Figure B-76. Aerobot Thermal Model

Table B-49. Electronics Power

Instrument	MEV Average Power (W)	Temp Limits (°C)
Aerosol Mass Spectrometer with Nephelometer (AMS-N)	Op: 13.5 Standby 0.2	Op: -40 °C to +80 °C Surv: -55 °C to + 125 °C
Fluorimetric Microscope (FM)	0.2	Op: -5 °C to +60 °C Surv: -55 °C to + 125 °C
Meteorological Suite (MET) (P, T, Radiometer, 3-d Wind Sensor Radiometer, dosimeter)	6.5	Op: -40 °C to +80 °C Surv: -55 °C to + 125 °C
Visible Imager (VI)	0	Op: -30 °C to +40 °C Surv: -135 °C to + 70 °C
Magnetometer (Mag)	0.7	Op: -180 °C to +80 °C Surv: -40 °C to + 40 °C
Avionics	23.4	Op: -20 °C to +50 °C Surv: -30 °C to + 60 °C
X-ponder	10.45	Op: -20 °C to +50 °C Surv: -30 °C to + 60 °C
SSPA	40.7	Op: -20 °C to +50 °C Surv: -30 °C to + 60 °C
IMU	13.2	Op: -20 °C to +50 °C Surv: -30 °C to + 60 °C

Units will need delta qualification for Venus Environment



### B.2.8.1.7.3 Thermal Concept of Operations

The Aerobot will cycle between a hotter ~50 km altitude and a much colder ~60 km altitude. While doing so the temperatures will remain within operating limits (without operational heaters). If instruments get too hot, they will be turned off until they are at an altitude where they can be turned on yet again. No survival heaters are needed on the Aerobot.

Temperature plots of a hot (50 km) altitude and a cold (60 km altitude for both daytime and nighttime) are shown in **Figure B-77**, **Figure B-78**, and **Figure B-79** respectively.

As shown in the figures, there is an appreciable difference in temperatures between 50km and 60km altitudes. At 50 km, box temperatures are getting very warm, probably over the maximum allowed temperature. It may be that boxes will have to be turned off, or the minimum altitude will have to be increased to where the electronics can be cooler.

### B.2.8.1.7.4 Technology Maturity

All thermal hardware used on the Aerobot is TRL 9. The thermal coating (Z93C55 white paint) is standard thermal coating used at GSFC for many missions. Thermistors are all TRL 9.

### B.2.8.2 Lander

The VFM Lander is designed to safely land the instrument payload in the tessera terrain of Venus and survive for at least 6 hours, with a goal of 8 hours. In order to land safely, the mechanical design needs to accommodate landing terrain uncertainty. To account for the uncertainty, the Lander is designed to land on a slope of up to 30° and accommodate a 0.5 m boulder beneath the sphere. With landing as the highest risk for the mission, the Lander includes both a Terrain Relative Navigation (TRN) and a Landing Hazard Avoidance (LHA) system. The TRN would be used to estimate the Lander local relative position by comparing terrain maps, which would be loaded into memory prior to separation, with terrain measurements from navigation sensors (LIDAR, engineering camera, laser altimeter). The LHA assesses the hazards in the projected landing site and uses fans to move the Lander laterally to avoid landing on the hazard. The TRN and LHA are discussed in more detail in **Section B.2.8.2.5**.

The Lander is designed to operate for at least 6 hours and up to 8 hours on the surface of Venus where the temperature of the atmosphere is 441°C and the pressure is 76 bar at West Ovda. The sphere is painted white with Z93C55 Conductive Coating. The sphere will start at -25°C in orbit around Venus before descent. During descent temperatures will steadily increase as the Lander descends into the atmosphere. As mentioned above, phase-change material (n-Eiocane (C<sub>20</sub>H<sub>42</sub>) +37°C) is used within the decks to flatten the temperature ramp.

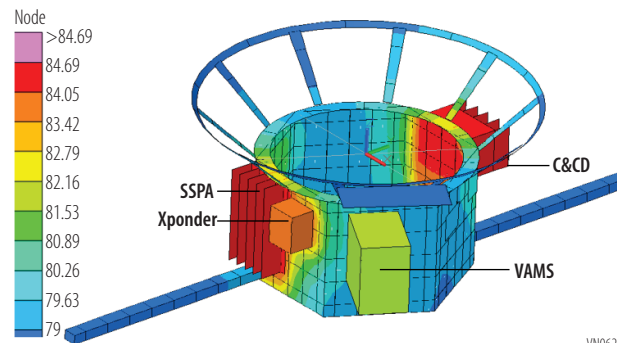


Figure B-77. Hot-biased Temperatures at 50km Altitude

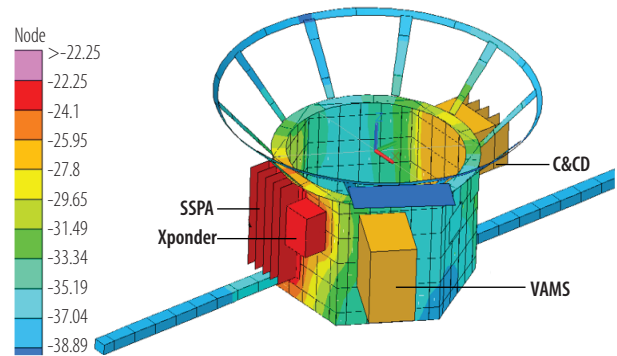


Figure B-78. Cold-biased Temperatures at 60km Altitude, Day-time

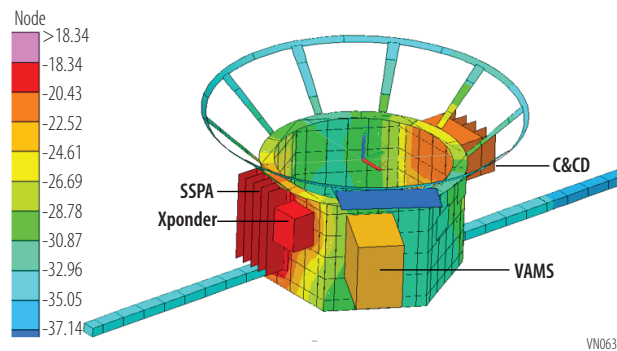
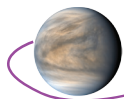


Figure B-79. Cold-biased Temperatures at 60km Altitude, Nighttime



The decks are thermally isolated from the sphere with a titanium flexure ring and all avionics and instruments are thermally coupled to the decks. The flexure ring is needed due to the CTE mismatch between the aluminium decks and the titanium stands. The flexures are designed to withstand the 50g entry loads. For the three triple-pane windows a low emissivity coating is used to reduce heating of the instrument optics. The emissivity is 0.15 on both sides of the inner window. The sphere is evacuated to high-vacuum ( $10^{-6}$  torr) conditions to reduce convective heat transfer and allow effective MLI blanketing. Zeolite is used to keep high vacuum during outgassing. Both high-temperature MLI blanketing and “Standard” Kapton MLI are used, with the high-temperature MLI blanketing being used on the inner walls of the sphere and the MLI used on the decks. All the thermal hardware has a high TRL level and has been used on many spaceflight programs.

The Lander avionics system provides a LCDH with a low power VORAGO ARM Cortex-M4 processor for commanding instruments, sample collection and the drill. The LCDH collects, processes and stores instrument and Lander health and safety data on the 8 Gbit solid state recorder. The LCDH also includes a high performance Spacecraft Computing (HPSC) ARM Cortex A53 for the processing of TRN and LHA algorithms. Timing with an accuracy of  $\geq 0.1$  msec with  $10^{-6}$  stability relative to ground station is provided by an ultrastable oscillator. A Mechanism, and Propulsion Unit (MPU) provides cards that interfaces with the aeroshell separation hardware, control deployments including: parachute, heat shield, backshell, leg deployments and fans.

The Lander power system consists of a primary (non-rechargeable) battery and supporting power electronics. The power system configuration is driven by lack of any usable solar flux at the Venus surface yielding no way to generate power to support loads or recharge a secondary battery. Saft LSH20 D 13000mAh 3.6V Lithium-Thionyl Chloride cells are used in a 9 series 9 parallel (9s9p) configuration to provide 200 AH of energy at 32V. The Power System Electronics (PSE) will be a heritage 28VDC battery dominated bus included as cards in the avionics package. The PSE will control switching and power distribution.

### B.2.8.2.1 Instrument Accommodations

The Lander sphere is built in three sections. The upper hemisphere supports the sample handling evacuation spheres and the PC cupola and provides an access port for integration. The PC cupola provides a FOV  $\geq 60^\circ$  per mirror (4) with  $240^\circ$  azimuth coverage and  $60^\circ$  below the nominal flat horizon and  $30^\circ$  above as shown in **Figure B-80**. The access port has plumbing for evacuating the sphere prior to launch. The lower hemisphere has the TLS and NMS inlet assembly and three windows.

The lowest window (**Figure B-81**) is for the DI and provides a Field of View  $> 90^\circ$ . Slightly higher is the window for the LHA system including the LIDAR, laser range finders, and the engineering camera (**Figure B-82**). The final window (**Figure B-83**) is for the R-LIBS. The equatorial ring has the electrical connection port, and a pass-through for the AS mounted on the outside of the sphere. The equatorial ring is the structural interface to the drag plate and legs. On the inside, it supports the thermally isolating ‘elephant stands’ which support the upper and lower decks. The equatorial ring is part of the spherical geometry to maintain as consistent a spherical shape as possible maximizing sphere strength.

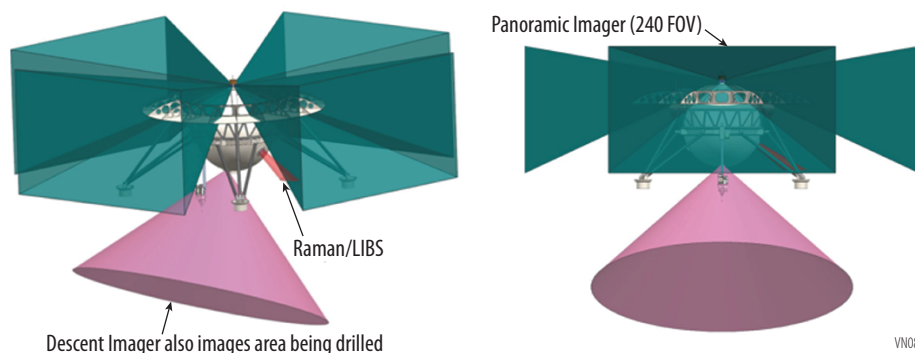
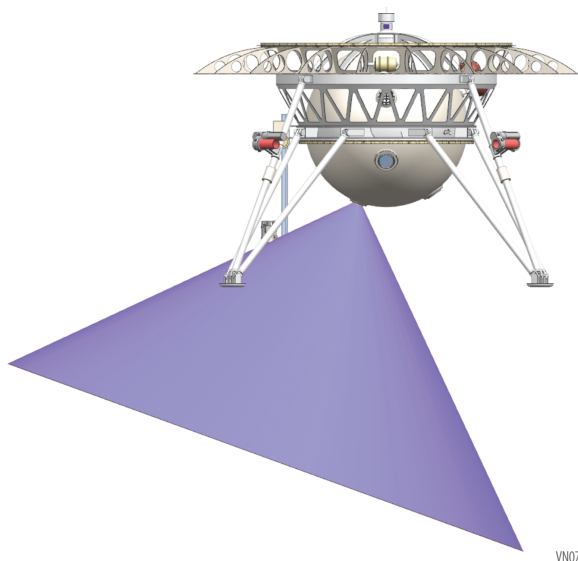
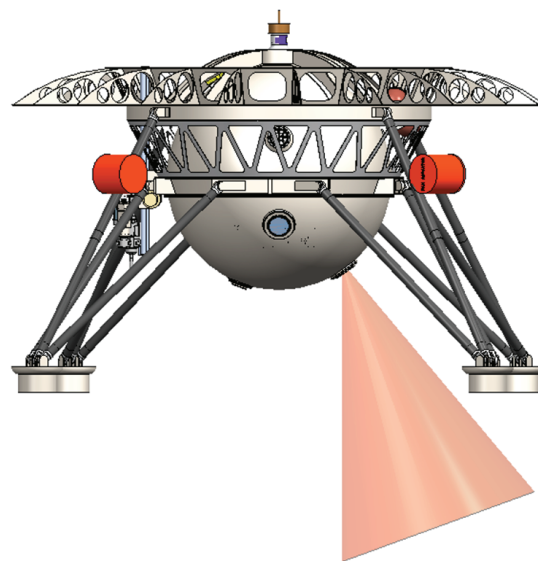


**Figure B-80.** Panoramic Camera FOV



VN076

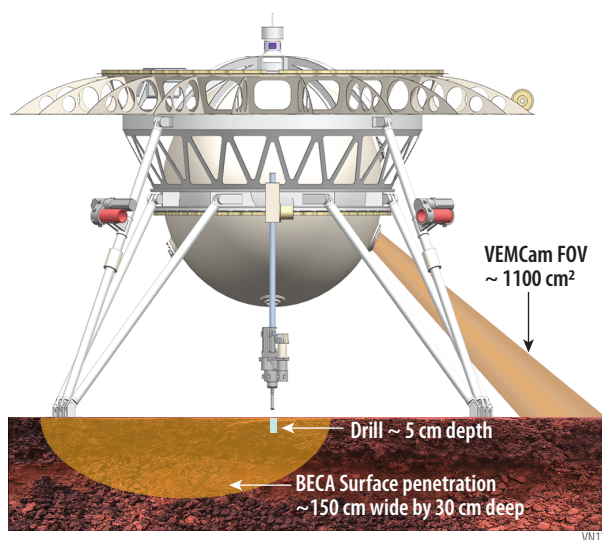
**Figure B-81.** Descent Imager has a view of the drill site



VN089

**Figure B-82.** LIDAR, laser range finders, and the engineering camera FOV

The upper and lower decks are isogrid aluminum. The isogrid pockets are used for embedding the phase-change material; and the aluminum provides high conductivity to the boxes and instruments. As required for thermal isolation of the decks, the ‘elephant stands’ are titanium which will require a flexure interface with the decks to mitigate CTE mismatch issues. Each deck has mounting interfaces on both top and bottom sides. A sheet metal aluminum retainer supports the sphere insulation. Metal C-seals will be required at all sphere ports and separation planes. The sphere will be launched evacuated which should simplify the sealing of all ports and pass-throughs as well as the sphere segments. Structural concepts developed for this study are within the current state-of-the-art and have heritage. It is likely that high pressure sealing and ports/pass-throughs will require additional development and testing. The following section provides information on the Lander instruments. **Table B-50** shows details for each instrument.



VN176

**Figure B-83.** Field of View for the R-LIBS and GRS. Note that the penetration is offset because of the location of the GRS within the Lander sphere.

## B.2.8.2.2 Instruments

### B.2.8.2.2.1 Neutral Mass Spectrometer (NMS)

NMS is an instrument on board the Lander that will collect data both in descent and on the surface. During descent the NMS is required to measure the abundances of SO<sub>2</sub>, SO, SO<sub>3</sub>, OCS, CO, H<sub>2</sub>O, HDO, NO, HCl, HF, and more at 0–60 km altitude. The desired sampling altitudes are approximately (i) above the cloud tops (60–70 km), (ii) just below the main cloud layer (~40–50 km), (iii) lower atmosphere (~20 km), (iv) just above the surface (~5 km), and (v) at the surface. The measurement requirements are ≥ 5 samples at 5 different altitudes including the sampling of the atmosphere at the surface. The goal of this data set is to determine isotopic ratios and abundances of hydrogen, noble gases, oxygen, nitrogen, and other chemical species in the atmosphere and below the cloud deck to the



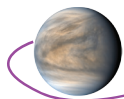


**Table B-50. Lander Instrument Details**

Item	Neutral Mass Spectrometer (NMS)	Tunable Laser Spectrometer (TLS)	Atmospheric Structure Suite (AS)	Descent NIR Imager (DI)	Neutron Generator/ Gamma Ray Spectrometer (GRS)	Nephelometer (Neph)	X-Ray Diffractometer (XRD)	Raman-LIBS Instrument (R-LIBS)	Panoramic Camera (PC)	X-ray Fluorescence Spectrometer (XFS)	LLISSE	Units
Type of instrument	Mass Spectrometer	Laser Spectrometer	Barometer, Temperature Sensor, Radiometer	NIR Camera	Neutron Generator/ Gamma Ray Spectrometer	Aerosol Light scattering	X-Ray Diffractometer	Raman, LIBS and camera	Visible Camera	X-Ray Fluorescence	Chem & Met. (P, T, Radiance and wind speed) sensors	
Number of channels	150 Da	4	Radiometer (7 science + 1 dark)	3	-	-	-	-	6	-	9 Chem 4 Met.	
Size/dimensions (for each instrument)	26x16x19	26x10x10	Radiance sensor : 11x31x14	20x10x10	GRS-7.62 dia x 18 PNG-6.35 dia. x 33 long	Optical head 30 x 15 x 4 (outside vessel)	30 x 18 x 15	Raman/ LIBS Spec 26x21x10 Imager 5x5x20 (lenses only)	5x5x11 (lenses and mirror only)	Sensor assembly ~26.4 W x 18.5 D x ~20.0 H		cm
Instrument mass <b>without</b> contingency (CBE*)	16.5	4.5	4.8	5	12	1.5	5	25	3	1	10	kg
Instrument mass contingency	30%	30%	30%	30%	30%	30%	30%	30%	30%	30%	30%	%
Instrument mass <b>with</b> contingency (CBE+Reserve)	21.5	5.9	6.2	6.5	15.6	2.0	6.5	32.5	3.9	1.3	13.0	kg
Instrument average payload power <b>without</b> contingency	60	26.1	6.9	40	45	6.6	29.5	61	12	15.1	10	W
Instrument average payload power contingency	30%	30%	30%	30%	30%	30%	30%	30%	30%	30%	30%	%
Instrument average payload power <b>with</b> contingency	78.0	33.9	9.0	52.0	58.5	8.6	38.4	79.3	15.6	19.6	13.0	W



Item	Neutral Mass Spectrometer (NMS)	Tunable Laser Spectrometer (TLS)	Atmospheric Structure Suite (AS)	Descent NIR Imager (DI)	Neutron Generator/ Gamma Ray Spectrometer (GRS)	Nephelometer (Neph)	X-Ray Diffractometer (XRD)	Raman-LIBS Instrument (R-LIBS)	Panoramic Camera (PC)	X-ray Fluorescence Spectrometer (XFS)	LLISSE	Units
Instrument average science data rate <b>without</b> contingency	1.6	2.1	557	333	0.87	0.1	8 Mbit/sample	117	1250	.7 Mbit/sample	0.2	kbit/sec
Instrument average science data rate contingency	30%	30%	30%	30%	30%	30%	30%	30%	30%	30%	30%	%
Instrument average science data rate <b>with</b> contingency	2.1	2.7	724.1	432.9	1.1	0.1	10.4 Mbit/sample	152.1	1625	0.91 Mbit/sample	0.3	kbit/sec
Instrument Fields of View	N/A	N/A	Radiometer. 10	40x40	N/A	N/A	N/A	N/A	30° above nominal flat horizon and 60° below	N/A	N/A	°
Pointing requirements (knowledge)	N/A	N/A	Loose	Loose	N/A	N/A	N/A	N/A	< 0.5	N/A	N/A	°
Pointing requirements (control)	N/A	N/A	± 45 from lander horizontal	Nadir	N/A	N/A	N/A	N/A	Loose	N/A	N/A	°
Pointing requirements (stability)	N/A	N/A	N/A	< 20	N/A	N/A	N/A	N/A	< 0.5	N/A	N/A	°/sec



surface. The **NMS** will determine the distribution and composition of atmospheric volatiles. A second scientific objective is to measure the abundances and isotopic ratios of Xe, Kr, Ar, and Ne to  $\pm 5$  per mil and certain stable gas isotopes, in particular  $^{15}\text{N}/^{14}\text{N}$  in  $\text{N}_2$  to  $\pm 5$  to  $\pm 10$  per mil, and, for comparison with the **TLS**, the isotopes of S (in  $\text{SO}_2$ ), C (in  $\text{CO}_2$ ), and D/H (in  $\text{H}_2\text{O}$ ).

#### **B.2.8.2.2.2 Tunable Laser Spectrometer (TLS)**

**TLS** is an instrument on board the Lander that is required to collect data in descent and on the surface. The **TLS** has 4 channels (lasers): Channel 1:  $\text{CO}_2$  and  $\text{H}_2\text{O}$  for isotopic ratio of  $^{18}\text{O}/^{17}\text{O}/^{16}\text{O}$  in  $\text{CO}_2$  and  $\text{H}_2\text{O}$ , D/H in  $\text{H}_2\text{O}$ , and  $^{13}\text{C}/^{12}\text{C}$  in  $\text{CO}_2$ , all to  $\pm 1$  per mil precision. Channel 2: CO and OCS for  $^{34}\text{S}/^{33}\text{S}/^{32}\text{S}$  in OCS,  $^{13}\text{C}/^{12}\text{C}$  in CO and OCS to  $\pm 5$  per mil precision. Note the precision can be relaxed to up to  $\pm 20$  per mil for  $^{33}\text{S}$ . Channel 3:  $\text{SO}_2$  abundance and  $^{34}\text{S}/^{33}\text{S}/^{32}\text{S}$  isotopes to  $\pm 5$  per mil. Channel 4: HCl and  $^{37}\text{Cl}/^{35}\text{Cl}$  to  $\pm 10$  per mil. The **TLS** will measure  $\geq 5$  samples at 5 different altitudes including sampling of the atmosphere at the surface. The intent of these data is to characterize the atmosphere from above the clouds to the surface which will aid in determining if Venus once hosted liquid water at the surface. The **TLS** is also required to measure the abundances of  $\text{SO}_2$ , SO,  $\text{SO}_3$ , OCS, CO,  $\text{H}_2\text{O}$ , HDO, NO, HCl, HF, and more at 0–60 km altitude during descent with vertical sampling of  $\leq 1$  km. The goal of these data is to determine the gaseous composition at 0–60 km altitude. The instrument used as the baseline is the **TLS** on Curiosity.

#### **B.2.8.2.2.3 Atmospheric Structure Suite (AS)**

**AS** consists of **air pressure and temperature sensors, and a radiometer** measuring up- and downwelling solar and thermal radiative fluxes, from the time of aeroshell release at  $\sim 60$  km altitude down to the surface. The purpose of this instrument is to measure the temperature structure of the atmosphere, revealing which parts of the atmosphere are in convective equilibrium, and providing context measurements for other atmospheric measurements. The **radiometer** measures up- and downwelling flux in seven spectral channels covering the full range from ultraviolet to long-wave infrared, to characterize radiative fluxes in the atmosphere. Most of the radiometer channels will be the same as those of the radiometer on the aerobot, allowing direct comparison of their datasets. The radiometer used as a baseline for this study is a modified version of the Net Flux Radiometer (NFR) developed for Ice Giant entry probes [Aslam et al., 2020].

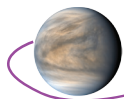
The **AS** will continue to sample at a low rate for one hour after touchdown. The main purpose of this continued operation is to provide meteorological context for other measurements, particularly composition measurements; also, the radiometer measures any dust clouds which may have been raised or any temporal variations in sky brightness due to cloud variability. After this one hour period of **AS** measurements on the surface, the remaining surface measurements of pressure, temperature, and radiative fluxes will be carried on by the **LLISSE** package.

#### **B.2.8.2.2.4 Descent NIR Imager (DI)**

**DI** is an imaging instrument on board the Lander which will collect data on descent and of the area being drilled once on the surface (**Figure B-80**). The instrument is required to collect data at 0.9 and 1.02 microns with an S/N of 30 and FOV of  $90^\circ$ . The **DI** will take  $\geq 20$  nested descent images from 20 km to surface (10 images/per band) with an S/N of 30. The required resolution of these images range from 100 m/pixel to 10 cm/pixel. This multispectral descent NIR imaging will view the Lander site and drill site before and after sample acquisition to examine the mineralogy and chemistry of tessera and ascertain rock type, as well as look for evidence of past water. The local and regional imaging of the landing site will search for evidence of surface features that might indicate a climatically different past (e.g., sedimentary structures, fluvial features).

#### **B.2.8.2.2.5 Neutron Generator/Gamma Ray Spectrometer (GRS)**

**GRS** is an instrument on board the Lander which is required to measure elemental abundances of major, minor, and trace rock forming elements, in particular Si, Al, Ti, Mg, Fe, Ca, Mn, Cr, Na, K, P, Cl, S, Ni, Rb, Sr, REEs, U, and Th. The **GRS** must have  $\sim 1.5$  hr integration time with limited interference from the lander structure. It will characterize the chemical elements of landing site bedrock (i.e., tessera material) to ascertain rock type. This instrument does not require a window to perform its analyses and can measure rock chemistry passively or actively with the neutron generator as a source.



The instrument used as the baseline for this flagship mission study is the Bulk Elemental Composition Analyzer (BECA)[Schweitzer et al., 2017].

#### **B.2.8.2.2.6 Nephelometer (Neph)**

**Neph** is an instrument on the Lander that will collect data on descent. The **Neph** is required to measure the effective size of particles to a resolution of 0.1  $\mu\text{m}$  and measure refractive index to a resolution of  $<0.02$ , as well as to identify non-spherical (non-liquid) particulates. These measurements are to be made with vertical sampling of  $\leq 1$  km between 0–48 km altitudes (below the  $\text{H}_2\text{SO}_4$  cloud layer). These data will contribute to the characterization of the vertical variation of composition from 0–62 km altitude which will, in turn, help determine the composition and distribution of volatiles in the atmosphere. The end result is a better understanding of the composition and climatological history of the surface of Venus and the present-day couplings between the surface and atmosphere.

#### **B.2.8.2.2.7 X-Ray Diffractometer (XRD)**

**XRD** is an instrument within the Lander designed to detect and quantify abundances of minerals within three ingested samples of surface rock material delivered by the drill system. If crystalline phases are present at high enough abundance, mineral compositions can be obtained using lattice parameter refinement [Morrison et al., 2018]. The **XRD** must be capable of quantifying major phases within  $\pm 10\%$ , and requires an integration time of 15 minutes per sample. The instrument is designed to measure the mineralogy of surface rocks with the scientific goal of mineralogical characterization of landing site bedrock, including mineral type and variability. By characterizing the surface materials in the landing site area, the **XRD** instrument will determine the oxidation state, chemistry and mineralogy of rocks in contact with the atmosphere. The **XRD** data will assist in determining if Venus once hosted liquid water at its surface. The instrument used as the baseline for this mission study is CheMin-V [Blake et al., 2019].

#### **B.2.8.2.2.8 X-Ray Fluorescence Spectrometer (XFS)**

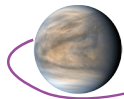
**XFS** is an instrument within the Lander, which will collect elemental abundance data on three ingested samples of surface rock material and analyze them with an integration time of 20 minutes per sample. The instrument is required to measure major, minor, and trace elements, in particular Si, Al, Ti, Mg, Fe, Ca, Mn, Cr, Na, K, P, Cl, S, F, Ni, Rb, Sr, and REEs. The primary goal of the **XFS** instrument is the chemical characterization of landing site bedrock (i.e., tessera material). This data will determine the chemistry of tessera to ascertain rock type. The VIXL instrument, which draws heritage from PIXL [Allwood et al., 2015], is used as the baseline for this study.

#### **B.2.8.2.2.9 Panoramic Camera (PC)**

**PC** is a multispectral imager that must image at least  $240^\circ$  azimuth with a vertical FOV  $60^\circ$  below the nominal flat horizon and  $30^\circ$  above the nominal flat horizon (**Figure B-80**), in 6 filters (440, 550, 630, 780, 900, and 1020 nm). A time-of-flight depth sensor for 3D information is desired. It is expected to collect the data of one complete multispectral image set  $\sim 15$  min after landing. The instrument's primary purpose is to take multispectral imaging of landing site rocks and rock formations to characterize the morphology of the Lander site. The **PC**'s data will assist in the search for evidence of surface features that might indicate a climatically different past (e.g., sedimentary structures, fluvial features).

#### **B.2.8.2.2.10 Raman-LIBS Instrument (R-LIBS)**

**R-LIBS** is an instrument on the Lander which will collect mineralogical (using Raman Spectroscopy) and chemical (using LIBS) information on surface rocks. The **R-LIBS** is required to measure the following elements: Si, Al, Ti, Mg, Fe, Ca, Mn, Cr, Na, K, P, Cl, S, F, Ni at the following levels: Major: 0.06–0.4 wt% Minor: 0.01–0.07 wt% Trace:  $\pm 10\%$ . The instrument must analyze a raster of four locations on a minimum of five samples to measure the variability of the chemistry and mineralogy of rock surfaces. **R-LIBS** plans to determine the mineralogy of a minimum of 5 samples with a detection limit of 1%. The instrument will address the weathering, chemistry and mineralogy of rocks in contact with the atmosphere, which can be used to understand the oxygen fugacity of the surface environment. The instrument used as the baseline for this flagship mission study is VEMCam [Clegg et al., 2019], which draws heritage from ChemCam on Curiosity.



### B.2.8.2.2.11 Sample Retrieval and Ingestion

Surface and subsurface particulate samples are provided to the instruments inside the lander by a combination of a rotary-percussive drill and a pneumatic-based sample transfer system (Figure B-84). The system is designed such that the samples transition from the high-temperature, high-pressure outside environment to a temperature (<40°C) and low pressure (<1 atm) environment at the instrument location inside the pressure vessel.

#### B.2.8.2.2.11.1 Rotary Percussion Drill

The drill has a powder-collection bit that collects drilled and pulverized rock material in the hollow core. The design features independent auger and percussor drive trains and incorporates a hollow drill stem for pneumatic transport of cuttings from the bit up through the center of the drill to a rotary coupling at the top. Brushless actuators provide feedback using a Pulsed Injection Position Sensor (PIPS) system for commutation, speed and position control. All elements are designed for full Venus temperature and pressure operation. A full-scale prototype drill from Honeybee Robotics (Figure B-85) has achieved a 5 cm drill depth in Saddleback Basalt in 15 minutes under full Venus conditions. The drill itself gets lowered to the surface after landing by a feed mechanism consisting of a lead screw driven by another high-temperature, brushless motor.

#### B.2.8.2.2.11.2 Sample Handling System

The pneumatic sample-transfer system uses the high-pressure Venus atmosphere to move particles from the drill-bit via gas entrainment in an impulsive, short-duration flow event, which is initiated by opening a pyrotechnic valve that connects a small lander-mounted dump tank with 1 atmosphere of internal pressure to the drill bit at 90 atmospheres external pressure. Atmospheric gas moves at high speed through the hollow drill bit, entraining the drill cuttings and then flowing through a small diameter tube to the lander. Inside the lander, the flow enters a cyclone particle separator after which the gas flows into the dump tank and the separated particles drop by gravity into a sample cup located in an airlock. The flow duration is only a few seconds, after which a second pyro-valve is actuated to close off the tank and isolate it from the system. Three such tank and valve systems are provided to enable three sequential sample transfer events from the same drill to the same airlock. This allows for samples at three different depths to be collected and provides for compositional analysis during the 15 minute drilling process.

The airlock is a piston-shaped structure that contains three sample cups for receiving the three samples. After each transfer event the piston translates a few centimeters to align the next cup with the tube bringing the sample from the cyclone. During these three sample transfer events, the cups are exposed to full Venus atmospheric pressure but are kept at near shirt-sleeve temperature by heat-sinking the airlock to the internal lander components. The tubing connecting the airlock with the cyclone is made of low thermal conductivity titanium tubing with a sufficiently long path-length to minimize the parasitic heat-leak to a tolerable amount for the several hour mission. After all three samples have been collected, the piston is translated further in the same direction, sliding through a set of o-ring seals in the surrounding structure and entering the low pressure region of the main lander itself. These samples

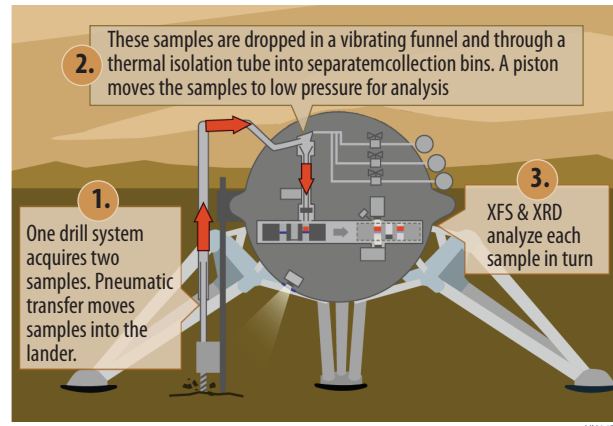


Figure B-84. Schematic of drill and sample transfer system modified from JPL graphic

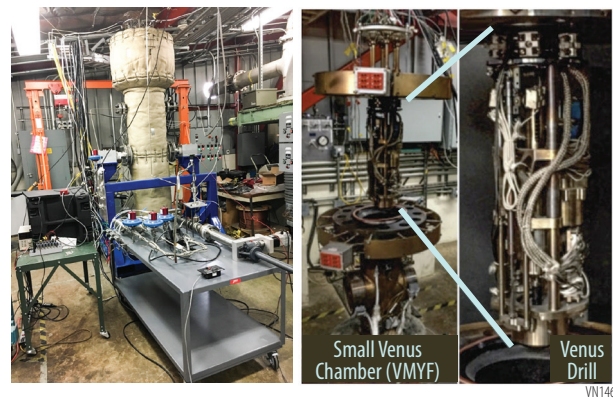
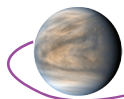


Figure B-85. (Left) JPL Large Venus Test Chamber (white cylinder) with prototype sample transfer system (foreground components on grey cart), (Right) Honeybee Robotics Venus drill being tested in the small Venus chamber at JPL.



**Table B-51.** Sample Acquisition and Ingestion Subsystem Mass, Power, and Data Rate

Sub-system	Drill	Sample Handling	
Type of Sub-system	Mechanism	Mechanism	
Size/dimensions			
Evacuation spheres (x3)	N/A	10 x 10 x 10 sphere	cm
Airlock cylinder	N/A	100 long, 10 diameter	cm
Cyclone	N/A	8 dia top, 1 dia bottom x 10 long	cm
Motor	N/A	5 dia, 5 long	cm
Drill	10 x 10 x 42	N/A	cm x cm x cm
Instrument mass <b>without</b> contingency (CBE*)	32	27	kg
Instrument mass contingency	30%	30%	%
Instrument mass <b>with</b> contingency (CBE+Reserve)	41.6	35.1	kg
Instrument average payload power <b>without</b> contingency	500	50	W
Instrument average payload power contingency	30%	30%	%
Instrument average payload power <b>with</b> contingency	650.0	65.0	W
Instrument average science data rate <b>without</b> contingency	10	10	kbit/sec
Instrument average science data rate contingency	30%	30%	%
Instrument average science data rate <b>with</b> contingency	13.0	13.0	kbit/sec

are then presented in sequence to the measuring instruments. A prototype sample transfer system from JPL has successfully demonstrated end-to-end performance in the laboratory at full Venus conditions when combined with the Honeybee Robotics rotary-percussive drill (**Figure B-85**).

The complete drilling and sample transfer system is operated via a timer that automatically sequences all of the steps in the process. The drill and feed mechanism are designed to tolerate variations in the surface under the lander and, in fact, operate much like a rugged, machine shop drill-press. The drilling speed is kept at a constant rate, independent of rock hardness, thereby allowing for a direct specification of the drilling depth with time and hence the sample transfer events. The large atmosphere pressure difference provides far more motive force than is required to move the samples, resulting in a very high-speed flow that efficiently moves the vast majority of particles through the system. The airlock movements are similarly synchronized to the transfer events and deliver samples to the instruments shortly after the end of drilling.

### **B.2.8.2.2.12 Long-Lived In Situ Solar System Explorer (LLISSE)**

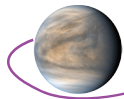
**LLISSE** is a payload carried externally on the Lander which will collect data for at least 60 Earth days. The **LLISSE** instrument measures surface winds and diurnal variations of light and temperature through a solar day (118 Earth days). The instrument also measures variability of key trace gases (SO<sub>x</sub>, CO, OCS, etc) to < 1 ppm sensitivity (2 ppm for SO<sub>x</sub>) to correlate with meteorology data. **LLISSE** will be searching for changes in near-surface atmospheric chemical composition. Another function of the instrument is to measure diurnal variation of surface winds, radiance, P, T, and trace gases to aid in the characterization of winds and determine their role in volatile transport. These data will help determine transport mechanisms from the solid surface to the upper atmosphere.

### **B.2.8.2.3 Entry, Descent, and Landing**

#### **B.2.8.2.3.1 Overview and Requirements**

The EDL subsystem includes the forebody and afterbody aeroshells with the TPS and the parachute(s), and within the mission's ConOps its primary performance is from entry interface to destination. It protects the Lander/instruments/payload from entry heating and deceleration forces during the entry into Venus's atmosphere. The EDL subsystem was designed to meet the following requirements:

1. Temperatures at the bondline not to exceed 260°C. This is driven by the temperature limits on the adhesive that bonds the TPS to the aeroshell structure.
2. Peak deceleration not to exceed 50 g. This requirement stems from the science instrumentation. This lower value (compared to prior missions) enables a wider array of science instrumentation to be used as part of this mission.



3. Achieve flight conditions to meet/deliver (a) a time of descent (from backshell separation to touchdown) of about 60 min, and (b) a terminal/touchdown speed less than 7.4 m/s.

The EDL subsystem must meet these requirements subject to entry conditions consistent with the interplanetary approach trajectory (**Table B-52**). The requirement on peak deceleration (for the nominal entry velocity of 10.08 km/s) yields an EPFA of  $-8.46^\circ$ , significantly shallower than prior missions (such as Pioneer Venus Large Probe,  $-32.4^\circ$ ) and mission concepts (such as VITaL,  $-23.5^\circ$ ).

The aeroshell shape is a  $70^\circ$  sphere-cone with a max diameter of 4.6 m. This geometry provides significantly better packaging and drag performance than the  $45^\circ$  sphere-cone (e.g., Pioneer Venus) and has a smaller surface area for a given diameter (thereby reducing the mass of the thermal protection system). The entry mass of 2031 kg (used for the analysis and design) results in a ballistic coefficient of  $94.3 \text{ kg/m}^2$ . The aeroshell structure is composite with a mass of 412 kg (not including the TPS), based on preliminary analysis. This estimate is conservative and detailed design could provide avenues of optimization and a reduction in mass.

The heat shield TPS is a tiled single-layer system of HEEET (Heatshield for Extreme Entry Environment Technology) with a mass of 215 kg and a uniform thickness of 0.6 inches. An alternative tiled dual-layer HEEET TPS is also viable, weighing 247 kg and made up of a 0.31" outer recession layer and a 0.27" inner insulative layer. HEEET is a 3-dimensional woven TPS system developed for extreme entry environments. A dual-layer HEEET features a denser recession layer (that is exposed to the atmosphere) and an insulation layer (underneath). The two layers are woven together. Single-layer HEEET only utilizes the insulation layer. Dual-layer HEEET is currently at TRL 6, while single-layer (insulation layer only) HEEET is the baseline material for the Mars Sample Return Earth Entry Vehicle, that will bring the samples back from Mars and land them safely on Earth.

**Table B-52.** Lander Entry Table (shows the information used to simulate the Entry Trajectory and design the Entry System)

	Item	Values	Units/Detail
Aeroshell	Aeroshell Geometry	70	$^\circ$ (sphere cone)
	Aeroshell max diameter	4.6	m
	Entry Mass	2030.9	kg
Entry Vector	Entry Interface	175	km
	Entry Velocity	10.076	km/s
	Peak Deceleration Requirement. Less than	50	g
	Entry Flight Path Angle	-8.47	$^\circ$
	Heading	270	$^\circ$ (relative to North)
	Entry Latitude	0.3592	$^\circ$ (relative to equator)
	Entry Longitude	70.1291	$^\circ$
	Entry time(s)	2464459.501	JED
	Descent	Main Parachute	10
Lander Aero		VISAx	Model
Lander Reference Diameter		1.25	model
Lander mass		1200.8	kg
Parachute deployment		1.4	Mach Number
Parachute deployment mechanism		Mortar Assembly/drogue	N/A
Drogue Parachute		None	N/A
Heatshield Separation		0.7	Mach Number
Backshell Separation		30	seconds (after separation)
Landing Site Elevation		1	km (above reference)
Landing Velocity Requirement. Less than		10	m/s
Landing time Requirement. No less than		60	min

\* The entry design assumes an entry flight path angle of  $-8.47^\circ$  (which results in a peak deceleration of 50 g) with the assumption that the nominal EPFA is  $-7.47^\circ$ , and the uncertainty is  $\pm 1^\circ$

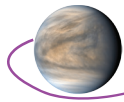


**Table B-53.** Shows the relevant information for the heatshield Thermal Protection System. Note that there are two possible designs/options, including either a single layer HEEET, or a dual-layer HEEET TPS.

TPS Material	TPS Thickness	Recession Layer Thickness	Insulative Layer Thickness	Aerial Density	Area	Mass
	(inch)	(inch)	(inch)	(kg/m <sup>2</sup> )	(m <sup>2</sup> )	(kg)
T/SL HEEET	0.583	–	0.583	12.15	17.7	<b>214.6</b>
T/DL HEEET	0.690	0.305	0.385	16.48	17.7	<b>291.2</b>

**Table B-54.** Shows the relevant information for the Lander backshell Thermal Protection System.

TPS Material	TPS Thickness	Aerial Density	Area	Mass
	(inch)	(kg/m <sup>2</sup> )	(m <sup>2</sup> )	(kg)
PICA	0.36	2.42	19.35	<b>46.9</b>

PICA (Phenolic Impregnated Carbon Ablator) is used as the backshell TPS. The tiles are expected to be bonded to the structure using HT-424 while RTV-560 fills gaps, using the same techniques as Mars Science Lab and Mars 2020. The backshell TPS mass is estimated to be 41 kg.

The aeroshell utilizes a supersonic parachute for deceleration prior to Lander separation and for stability near Mach 1. The parachute designed is a 10.04 m diameter Disk-Gap-Band parachute deployed at Mach 1.4, and is expected to weigh 35.6 kg. This parachute design has been used on every US mission to Mars since Viking (including the Perseverance mission, and the Mars Sample Return's Sample Retrieval Lander). In addition, supersonic DGBs have been used as the drogue parachutes on Earth reentry missions such as Stardust. Supersonic DGBs have been tested multiple times at Earth via high-altitude tests (starting with Viking Balloon Launched Decelerator Test (BLDT), Planetary Entry Parachute Program (PEPP), Supersonic Planetary Entry Decelerator (SPED), and with the recent ASPIRE test series). Huygens also featured a DGB parachute.

The Lander is composed of a pressure vessel and a drag plate. The drag (and stability) performance is uniquely dependent on the final design including the size of the pressure vessel, the number/shape/size of the legs, the position and size of the drag plate. To meet the required descent time of not less than 1 hour, the Lander must have a drag area (CdA) of 7.63 m<sup>2</sup>. Referenced to a 1.2 m diameter circle, this implies a drag coefficient of 6.75 which is comparable to drag coefficients of landers studied for prior Venus missions (e.g., wind tunnel testing for VISAGE [O'Farrell et al., 2017]). While wind tunnel testing is required to determine the drag characteristics, the proposed aeroshell geometry should provide opportunities to increase the drag area of the drag plate if necessary.

### B.2.8.2.3.2 Lander Aeroshell Structure

The Aeroshell structure is designed to withstand the high deceleration loads (~50 g) during entry. The Thermal Protection system is designed to not let the internal/bondline temperature exceed 260° C during the entry pulse. Expected peak heating during the entry is 1734 W/cm<sup>2</sup> (convective, rough wall, margined, at the shoulder) with an integrated heat load of 23,875 J/cm<sup>2</sup>. The shoulder also sees a peak radiative heating of 87.3 W/cm<sup>2</sup> (margined) with a corresponding heat load of 1379 J/cm<sup>2</sup>.

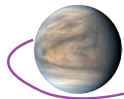
### B.2.8.2.3.3 Concept of Operations

**Table B-55** provides a summary of main events and concept of operations from entry interface to the descent of the Lander to the desired altitude.

**Table B-55.** Lander Entry, Descent, and Landing Timeline

Event	Trigger	Time from Entry (sec)	Altitude (km)	Altitude Rate (m/s)	Total Mass (kg)
Entry Interface	Altitude	0	174.852	-1480.74	2030.9
Chute Deploy	M=1.4	125.3	75.33928	-178.467	2030.9
Chute Inflated	Deploy + 0.3 s	125.526	75.29903	-176.983	2030.9
Heatshield Sep	Altitude	358.6	59.9982	-36.2916	1372.18
Backshell Sep	HSS + 30 s	388.6	59.12406	-27.8747	1082.19
Lander Touchdown	Altitude	3697.446	1	-7.83508	1082.19





The aeroshell enters the atmosphere from orbit, at a relative velocity of 10.076 km/s (**Figure B-86**). The entry flight path angle is designed to be  $-8.5^\circ$  to limit the peak deceleration to 50 times Earth-g. The heat pulse lasts for about 2 min, slowing down the capsule. The supersonic parachute deploys at Mach 1.4 (and an altitude of 75.3 km), fully inflating within 0.3 seconds. The capsule descends under the parachute for the next 4 minutes, followed by heat-shield separation at a 60.0 km altitude. 30 seconds later, the parachute and backshell separate from the Lander which continues to descend towards the surface. The Lander reaches the surface at a speed of 7.21 m/s after roughly an hour, assuming a drag area of  $7.63\text{m}^2$ . Note that the requirements on touchdown velocity and descent time are linked. Further reduction in touchdown speed is possible by modifying the drag performance of the Lander, but will be accompanied by an increase in the descent time.

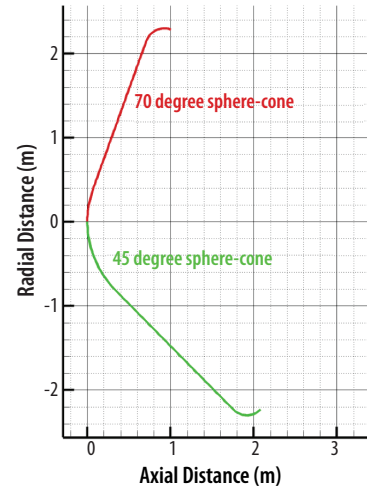


**Figure B-86.** Figure compares the two heatshield geometries—a  $45^\circ$  sphere-cone, and a  $70^\circ$  sphere-cone.

Previous missions to Venus (as well as studies) were designed with a requirement on peak deceleration much higher than the current value of 50 g. This results in a significantly different entry flight path angle ( $-8.5^\circ$ , as opposed to Pioneer Venus's value of  $-32.4^\circ$ ). An upper limit on EFPA was conservatively chosen as  $-6.4^\circ$ . This is the angle at which lofting, or flight up from the surface, occurs. Limiting the EFPA to the lofting condition ensures that the entry vehicle will not skip out and protects against very large footprint dispersions.

#### B.2.8.2.3.4 EDL ConOps Trigger(s)

The parachute deployment event is triggered on navigated velocity. Heatshield separation is triggered on altitude and backshell separation is a fixed time from heatshield separation. The EDL sequence is not expected to be sensitive to reasonable errors in the navigated state. It is possible that simple timers and g-sensors could be used for all trigger events, but it has not yet been studied.

#### B.2.8.2.3.5 Key Trades

Early in the design process, trades involved EPFA and the resulting heating and the peak deceleration. Steeper entries resulted in higher peak deceleration, reduced entry pulse width (time), and higher peak heating. At an entry velocity of 10.076 km/s, an entry flight path angle of  $-8.5^\circ$  provided 50 g of peak deceleration, with a narrow entry corridor (between the designed EFPA and skip out, at  $-6.4^\circ$ ).

##### B.2.8.2.3.5.1 $45^\circ$ vs $70^\circ$ Geometry

Almost all previous missions and studies to Venus were designed with a  $45^\circ$  geometry (**Figure B-86**). This legacy geometry provides unconditional stability during the entry and descent (down to subsonic speeds, provided appropriate packaging and the desired c.g. location). Since the current mission design called for an entry-from-orbit at a somewhat lower entry speed of 10.076 km/s (compared to Pioneer Venus's entry speed of 11.5 km/s), other geometries were considered. A  $70^\circ$  sphere-cone offers better packaging and increased drag, and has been successfully used at Mars (with similar atmospheric composition as Venus). Early aerothermal analysis showed that (a) while the  $70^\circ$  geometry results in higher radiative heating near the shoulder compared to the  $45^\circ$  geometry, the total heating is still within the capability of the thermal protection system, (b) that the  $70^\circ$  sphere-cone, by virtue of smaller surface area, results in a lighter heat shield, and (c) while the  $70^\circ$  geometry requires a supersonic parachute, the loads and deployment conditions for such a parachute are within recently demonstrated limits in the ASPIRE test program [O'Farrell et al., 2017] where supersonic DGB parachutes were tested/deployed at high altitudes over Earth through three different flight tests during 2017 and 2018. The second flight test featured a parachute deployment at Mach 2.0 and the third one featured a deployment at a high dynamic pressure of over 1000 Pa.

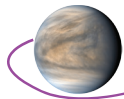


**Table B-56.** Areas and Backshell TPS masses corresponding to various backshell geometries

Backshell Geometry	Area [m*m]	Backshell TPS mass [kg]
VFM Lander	19.35	46.9
M2020	23.41	56.7
Mars Insight	23.02	55.8
Marsh Phoenix	23.02	55.8
Stardust	27.54	66.8
Dragonfly	25.36	61.5
Pathfinder	21.58	52.3

### B.2.8.2.3.6 Backshell Geometry

The backshell geometry used in the current design, shown in **Figure B-87** is driven by packaging constraints: i.e., the smallest backshell that can package all the components inside the aeroshell. The TPS mass estimates (**Table B-56**) are consistent with this geometry. This being a novel geometry, an aerodynamic database has to be generated early in the project (likely including CFD, wind tunnel testing and ballistic range testing) both to establish the aerodynamic characteristics as well as to ensure desired static and dynamic stability features. Use of a legacy backshell geometry permits taking advantage of existing knowledge and aerodynamic databases. **Figure B-87** also shows a few legacy geometries, scaled appropriately. These geometries provide larger packing volume and exhibit a larger surface area (increasing the backshell TPS mass). For the same backshell TPS thickness, the TPS masses for these other geometries range from 52.3 kg to 66.8 kg.

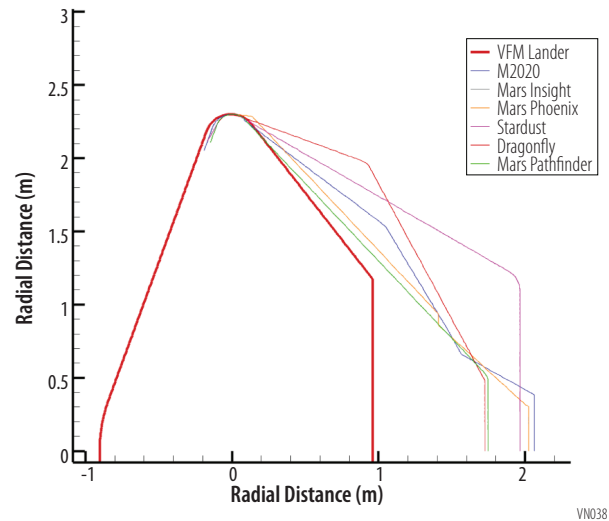


**Figure B-87.** Geometry of the current design of the backshell along with a few legacy backshells scaled up to match the aeroshell diameter.

### B.2.8.2.3.7 Navigated State Triggers vs Timers

Use of g-sensors and timers would simplify the design and operations of the EDL system, though it would likely increase dispersions in parachute deploy conditions. A full Monte Carlo study is needed to determine whether such dispersions would be acceptable.

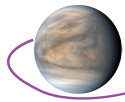
### B.2.8.2.3.8 Suggested Later Trade: Drogue Parachute, or Mortar Deployment

We suggest an early analysis and design trade of the parachute deployment system: whether the main supersonic parachute is extracted through a drogue parachute (supersonic, above Mach 1.4) or is deployed by a mortar. Both are viable and have been shown to be successful (at Mars, Venus, and at Earth).

### B.2.8.2.3.9 Recommended Future Studies

#### B.2.8.2.3.9.1 Lander Drag and Stability Characteristics

A significant portion of the EDL ConOps is characterized by the descent of the Lander after backshell separation. This period is highly dependent on the drag performance and the stability characteristics of the Lander geometry—essentially a spherical pressure vessel and a drag plate. The current ConOps assumes a drag area of 7.63 m<sup>2</sup> which is viable, based on recent experimental work [O'Farrell et al., 2017]. Wind tunnel testing of the final Lander geometry (or trades on different geometries) are required to assess/evaluate the aerodynamic behavior.



### B.2.8.2.3.9.2 Aeroshell cg and Mass Properties

Mass properties of the aeroshell (heatshield + backshell + aeroshell structure + payload) need to be evaluated to ensure that it has the desirable attributes (location of the center of gravity) to allow a stable hypersonic and supersonic flight.

### B.2.8.2.4 Lander Structure

#### B.2.8.2.4.1 Packaging Drivers

The Lander packaging had a diverse set of driving requirements; all design considerations for the Lander plus the need to safely deliver the Lander to a potentially rugged surface of Venus. Because of the Venus surface environment, all structures that are not thermally controlled are required to be titanium since aluminum alloys lose significant amounts of strength at these high temperatures. The aeroshell cone-angle and interior volume/diameter enabled a very simple leg design with a telescoping upper arm. This allows for both a single motion deployment and for energy absorption with the use of a crushable canister inside the leg tube. The legs also provide mounting for the fan actuation system (**Figure B-88**). The addition of hazard avoidance capability for the Lander opened up the possibility for a smaller, simpler leg design. A drive system, used to deploy the legs, can also be used to stabilize the landed craft after landing. It should be noted that the width of the leg stance could be greatly increased, thereby improving landing stability, by implementing a multi-fold leg design. This would also allow a smaller diameter entry system. This optimization was left for future work. At the base of the legs are landing pads. Additional work needs to be done to determine the type of foot interface needed based upon the expected terrain. For example, spikes might be more appropriate if landing on scree. Energy absorbing material can be added to the pads if landing on harder surfaces or some combination of the two.

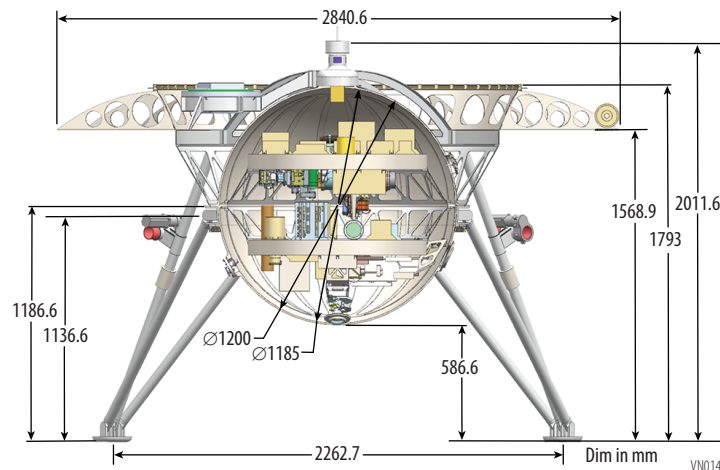
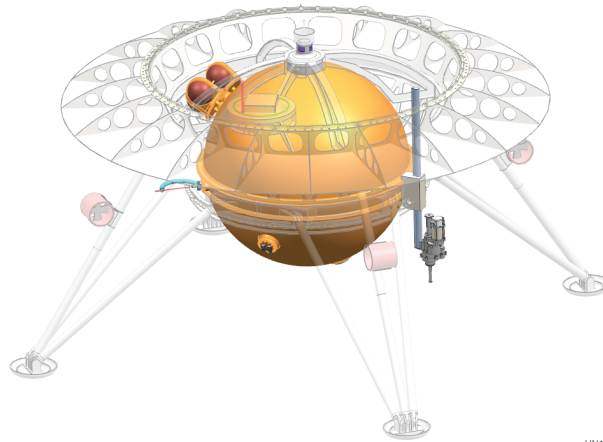
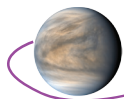


**Figure B-88.** Lander interior: upper deck primarily holds Lander operational boxes such as communication and power boxes; between decks is dominated by instrument boxes with the exception of the LCDH box; lower volume has both instrument components and the hazard avoidance boxes. (Exterior dimension shown)

The equatorial ring of the sphere is the primary backbone of the Lander design shown in **Figure B-89**. On the exterior, it provides the interface to the drag plate, the legs, and the instrument sphere. A bridging structure (**Figure B-90**), which does not interface with the instrument sphere, is used to bridge the leg loads and isolate the sphere during landing. The bridge also provides mounting of the **LLISSE** instrument. The drag plate is used to control the terminal velocity during descent. Detailed flight dynamics of the drag plate have not been performed but some approximate calculations were done and used in the EDL design that is discussed in **Section B.2.8.2.3**. The field of view of the **PC** is comprised of 4 distinct 60° FOVs through the use of four mirrors in the cupola. Because the drag plate is within the FOV, additional options to increase the **PC** FOV, such as a drag plate that folds out of the way after landing or a deployable drag plate that sits above the Lander, are left to future studies. The drag plate provides mounting for the **radiance sensor**.



VN164

Figure B-89. Lander Sphere showing drill and evacuation spheres (shown in Red)

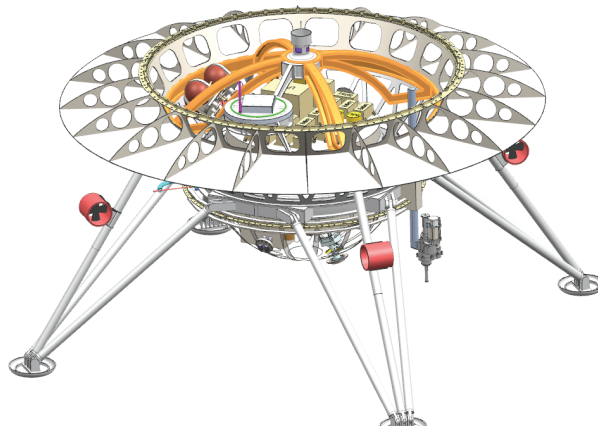
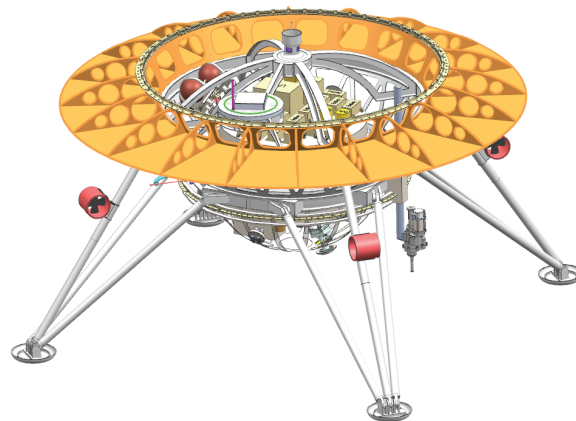


Figure B-90. Lander Bridge shown in orange



VN166

Figure B-91. Lander Drag Plate shown in orange

The Lander sphere is built in three sections. The upper hemisphere supports the sample handling tanks and the PC cupola and provides an access port for integration. The access port has plumbing for evacuating the sphere prior to launch. The lower hemisphere has the NMS inlet assembly and three windows. The lowest window is for the DI. Slightly higher is the window for the hazard avoidance systems including the LIDARs, laser range finders, and the engineering camera. The final window is

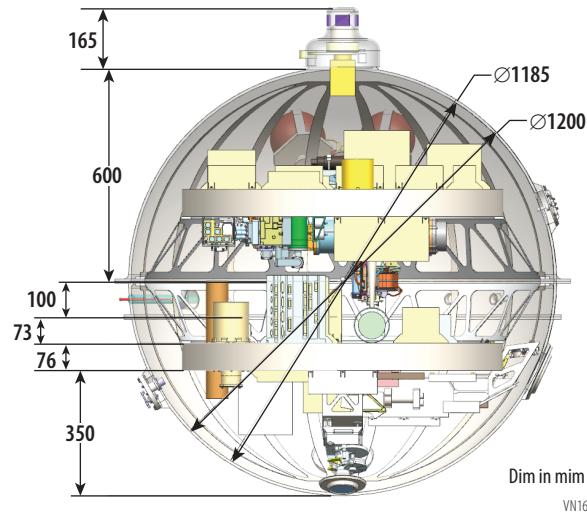
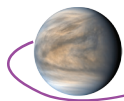


Figure B-92. Lander Sphere Cutaway to show Decks, which hold the avionics and instruments

for the **R-LIBS**. The equatorial ring has the electrical connection port, and a pass-through for the pressure/temperature sensors and the equatorial ring is the structural interface to the drag plate and legs. On the inside, it supports the thermally isolating ‘elephant stands’ which support the upper and lower decks. The equatorial ring is part of the spherical geometry to maintain as consistent a spherical shape as possible, maximizing sphere strength.

The upper and lower decks are isogrid aluminum. The isogrid pockets are used for embedding the phase-change material; and the aluminum provides high conductivity to the boxes and instruments. As required for thermal isolation of the decks, the ‘elephant stands’ are titanium which will require a flexure interface (**Figure B-93**) with the decks to mitigate CTE mismatch issues. The flexure interface has 36 titanium blades, the same size as the ‘elephant stand’ legs, between the deck and the stand with room to grow if a future detailed analysis reveals a change is needed. The flexures are designed to withstand the 50g entry load and the loads imparted by the CTE mismatch as it experiences the temperature delta of 78° C  $\Delta T$  over the 8 hour Lander lifetime (displacement of the flexure is only 0.55 mm). Each deck has mounting interfaces on both top and bottom sides. A sheet-metal aluminum retainer supports the sphere insulation. Metal C-seals will be required at all sphere ports and separation planes. The sphere will be launched evacuated (to  $10^{-6}$  torr), which should simplify the sealing of all ports and pass-throughs as well as the sphere segments.

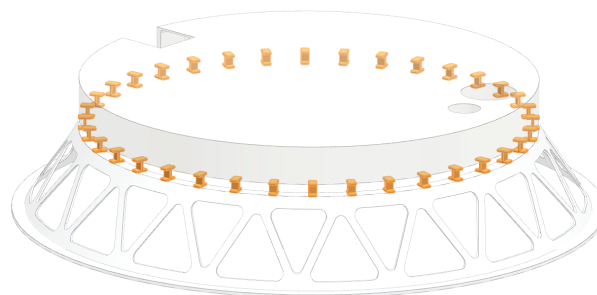
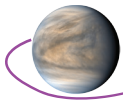


Figure B-93. Elephant Stand Thermal Flexures

Deck components are grouped by function whenever possible. The upper deck primarily holds Lander operational boxes such as communication and power boxes. Between decks is dominated by instrument boxes with the exception of the LCDH box. The lower volume has both instrument components and the hazard avoidance boxes.



#### B.2.8.2.4.2 Load Path, Sizing and Analysis – Lander

The load path of the Lander within the aeroshell conceptually requires one support structure between the Lander and the backshell for launch loads and a second support structure between the Lander and the aeroshell (forward shell) during atmosphere entry. On smaller entry systems, such as the Galileo Probe, a common support structure for both launch and entry loads was utilized around the outer perimeter of the aeroshell. The large diameter of the entry system for VFM suggests a backshell interface for launch and forward shell interface for entry would be more mass efficient. The drawback of this concept is defining the mounting or the operations to avoid over-constraining the Lander. The aeroshell/Lander interface and mounting/release concepts are considered future work.

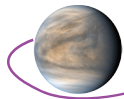
Hand calculation sizing was done for the sphere based on a pressure differential 9.2 MPa and ambient temperature of 441°C. A few other major structural platforms were also sized in a similar way including the legs, deck ‘elephant stands’ and aeroshell interface trusses. The entry loading of 50 g dominates both launch and landing loads and was used for sizing calculations. The support load path for the Lander for atmospheric entry is through the equatorial ring, which is the same as landing loads. Launch loads are significantly less but are in the opposite direction through the drag plate support truss. The current concept has a sheet-metal drag-plate constructed similarly to an aircraft wing with skin and ribs. Since an aerodynamic analysis was not done, it may be possible that the sheet metal skin could be replaced with ribs and a high temperature membrane.

Basic tip-over geometry was briefly studied and the current leg configuration works with the assumption that the fan actuation system is able to compensate for the ground level wind speed of 1–3 m/s and energy absorption systems in the legs remove enough of the kinetic energy at impact to prevent tip-over. Eliminating the lateral velocity during impact greatly simplifies the landing cases. It was further assumed that the landing hazard avoidance system could avoid large rocks. These idealizations, along with the assumption that the kinetic energy at impact can be fully absorbed by the legs and crushable material, made the current notional leg design conceptually feasible. It is very unlikely that these assumptions are conservative enough. A more robust design, with additional energy absorbing capabilities and increased leg span will need to be studied along with a full and detailed landing dynamics analysis. The kinetic energy in the lander must be absorbed to ensure a stable landing. The conceptual design of the landing legs uses crushable structures. Although a detailed design of the crush system was not done, a simple approximation using a cylinder on the bottom of the landing pads showed that the energy could successfully be absorbed on impact within the limits of the idealized version of the impact.

The baseline design has the crushable material notionally within the telescoping legs. It was assumed that the landing pad crush cylinder concept, as analyzed, could be incorporated into the landing legs. The design of the crushable material geometry will need to be considered since the crushable material will only begin to absorb energy when the load on the crushable material reaches the crush strength. Since the crush strength is constant, varying the crush system geometry will be needed. Flexing the landing legs during impact should be avoided since energy stored in the landing legs will be like a spring. This energy will be released when the crushable material reaches its full stroke resulting in a potential bounce. Therefore it is likely that the geometry of the crushable material will need to be varied, such as a conical structure, to avoid a stepwise build-up of energy in the legs. It is also clear from the analysis that increasing the span of the legs using folding or deployable systems would be a significant advantage to the stability of the landing. The design as shown is theoretically viable with the caveats indicated above.

#### B.2.8.2.4.3 Key Trades

1. **Options for number of legs.** The number of legs increases the tip-over distance and increases stability at the cost of mass and packaging complexity. Studies of net gain in stability compared to the mass cost drove the design to a four-leg layout.
2. **Leg design.** The larger (4.6 m) aeroshell allowed for a simple Viking style tripod leg concept. Other leg designs were considered for saving mass by reducing the aeroshell diameter and increasing the leg stance. The addition of the hazard avoidance system obviates the need for a wider leg stance for the preliminary concept although future work is needed on optimizing landing stability as the current design, while viable, is not as conservative as could be wished.



- 3. **Lander diameters.** Increased diameter of the sphere simplifies packaging, interrogation, and assembly at the cost of increased mass as well as surface area. Increasing the surface area increases the heat flow into the sphere.

### B.2.8.2.4.4 Recommend Future Studies

- 1. Aeroshell mounting/interface/release concepts.
- 2. Landing dynamics—as mentioned above, the need to maintain stability while landing on an unknown surface will require extensive testing and study.
- 3. Drag plate design to reduce landing velocity and oscillation.
- 4. Kinetic energy absorption methodologies.
- 5. Leg deployment concepts for increasing leg span for stabilization.
- 6. Landing pad interface to the ground.
- 7. Number of legs.
- 8. Leveling methods.

### B.2.8.2.5 Lander Attitude Control System

Prior to separation, the Lander ACS is provided with the initial attitude state information. After separation the Lander ACS will begin monitoring the attitude of the Lander and updating the attitude state. For most of the descent the ACS is monitoring and updating state information. Once the Lander gets to roughly 5 km altitude, the ACS can initialize the TRN and LHA subsystem discussed in the following sections. Once safely landed the ACS is turned off. The Lander ACS block diagram is shown in **Figure B-94**.

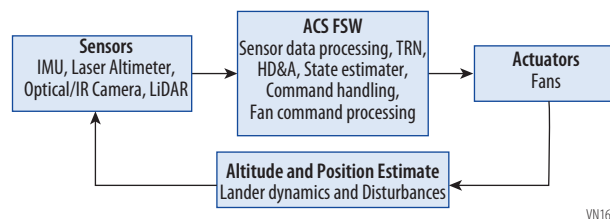


Figure B-94. Lander Block Diagram

The Landing mode, which is the only mode of operation, receives the current attitude state at separation from the Orbiter and then uses sensor data. The only sensor available for the majority of the landing is the IMU. TRN and LHA sensors can be used once below the clouds at approximately 5 km. The ACS software receives the sensor data and updates its state and issues commands to the Fans. Then the Attitude and Position Estimate (APE) utilizes the sensors to estimate the Lander position relative to the landing target/landmark. The APE architecture for the Venus Flagship Mission (VFM) is shown in **Figure B-95**.

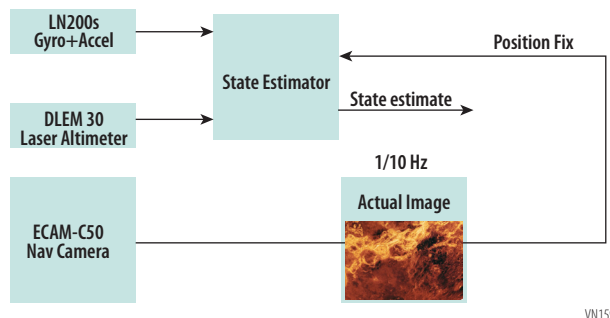
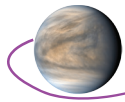


Figure B-95. Attitude and Position Estimate (APE) architecture



In addition to APE, the Landers flight software will also contain a Terrain and Relative Navigation (TRN) and Hazard Detection and Avoidance (HD&A) function.

#### **B.2.8.2.5.1 Terrain Relative Navigation and Hazard Detection and Avoidance**

The VFM Lander is designed to safely land the instrument payload in a tessera terrain and survive for at least 6 hours, with a goal of 8 hours. In order to land safely, the mechanical design needs to accommodate landing terrain uncertainty. To account for the uncertainty the Lander is designed to land on a slope of up to 30° and accommodate a 0.5 m beneath the sphere. With landing as the highest risk for the mission the Lander includes both a Terrain Relative Navigation (TRN) and a Hazard Detection and Avoidance (HD&A) system. The HD&A assess the hazards in the projected landing site and uses the fan actuators to move the Lander laterally to avoid landing on the hazard.

In general, HD&A is used to avoid known or unknown (no preflight knowledge) hazards within the landing site and consists of algorithms, image sensors and position/attitude actuators. To evaluate the feasibility of the HD&A for the Venus environment, a baseline architecture and hardware is designed and discussed. This baseline is not the only HD&A solution, but illustrates feasibility. The Detection and Actuator sections provide a detailed description of the baseline hardware that is appropriate for VFM.

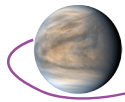
#### **B.2.8.2.5.2 HD&A Requirements**

For VFM, hazards are defined as slopes greater than 30° and/or boulders with diameters greater than 0.5m. The HD&A software must have the ability to identify these hazards [Furfaro et al., 2012; Carson et al., 2015]. Based on the proposed baseline operation and the expected performance of known detection systems, the VFM team adopted an image resolution of 0.1m at 2km based on Moroz [2002]. Once identified, the lander must enact a correction that minimizes hazard impact; this is often treated as an optimization problem [e.g., Furfaro et al., 2012; Lunghi et al., 2015; Yuan et al., 2018]. For the VFM, a 0.5 Hz–0.05Hz HD&A cycle should be sufficient to generate an image, identify a hazard, and generate the appropriate action to avoid the hazard. This requirement will drive the memory/processing capability. Functionally, the HD&A algorithms must account for deviations from the Lander’s intended course, and for uncertainty/noise in the image. Without accounting for uncertainties, a HD&A system may attempt to “thread the needle” beyond the Lander’s capabilities or engage in wasteful avoidance maneuvers if given overly strict constraints [Furfaro et al., 2012; Carson et al., 2015; Yuan et al., 2018]. The orientation of the Lander during descent changes with time due to atmospheric effects and adds to the smearing problem. Lorenz [2010] reported angular deviations and rates of angular deviation of previous planetary landers from nadir (vertical). This variation in orientation will reduce the knowledge of the hazard relative position. As the amplitude and frequency of the variations increase, so will the smearing of the image and will reduce the effectiveness of the HD&A. In addition to the noise/uncertainties, the ACS system must be designed to reduce rate stability errors, which can induce blurring. The ACS attitude rate stability requirement is 10 pixel per HD&A cycle.

#### **B.2.8.2.5.3 HD&A Operation**

The HD&A operation assumes that the landing site/corridor size will account for all uncertainties and errors (navigation errors, timing errors, wind uncertainties, drag errors, etc.) associated with the descent prior to HD&A turn-on altitude. A discussion of the corridor design can be found in the Mission Design **Section B.2.7**. The HD&A turn-on altitude is determined by the altitude where sensors can generate accurate terrain images with the desired resolution, which are used by the HD&A to identify and assess hazards in the expected landing site. Based on the assessment, a safety correction is generated by the HD&A and used by the Guidance Navigation and Control (GN&C) Systems to avoid the hazard. Since all corrections are not feasible, the HD&A assesses the feasibility of the correction based on the Lander actuator capability, Lander constraints, and safety criteria. During the final stage of the descent (free fall), corrections are nulled. If possible, the descent and landing data is transmitted (or stored for later transmission) to the Orbiter. The HD&A cycle is based on the mission requirements, and is expected to be between 5 seconds to 2 minutes.





#### B.2.8.2.5.4 Venus Environment

The Venus atmosphere is very thick and ~80 times the pressure of Earth's atmosphere on the tessera, where the surface temperature is on the order of 440°C. Optically, Venus is similar to looking through a murky fluid consisting of mostly carbon dioxide gas (~96%), nitrogen (~3%), and water vapor (0.003%) under a thick layer of sulfuric acid clouds at ~50–60 km altitude. This type of environment reduces the optical effectiveness of various sensors. Utilizing ongoing work B. Grieger, and Nat Gill, GSFC LIDAR engineers, and Colin Wilson, a Senior Research Fellow at the University of Oxford, came up with baseline assumptions which are used in the design process for a Venus LIDAR. These assumptions are listed below.

- Laser must transmit through a thermal window with 80% efficiency at 1064 nm.
- Atmospheric Extinction Coefficient (1/m) 0.002.
- Solar Spectral Radiance (W/(m<sup>2</sup>\* μm)) 251.
- Background reflectance 20%, target reflectance 10%.
- 0.8 mrad laser divergence = 10 cm spot size (1/e<sup>2</sup>) at 125m.
- Relative velocity to ground is 0.5m/s which limits integration time.
- Optimizing for maximum range, FOV, and frame rate.

The LIDAR design will be similar to On-orbit Servicing, Assembly, and Manufacturing Mission 1 (OSAM-1) Kodiak system, except at 1064 nm, SiAPD (Silicon avalanche photodiodes), 1 receiver 2 box system. The design trade will consist of 4 cases investigated with 3 mm or 5 mm detector, 31 mm or 50 mm aperture. The 5 mm detector performance is CBE for the prototype of the OSAM-1 system.

#### B.2.8.2.5.5 Detection Systems

Recent successful automated HD&A systems have relied on a dual sensor approach [Jiang et al., 2016; Lunghi et al., 2016], which this mission study adopted. Generally, a descent imager is used to determine broad-scale hazards (e.g., regions of shadow) at a relatively high altitude where small course corrections can propagate into large changes in the landing area, while a flash LIDAR system is used for fine tuning at a relatively low altitude [Jiang et al., 2016; Lunghi et al., 2016]. Our selected descent imager and flash LIDAR systems are a combined system from GSFC.

A flash LIDAR system is the 3D imager baseline system. A simplistic analogy is that a flash LIDAR is the camera version of more contemporary LIDAR systems. Whereas more traditional LIDAR systems obtain topographic information by consecutively scanning different locations using a series of small diameter laser pulses which are then combined to form a single Digital Elevation Model (DEM), a flash LIDAR acquires topographic information over a distributed area using a single large diameter pulse [Jiang et al., 2016; McManamon et al., 2017; Xiao et al., 2019]. This has several benefits. Flash LIDAR reduces the computational power required compared to other LIDAR methods. Only a single correction for the lander orientation is required for the DEM extracted at each altitude as opposed to the correction for each LIDAR point required by scanning LIDAR systems. Flash LIDAR has fewer moving parts, which generally results in fewer complications and equipment breakdowns. Moreover, flash LIDAR is a technology which NASA has already developed and licensed for commercial use in autonomous rover and robot guidance and control and usage in space [NASA Technology Transfer Program; patents 8,655,513; 8,494,687; 9,354,880; <https://technology.nasa.gov/patent/LAR-TOPS-168>] and is already in use in the Autonomous Landing Hazard Avoidance Technology (ALHAT) program [Carson et al., 2015]. Flash LIDAR also has several potential detriments that must be explored before a full recommendation for this technology can be made. The key technology development is a stronger laser pulse. This is particularly important for flash LIDAR systems that use a single laser pulse to form a DEM of the surface [McManamon et al., 2017]. Common flash LIDAR systems require cooling, which increases energy requirements and mass [McManamon et al., 2017]. Individual locations in each return pulse can also suffer from smearing effects, resulting in a convolution of nearby elevation values and a DEM that is smoothed compared to the true ground surface.

Based on the VFM requirements, further LIDAR technology development is needed to increase the range relative to the Venus atmosphere. To achieve the Venus LIDAR requirements, the next generation LIDAR must exceed the ALHAT next generation LIDAR.

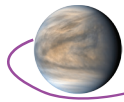


Table B-57. ALHAT/Next Generation LIDAR specifications

Parameter	ALHAT Flash LIDAR	Next Generation LIDAR
Detector Array Size	16 K	> 65 K
Range Precision within a frame (1-sigma)	7 cm	3 cm
Frame Rate	20 Hz	20 Hz
Operational Wavelength	1.06 micron	Eye-safe 1.57 micron
Max Operational Range (for diffuse target with 30% reflectivity at normal look angle)	1,800 m	3,000 m

Ref: <https://ntrs.nasa.gov/search.jsp?R=20160011575> 2020-07-19T21:00:39+00:00Z

Assuming a decrease in performance due to the thick Venus atmosphere, the Flash LIDAR should be able to detect hazards smaller than 50 cm from about 1.8 km distance.

### B.2.8.2.5.6 HD&A Algorithm

Following data collection, the HD&A algorithm must account for and address the physical limitations of the descent imager and LIDAR that reduce the data quality, identify hazards, account for actuator limitations, and plot/enact course trajectories corrections to minimize hazards. The process of autonomously detecting and identifying hazards on a rocky, monochromatic surface is feasible and has been demonstrated effectively (e.g., the successful landing of Chang'e-3 on the farside of the Moon [Jiang et al., 2016] and Morpheus test flights [Carson et al., 2015].

Autonomous HD&A generally falls into a deterministic set of rules, or cognitive processes meant to mimic human interactions. Deterministic methods often overfit safety concerns, resulting in a reduced number of identified safe paths [Lunghi et al., 2016] and excessive energy usage [Yuan et al., 2018]. Alternatively, cognitive processes techniques like neural networks (or fuzzy logic) exist that mitigate the problems encountered by deterministic systems via their ability to adapt to new situations [Furfaro et al., 2012] and demonstrated short computation times Lunghi et al. [2016]. These techniques allowed the HD&A system to avoid excessive energy usage for hazard avoidance maneuvers (e.g., avoiding a path that is safe to 2.9  $\sigma$  because of a required safety limit of 3  $\sigma$ ) while also reducing the failure rate as compared to deterministic methods [Yuan et al., 2018].

### B.2.8.2.5.7 HD&A Actuation

The capability of the HD&A system is based on the sensor, algorithm and the actuation. The possible physical trajectory corrections the HD&A can produce is defined by the HD&A actuators and associated constraints. The actuator choice is a function of the environment, mass, power, and needed control effort. In many cases, the HD&A will utilize the Attitude Control system (ACS) and position actuators. In typical cases, the lander HD&A will utilize the spacecraft thrusters as the primary actuator. If the thruster cannot provide the needed controllability, then a typical spacecraft will use reaction wheels to augment the actuation system to produce the needed controllability. For the VFM Lander thrusters and reaction wheels are not available and another actuator must be identified.

### Venus specific HD&A Operation

For the VFM, hazard avoidance algorithm is initialized at approximately 5.0 km. It will remain in initialized and in standby until the detection can produce the needed resolution. Extrapolating from the next generation ALHAT system [Amzajerjian et al., 2020] and accounting for the range reduction associated with the Venus atmosphere, the expected performance range is reduced from 3 km to 2 km. The altitude is based on the steepness of the trajectory. For a vertical descent, the altitude and range will be the same. This range will be used to define the baseline HD&A altitude. NASA LaRC and GFSC LIDAR experts are currently working to determine the best LIDAR wavelength to ensure and improve upon this capability. It would be advantageous to have hazard avoidance begin at higher altitudes and future studies should look at increasing the starting altitude to at least 9 km to allow time for a second hazard avoidance maneuver. **Figure B-96** provides a single trajectory depiction of the descent with HD&A.

Below 5 km, the HD&A will remain in standby until the 2.5 km range where the HD&A will begin to process images, provide initial assessments of the hazards and null the corrections. Prior to

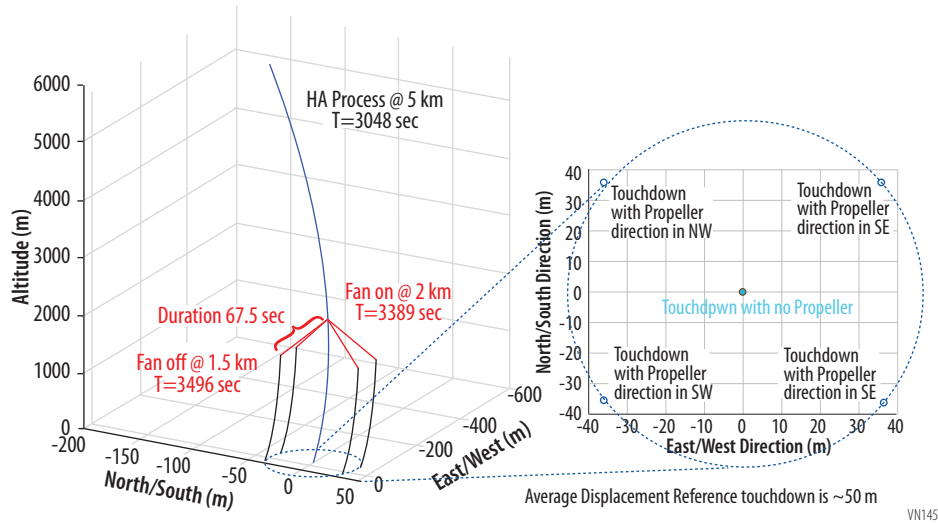
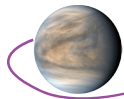


Figure B-96. Single trajectory depiction of the descent with HD&A to touchdown

the 5km range, other instrumentation will provide a local terrain map of the expected landing site. At the 2 km range, the HD&A will use the current hazard estimates and the previously determined landing site terrain map to determine the appropriate correction. Once the direction and magnitude is determined, the HD&A correction is processed and commands are sent to the actuators. As seen in **Figure B-96**, the actuation system should provide 50 m of lateral change from the nominal touchdown position. To achieve this divert distance in one maneuver, a 68 s maneuver is needed. As new information is obtained at lower altitude, an update to the maneuver can be initiated until the actuation turnoff altitude. This divert distance can be broken into two maneuvers. The HD&A can operate until the predefined cutoff altitude of 100 m.

During the mission study, a trade study was conducted to determine the appropriate actuator that would work in the Venus environment that surveyed five types of actuators, which consisted of: Control Moment Gyro, High Pressure Cold Gas Thrusters, Electronic Thrusters, Control Surface Actuation System and VTF (Venus Thrust Fan). The VTF concept was initially proposed during a GSFC MDL study. It uses a version of the motor, already developed for the Lander drill and tested in a Venus environment. Out of the five types of actuators the Control Moment Gyro, High Pressure Cold gas Thrusters and Electronic thrusters were ruled out as infeasible due to extreme Venus atmosphere temperature and pressure. Although Control Surface (i.e., wings) were not sensitive to atmosphere, they required a challenging mechanical actuation system as opposed to the VTF system which simply mounted to the landing structure and did not need any additional actuation. In terms of feasibility, the VTF system was selected for the VFM baseline control actuation system, mainly due to its relative simplicity. For the VFM, the HD&A actuators are sized based on the divert capability, the allowable size, and the power. A brief description of the sizing methodology and a divert vs fan vs power trade is discussed in the next section.

**Methodology for sizing propeller**

The concept of the VTF is a spinoff of the trolling motor for fishing boats. To reduce the impact of gas motors on lakes and reservoirs, a trolling motor, which is a self-contained electric motor with control electronics and a propeller, control electronics and propeller, is used instead of the higher horse power gas motor. The trolling motors are usually at the bow or stern. The figure (**Figure B-97**) shows the schematic of propeller.

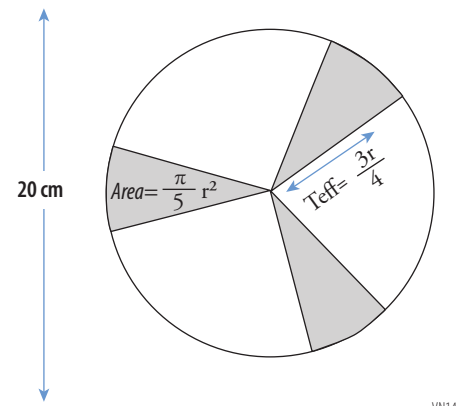
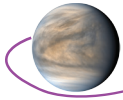


Figure B-97. VTF geometry and Size



Assuming that there are total of 2 propellers active at one time with each propeller consisting of 3 blades, one can come with expression of required angular velocity in terms of these forces. Recall that Aerodynamic lift contribution due to each blade is:

$$L = \frac{1}{2} \eta \rho C_L A_{blade} (\omega r_{blade})^2$$

- Where  $L$  = Aerodynamic Lift
- $\rho$  = atmospheric density
- $A_{blade}$  = area of the blade
- $C_L$  = Coefficient of Lift
- $\omega r_{blade}$  = Velocity of the blade at  $r_{blade}$
- $r_{blade}$  = Radius of blade
- $\omega$  = Velocity of blade

Hence, Aerodynamic contribution due to single Fan is

$$\frac{F_{prop}}{2} = \frac{1}{2} \rho C_L A_{blade} (\omega r_{blade})^2$$

- Where  $F_{prop}$  = Force of a single propeller
- $r_{blade}$  = Radius of blade

Equation above can be solve for  $\omega$ , and we get

$$\omega = \sqrt{\frac{F_{prop}}{\eta \rho C_L A_{blade} r_{blade}^2}}$$

With assumption that  $C_L = 1.2$ , minimum drag ( $\rho$ ) of  $64 \text{ kg/m}^3$ , efficiency of 70% and  $r_{blade} = 3r/4$ . Furthermore, torque required to keep motor running at constant speed is  $\sim 25 \text{ mNM}$ , which can be computed using the following equation:

$$P = \tau \omega$$

- Where  $P$  = Power
- $\tau$  = torque

Utilizing the equations described above and engineering judgment, the following trade study plots were generated to illustrate the trade space and provide options to the proposer for the VTF actuators. **Figure B-98** looks at the motor size vs the required power.

Assumes a displacement of 50 m and compares the motor size vs power. The result is that a larger motor will result in lower required power to achieve the 50 m divert maneuver. The next three plots (**Figure B-99**) show the effect of the blade.

The plots above allow the user flexibility in sizing the VTF to meet the requirements and constraints associated with power, mass, and size. The baseline for this study is a 20 cm propeller.

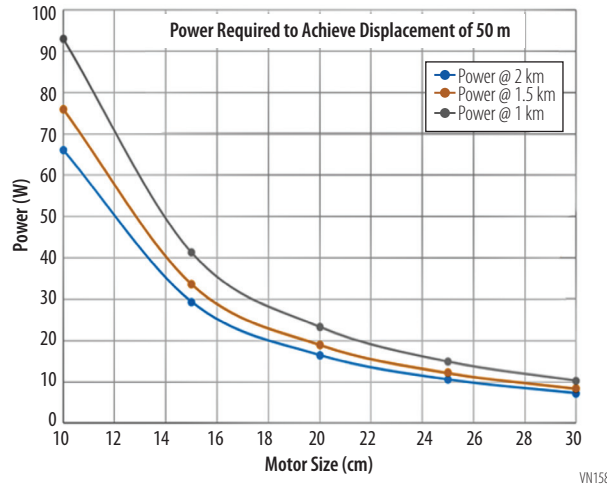
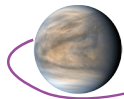


Figure B-98. Required Power

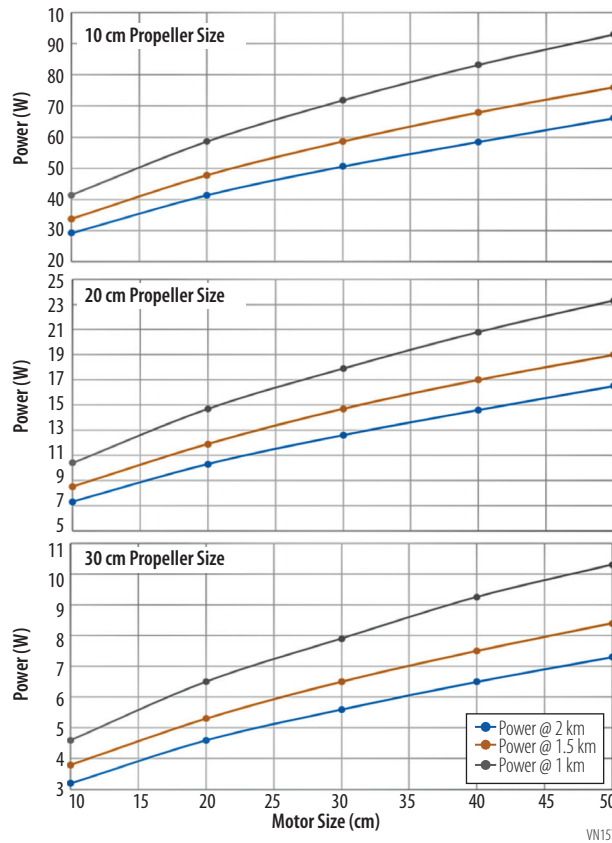
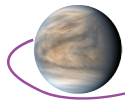


Figure B-99. (Top) 10 cm Propeller size, (Middle) 20 cm Propeller size, (Bottom) 30 cm Propeller size

### B.2.8.2.5.8 TRN and HD&A Technology Maturity

The Mars Exploration Rover (MER) mission flew the JPL Descent Image Motion Estimation System (DIMES), which tracked features in descent images and fused that with information from an IMU and a RADAR altimeter to estimate terrain relative horizontal velocity as part of control logic for firing rockets to reduce horizontal velocity before touchdown.

The JPL Lander Vision System (LVS) Terrain Relative Navigation (TRN) technology is flying on Perseverance with Entry Descent and Landing (EDL) occurring on February 18th, 2021. LVS uses an *a priori* map generated from images taken on orbit to correct gross errors in EDL. It is ideal for fast dynamics to correct to a nominal ground planned trajectory and has an accuracy of ~ 40 m. With sup-



port from JPL a similar capability is in development for the Moon by Astrobotics. The LVS requires a dedicated processor with hardware acceleration and a fast, wide field of view camera.

Technology development in process for Europa landing is extending LVS and DIMES to combine landmark recognition for terrain-relative position estimation and visual feature tracking for terrain-relative velocity estimation. This work is also developing a dual-mode LIDAR to provide altimetry at high altitude and landing hazard detection at lower altitude.

There are new systems that are soon to be flown by industry and NASA. The Natural Feature Tracker (NFT) developed by Lockheed and Draper and GSFC Retina have similar capabilities to perform on-board identification of predetermined (ground) landmarks feeding into a navigation filter that enables precision targeting of a predefined ground target. This capability is best suited for slow dynamics where extreme precision and accuracy are needed (<5 m error ellipse). The drawback to this method is that it requires extensive surveying of the target from orbit first so landmarks can be properly characterized. The algorithms run on dedicated processors or on highly-capable central processors.

Current research and development includes Goddard Fellows Innovation Challenge (GFIC) work on opportunistic landmarks and James McCabe's finite set work. They are developing fully autonomous navigation algorithms using opportunistic landmarks (not pre-defined) that essentially provide dead reckoning for EDL. A current challenge in image processing is identifying the same feature over a range of lighting conditions. Possible solutions include machine learning and artificial intelligence. In addition, many techniques are being developed for lunar missions focused primarily on accelerating the image processing (i.e., extracting terrain features and correlating/comparing them to onboard maps) but also on the navigation algorithms (i.e., leveraging visual odometry to track random features rather than known features to navigate without onboard maps and avoid the time-consuming feature correspondence step).

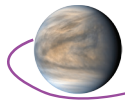
NASA projects that are currently working on TRN tech development are: SPLICE (Lunar EDL), O-rex (asteroid), Perseverance (Mars EDL). Some lunar missions are likely to require hazard detection and avoidance systems, but not all. Depending on mission requirements, some missions will need to land as close as possible to their intended target (using TRN) and at the same time avoid crashing into hazards. Other missions might be able to land 'close enough' to the target and focus on avoiding hazards at the last minute. The ALHAT project in 2014 tested a hazard detection & avoidance system onboard the experimental Morpheus Lander at KSC. For ALHAT, a Flash LIDAR developed at LaRC was used on a gimbal. The gimbal pointed the LIDAR to the ground in a mosaic-like pattern with a pre-designed overlap between range images. The range images were then stitched together to form a larger DEM of the area surrounding the landing site at 10 cm/pixel. Once this DEM was created, the hazard-relative navigation phase began by taking single flash range images every second matching each image to the main DEM to correct the vehicle's estimated position. Some missions/companies might adopt this ALHAT LIDAR and concept in the future. The SPLICE project is currently developing a different Hazard Detection LIDAR at GSFC (code 600) for hazard detection at an altitude of about 500 m and 5 cm/pixel resolution for a circular area of about 100 m in diameter. However, the SPLICE project is not currently planning on a hazard relative navigation phase, so any divert maneuvers will be performed based on the single DEM created with the HD LIDAR at the start of the terminal descent phase. The flight conditions at the time of the LIDAR scan are going to be a challenging systems engineering problem when optimizing the trajectory and sensor pointing needs for both TRN and HD.

NASA projects have partnered with Draper, Lockheed Martin, and Blue Origin to develop TRN/HD systems as well as specific CLPS providers so the state-of-the-art is a combination of all these parties with the additional novel algorithm development that is ongoing in several NASA Centers and academia (and private company partnerships).

## **B.2.8.2.6 Lander Avionics**

### **B.2.8.2.6.1 Overview**

The avionics for the Venus Lander portion of the mission is a single-string system because of the mission duration (eight hours) and because of the extreme mass, volume, and power restrictions of the Lander. The avionics consists of the following functions: Command and Data Handling (C&DH), attitude control sensors, power distribution, mechanisms for launch locks, deployments and motors, and control of main engine propulsion and Attitude Control System (ACS). The avionics implementation



consists of two enclosures, the C&DH Unit and the Mechanism, and the Propulsion Unit (MPU). All units are single-string.

The functions of the C&DH portion of the avionics performs basic command and control of the Lander including Entry, Descent and Landing (EDL) to the venusian surface. This phase is the highest risk phase because a fault of some portions of the system during this phase may result in a destruction of the Lander. Because of the short duration of the EDL phase of the mission and therefore the low probability for a fault in the portions of the system that could end the mission, the avionics is designed to fly-through any fault.

The C&DH is comprised of a low-power processor based upon the VORAGO ARM Cortex-M4, the processor chip has a power of less than 1W (the board peripherals are about 3W additional), which is used for the surface (science) operation phase of the mission. This is important to reduce the power requirements and therefore mass of the primary battery. During this phase of the mission, the processor gathers science data and stores it to the Solid-State Recorder (SSR) card for transmission to the Orbiter. The processor executes stored commands and gathers telemetry during the science phase of the mission. The processor performed CCSDS AOS transfer frame generation of telemetry data and passes it to the Multi Interface Card (MIC), which has the communication interface function and performs Forward Error Correction (FEC) encoding (Reed Solomon or Turbo) and has the interface to the S-band transponder.

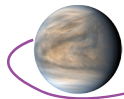
For the EDL portion of the mission, a second Single Board Computer (SBC) is used, which is based upon the High Performance Spacecraft Computing (HPSC) chip that has several ARM Cortex A53 64 bit processors or other rad hard high performance processor for the Terrain Relative Navigation (TRN) processing. This SBC is higher power and, therefore, only used during the EDL portion of the mission. After landing, it is powered down. Terrain Relative Navigation and Hazard Avoidance processor card uses parts that are readily available, except for the HPSC chip and the overall board design. This has flown on Perseverance and is TRL 7.

The MIC has the interface to the instruments, which are many low data rate (10s of kbits/sec average) and some high-rate several Mbit/s instruments, these include various different mass spectrometers, a nephelometer, various mineralogy instruments and cameras. The C&DH has the ability to handle the typical spacecraft interfaces such as RS-422 UART interface, I2C, LVDS interfaces, SpaceWire and Mil-Std 1553B. The lowest power option is RS-422 UART option so this will probably be the solution unless there is a heritage instrument that dictates a different solution. The instrument interfaces reside on the MIC along with the communication interface. The MIC board also has the GN&C sensor interfaces such as sun sensors, IMU, accelerometers, star tracker, etc., as well as Mil-Std 1553B, I2C, RS-422 or SpaceWire data interface for other avionic units.

#### **B.2.8.2.6.2 C&DH Unit**

The functions of the C&DH portion of the avionics performs basic command and control of the Orbiter. The C&DH implements the VORAGO ARM Cortex-M4 processor. The processor runs the flight software to command GN&C effectors based upon the GN&C sensors and algorithms, the power distribution switches to various spacecraft loads. The Lander runs on a scheduled timeline uploaded in advance to perform autonomous operations. The processor works as the file manager for the memory on the MIC that stores the packets from the Lander for reliable forwarding to the Orbiter, i.e., DTN bundle protocol operations for reliable communication. The functions of the various cards in the C&DH system are internally redundant. Note: for the EDL portion of the mission, both processors are running VORAGO Arm Cortex-M4 and the HPSC for the TRN.

The MIC is a multi-function card. It has the high-speed interfaces, Mil-Std 1553B interface as well as RS-422 interfaces to support the nominal interfaces found on a spacecraft. It also has the communication functions (transfer frame FEC encoding, hardware command decoding and execution as well as the transponder interface and transmitter interface for the different RF bands); GN&C interfaces for sun sensors and IMU; and non-volatile memory of 50 GBytes to serve as the SSR (need update on memory size requirement). The MIC also has the Mission Elapsed Timer (MET) and provides the One Pulse Per Second interface (1 PPS) to spacecraft subsystems as well. The Analog Telemetry Card (ATC) has the analog digital converter (ADC) and analog multiplexers to gather temperature and other analog telemetry for the spacecraft. The Analog Telemetry Card (ATC) has the analog digital converter (ADC) and analog multiplexers to gather temperature and other analog telemetry for the spacecraft.



The power switch function uses three Generic Switch Module (GSM) cards. Lastly, the C&DH enclosure has the Low Voltage Power Supply (LVPS) to power the cards in the C&DH.

### B.2.8.2.6.3 Mechanism, and Propulsion Unit (MPU)

The MPU has functions for mechanisms, which include the launch locks, motors and propulsion valve drive. Pressure sensor telemetry goes to the C&DH Unit. All cards have I2C interfaces. The Motor Controller Card (MCC) has the H-bridge circuits and the relays to control 3 phase stepper motors. Each MCC has the ability to drive four motors. Currently one MCC is baselined for antenna and solar array gimbals. Two MCCs are baselined. The Mechanism Release Card (MRC) has the ability to control eight mechanisms switching both high and low side with an arm switch. Two MRC are currently baselined. The Propulsion Drive Card (PDC) has the ability to control eight valves switching both high and low side with an arm switch. Three PDC is currently baselined. Lastly, the MPU has a LVPS card to provide secondary voltages to the MPU cards.

### B.2.8.2.6.4 Concept of Operations

The EDL operation uses a high performance processor during this phase for Terrain Relevant Navigation (TRN) and Hazard Avoidance along with the low power C&DH processor. After landing, the high performance processor is powered down and a low powered processor is used for Venus surface operations (science operation). The data can be stored if necessary (if the Orbiter or SmallSat communication relay is not available) but the mission is designed to handle direct contact during most of the Lander operation.

### B.2.8.2.7 Lander Power

The Lander power system consists of a primary (non-rechargeable) battery and supporting power electronics. The power system configuration is driven by lack of any usable solar flux at the Venus surface yielding no way to generate power to support loads or recharge a secondary battery. Saft LSH20 D 13000mAh 3.6V Lithium-Thionyl Chloride cells are used in a 9 series 9 parallel (9s9p) configuration to provide 200 AH of energy at 32V. The Power System Electronics (PSE) will be a heritage 28VDC battery dominated bus included as cards in the avionics package. The PSE will control switching and power distribution. The Lander battery PSE, 28VDC battery-dominated bus, and harness are all TRL 7.

### B.2.8.2.8 Lander Thermal

#### B.2.8.2.8.1 Thermal Overview

The Lander descends through a progressively hot, high pressure atmosphere, to land on a surface where the temperature approaches +445°C. While on the surface, it needs to survive up to 7 hours for science operations.

During descent, the atmosphere gets progressively denser (and hotter). Heat transfer coefficients can be calculated from the Reynolds Number (based on atmospheric thermal properties and descent velocities. **Figure B-100** and **Figure B-101** shows a plot of temperature and heat transfer coefficients.

A summary of the Lander's Thermal Design is shown below:

- The sphere is painted white with Z93C55 Conductive Coating.
  - Sphere will stay at -25°C in orbit around Venus before descent.
- Temperatures will steadily increase as it descends into the Atmosphere.
- Phase Change Material (+37°C) used within the Decks to flatten temperature ramp.
  - 76kg of n-Eiocene (C<sub>20</sub>H<sub>42</sub>) wax.

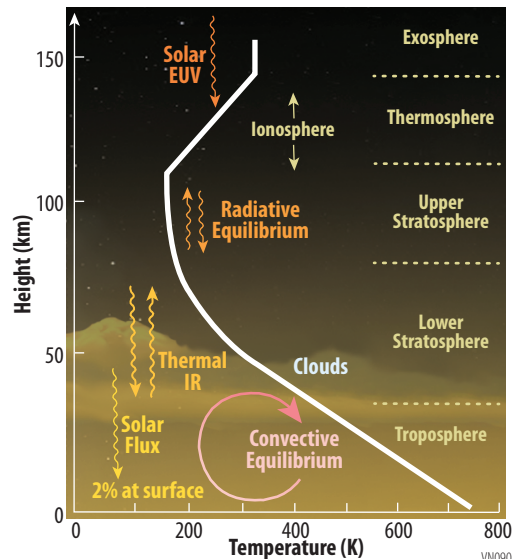
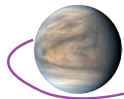


Figure B-100. Venus Temperature vs. Altitude. After Taylor [2014].





- Decks thermally isolated from sphere with a titanium flexure ring.
- All avionics and instruments thermally coupled to the 2 decks.
- Low emissivity coating put on double-pane sapphire windows.
  - Reduce heating onto instrument optics.
  - Assumed emissivity of 0.15 on both sides of inner window.
- Sphere evacuated to high-vacuum conditions.
  - Reduce convective heat transfer.
  - Allow effective MLI blanketing.
  - Zeolite used to keep high-vacuum during outgassing.
- **MLI blanketing**
  - High-temperature MLI blanketing put on inner walls of sphere.
  - “Standard” Kapton MLI put on decks.

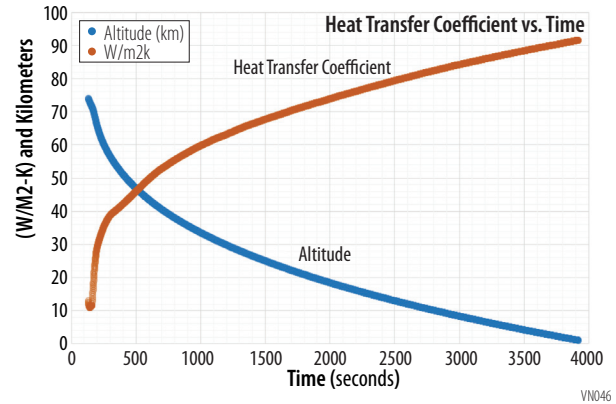


Figure B-101. Heat Transfer Coefficient during Descent

A thermal model of the Lander is shown in **Figure B-102**. It consists of two aluminum decks, packed with Phase Change Material (PCM) which melts at +37°C. The two decks are thermally isolated from the titanium Lander sphere walls by low conductance titanium flexures, as well as MLI blanketing. The sphere internal volume remains at high vacuum ( $10^{-6}$  torr) in order to eliminate convective heating.

### B.2.8.2.8.2 Concept of Operations

The Lander is painted white in order to keep the sphere cold (but above survival limits) during the orbits around Venus prior to descent (limit solar heating), but cold-biased so that it increases science time while on the Venus surface.

As the Lander descends through the atmosphere, the sphere walls heat up due to convective (and radiative) heating. **Figure B-103** shows the temperature of the outer sphere walls during descent.

While on the surface, the temperatures of the instruments located on the two decks continue to warm up due to electronics power being dissipated as well as conduction/radiation from the sphere walls.

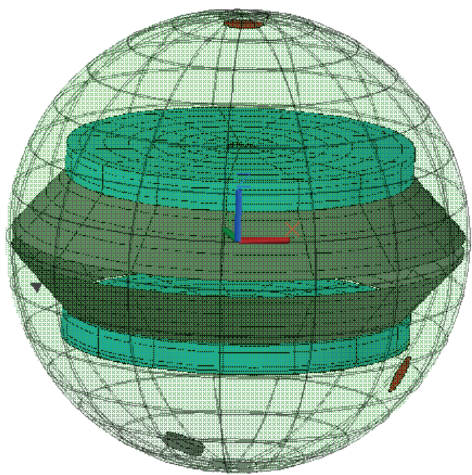


Figure B-102. Lander Thermal Model

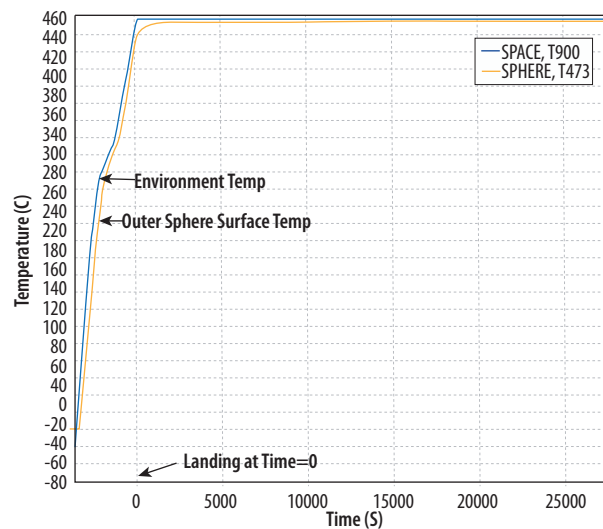


Figure B-103. Sphere Temperature during Descent and Surface Ops

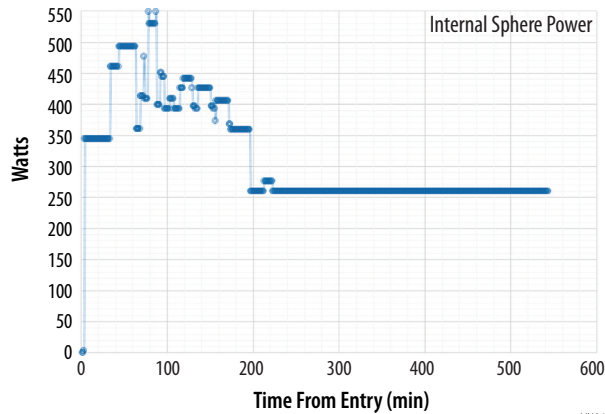
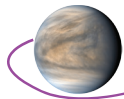


Figure B-104. Internal Sphere Power dissipation

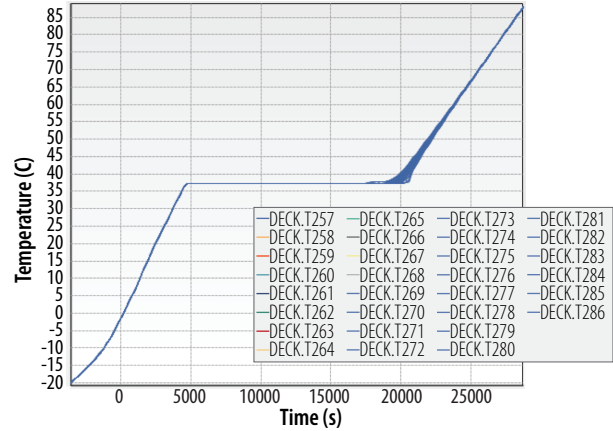


Figure B-105. Deck Temperature during Descent and Surface Ops

Figure B-104 shows the power being dissipated by the deck-mounted instruments and the avionics as a function of time. And Figure B-105 shows the temperature of the decks as a function of time. Once the PCM melts, the temperature of the electronics continue to increase until the mission ends.

As shown in the plots, the PCM keeps the electronics at +37°C until about 5.8 hours after landing (6.8 hours from the start of descent). After that the temperatures increase steadily, but still remain below +65°C until almost 7 hours after landing. Figure B-106 shows the temperature of a double-pane sapphire window. If the inner window's temperature is too high for instruments, a triple-pane window can be used. All thermal hardware has a high TRL level. MLI, whether high temperature or standard temperature, has been used on many spaceflight programs as has the white coating. Phase-change material has been used at GSFC as recently as the NICER program and is used elsewhere in the space industry.

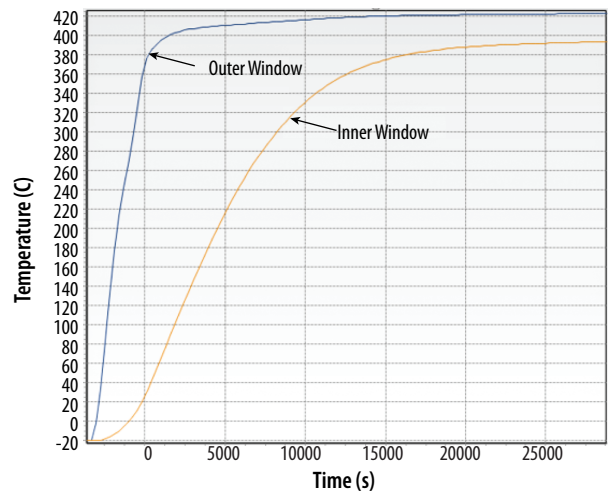


Figure B-106. Sapphire Window Temperature during Descent and Surface Ops

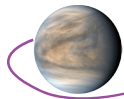
### B.2.8.3 Orbiter

The VFM Orbiter functions as a carrier and propulsion system for the other mission platforms, communication relay for the Lander and Aerobot and a science platform. The instruments on the Orbiter include a SAR, NIR-I, S-mm, Mag, two ESA-i, two ESA-e, and the two NMS.

#### B.2.8.3.1 Instrument Accommodations

The NIR-I instrument has a wide FOV of 45° perpendicular to the spacecraft velocity vector and its boresight is pointed at nadir. The S-mm instrument includes its own scan mirror which is used to scan the FOV across different tangent altitudes at the limb of the planet, and also to view space views (for calibration) and nadir views (for deep sounding). It is mounted on a turntable to provide the ability to look at the limb in both along-track and cross-track directions. The Mag is deployed on a 2 m boom. The two ESA-I, ESA-e, and NMSs are mounted on the + and -x panel since the latter instruments need to be in the velocity direction and twice a year the Orbiter must rotate 180° to keep the radiator pointed away from the sun.

A 5 m deployable mesh reflector antenna functions as both the SAR and the communication antenna for S-band, X-band, and Ka-band systems. The Orbiter also has two X-band omni antennas and



a medium gain X-band antenna. The 5 m antenna stows into a very compact package with enough clearance to mount it on the  $-y$  panel. The antenna is a smaller version of the 6m antenna flown in 2015 on Soil Moisture Active Passive (SMAP). The deployment system is the same as used on SMAP without the added turntable that SMAP required. The antenna is oriented to allow the SAR to observe at its viewing angle of  $45^\circ$  off nadir, perpendicular to the spacecraft velocity vector. During the mapping orbit the look angle is  $45^\circ$ . During the elliptical orbit the look angle varies from  $17^\circ$ – $45^\circ$  depending on the altitude (300–1000 km).

### B.2.8.3.2 Orbiter Instruments

#### B.2.8.3.2.1 Synthetic Aperture Radar (SAR)

To achieve our science objectives (see **STM Table 2**) we require the SAR to have the ability to image at 10 m resolution for limited areas, preferably with a wide enough swath width to allow contiguous imaging when we are in our final science orbit, which will move the equatorial ground longitude  $\sim 10$  km each orbit. In many cases we would also like to collect context imaging with a wide swath width but at an intermediate resolution ( $\sim 30$  m) to understand the areas surrounding the high-resolution swath and better enable tying the new data to the global imaging from Magellan. The SAR will operate in two modes—narrow beam (20 km swath width) and wide beam (40 km swath width). The array is shown in **Figure B-107**. **Table B-58** shows the SAR details.

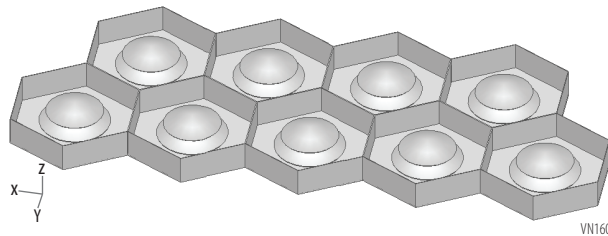
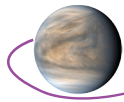


**Figure B-107.** SAR feed array consists of 9 antenna elements, arranged with two columns of 4 and 5 elements respectively, nestled side by side in a triangular grid spacing.

**Table B-58.** Synthetic Aperture RADAR (SAR) Instrument Table

Item	Value	Units
Type of instrument	SAR	
Number of feeds	9	
Size/dimensions (for each instrument)	Reflector antenna: 5.4 x 5.0 Feed Array: 0.2 x 0.5 x 0.08. Radar Electronics: .75 x .33 x .25	m x m m x m x m m x m x m
Mass without contingency (CBE*)	85	kg
Mass contingency	30	%
Mass with contingency (CBE+Reserve)	111	kg
Average payload power without contingency	73	W
Average payload power contingency	30	%
Average payload power with contingency	94	W
Operating Frequency	2.385	GHz
Chirp bandwidth		
• Narrow beam mode @ 5 m resolution	52	MHz
• Narrow beam mode @ 10 m resolution	26	
• Wide beam mode @ 30 m resolution	9	
NESZ		
• Narrow beam mode @ 5 m resolution at 300 km	-25	dB
• Narrow beam mode @ 10 m resolution at 300 km	-25	
• Wide beam mode @ 30 m resolution at 300 km	-25	
Beam Tilt	45	$^\circ$ from Nadir
Pulse repetition frequency	2900	kHz



Item	Value	Units
Duty Cycle	2	%
Polarization	Dual linear	VV, VH
Swath Width		
• Narrow beam mode @ 300 km	20	km
• Wide beam mode @ 300 km	40	km
Bandwidth		
• Narrow beam mode @ 5 m resolution	52.0	MHz
• Narrow beam mode @ 10 m resolution	26.0	MHz
• Wide beam mode @ 30 m resolution	9.0	
Average science data rate <sup>^</sup> without contingency (with onboard 8 bit to 4 bit compression)		
• Narrow beam mode @ 300 km, 5 m resolution	163	Mbps
• Narrow beam mode @ 300 km, 10 m resolution	86	Mbps
• Wide beam mode @ 300 km, 30 m resolution	53	Mbps
Average science data <sup>^</sup> rate contingency	30	%
Average science data <sup>^</sup> rate with contingency (with onboard 8 bit to 4 bit compression)		
• Narrow beam mode @ 300 km, 5 m resolution	211.9	Mbps
• Narrow beam mode @ 300 km, 10 m resolution	111.8	Mbps
• Wide beam mode @ 300 km, 30 m resolution	68.9	Mbps
Fields of View		
• Narrow beam mode @ 300 km	1.82 x 1.71	°
• Wide beam mode @ 300 km	3.65 x 1.60	°
Pointing requirements (knowledge)	0.5	Arcmin
Pointing requirements (control)	1.5	Arcmin
Pointing requirements (stability)	0.1	° over 1,000 sec

\*CBE = Current Best Estimate.

<sup>^</sup>Instrument data rate defined as science data rate prior to on-board processing

Resolution and signal-to-noise requirements from the STM can be met through varying pulse length (longer pulse duration improves resolution and increases data rate) and onboard summing of multiple looks (which decreases resolution but increases signal-to-noise).

### B.2.8.3.2.2 Near IR Imager (NIR-I)

The NIR-I is a multispectral pushbroom imager with 14 different spectral filters spanning a spectral range from 0.7–1.5  $\mu\text{m}$ . Six filters are centered on atmospheric spectral windows in which surface emission is detected. The other spectral filters measure cloud properties, water abundance, air glow and stray light. The instrument has a wide field of view ( $45^\circ$ ), optimized for an orbiter in low Venus orbit. NIR-I is designed to operate at all times when the following conditions are met: the boresight is pointed at nadir (or within  $20^\circ$  of nadir), its target is on the nightside of Venus and its FOV is perpendicular to the spacecraft velocity vector (to enable pushbroom imaging). The STM and associated text shows that successful evaluation of rock type from orbit requires a multiband imager over a wavelength range that spans the atmospheric near-infrared spectral windows. The imager needs to have enough channels to cover each of the windows and the additional channels necessary to remove atmospheric contamination and stray light from the surface-imaging channels. Between the field of view and the detector's pixel dimensions, the camera needs to image the surface with fine enough sampling to achieve the scattering-limited 100 km resolution of the surface. Through a combination of multiple looks and the dynamic range of the detector, the imaging needs to achieve adequate SNR to evaluate surface emissivity with an accuracy and precision of better than 3%. If it is not possible to operate continuously, NIR-I should operate in blocks of at least 5 consecutive orbits as the overlapping fields of view of the pushbroom imager are crucial to disentangle the effects of surface emissions from those associated with cloud variability. The strawman NIR mapper instrument used for VFM is the Venus Emissivity mapper as designed for VERITAS and EnVision orbiters.

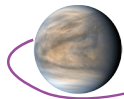


**Table B-59.** Near IR imager (NIR-I) Instrument Table

Item	Value	Units
Type of instrument	Near IR imager	
Number of channels	14	
Size/dimensions (for each instrument)	600 x 220 x 210	mm x mm x mm
Instrument mass without contingency (CBE*)	3.4	kg
Instrument mass contingency	30	%
600Instrument mass with contingency (CBE+Reserve)	4.42	kg
Instrument average payload power without contingency	13	W
Instrument average payload power contingency	30	%
Instrument average payload power with contingency	16.9	W
Instrument average science data rate <sup>^</sup> without contingency	115.74	kbps
Instrument average science data <sup>^</sup> rate contingency	30	%
Instrument average science data <sup>^</sup> rate with contingency	150.46	kbps
Instrument Fields of View (if appropriate)	45 x 2.3	°
Pointing requirements (knowledge)	1	arcmin
Pointing requirements (control)	10	arcmin
Pointing requirements (stability)	0.02	°/sec

\*CBE = Current Best Estimate.

<sup>^</sup>Instrument data rate defined as science data rate prior to on-board processing

### B.2.8.3.2.3 Sub-MM Spectrometer (S-mm)

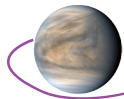
The **S-mm** instrument measures trace gas abundances, temperature structure and winds. The instrument is required to measure spectra in the wavelength ranges around 520  $\mu\text{m}$  (530 GHz–625 GHz) and 250  $\mu\text{m}$  (1080–1275 GHz) with a spectral resolution of  $10^7$ . It will primarily view the atmospheric limb of the planet, measuring temperatures, trace gas species abundances, and line-of-sight Doppler wind velocities at altitudes of ~70 to 140 km. Target species to be measured include CO and H<sub>2</sub>O isotopologues, ClO, HCl, H<sub>2</sub>SO<sub>4</sub>, O<sub>2</sub>, O<sub>3</sub>, NO, OCS, SO, and SO<sub>2</sub>. Vertical resolution is 1.5–3 km at the limb of Venus, from the final circular mapping orbit. The JUICE/SWI instrument used as the baseline for this flagship study is currently at TRL 8; its flight model is undergoing final calibration at time of writing in preparation for launch to Jupiter in May 2020. Some redesign for the Venus environment may be necessary, in particular to enable operation at the high solar fluxes found in Venus orbit (JUICE/SWI was designed to survive a Venus flyby, during which it will be exposed to Venus sunlight, but it was not designed for scientific observation in these conditions). The SWI instrument has a radiator, which may need redesign for use on the VFM platform. There are also heterodyne

**Table B-60.** Sub-mm spectrometer Instrument Table

Item	Value	Units
Type of instrument	Sub-mm spectrometer	
Number of channels	2	
Size/dimensions (for each instrument)	500 x 300 x 300	mm x mm x mm
Instrument mass <b>without</b> contingency (CBE*)	19.3	kg
Instrument mass contingency	30	%
Instrument mass <b>with</b> contingency (CBE+Reserve)	25.09	kg
Instrument average payload power <b>without</b> contingency	55	W
Instrument average payload power contingency	30	%
Instrument average payload power <b>with</b> contingency	71.5	W
Instrument average science data rate <sup>^</sup> <b>without</b> contingency	80	kbps
Instrument average science data <sup>^</sup> rate contingency	30	%
Instrument average science data <sup>^</sup> rate <b>with</b> contingency	104	kbps
Instrument Fields of View (if appropriate)	0.05 x 0.05	°
Pointing requirements (knowledge)	10	arcmin
Pointing requirements (control)	10	arcmin
Pointing requirements (stability)	0.01	°/sec

\*CBE = Current Best Estimate.

<sup>^</sup>Instrument data rate defined as science data rate prior to on-board processing



instrument developments in the USA, e.g., MATISSE development by G. Chattopadhyay (JPL). Although currently at lower TRL, their CMOS all-digital back-end may yield significantly lower mass and power requirements.

#### B.2.8.3.2.4 Magnetometer (Mag)

**Mag** is an instrument capable of measuring the magnetic field of Venus. The instrument is part of the payload for four of the five Venus Flagship Mission assets—the Aerobot, Orbiter, and the two SmallSats. The instrument must be magnetically clean and requires a >1 meter boom with 32 Hz sampling and a resolution of  $\pm 5$  nT. The fluxgate magnetometer data will be used to characterize the magnetic field topology and strength as well as search for evidence of a past or current magnetic field. These data, in concert with other instruments aboard the five assets will aid in the understanding the history of the liquid water and volatiles on Venus. The instrumentation used as a baseline for this mission study is currently at TRL 9 and has heritage on three flight missions—MAVEN, Parker Solar Probe, and Juno.

**Table B-61.** Magnetometer (MAG) Instrument Table

Item	Value	Units
Type of instrument	Magnetometer	
Number of channels	N/A	
Size/dimensions (for each instrument)	127 x 76 x 91	mm x mm x mm
Instrument mass <b>without</b> contingency (CBE*)	1	kg
Instrument mass contingency	30	%
Instrument mass <b>with</b> contingency (CBE+Reserve)	1.3	kg
Instrument average payload power <b>without</b> contingency	1	W
Instrument average payload power contingency	30	%
Instrument average payload power <b>with</b> contingency	1.3	W
Instrument average science data rate <sup>^</sup> <b>without</b> contingency	4.63	kbps
Instrument average science data <sup>^</sup> rate contingency	30	%
Instrument average science data <sup>^</sup> rate <b>with</b> contingency	6.02	kbps
Instrument Fields of View (if appropriate)	N/A	°
Pointing requirements (knowledge)	N/A	arcmin
Pointing requirements (control)	N/A	arcmin
Pointing requirements (stability)	N/A	°/sec

\*CBE = Current Best Estimate.

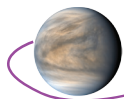
<sup>^</sup>Instrument data rate defined as science data rate prior to on-board processing

#### B.2.8.3.2.5 The Ion Electrostatic Analyzer (ESA-i)

**ESA-i** is an instrument capable of measuring *in situ* escaping Venus atmospheric ions and solar wind ions. This instrument is part of the payload for three of the five Venus Flagship Mission assets—the SmallSats and the Orbiter. The **ESA-i** is required to study how ions are accelerated from rest; to measure minor species escape rates; to measure precipitating ion flux (sputtering), and to measure the solar wind. Collecting these data will aid in understanding the history of volatiles and liquid water on Venus and determining if Venus was habitable and if Venus once hosted liquid water on its surface. The instrumentation used as a baseline for this mission study is currently at TRL 6 and has heritage on two flight missions—MAVEN and Solar Parker Probe.

**Table B-62.** Ion Electrostatic Analyzer Instrument Table (ESA-i)

Item	Value	Units
Type of instrument	Ion Electrostatic Analyzer	
Number of channels	N/A	
Size/dimensions (for each instrument)	240 x 170 x 150	mm x mm x mm
Instrument mass <b>without</b> contingency (CBE*)	3.2	kg
Instrument mass contingency	30	%
Instrument mass <b>with</b> contingency (CBE+Reserve)	4.16	kg
Instrument average payload power <b>without</b> contingency	3.7	W



Item	Value	Units
Instrument average payload power contingency	30	%
Instrument average payload power <b>with</b> contingency	4.81	W
Instrument average science data rate <sup>^</sup> <b>without</b> contingency	34.6	kbps
Instrument average science data <sup>^</sup> rate contingency	30	%
Instrument average science data <sup>^</sup> rate <b>with</b> contingency	44.98	kbps
Instrument Fields of View (if appropriate)	260 x 90	°
Pointing requirements (knowledge)	N/A	arcmin
Pointing requirements (control)	N/A	arcmin
Pointing requirements (stability)	N/A	°/sec

\*CBE = Current Best Estimate.

<sup>^</sup>Instrument data rate defined as science data rate prior to on-board processing

### B.2.8.3.2.6 The Electron Electrostatic Analyzer (ESA-e)

**ESA-e** is an instrument capable of measuring *in situ* solar wind electrons and photoelectrons. This instrument is part of the payload for three of the five Venus Flagship Mission assets—two SmallSats and the Orbiter. The **ESA-e** is required to measure *in situ* the solar wind electrons and photoelectrons to characterize the solar winds and the magnetic field topology and strength. The collection of these data will aid in the search for evidence of a current or past magnetic field and assist in determining the atmospheric escape rates over a full solar cycle. These data, in turn, will aid in understanding the history of volatiles and liquid water on Venus and determining if Venus was habitable and if Venus once hosted liquid water on its surface. The instrumentation used as a baseline for this mission is currently at TRL 7 and has heritage on two flight missions—Themis and Solar Parker Probe.

**Table B-63.** Electron Electrostatic Analyzer Instrument Table (ESA-e)

Item	Value	Units
Type of instrument	Electron Electrostatic Analyzer	
Number of channels	N/A	
Size/dimensions (for each instrument)	160 x 190 x 150	mm x mm x mm
Instrument mass <b>without</b> contingency (CBE*)	2.2	kg
Instrument mass contingency	30	%
Instrument mass <b>with</b> contingency (CBE+Reserve)	2.86	kg
Instrument average payload power <b>without</b> contingency	2.1	W
Instrument average payload power contingency	30	%
Instrument average payload power <b>with</b> contingency	2.73	W
Instrument average science data rate <sup>^</sup> <b>without</b> contingency	4.39	kbps
Instrument average science data <sup>^</sup> rate contingency	30	%
Instrument average science data <sup>^</sup> rate <b>with</b> contingency	5.71	kbps
Instrument Fields of View (if appropriate)	360 x 120	°
Pointing requirements (knowledge)	N/A	arcmin
Pointing requirements (control)	N/A	arcmin
Pointing requirements (stability)	N/A	°/sec

\*CBE = Current Best Estimate.

<sup>^</sup>Instrument data rate defined as science data rate prior to on-board processing

### B.2.8.3.2.7 The Neutral Mass Spectrometer (NMS)

**NMS** is an instrument capable of measuring *in situ* the neutral constituents that are the source of ion escape. This instrument is part of the payload for the Orbiter. The **NMS** is required to measure neutrals from 2–150 Daltons throughout the polar elliptical orbit; during aerobraking, which would secure excellent upper atmosphere data; and, finally, in the circular science orbit. The instrument levies the requirement of RAM pointing, which necessitates the use of two because of the required rotation of the s/c. The measurements from the **NMS**, in concert with instruments on the Small Satellites and the orbiter will characterize ion escape which will aid in the determination of the Venus atmospheric escape rates over a full solar cycle. It will also measure the atmospheric species as a function of the aero-

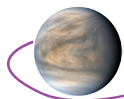


**Table B-64.** Neutral Mass Spectrometer (NMS) Instrument Table

Item	Value	Units
Type of instrument	Neutral Mass Spectrometer (NMS)	
Number of channels	150	Daltons
Size/dimensions (for each instrument)	414 x 396 x 218	mm x mm x mm
Instrument mass <b>without</b> contingency (CBE*)	14	kg
Instrument mass contingency	30	%
Instrument mass <b>with</b> contingency (CBE+Reserve)	18.2	kg
Instrument average payload power <b>without</b> contingency	1.2	W
Instrument average payload power contingency	30	%
Instrument average payload power <b>with</b> contingency	1.56	W
Instrument average science data rate <sup>^</sup> <b>without</b> contingency	4.64	kbps
Instrument average science data <sup>^</sup> rate contingency	30	%
Instrument average science data <sup>^</sup> rate <b>with</b> contingency	6.03	kbps
Instrument Fields of View (if appropriate)	RAM Direction	
Pointing requirements (knowledge)	N/A	arcmin
Pointing requirements (control)	N/A	arcmin
Pointing requirements (stability)	N/A	°/sec

\*CBE = Current Best Estimate.

<sup>^</sup>Instrument data rate defined as science data rate prior to on-board processing

braking maneuver. The instrumentation used as a baseline for this mission study is currently at TRL 8 and has heritage on one flight mission—MAVEN.

### B.2.8.3.3 Orbiter Structure

The Orbiter structural design was driven by carrying the launch loads of the other mission platforms through to the launch vehicle. The Aerobot is mounted beneath the Orbiter and inside the 3.1 m PAF used to attach to the upper stage of the Falcon 9 Heavy Expendable. The Orbiter structural radials are the transition load path from the 3.1 m interface to the launch vehicle and the central cylinder, which carries the launch loads for both the Lander and the Aerobot. The Orbiter structure was designed with composite face-sheet/aluminum honeycomb core panels using the clip and post method employed on other composite structures such as Lunar Reconnaissance Orbiter (LRO). The basic structure of a central cylinder, upper and lower deck, radials and equipment panels is very common and well understood. The dry mass efficiency of the structure is approximately 12%.

To accommodate the placement of the Aerobot under the Orbiter the main engines were moved outboard. This had the added benefit of providing significant ACS capability. The octagon design provided an efficient mount for the large oxidizer tank and the central cylinder and bays for mounting the four fuel tanks. The central cylinder is the primary support for the Lander. The Lander inside its aeroshell is attached to the top deck of the Orbiter using COTS separation rings and the SmallSats are tucked in between the Lander and the top deck of the Orbiter. The SmallSats are attached via separation rings to a vertical bracket, similar in concept to a Moog's Evolved Secondary Payload Adapter (ESPA). All structural components are well within the state-of-the-art.

### B.2.8.3.4 Orbiter Propulsion

The Orbiter propulsion subsystem is a large regulated bipropellant system. The propellant is stored in COTS tanks. The main engines are a set of four 4,000 N engines (AJ PN R-40B, see **Figure B-108**). Two redundant sets of  $2 \times 450$  N engines (AJ PN R-4D-15 HIPAT, see **Figure B-108**) are used for roll control during maneuvers. Separate



**Figure B-108.** R-40B 4,000N (left) and R-4D-15 450N (HiPAT, right) rocket engines (not to scale)



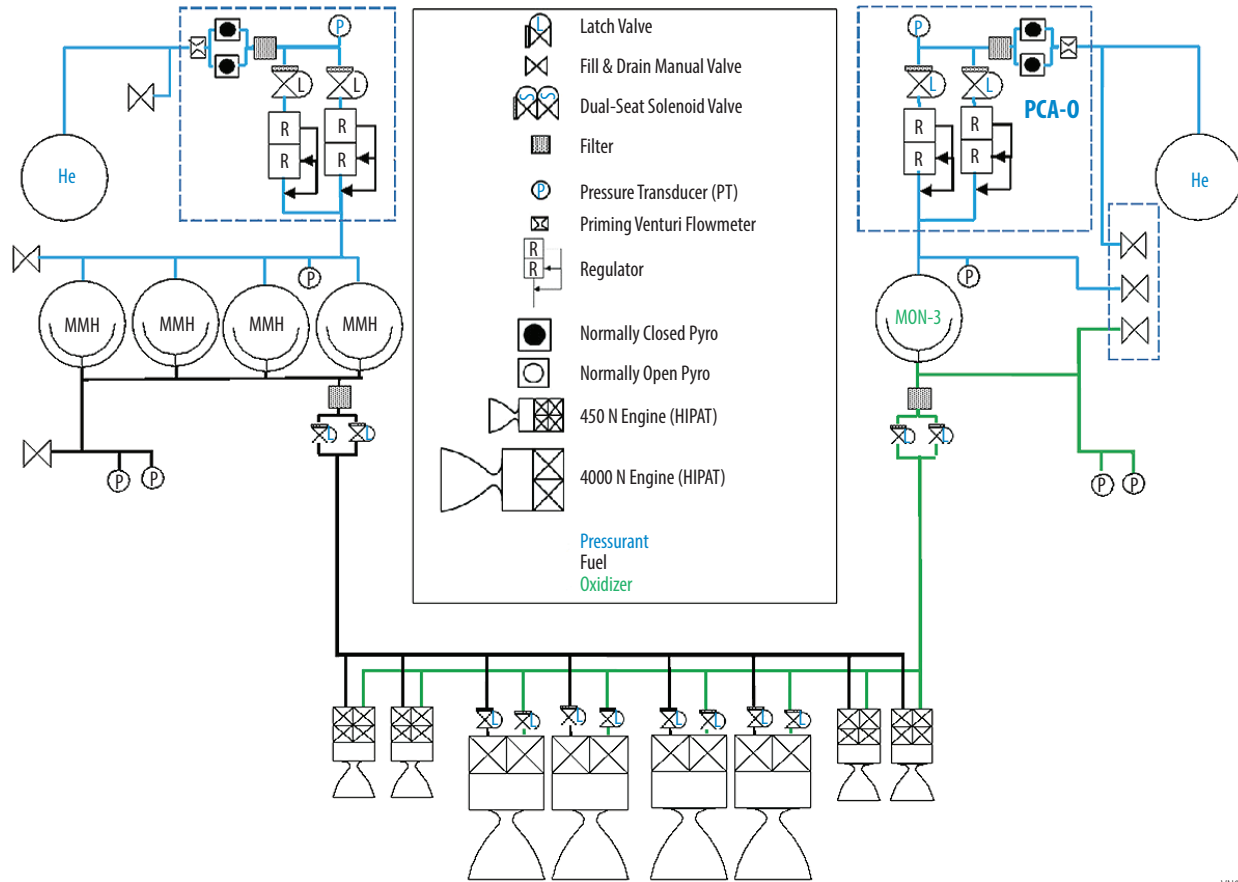
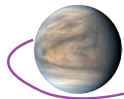


Figure B-109. Schematic of the Propulsion Subsystem

VN091

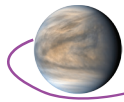
pressurization manifolds are used to provide regulated pressure to both the fuel and oxidizer tanks. All of the components are COTS.

The system is single fault tolerant. Each pressurization string is fully redundant, and there are separate strings of redundant attitude control thrusters. A schematic of the subsystem is shown in **Figure B-109**.

**Table B-65** shows the calculation of the Orbiter propellant mass. The Isp of the thruster is 293 but a knockdown value of 290 is used for margin. In addition, all propellant masses have a 10% margin

Table B-65. Orbiter Propellant

Propellant Sizing	Platforms in Mass	ΔV for each Launch Date (m/s)		ΔV Max m/s	MEV WET Mass of Orbiter (kg)	2031 Prop Mass (kg)	2031 Prop Mass with 10% margin (kg)	2032 Prop Mass (kg)	2032 Prop Mass with 10% contingency (kg)	Max Propellant Mass (kg)
		Jun. 2031	Jun. 2032							
Science Orbit Maintenance	Orbiter	0.0	0.0	0.0	1,930.2	0.0	0.0	0.0	0.0	0.0
Aerobraking Operations	Orbiter	50.0	50.0	50.0	1,930.2	37.7	41.5	37.7	41.5	37.7
Divert Maneuver after releasing Lander	Orbiter	130.0	130.0	130.0	1,930.2	99.4	109.3	99.4	109.3	99.4



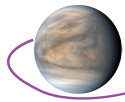
Propellant Sizing	Platforms in Mass	ΔV for each Launch Date (m/s)		ΔV Max m/s	MEV WET Mass of Orbiter (kg)	2031 Prop Mass (kg)	2031 Prop Mass with 10% margin (kg)	2032 Prop Mass (kg)	2032 Prop Mass with 10% contingency (kg)	Max Propellant Mass (kg)
		Jun. 2031	Jun. 2032							
Lander Deployment	Orbiter			0.0		0.0	0.0	0.0	0.0	0.0
Lander Entry Targeting	Orbiter plus Lander	1.7	9.8	9.8	3,932.4	2.6	2.8	14.9	16.4	14.9
Orbiter Periapsis Adjustment	Orbiter plus Lander	45.0	20.0	45.0	3,932.4	69.0	75.9	30.5	33.6	69.0
Landing site Analysis 2	Orbiter plus Lander	0.0	0.0	0.0	3,932.4	0.0	0.0	0.0	0.0	0.0
Landing Site Analysis 1	Orbiter plus Lander	0.0	0.0	0.0	3,932.4	0.0	0.0	0.0	0.0	0.0
VOI Insertion	Orbiter plus Lander	530.0	158.0	530.0	3,932.4	886.8	975.5	247.3	272.0	886.8
Orbiter VOI Targeting	Orbiter plus Lander	10.0	17.0	17.0	3,932.4	15.2	16.8	26.0	28.5	26.0
Aerobot Deployment	Orbiter plus Lander			0.0	3,932.4	0.0	0.0	0.0	0.0	0.0
Aerobot TCM for Entry	Orbiter, Lander, and Aerobot	2.0	2.0	2.0	5,365.6	4.2	4.6	4.2	4.6	4.2
Aerobot Targeting	Orbiter, Lander, and Aerobot	10.0	10.0	10.0	5,365.6	20.8	22.9	20.8	22.9	20.8
DSM	Orbiter, Lander, and Aerobot	115.0	966.0	966.0	5,365.6	243.7	268.1	2,389.3	2,628.2	2,389.3
SmallSat Deployment	Orbiter, Lander, and Aerobot			0.0	5,365.6	0.0	0.0	0.0	0.0	0.0
SmallSat Targeting	Orbiter, Lander, Aerobot and SmallSats	0.0	0.0	0.0	5,965.6	0.0	0.0	0.0	0.0	0.0
<b>Total</b>		<b>893.7 m/s</b>	<b>1,362 m/s</b>	<b>1,759.8</b>	<b>N/A</b>	<b>1,379.4</b>	<b>1,517.4</b>	<b>2,870.0</b>	<b>3,157.0</b>	<b>3,548.0</b>

added. Moreover, the propellant mass is calculated for the worst case ΔV totals of the primary and backup orbits.

The pressurant tanks are isolated by redundant pyro valves during launch. The system is pressurized during the transfer to lunar orbit insertion and a calibration maneuver is performed. All maneuvers are performed with the main engines, except for smaller orbit maintenance maneuvers. All of the components in the subsystem (**Figure B-109**) are TRL-9.

### B.2.8.3.5 Orbiter Power

The Orbiter power system consists of solar arrays, a secondary battery, and supporting power electronics. TJGaAs solar cells with bare cell efficiency of 29.5% are used. The solar constant at Venus is 2263 W/m<sup>2</sup>, and the arrays operate at 140°C. Space Environmental Effects and Education System (SPENVIS) solar array radiation factors were used to derive the array area. A single two axis tracking panel with 5.4m<sup>2</sup> active area (5.9 m<sup>2</sup> total substrate area) will provide 1,845 W of power to support loads and battery recharge. A high energy density 38AH Li Ion battery is used to support night loads. The Power System Electronics (PSE) will be a heritage 28VDC battery dominated bus included as cards in the avionics package. All Orbiter power components are greater than TRL 7.



### **B.2.8.3.6 Orbiter Avionics**

#### **B.2.8.3.6.1 Avionics Overview**

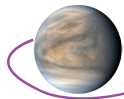
The avionics for the Orbiter are a block redundant system to meet the reliability for a Class A Flagship Mission, consisting of the following functions: Command and Data Handling (C&DH), attitude control sensors and thrusters, power conditioning and distribution, mechanisms for launch locks, deployments and motors, and control of main engine propulsion. The avionics implementation consists of three enclosures, C&DH Unit, the Power System Electronics (PSE) and the Mechanism, and Propulsion Unit (MPU). Only one block side is hot (powered) at a time and the other block side is cold (un-powered). The mechanism for switching over from one block side to the other occurs by two different mechanisms. These include autonomous switch-over or switch-over via hardware ground command. The autonomous switch-over occurs based upon missing heartbeats from a processor to the Multi-Interface Cards (MICs), which performs the decision between them. The MIC implements the hardware command decoder, Forward Error Correction (FEC) encoding of telemetry transfer frames and has the communication interface to the transponder or transmitter among other functions. See MIC description below.

The Venus Orbiter, for most of the mission, functions as a communication relay between Earth and the Lander, and the Aerobot. The Venus Orbiter utilizes a store and forward protocol called Delayed Tolerant Network (DTN), which has the ability to store packets from the Lander, and Aerobot and forward them to Earth or receive commands from Earth and forward them to the Lander and Aerobot. DTN is a protocol implemented by the C&DH system independent of the implementation of the RF system. The Orbiter receives communication from Earth and stores the data until it has line-of-sight (LOS) to the other assets at which time it transmits the data to them in a reliable manner (with acknowledgments from the assets and possible retransmissions from the Orbiter until all the data is acknowledged as being received correctly). The same happens in the reverse direction from the Venus assets to the Orbiter to Earth, where each hop in the communication is reliability transferred and stored before forwarded to the next destination until it reaches the final destination based upon communication availability, i.e., LOS. If the next hop in the communication is unavailable, delay in communication occurs until LOS is established. For the Orbiter there are only two hops (Earth to Orbiter and Orbiter to Venus platforms, and the reverse direction).

#### **B.2.8.3.6.2 C&DH Unit**

The functions of the C&DH portion of the avionics performs basic command and control of the Orbiter. The C&DH implements the RAD750 v3 processor. The processor runs the flight software to command GN&C effectors based upon the GN&C sensors and algorithms. It also gathers house-keeping telemetry and performs fault detection isolation and recovery (FDIR) autonomously. The Orbiter runs on a scheduled timeline uploaded in advance to perform autonomous operations. The spacecraft processor works as the file manager for the Solid-State Recorder (SSR) card that stores the packets from Earth and the Landers for reliable forwarding to their respective destination (Lander or Earth), i.e., DTN bundle protocol operations for reliable communication. The functions of the various cards in the C&DH system are internally redundant and are as follows:

The processor based upon the RAD750 v3 or next generation runs the flight software to control the Orbiter and has the cPCI interface to communicate with the MIC and SSR; two of each for redundancy. The MIC is a multi-function card. It has high-speed interfaces, the Mil-Std 1553B interface as well as RS-422 interfaces to support the nominal interfaces found on a spacecraft. It also has the communication functions (transfer frame FEC encoding, hardware command decoding and execution as well transponder interface and transmitter interface for the different RF bands; GN&C interfaces for a sun sensor, IMU and reaction wheels; and the non-volatile memory that may be used to supplement or replace the SSR depending upon the memory size requirements. The MIC has the Mission Elapsed Timer (MET) and provides the One Pulse Per Second interface (1 PPS) to spacecraft subsystems as well as the watch-dog timers and logic to determine block switch-over. The MIC is the only card that is powered on both sides for this reason. Both MICs communicate to help determine the switch-over condition using Triple Modular Redundant (TMR) logic. Note the LVPS is powered on both sides as well to support powering of the redundant side MIC. There are two MICs for redundancy.



The Analog Telemetry Card (ATC) has the analog digital converter (ADC) and analog multiplexers to gather temperature and other analog telemetry for the spacecraft. There are two for redundancy.

The Solid State Recorder (SSR) has the non-volatile memory (Flash) 4 TBytes of data for the DTN relay communication storage. There are two for redundancy.

Lastly, the C&DH enclosure has the Low Voltage Power Supply (LVPS) to power the cards in the C&DH and there are two for redundancy.

### B.2.8.3.6.3 Power Supply Electronics (PSE)

The functions of the Power System Electronics (PSE) portion of the avionics perform solar array current regulation for the spacecraft loads and control the battery charging, the power distribution switches to various spacecraft loads and telemetry for power system functions. Note that the PSE functions are redundant within the same enclosure. The Solar Array Regulation Module (SARM) has the Field Effect Transistors (FETS) to switch the solar array strings for current regulation. There are two SARM cards in the PSE for redundancy. The Battery Charge Module (BCM) card performs battery charge control and depending on whether there are one or two batteries determines how many BCMs are present (one per battery), although there are examples where a redundant systems use a single battery, i.e., Lucy (Discovery class mission). There are two Analog Telemetry Card (ATC) cards in the PSE, one primary and one redundant to read analog telemetry for the PSE. The power switch function uses six Generic Switch Module (GSM) cards. Three for primary side and three for redundant side. Lastly, the PSE has one house-keeping power supply, which is internally redundant.

### B.2.8.3.6.4 Mechanism, and Propulsion Unit (MPU)

The MPU has the functions for mechanisms, which include the launch locks, motors and propulsion valve drive. Please note that the pressure sensor telemetry goes to the C&DH Unit. All cards have I2C interfaces. The Motor Controller Card (MCC) has the H-bridge circuits and the relays to control 3 phase stepper motors. Each MCC has the ability to drive four motors. Currently one MCC is baselined for antenna and solar array gimbals. One MCC is baselined. The Mechanism Release Card (MRC) has the ability to control eight mechanisms switching both high and low side with an arm switch. One MRC is currently baselined. The Propulsion Drive Card (PDC) has the ability to control eight valves switching both high and low side with an arm switch. Three PDC is currently baselined. Lastly, the MPU has a LVPS card to provide secondary voltages to the MPU cards.

### B.2.8.3.7 Orbiter Communications

The Orbiter, for most of the mission, functions as a communication relay between Earth and the Lander, and Earth and the Aerobot and utilizes a store and forward protocol called Delayed Tolerant Network (DTN), which has the ability to store packets from the Lander, and Aerobot and forward them to Earth or receive commands from Earth and forward them to the Lander and Aerobot. The Venus atmosphere attenuates the S-band link as a function of elevation as shown in **Figure B-110**. For this reason a margin of at least 4dB is required at 15° elevation and 1dB at 80° elevation for Lander and Aerobot links. **Figure B-111** shows the X-Band and Ka-Band communication diagram.

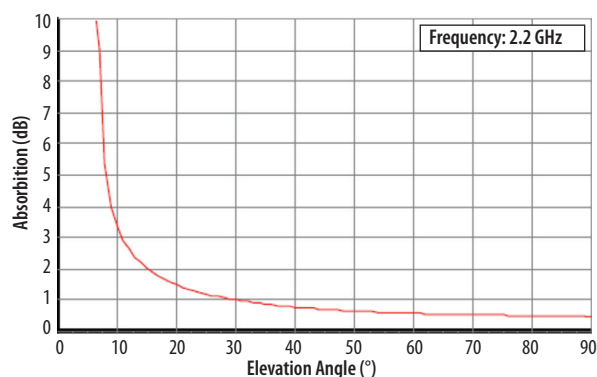


Figure B-110. S-Band Absorption in Venus Atmosphere

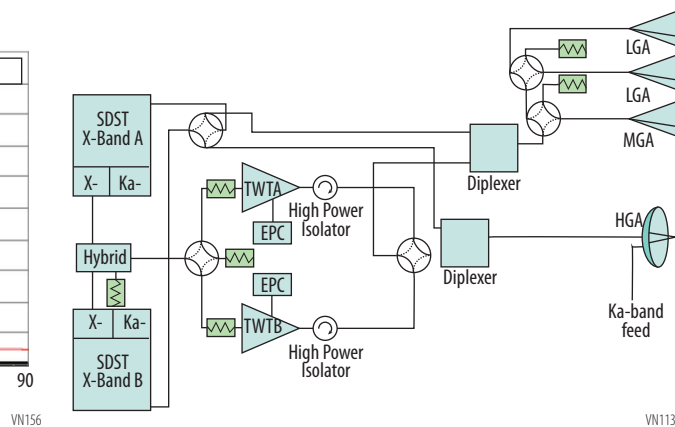
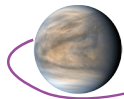


Figure B-111. Orbiter X-Band and Ka-Band Diagram



### B.2.8.3.8 Orbiter Attitude Control

The Orbiter is three-axis stabilized with significant momentum and torque capabilities to account for the large inertia associated with the stacked configuration. The Attitude Control System (ACS) must maintain control of the Orbiter during cruise, SmallSat and Aerobot separations, VOI, the elliptical polar orbit, Lander separation, the elliptical polar orbit prior to and during aerobraking, and during the final circular polar orbit. The Orbiter must point the large 5m antenna at Earth for communication, at the Aerobot, Lander and SmallSats for communication and at Venus for RADAR observations. This drives the Orbiter towards a three-axis stabilized ACS with significant momentum and torque capabilities. The requirements derived to meet the mission needs are shown in **Table B-66**.

**Table B-66.** Orbiter Attitude Control Requirements

Attitude Control	3 arcmin 3-axis 3-sigma
Attitude Knowledge	0.5 arcmin 3-axis 3-sigma

### B.2.8.3.9 Operations Concept

This section discusses the concept of operation in mission phase order. At launch the Orbiter is carrying the SmallSats, Lander, and Aerobot as depicted in **Figure B-12**. After Launch Vehicle (LV) separation, the Orbiter ACS system controls any tipoff rates and slews to a power/communication positive attitude. The solar arrays and antenna are deployed followed by the SmallSats. Then the Orbiter, carrying the Aerobot and Lander, begins its cruise to Venus. Upon arrival at Venus, the Orbiter separates the Aerobot and then performs the Venus Orbit Insertion (VOI) maneuver to place the Orbiter with Lander into the Venus elliptical polar orbit. While in orbit, the Orbiter will align its body axis with the Local Vertical Local Horizontal (LVLH) Frame.

The Orbiter acts as both a communication relay and a platform for its instruments. The Orbiter concept of operation has some flight heritage (LRO). However, the major difference between VFM and previous missions is the control of the Orbiter with Aerobot and Lander configurations and the needed control authority (significantly higher inertia/tipoff momentum, slew torques).

The Orbiter ACS block diagram is based on previous missions and shown in **Figure B-112**.

The navigation portion of the Orbiter Flight Software (FSW) is required to estimate and control the spacecraft position, which reduces the need for additional ground processing to ensure a precise Lander separation point/time. The Orbiter's ACS has five modes: Mission (nadir, and inertial point), Separation,  $\Delta V$ ,  $\Delta H$ , Sun Safe (Sun Acq, Rate Null). The new mode in this architecture is the separation mode. The other modes are based on heritage algorithms/modes. The separation mode is designed to facilitate the safe and accurate ejection of the Lander. This mode places the momentum vector in the correct direction and removes excessive separation disturbance torques with thrusters. After Lander separation, the Orbiter will perform a post-separation checkout, which includes sensor and actuator calibrations. These calibrations are used to determine scale factors for the thruster commanding.

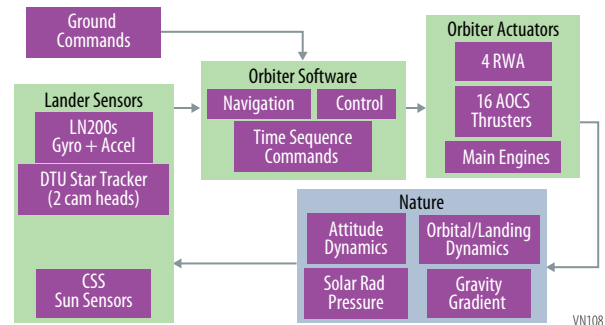
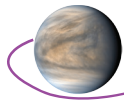


**Figure B-112.** Orbiter ACS block diagram

### B.2.8.3.10 Orbiter Thermal

The VFM Orbiter thermal design consists of radiators on the Orbiter -z surface, bottom deck to dissipate electronics heat while keeping the radiators out of the Sun (and view of the hot Venus surface). Approximately 358 watts of heat needs to be dissipated from the Instruments, Avionics, and Comm system with radiator patches on the Orbiter's bottom deck body. A toasty cavity approach eliminates propulsion system heaters on the fuel tanks and lines while orbiting Venus. Heater patches are used on the Orbiter's bottom deck and  $\sim 0.67 \text{ m}^2$  of radiator area is needed to dissipate the 358 watts (orbit average) of the Orbiter's electronics heat. Small patch radiators can be used for every box, or spreader heat pipes can be embedded in the Orbiter's lower deck to help spread heat from the deck to radiator patches. MLI blanketing is placed over the lower deck electronics to prevent heat from Sun and Venus



facing surfaces from dumping extra heat into the boxes. The thrust tube is painted black (internal and external surfaces) to radiate heat into the propulsion tanks. The internal walls of the Orbiter are painted black as well to keep the tanks warm. During cruise phase, the attached aeroshell will somewhat cover the radiators' view to space, but no enhancements to the thermal system are needed; the radiators can still dissipate the requisite cruise phase heat. White MLI blanketing covers the entire external surface of the Orbiter, except for the radiator patches, which are made up of OSR tiles.

**Figure B-113** shows the external thermal model of the Orbiter with the Aerobot attached, **Figure B-114** shows the external thermal model during aerobraking and the circular orbit, while **Figure B-115** shows the internal view of the Orbiter, including the propulsion tanks within the torque tube, as well as the 4 external to the torque tube.

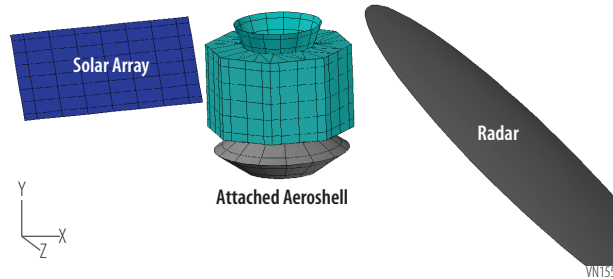


**Figure B-113.** External Thermal Model Components with Aerobot

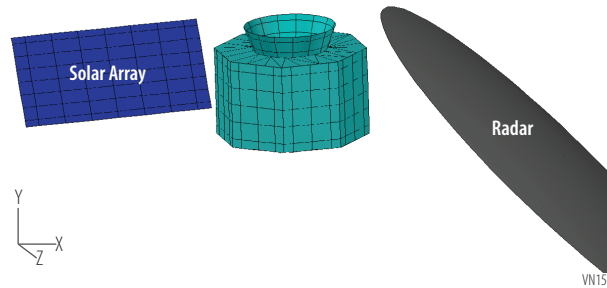


**Figure B-114.** External Thermal Model Components, Orbit Phase

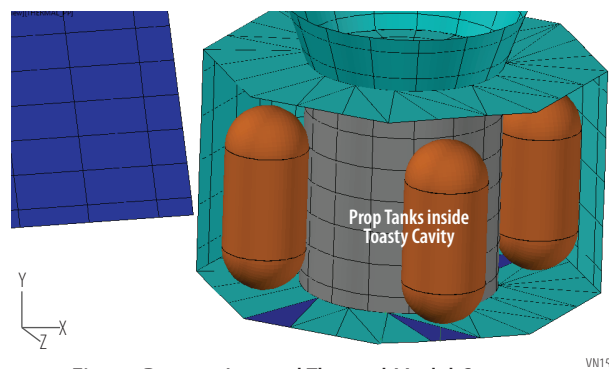


**Figure B-115.** Internal Thermal Model Components

The Orbiter must keep the electronics boxes (instruments, communication system, and avionics) below their operating temperature limits during the Venus orbits. To do this, the bottom deck (-y axis) remains parallel to the Sun at all times (beta angles 0° through 90°). The two axis solar array will rotate to keep it perpendicular to the Sun. Twice a year the Orbiter will rotate about the z-axis to keep the bottom deck pointed away from the sun. **Figure B-116**, **Figure B-117**, and **Figure B-118** show plots of the radiator temperatures as a function of time throughout the orbit. The propulsion system (tanks and lines) stay warm by sharing thermal heat from the radiators, keeping them above the hydrazine freezing point at all times. All thermal hardware has a high TRL level. It should be noted that to keep

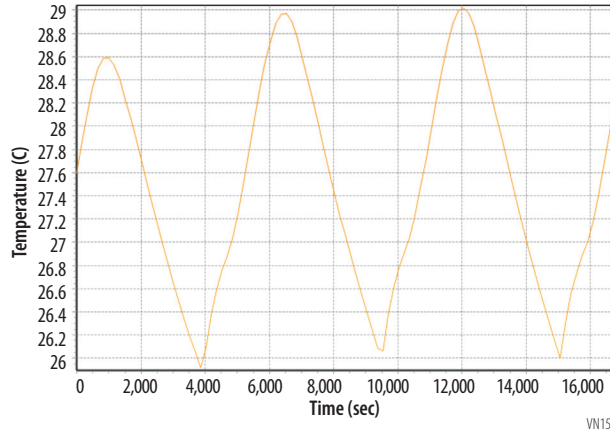
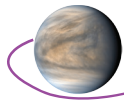


Figure B-116. Lower Deck Radiator Temperature, Beta=0° Circular Orbit

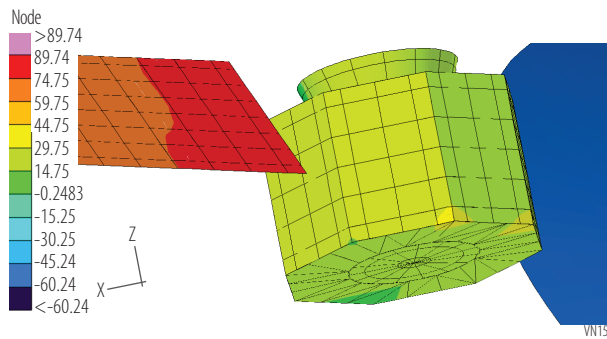


Figure B-117. Orbital Temperatures during Hot Beta=90°

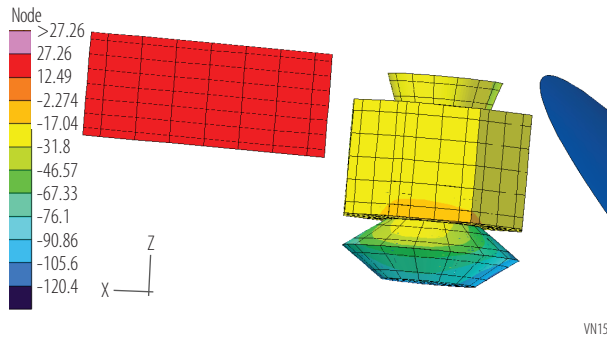


Figure B-118. Cold Biased Cruise Phase

the electronics within operating temperature range while orbiting Venus (hot-biased conditions), there needs to be 129 W of heat (electronics power + heater power) to keep the boxes above survival limits during the cold cruise phase.

### B.2.8.4 SmallSats

The Venus Flagship Mission uses two SmallSats (Figure B-119) that provide scientific data from the instruments and provide communications coverage for the Aerobot and Lander. SmallSats are at CML 2. The SmallSats are physically identical, but will be deployed in different venusian orbits: SmallSat-1’s orbit inclination is 22.5° (ICRF), and SmallSat-2’s orbit inclination is 65°. They detach from the Orbiter a few hours after launch and guide themselves to Venus, each using solar electric propulsion. After arrival at Venus they follow a low-thrust spiral down to their final Venus orbits. Besides their science requirements, the SmallSats need to provide communication access to the Aerobot and Lander. Therefore, both have to be orbiting Venus prior to the arrival of the other platforms. Details of the trajectory design for the SmallSats is shown in Section B.2.7.4. The trajectory design assumed a

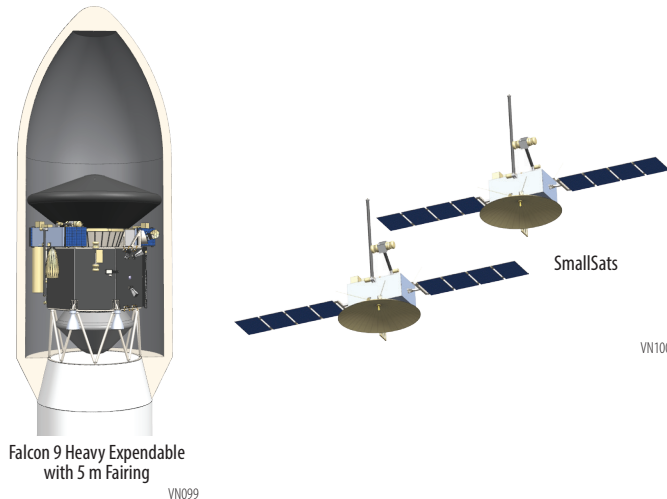
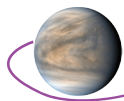


Figure B-119. SmallSats in the stowed and deployed configuration

Solar Electric Propulsion system with two (2) Engines with a thrust (N) of 0.0674 and Propellant Isp (s) of 1,750. For a CBE dry mass of 134.6 kg, 104.0 kg of fuel will be needed resulting in a total CBE launch mass of 238.6 kg which is less than the 300 kg requirement.

### B.2.8.4.1 SmallSat Overview

#### B.2.8.4.2 SmallSat Instruments (Tables follow descriptions)

The two SmallSat payloads were selected to focus on the science of understanding atmospheric evolution via the interaction of the Venus atmosphere and the solar wind. To accomplish this science goal, the payloads consist of plasma and fields instruments—**magnetometers, electrostatic analyzers, Langmuir Probe, an electric field detector, and extreme ultraviolet detectors.** This suite of instruments aboard two SmallSats provide the means to collect data simultaneously on both the day and night side as well as previously unsampled southern latitudes. A detailed description of each instrument is provided in this section.

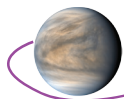
##### B.2.8.4.2.1 Langmuir Probe (LP)

The LP on each SmallSat is an instrument capable of measuring thermal ions. This instrument is part of the payload for both SmallSats. The LP is required to measure thermal ions and electrons from 0.01 eV–5 eV with 0.3 mV/m resolution and must be magnetically clean to ensure accurate measurements. The data from this instrument will aid in characterizing the ion escape rate from the Venus atmosphere over a full solar year. Collection of this data plays a crucial role in determining if Venus once hosted

Table B-67. Langmuir Probe (LP) Instrument Table

Item	Value	Units
Type of instrument	Langmuir Probe (LP)	
Number of channels	n/a	
Size/dimensions (for each instrument)	0.635 cm dia, 40 cm long	cm
Instrument mass <b>without</b> contingency (CBE*)	2.6	kg
Instrument mass contingency	30	%
Instrument mass <b>with</b> contingency (CBE+Reserve)	3.38	kg
Instrument average payload power <b>without</b> contingency	2.7	W
Instrument average payload power contingency	30	%
Instrument average payload power <b>with</b> contingency	3.51	W
Instrument average science data rate <sup>^</sup> <b>without</b> contingency	0.21	kbps
Instrument average science data <sup>^</sup> rate contingency	30	%
Instrument average science data <sup>^</sup> rate <b>with</b> contingency	0.27	kbps
Instrument Fields of View (if appropriate)	n/a	
Pointing requirements (knowledge)	n/a	





Item	Value	Units
Pointing requirements (control)	n/a	
Pointing requirements (stability)	magnetically clean	

\*CBE = Current Best Estimate.

^Instrument data rate defined as science data rate prior to on-board processing

liquid water at the surface. The instrumentation used as a baseline for this mission study is currently at TRL 7 and has heritage on a flight mission—MAVEN.

### B.2.8.4.2.2 Ion Electrostatic Analyzer (ESA-i)

The **ESA-i** is an instrument capable of measuring *in situ* escaping Venus atmospheric ions and solar wind ions. This instrument is part of the payload for three of the five Venus Flagship Mission assets—two SmallSats and the Orbiter. The **ESA-i** is required to study how ions are accelerated from rest; to measure minor species escape rates; to measure precipitating ion flux (sputtering), and to measure the solar wind. Collecting these data will aid in understanding the history of volatiles and liquid water on Venus and determining if Venus was habitable and if Venus once hosted liquid water on its surface. The instrumentation used as a baseline for this mission study is currently at TRL 6 and has heritage on two flight missions—MAVEN and Solar Parker Probe.

**Table B-68.** Ion Electrostatic Analyzer Instrument Table (ESA-i)

Item	Value	Units
Type of instrument	Ion Electrostatic Analyzer	
Number of channels	n/a	
Size/dimensions (for each instrument)	240 x 170 x 150	mm x mm x mm
Instrument mass <b>without</b> contingency (CBE*)	3.2	kg
Instrument mass contingency	30	%
Instrument mass <b>with</b> contingency (CBE+Reserve)	4.16	kg
Instrument average payload power <b>without</b> contingency	3.7	W
Instrument average payload power contingency	30	%
Instrument average payload power <b>with</b> contingency	4.81	W
Instrument average science data rate^ <b>without</b> contingency	34.61	kbps
Instrument average science data^ rate contingency	30	%
Instrument average science data^ rate <b>with</b> contingency	44.93	kbps
Instrument Fields of View (if appropriate)	360 x 120	°
Pointing requirements (knowledge)	n/a	
Pointing requirements (control)	n/a	
Pointing requirements (stability)	n/a	

\*CBE = Current Best Estimate.

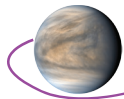
^Instrument data rate defined as science data rate prior to on-board processing

### B.2.8.4.2.3 Electron Electrostatic Analyzer (ESA-e)

The **ESA-e** is an instrument capable of measuring *in situ* solar wind electrons and photoelectrons. This instrument is part of the payload for three of the five Venus Flagship Mission assets—two SmallSat and the Orbiter. The **ESA-e** is required to measure *in situ* the solar wind electrons and photoelectrons to characterize the solar winds and the magnetic field topology and strength. The collection of these

**Table B-69.** Electron Electrostatic Analyzer (ESA-e) Instrument Table

Item	Value	Units
Type of instrument	Electron Electrostatic Analyzer	
Number of channels	n/a	
Size/dimensions (for each instrument)	160 x 190 x 150	mm x mm x mm
Instrument mass <b>without</b> contingency (CBE*)	2.2	kg
Instrument mass contingency	30	%
Instrument mass <b>with</b> contingency (CBE+Reserve)	2.86	kg
Instrument average payload power <b>without</b> contingency	2.1	W
Instrument average payload power contingency	30	%
Instrument average payload power <b>with</b> contingency	2.73	W



Item	Value	Units
Instrument average science data rate <sup>^</sup> <b>without</b> contingency	4.4	kbps
Instrument average science data <sup>^</sup> rate contingency	30	%
Instrument average science data <sup>^</sup> rate <b>with</b> contingency	5.72	kbps
Instrument Fields of View (if appropriate)	360 x 120	°
Pointing requirements (knowledge)	n/a	
Pointing requirements (control)	n/a	
Pointing requirements (stability)	n/a	

\*CBE = Current Best Estimate.

<sup>^</sup>Instrument data rate defined as science data rate prior to on-board processing

data will aid in the search for evidence of a current or past magnetic field and assist in determining the atmospheric escape rates over a full solar cycle. These data, in turn, will aid in understanding the history of volatiles and liquid water on Venus and determining if Venus was habitable and if Venus once hosted liquid water on its surface. The instrumentation used as a baseline for this mission is currently at TRL 7 and has heritage on two flight missions—Themis and Solar Parker Probe.

#### B.2.8.4.2.4 Solar Energetic Particle Detector (SEPD)

The **SEPD** is an instrument capable of measuring *in situ* the solar wind protons at high energies. This instrument is part of the payload for two of the five Venus Flagship Mission assets—the two SmallSats. The **SEPD** is required to measure protons and electrons from 20 keV–12 MeV, with a  $\Delta E/E$  of < 25 to characterize the solar winds. The collection of these data will assist in determining the atmospheric escape rates over a full solar cycle, which, will aid in understanding the history of volatiles and liquid water on Venus determining if Venus was habitable and if Venus once hosted liquid water on its surface. The instrumentation used as a baseline for this mission is currently at TRL 7 and has heritage on one flight mission—MAVEN.

**Table B-70.** Solar Energetic Particle Detector (SEPD) Instrument Table

Item	Value	Units
Type of instrument	Solar Energetic Particle Detector (SEPD)	
Number of channels	n/a	
Size/dimensions (for each instrument)	240 x 240 x 200, 250 x 200 x 50	mm x mm x mm
Instrument mass <b>without</b> contingency (CBE*)	2	kg
Instrument mass contingency	30	%
Instrument mass <b>with</b> contingency (CBE+Reserve)	2.6	kg
Instrument average payload power <b>without</b> contingency	2.6	W
Instrument average payload power contingency	30	%
Instrument average payload power <b>with</b> contingency	3.38	W
Instrument average science data rate <sup>^</sup> <b>without</b> contingency	0.2	kbps
Instrument average science data <sup>^</sup> rate contingency	30	%
Instrument average science data <sup>^</sup> rate <b>with</b> contingency	0.26	kbps
Instrument Fields of View (if appropriate)	n/a	
Pointing requirements (knowledge)	n/a	
Pointing requirements (control)	n/a	
Pointing requirements (stability)	n/a	

\*CBE = Current Best Estimate.

<sup>^</sup>Instrument data rate defined as science data rate prior to on-board processing

#### B.2.8.4.2.5 Magnetometer (Mag)

The **Mag** measures the magnetic field of Venus. The instrument is part of the payload for 4 of the 5 Venus Flagship Mission assets—the Aerobot, Orbiter, and the two SmallSats. The instrument must be magnetically clean and requires a > 1 meter boom with 32 Hz sampling and a resolution of  $\pm 5$  nT. The **fluxgate magnetometer** data will be used to characterize the magnetic field topology and strength as well as search for evidence of a past or current magnetic field. These data, in concert with other instruments aboard the five assets will aid in the understanding the history of the liquid water and volatiles

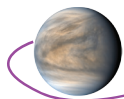


**Table B-71. Magnetometer (MAG) Instrument Table**

Item	Value	Units
Type of instrument	Magnetometer (MAG)	
Number of channels	1	
Size/dimensions (for each instrument)	127 x 76 x 91	mm x mm x mm
Instrument mass <b>without</b> contingency (CBE*)	1	kg
Instrument mass contingency	30	%
Instrument mass <b>with</b> contingency (CBE+Reserve)	1.3	kg
Instrument average payload power <b>without</b> contingency	1	W
Instrument average payload power contingency	30	%
Instrument average payload power <b>with</b> contingency	1.3	W
Instrument average science data rate <sup>^</sup> <b>without</b> contingency	2	kbps
Instrument average science data <sup>^</sup> rate contingency	30	%
Instrument average science data <sup>^</sup> rate <b>with</b> contingency	2.6	kbps
Instrument Fields of View (if appropriate)	magnetically clean	
Pointing requirements (knowledge)	n/a	
Pointing requirements (control)	n/a	
Pointing requirements (stability)	n/a	

\*CBE = Current Best Estimate.

<sup>^</sup>Instrument data rate defined as science data rate prior to on-board processing

on Venus. The instrumentation used as a baseline for this mission study is currently at TRL 9 and has heritage on three flight missions—MAVEN, Parker Solar Probe, and Juno.

#### B.2.8.4.2.6 Extreme Ultraviolet (EUV)

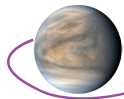
The EUV measures the EUV radiation and is part of the payload on both SmallSats. The instrument has three channels (A, B, and C) which are designed to measure the following ranges 0.1–3 nm and 17–22 nm; 0.1–7 nm; and 121–122 nm, respectively. The instrument levies the requirement of sun pointing on its host assets. The EUV will aid in characterizing the solar wind conditions and determining the solar wind variations. These data, in concert with data from other instruments, will determine the atmospheric escape rate over a solar year. The instrumentation used as a baseline for this mission study is currently at TRL 6 and has heritage on one flight mission—MAVEN.

**Table B-72. Extreme Ultraviolet (EUV) Instrument Table**

Item	Value	Units
Type of instrument	Extreme UltraViolet (EUV)	
Number of channels	3	
Size/dimensions (for each instrument)	97x145x109	mm x mm x mm
Instrument mass <b>without</b> contingency (CBE*)	7	kg
Instrument mass contingency	30	%
Instrument mass <b>with</b> contingency (CBE+Reserve)	9.1	kg
Instrument average payload power <b>without</b> contingency	14	W
Instrument average payload power contingency	30	%
Instrument average payload power <b>with</b> contingency	18.2	W
Instrument average science data rate <sup>^</sup> <b>without</b> contingency	1.6	kbps
Instrument average science data <sup>^</sup> rate contingency	30	%
Instrument average science data <sup>^</sup> rate <b>with</b> contingency	2.1	kbps
Instrument Fields of View (if appropriate)	sun pointed	°
Pointing requirements (knowledge)	n/a	
Pointing requirements (control)	n/a	
Pointing requirements (stability)	n/a	

\*CBE = Current Best Estimate.

<sup>^</sup>Instrument data rate defined as science data rate prior to on-board processing



### B.2.8.4.2.7 Electric Fields Detector (E-FD)

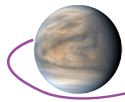
The **E-FD** is an instrument that can directly measure and map the electric fields that accelerate plasma and drive atmospheric escape and is part of the payload of both SmallSats. The **E-FD** measures the electric fields with a resolution of 1 mV/m-50 mV/m and must be magnetically clean. This data will be used to characterize ion escape and in concert with data from other instruments, will determine the atmospheric escape rate over a solar year. The instrumentation used as a baseline for this mission study is currently at TRL 9 and has heritage on one flight mission—Parker Solar Probe.

**Table B-73.** Electric Fields Detector (E-Fd) instrument table

Item	Value	Units
Type of instrument	Electric Fields Detector (E-Fd)	
Number of channels	n/a	
Size/dimensions (for each instrument)	30 mm diameter x 2 m	
Instrument mass <b>without</b> contingency (CBE*)	3	kg
Instrument mass contingency	30	%
Instrument mass <b>with</b> contingency (CBE+Reserve)	3.9	kg
Instrument average payload power <b>without</b> contingency	3	W
Instrument average payload power contingency	30	%
Instrument average payload power <b>with</b> contingency	3.9	W
Instrument average science data rate <sup>^</sup> <b>without</b> contingency	3.5	kbps
Instrument average science data <sup>^</sup> rate contingency	30	%
Instrument average science data <sup>^</sup> rate <b>with</b> contingency	4.5	kbps
Instrument Fields of View (if appropriate)	magnetically clean	°
Pointing requirements (knowledge)	n/a	
Pointing requirements (control)	n/a	
Pointing requirements (stability)	n/a	

\*CBE = Current Best Estimate.

<sup>^</sup>Instrument data rate defined as science data rate prior to on-board processing



## Appendix C. Special Technical Analyses – Approaches to Safe Landing on Tessera Terrain

### C.1 Overview

Landing on tesserae is essential to the question of habitability. The Magellan SAR data provide images at ~100 m resolution in which we see ubiquitous faults, folds and structural elements down to the scale of the images. Stereo topography is available for ~20% of the planet yielding ~1 km resolution [Herrick et al., 2012]. These data show that km scale slopes are generally <15° on tesserae (**Figure C-1**) but lander scale roughness elements are poorly known. A better understanding of hazardous topography can be obtained from VFM during its elliptical orbit prior to Lander separation, but would be profoundly advanced by the VERITAS (SAR and topography) and DAVINCI+ (meter-scale roughness) missions.

Since safe landing on tessera terrain is a critical enabler for the future exploration of Venus, the VFM study spent some time considering this problem and here we summarize the results of this discussion and make recommendations for further geologic study and technology development that can reduce the risk of tessera landing.

**Geological assessment.** We assume there are two primary types of geological hazards in the tesserae terrain:

**Slopes.** While km scale slopes are generally less than 15° on tesserae (**Figure C-1**), the Magellan data show a terrain rich with faults. Anderson’s [1951] theory on fault mechanics predicts fresh normal and reverse fault scarps to have slopes of 60°, but could be as high as 75°. Vertical scarps may exist if the lineaments are strike-slip faults or open tensile fractures as modeled by Hansen et al. [2000]. At Magellan scale, we can estimate the likelihood of encountering a fault scarp by counting the number of lineaments in a given area. For the western Ovda landing site (typical of most tessera), this percentage is low, on the order of ~1% of the VFM landing ellipse. Thus the chances of landing on a known steep fault scarp are low.

Weathering processes on planets work to reduce the slope of fresh faults over time. The primary mechanisms for physical weathering on modern Venus are mass wasting and the deposition of sediments from impact craters. Chemical weathering of the surface and seismicity will weaken materials and facilitate physical weathering. Connors and Suppe [2001] used Magellan stereo images of 170 extensional faults on the Venus plains and calculated their average slopes to be 36.4° ± 1.2°. Connors [1995] also performed detailed analysis of 4 individual scarp faces and calculated slopes that ranged from ~17°–57°. This suggests that most faults are weathering by mass wasting to the angle of repose. It is therefore likely that the fault scarps in the tesserae, which are older than the plains, are less than 60° generally.

**Decimeter to meter scale surface roughness.** The brightness of tessera terrain in Magellan RADAR are the result of roughness elements at the cm to m scale. The rock-size distribution of tessera terrain is unknown. An Earth analogue for tesserae could be dry mountainous regions, where the primary mechanisms of rock production are freeze-thaw and gravity processes without significant fluvial processes that would sort and round the rocks. These surfaces result in slopes covered by scree and rocks that fall by toppling and rolling. Magellan surveys of the planet show a limited number of landslide deposits that might produce boulders of unknown size [Malin, 1992].

Both of these issues can be mitigated with higher resolution data. Slope measurements can be significantly improved with VERITAS topography and InSAR data. Surface roughness can be assessed by targeted VERITAS SAR images at 15 m resolution. DAVINCI+ will collect descent images over

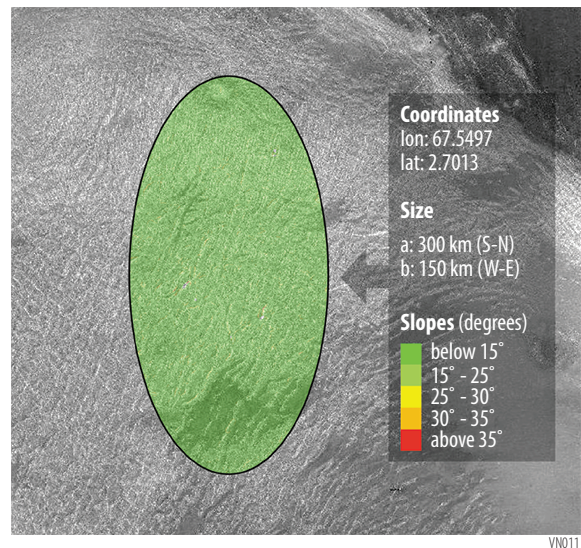
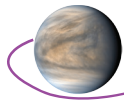


**Figure C-1.** Slope analysis over VFM landing ellipse using radargrammetric data from Herrick et al., [2012].



tessera terrain that would provide sub-meter resolution with a NIR camera providing critical insight into the surface elements that we see with the SAR data. These images would allow analysis of rock size distribution similar to what has been done for Mars [e.g., Golombek et al., 2003]. Assuming a nominal launch date for these missions of 2026, such data could be available to help select safe landing sites for VFM.

Because of the importance of this problem, we studied several approaches to safe-landing in tessera terrain. They include:

1. Regional SAR mapping by VFM to select a landing site.
2. Robust lander design.
3. Autonomous hazard detection and avoidance during lander descent.
4. Landing site analyses—slope, roughness, and mantling maps of tessera terrains.
5. Recommendations for analysis and investments.

We hope that these studies will assist any and all missions that seek to land on this critical terrain type.

## C.2 Approaches to Safe Landing

### C.2.1 Regional SAR Mapping by VFM to Select Landing Site – Equatorial Mapping Orbit Study

We studied whether we could collect imaging data of potential landing sites with the VFM prior to deorbiting the Lander to select a safe landing site (as done for Viking) because we decided to design the VFM as if it would not have any prior Venus missions (worst case scenario). To this end, we investigated whether we could enter into a landing site mapping orbit, deploy the Lander and then adjust the orbit to a circular science orbit. We considered two options: 1) capture into a 5 day elliptical *equatorial* orbit prior to deploying the Lander, and 2) capture into a 5 day elliptical *polar* orbit prior to deploying the Lander.

*Elliptical equatorial orbit capture.* To maximize the mapping of western Ovda Regio at a latitude of  $\sim 3^\circ$ , it was necessary to attain an equatorial orbit. The SAR system could acquire imaging when the Orbiter was below 1000 km. With the elliptical equatorial orbit, the SAR could image the landing site twice, acquiring 41.73% and 34.33% of the  $150 \times 300$  km target ellipse in the two passes summing to 76.06% of the ellipse and images of other areas at the same latitude, yielding SAR coverage for a total of 4.47% of the planet. In this study, these data could be collected in 6 months for a VOI of 29 Jun 2032, where targets acquired 31 Dec 2033, then Lander deployment 28 Jan 2034. However, because other science objectives (imaging, gravity) require a low polar orbit, in this scenario the spacecraft would have to alter its orbit from equatorial to polar, requiring roughly 500 m/s of  $\Delta v$  to perform an inclination change of nearly 90 degrees. We found this maneuver resulted in a very poor mass margin for the Orbiter due to the amount of fuel required.

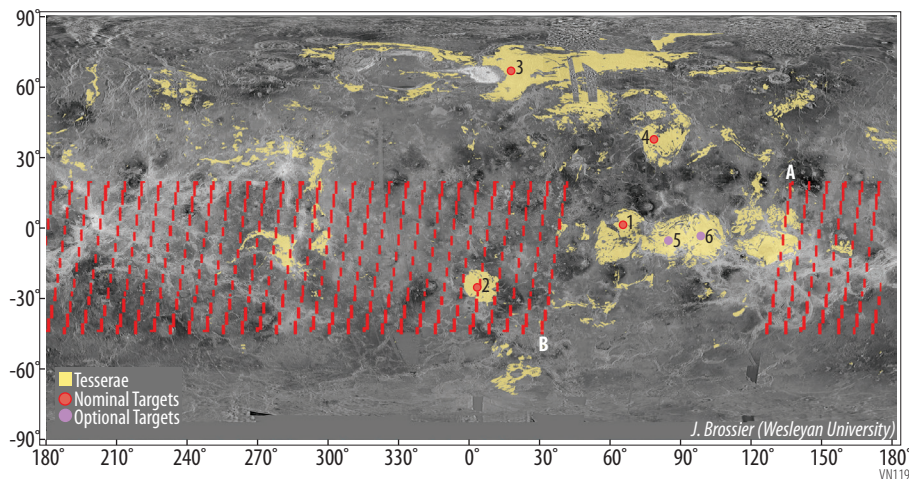
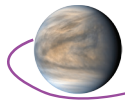


**Figure C-2.** VFM SAR imaging passes during the elliptical polar orbit prior to Lander deployment during the current baseline. Mapping starts at  $\sim 120^\circ$  longitude and moves eastward to  $\sim 30^\circ$ . The number of passes can be extended by lengthening the time of the elliptical orbit, if desired.



*Elliptical polar orbit capture.* Entering into a 5 day elliptical polar orbit allows the same total SAR coverage of 4.47% during a 6 month encounter. However, in the polar orbit, the planet's rotation results in ~782 km distance between swaths. In 6 months, this results in a single pass over some occurrences of tessera terrain. In the widebeam mode, the RADAR could acquire a maximum 76 km swath (~50% of the ellipse) of 10 m SAR data with a look angle of 17°, however higher power (narrow beam) or higher look angles (to 45°, more similar to Magellan) would result in smaller swath widths. The polar orbit was selected as the current baseline to avoid the inclination change maneuver and preserve mass margin. Although it provides less coverage of a particular landing site than the equatorial it will still provide high resolution SAR imaging of several candidate landing sites as well as other regions of tessera terrain, all of which critically inform landing site hazard assessment in the absence of other SAR data sets (e.g., from VERITAS). However, in the current mission design, the west Ovda landing site would not be imaged prior to the deployment of the Lander (**Figure C-2**). This can be mitigated by 1) leveraging images of other tessera terrain occurrences to estimate risk and train the hazard detection and avoidance (HD&A) system, and/or 2) extend the elliptical orbit duration to cover more of the planet. With the requirement to land on the dayside, it would take an additional 243 days to image the west Ovda landing site and then return to deploy the Lander to that site on 15 Jan 2036. Other tessera landing sites can also be reached in daylight including landing site #2 (**Appendix B, Figure B-1**) in Alpha Regio on 13 Dec 2035. The ample fuel margin of the Orbiter in the current design provides the flexibility to allow for this imaging strategy. This strategy also reduces risk in the case that high resolution imaging of the tesserae reveal it to be too dangerous for the Lander as designed. In this case, a landing site in the plains could be selected but would result in a significant loss to achieving the VFM science objectives.

The high resolution SAR and topography data collected by VERITAS would obviate the need to rely on VFM imaging for landing site hazard assessment by providing global maps of the planet at the 10s m scale. Descent images of Alpha Regio tessera from DAVINCI+ would provide unparalleled information about sub-m scale features. Either mission would be a crucial pathfinder and significantly reduce risk for all future Venus lander missions including VFM, New Frontiers proposals, and Venera-D.

## C.2.2 Robust Lander Design configurations

Our current knowledge of tessera morphology of < 30° slopes and boulders  $\leq 0.5$  m as described above were used to drive the design for the Lander. The lander structural design is described in detail in **Section 2.8.2.4** in **Appendix B**.

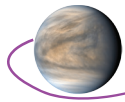
## C.2.3 Hazard Detection & Avoidance (HD&A)

Autonomous systems for HD&A include the base requirements, detection systems, and software for translating data into a hazard map.

**Base Requirements:** We divided the base requirements of our HD&A system into 2 general categories: those relevant to all landers traveling to a body outside of immediate radio contact with Earth, and those specific to safely landing in the tessera terrain of Venus.

Due to its distance from Earth, the HD&A system of the Venus Lander requires **complete autonomy**. The HD&A software **must identify hazards** (e.g., boulders >0.5 m in diameter) **and high-priority science targets** from data acquired as the lander descends [Furfaro et al., 2012; Carson et al., 2015]. Once identified, the lander **must plot and enact a course that maximizes science return and minimizes hazards**; this is often treated as an optimization problem [e.g., Furfaro et al., 2012; Lunghi et al., 2015; Yuan et al., 2018]. The Lander must then account for deviations from its intended course. This means the HD&A system must be closed-loop, a type of system in which new or updated data is incorporated to adjust for deviations from the desired or reference state [Carson et al., 2015; Yuan et al., 2018]. Furthermore, the HD&A system must be able to account for uncertainty. The true position of the lander during descent, and therefore its true proximity to hazards, will be unknown. Without accounting for this, an HD&A system may attempt to “thread the needle” beyond the lander’s capabilities or engage in wasteful avoidance maneuvers if given overly strict constraints [Furfaro et al., 2012; Carson et al., 2015; Yuan et al., 2018].

Venus has several specific issues that complicate hazard detection and avoidance. The highly scattering nature of the atmosphere results in **near isotropic lighting** conditions [Campbell & Shepard,

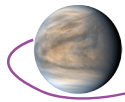


1997], a stark contrast to the predominantly directional illumination conditions of Earth, Mars, and the Moon. Because of this isotropic lighting, there are unlikely to be any true shadows on the surface of Venus (excluding extreme geometries such as cave systems). This will likely result in a more homogeneous surface appearance [Campbell & Shepard, 1997] and increased difficulty in identifying and tracking surface features [Petry et al., 2013]. The atmosphere also causes **strong signal attenuation** and a potentially large **scattering footprint** [Moroz, 2002], even beneath the cloud deck [Knically & Herrick, 2019]. The amount of signal attenuation determines the effective range of any LIDAR or imagery system used; the atmospheric scattering causes blur and expansion of the scattering footprint [Moroz, 2002; Knically & Herrick, 2019]. Moroz [2002] found that the 0.85 and 1.02  $\mu\text{m}$  windows are useful for imaging the surface at altitudes of  $\sim 5$  and 15 km respectively, if we assume a value of  $\sim 0.1$  is acceptable for the ratio of upwelling surface radiation to total upwelling radiation measured by the sensor. Elevated surfaces, such as the tessera terrains we have targeted, have improved visibility as their elevation puts them above the densest and most scattering portions of the atmosphere [Moroz, 2002; Knically & Herrick, 2019]. The **orientation of the lander during descent changes with time** due to atmospheric effects and adds to the smearing problem [Moroz, 2002; Lorenz, 2010]. Lorenz [2010] reported angular deviations and rates of angular deviation of previous planetary landers from nadir (vertical). For Venus landers, angular deviation ranges from as little as  $8^\circ$  to as much as  $30^\circ$  with angular deviation rates from  $10^\circ/\text{s}$ . up to  $20^\circ/\text{s}$ . Though the rate of deviation may be curtailed by a sufficiently short measurement integration time, any HD&A system must be able to deal with the distortions in both the LIDAR and descent imagery data caused by these deviations from vertical. This requires a system that can accurately and precisely sharpen (also known as deblur or de-smear) blurred imagery and correct for geometric distortions. The selected landing target, tessera terrain, may have a **monochromatic surface**. Combined with the ubiquitous lighting, this can make the reliable delineation of objects extremely difficult. The last issue with which to contend is the descent rate, rotation and sway; this, combined with the specifics of the descent control mechanism (e.g., drag skirt, fans, retro rockets) and our starting altitude of 20 km for initial hazard detection, places constraints on the amount of time the HD&A software has in order to detect hazards and enact a new descent path. The large Pioneer Venus probe provides a minimum time estimate; it took  $\sim 35$  minutes to free-fall from 45 km [Lorenz, 2010] for an average descent rate of  $\sim 21$  m/s. Based on the PV probe rate of descent, a free-falling lander will reach the surface in  $\sim 15.5$  minutes with new data acquired every  $\sim 45$  seconds or 1 km of descent. Estimates of descent rate for our specific Lander configuration range from  $\sim 13$  m/s at 20 km to  $\sim 7$  m/s at touchdown, acquiring new data every  $\sim 75$ – $140$ s if collected at the same 1 km interval. As we need as much time as possible for the descent control mechanism to alter the lander's trajectory, our HD&A software must be able to react to new data within a few seconds up to  $\sim 10$  seconds [Carson et al., 2015].

**Detection Systems:** Recent successful automated HD&A systems have relied on a **dual sensor approach** [Jiang et al., 2016; Lunghi et al., 2016], which this mission study adopted. Generally, an engineering descent imager (separate from the DI instrument for providing context images of the landing site) is used to determine broad-scale hazards (e.g., regions of shadow) at a relatively high altitude where small course corrections can propagate into large changes in the landing area, while a **LIDAR** system is used for fine tuning at a relatively low altitude [Jiang et al., 2016; Lunghi et al., 2016]. This was used for the automated far-side landing of Chang'e-3 and a similar, though slightly modified, hazard detection system is planned for future Chinese missions [Jiang et al., 2016]. Our selected engineering descent imager and LIDAR systems are a combined system from the GSFC.

Both of these systems will be affected by the absorption and scattering of the Venus atmosphere, though the increased elevation of our selected landing site helps to reduce these effects [Moroz, 2002; Knically & Herrick, 2019]. Of our selected landing sites, Alpha Regio has some of the lowest elevations:  $\sim 1$  km above MPR; western Ovda Regio, our target, reaches a minimum of  $\sim 1$  km above MPR and as high as  $4+$  km in some areas. The **increased surface elevation of the tessera terrains helps mitigate the effects of the venusian atmosphere** by increasing the amount of downwelling radiation that reaches the surface and hence increasing the upwelling radiation (i.e., the signal reflected from the surface that we intend to measure), as well as by reducing the amount of upwelling radiation that is scattered away from the detectors [Moroz, 2002; Knically & Herrick, 2019]. However, despite these improvements thanks to the increased surface elevation, it appears that only the 1.02 micron wavelength will be useful for viewing the surface at distances  $>15$  km [Moroz, 2002]. An increase





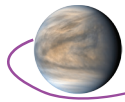
in the surface elevation from 0 to 6 km increased the cutoff for visibility as defined in Moroz [2002] for a descending probe viewing the 1.02 micron wavelength from ~16 km to ~22 km. For the 0.85 micron wavelength, the cutoff increased from ~5 to ~7.5 km. It **may be beneficial to make use of** a longer wavelength atmospheric window for secondary imaging, such as **the 1.27 micron window** as suggested by Knicely & Herrick [2019], as it would be less affected by the deleterious effects of the atmosphere compared to the 0.90 micron wavelength.

The descent imager has a 40° field of view and collects 40 kpixel images with an image integration time of 81 ms. Although the **current field of view** exceeds the previously reported maximum angular deviation by 10°, this **threatens to limit identifiable features from one frame to the next** to a 10° field of view beneath the craft and may hide low hazard and high science value landing sites that could be easily reached. The integration time of 81 ms and maximum angular deviation rate of 20°/s results in ~1.6° change in the orientation of the spacecraft. At 20 km, this blurs ~565 m of the surface into the nadir pixel; at 1 km, ~28 m. This estimate does not include any blurring caused by scattering of light by the atmosphere, which may be significant [Moroz, 2002; Knicely & Herrick, 2019].

Our LIDAR system integrates multiple laser pulses over the same period of time as the descent imager: 81 ms. Individual pulses are negligibly affected by the angular deviation rate; the resultant angular deviation over the course of time it takes for a single pulse to return traveling at the speed of light in a vacuum is ~10<sup>-5</sup>°. Like the descent imager, the integrated pulses can be severely affected by angular deviations from vertical. Assuming 81 ms of integration time at an altitude of 1 km with the maximum angular deviation rate of 20°/s, a nadir LIDAR point will experience ~28 m of lateral travel; at 250 m, the lateral travel decreases to ~7 m. This system currently operates at the **1.55 micron wavelength**. Within the venusian atmosphere, this wavelength is **particularly vulnerable to signal attenuation** [Knicely & Herrick, 2019] and beam spreading due to the higher level of interaction of this wavelength with the atmosphere. A **better wavelength** for the specific conditions of Venus is the **1.27 micron window** [Knicely & Herrick, 2019], though investigation is required to ascertain the exact detriments and benefits, and therefore if changing the wavelength of the LIDAR is necessary. As this is a scanning LIDAR, **geometric corrections are required** to place the LIDAR returns in their correct positions, which can be a **computationally expensive process** [Jiang et al., 2016; Xiao et al., 2019] that requires excessive power, hardware, and mass [Carson et al., 2015].

This **scanning LIDAR system could potentially be replaced by a flash LIDAR** system. A simplistic analogy is that a flash LIDAR is the camera version of more contemporary LIDAR systems. Whereas more traditional LIDAR systems obtain topographic information by consecutively scanning different locations using a series of small diameter laser pulse which are then combined to form a single DEM, a flash LIDAR acquires topographic information over a distributed area using a single large diameter pulse [Jiang et al., 2016; McManamon et al., 2017; Xiao et al., 2019]. This has several benefits. Flash LIDAR reduces the computational power required as compared to other LIDAR methods. Only a single correction for the lander orientation is required for the DEM extracted at each altitude as opposed to the correction for each LIDAR point required by scanning LIDAR systems. Flash LIDAR has fewer moving parts which, generally, results in fewer complications and equipment breakdowns. Finally, flash LIDAR is a technology for which NASA has already developed and licensed for commercial use in autonomous rover and robot guidance and control and usage in space [NASA Technology Transfer Program; patents 8,655,513; 8,494,687; 9,354,880; <https://technology.nasa.gov/patent/LAR-TOPS-168>] and is already in use in the ALHAT program [Carson et al., 2015]. Flash LIDAR also has several **potential detriments that must be explored before a full recommendation for this technology can be made**. This system must fire a stronger pulse or more pulses (which would then require more corrections for lander orientation) as it is distributed over a larger area and must also contend with background noise and signal attenuation caused by the venusian atmosphere and surface; this is particularly important for flash LIDAR systems that use a single laser pulse to form a DEM of the surface [McManamon et al., 2017]. Common flash LIDAR systems require cooling, which increases energy requirements and mass [McManamon et al., 2017], though flash LIDAR systems used in ALHAT can be air cooled [Carson et al., 2015]. Individual locations in each return pulse will also suffer from smearing effects, resulting in a convolution of nearby elevation values and a DEM that is smoothed compared to the true ground surface.

**HD&A Software:** Following data collection, the HD&A software must account for and address the physical limitations of the descent imager and LIDAR that reduce the data quality (smearing of



pixel values due to the scattering nature of the atmosphere and rapid changes in lander orientation; geometric distortions in the imagery and LIDAR data caused by deviations from nadir (vertical)), identify hazards and high-value science targets from the acquired data, and plot and enact course trajectories to minimize hazards and maximize science return despite uncertainties in the position of the landing craft, hazards, and high value science targets.

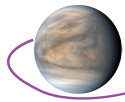
The process of autonomously detecting and identifying hazards on a rocky, monochromatic surface has been demonstrated effectively (e.g., the successful landing of Chang'e-3 on the farside of the Moon [Jiang et al., 2016] and Morpheus test flights [Carson et al., 2015]). For this reason, we limited this discussion to the specific difficulties presented by Venus, which are the smearing of pixel values and the isotropic lighting caused by the highly scattering atmosphere.

Numerous, relatively simple methods exist to sharpen imagery affected by motion blur (as well as other sources of blur), both in the spatial domain (e.g., adding the Laplacian of the original image to itself to sharpen blurred edges; subtracting the dilated or eroded image from itself to find edges) and the frequency domain (e.g., downward continuation to sharpen edges), and are easily implemented and/or widely available in existing software packages. More complicated and robust methods exist as well [e.g., Iglesias et al., 2015; Wang et al., 2018]. Tabel & Stechele [2017] summarized 4 different smear correction methods and found that, given onboard parallel computing and/or onboard Fast Fourier Transforms [Carson et al., 2015] to reduce complexity, **smear could be removed from descent imagery for autonomous missions.**

**Complex lighting is a difficult problem** in image processing, especially in the identification of edges of rocky objects in low contrast imagery, as is expected for the descent imager. Most software and methods assume a singular illumination source (e.g., Scale Invariant Feature Transform (SIFT)), and those methods that can address more complicated lighting conditions have significantly increased computational requirements [e.g., Petry et al., 2013]. **One potential solution to this problem is texture analysis.** Texture is any metric that describes local patterns in an image and has been used to partition images into regions of interest for segmentation and classification [Campbell & Shepard, 1997; Niekum, 2008]. Large boulders, regolith, and bedrock (our ideal target) will each exhibit different textures at different scales. Campbell & Shepard [1997] examined the possible effects of the isotropic lighting of Venus for two end-member rock surfaces: a diffusive (Lambertian; matte-like surface) surface and a specular (Lommel-Seeliger; mirror-like) surface. Their initial work suggests that the various textures (AKA moments) will be distinct and separable for various surfaces, and that some slope information can be extracted as well. Additionally, simple image processing techniques may potentially help address the problem of isotropic lighting and make texture analysis more robust. Niekum [2008] noted that **histogram equalization helped image segmentation in low contrast imagery for the autonomous detection and classification of rocks** by a mock Mars rover; it has also been used to help improve edge detection for bulk rock material [Iwaszenko & Smolinski, 2020]. The isotropic lighting conditions of Venus are likely to result in a reduction in the standard deviation of mean brightness, also known as low contrast [Campbell & Shepherd, 1997]; in other words, the pixel values obtained by the descent imager will likely be confined to a relatively small range of values compared to the total range that the imager could measure. Histogram equalization reassigns the absolute values of the measured pixels so their values are equally spread across the total range, rather than concentrated in a small subset of values, resulting in more robust evaluations of textures. These **textural variations** then **provide the basis for segmentation** of various parts of the collected imagery into different classes via methods such as region merging; this method generally requires a secondary algorithm to classify the regions [Niekum, 2008] and hence where the hazardous features and high science value targets are. This secondary algorithm is discussed below.

Once corrected, autonomous analysis of the data must accurately and precisely identify hazards, their relative danger, and high-value science targets, and then plot and enact a safe course [Carson et al., 2015; Lunghi et al., 2016]. Without all of these components, it is entirely possible for a lander to select a low science target because it is the lowest hazard, which, while safe, may limit the degree to which the lander can address some of the VFM objectives.

The types of autonomous HD&A software generally fall into a deterministic set of rules or a neural network meant to mimic human cognitive processes. **Deterministic methods would likely perform poorly** due to their strict adherence to given constraints. The descent data will have some uncertainty in locating hazards and science targets [Carson et al., 2015]. Systems using deterministic methods of-



ten overfit safety concerns, resulting in a reduced number of identified safe paths [Lunghi et al., 2016] and excessive energy usage [Yuan et al., 2018]. A deterministic system will also only identify those hazards that we specifically mark *a priori* as hazards. The inability of this method to address uncertainties in the descent data and adapt to the unknowns of the venusian environment are significant problems.

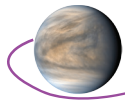
Alternatively, **various types of neural networks exist that mitigate the problems encountered by deterministic systems** via their ability to adapt to new situations [Furfaro et al., 2012]. Lunghi et al. [2016] examined a pair of artificial neural networks. This demonstrated short computation times (on the order of 1 second). Furfaro et al. [2012] explored the ability of an Evolutionary Fuzzy Cognitive Map (E-FCM), a type of fuzzy cognitive map that can adjust its rules with time, to identify and select low hazard, high science targets. E-FCMs are based on fuzzy logic, which, at its core, mimics the fuzzy nature of human thinking. With the proper inputs, fuzzy logic rules can be devised that mimic the thinking of a group of planetary scientists. This allows the effective transport of the decision-making capability of the design team with the lander. Yuan et al. [2018] demonstrated a Bayesian-based neural network. They derived fully analytical expressions, which reduces the required computation, and included the effects of uncertainty. This allowed their simulated HD&A system to avoid excessive energy usage for hazard avoidance maneuvers (e.g., avoiding a path that is safe to  $2.9\sigma$  because of a required safety limit of  $3\sigma$ ) while also reducing the failure rate as compared to deterministic methods [Yuan et al., 2018]. The ALHAT program used a conceptually similar probability-based hazard assessment in successful Morpheus test flights [Carson et al., 2015]. The use of Bayes Theorem does render this susceptible to failure in the event that the rules used in the probability assessment reach different conclusions [Furfaro et al., 2012].

Below, we briefly describe 2 methods by which the **usefulness of our LIDAR system could be expanded by making unusual use of the returned data**. One potential method involves using the amplitude of the profile of the return pulse **to characterize surface roughness**. This concept, and a number of assumptions about the physical characteristics of the surface, was applied to Magellan RADAR altimetry data to simultaneously estimate planetary radius, Fresnel reflectivity, and root mean square (RMS) slope (a measure of surface roughness) [Plaut, 1993]. This involved pre-computing time-dependent return profiles for various surface characteristics and loading these into Magellan. Once at Venus, Magellan compared the returned RADAR altimeter pulses to the pre-computed templates to determine the variables that resulted in the best template match. A similar concept could be applied to the LIDAR data. The surface roughness information acquired would be representative of the area within the LIDAR pulse's instantaneous field of view (IFOV). This method would **require** a system that could measure a return pulse (or integrated pulses) accurately enough to capture its (their) **amplitude changes through time**, as well as highly accurate **characterization of the atmosphere's effect on the amplitude profile** as atmospheric scattering stretches the return time by causing some photons to take slightly longer path lengths.

Examination of the return pulse could **potentially detect dangerously large boulders within a single LIDAR point** without using the DEM. Any LIDAR return with multiple strong peaks would indicate multiple surface elevations within the LIDAR footprint. This usage has 3 **requirements**. The first and second are the same as above: 1) **the ground projected footprint of the LIDAR must be larger than the target of interest**; i.e., boulders  $>0.5$  m; and 2) **the time-dependent effect of the atmosphere on the return profile must be accurately characterized**. Third, it would require a LIDAR system capable of **accurately and precisely characterizing the return pulse down to less than 1.5 ns** (half the approximate time for light to travel 0.5 m and back as required by Shannon's sampling theorem [Everett, 2013]). The ability to directly measure the amplitude of the return pulse and pulses separated by a nanosecond has been demonstrated for some flash LIDAR systems [McManamon et al., 2017]. This third requirement could place constraints on the sampling frequency as the LIDAR returns cannot overlap over the distance of interest. For example, to detect a 3 meter tall boulder requires a minimum pulse separation time of 10 nanoseconds; if less than this time, the return signal from 2 pulses will overlap and prevent detection of the boulder.

## C.2.4 Landing Site Analyses – Slope, Roughness, and Mantling Maps of Tessera Terrains

We have compiled 3 broad requirements for our landing site, which drove our landing site analyses. These are: 1) **a surface with slopes  $<30^\circ$** , 2) **an area free of boulders  $>0.5$  m**, and 3) **an area in which the drill can sample tessera material** (i.e., an area without thick regolith or impact crater debris man-



ting the surface). Two datasets are necessary to fully evaluate tessera terrains based on these criteria: slope and roughness maps, and mantling/regolith maps.

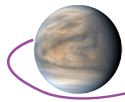
**Slope & Roughness Maps:** We have combined our discussion of the slope and roughness maps as we considered them different descriptors of the same parameter. Both are scale dependent measures of topographic variation: the slope over some distance will be related to the roughness across that same distance, given the same step size is used in calculating the values of slope and surface roughness. In some cases, roughness maps are derived by calculating the residual of the DEM subtracted from a datum or best-fit local plane [Xiao et al., 2019]. This essentially removes the large scale slopes (as might be caused by a regional trend) to retain the small scale slopes, which is then often called surface roughness.

Currently, **our best data for slope analysis comes from the Magellan mission.** The Global Topographic Data Record (GTDR) has a pixel size of  $\sim 5$  km and was derived from altimetry measurements, which have a footprint ranging from as little as  $12 \times 8$  km at  $10^\circ\text{N}$  up to  $27 \times 15$  km at  $80^\circ\text{N}$  and  $60^\circ\text{S}$  (the maximum extents north and south) [Plaut, 1993]. This large footprint, combined with the known undulations on the order of 2–6 km of some tessera terrain [Ghent & Tibuleac, 2002], renders the GTDR inadequate for characterizing slope in tessera terrains as it smears fine detail. A higher resolution set of topography exists in the form of stereo-derived topography. Stereo-derived topography of Venus has a horizontal resolution of  $\sim 1\text{--}2$  km and a vertical resolution of  $\sim 50\text{--}100$  m [Herrick et al., 2012], making it sufficient to characterize broad-scale slopes in tessera terrains. Stereo-derived DEMs have been created using automated methods for those regions with overlapping imagery with the same-look direction (Cycle 1 and Cycle 3 imagery); this same-look imagery covers  $\sim 20\%$  of Venus [Herrick et al., 2012]. We derived simple slope maps from the stereo-derived DEMs using ArcGIS in 3 tessera terrains near  $66^\circ\text{N } 006^\circ\text{E}$ ,  $40^\circ\text{N } 079^\circ\text{E}$ , and  $10^\circ\text{N } 065^\circ\text{E}$ . Our preliminary analysis of the slope maps for these regions found **median slopes of  $\sim 5^\circ$  and maximums of  $\sim 30^\circ$ . Over 90% of the areas examined have slopes below  $20^\circ$** , well within the requisite slope of  $35^\circ$ , **indicating the vast majority of tessera terrains are suitable as landing sites with respect to slope.**

The derived slope maps only include data from same-look imagery. Topography, and therefore **slope, can also be extracted from opposite-look imagery pairs** (i.e., Cycle 1 and Cycle 2). Slopes extracted using opposite-look imagery would provide a check of the slope maps derived from same-look imagery as Cycle 2 overlaps with the majority of the Cycle 3 imagery, as well as provide slope information for an additional  $\sim 20\%$  of Venus. This currently would require manual selection of match points, a time consuming effort, though automation of match point selection may be possible using more advanced techniques than cross correlation such as mutual information. We recommend detailed analysis of the slopes of tessera terrains derived using the already completed, same-look direction stereo-derived DEMs, and the development of automated methods to acquire topographic information from opposite-look Magellan imagery followed by the extraction and analysis of that slope information.

The Global Slope Data Record (GSDR; often referred to as RMS slope) and Magellan RADAR imagery represent our best global data on small scale (less than several meters) topographic variation, often called surface roughness, though these data sets lack the resolution necessary to extract information at our desired scale of  $\leq 0.5$  m. The former suffers from the same problem as the GTDR: a footprint  $\sim 10\text{--}20$  km in diameter that smears pixel values. The latter (RADAR imagery) is convoluted with effects from topography (i.e., local slope relative to the RADAR incidence angle) and the electrical properties of the surface [Ford & Plaut, 1993], as well as a minimum pixel size of 75 m. In addition to these, we have data in the form of imagery of the surface taken by the Venera and Vega landers, though these most likely landed in the plains and cannot provide useful information on the surface roughness of tessera terrain [Weitz & Basilevsky, 1993; Abdrakhimov & Basilevsky, 2002]. Both the GSDR and RADAR imagery of tessera terrains indicate high surface roughness in the decimeter to decameter range [Ford & Plaut, 1993; Tanaka et al., 1997]. RMS slopes in tessera terrains taken from the GSDR range from as little as  $<1^\circ$  up to  $>11^\circ$ . These are relative values, and, without ground truth, provide only a vague idea that the tessera terrain is rough in comparison to the plains and other venusian features. For these reasons, **our primary sources of data on the surface roughness will likely come from the engineering descent imager and LIDAR aboard the lander.**

The engineering camera could potentially obtain a measure of surface roughness by calculating the standard deviation of grayscale values in a region [Campbell & Shepard, 1997]. The work of Campbell & Shepard [1997] indicates that the mean and standard deviation of grayscale values are dependent



on the broad-scale surface slope and small-scale surface roughness. Obtaining values of surface slope and roughness would require their simultaneous determination, similar to the simultaneous solution for the planetary radius, Fresnel reflectivity, and surface RMS slope as done for the Magellan mission [Plaut, 1993]. This relation could be further exploited by determining a robust method by which to relate the standard deviation of grayscale values to our already existing RMS slope values of Venus and some other, more standardized roughness parameter like autocorrelation length [Shepard et al., 2001]. The LIDAR DEMs may also provide the basis for surface roughness determination by removing regional slopes as described above [Xiao et al., 2019] or some other method such as subtracting a low-pass filtered version of the DEM from itself.

**Mantling & Regolith Maps:** Part of the main goal of the Lander is to sample material representative of the rock that composes tessera terrain. This **requires landing in an area** in which the drill can reach rock **free of mantling material** or regolith, or with only a very thin covering of material. Information derived from polarimetric analysis of RADAR returns can be used to identify regions of tessera terrain with thick mantling material prior to mission launch.

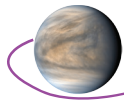
**A unique characteristic of RADAR is its polarization direction.** At RADAR wavelengths, mantling material and regolith act as volume scatterers, a type of scatterer in which the individual pieces of material are smaller than the wavelength of the signal. Furthermore, volume scatterers redistribute the energy of an incident wave polarized in a single direction into other orientations. Given returns from multiple polarization returns (e.g., horizontal transmit and receive (HH) followed by horizontal transmit and vertical receive (HV) for the same location), the quantity of volume scattering, and hence the amount of mantling material, can be constrained. The Magellan RADAR used a horizontal transmit and receive (HH) polarity [Ford, 1993]. This polarity is sensitive to double bounces, a reflection from a continuous surface with a right angle (e.g., urban structures and tree trunks), and is insensitive to volume scattering. This has made detection of mantling layers on Venus using Magellan RADAR imagery difficult, though it is possible for relatively thick deposits or when combined with the Magellan emissivity data [e.g., Campbell et al., 1992; Herrick & Phillips, 1994]. **Arecibo Observatory may provide the necessary data to constrain the quantity of mantling material.**

Campbell et al. [2015] combined same sense circularly-polarized RADAR data from Arecibo with the horizontally polarized Magellan RADAR data to search for crater mantling deposits on tessera terrain. **The Arecibo data is particularly sensitive to** the type of **volume scattering** that would be caused by a layer of regolith or impact ejecta, as are hybrid polarity schemes (e.g., horizontal transmit and vertical receive (HV)). Their analysis indicates that **mantling deposits from crater ejecta may be as thin as 5 cm in some areas and greater than 12 cm in other parts** of tessera terrain. Avoiding regions of thick mantling deposits is necessary to acquire surface samples representative of the tessera rather than plains material from crater ejecta or other erosional material. This also has important implications for accurately interpreting any NIR emissivity data, as a mantling of plains material over tessera terrain from a nearby impact crater would drastically alter the measured NIR emissivities [Campbell et al., 2015].

### C.2.5 Recommendations for study

First, **the distribution of mantling deposits over tessera terrains requires further investigation.** For use in selecting a landing site, we would ideally acquire same-sense circularly polarized or hybrid polarity RADAR data of the entirety of Venus and use it to find tessera terrains free of, or only with, thin mantling deposits. However, Arecibo can only image a single hemisphere of Venus, and sending a RADAR capable of acquiring data sensitive to volume scatterers would require at least 1 year of data collection and mapping prior to release of the lander, if not longer. Campbell et al. [2015] examined only 3 regions of tessera terrain across the Earth-facing hemisphere of Venus near identified impact craters. Further investigation along these lines can help constrain acceptable tessera landing sites.

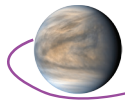
Second, and perhaps only an extension of the first, we recommend **analyzing currently available datasets for an alternative method by which to find mantling deposits** across other portions of Venus. This could involve correlating mantling deposits detected using the Arecibo and Magellan data to emissivity data acquired by the Venus Express Mission or another source, as alluded to in Carter et al. [2011] and Gilmore & Stein [2017]. Such an attempt would suffer from the large footprint of the emissivity data, making it unable to locate areally small mantling deposits as might result from local



mass wasting processes, but sufficient for finding areally large deposits that would result from events such as cratering or ubiquitous processes like chemical weathering.

Third, we recommend **investing in research into the effects of the isotropic lighting conditions of Venus on image interpretation and feature tracking**. To our knowledge, Campbell & Shephard [1997] represents the only published research into how the near-isotropic lighting conditions of Venus will affect imagery of the surface and the interpretation and analysis of that imagery. Further examination of the effects of these lighting conditions into our ability to differentiate the causative surfaces, and of how to reliably identify and track surface features in these conditions, is necessary.

Fourth, **we recommend investing in the development of automated matching algorithms for opposite-look RADAR imagery**. Additional high-resolution DEMs can be derived from opposite-look Magellan imagery pairs, which would result in better constraints on the surface slopes (and therefore the hazardous nature) of venusian tessera terrains. Currently, matching opposite-look RADAR imagery requires time-consuming manual intervention. Preliminary investigations suggest mutual information would be able to autonomously identify matching locations and permit the automated extraction of stereo-derived DEMs from opposite-look RADAR imagery.



## Appendix D. Additional Information on Technologies and Techniques

Although the VFM can be accomplished with limited technology development that is identified in the Technology Development Plan in **Section 4.2** of the final report (**Table 14**), the mission could benefit substantially from sustained investment in ancillary technologies that could reduce the cost and complexity of the mission. Specific technologies that would reduce cost and/or improve science data return for this Venus Flagship Mission are:

### Lander

1. Investments in Autonomy; both system (including goal-based sequencing and fault protection) and functional level to operate on the surface for eight hours without substantial communication with Earth [VDRT, 2018].
2. Passive thermal management techniques to enable longer-lived surface vehicles.
3. Higher density batteries – higher W-hr/kg performance, higher operating temperature.
4. High performance computing.

### Orbiter

1. Next generation reprogrammable RF transponders with reduced SWaP dual-band architecture, supporting UHF, S, X, and Ka-band options, a multitude of modulation types, turbo and LDPC coding, regenerative ranging, and open-loop recording.
2. Optical Communications and ground based assets needed to support it.
3. Spaceborne atomic clocks to revolutionize spacecraft tracking methods.
4. Compression for SAR and other targeted data types.

### SmallSats

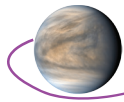
1. Next generation reprogrammable RF transponders with reduced SWaP.

**Appendix C** also outlines needed research that could improve landing site identification, which would support the development of Landing Hazard Detection and Avoidance technologies.

In addition, one can envision mission and payload enhancements for extraordinary science return. These were described in detail in the 2009 Venus Flagship Mission Study and **Table D-1** below updates the community on the advancements of those technologies since that time. Some, e.g. refrigeration at the kilowatt level, for example, is only valuable if you have something like a nuclear power source, which is currently unavailable for the Venus surface. Others have undergone development in the last decade, e.g., high-temperature electronics, sensors, and batteries, which have proceeded under the HOTech program, although further work is needed before a scientifically viable, stand-alone Venus surface mission can be accomplished, particularly in the area of computing, memory and communications. The VEXAG Technology Plan [Hunter et al., 2019] also details technologies needed for future Venus exploration.

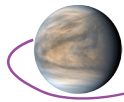
**Table D-1.** Technology Enhancements for possible future Venus Missions

Capability	Requirements	State-of-the-Art 2009	Development focus	References	State-of-the-Art 2019
Refrigeration	<ul style="list-style-type: none"> <li>• long life in Venus environment (months)</li> <li>• high efficiency</li> <li>• capable of ~3kW total heat rejection</li> <li>• suitable for integration with lander and low altitude balloon pressure vessels</li> <li>• minimized mechanical vibration</li> </ul>	<p><b>TRL ~3</b></p> <ul style="list-style-type: none"> <li>• high temp operation not demonstrated at system level</li> </ul>	<ul style="list-style-type: none"> <li>• Stirling machines need to be adapted for Venus environment</li> <li>• duplex Stirling machine must be produced that integrates the heat engine and refrigerator functions into a high efficiency and high reliability device</li> </ul>	<ul style="list-style-type: none"> <li>• Lewandowski et al., 2008</li> <li>• Landis, 2007</li> <li>• Penswitch, 1984</li> <li>• Shaltens, 2007</li> <li>• Wierzchos and Ascaso, 2002</li> <li>• Radebaugh 2000</li> <li>• Dudzinski 2008</li> </ul>	<p>See table below (page D-4)</p> <p><b>TRL ~4</b></p>

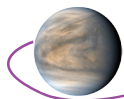


Capability	Requirements	State-of-the-Art 2009	Development focus	References	State-of-the-Art 2019
High-temp power system	<ul style="list-style-type: none"> <li>• long life in Venus environment</li> <li>• high conversion efficiency</li> <li>• low mass</li> </ul>	<p><b>TRL ~3</b></p> <ul style="list-style-type: none"> <li>• demonstrated single Stirling converter for 300 hours operation with a 850 °C hot-end temp and 90 °C cold-end, 38% efficiency and 88 W power output with heat input equivalent to 1 GPHS.</li> </ul>	<ul style="list-style-type: none"> <li>• cold end operation needs to be raised from 90 °C to 480 °C with high conversion efficiency preserved</li> <li>• material testing, system development and validation for reliable operation in Venus surface environment.</li> </ul>	<ul style="list-style-type: none"> <li>• Mason 2006, Balint 2007</li> <li>• Balint, 2006 Hyder 2000, Landis 2007, Mellot 2004, Landis and Mellot 2007, Schreiber 2006, Lewandowski 2008, Schreiber 2000</li> <li>• Balint et al., 2008</li> <li>• Dochat, 1992</li> <li>• Dudzinski, 2008</li> </ul>	<p>See table below (page D-4)</p> <p><b>TRL ~ 3</b></p>
High-temp energy storage	<ul style="list-style-type: none"> <li>• long life in Venus environment (117 days min.)</li> <li>• high specific energy rechargeable and primary batteries</li> </ul>	<p><b>TRL 4</b></p> <ul style="list-style-type: none"> <li>• demonstrated LiAl-FeS<sub>2</sub>, Na-S, and Na-metal chloride secondary batteries with specific energy in the 100-200 Wh/kg range</li> </ul>	<ul style="list-style-type: none"> <li>• adapt cell and battery designs for space applications</li> <li>• stability of seals and terminals</li> <li>• minimize the corrosion of current collectors at high temperatures</li> <li>• optimize the electrolyte composition to improve performance and reliability</li> </ul>	<ul style="list-style-type: none"> <li>• Kolawa et al., 2007-EE tech report</li> <li>• Hagedorn 1993</li> <li>• Mondt, 2004</li> </ul>	<p>See table below (page D-4)</p> <p><b>TRL ~4-5</b></p>
High-temp sensors	<ul style="list-style-type: none"> <li>• long life in Venus environment (117 days min.)</li> </ul> <p><b>Seismometers:</b></p> <ul style="list-style-type: none"> <li>• 0.3 mHz to 10 Hz frequency range</li> <li>• 10<sup>-8</sup> to 10<sup>-9</sup> msec</li> <li>• 2Hz<sup>1/2</sup> amplitude sensitivity</li> </ul> <p><b>Other sensors:</b></p> <ul style="list-style-type: none"> <li>• pressure, temperature, wind speed, gas species variation in time</li> </ul>	<p><b>TRL 2-6</b></p> <ul style="list-style-type: none"> <li>• geophones operating up to 260 °C</li> <li>• high-temperature pressure, temperature, and anemometers used on Venera/VEGA and Pioneer</li> </ul>	<ul style="list-style-type: none"> <li>• high-temperature MEMS technology for seismometers</li> <li>• SiC and GaN high temperature sensors</li> </ul>	<ul style="list-style-type: none"> <li>• Waite et al., 2006</li> <li>• Hunter, 2007</li> </ul> <p><b>5.4.2.4.1 Pressure sensors:</b></p> <ul style="list-style-type: none"> <li>• Okojie, 2006 &amp; 2003</li> <li>• Son, 2005</li> <li>• Liu, 2006</li> <li>• Ni, 2007</li> <li>• Guhel, 2002</li> </ul> <p><b>5.4.2.4.2 Physical Sensors:</b></p> <ul style="list-style-type: none"> <li>• Wrbanek, 2006</li> <li>• Lei, 1999</li> </ul> <p><b>5.4.2.4.3 Chemical Sensors:</b></p> <ul style="list-style-type: none"> <li>• Hunter, 2006</li> <li>• Navair, 2007</li> <li>• Schluwig, 2002</li> <li>• Son, 2007</li> <li>• Kang, 2004</li> <li>• Son, 2008</li> </ul>	<p>See table below (page D-4)</p> <p><b>TRL ~4</b></p>

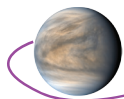




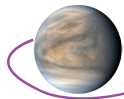
Capability	Requirements	State-of-the-Art 2009	Development focus	References	State-of-the-Art 2019
High-temperature Electronics (500 °C)	<ul style="list-style-type: none"> <li>• long life at Venus environment (117 days min.)</li> <li>• data acquisition, processing, and storage capability</li> <li>• power management</li> </ul>	<ul style="list-style-type: none"> <li>• long life at Venus environment (117 days min.)</li> <li>• data acquisition, processing, and storage capability</li> <li>• power management</li> </ul>	<ul style="list-style-type: none"> <li>• SiC-based electronics</li> <li>• GaN-based and miniaturized vacuum electronics</li> <li>• high-temperature electronic packaging, passive components</li> <li>• reliability, long life</li> </ul>	<ul style="list-style-type: none"> <li>• Neudeck, 2000</li> <li>• Neudeck, 2002</li> <li>• Daumuller, 1999</li> <li>• Wurfl, 2000</li> <li>• Wilson 1995</li> <li>• Ward, 2005</li> <li>• Chen, 2008</li> <li>• Neudeck, 2008</li> <li>• Spry, 2008</li> <li>• McCluskey, 1996</li> <li>• DelCastillo, 2007</li> <li>• Manohara, 2008 &amp; 2009</li> <li>• Delcastillo, 2008</li> <li>• Johnson, 2007</li> <li>• Delcastillo, 2006</li> </ul>	<p>See table below (page D-4)</p> <p><b>TRL ~4-5</b></p>
Medium-Temperature electronics (300 °C)	<ul style="list-style-type: none"> <li>• low power dissipation at 300 °C</li> <li>• long life and reliability</li> </ul>	<p><b>TRL 4</b></p> <ul style="list-style-type: none"> <li>• medium temperature components developed for automotive and oil drilling industry</li> </ul>	<ul style="list-style-type: none"> <li>• HT SOI CMOS electronic components</li> <li>• low power</li> <li>• test, validation, and reliability</li> </ul>	<ul style="list-style-type: none"> <li>• Neudeck, 2002 &amp; 2000</li> <li>• Powell, 2008</li> </ul>	<p>See table below (page D-4)</p> <p><b>TRL ~5-6</b></p>
High-temperature telecom	<ul style="list-style-type: none"> <li>• long life at Venus environment (117 days min.)</li> <li>• high data rate (~4.5 kbs)</li> </ul>	<p><b>TRL 2</b></p> <ul style="list-style-type: none"> <li>• demonstrated 2 GHz operation at 275 °C using SiC</li> <li>• SiC and vacuum tube based oscillator demonstrated at ~500°C</li> </ul>	<ul style="list-style-type: none"> <li>• SiC based RF components for transmitters</li> <li>• miniaturized vacuum tube technology for power amplifiers</li> <li>• SiC based RF components for transmitters</li> </ul>	<ul style="list-style-type: none"> <li>• Sternowski, 2008</li> <li>• McCluskey 1996,</li> <li>• Schwartz, 2005</li> <li>• Wang, 2005</li> <li>• Gao, 1994</li> <li>• Daumiller, 1999</li> <li>• Jimenez, 2006</li> <li>• Neudeck, 2002</li> <li>• Dzewonski, 1997</li> </ul>	<p>See Table D-2 below (page D-4)</p> <p><b>TRL ~4-7</b></p>



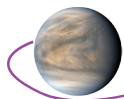
<p>Refrigeration</p>	<p>HoneyBee Robotics 2017 SBIR: High Temperature Stirling Cooler <a href="https://www.sbir.gov/sbirsearch/detail/1426373">https://www.sbir.gov/sbirsearch/detail/1426373</a></p> <ul style="list-style-type: none"> <li>“developing a miniature Stirling cooler, suitable for integration with a sensor package at the end of an effector or robot arm, which is capable of keeping conventional electronics cool outside of the spacecraft body in the high temperature Venus environment.”</li> </ul> <p>Anderson &amp; Gross (2018) Venus Lander Electronics Payload Thermal Management Using a Multistage Refrigeration System <a href="https://drive.google.com/drive/folders/14piu2TESXt4kjWo-wfR6cEWZ7QMJfelf">https://drive.google.com/drive/folders/14piu2TESXt4kjWo-wfR6cEWZ7QMJfelf</a></p> <ul style="list-style-type: none"> <li>“combination of supercritical fluids (TCO<sub>2</sub> and SCO<sub>2</sub>) in conjunction with a biodiesel type of working fluid (FAME-MLL) along with NH<sub>3</sub> to realize an effective cascaded cycle. The four-stage cascade cycle is designed to be operated continuously while on-station powering Venus science missions, thus acting as the primary thermal control management system...The results for the optimized cascaded cycle presented herein indicate a COP of 0.87 for the cycle to have a refrigeration capacity of 100 W at 100°C.”</li> </ul> <p>Anderson et al (2017) Actively Cooled Venus Lander Instrument Payload Using a Multi-Cascade Refrigeration Cycle <a href="https://www.hou.usra.edu/meetings/lpsc2017/eposter/1015.pdf">https://www.hou.usra.edu/meetings/lpsc2017/eposter/1015.pdf</a></p> <p>Makel Engineering Inc. (2017–2019) SBIR: High Temperature, Radiation Hard Electronics Architecture for a Chemical Sensor Suite for Venus Atmospheric Measurements <a href="https://www.sbir.gov/sbirsearch/detail/1426369">https://www.sbir.gov/sbirsearch/detail/1426369</a></p> <p>Qiu &amp; Solomon (2018) Free-Piston Stirling Engine Generators <a href="https://www.intechopen.com/books/energy-conversion-current-technologies-and-future-trends/free-piston-stirling-engine-generators">https://www.intechopen.com/books/energy-conversion-current-technologies-and-future-trends/free-piston-stirling-engine-generators</a></p> <p>Need access: Erbay et al. 2016 Overall performance of the duplex Stirling refrigerator <a href="https://www.sciencedirect.com/science/article/pii/S0196890416310792">https://www.sciencedirect.com/science/article/pii/S0196890416310792</a></p> <p>Wood 2013 Patent: FREE-PISTON STIRLING MACHINE FOR EXTREME TEMPERATURES <a href="https://patentimages.storage.googleapis.com/36/5a/ea/94448d317bee3e/US8590301.pdf">https://patentimages.storage.googleapis.com/36/5a/ea/94448d317bee3e/US8590301.pdf</a></p> <p>SBIR Advanced Cooling Technologies; Tarau et al (2011) Thermal Management System for Long-Lived Venus Landers</p> <ul style="list-style-type: none"> <li>“The five-feature VCHP model predicts that the Stirling convertor can: 1) rest during transit at ~100°C lower temperature than the nominal one (~1000°C); 2) pre-cool the modules before the entry into the Venus atmosphere, lowering the temperature by another ~85°C; 3) work at nominal temperature of ~1000°C on Venus surface; 4) stop working (for short periods of time on Venus surface with a relatively small vapor temperature increase of ~ 6–9°C and 5) reject excess heat during the entire mission if short-lived isotopes are used.”</li> </ul> <p>Advanced Cooling Technologies Inc SBIR 2018-19 <a href="https://www.sbir.gov/sbirsearch/detail/1560071">https://www.sbir.gov/sbirsearch/detail/1560071</a></p>
<p>High temp power system</p>	<p>Physical Sciences Inc SBIR 2019–20:</p> <p>Electrical Power from Thermal Energy Scavenging in High Temperature Environments <a href="https://www.sbir.gov/sbirsearch/detail/1561949">https://www.sbir.gov/sbirsearch/detail/1561949</a></p> <ul style="list-style-type: none"> <li>“develop an integrated metal hydride (MH) system and spectrally-tuned thermophotovoltaic power converter (PC) system that can extract heat during periods of high thermal intensity and convert it to electricity at greater than 25 percent efficiency. . . In Phase II, we will produce and functionally characterize an integrated engineering prototype of the MH-PC heat scavenging electrical power generator system, fully tested in the laboratory and in simulated thermal-vacuum environments, together with an analytical model of the functional system. We will identify candidate facilities (e.g., NASA/Stennis) for field testing of the system in Phase III”</li> </ul> <p>Sierra Lobo Inc SBIR 2013 Thermoacoustic Duplex Technology for Cooling and Powering a Venus Lander <a href="https://www.sbir.gov/sbirsearch/detail/411683">https://www.sbir.gov/sbirsearch/detail/411683</a></p> <ul style="list-style-type: none"> <li>“The system can potentially be used with the gas from the atmosphere of Venus, which is primarily composed of CO<sub>2</sub>, as a working fluid. This provides two key advantages: (1) The system can make the transit to Venus in a low-pressure state, which significantly decreases system mass, and (2) the effect of leakage during operation is minimized”</li> </ul> <p><a href="https://www.sciencedirect.com/science/article/abs/pii/S0094576518303941">https://www.sciencedirect.com/science/article/abs/pii/S0094576518303941</a></p> <p>Hot Operating Temperature Lithium combustion IN situ Energy and Power System (HOTLINE Power System)</p>



<p>High temp energy storage</p>	<p>Glass et al 2020  <a href="https://www.sciencedirect.com/science/article/pii/S0378775319314855">https://www.sciencedirect.com/science/article/pii/S0378775319314855</a></p> <ul style="list-style-type: none"> <li>• “FeS has emerged as the most suitable cathode. With optimized cell components, cell design, and operational parameters, laboratory test cells were fabricated, which demonstrated continuous operation of ~26 days at 475 °C.”</li> </ul> <p>Lynntech Inc SBIR 2019–20:          Fluoride Ion Solid State Battery for Terrestrial Venus Applications <a href="https://www.sbir.gov/sbirsearch/detail/1670949#">https://www.sbir.gov/sbirsearch/detail/1670949#</a></p> <ul style="list-style-type: none"> <li>• “Lynntech proposes to develop high temperature all solid-state Fluoride-ion batteries (FIB) using a solid-state electrolyte, and high capacity electrodes with excellent chemical and thermal compatibility with the electrolyte... over a wide temperature range of 150 to 500 Celsius.”</li> </ul>
<p>High temp sensors</p>	<p>Makel Engineering</p> <ul style="list-style-type: none"> <li>• 2018–19 SBIR: Solid-State, Electrochemical Micro-Sensors for Atmospheric Nitrogen and Carbon Dioxide Measurements at the Surface of Venus <a href="https://www.sbir.gov/sbirsearch/detail/1670337">https://www.sbir.gov/sbirsearch/detail/1670337</a></li> <li>• “Prototype sensors were fabricated and tested in relevant laboratory conditions, demonstrating the technology to TRL 4.”</li> <li>• 2019–20 SBIR: Venus In situ Mineralogy Reaction Array (VIMRA) Sensor Platform <a href="https://www.sbir.gov/sbirsearch/detail/1670995">https://www.sbir.gov/sbirsearch/detail/1670995</a></li> <li>• “Prototype mineral sensors will be fabricated and tested in Phase I to demonstrate the technology to TRL 4 by testing in relevant laboratory conditions. In Phase II, the VIMRA sensor platform will be combined with SiC electronics to provide a high temperature capable payload suitable for extended operation on the surface of Venus.”</li> <li>• 2017–19 SBIR: High Temperature, Radiation Hard Electronics Architecture for a Chemical Sensor Suite for Venus Atmospheric Measurements, Phase II <a href="https://www.sbir.gov/sbirsearch/detail/1426369">https://www.sbir.gov/sbirsearch/detail/1426369</a></li> </ul> <p>Sporian Microsystems 2018-21 SBIR:          Pressure Sensors for Glenn Extreme Environment Rig and Planetary Science Applications  <a href="https://www.sbir.gov/sbirsearch/detail/1670711">https://www.sbir.gov/sbirsearch/detail/1670711</a></p> <ul style="list-style-type: none"> <li>• “. . .will be beneficial to NASA’s planetary science mission by facilitating environmental chamber testing/ validation, and pressure measurements in the Venus atmosphere and on the surface. The Phase I effort focused on heavily leveraging prior harsh environment, in situ instrumentation development and, with input from current/prior NASA partners, successfully constructing and characterizing prototype sensor suites”</li> </ul>
<p>High temp electronics (500C)</p>	<p>Ozark IC (PI: Franics, Anthony) 2018–19 SBIR: Integrated Silicon Carbide Electronics for Venus Surface Actuation</p> <ul style="list-style-type: none"> <li>• Phase I TRL end: 6 <a href="https://sbir.nasa.gov/SBIR/abstracts/18/sbir/phase2/SBIR-18-2-S4.04-1268.html">https://sbir.nasa.gov/SBIR/abstracts/18/sbir/phase2/SBIR-18-2-S4.04-1268.html</a></li> <li>• Phase II: <a href="https://www.sbir.gov/sbirsearch/detail/1670909">https://www.sbir.gov/sbirsearch/detail/1670909</a></li> <li>• “In Phase I of this effort, Ozark IC showed, through a laboratory demonstration, that NASA’s JFET-R technology can continuously run a stepper motor for over 1,000 hours of operation at 470°C. In parallel, Honeybee Robotics demonstrated that its TRL-6 level Venus motors are capable of being used in a stepper configuration to achieve the required auger needs for a Venus drill.”</li> </ul> <p>Advent Diamond Inc SBIR 2017–18: SBIR Phase I: Advancing High-Power Diamond Devices Towards Commercialization  <a href="https://www.sbir.gov/sbirsearch/detail/1499847">https://www.sbir.gov/sbirsearch/detail/1499847</a></p>
<p>Mid temp electronics (300C)</p>	<p>Ozark IC (PI: Holmes) SBIR 2019–2020: Ruggedized Communication Technology for Enabling High-Temperature Directional Drilling  <a href="https://www.sbir.gov/sbirsearch/detail/1640779">https://www.sbir.gov/sbirsearch/detail/1640779</a></p> <ul style="list-style-type: none"> <li>• “Ozark IC achieves these operating temperatures using a range of technologies at various Technology Readiness Levels (TRL), including silicon-on-insulator (GEN1: TRL 8) and silicon carbide semiconductors (GEN2: TRL 6), advanced ceramic packaging (GEN1: TRL 6-8), and advanced/additive manufacturing techniques (GEN2: TRL 5) To achieve high-temperature (HT) directional drilling, the team proposes to modify the state-of-the-art (SOA) 160°C wireline telemetry system with a novel, surface- powered wireline capable of 1000-hour operation at 250°C.”</li> </ul>

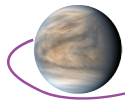


<p>High temp telecom</p>	<p>INNOSYS Inc SBIR 2019–2020 Space Exploration Extreme Environment Communication Transceiver <a href="https://sbir.nasa.gov/SBIR/abstracts/19/sbir/phase1/SBIR-19-1-S4.04-3555.html">https://sbir.nasa.gov/SBIR/abstracts/19/sbir/phase1/SBIR-19-1-S4.04-3555.html</a></p> <ul style="list-style-type: none"><li>• TRL begin: 4 end: 7</li><li>• “This will be based on the transmitter that InnoSys has developed based on its proprietary SSVDTM technology, which has been proven to operate at S band and survive a 500°C environment.”</li></ul> <p>Senesky (Stanford) SBIR 2017–19: Passively Compensated Low-Power Chip-Scale Clocks for Wireless Communication in Harsh Environments</p> <p><a href="https://data.nasa.gov/dataset/Passively-Compensated-Low-Power-Chip-Scale-Clocks-/rngz-v4km">https://data.nasa.gov/dataset/Passively-Compensated-Low-Power-Chip-Scale-Clocks-/rngz-v4km</a></p> <ul style="list-style-type: none"><li>• “InAlN/GaN high electron mobility transistors are proven to be operable up to 1000C and resonators in GaN and other III-Vs are shown to offer high-temperature operation, high power stability, high Q, and designable zero-bias TCF values in a wide temperature range (up to 600C).</li><li>• “The design and implementation of the chip-scale clock has an entry technology readiness level (TRL) of 2 and exit TRL of 4”</li></ul>
--------------------------	---

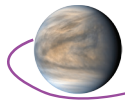


## Appendix E. References

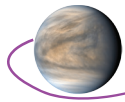
- Abdrakhimov, A. M., & A. T. Basilevsky. 2002. "Geology of the Venera and Vega landing-site regions." *Solar System Research*, 36, 136-159. <https://doi.org/10.1023/A:1015222316518>
- Allwood, A., Clark, B., Flannery, D., Hurowitz, J., Wade, L., Elam, T., Foote, M., Knowles, E., Texture-specific elemental analysis of rocks and soils with PIXL: The Planetary Instrument for X-ray Lithochemistry on Mars 2020. 2015 IEEE Aerospace Conference, 2015, pp. 1-13.
- Amzajerjian, Farzin & Pierrottet, Diego & Petway, Larry & Hines, Glenn & Roback, Vincent. (2011). Lidar systems for precision navigation and safe landing on planetary bodies. Proceedings of SPIE - The International Society for *Optical Engineering*. 8192. [10.1117/12.904062](https://doi.org/10.1117/12.904062).
- Anderson, E. M. 1951. *The Dynamics of Faulting*. Oliver and Boyd, London.
- Anderson, A.W., Nordan, H.C., Cain, R.F., Parrish, G., and Duggan, D. 1956. Studies on a radio-resistant micrococcus. I. Isolation, morphology, cultural characteristics, and resistance to gamma radiation. *Food Technology* 10(1):575-577.
- Anderson, Kevin R., et al. "Venus Lander Electronics Payload Thermal Management Using a Multi-Stage Refrigeration System." 47th AIAA Thermophysics Conference, 2017, doi:[10.2514/6.2017-4344](https://doi.org/10.2514/6.2017-4344).
- Anderson, Kevin R., et al. "Venus Lander Electronics Payload Thermal Management Using a Multistage Refrigeration System." *Journal of Thermophysics and Heat Transfer*, vol. 32, no. 3, 2018, pp. 659–668., doi:[10.2514/1.5286](https://doi.org/10.2514/1.5286).
- Ando, H., T. Imamura, N. Sugimoto, M. Takagi, H. Kashimura, S. Tellmann, M. Pätzold, B. Häusler, and Y. Matsuda (2017), Vertical structure of the axi-asymmetric temperature disturbance in the Venusian polar atmosphere: Comparison between radio occultation measurements and GCM results, *J. Geophys. Res. Planets*, 122, pp. 1687–1703, doi:[10.1002/2016JE005213](https://doi.org/10.1002/2016JE005213)
- Aslam et al. (2020), Advanced Net Flux Radiometer for the Ice Giants. *Space Science Reviews*, doi:[10.1007/s11214-019-0630-x](https://doi.org/10.1007/s11214-019-0630-x)
- Atreya, S. K., M.G. Trainer, H.B. Franz, M.H. Wong, H.L.K. Manning, C.A. Malespin, P.R. Mahaffy, P.G. Conrad, A.E. Brunner, L.A. Leshin, J.H. Jones, C.R. Webster, T.C. Owen, R.O. Pepin, and R. Navarro-González (2013). Primordial Argon Isotope Fractionation in the Atmosphere of Mars Measured by the SAM Instrument on Curiosity, and Implications for Atmospheric Loss, *Geophys. Res. Lett.*, 40(21):5605-5609, doi:[10.1002/2013GL057763](https://doi.org/10.1002/2013GL057763), 2013.
- Baines et al. 2013. The Atmospheres of the Terrestrial Planets: Clues to the Origins and Early Evolution of Venus, Earth and Mars, in *Comparative Climatology of Terrestrial Planets* (S. J. Mackwell, et al., eds.), pp137-160, University of Arizona Press.
- Balint, T. S., and K. H. Baines. "Nuclear polar VALOR: an ASRG-enabled Venus balloon mission concept." AGU Fall Meeting Abstracts. 2008.
- Balint, T. S., Cutts, J. A., Kolawa, E. A., Kwok, J. H. "Mitigating extreme environments for long-lived Venus in-situ missions." European Geosciences Union (EGU) General Assembly, Vienna, Austria, 13–18. April 2008.
- Banerdt, W.B., Smrekar, S.E., Banfield, D. et al. Initial results from the InSight mission on Mars. *Nat. Geosci.* 13, 183–189 (2020). <https://doi.org/10.1038/s41561-020-0544-y>
- Barabash, S., et al. 2007. The Analyser of Space Plasmas and Energetic Atoms (ASPERA-4) for the Venus Express mission, *Planet. Space Sci.*, 55, 1772–1792.
- Basilevsky A.T., and Head J.W. III (1998) The geologic history of Venus: A stratigraphic view. *Journal of Geophysical Research: Planets* 103, 8531-8544, doi:[10.1029/98je00487](https://doi.org/10.1029/98je00487).
- Bertaux, J.-L. and Clarke, J.T., 1989. Deuterium content of the Venus atmosphere. *Nature* 338:567-568.
- Bertaux, J.L. et al. 2007. A warm layer in Venus' cryosphere and high-altitude measurements of HF, HCl, H<sub>2</sub>O and HDO. *Nature* 450, 646.
- Bezard, B. et al. 1990. The deep atmosphere of Venus revealed by high resolution nightside spectra. *Nature* 345, 508.
- Bhartia, R., W. F. Hug, E. C. Salas, R. D. Reid, K. K. Sijapati, A. Tsapin, W. Abbey, K. H. Nealson, A. L. Lane, and P. G. Conrad. 2008. Classification of organic and biological materials with deep ultraviolet excitation. *Appl. Spectrosc.* 62:1070–1077.



- Bhartia, R., Salas, E.C., Hug, W.F., Reid, R.D., Lane, A.L. Edwards, K.J., and Neelson, K.H. (2010) Label-free bacterial imaging with Deep-UV Laser-Induced Native Fluorescence. *Applied & Environmental Microbiology* 76(21):7231–7237.
- Bjoraker, G. L., Larson, H. P., Mumma, M. J., Timmermann, R., & Montani, J. L. (1992). Airborne observations of the gas composition of Venus above the cloud tops: Measurements of H<sub>2</sub>O, HDO, HF, and the D/H and <sup>18</sup>O/<sup>16</sup>O isotopic ratios. In *Bulletin of the American Astronomical Society* (Vol. 24, p. 995).
- Blake, D., Vaniman, D., Achilles, C., Anderson, R., Bish, D., Bristow, T., Chen, C., Chipera, S., Crisp, J. and Des Marais, D. (2012) Characterization and calibration of the CheMin mineralogical instrument on Mars Science Laboratory. *Space Science Reviews* 170, 341-399.
- Blake D., Sarrazin, P., Bristow, T. S., Walroth, R. Downs, R., Gailhanou, M., Yen, A., Zacny, K., (2019) CheMin-V: A definitive mineralogy instrument for the Venera-D mission, Lun. Plan. Sci. Conf. 50 (LPI Contrib. No. 2132), #1468.
- Blamont, J., et al. “Balloons on planet Venus: final results.” *Advances in Space Research* 13.2 (1993): 145-152.
- Bocanegra-Bahamon, T. M., et al. (2019), Venus Express radio occultations observed by PRIDE, *Astronomy and Astrophysics*, 626, A59, <https://doi.org/10.1051/0004-6361/201833160>
- Bogard, D.D. and Johnson, P., 1983. Martian gases in an Antarctic meteorite?. *Science*, 221(4611), pp.651-654.
- Borg, L.E., Connelly, J.N., Nyquist, L.E., Shih, C.Y., Wiesmann, H. and Reese, Y., 1999. The age of the carbonates in Martian meteorite ALH84001. *Science*, 286(5437), pp.90-94.
- Bouvier, L.C., Costa, M.M., Connelly, J.N. et al. Evidence for extremely rapid magma ocean crystallization and crust formation on Mars. *Nature* 558, 586–589 (2018). <https://doi.org/10.1038/s41586-018-0222-z>
- Brace, L. H., Kasprzak, W. T., Taylor, H. A., Theis, R. F., Russell, C. T., Barnes, A., Mihalov, J. D., and Hunten, D. M. 1987. The ionotail of Venus: Its configuration and evidence for ion escape, *J. Geophys. Res.*, 92(A1), 15– 26.
- Brissaud, Q., R. Martin, R. F. Garcia and D. Komatitsch (2017). *Geophys. J. Int.* 210. <https://doi.org/10.1093/gji/ggx185>
- Bullock, M. A., and D. H. Grinspoon. 2001. The recent evolution of climate on Venus, *Icarus*, 150, 19-37.
- Byrne P.K., Ghail R. C., Gilmore M. S., Celâl Şengör A. M., Klimczak C., Senske D. A., Whitten J. L., Khawja S., Ernst R. E., Solomon S. C. (2020) Venus tesserae feature layered, folded, and eroded rocks. *Geology*, in press.
- Calgary, O. “Passively Compensated Low-Power Chip-Scale Clocks for Wireless Communication in Harsh Environments.” NASA, NASA, [data.nasa.gov/dataset/Passively-Compensated-Low-Power-Chip-Scale-Clocks-/rngz-v4km](https://data.nasa.gov/dataset/Passively-Compensated-Low-Power-Chip-Scale-Clocks-/rngz-v4km).
- Campbell, B. A., D. B. Campbell, G. A. Morgan, L. M. Carter, M. C. Nolan, & J. F. Chandler. 2015. “Evidence for crater ejecta on Venus tessera terrain from Earth-based radar images.” *Icarus*, 250, 123-130. <http://dx.doi.org/10.1016/j.icarus.2014.11.025>
- Campbell, B. A., & M. K. Shepard. 1997. “Effect of Venus surface illumination on photographic image texture.” *Geophysical Research Letters*, 24, 731-734. doi: [10.1029/97GL00598](https://doi.org/10.1029/97GL00598)
- Campbell, D. B., N. J. S. Stacy, W. I. Newman, R. E. Arvidson, E. M. Jones, G. S. Musser, A. Y. Roper, & C. Shaller. 1992. “Magellan observations of extended impact crater related features on the surface of Venus.” *Journal of Geophysical Research: Planets*, 97, 16249-16277. <https://doi.org/10.1029/92JE01634>
- Campbell, I.H., Taylor, S.R., 1983. No water, no granites – No oceans, no continents. *Geophys. Res. Lett.* 10, 1061–1064.
- Canfield, D. E., & Raiswell, R. (1999). The evolution of the sulfur cycle. *American Journal of Science*, 299(7-9), 697-723.
- Canfield, D. E., Rosing, M. T., & Bjerrum, C. (2006). Early anaerobic metabolisms. *Philosophical Transactions of the Royal Society B: Biological Sciences*, 361(1474), 1819-1836.
- CAPS (Committee on Astrobiology and Planetary Science of the National Academies of Sciences, Engineering, and Medicine) 2017. Report Series: Getting Ready for the Next Planetary

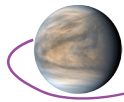


- Science Decadal Survey. Washington, DC: The National Academies Press. <https://doi.org/10.17226/24843>.
- Carson III, J. M., E. A. Robertson, N. Trawny, & F. Amzajerdian. 2015. "Flight testing ALHAT precision landing technologies integrated onboard the Morpheus rocket vehicle." AIAA SPACE 2015 Conference and Exposition. <https://doi.org/10.2514/6.2015-4417>
- Carter, L. M., D. B. Campbell, & B. A. Campbell. 2011. "Geologic studies of planetary surfaces using radar polarimetric imaging." Proceedings of the IEEE, 99. doi: [10.1109/JPROC.2010.2099090](https://doi.org/10.1109/JPROC.2010.2099090)
- Cathey, Henry. "Evolution of the NASA ultra long duration balloon." AIAA Balloon Systems Conference. 2007.
- Chen, Y., Castillo, L., Aranki, N., Assad, C., Mazzola, M., Mojarradi, M., Kolawa, E. "Reliability assessment of high temperature electronics and packaging technology for Venus missions." Digests of IEEE 2008 International Reliability Physics Symposium IRPS. pp 641-642. 2008.
- Clark I. and C. Tanner, "A historical summary of the design, development, and analysis of the disk-gap-band parachute," 2017 IEEE Aerospace Conference, Big Sky, MT, 2017, pp. 1-17, doi: [10.1109/AERO.2017.7943854](https://doi.org/10.1109/AERO.2017.7943854).
- Clegg, S. M., B. S. Okhuysen, D. S. DeCroix, R. T. Newell, R. C. Weins, S. K. Sharma, S. Maurice, R. K., Martinez, A. Reyes-Newell, M. D. Dyar (2019) Venus Elemental and Mineralogical Camera (VEMCam), EPSC-DPS Joint Meeting 2019, Vol. 13, EPSC-DPS2019-827-1.
- Cockell, C. S., 1999. Life on Venus. *Planetary and Space Science*. 47, 1487-1501.
- Connerney, J. E. P., M. H. Acuña, P. J. Wasilewski, N. F. Ness, H. Rème, C. Mazelle, D. Vignes, R. P. Lin, D. L. Mitchell, P. A. Cloutier Magnetic Lineations in the Ancient Crust of Mars Science 30 Apr 1999: Vol. 284, Issue 5415, pp. 794-798 DOI: [10.1126/science.284.5415.794](https://doi.org/10.1126/science.284.5415.794)
- Connors C. (1995) Determining heights and slopes of faults scarps and other surfaces on Venus using Magellan stereo radar, *J. Geophys. Res.* 100, 14361-14381.
- Connors, C., and Suppe, J. (2001), Constraints on magnitudes of extension on Venus from slope measurements, *J. Geophys. Res.*, 106( E2), 3237– 3260, doi:[10.1029/2000JE001256](https://doi.org/10.1029/2000JE001256).
- Conrad, P. G., C.A. Malespin, H.B. Franz, R.O. Pepin, M.G. Trainer, S.P. Schwenzer, S.K. Atreya, Freissinet, J.H. Jones, H. Manning, T. Owen, A.A. Pavlov, R.C. Wiens, M.H. Wong, P.R. Mahaffy (2016). In Situ Measurement of Atmospheric Krypton and Xenon on Mars with Mars Science Laboratory, with Earth and Planetary Science Letters, 454, 1–9, 2016.
- Crumpler, L. S., J. C. Aubele, D. A. Senske, S. T. Keddie, K. P. Magee, and J. W. Head. 1997. Volcanoes and centers of volcanism on Venus, in Venus II, edited by S. W. Bougher et al., pp. 697–756, Univ. of Ariz. Press, Tucson.
- Cutts et al. (2015). Probing the Interior Structure of Venus. Keck Institute for Space Studies Final Report.
- Cutts, Jim, et al. "Aerial Platforms for the Scientific Exploration of Venus", JPL D-102569, October, 2018. Loon LLC. "Project Loon." <https://loon.co/> (Retrieved March 2019).
- Dartnell, L. R., Nordheim, T. A., Patel, M. R., Mason, J. P., Coates, A. J., & Jones, G. H. (2015). Constraints on a potential aerial biosphere on Venus: I. Cosmic rays. *Icarus*, 257, 396-405.
- Daumiller, I., C. Kirchner, M. Kamp, K. J. Ebeling and E. Kohn. "Evaluation of the temperature stability of AlGaIn/GaN heterostructure FETs." IEEE Electron Device Letters, Vol. 20, No. 9, pp 448-450. September 1999.
- Davaille, A., S.E. Smrekar, S. Tomlinson, Experimental and observational evidence for plume-induced subduction on Venus. *Nat. Geosci.* 10, 349–355 (2017)
- de Bergh, C., Lutz, B.-L., Owen, T., Maillard, J.-P. 1989. Measurements of the D/H ratio in planetary atmospheres by ground based infrared spectroscopy. *Infrared Spectroscopy in Astronomy* 41.
- de Bergh, C., Bezard, B., Owen, T., Crisp, D., Maillard, J. P., & Lutz, B. L. (1991). Deuterium on Venus: observations from Earth. *Science*, 251(4993), 547-549.
- de Bergh, C. 1993. The D/H ratio and the evolution of water in the terrestrial planets. *Origins Life Evol Biosphere* 23: 11. <https://doi.org/10.1007/BF01581986>.
- De Jong, Maxim, "Systems and Methods Including Elevation Control", United States Patent Application US 2017/0129579 A1, Assignee: Thin Red Line Aerospace Ltd., May 11, 2017.

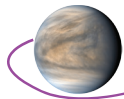


- Del Castillo, L., T. Hatake, M. Mojarradi, T. Vo, W. West, J. Yager. “Extreme Temperature Sensing System for the Venus Ambient Environment.” R&TD Annual Report. September 2007.
- Del Castillo, L., T. W. Johnson, T. Hatake, M. M. Mojarradi and E. A. Kolawa. “Sensor amplifier for the Venus ground ambient.” International Conference on High Temperature Electronics (HiTEC), May 15–18, 2006, Santa Fe, NM: International Microelectronics and Packaging Society. 2008.
- Dochat, G. “Venus lander stirling cooler.” Mechanical Technology Inc. Company Report. August 1992.
- Delort, A-M., Väitilingom, M., Amato, P., Sancelme, M., Parazols, M., Mailhot, G., and Deguillaume, L. (2010) A short overview of the microbial population in clouds: Potential roles in atmospheric chemistry and nucleation processes. *Atmospheric Research* 98(2–4):249-260.
- Delort, A-M., P. Amato (eds), *Microbiology of Aerosols*, John Wiley & Sons, Nov 13, 2017.
- Doglioni, C., Pignatti, J. and Coleman, M., 2016. Why did life develop on the surface of the Earth in the Cambrian?. *Geoscience Frontiers*, 7(6), pp.865-873.
- Donahue, T. M., Grinspoon, D. H., Hartle, R. E., & Hodges, R. R. Jr. (1997). Ion/neutral escape of hydrogen and deuterium: Evolution of water. In S. W. Bougher, D. M. Hunten, & R. J. Phillips (Eds.), *Venus II: Geology, Geophysics, Atmosphere, and Solar Wind Environment* (p. 385–414). Tucson: The University of Arizona Press.
- Donahue, T. M. 1999. New analysis of hydrogen and deuterium escape from Venus. *Icarus* 141:226-235.
- Donahue, T. M. et al. 1982. Venus was wet—a measurement of the ratio of deuterium to hydrogen. *Science*, 216, 630.
- Dudzinski, L. “Radioisotope Power for NASA’s Space Science Missions.” NASA briefing to the Outer Planets Advisory Group. March 31, 2008.
- Dyar M. D., S. E. Smrekar and S. R. Kane. 2019. How Visiting Venus Will Help Us Find Life on Distant Planets, *Scientific American* 320, 2, 56-63 (February 2019) doi:10.1038/scientificamerican0219-56
- Dziewonski, A. M. and D. L. Anderson. “Preliminary Reference Earth Model.” *Phys. Earth Planet. Int.* 25, 297-356. 1981.
- Elkins-Tanton, L. T., S.E. Smrekar, P.C. Hess, E.M. Parmentier, Volcanism and volatile recycling on a one-plate planet: applications to Venus. *J. Geophys. Res.* 112, E04S06 (2007). <https://doi.org/10.1029/2006JE002793>
- Erbay, L. Berrin, et al. “Overall Performance of the Duplex Stirling Refrigerator.” *Energy Conversion and Management*, vol. 133, 2017, pp. 196–203., doi:10.1016/j.enconman.2016.12.003.
- Everett, M. E. 2013. “Appendix A: Shannon sampling theorem.” In: Everett, M. E. (Ed). *Near-Surface Applied Geophysics*. Cambridge University Press, Cambridge, UK. Pg 359-362
- Failor, K.C., Schmale, D.G. III, Vinatzer, B.A., and Monteil, C.L. (2017). Ice nucleation active bacteria in precipitation are genetically diverse and nucleate ice by employing different mechanisms. *ISME Journal* 11:2740–2753.
- Fee, D., Matoza, R.S. (2013). An overview of volcano infrasound: From Hawaiian to Plinian, local to global. *Journal of Volcanology and Geothermal Research* 249, 123–139. <https://doi.org/10.1016/j.jvolgeores.2012.09.002>
- Fegley, B., Zolotov, M.Y., & Lodders, K. 1997. The Oxidation State of the Lower Atmosphere and Surface of Venus, *Icarus*, 125, 416.
- Filiberto, J., D. Trang, Al. H. Treiman, M. S. Gilmore (2020). Present-day volcanism on Venus as evidenced from weathering rates of olivine. *Science Advances* 6, doi: [10.1126/sciadv.aax7445](https://doi.org/10.1126/sciadv.aax7445)
- Fjeldbo, G., B. Seidel, D. Sweetnam (1975), The Mariner 10 radio occultation measurements of the ionosphere of Venus, *J. Atmos. Sci.*, 32, pp. 1232-1236
- Ford, J. P., & J. J. Plaut. 1993. “Magellan Image Data.” In: Ford, J. P., J. J. Plaut, C. M. Weitz, T. G. Farr, D. A. Senske, E. R. Stofan, G. Michaels, & T. J. Parker. “Guide to Magellan Image Interpretation.” JPL Publication 93-24.
- Frandsen, B. N., Wennberg, P. O., Kjaergaard, H. G., 2016. Identification of OSSO as a near-UV absorber in the Venusian atmosphere. *Geophysical Research Letters*. 43, 11.

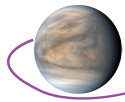




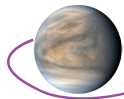
- Fukuhara, T., Futaguchi, M., Hashimoto, G. L., Horinouchi, T., Imamura, T., Iwagami, N., ... & Sato, M. (2017). Large stationary gravity wave in the atmosphere of Venus. *Nature Geoscience*, 10(2), 85-88.
- Furfaro, R. W. Fink, & J. S. Kargel. 2012. "Autonomous real-time landing site selection for Venus and Titan using Evolutionary Fuzzy Cognitive Maps." *Applied Soft Computing*, 12, 3825-3839. doi:10.1016/j.asoc.2012.01.014
- Futaana, Y. et al. 2017. Solar Wind Interaction and Impact on the Venus Atmosphere, *Space Science Reviews*, 212, 1453-1509.
- Gao, G.-b., J. Sterner, H. Morkoc. "High frequency performance of SiC heterojunction bipolar transistors." *IEEE Transactions on Electron Devices*, vol. 41, pp 1092-1097. 1994.
- Garvin, J. B., J. W. Head, M. T. Zuber, and P. Helfenstein. 1984. Venus: The nature of the surface from Venera panoramas, *J. Geophys. Res.*, 89, 3381-3399.
- Garvin, J. B., et al. 2020, DAVINCI+: Deep Atmosphere of Venus Investigation of Noble Gases, Chemistry & Imaging, Plus, *Lunar. Plan. Sci.*, 51, Abstract #2599.
- Genova A. et al. 2019. Geodetic Evidence That Mercury Has A Solid Inner Core, *GRL* 46, <https://doi.org/10.1029/2018GL081135>
- Ghail, Richard and Wilson, Colin and Widemann, Thomas and Titov, Dmitrij and Bruzzone, Lorenzo and Helbert, Jörn and Carine Vandaele, Ann and Marcq, Emmanuel and Dumoulin, Caroline and Rosenblatt, Pascal (2019) Envision M5 Venus orbiter proposal. EPSC-DPS Joint Meeting 2019, 15–20 September 2019, Geneva, Switzerland. <https://elib.dlr.de/131751>
- Ghent, R. R., & I. M. Tibuleac. 2002. "Ribbon spacing in Venusian tessera: Implications for layer thickness and thermal state." *Geophysical Research Letters*, 29. <https://doi.org/10.1029/2002GL015994>
- Giardini et al. (2020). The seismicity of Mars. *Nature Geoscience* 13, 205–212.
- Gillmann et al. (2020). Dry late accretion inferred from Venus's coupled atmosphere and internal evolution. *Nat. Geosci.* <https://doi.org/10.1038/s41561-020-0561-x>
- Gilmore, M. S., & A. J. Stein. 2017. "Variability of tessera radar emissivity on Venus." LPSC XLVIII. Abstract #2523.
- Gilmore M.S., Mueller N., and Helbert J. (2015) VIRTIS emissivity of Alpha Regio, Venus, with implications for tessera composition. *Icarus*, 254, 350-361.
- Gilmore M. S., A. Treiman, J. Helbert and S. Smrekar. 2017. Venus Surface Composition Constrained by Observation and Experiment, *Space Sci. Rev.*, 11, pp. 1-30, in Venus III (eds. B. Bézard, C. T. Russell, T. Satoh, S. Smrekar), doi:10.1007/s11214-017-0370-8.
- Gladman BJ, Burns JA, Duncan M, Lee P, Levinson HF, The exchange of impact ejecta between terrestrial planets. *Science*, 1996;271:1387–1392.
- Glass, Dean E., et al. "High Temperature Primary Battery for Venus Surface Missions." *Journal of Power Sources*, vol. 449, 2020, p. 227492., doi:10.1016/j.jpowsour.2019.227492.
- Golombek, M. P., Haldemann, A. F. C., Forsberg-Taylor, N. K., DiMaggio, E. N., Schroeder, R. D., Jakosky, B. M., Mellon, M. T., and Matijevic, J. R. (2003), Rock size-frequency distributions on Mars and implications for Mars Exploration Rover landing safety and operations, *J. Geophys. Res.*, 108, 8086, doi:10.1029/2002JE002035, E12.
- Greeley, R., Arvidson, R.E., Elachi, C., Geringer, M.A., Plaut, J.J., Saunders, R.S., Schubert, G., Stofan, E.R., Thouvenot, E.J., Wall, S.D. and Weitz, C.M., 1992. Aeolian features on Venus: preliminary Magellan results. *Journal of Geophysical Research: Planets*, 97(E8), pp.13319-13345.
- Green II, H., P. Burnley. 1989. A new self-organizing mechanism for deep-focus earthquakes. *Nature* 341, 733–737.
- Greenwood, J.P., Karato, S., Vander Kaaden, K.E. et al. Water and Volatile Inventories of Mercury, Venus, the Moon, and Mars. *Space Sci Rev* 214, 92 (2018). <https://doi.org/10.1007/s11214-018-0526-1>
- Greenwood, R. C., & Anand, M. (2020). What is the oxygen isotope composition of Venus? The scientific case for sample return from Earth's "sister" planet. *Space Sci Rev*, 216, 52.
- Grieger, B.; Ignatiev, N. I.; Hoekzema, N. M.; Keller, H. U. 2004. Indication of a near surface cloud layer on Venus from reanalysis of Venera 13/14 spectrophotometer data. Proceedings of the International Workshop Planetary Probe Atmospheric Entry and Descent Trajectory



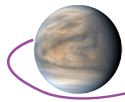
- Analysis and Science, 6-9 October 2003, Lisbon, Portugal. Edited by A. Wilson. ESA SP-544, Noordwijk, Netherlands: ESA Publications Division, ISBN 92-9092-855-7, 2004, p. 63–70
- Grindrod P. M., E. R. Stofan and J. E. Guest. 2010. Volcanism and resurfacing on Venus at the full resolution of Magellan SAR data, *GRL*, 37 <https://doi.org/10.1029/2010GL043424>
- Grinspoon, D. H. (1997). Venus revealed: a new look below the clouds of our mysterious twin planet.
- Grinspoon, D. H., Bullock, M. A., 2003. Did Venus experience one great transition or two? *B.A.A.S.* 35. <https://ui.adsabs.harvard.edu/abs/2003DPS....35.4403G/abstract>
- Grinspoon, D.H. and Bullock, M.A. (2013). Astrobiology and Venus Exploration. In *Exploring Venus as a Terrestrial Planet* (eds L.W. Esposito, E.R. Stofan and T.E. Cravens). doi:10.1029/176GM12
- Grinspoon, D., Amato, M., Adams, M., and Balint, T. “Venus Climate Mission Study Final Report” (2010).
- Guest J.E., and Stofan E.R. (1999), A new view of the stratigraphic history of Venus, *Icarus*, 139, 55-66.
- Guhel Y., B. Boudart, V. Hoel, M. Werquin, C. Gaquiere, J. C. De Jaeger, M. A. Poisson, I. Daumiller, and E. Kohn. “Effects of High Temperature on the Electrical Behavior of AlGaIn/GaN HEMTs.” *Microwave Opt. Technol. Lett.* 34, 4. 2002.
- Gülcher, A.J.P., Gerya, T.V., Montési, L.G.J. et al. Corona structures driven by plume–lithosphere interactions and evidence for ongoing plume activity on Venus. *Nat. Geosci.* (2020). <https://doi.org/10.1038/s41561-020-0606-1>
- Hagedorn, N.H. “Alkali metal carbon dioxide electrochemical system for energy storage and/or conversion of carbon dioxide to oxygen.” Patent 5213908, 1993.
- Hall, Jeffery L., et al. “Altitude-Controlled Light Gas Balloons for Venus and Titan Exploration.” AIAA Aviation 2019 Forum. 2019-3194.
- Hall, J. L., et al. “Prototype design and testing of a Venus long duration, high altitude balloon.” *Advances in Space Research* 42.10 (2008): 1648-1655.
- Hansen, V., Phillips, R., Willis, J. & Ghent, R. (2000). Structures in tessera terrain, Venus: Issues and answers. *Journal of Geophysical Research*. 105. 4135-4152. 10.1029/1999JE001137.
- Hansen V.L., and Young D.A. (2007) Venus’s evolution: A synthesis. Geological Society of America Special Papers 419, 255-273, doi:10.1130/2006.2419(13).
- Hashimoto G.L., Roos-Serote M., Sugita S., Gilmore M.S., Kamp L.W., Carlson R.W., and Baines K.H. (2008) Felsic highland crust on Venus suggested by Galileo Near-Infrared Mapping Spectrometer data. *Journal of Geophysical Research: Planets*, 113(E5). E00B24, doi:10.1029/2008JE003134.
- Helbert, J., N. Müller, P. Kostama, L. Marinangeli, G. Piccioni, and P. Drossart. 2008. Surface brightness variations seen by VIRTIS on Venus Express and implications for the evolution of the Lada Terra region, Venus, *Geophys. Res. Lett.*, 35, L11201, doi: 10.1029/2008GL033609.
- Helbert, J., Dennis Wendler, Ingo Walter, Thomas Widemann, Emmanuel Marcq, Gabriel Guignan, Sabrina Ferrari, Alessandro Maturilli, Nils Mueller, David Kappel, Judit Jaenchen, Mario D’Amore, Anko Boerner, Darby Dyar, Gabriele E. Arnold, Suzanne Smrekar, “The Venus Emissivity Mapper (VEM) concept,” *Proc. SPIE* 9973, Infrared Remote Sensing and Instrumentation XXIV, 99730R (14 September 2016); <https://doi.org/10.1117/12.2237568>
- Helbert, J., Maturilli, A., Dyar, M.D., Ferrari, S., Mueller, N. and Smrekar, S., 2017, March. First set of laboratory Venus analog spectra for all atmospheric windows. In *Lunar Planet. Sci. Conf. Abstr* (Vol. 48, p. 1512).
- Helbert, J., A. C. Vandaele, E. Marcq, S. Robert, C. Ryan, G. Guignan, Y. Rosas-Ortiz, E. Neefs, I. R. Thomas, G. Arnold, G. Peter, T. Widemann, L. Lara, “The VenSpec suite on the ESA EnVision mission to Venus,” *Proc. SPIE* 11128, Infrared Remote Sensing and Instrumentation XXVII, 1112804 (9 September 2019); <https://doi.org/10.1117/12.2529248>
- Herrick R.R., and Rumpf M.E. (2011) Postimpact modification by volcanic or tectonic processes as the rule, not the exception, for Venusian craters. *Journal of Geophysical Research* 116, doi:10.1029/2010je00372.
- Herrick, R. R., D. L. Stahlke, & V. L. Sharpton. 2012. “Fine-scale Venusian topography from Magellan stereo data.” *Eos*, 93. <https://doi.org/10.1029/2012EO120002>



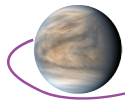
- Herrick, R. R., & R. J. Phillips. 1994. "Implications of a global survey of Venusian impact craters." *Icarus*, 111, 387-416.
- Herrick, R.R. et al. 2009. The Rationale for a New High-resolution Imaging Radar Mission to Venus. AGU Fall Meeting Abstracts. P33A1281H.
- Hickey, M.P., G. Schubert, and R.L. Walterscheid (2009). Propagation of tsunami-driven gravity waves into the thermosphere and ionosphere. *J. Geophys. Res.* 114, A08304, doi: [10.1029/2009JA014105](https://doi.org/10.1029/2009JA014105)
- Hill, S.C., Pinnick, R.G., Niles, S., Pan, Y-L., Holler, S., Chang, R.K., Bottiger, J., Chen, B.T., Orr, C-S., and Feather, G. (1999). Real-Time Measurement of Fluorescence Spectra from Single Airborne Biological Particles. *Field Analyt Chem & Tech* 3(4-5):221-239, 1999
- Horinouchi, Takeshi, Yoshi-yuki Hayashi, Shigeto Watanabe, Manabu Yamada, Atsushi Yamazaki, Toru Kouyama, Makoto Taguchi, Tetsuya Fukuhara, Masahiro Takagi, Kazunori Ogohara, Shinya Murakami, Javier Peralta, Sanjay S. Limaye, Takeshi Imamura, Masato Nakamura, Takao M. Sato, Takehiko Satoh, 2020, How waves and turbulence maintain the super-rotation of Venus' atmosphere, *Science*, Vol. 368, Issue 6489, pp. 405-409 DOI: 10.1126/science.aaz4439
- Hunter, G, J. Balcerski, S. Clegg, J. Cutts, C. Gray, N. Izenberg, N. Johnson, T. Kremic, L. Matthies, J. O'Rourke, and E. Venkatapathy (2019) VEXAG Venus Technology Plan. [https://www.lpi.usra.edu/vexag/reports/VEXAG\\_Venus\\_Techplan\\_Current.pdf](https://www.lpi.usra.edu/vexag/reports/VEXAG_Venus_Techplan_Current.pdf)
- Hunter, G.W., Okojie, R.S., Neudeck, P.G., Beheim, G.M., Ponchak, G.E., Fralick, G., Wrbanek, J. and Chen, L.Y., 2006. High temperature electronics, communications, and supporting technologies for Venus missions. *Electr. Eng.*, 8.
- Hunter, G. W., Liu C. C., Makel D. "MEMS handbook, second edition, design and fabrication." CRC Press LLC, ed. M. Gad-el-Hak, Boca Raton, FL, Ch. 11. 2006.
- Hunter, G. W., P. G. Neudeck, R. S. Okojie, G. M. Beheim, M. Kraskowski, G. E. Ponchak and L. Y.Chen. "High temperature electronics, communications, and supporting technologies for Venus missions." 5th International Planetary Probe Workshop, Bordeaux, France. June 23-29, 2007.
- Hyder, A. K., Wiley, R. L., Halpert, G., Flood, D. J., and Sabripour, S. "Spacecraft power technologies." Imperial College Press, London, Ch. 5-6. 2000.
- Iglesias, F. A., A. Feller, & K. Nagaraju. 2015. "Smear correction of highly-variable, frame-transfer-CCD images with application to polarimetry." *Applied Optics*, 54, 5970-5975. <https://doi.org/10.1364/AO.54.005970>
- Imamura, T., Higuchi, T., Maejima, Y., Takagi, M., Sugimoto, N., Ikeda, K., & Ando, H. (2014). Inverse insolation dependence of Venus' cloud-level convection. *Icarus*, 228, 181-188.
- Imamura, T., et al. (2017), Initial performance of the radio occultation experiment in the Venus orbiter mission Akatsuki, *Earth, Planets, and Space*, 69, doi:10.1186/s40623-017-0722-3.
- Ivanov, M.A., Basilevsky, A.T., 1993. Density and morphology of impact craters on tesserae terrain. *Geophys. Res. Lett.* 20, 2579-2582.
- Ivanov, M.A., Head, J.W., 1996. Tessera terrain on Venus: A survey of the global distribution, characteristics, and relation to surrounding units from Magellan data. *J. Geophys. Res.* 101, 14861-14908.
- Ivanov M.A., and Head J. W. (2011) Global geological map of Venus. *Planetary and Space Science* 59, 1559-1600, doi:<http://dx.doi.org/10.1016/j.pss.2011.07.008>.
- Iwagami, N., Hashimoto, G. L., Ohtsuki, S., Takagi, S., Robert, S., 2015. Ground-based IR observation of oxygen isotope ratios in Venus's atmosphere. *Planetary and Space Science*. 113-114, 292-297. <http://dx.doi.org/10.1016/j.pss.2014.10.004>
- Iwaszenko, S., & A. Smolinski. 2020. "Texture features for bulk rock material grain boundary segmentation." *Journal of King Saud University – Engineering Sciences*. <https://doi.org/10.1016/j.jksues.2020.03.001>
- Jackson, J.M., V.H. Lai, and D.C. Bowman. 2018. Detection of Artificial Earthquakes from balloon-borne infrasound sensors, *Geophysical Research Letters*, 45. <https://doi.org/10.1002/2018GL077481>.
- James, P. B., M. T. Zuber, & R. J. Phillips. (2013). "Crustal thickness and support of topography on Venus." *Journal of Geophysical Research: Planets*. Vol 118. doi: [10.1029/2012JE004237](https://doi.org/10.1029/2012JE004237).



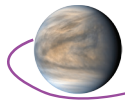
- Jenkins, J. M., P. G. Steffes, D. P. Hinson, J. D. Twicken, and G. L. Tyler (1994), Radio Occultation Studies of the Venus Atmosphere with the Magellan Spacecraft: 2. Results from the October 1991 Experiments, *Icarus*, 110, pp. 79-94, <https://doi.org/10.1006/icar.1994.1108>
- Jiang, X., S. Li, & T. Tao. 2016. "Innovative hazard detection and avoidance strategy for autonomous safe planetary landing." *Acta Astronautica*, 126, 66-76. <http://dx.doi.org/10.1016/j.actaastro.2016.02.028>
- Jimenez, J. L. and U. Chowdhury. "X-band GaN FET reliability." IEEE 46th Int. Reliability Physics Symp., Phoenix, AZ, pp 429-435. 2006.
- Johnson, J. B., R. C. Aster, and P. R. Kyle (2004), Volcanic eruptions observed with infrasound, *Geophys. Res. Lett.* 31, L14604, doi:[10.1029/2004GL020020](https://doi.org/10.1029/2004GL020020)
- Johnson, R. W., Wang, C., Liu, Y., Scofield, J. D. "Power Device Packaging Technologies for Extreme Environments." *Electronics Packaging Manufacturing*, IEEE Transactions on (1521-334X), Vol. 30, Issue 3; p. 182. July 2007.
- Kane, S.R. and 11 colleagues 2019. Venus as a Laboratory for Exoplanetary Science. *Journal of Geophysical Research (Planets)* 124, 2015–2028.
- Kane, S.R., Barclay, T., Gelino, D.M. 2013. A Potential Super-Venus in the Kepler-69 System. *The Astrophysical Journal* 770.
- Kane, S.R., Ceja, A.Y., Way, M.J., Quintana, E.V. 2018. Climate Modeling of a Potential ExoVenus. *The Astrophysical Journal* 869.
- Kane S. R., R. K. Kopparapu, S. D. Domagal-Goldman. 2014. On the frequency of potential Venus analogs from Kepler data. *Ap.J.Lett.* 794:L5.
- Kang B. S., F. Ren, B. P. Gila, C. R. Abernathy, J. Lin, S. N. G. Chu. "GaN-based diodes and transistors for chemical, gas, biological and pressure sensing." *J. Phys. Condens. Matter* 16 R961-R994. 2004.
- Kaula, W.M., 1999. Constraints on Venus evolution from radiogenic argon. *Icarus*, 139, 32-39.
- Kempton, E.M.R. and 42 colleagues 2018. A Framework for Prioritizing the TESS Planetary Candidates Most Amenable to Atmospheric Characterization. *Publications of the Astronomical Society of the Pacific* 130, 114401.
- KISS (Keck Institute for Space Studies), Venus Seismology Study Team. 2015. Probing the Interior Structure of Venus, Keck Institute for Space Studies, Pasadena, Calif. <http://resolver.caltech.edu/CaltechAUTHORS:20150727-150921873>.
- Kite, E.S., M. N. Barnett (2020) Exoplanet secondary atmosphere loss and revival, Proceedings of the National Academy of Sciences Jul 2020, 202006177; DOI: 10.1073/pnas.2006177117
- Kempton, E.M.R. and 42 colleagues 2018. A Framework for Prioritizing the TESS Planetary Candidates Most Amenable to Atmospheric Characterization. *Publications of the Astronomical Society of the Pacific* 130, 114401
- Klaasen, K. P., and R. Greeley. "VEVA Discovery mission to Venus: exploration of volcanoes and atmosphere." *Acta Astronautica* 52.2-6 (2003): 151-158.
- Kliore, A. J. (1985), Recent results on the Venus atmosphere from pioneer Venus radio occultations, *Advances in Space Research*, 5, pp. 41-49, [https://doi.org/10.1016/0273-1177\(85\)90269-8](https://doi.org/10.1016/0273-1177(85)90269-8)
- Klotz, M. G., Bryant, D. A., & Hanson, T. E. (2011). The microbial sulfur cycle. *Frontiers in microbiology*, 2, 241.
- Knicely, J. J., & R. R. Herrick. 2019. "Evaluation of the bandwidths and spatial resolutions achievable with near-infrared observations of Venus below the cloud deck." *Planetary and Space Science*, 181. <https://doi.org/10.1016/j.pss.2019.104787>
- Knollenberg R. G. and D. M. Hunten, 1980. The microphysics of the clouds of Venus: Results of the Pioneer Venus Particle Size Spectrometer Experiment, *JGR, Space Physics*, 85, 8039-8058, <https://doi.org/10.1029/JA085iA13p08039>
- Konopliv, A.S. and Sjogren, W.L., 1996. Venus Gravity Handbook, JPL Publication 96-2, 66 pp.
- Konopliv, A. S., W.B. Banerdt, W.L. Sjogren, Venus Gravity: 180th Degree and Order Model, *Icarus*, Volume 139, Issue 1, 1999, Pages 3-18, <https://doi.org/10.1006/icar.1999.6086>.
- Kotiranta, M., Jacob, K., Kim, H., Hartogh, P. and Murk, A., 2018. Optical Design and Analysis of the Submillimeter-Wave Instrument on JUICE. *IEEE transactions on terahertz science and technology*, 8(6), pp.588-595.



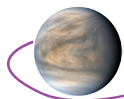
- Krasnopolsky, V. A. (2006). Chemical composition of Venus atmosphere and clouds: Some unsolved problems. *Planetary and Space Science*, 54(13-14), 1352-1359.
- Krasnopolsky, V. A., 2017. On the iron chloride aerosol in the clouds of Venus. *Icarus*. 286, 134-137.
- Kremic et al. (2020) Long-Lived In situ Solar System Explorer (LLISSE): Potential contributions to the next decade of Solar System exploration, Planetary Science and Astrobiology Decadal Survey White Paper.
- Kremic T., R. Ghail, M. Gilmore, G. Hunter, W. Kiefer, S. Limaye, M. Pauken, C. Tolbert, C. Wilson (2020) Long-duration Venus lander for seismic and atmospheric science, *Plan. Space Sci.*, 190, 104961.
- Krishnamoorthy, S., A. Komjathy, J. A. Cutts, M. T. Pauken, L. Martire, R. F. Garcia, D. Mimoun, V. H. Lai, J. M. Jackson, D. C. Bowman, S. Kedar, S. E. Smrekar and J. L. Hall (2018a). Seismic infrasound as a geophysical probe for Venus. 49th Lunar and Planetary Science Conference 2018 (LPI Contrib. No. 2083).
- Krishnamoorthy, S., A. Komjathy, M.T. Pauken, J.A. Cutts, R.F. Garcia, D. Mimoun, A. Cadu, A. Sournac, J.M. Jackson, V.H. Lai, and D.C. Bowman (2018b): Detection of Artificial Earthquakes from balloon-borne infrasound sensors, *Geophysical Research Letters*, 45. <https://doi.org/10.1002/2018GL077481>
- Krishnamoorthy, S., V.H. Lai, A. Komjathy, M.T. Pauken, J.A. Cutts, R.F. Garcia, D. Mimoun, J.M. Jackson, D.C. Bowman, E. Kassarian, L. Martire, A. Sournac, and A. Cadu (2019): Aerial Seismology using Balloon-Based Barometers, *IEEE Transactions on Geoscience and Remote Sensing*, doi: [10.1109/TGRS.2019.2931831](https://doi.org/10.1109/TGRS.2019.2931831)
- Krishnamoorthy, S. et al. (2020) Seismology on Venus with infrasound observations from balloon and orbit, Planetary Science and Astrobiology Decadal Survey White Paper.
- Lai, V. H., Z. Zhan and Q. Brissaud (2019). Insight on the Kilauea caldera evolution through the 2018 earthquake sequence, in V43C-0204, Fall Meeting of the American Geophysical Union.
- Landis, G. and K. C. Mellott. "Venus surface power and cooling system design." Paper IAC-04-R.2.06, *Acta Astronautica*, Vol. 61, No. 11-12, pp 995-1001. 2007.
- Lebonnois S. and G. Schubert. 2017. The deep atmosphere of Venus and the possible role of density-driven separation of CO<sub>2</sub> and N<sub>2</sub>, *Nature Geosci.* 10, 473-477.
- Lebonnois, S., Schubert, G., Forget, F. and Spiga, A., 2018. Planetary boundary layer and slope winds on Venus. *Icarus*, 314, pp.149-158.
- Lebonnois, S., G. Schubert, T. Kremic, L. M. Nakley, K. G. Phillips, J. Bellan, D. Cordier (2020). An experimental study of the mixing of CO<sub>2</sub> and N<sub>2</sub> under conditions found at the surface of Venus. *Icarus* 338, 113550.
- Lei, J. F., Fralick G. C., Krasowski M. J. "Microfabricated multifunction strain-temperature gauge." US Patent 5,979,243, November 9, 1999.
- Lewandowski. E. J., J. G. Schreiber, S. D. Wilson, S. M. Oriti, P. Cornell, N. Schifer. "Extended operation testing of Stirling convertors in support of Stirling radioisotope power system development." 6th International Energy Conversion Engineering Conference (IECEC), AIAA 2008-5791, Cleveland, OH. July 2008.
- Li, C., Z. Peng, S. Yao, H. Guo, Z. Zhan, and H. Zhang (2018). Abundant aftershock sequence of the 2015 Mw7.5 Hindu Kush intermediate-depth earthquake. *Geophys. J. Int.*, 213, 2, 1121-1134, <https://doi.org/10.1093/gji/ggy016>
- Limaye, S.S., Mogul, R., Smith, D.J., Ansari, A.H., Słowik, G.P. and Vaishampayan, P., 2018. Venus' Spectral Signatures and the Potential for Life in the Clouds. *Astrobiology*, 18(9), pp.1181-1198.
- Liu Y., M. Z. Kauser, D. D. Schroepfer, P. P. Ruden, J. Xie, Y. T. Moon, N. Onojima, H. Morkoç, K.-A. Son, M. I. Nathan. "Effect of hydrostatic pressure on the current-voltage characteristics of GaN/AlGaN/GaN heterostructure devices." *J. Appl. Phys.* 99, 113706. 2006.
- Lognonné, P. et al. (2006). Ground-based GPS imaging of ionospheric post-seismic signal, *Planet. Space Sci.* 54, 528–540, doi:[10.1016/j.pss.2005.10.021](https://doi.org/10.1016/j.pss.2005.10.021).
- Lognonné, P. and C.L. Johnson (2007). Planetary Seismology, in Treatise, *Geophysics* 10, 4.
- Loper, D.E., P.H. Roberts, Compositional convection and the gravitationally powered dynamo. *Stellar & Planetary Magnetism* (Ed: A.M. Soward). Gordon & Breach, 1983, 297-327.



- Lorenz, R. D. 2010. "Attitude and angular rates of planetary probes during atmospheric descent: Implications for imaging." *Planetary and Space Science*, 58, 838-846. doi:10.1016/j.pss.2010.01.003
- Lorenz, R. D. 2012. Planetary seismology—Expectations for lander and wind noise with application to Venus, *Planetary and Space Science*, 62, 86-96.
- Lorenz, R. D., & Panning, M. (2018). Empirical recurrence rates for ground motion signals on planetary surfaces. *Icarus*, 303, 273-279.
- Luhmann, J. G., et al. 2008. Venus Express observations of atmospheric oxygen escape during the passage of several coronal mass ejections, *Journal of Geophysical Research*, 113, doi:10.1029/2008je003092.
- Lunghi, P., M. Lavagna, & R. Armellin. 2015. "A semi-analytical guidance algorithm for autonomous landing." *Advances in Space Research*, 55, 2719-2738. <http://dx.doi.org/10.1016/j.asr.2015.02.022>
- Lunghi, P. M. Ciarambino, & M. Lavagna. 2016. "A multilayer perceptron hazard detector for vision-based autonomous planetary landing." *Advances in Space Research*, 58, 131-144. <http://dx.doi.org/10.1016/j.asr.2016.04.012>
- Lustig-Yaeger, J., Meadows, V.S., Lincowski, A.P. 2019. The Detectability and Characterization of the TRAPPIST-1 Exoplanet Atmospheres with JWST. *The Astronomical Journal* 158.
- Mahaffy, P. R., et al., 2012. The Sample Analysis at Mars Investigation and Instrument Suite. *Space Science Reviews*. 170, 401-478.
- Malin, M. C. (1992), Mass movements on Venus: Preliminary results from Magellan cycle 1 observations, *J. Geophys. Res.*, 97( E10), 16337– 16352, doi:10.1029/92JE01343.
- Marcq, E., J.-L. Bertaux, F. Montmessin and D. Belyaev. 2013. Variations of sulfur dioxide at the cloud top of Venus's dynamic atmosphere, *Nature Geoscience*, 6, 5–28.
- Martire, L., Q. Brissaud, V.H. Lai, R.F. Garcia, R. Martin, S. Krishnamoorthy, A. Komjathy, A. Cadu, J.A. Cutts, J.M. Jackson, D. Mimoun, M.T. Pauken, and A. Sournac (2018): Numerical simulation of the atmospheric signature of artificial and natural seismic events, *Geophysical Research Letters*, 45, 12,085–12,093, <https://doi.org/10.1029/2018GL080485>
- Mason, S. "Realistic specific power expectations for advanced radioisotope power systems." Proceedings of the 4th International Energy Conversion Engineering Conference (IECEC-2006), San Diego, CA. June 2006.
- Mazel C. H., and Fuchs E. (2003) Contribution of fluorescence to the spectral signature and perceived color of corals. *Limnol Oceanog*, 48, 390.
- McCluskey, F. P., R. Grzybowski, T. Podlesak. "High temperature electronics." CRC Press, Boca Raton, FL. 1996.
- McGovern, P. J., M. E. Rumpf, and J. R. Zimbelman (2013), The influence of lithospheric flexure on magma ascent at large volcanoes on Venus, *J. Geophys. Res. Planets*, 118, 2423–2437, doi:10.1002/2013JE004455
- McKinnon, W. B., K. J. Zahnle, B. I. Ivanov, and H. J. Melosh (1997) Cratering on Venus: Models and observations, in Venus II, edited by S. W. Bougher, D. M. Hunten, and R. J. Phillips, pp. 969-1014, Univ. of Ariz. Press, Tucson.
- McManamon, P. F., P. Banks, J. Beck, D. G. Fried, A. S. Huntington, & E. A. Watson. 2017. "Comparison of flash LIDAR detector options." *Optical Engineering*, 56. doi: 10.1117/1.OE.56.3.03122
- Mellott, K. D. "Electronics and sensor cooling with a Stirling cycle for Venus surface mission," AIAA 2nd International Energy Conversion Engineering Conference, AIAA 2004-5610, Providence, RI. August 2004.
- Melosh, H.J., Tonks, W.B. (1993) Swapping Rocks: Ejection and Exchange of Surface Material Among the Terrestrial Planets. *Meteoritics* 28, 398–398.
- Mendonça, J. M., Read, P. L., Wilson, C. F., & Lewis, S. R. (2012). Zonal winds at high latitudes on Venus: An improved application of cyclostrophic balance to Venus Express observations. *Icarus*, 217(2), 629-639. Meng, X., Verkhoglyadova, O. P., Komjathy, A., Savastano, G., and Mannucci, A. J. (2018). Physics-based modeling of earthquake-induced ionospheric disturbances, *J. Geophys. Res.: Space Physics*, 123, pp. 8021–8038, <https://doi.org/10.1029/2018JA025253>

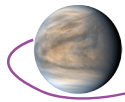


- Meng, X., Vergados, P., Komjathy, A., and Verkhoglyadova, O. (2019), Upper atmospheric responses to surface disturbances: An observational perspective, *Radio Sci.*, 54, pp. 1076–1098, <https://doi.org/10.1029/2019RS006858>
- Meyer, F.J. and Sandwell, D.T., 2012. SAR interferometry at Venus for topography and change detection. *Planetary and Space Science*, 73(1), pp.130-144.
- Mondt, J., Burke, K., Bragg, B., Rao, G., Vukson, S. “Energy storage technology for future space science missions.” National Aeronautics and Space Administration, Technical Report, JPL D-30268 Rev. A. 2004.
- Morbidelli, A., J.I. Lunine, D.P. O’Brien, S.N. Raymond, K.J. Walsh, Building terrestrial planets, *Annual Review of Earth and Planetary Sciences* 2012 40:1, 251-275
- Morowitz, H., Sagan, C. Life in the Clouds of Venus?. *Nature* 215, 1259–1260 (1967). <https://doi.org/10.1038/2151259a0>
- Moroz, V. I. (2002). “Estimates of visibility of the surface of Venus from descent probes and balloons.” *Planetary and Space Science*, 50, pp. 287-297, [https://doi.org/10.1016/S0032-0633\(01\)00128-3](https://doi.org/10.1016/S0032-0633(01)00128-3)
- Morrison, S. M., Downs, R. T., Blake, D. F., Prabhu, A., Eleish, A., Vaniman, D. T., ... & Treiman, A. H. (2018). Relationships between unit-cell parameters and composition for rock-forming minerals on Earth, Mars, and other extraterrestrial bodies. *American Mineralogist*, 103(6), 848-856
- Mueller, N., Helbert, J., Hashimoto, G. L., Tsang, C. C. C., Erard, S., Piccioni, G., & Drossart, P. (2008). Venus surface thermal emission at 1  $\mu\text{m}$  in VIRTIS imaging observations: Evidence for variation of crust and mantle differentiation conditions. *Journal of Geophysical Research: Planets*, 113(E5).
- NASEM (National Academies of Sciences, Engineering, and Medicine). 2017. Powering Science—NASA’s Large Strategic Science Missions. Washington, DC: The National Academies Press. <https://doi.org/10.17226/24857>.
- NASEM (National Academies of Sciences, Engineering, and Medicine). 2018. Visions into Voyages for Planetary Science in the Decade 2013-2022: A Midterm Review. Washington, DC: The National Academies Press. <https://doi.org/10.17226/25186>.
- NASEM (National Academies of Sciences Engineering and Medicine). Assessment of Planetary Protection Requirements for Venus Missions: Letter Report (2006). National Academies Press, 2006; 16p.
- Navair, Multi-Species Gas Sensor Array project, Test and Evaluation/Science and Technology Program, Navair, Naval Undersea Warfare Center, Newport, RI, contract N66604-07-C-1828
- Neudeck, P. G. “SiC technology.” *The VLSI Handbook, the Electrical Engineering Handbook Series* (W.-K. Chen, Ed.), pp 6.1-6.24. CRC Press and IEEE Press, Boca Raton, FL. 2000.
- Neudeck, P. G., Okojie, R. S., Chen, L.-Y. “High-temperature electronics—A role for wide bandgap semiconductors.” *Proceedings of the IEEE*, vol. 90, pp 1065-1076. 2002.
- Neudeck, P. G., D. J. Spry, L.-Y. Chen, C. W. Chang, G. M. Beheim, R. S. Okojie, L. J. Evans, R. Meredith, T. Ferrier, M. J. Krasowski, N. F. Prokop. “Long-term characterization of 6H- SiC transistor integrated circuit technology operating at 500 °C.” *Silicon Carbide 2008 - Materials, Processing and Devices*, vol. 1069, Materials Research Society Symposium Proceedings (M. Dudley, A. R. Powell, C. M. Johnson, and S.-H. Ryu, Eds). Warrendale, PA: Materials Research Society. 2008.
- Ni, X., J. Xie, Y. Fu, H. Morkoç, I.P. Steinke, Y. Liu, P.P. Ruden, K.-A. Son, B. Yang. “Investigation of current-voltage characteristics of n-GaN/i-Al<sub>x</sub>Ga<sub>1-x</sub>N/n-GaN structures.” *SPIE* 6473, 11. 2007.
- Niekum, S. 2008. “Reliable rock detection and classification for autonomous science.” Honor Bachelor Thesis, Carnegie Mellon University.
- Niemann, H. B., Hartle, R. E., Kasprzak, W. T., Spencer, N. W., Hunten, D. M., & Carignan, G. R. (1979). Venus upper atmosphere neutral composition: Preliminary results from the Pioneer Venus orbiter. *Science*, 203(4382), 770-772.
- Nimmo, F., and D. McKenzie (1998), Volcanism and tectonics on Venus, *Annu. Rev. Earth Planet. Sci.*, 26, 23–51.

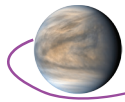


- NRC (National Research Council). 2011. Vision and Voyages for Planetary Science in the Decade 2013-2022. The National Academies Press. Washington, DC.
- O'Brien, D.P. A. Izidoro, S.A. Jacobson, S.N. Raymond, D.C. Rubie, The delivery of water during terrestrial planet formation. *Space Sci Rev.* 214, 47 (2018). <https://doi.org/10.1007/s11214-018-0475-8>
- Occhipinti, G., P. Coïsson, J.J. Makela, S. Allgeyer, A. Kherani, H. Hébert, and P. Lognonné (2011). Three-dimensional numerical modeling of tsunami-related internal gravity waves in the Hawaiian atmosphere, *Earth Planets Space* 63 (7): 847–851, doi:10.5047/eps.2011.06.051
- O'Farrell et al, 'Static Wind Tunnel Testing of a Legged Venus Lander', AIAA Paper 2017-3726.
- O'Farrell C., B. S. Sonneveldt, C. Karhgaard, J. A. Tynis and I. G. Clark, "Overview of the ASPIRE Project's Supersonic Flight Tests of a Strengthened DGB Parachute," 2019 IEEE Aerospace Conference, Big Sky, MT, USA, 2019, pp. 1-18, doi: 10.1109/AERO.2019.8741611.
- Okojie, R. S., Fralick G. C., Saad G. J., Blaha C. A., Adamczyk J. J., Feiereisen J. M. "A single crystal SiC plug-and-play high temperature drag force transducer." Digest of Technical Papers for Transducers 2003, pp. 400-403, IEEE Catalog Number 03TH8664C, The 12th International Conference on Solid State Sensors, Actuators and Microsystems, Boston, MA. June 2003.
- Okojie, R. S., S. M. Page, M. Wolff. "Performance of MEMS-DCA SiC pressure transducers under various dynamic conditions." 2006 IMAPS International High Temperature Electronics Conference, Santa Fe, NM, pp 70-75. May 2006.
- O'Rourke, J. G., Korenaga, J., 2015. Thermal evolution of Venus with argon degassing. *Icarus.* 260, 128-140.
- O'Rourke, J.G. and Stevenson, D. J. 2016. Powering Earth's Dynamo with Magnesium Precipitation from the Core. *Nature* 529, 387–389.
- O'Rourke, J.G., Wolf, A.S. and Ehlmann, B.L., 2014. Venus: Interpreting the spatial distribution of volcanically modified craters. *Geophysical Research Letters*, 41(23), pp.8252-8260.
- O'Rourke, J. G., Buz, J., Fu, R. R., & Lillis, R. J. (2019). Detectability of remanent magnetism in the crust of Venus. *Geophysical Research Letters*, 46, 5768– 5777. <https://doi.org/10.1029/2019GL082725>.
- O'Rourke, J. G. (2020) Searching for crustal remanent magnetism on Venus is a high-impact science objective, Planetary Science and Astrobiology Decadal Survey White Paper.
- Oschlisniok J, B. Häusler, M. Pätzold, G. L. Tyler, M. K. Bird, S. Tellmann, S. Remus, T. Andert (2012), Microwave absorptivity by sulfuric acid in the Venus atmosphere: first results from the Venus Express Radio Science experiment VeRa, *Icarus*, 221, pp. 940–948, <https://doi.org/10.1016/j.icarus.2012.09.029>
- Ostberg, C., & Kane, S. R. (2019). Predicting the Yield of Potential Venus Analogs from TESS and Their Potential for Atmospheric Characterization. *The Astronomical Journal*, 158(5), 195.
- Papike, J.J., Karner, J.M. and Shearer, C.K., 2003. Determination of planetary basalt parentage: A simple technique using the electron microprobe. *American Mineralogist*, 88(2-3), pp.469-472.
- Penswich, L. B. and I. Urieli. "Duplex Stirling machines." QP-051082-A presented at the 19th Annual Intersociety Energy Conversion Engineering Conference, San Francisco, CA. 1984.
- Pepin, R. 1991. On the origin and early evolution of terrestrial planet atmospheres and meteoritic volatiles. *Icarus*, 92, 2–79.
- Peplowski, P.N., Lawrence, D.J. & Wilson, J.T. Chemically distinct regions of Venus's atmosphere revealed by measured N2 concentrations. *Nat Astron* (2020). <https://doi.org/10.1038/s41550-020-1079-2>
- Pepper, I.L., and Dowd, S.E. 2009, . Aeromicrobiology. Environmental Microbiology. Academic Press, NYNY. Pp. 83-101.
- Pereira, M.L., Knibbs, L.D., He, C., Grzybowski, P., Johnson, G.R., Huffman, J.A., Bell, S.C., Wainwright, C.E., Matte, D.L., Dominski, F.H., Andrade, A., and Morawska, L. (2017) Sources and dynamics of fluorescent particles in hospitals. *Indoor Air* 27:988–1000.
- Perez, T., G.J. Finkelstein, O. Pardo, N.V. Solomatova, and J.M. Jackson (2020): A Synchrotron Mössbauer Spectroscopy Study of a Hydrated Iron-Sulfate at High Pressures. *Minerals*, 10, 46, <https://doi.org/10.3390/min10020146>

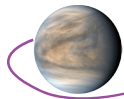




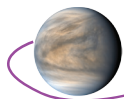
- Perez-Hoyos, S., Sanchez-Lavega, A., Garcia-Munoz, A., Irwin, P.G.J., Peralta, J., Holsclaw, G., McClintock, W.M., and Sanz-Requena, J.F. (2018) Venus upper clouds and the UV-absorber from MESSENGER/MASCS observations. arXiv 1801.03820.
- Petry, M. R., A. P. Moreira, & L. P. Reis. 2013. "Increasing illumination invariance of SURF feature detector through color constancy." In: Correia L., Reis L. P., Cascalho J. (eds) Progress in Artificial Intelligence. EPIA 2013. Lecture Notes in Computer Science, 8154. [https://doi.org/10.1007/978-3-642-40669-0\\_23](https://doi.org/10.1007/978-3-642-40669-0_23)
- Phillips R.J., and Hansen V.L. (1998) Geological evolution of Venus: Rises, plains, plumes, and plateaus. *Science*, 279(5356), 1492-1497.
- Phillips, R. J., R. E. Grimm, and M. C. Malin (1991), Hot-spot evolution and the global tectonics of Venus, *Science*, 252(5006), 651-658.
- Phillips R.J., Raubertas R.F., Arvidson R.E., Sarkar I.C., Herrick R.R., Izenberg N., and Grimm R.E. (1992) Impact crater distribution and the resurfacing history of Venus, *J. Geophys. Res.*, 97, 15,923-15948.
- Plaut, J. J. 1993. "The Non-SAR Experiments." In: Ford, J. P., J. J. Plaut, C. M. Weitz, T. G. Farr, D. A. Senske, E. R. Stofan, G. Michaels, & T. J. Parker. "Guide to Magellan Image Interpretation." JPL Publication 93-24.
- Pollack, J.B., Toon, O.B., Whitten, R.C., Boese, R., Ragent, B., Tomasko, M., Esposito, L., Travis, L., and Wiedman, D., 1980, Distribution and source of the UV absorption in Venus' atmosphere: *Journal of Geophysical Research: Space Physics* (1978–2012), v. 85, p. 8141–8150, doi:10.1029/ja085ia13p08141.
- Powell, A.J., Neudeck, P. G., Trunek, A. J., Spry, D. J. "Method for the growth of large low-defect single crystals." United States Patent 7449065. 2008 PPIRB, NASA Planetary Protection Independent Review Board Final Report. NASA Science Mission Directorate, Washington, DC, 2019.
- Qiu, Songgang, and Laura Solomon. "Free-Piston Stirling Engine Generators." Energy Conversion - Current Technologies and Future Trends, 2019, doi:10.5772/intechopen.79413.
- Radebaugh, R. "Pulse tube cryocoolers for cooling infrared sensors." Proceedings of SPIE, The International Society for Optical Engineering, Infrared Technology and Applications XXVI, Vol. 4130, pp 363-379 (see in particular Fig. 7). 2000.
- Rappaport, N.J., Konopliv, A.S., Kucinskis, A.B. and Ford, P.G., 1999. An improved 360 degree and order model of Venus topography. *Icarus*, 139(1), pp.19-31.
- Romeo I., and Turcotte D. (2008) Pulsating continents on Venus: an explanation for crustal plateaus and Tessera terrains, *Earth Planet. Sci. Lett.* 276, 85–97.
- Rost, F.W.D. (1992) Fluorescence Microscopy, Volume 2. Cambridge Univ. Press, 473 pp.
- Russell, C. T., R. C. Elphic, and J. A. Slavin (1979), Initial Pioneer Venus magnetometer observations, Proc. Lunar Planet. Sci. Conf. 10th, 2277-2290.
- Santos A. R. et al., (2020) Venus Petrology: The Need for New Data, Planetary Science and Astrobiology Decadal Survey White Paper.
- Schubert, G., C. Covey, A. Del Genio, L.S. Elson, G. Keating, A. Seiff, R.E. Young, J. Apt, C.C. Counselman, III, A.J. Kliore, S.S. Limaye, H.E. Revercomb, L.A. Sromovsky, V.E. Suomi, F. Taylor, R. Woo, and U. von Zahn, 1980: Structure and circulation of the Venus atmosphere. *J. Geophys. Res.*, 85, 8007-8025, doi:10.1029/JA085iA13p08007.
- Schulze-Makuch, D., Grinspoon, D. H., Abbas, O., Irwin, L. N., & Bullock, M. A. (2004). A sulfur-based survival strategy for putative phototrophic life in the Venusian atmosphere. *Astrobiology*, 4(1), 11-18.
- Schweitzer J. S., A. M. Parsons, J. Grau, D. J. Lawrence, T. P. McClanahan, J. Miles, P. Peplowski, L. Perkins, R. Starr (2017) Measuring surface bulk elemental composition on Venus, *Physics Procedia*, 90, 180-186.
- Schwig J., G. Muller, M. Eickhoff, O. Ambacher, M. Stutzmann. "Gas sensitive GaN/AlGaN heterostructures." Sensors and Actuators B87, 425-430. 2002.
- Schreiber, J. G. "Assessment of the free-piston Stirling convertor as a long life power convertor for space." AIAA-2000-3021. 2000.



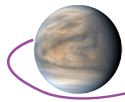
- Schreiber, J. G. "Developmental considerations on the free-piston Stirling power convertor for use in space." Proceedings of the 4th International Energy Conversion Engineering Conference (IECEC-2006), San Diego, CA. June 2006
- Schwartz, Z. D. and G. E. Ponchak, "High temperature performance of a SiC MESFET based oscillator," 2005 IEEE MTT-S Int. Microwave Symp. Dig. Long Beach, CA, pp 1179-1182. June 2005.
- Seager S, Petkowski JJ, Gao P, Bains W, Bryan NC, Ranjan S, Greaves J. The Venusian lower atmosphere haze as a depot for desiccated microbial life: a proposed life cycle for persistence of the Venusian aerial biosphere," *Astrobiology*, 2020; in press.
- Seiff A. for the Vega Science Balloon Team (1987) Further information on structure of the atmosphere of Venus derived from the VEGA Venus balloon and Lander mission, *Advances in Space Research*, 7, 323-328, [https://doi.org/10.1016/0273-1177\(87\)90239-0](https://doi.org/10.1016/0273-1177(87)90239-0).
- Semprich, J., Filiberto, J., Treiman, A. H. (2020). Venus: A phase equilibria approach to model surface alteration as a function of rock composition, oxygen-and sulfur fugacities. *Icarus*, 113779.
- Senske, D. A., and J. J. Plaut. 2000. The Tellus Region of Venus: Processes in the Formation and Modification of Tessera Terrain, LPSC 31, Abstract # 1496.
- Sergeev, D.E., Lambert, F.H., Mayne, N.J., Boutle, I.A., Manners, J., Kohary, K. (2020) Atmospheric Convection Plays a Key Role in the Climate of Tidally Locked Terrestrial Exoplanets: Insights from High-resolution Simulations. *The Astrophysical Journal* 894, <https://doi.org/10.3847/1538-4357/ab8882>
- Shaltens, R. K. and W. A. Wong. "Advanced Stirling technology development at NASA Glenn Research Center." NASA/TM—2007-214930. 2007.
- Shalygin, E.V., Markiewicz, W.J., Basilevsky, A.T., Titov, D.V., Ignatiev, N.I. and Head, J.W., 2015. Active volcanism on Venus in the Ganiki Chasma rift zone. *Geophysical Research Letters*, 42(12), pp.4762-4769.
- Sharpton, V.L., Esposito, L. and Sotin, C. 2014. Venus Exploration Targets Workshop, Final Report, Houston, TX.
- Shen, Z. and Z. Zhan (2020). Metastable Olivine Wedge Beneath the Japan Sea Imaged by Seismic Interferometry. *Geophys. Res. Lett.* <https://doi.org/10.1029/2019GL085665>
- Shepard, M. K., B. A. Campbell, M. H. Bulmer, T. G. Farr, L. R. Gaddis, & J. J. Plaut. 2001. "The roughness of natural terrain: A planetary and remote sensing perspective." *Journal of Geophysical Research*, 106, 32,777-32,795.
- Smith D.J., Microbes in the upper atmosphere and unique opportunities for astrobiology research. *Astrobiology* 2013;13(10): 981-990.
- Smrekar, S., R.J. Phillips, Venusian highlands: geoid to topography ratios and their implications. *Earth Planet. Sci. Lett.* 107, 582-597 (1991)
- Smrekar, S.E., Stofan, E.R., Mueller, N., Treiman, A., Elkins-Tanton, L., Helbert, J., Piccioni, G., Drossart, P., 2010. Recent hot spot volcanism on Venus from VIRTIS emissivity data. *Science*, 328, 605-608.
- Smrekar, S.E., et al., (2020) VERITAS (Venus Emissivity Radio Science, InSAR, Topography and Spectroscopy): A proposed Discovery mission, *Lunar. Plan. Sci.*, 51, Abstract #1449.
- Smrekar, S.E., Davaille, A. & Sotin, C. Venus Interior Structure and Dynamics. *Space Sci Rev* 214, 88 (2018). <https://doi.org/10.1007/s11214-018-0518-1>
- Smrekar, S. E., L. Elkins-Tanton, J.J. Leitner, A. Lenardic, S. Mackwell, L. Moresi, C. Sotin, E.R. Stofan, Tectonic and volcanic evolution of Venus and the role of volatiles: implications for understanding the terrestrial planets, in Exploring Venus as a Terrestrial Planet, ed. by L.W. Esposito et al.. AGU Geophysical Monograph Series, vol. 176 (2007), pp. 45-71
- Solomatov, V.S., Moresi, L.N., 1996. Stagnant lid convection on Venus. *J. Geophys. Res.: Planets* 101, 4737-4753.
- Solomon, S.C., Smrekar, S.E., Bindshadler, D.L., Grimm, R.E., Kaula, W.M., McGill, G.E., Phillips, R.J., Saunders, R.S., Schubert, G., Squyres, S.W. and Stofan, E.R., (1992), Venus tectonics: An overview of Magellan observations. *Journal of Geophysical Research: Planets*, 97(E8), pp.13199-13255.



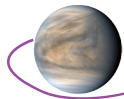
- Son K.-A., Y. Liu, P. P. Ruden, J. Xie, N. Biyikli, Y. T. Moon, N. Onojima, H. Morkoç. “GaN-based micro pressure sensor for extreme environments.” *Proc. IEEE Sensors*, 1259. 2005.
- Son K.-A., B. Yang, N. Prokopuk, J.S. Moon, A. Liao, M. Gallegos, J. Yan, M.A. Khan. “GaN-based micro chemical sensor nodes for early warning of chemical agents.” *Proceedings of SPIE 6556 Micro (MEMS) and Nanotechnologies for Defense and Security*, paper # 6556-36. 2007.
- Son K.-A., B. H. Yang, A. Liao, N. Prokopuk, J. S. Moon, T. M. Katona, M. A. Khan. “Novel GaN micro chemical sensor nodes for long-range trace chemical agent detection and mapping.” *Proceedings of 2008 Chemical and Biological Defense Physical Science and Technology*. 2008.
- Spencer, M., Chan, S., Veilleux, L. and Wheeler, K., 2009, May. The soil moisture active/passive (SMAP) mission radar: A novel conically scanning SAR. In *2009 IEEE Radar Conference* (pp. 1-4).
- Spry, D. J., P. G. Neudeck, L.-Y. Chen, G. M. Beheim, R. S. Okojie, C. W. Chang, R. D. Meredith, T. L. Ferrier, L. J. Evans. “Fabrication and testing of 6H-SiC JFETs for prolonged 500 °C operation in air ambient.” *Silicon Carbide and Related Materials 2007*, Materials Science Forum, T. Kimoto, Ed., Switzerland: Trans Tech Publications. 2008.
- Steffes, P. G., J. M. Jenkins, R. S. Austin, S. W. Asmar, D. T. Lyons, E. H. Seale, and G. L. Tyler (1994), Radio Occultation Studies of the Venus Atmosphere with the Magellan Spacecraft: 1. Experimental Description and Performance, *Icarus*, 110, pp. 71-78, <https://doi.org/10.1006/icar.1994.1107>
- Sternowski, R. H. “Extreme temperature design techniques for a Venus exploration S-band transmitter.” 6th International Planetary Probe Workshop, Atlanta, GA. June 2008.
- Stevenson, D.J., Spohn, T., and Schubert, G. 1983. Magnetism and thermal evolution of the terrestrial planets. *Icarus* 54, 466-489.
- Sukhanov, A.L., 1992. Tesseræ. In: Bursukov, V.L., Basilevsky, A.T., Volkov, V.P., Zharkov, V.N. (Eds.), *Venus Geology, Geochemistry, and Geophysics*, Research Results from the USSR. Univ. of Arizona Press, Tuscon, pp. 82–95.
- Sutin, B. M., et al. 2018. VAMOS: a SmallSat mission concept for remote sensing of Venusian seismic activity from orbit. *Proc. SPIE 10698, Space Telescopes and Instrumentation 2018: Optical, Infrared, and Millimeter Wave*, 106985T (6 July 2018); doi: [10.1117/12.2309439](https://doi.org/10.1117/12.2309439)
- Tabel, S., & W. Stechele. 2017. “Fast computation of readout smear correction for framestore CCD based images.” *Proceedings of the 2017 International Conference on Computer Graphics and Digital Image Processing*. <https://doi.org/10.1145/3110224.3110233>
- Tanaka, K. L., D. A. Senske, M. Price, & R. L. Kirk. 1997. “Physiography, geomorphic/geologic mapping and stratigraphy of Venus.” In: Bougher, S. W., Hunten, D. M., & Phillips, R. J. (Eds.). *Venus II: Geology, Geophysics, Atmosphere, and Solar Wind Environment*. The University of Arizona Press, Tucson. Pg 667-696.
- Tarau, C., et al. “Thermal Management System for Long-Lived Venus Landers.” 9th Annual International Energy Conversion Engineering Conference, 2011, doi:[10.2514/6.2011-5643](https://doi.org/10.2514/6.2011-5643).
- Taylor, G.J. 2013. The bulk composition of Mars. *Chemie der Erde-Geochemistry* 73, 401-420.
- Taylor F. W. (2014) *The Scientific Exploration of Venus*, Cambridge University Press, 295 pp.
- Taylor, F. W., Svedhem, H., & Head, J. W. (2018). Venus: The atmosphere, climate, surface, interior and near-space environment of an Earth-like planet. *Space Science Reviews*, 214(1), 35. <https://doi.org/10.1007/s11214-018-0467-8>
- Tellmann, S., M. Patzold, B. Hausler, M. K. Bird, and G. L. Tyler (2009), Structure of the Venus neutral atmosphere as observed by the Radio Science experiment VeRa on Venus Express, *J. Geophys. Res.*, 114, E00B36, doi:[10.1029/2008JE003204](https://doi.org/10.1029/2008JE003204)
- Titov, D. V., Ignatiev, N. I., McGouldrick, K., Wilquet, V., & Wilson, C. F. (2018). Clouds and hazes of Venus. *Space Science Reviews*, 214(8), 126.
- Tomasko, M. G., Doose, L. R., Smith, P. H., & Odell, A. P. (1980). Measurements of the flux of sunlight in the atmosphere of Venus. *Journal of Geophysical Research: Space Physics*, 85(A13), 8167-8186.
- Toon, O. B., Turco, R. P., Pollack, J. B., 1982. The ultraviolet absorber on Venus: Amorphous sulfur. *Icarus*. 51, 358-373.
- Treiman, A. and Filiberto, J. 2016. How Good is Good Enough? Major Element Chemical Analyses of Basalt by Spacecraft Instruments, Lunar and Planetary Science Conference, p. 1029.



- Treiman, A. H. (2007) Geochemistry of Venus' surface: Current limitations as future opportunities, in *Exploring Venus as a Terrestrial Planet*, edited by LW. Esposito et al., pp. 7-22, AGU Geophysical Monograph Series 176, Washington, D.C.
- Treiman, A.H., Gleason, J.D. and Bogard, D.D., 2000. The SNC meteorites are from Mars. *Planetary and Space Science*, 48(12-14), pp.1213-1230.
- Treiman A. H. et al. (2020) Laboratory Studies in Support of Venus Exploration: Surface and Near-Surface, Planetary Science and Astrobiology Decadal Survey White Paper.
- Turcotte D.L. (1993) An episodic hypothesis for Venusian tectonics. *J. Geophys. Res.* 98, 17061–17068.
- Turcotte D.L., Morein G., Roberts D., and Malamud B.D. (1999) Catastrophic resurfacing and episodic subduction on Venus. *Icarus* 139, 49–54.
- Ueno, Y., Johnson, M. S., Danielache, S. O., Eskebjerg, C., Pandey, A., Yoshida, N., 2009. Geological sulfur isotopes indicate elevated OCS in the Archean atmosphere, solving faint young sun paradox. *Proceedings of the National Academy of Sciences*. 106, 14784-14789. doi:10.1073/pnas.0903518106.
- Vandaele, A.C., Korablev, O., Belyaev, D., Chamberlain, S., Evdokimova, D., Encrenaz, T., Esposito, L., Jessup, K.L., Lefevre, F., Limaye, S. and Mahieux, A., 2017. Sulfur dioxide in the Venus Atmosphere: II. Spatial and temporal variability. *Icarus*, 295, pp.1-15.
- Vaniman, D. T., et al, 2014. Mineralogy of a Mudstone at Yellowknife Bay, Gale Crater, Mars. *Science*, 343.
- VBST (Venus Bridge Study Team). 2018. Venus Bridge: A concept for the low cost exploration of Venus. Delivered to the NASA AA, public briefing available here: [https://www.lpi.usra.edu/vexag/meetings/archive/vexag\\_15/presentations/19-Grimm-Venus-Bridge-Focus-Group.pdf](https://www.lpi.usra.edu/vexag/meetings/archive/vexag_15/presentations/19-Grimm-Venus-Bridge-Focus-Group.pdf)
- Venera-D JSDT (Venera-D Joint Science Definition Team). 2019, Venera-D: Expanding Our Horizon of Terrestrial Planet Climate and Geology Through the Comprehensive Exploration of Venus, Phase II Final Report, <https://www.lpi.usra.edu/vexag/reports/Venera-DPhaseIIFinalReport.pdf>
- VDRM (Venus Design Reference Team) 2018, 2018 Workshop on Autonomy for Future NASA Science Missions: Venus Design Reference Mission Reports, <https://science.nasa.gov/science-red/s3fs-public/atoms/files/NASA%202018%20Autonomy%20Workshop%20Venus%20DRM%20reports.pdf>
- Vergados, P., Komjathy, A., and X. Meng (2019), “Ionosphere Remote Sensing I: TID for Detection, Monitoring, and Forecasting Natural and Manmade Hazardous Events”, Book Chapter in *Position, Navigation, and Timing Technologies in the 21st Century, Integrated Satellite Navigation, Sensor Systems and Civil Applications*, Editors: Jade Morton, Frank van Diggelen, James Spilker Jr., Bradford Parkinson (in press).
- VEXAG GOI ([https://www.lpi.usra.edu/vexag/reports/VEXAG\\_Venus\\_GOI\\_Current.pdf](https://www.lpi.usra.edu/vexag/reports/VEXAG_Venus_GOI_Current.pdf))
- VFMS (Venus Flagship Mission Study). 2009. <https://vmf.jpl.nasa.gov/files/Venus+Flagship+Mission+Study+090501-compressed.pdf>
- von Zahn, U. et al. 1983. Composition of the Venus atmosphere, in *Venus* (D. M. Hunten et al, eds.) pp. 299-430, University of Arizona Press.
- Voss, Paul. “Advances in Controlled Meteorological (CMET) balloon systems.” AIAA Balloon Systems Conference. 2009.
- Wacey, D., Kilburn, M. R., Saunders, M., Cliff, J., & Brasier, M. D. (2011). Microfossils of sulphur-metabolizing cells in 3.4-billion-year-old rocks of Western Australia. *Nature Geoscience*, 4(10), 698-702.
- Wächtershäuser, G. (1988). Before enzymes and templates: theory of surface metabolism. *Microbiological reviews*, 52(4), 452.
- Wächtershäuser, G. (2007). On the chemistry and evolution of the pioneer organism. *Chemistry & Biodiversity*, 4(4), 584-602.
- Waite, J. H., Jr., Combi, M. R., Ip, W.-H., Cravens, T. E., McNutt, R. L., Jr., Kasprzak, W., Yelle, R., Luhmann, J., Niemann, H., Gell, D., Magee, B., Fletcher, G., Lunine, J., Tseng, W.-L. “Cassini Ion and Neutral Mass Spectrometer: Enceladus plume composition and structure. *Science* 311, 1419-1422. 2006.



- Waksman, S. A., & Joffe, J. S. (1922). Microorganisms concerned in the oxidation of sulfur in the soil: II. Thiobacillus Thiooxidans, a new sulfur-oxidizing organism isolated from the soil 1. *Journal of bacteriology*, 7(2), 239.
- Wang, R., G. Ma, Q. Qin, Q. Shi, & J. Huang. 2018. "Blind UAV images deblurring based on discriminative networks." *Sensors*, 18, 2874-2897. doi: [10.3390/s18092874](https://doi.org/10.3390/s18092874)
- Wang, R., W. H. Ko, D. J. Young. "Silicon-carbide MESFET-based 400 °C MEMS sensing and data telemetry." *IEEE Sensors Journal*, Vol. 5, No. 6, pp 1389-1394. Dec. 2005.
- Ward, S. T. Allen and J. Palmour. "Reliability assessment of production SiC MESFETS." GaAs MANTECH Technical Digest, New Orleans, LA. 2005
- Wasmund, K., Mußmann, M., and Loy, A. 2017. The life sulfuric: microbial ecology of sulfur cycling in marine sediments. *Environ Microbiol Reports* (4): 323–344. doi: [10.1111/1758-2229.12538](https://doi.org/10.1111/1758-2229.12538)
- Watson, E. B., Thomas, J. B., Cherniak, D. J., 2007. 40Ar retention in the terrestrial planets. *Nature*. 449, 299-304.
- Way, M.J., and A.D. Del Genio, 2020: Venusian habitable climate scenarios: Modeling Venus through time and applications to slowly rotating Venus-like exoplanets. *J. Geophys. Res. Planets*, 125, no. 5, e2019JE006276, doi:[10.1029/2019JE006276](https://doi.org/10.1029/2019JE006276).
- Way, M. J., Del Genio, A. D., Kiang, N. Y., Sohl, L. E., Grinspoon, D. H., Aleinov, I., Kelley M., Clune, T. 2016. Was Venus the First Habitable World of our Solar System? *Geophys. Res. Lett.*, 43:8376–8383. doi:10.1002/2016GL06979
- Weitz, C. M., & A. T. Basilevsky. 1993. "Magellan observations of the Venera and Vega landing site regions." *Journal of Geophysical Research: Planets*, 98, 17069-17097. <https://doi.org/10.1029/93JE01776>
- Whitten et al. (2020) Venus Tesserae: The importance of Venus tesserae and remaining open questions, Planetary Science and Astrobiology Decadal Survey White Paper.
- Wiens, R. et al. 2012. The ChemCam Instrument Suite on the Mars Science Laboratory (MSL) Rover: Body Unit and Combined System Tests. *Space Science Reviews*. 170, 167-227.
- Wiens, R.C., S. Maurice, J. Lasue, O. Forni, R.B. Anderson, S. Clegg, et al. Pre-flight calibration and initial data processing for the ChemCam laser-induced breakdown spectroscopy instrument on the Mars Science Laboratory rover, *Spectrochim. Acta Part B*, 82 (2013), pp. 1-27.
- Wierzchos, D. M. and C. Ascaso. "Microbial fossil record of rocks from the Ross Desert, Antarctica: Implications in the search for past life on Mars." *International Journal of Astrobiology* 1, 51-59. 2002.
- Wilson, C., O'Neill, A., Baier, S., Nohawa, J. "A complementary III–V heterostructure field effect transistor technology for high temperature integrated circuits." vol.29, p.54-57. 1995.
- Wolcott, J.H., D.J. Simons, D.D. Lee, and R.A. Nelson (1984). Observations of an ionospheric perturbation arising from the Coalinga earthquake of May 2. *J. Geophys. Res.* 89, 6835–6839, 1984.
- Wong, M.H., S. K. Atreya, P.R. Mahaffy, H.B. Franz, C. Malespin, M.G. Trainer, J.C. Stern, P.G. Conrad, H.L.K. Manning, R.O. Pepin, R.H. Becker, C.P. McKay, T.C. Owen, R. Navarro-González, J.H. Jones, B.M. Jakosky, and A. Steele (2013). Isotopes of Nitrogen on Mars: Atmospheric measurements by Curiosity's mass spectrometer, with *Geophys. Res. Lett.*, 40(23):6033-6037, doi:[10.1002/2013GL057840](https://doi.org/10.1002/2013GL057840), 2013.
- World View Enterprises. <https://worldview.space/> (Retrieved March 2019).
- Wrbanek, J.D. and G. C. Fralick. "Thin film physical sensor instrumentation research and development at NASA Glenn Research Center." NASA TM-2006-214395, ISA# TP06IIS023. September 2006.
- Wu et al (2018). The near-UV absorber OSSO and its isomers. *Chem. Commun.*, DOI: 10.1039/c8cc00999f.
- Würfl, J., Hilsenbeck, J., Nebauer, E., Tränkle, G., Obloh, H., Österlem W. "Reliability of AlGaIn/GaN HFETs comprising refractory ohmic and Schottky contacts." *Microelectronics Reliability*, Volume 40, Issues 8-10, pp 1689-1693. 2000.
- Xiao, X., M. Yao, H. Cui, & Y. Fu. 2019. "Safe Mars landing strategy: Towards LIDAR-based high altitude hazard detection." *Advances in Space Research*, 63, 2535-2550. <https://doi.org/10.1016/j.asr.2019.01.005>



- Yuan, X., Z. Yu, P. Cui, R. Xu, S. Zhu, M. Cao, & E. Luan. 2018. "Probability-based hazard avoidance guidance for planetary landing." *Acta Astronautica*, 144, 12-22. <https://doi.org/10.1016/j.actaastro.2017.11.039>
- Yung, Y. L., W. B. Demore (1982). Photochemistry of the Stratosphere of Venus: Implications for Atmospheric Evolution. *Icarus* 51, 199-247.
- Zahnle, K. J., Planetary noble gases. E. H. Levy, J. I. Lunine, Eds., Protostars and Planets III. University of Arizona Press, Tucson, 1993, pp. 1305-1338.
- Zhan, Z. & H. Kanamori (2016). Recurring large deep earthquakes in Hindu Kush driven by a sinking slab. *Geophys. Res. Lett.* 43, 14, 7433-7441, <https://doi.org/10.1002/2016GL069603>
- Zhang, X., Liang, M.C., Montmessin, F., Bertaux, J.L., Parkinson, C. and Yung, Y.L., 2010. Photolysis of sulfuric acid as the source of sulfur oxides in the mesosphere of Venus. *Nature Geoscience*, 3(12), p.834.
- Zolotov, M.Y. 2018. Gas–solid interactions on Venus and other Solar System bodies. *Reviews in Mineralogy and Geochemistry* 84, 351-392.